Advances in Experimental Medicine and Biology 981

Joachim Krebs *Editor*

Membrane Dynamics and Calcium Signaling

Springer

Advances in Experimental Medicine and Biology

Volume 981

More information about this series at http://www.springer.com/series/5584

Joachim Krebs
Editor

Membrane Dynamics and Calcium Signaling

Springer

Editor
Joachim Krebs
MPI for Biophysical Chemistry
Göttingen, Germany

ISSN 0065-2598 ISSN 2214-8019 (electronic)
Advances in Experimental Medicine and Biology
ISBN 978-3-319-55857-8 ISBN 978-3-319-55858-5 (eBook)
https://doi.org/10.1007/978-3-319-55858-5

Library of Congress Control Number: 2018934719

Printed on acid-free paper

This Springer imprint is published by the registered company Springer International Publishing AG part of Springer Nature.
The registered company address is: Gewerbestrasse 11, 6330 Cham, Switzerland

Preface

Calcium as a versatile carrier of many signals can lead to cell-specific Ca^{2+} signalosomes delivering Ca^{2+} signals with spatial and temporal characteristics. These are especially true for membrane contact sites (MCSs) creating microdomains where two membranes of different organelles are closely apposed to facilitate molecular communication to promote Ca^{2+} signaling. The formation of MCSs is a highly dynamic process which is important to regulate Ca^{2+} homeostasis controlled by a plethora of Ca^{2+} channels, pumps, and exchangers. MCSs probably emerged early during eukaryotic evolution (Jain A, Holthuis JCM (2017) *BBA Mol Cell Res* 1864:1450–1458). They could be visualized early on by electron microscopy (see Fig. 1; Palade 1953), but their functional importance became evident much later.

Calcium controls a large number of cellular functions reflected by the numerous proteins regulating Ca^{2+} homeostasis. The recent significant improvement of different techniques to solve structures of large and complex proteins at high resolution and their involvement in the function of different MCSs increased our understanding of Ca^{2+} signaling to regulate cellular functions. This is due to highly specific interaction of Ca^{2+} with proteins resulting in specific modulations of protein–protein interactions which are followed by conformational changes of the participants. In recent years, it became evident that calcium often fulfills its signaling function within microdomains due to MCSs between different intracellular organelles such as the endo/sarcoplasmic reticulum and mitochondria or between intracellular organelles and the plasma membrane. Knowledge about the details of these dynamic processes rapidly increased in recent years. In this book, we review the most recent developments by leading experts in the field. It is a state-of-the-art summary of our present knowledge in this quickly growing field of calcium signaling in connection with dynamic membrane processes. The book provides insight into the impressive progress made in many areas of calcium signaling but also reminds us of how much remains to be learned.

I am grateful to all participants of this book for their support and their excellent contributions. I am indebted to Springer International for giving me the opportunity to edit this book. I hope it provides a stimulating guide to workers in this research

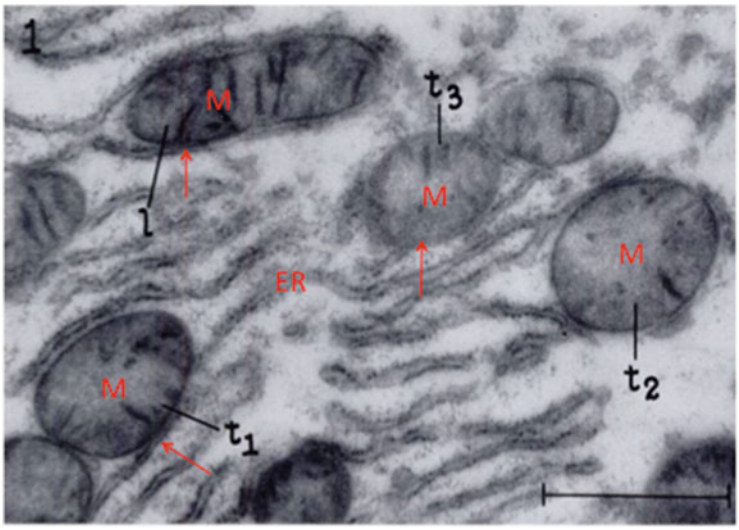

Fig. 1 The figure shows the electron micrograph of a small section of the cytoplasm of a rat liver cell as taken from Palade GE (1953) *J Histochem Cytochem* 1:188–211, with the permission of the publisher. *M* mitochondria, *ER* endoplasmic reticulum. The arrows point to possible membrane contact sites between the ER and a mitochondrion

area and to a broader scientific community with a general interest in the fascinating field of calcium signaling. My sincere thanks also go to Amrei Strehl, Claus-Dieter Bachem, and Rakesh Jotheeswaran from Springer who kindly helped in all aspects of editing this book. I am very grateful to Christian Griesinger, Head of the Department of NMR-Based Structural Biology at the Max Planck Institute for Biophysical Chemistry, for his long-standing support. Last but not least, I am very thankful to my wife, Eva Krebs-Roubicek, for her patience and understanding during the process of editing this book.

Göttingen, Germany Joachim Krebs
August 2017

Contents

Part I
Plasma Membrane

Chapter 1
The Plasma Membrane Calcium Pump (PMCA): Regulation of Cytosolic Ca^{2+}, Genetic Diversities and Its Role in Sub-plasma Membrane Microdomains

Joachim Krebs

Abstract In this chapter the four different genes of the mammalian plasma membrane calcium ATPase (PMCA) and their spliced isoforms are discussed with respect to the structural and functional properties of PMCA, the tissue distribution of the different isoforms, including their differences during development. The importance of PMCA for regulating Ca^{2+} signaling in microdomains under different conditions is also discussed.

Keywords PMCA · Ca^{2+} signaling · Calcium homeostasis · Second messenger · Ca^{2+} microdomains · CaMKIV · Alternative splicing

1.1 Introduction

Cells are activated by a variety of stimuli to which they must respond. This results in the cellular ability to change its functions rapidly depending on the signal. One of the most versatile carrier of many signals is calcium within and outside cells. In the extracellular body fluid (ECF) Ca^{2+} is in equilibrium between its free (ionized as Ca^{2+}) and bound forms which is controlled by a highly integrated and complex endocrine system. This involves the interplay between three hormones: parathyroid hormone, calcitonin and Vitamin D which regulate the calcium homeostasis of ECF [1]. Due to its high flexibility as a ligand with its unique coordination chemistry (coordination numbers are usually 6–8, but up to 12 are possible) and its polarizability, Ca^{2+} can regulate many important aspects of cellular activity. As one of the second messengers calcium participates in many different signal transduction pathways leading to protein phosphorylation and dephosphorylation, cell proliferation, differentiation, gene transcription, cell motility, neurotransmission and programmed cell death [2]. Therefore it is probably fair to say that calcium-dependent processes are beginning with fertilization to create new life and ending life with the

J. Krebs (✉)
Max Planck Institute for Biophysical Chemistry, Göttingen, Germany
e-mail: jkrebs@nmr.mpibpc.mpg.de

J. Krebs (ed.), *Membrane Dynamics and Calcium Signaling*, Advances in Experimental Medicine and Biology 981,
https://doi.org/10.1007/978-3-319-55858-5_1

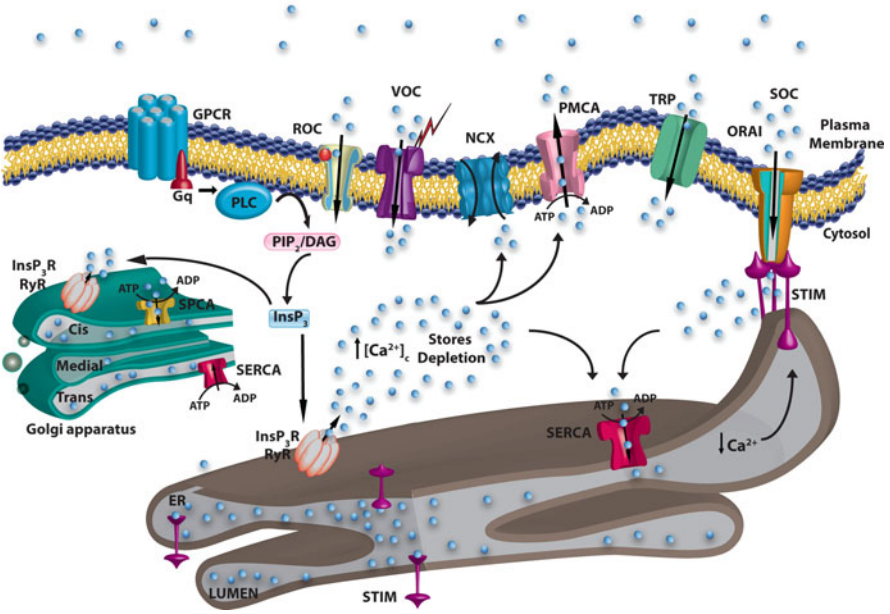

Fig. 1.1 Schematic representation of Ca^{2+} transporters and channels in the plasma membrane and in intracellular organelles. The Figure has been reproduced from Carafoli, E., Krebs, J. (2016) Calcium and Calmodulin Signaling, in: Encyclopedia of Cell Biology (R.A. Bradshaw, P.D. Stahl, eds.), Volume 3, pp. 161–169. Elsevier Inc. with permission from the publishers

programmed cell death [3].Thus, the maintenance of calcium homeostasis is a highly integrated process consisting of a number of hormonally controlled feedback loops and an elaborate system of Ca^{2+}-transporters, -channels, -exchangers, Ca^{2+}-binding/buffering proteins and Ca^{2+}-pumps. It is of central importance that Ca^{2+} fluxes into and out of the cell are tightly regulated (see Fig. 1.1).

The response to cellular activation by signal-accepting receptors can lead up to a 100-fold increase in intracellular free Ca^{2+} concentration which in a resting cell is in the order of 100–200 nM. In order that changes of intracellular Ca^{2+} concentration either as uptake from extracellular Ca^{2+} or as release from intracellular stores can fulfill the properties of an intracellular messenger, this is accomplished due to the interaction of Ca^{2+} with proteins which specifically interact with Ca^{2+} with high efficiency and within a background of mM Mg^{2+} concentrations, the so-called EF-hand proteins [4]. At variance with extracellular proteins which bind Ca^{2+} with low affinity, the EF-hand proteins like calmodulin and related proteins bind Ca^{2+} with high affinity and cooperativity. The characteristics of these proteins is the content of a helix-loop-helix motif which is now known as the EF-hand as introduced by Kretsinger [5] based on the crystal structure of parvalbumin (PV) [6]. The structure of PV contains six alpha helices, named A to F of which helices E and F enclose a Ca^{2+}-binding loop resembling a human hand, the "EF-hand". This motif was later discovered in numerous other proteins (see [4]) as a highly conserved structural Ca^{2+}-binding arrangement for intracellular proteins mediating Ca^{2+}-dependent

cellular responses. Most recent examples of EF-hand containing proteins include the calcium release channel known as ryanodine receptor [7–9] and the MCU complex of the mitochondrial Ca^{2+} uniporter [10–12]. In these proteins EF-hand motifs are proposed to regulate the gating mechanism of the Ca^{2+} transport (see Chaps. 8 and 12).

Key to control the level of intracellular Ca^{2+} concentration are several membrane-bound calcium transport systems of different capacity and affinity for Ca^{2+}: the plasma membrane sodium/calcium exchanger (NCX) and the mitochondrial calcium uniporter, both proteins of high capacity, but low affinity for Ca^{2+}; and the calcium pumps of the sarco/endoplasmic reticulum (SERCA) and the plasma membrane (PMCA), both of high affinity for Ca^{2+} and responsible for the fine tuning of the Ca^{2+} level in a resting cell. This was especially assumed for the PMCA of which some isoforms have a higher affinity measured for Ca^{2+}-transporting systems (e.g. see [13]), but due to its low abundance it is more reasonable to assume that its function is more effective in Ca^{2+} microdomains (for recent reviews see [14–16]). In this chapter I will summarize the general properties of PMCA, its genetic differences with special emphasis on differences in tissue distribution, development and pathology, a variety which is due to differences of genetic and spliced isoforms. Finally, I will discuss the functional importance of PMCA isoforms in Ca^{2+} microdomains.

1.2 General Properties of PMCA

In 1961 Dunham and Glynn first reported the existence of a Ca^{2+}-dependent ATPase in erythrocytes [17] which was later confirmed by Schatzmann who provided evidence that Ca^{2+} is pumped out of human red blood cells against a Ca^{2+} gradient on the expense of ATP [18]. Later it was demonstrated that P-type ATPases ([19, 20]; see also [21]) typically form a phosphorylated high-energy intermediate, i.e. an acyl-phosphate (usually aspartyl-phophate) to provide the enzyme with sufficient energy to pump ions across the membrane against its gradient. 1977 two independent Labs reported that the PMCA from erythrocytes could be stimulated by calmodulin [22, 23]. This finding encouraged Niggli et al. to purify PMCA from erythrocytes using a calmodulin affinity column [24]. The purification of the enzyme permitted the detailed investigation of the properties of PMCA. It could be documented that among the numerous activators of the PMCA like acidic phospholipids and others [25] calmodulin is the major regulator of the plasma membrane calcium pump leading to the identification of a calmodulin-binding domain of the pump [26], and solving the primary structure of the enzyme [27, 28].

PMCA, with a size between 120 and 140 kDa due to genetic diversity and alternatively spliced isoforms (see later), is a membrane protein with ten transmembrane helices, and the N- and C-termini both located in the cytosol. The enzyme is an essential component of all mammalian plasma membranes, and seems to be present in all animal cells and in plants ([16]; see also [29]). Mammals contain four different

genes encoding PMCA. Additional isoforms are obtained due to alternative splicing of the primary transcript as first demonstrated by Strehler et al. [30]. The four genes contain two splice sites, characterized as splice site "A" and splice site "C" (the original identified additional splice site "B" turned out to be a product of aberrant splicing; see [31]). These are both located close to or within regulatory domains of the enzyme giving rise to more than 30 different isoforms of slightly different molecular weights [16, 31, 32]. As can be noticed from Fig. 1.2 the major protein mass protrudes into the cytosol enclosing two cytosolic loops and a long C-terminal tail containing the calmodulin-binding domain [26] and other regulatory sites [16]. In plants the calmodulin-binding domain is located close to the N-terminus of the enzyme [29, 33]. Splice site "A" is located closely upstream of the phospholipid binding site thereby changing the length of the first intracellular loop, the

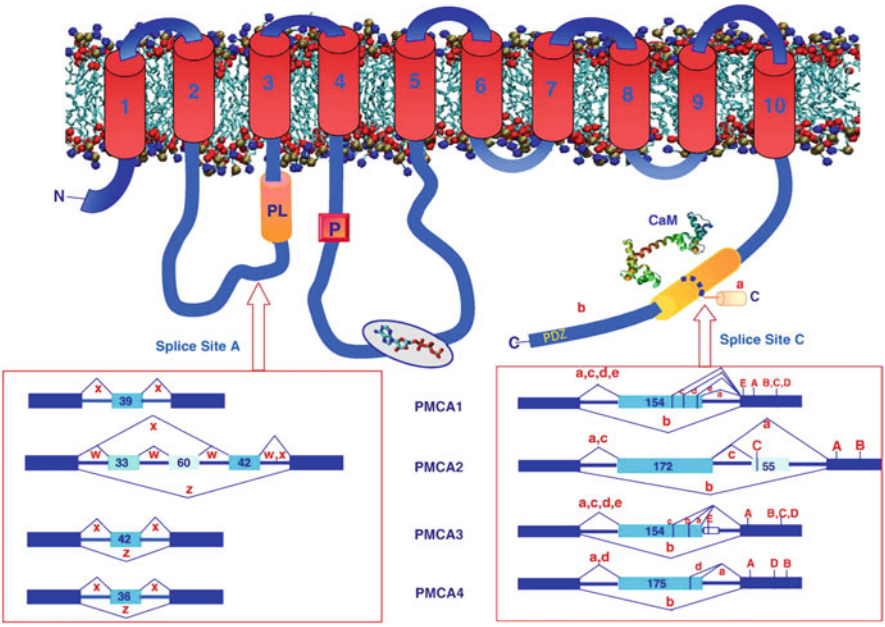

Fig. 1.2 Topology domains and splicing variants of the human PMCA isoforms. The ten transmembrane domains of the pump are numbered and indicated by red boxes. Splice sites "A" (first cytosolic loop) and "C" (C-terminal tail) are indicated by red arrows. Splice site "C" lies within the calmodulin-binding domain (yellow cylinder; defined by the structural model of *CaM* calmodulin). The exon structure of the different regions affected by alternative splicing is shown for each of the four different PMCA genes. Constitutively spliced exons are indicated as dark blue boxes, alternatively inserted exons are shown in light blue; the resulting splice variants are labeled by their lower case symbols, the positions of the translation stop codons for each splice form are indicated by the corresponding capital letters. In PMCA3, splice variant "e" results from a read-through of the 154-nt exon into the following intron (indicated as small open box). The sizes of alternatively spliced exons are given as nucleotide numbers. *PL* phospholipid binding domain, *P* location of the aspartyl-phosphate formation, *PDZ* consensus sequence recognizing PDZ domains of interacting targets. Reproduced from Krebs [32] with permission of the publishers

second loop encloses the catalytic center with the ATP binding site and the aspartate essential for building the high energy acyl-phosphate (Fig. 1.2). Interestingly, splice site "C" was identified within the calmodulin-binding domain giving rise to isoforms with markedly different amino acid sequences due to a shift of the reading frame resulting in a change of sensitivity towards calmodulin regulation [32]. PMCA is the only calmodulin-dependent enzyme known to date producing spliced isoforms with distinct regulatory properties. On the other hand, in the absence of calmodulin the calmodulin-binding domain is interacting with two internal receptor sites located within the catalytic center of the enzyme to keep the PMCA in an autoinhibited state [34, 35]. In plants, the calmodulin-binding domain of the plasma membrane calcium pump, located in the N-terminal cytoplasmic domain of the pump, is overlapping with the autoinhibitory region of the enzyme [29].

1.3 Structural Details of PMCA

As mentioned before, the calcium pump of the plasma membrane belongs to the class of P-type ATPases [19–21] like the calcium pump of the sarcoplasmic/endoplasmic reticulum. Both enzymes undergo conformational changes during the reaction cycle for which energy is provided by ATP forming a high energy acylphosphate to enable the pumps to transfer Ca^{2+} across the membrane against a steep Ca^{2+} ion gradient. For some time the basic conformational differences recognized as the Ca^{2+}-high affinity and Ca^{2+}-low affinity types were called the E1 and E2-forms of the pumps [36, 37]. Due to the seminal work of Toyoshima and coworkers structural details of the reaction cycle have been solved for the SERCA pump leading to a general understanding of the function of P-type ATPases ([38]; for review see [21, 39]). Based on the solved crystal structures of the different conformations during the reaction cycle three major cytosolic domains of the SERCA pump have been identified: the actuator (A), the nucleotide-binding (N) and the phosphorylation domain (P; see [39]). Large domain movements could be observed if the pump changes from the E1 to the E2 form (see [39]). After binding of ATP to the nucleotide binding domain conformational change brings this site close to the catalytic aspartate to form the Ca^{2+}-dependent high energy acyl-phosphate. The conformational change of the cytosolic part of the pump is transmitted to the transmembrane helices where the high affinity calcium binding site is then rearranged to decrease its affinity for calcium which is thus released to the extracellular side of the membrane. Interestingly, it has been noted for PMCA that per each reaction cycle the use of one ATP transports one Ca^{2+} across the membrane of reconstituted liposomes [40]. This is in contrast to the SERCA pump which operates at a stoichiometry of two Ca^{2+}/ATP [41].

Considerable attempts have been made over the years to crystallize PMCA, but those have failed so far, even if preliminary reports crystallizing a homologous PMCA from plants have been published [33]. The failure to crystalize protein isoforms of the PMCA from higher organisms is probably due to the properties of

the C-terminal sequence containing the calmodulin-binding domain which permits the pump to oligomerize [42]. This peculiar property of PMCA may prevent the building of defined crystal structures. Nevertheless, structural homology between the SERCA and the PMCA pumps permitted homology modeling of the PMCA pump (omitting the 37 N-terminal and the 144 C-terminal amino acids of PMCA which have no correspondence in the SERCA pump; [43]). The model demonstrates the conformational differences between the Ca^{2+} low affinity E2 form (Fig. 1.3a) and the Ca^{2+} high affinity form E1 of PMCA (Fig. 1.3b).

In order to evaluate the structural impact of calmodulin on its interaction with the PMCA pump the structure of complexes of calmodulin with synthetic peptides, C20W and C24W, have been investigated. These peptides correspond to different parts of the calmodulin-binding domain of the PMCA with an estimated length of 28 amino acids [26]. These complexes have been studied by small-angle X-ray scattering (SAXS; [45]) and NMR [46]. The SAXS experiments demonstrated that

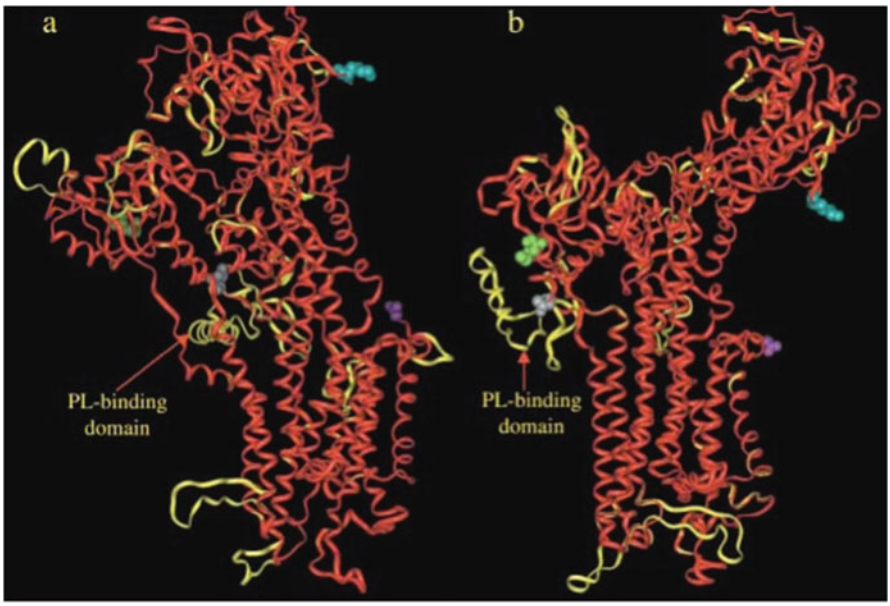

Fig. 1.3 Homology modeling of the PMCA pump based on the structures of the SERCA pump (see [39]) in (**a**) the Ca^{2+}-free (E2) and (**b**) the Ca^{2+}-bound (E1) forms. The models were generated with the automatic SWISS-MODEL server [43]. The amino acid sequences used for PMCA and SERCA were obtained from the SWISSPROT database (omitting the 37 N-terminal and the 144 C-terminal amino acid sequences of PMCA which have no correspondence in the SERCA pump). The two structures are shown as an overlay of the backbones in ribbon representation, SERCA in red, PMCA in yellow. The following amino acids of the SERCA pump are depicted as CPK models: N-terminal Met1 (green), Thr242 (gray, phospholipid binding domain of PMCA), and the C-terminal Gly994 (purple). The structures of the SERCA pump have been obtained from the PDB platform. The Ca^{2+}-free or E2 conformation is 1IWO, the Ca^{2+}-bound or E1 conformation is 1EUL. Reproduced from Krebs et al. [42] with permission from the publishers

the complex between calmodulin and C20W revealed an extended structure similar to calmodulin alone, whereas the complex with C24W resulted in the formation of a globular structure similar to those observed with many other calmodulin binding peptides (see [47]).

The detailed structure of calmodulin in complex with the peptide C20W was solved by NMR [46]. C20W corresponds to the conserved N-terminal part of the calmodulin-binding domain of PMCA (see below). It was shown that the C20W peptide bound selectively to the C-terminal half of calmodulin in agreement with the biochemical observation that PMCA can be activated by the C-terminal half of calmodulin alone, but not by its N-terminal half ([48]; see also [49]). The global structure of the calmodulin/C20W complex revealed an unusual extended structure similar to the dumbbell shape of calmodulin as observed by SAXS measurements ([45]; see also [50, 51]) which is different from the collapsed structure of the complex of calmodulin with the peptide M13 corresponding to the calmodulin-binding domain of myosin light chain kinase [52]. Later the group of Strehler solved the structure of the complex between calmodulin and the peptide C28W which corresponds to the entire length of the calmodulin-binding domain of the PMCA isoform 4b [53]. In this complex calmodulin is wrapped around the full-length calmodulin-binding domain.

The regulation of the PMCA activity by calmodulin is an impressive example for the autoregulatory properties of the Ca^{2+} signal. As soon as the pump is activated by calmodulin the concentration of Ca^{2+} in the direct environment of the cytosolic part of the pump decreases resulting in an at least partial dissociation of calmodulin (most likely the N-terminal domain of calmodulin from the C-terminal part of its binding site) with the consequent decrease of the pump activity. However, decreasing the activity of PMCA would consequently increase the Ca^{2+} concentration in its direct environment and promoting the rebinding of calmodulin to the pump demonstrating the oscillatory character of binding and regulating PMCA by calmodulin [54]. Therefore, the structure of the calmodulin/C20W complex may have a special significance for the function of the Ca^{2+} pump demonstrating the differences in affinity of calmodulin for the two halves of the calmodulin-binding domain (see also [48]). These differences in calmodulin sensitivity of the pump become even more visible due to alternative splicing within the calmodulin-binding domain [32] which results in striking differences of PMCA for its regulation by calmodulin. These variations lead to different activation profiles of the pump which possibly can influence the apparent affinity of the enzyme for Ca^{2+} [55], a property which may become important for tuning Ca^{2+} homeostasis in different microdomains of the cell (see below).

1.4 Genetic Diversity of PMCA in Health and Disease

In mammals four different genes encode the plasma membrane calcium pump (named ATP2B1-4 according to the genome database nomenclature) which in humans are located on four different chromosomes [16, 32]. Splice sites "A" and "C" give rise to numerous RNA splice variants encoding proteins of different length

and regulatory properties ([31]; see Fig. 1.2). In addition, alternative splicing can also occur in the 5′ untranslated region as described by Silverstein and Tempel [56] for ATP2B2.

Of the four different gene products PMCA 1 and 4 are generally described as the housekeeping forms of PMCA since their expression is widely distributed in tissues, but this view has changed in recent years as discussed by Brini et al. [57]. On the other hand, knock out mice of PMCA1 are the only phenotypes of PMCA which are embryonically lethal [58]. PMCA2 and 3 are specifically expressed in highly specialized tissues. PMCA2 is especially abundant in the Purkinje and granular cells of the cerebellum [59], in the outer hair cells of the inner ear [60], localized in the stereocilia [61], and in mammary glands [56]. PMCA3 is like PMCA2 mainly restricted to the nervous system, but in contrast to PMCA2 which is mainly abundant in postsynaptic densities, PMCA3 can be mainly found in presynaptic terminals of the cerebellum and the choroid plexus [62, 63], but also in skeletal muscle [64].

As can be realized from Fig. 1.2 splicing at site "A" affects exons of different sizes and complexity by comparing the different gene products. The splicing pattern of splice site "C" is even more complex as can be noticed from Fig. 1.2. One important difference between the splicing "a" and "b" variants should be made here: the "a" splicing variant of all four genes includes an extra exon which, if the entire exon is inserted, the reading frame is changed resulting in a protein with shorter C-terminal amino acid sequences due to an early stop codon. As mentioned before, since splice site "C" is located within the calmodulin binding domain, such a shift in the reading frame influences the property of the calmodulin binding domain resulting in a change in the sensitivity of regulating PMCA by calmodulin. The "b" variant of all four human genes do not include the spliced-in exons as discussed before for the "a" variant (Fig. 1.2) leading to a highly conserved C-terminal protein amino acid sequence with an identical calmodulin binding domain for all four "b" isoforms. Another interesting property of the "b" variants is that they all contain a PDZ domain-interacting sequence [65, 66] which is absent in all "a" variants due to the truncated C-terminal amino acid sequences. These PDZ domain-interacting sequences enable the PMCA "b" isoforms to form interacting complexes in Ca^{2+} signaling microdomains as discussed below [67, 68].

1.4.1 PMCA1

PMCA1 is widely distributed in most tissues of humans and animals. From all four PMCA genes PMCA1 seems to be the gene encoding the essential plasma membrane calcium pump, i.e. if knocked out it is the only isoform which leads to embryonic lethality in mice [58]. Therefore it can not be compensated by any of the other PMCA genes, especially during the early stages of development [69]. The importance of PMCA1 is underlined by the finding that PMCA1b can be detected during neural development of the rat already at the earliest days studied (E10; [70]). Brandt and Neve also observed that at E10 next to isoform PMCA1b PMCA1a was

only faintly visible, but during further development of the rat brain the expression of PMCA1b mRNA declined and the expression of variant 1a continuously increased suggesting that PMCA1a is an important isoform for brain development. This specific splice shift was later confirmed by Kip et al. [71]. The importance of this observation was underlined by the report of Strehler and co-workers [72] who provided evidence that PMCA1a is specifically expressed in the plasma membranes of neurons in different areas of the brain concentrating in somata, dendrites and spines. In these areas PMCA1a contributes to the modulation of soma-dendritic Ca^{2+} transients shaping the signals with high spatial and temporal resolution [73], but which according to Kenyon et al. [72] is not valid for all neurons investigated. This observation may indicate that PMCA1a contributes to the functional optimization of Ca^{2+} handling only in particular neurons [72].

One of the functional consequences by comparing PMCA1a with the "b" isoform is the considerable difference in the C-terminal amino acid sequence resulting in a lower calmodulin sensitivity for PMCA1a which could influence the basic Ca^{2+}-pumping activity of the enzyme. Caride et al. [13] compared in detail the difference between "a" and "b" isoforms in calmodulin binding and activation for PMCA4. They demonstrated that PMCA4a is more efficient than PMCA4b in reducing cytosolic Ca^{2+} concentrations after a Ca^{2+} spike due to its higher basic Ca^{2+} activity. Similar conclusions could be drawn for the activation kinetics of PMCA1a in comparison to PMCA1b.

Considering the surprising result of switching from PMCA1b to 1a during embryonal development one may ask what signal regulates this switch in expression between the two isoforms. Even if this regulation is far from being understood in detail, certain aspects may become clear due to some recent reports. In 2001 Xie and Black demonstrated that the Ca^{2+}-calmodulin dependent protein kinase IV (CaMKIV), known to be responsible for regulating Ca^{2+}-dependent gene transcription [74] is also involved in Ca^{2+}-dependent regulation of alternative splicing ([75]; for further details see [32]). It was realized that the CaMKIV-dependent splicing was made possible using a common consensus sequence that was recognized by a heterogeneous nuclear ribonucleoprotein (hnRNP L) which if phosphorylated by CaMKIV regulated alternative splicing as demonstrated for calcium-dependent potassium channels [76]. By examining the human genome database a number of exons matching the consensus sequence have been identified [77] including exon 21 of PMCA1. This exon contains two internal splice donor sites (see [30]), the consensus recognition sequence for CaMKIV can be identified at the second splice donor site of exon 21, which is unique for PMCA1 [32]. Thus, if PMCA1a should be expressed appropriately the total sequence of exon 21 containing 154 nt has to be transcribed (Fig. 1.2) and the internal splice donor sites have to be suppressed which would be achieved by CaMKIV [32]. This regulation of alternative splicing for PMCA1 may explain why PMCA1a became the specific neuronal isoform as documented by Kenyon et al. [72]. Another interesting aspect of such a regulation by CaMKIV may be considered here. In a detailed study we demonstrated that in a fetal rat brain primary cell culture system the expression of CaMKIV was directly induced by the thyroid hormone T_3 in a time- and concentration-dependent manner [78]. Since it is

well documented that T_3 is very important for neural development, the T_3-dependent induction of CaMKIV would thus be responsible for regulating the expression of the neural specific isoform PMCA1a important for Ca^{2+} homeostasis in the developing brain [79].

To date, PMCA1 is the only isoform for which no mutations have been described [32]. The essential role of PMCA1 is not only documented by the fact that it is the only isoform of PMCA which, if knocked out, is embryonically lethal [58, 69], but also by the finding that it can compensate for the absence of other isoforms like PMCA4 [69]. Large scale genomic studies in mice and human detected a special link between PMCA1 and its role controlling Ca^{2+} homeostasis in smooth muscles and influencing the regulation of blood pressure as reviewed by Brini et al. [14].

1.4.2 PMCA2

Early on it was recognized that PMCA2, as well as PMCA3 (see below), are specifically expressed only in highly specialized tissues. PMCA2 is mainly expressed in the nervous system, in the mammary gland or in other specialized tissues. As can be noticed from Fig. 1.2 several spliced isoforms may occur. In the PMCA2w/a isoform all possible exons of splice sites "A" and "C" are spliced in leading to a truncated form of the pump due to a frame shift caused by the "a" variant. In 1998 a mouse model was described which phenotypically was characterized with severe symptoms such as deafness and other neural disorders which resulted from a glycine to serine mutation (G283S) of PMCA2w/a located in a highly conserved amino acid sequence of PMCA2 [80]. PMCA2w/a is selectively expressed in the outer hair cells of the inner ear where it is localized in the stereocilia containing the sensory transduction apparatus responsible for hearing and balance of the mice [60, 61]. Similar results have been reported by Kozel et al. [81] for PMCA2-deficient mice. In humans a deafness phenotype has been reported for a G293S mutation of PMCA2w/a together with a simultaneous mutation in cadherin 23 critical for the correct functioning of the transduction complex [82].

Of special interest is the 5′ untranslated region of PMCA2 containing different regulatory domains as indicated before. By using different transcriptional start regions the enzyme is directed into different cell types such as Purkinje neurons, cerebellar granular cells, outer hair cells or epithelia cells of the lactating mammary gland [56]. To transport milk Ca^{2+} in the lactating mammary gland PMCA2 is expressed in the apical membrane of the epithelia only during lactation to become one of the most active pumps measured in an organism [83]. Recently it was reported that the expression level of PMCA2 correlates with HER2, a human epidermal growth factor receptor kinase and a specific marker for breast cancer [84]. PMCA2 interacts with HER2 in specific actin-rich membranes important for the localization of HER2 and its partners thereby influencing HER2-mediated cancer. This conclusion became apparent due to the finding that manipulating PMCA2 levels alters the

proliferation of breast cancer cells and knocking out PMCA2 inhibits the development of tumors in mice [84].

1.4.3 PMCA3

PMCA3, the least characterized isoform of the plasma membrane calcium pump, is like PMCA2 mainly expressed in the nervous system, basically located at presynaptic terminals of cerebellar granule cells [31], but also in the choroid plexus and in the hippocampus [62, 63]. In addition, PMCA3 is also expressed in skeletal muscles [64]. Recently, mutations of PMCA3 have been reported which could be connected with specific human diseases. In an extensive clinical study of patients suffering from hypertension it was shown that the ion homeostasis of cells have been impaired which was due to mutations of Na^+/K^+-ATPase (ATP1A1) and PMCA3 (ATP2B3) [85, 86]. The mutations of PMCA3 were located in the transmembrane domain leading to a distortion which probably affected the Ca^{2+} binding site of the pump. Zanni et al. [87] reported a missense mutation of PMCA3, the gene of which is located on the X chromosome [88]. It was interesting to observe that this missense mutation (G1107D) was discovered in two families with X-linked congenital cerebellar ataxia [87, 89]. The mutation G1107D is located within the calmodulin-binding domain leading to a decreased calmodulin-sensitivity of the pump and a reduced ability to control Ca^{2+} homeostasis of cells. These effects were demonstrated by overexpression of the mutated pump in HeLa cells [87]. Mice in which PMCA3 has been knocked out demonstrated a kind of sleep disorder, but no additional behavioral or histological defects were reported [90].

1.4.4 PMCA4

Next to PMCA1 PMCA4 has been detected in all tissues examined, but in contrast to PMCA1 PMCA4 is not embryonically lethal if knocked out, and mice carrying a PMCA4 null mutation showed a normal appearance and behavior [69]. Nevertheless, it has been reported that PMCA4 is of critical importance for specific cellular functions. Thus, it was shown that the activity of PMCA was critical to maintain a resting Ca^{2+} level in sperm cells [91] which later was identified as PMCA4b by the group of Neyses [92]. It was further demonstrated that loss of PMCA4 in male mice caused a sperm motility defect and infertility of those mice [69, 92]. In this context, another observation is of interest. Brandenburger et al. [93] found that during the sperm maturation process a switch from PMCA4b to 4a occurred suggesting that sperm maturation requires a shift from the slow PMCA4b to the faster PMCA4a variant due to its higher basic Ca^{2+} activity as reported by Caride et al. [13]. Similar observations have been made for a switch from PMCA1b to 1a during neural development as described before. In another study it was reported that PMCA4

ablation can prevent development of hypertrophic cardiomyopathy in transgenic mice expressing a tropomyosin E180G mutant in heart ([94]; see also [95]). Recently it was reported by Ho and co-workers [96, 97] that in a Chinese family with autosomal familial spastic paraplegia (FSP) a missense mutation of PMCA4 was discovered. They detected a R268Q mutation in six family members suffering from FSP which has not been described so far in any databank. The R268Q mutation is located closely to splice site "A" of PMCA and in the neighborhood of the phospholipid binding domain (see Fig. 1.2), a mutation which due to computational modeling may lead to a partly misfolded protein [97]. Therefore it was speculated that this mutation may be responsible for dysregulation of Ca^{2+} signaling causing neuronal deficits associated with FSP.

1.5 PMCA and Microdomains of Ca^{2+} Signaling

Considering the numerous isoforms of PMCA and its usual low abundance the question arises how significant is the participation of the plasma membrane calcium pump in regulating cytosolic Ca^{2+} homeostasis in the presence of the more efficient SERCA pump due to its greater abundance. In addition, the high transport capacity of the Na^+/Ca^{2+} exchanger can efficiently restore the cytosolic Ca^{2+} concentration to values typical for a cell at rest, especially in excitable tissues like the heart or the nervous system. In view of the specific tissue distribution of a number of different isoforms it is more likely that the main role of the PMCA pump is regulating the Ca^{2+} concentration in selected microdomains as discussed in detail in this section.

All "b" spliced isoforms contain a specific consensus sequence at the C-terminus of the protein for interacting with PDZ-domains of target proteins ([66]; see Fig. 1.2). As discussed in detail by Strehler [16] the identification of such a consensus sequence for direct recognition of PDZ-containing proteins led to the identification of a number of proteins such as the membrane-associated guanylate kinases (MAGUKs), PSD95, NOS-1 and other regulatory proteins which have been found to directly interact with PMCA"b" (and c/d; see Fig. 1.2) splice variants, but not with the "a" spliced isoforms due to the shift of the reading frame as mentioned before. This specific property, especially of the "b" splice variants of PMCAs enables the protein to be selectively incorporated into signaling complexes with specific functions concentrated in caveolae [67] or lipid rafts [68, 98]. The importance of the ability to recruit PMCA to such specific microdomains via its PDZ-domains recognizing amino acid sequence has been first demonstrated by the group of Neyses [99]. These authors provided evidence that PMCA4b interacted with the neuronal form of the NO synthase (nNOS) thereby tightly regulating the enzyme by altering local Ca^{2+} concentration. In a later study the same group generated transgenic mice overexpressing either full-length PMCA4b or a mutant lacking the last 120 amino acids at the C-terminus of the pump including the (autoinhibitory) calmodulin-binding domain and the consensus amino acid sequence recognizing PDZ-domains of target proteins ([100, 101]). This

mutant pump is highly active but is unable to regulate nNOS activity. In this way it was demonstrated in vivo that PMCA4b controls cardiac contractility through the interaction with nNOS regulating NO production and cAMP and cGMP signaling. Such a recruitment of PDZ-mediated PMCA to different membrane microdomains has been demonstrated also for other PMCA-PDZ protein interactions important for platelet activation [102], for activation of the muscarinic G-protein coupled receptor [103] or for interneuron calcium signaling mediated by the nicotinic acetylcholine receptor [104] as discussed by Strehler [16]. Thus it became obvious that locating PMCAs to different membrane microdomains has to be precisely organized to control the changing demands of Ca^{2+} signaling indicating that protein-protein interactions of PMCAs are dynamic processes with short-term and long-term regulations.

Another example of recruiting PMCA into specific microenvironments is its property to interact and be activated by acidic phospholipids [25], especially by phosphatidylinositol-4,5-bisphosphate (PIP_2; [105, 106]) which is as active as calmodulin [106] interacting with PMCA at a 1:1 molar ratio [105]. This observation may privilege PMCA to fine tune Ca^{2+} concentrations at ER-PM micro domains. It has been shown that depletion of the ER Ca^{2+} stores results in Orai-STIM1 clustering in ER-PM microdomains (for recent reviews see [107, 108]) which are reported to be shaped by PIP_2 PM lipid rafts domains [109], important modulators in Ca^{2+} signaling as mentioned before [68]. This is of interest since it is well documented that next to PMCA also STIM1 has a high affinity for PIP_2 [110]. Therefore, according to the group of Ambudkar ([111]; see also Chap. 11) there is ample evidence for microdomains representing the close proximity between ER and PM membranes in which regulators of SOCE, i.e. STIM1, Orai1 and TRPC1, are tightly associated in a functional complex with regulators of intracellular Ca^{2+}, i.e. PMCA and SERCA. Thus it is evident that modulation of Ca^{2+} signals reveal a dynamic Ca^{2+} signaling complex in which a number of different Ca^{2+} regulators in closed spatial environment are involved to control Ca^{2+} homeostasis of the cell.

1.6 Conclusions

In this chapter I summarized the structural and functional properties of the plasma membrane calcium pump pointing to the different ways how the enzyme is regulated. In recent years it became increasingly evident that PMCA is less participating in the control of the bulk cellular Ca^{2+} rather than controlling different aspects of local Ca^{2+} signaling. This specific role is underlined by the fact that the PMCA isoforms not only are translated from four different genes in mammals, but in addition numerous spliced isoforms enable the pump to control Ca^{2+} signaling spatially and temporarily restricted within microdomains in a cellular and tissue selective way [32]. Due to the specific property how the pump can interact with other partners within those microdomain complexes, for instance by recognizing PDZ-domains of interacting targets [66], this may transduce the regulation of local

Ca^{2+} signaling to modulate the activities of its local partners. In turn, mutations at critical sites of PMCA can lead to severe dysfunction and diseases as discussed above. Nevertheless, some of the molecular aspects with respect to the complexity of those microdomains and the role of the different isoforms of PMCA are still not completely understood and need further clarification.

Acknowledgement Thanks are due to Marek Michalak for critically reading the manuscript.

Conflict of Interest The author declares no conflict of interests.

References

1. Krebs J (1995) Calcium, biochemistry. In: Meyers RA (ed) Encyclopedia of molecular biology and molecular medicine, vol 1. VCH, Weinheim, pp 237–250
2. Carafoli E, Krebs J (2016) Why calcium? How calcium became the best communicator. J Biol Chem 291:20849–20857
3. Krebs J, Michalak M (2007) Calcium: a matter of life or death. Elsevier, Amsterdam
4. Kawasaki H, Nakayama S, Kretsinger RH (1998) Classification and evolution of EF-hand proteins. Biometals 11:277–295
5. Kretsinger RH (1975) Hypothesis: calcium modulated proteins contain EF hands. In: Carafoli E, Clementi F, Drabikowski W, Margreth A (eds) Calcium transport in contraction and secretion. Elsevier, Amsterdam, pp 469–478
6. Kretsinger RH, Nockolds CE (1973) Carp muscle calcium-binding protein. II. Structure determination and general description. J Biol Chem 248:3313–3326
7. Efremov RG, Leitner A, Aebersold R, Raunser S (2015) Architecture and conformational switch mechanism of the ryanodine receptor. Nature 517:39–43
8. Yan Z et al (2015) Structure of the rabbit ryanodine receptor RyR1 at near-atomic resolution. Nature 517:50–55
9. Zalk R et al (2015) Structure of a mammalian ryanodine receptor. Nature 517:44–49
10. Baughman JM et al (2011) Integrative genomics identifies MCU as an essential component of the mitochondrial calcium uniporter. Nature 476:341–345
11. De Stefani D, Raffaello A, Teardo E, Szabo I, Rizzuto R (2011) A forty-kilodalton protein of the inner membrane is the mitochondrial calcium uniporter. Nature 476:336–340
12. Perocchi F et al (2010) MICU1 encodes a mitochondrial EF hand protein required for Ca(2+) uptake. Nature 467:291–296
13. Caride AJ, Filoteo AG, Penniston JT, Strehler EE (2007) The plasma membrane Ca^{2+} pump isoform 4a differs from isoform 4b in the mechanism of calmodulin binding and activation kinetics. Implications for Ca^{2+} signaling. J Biol Chem 282:25640–25648
14. Brini M, Carafoli E, Cali T (2017) The plasma membrane calcium pumps: focus on the role in (neuro) pathology. Biochem Biophys Res Commun 483:1116–1124
15. Lopreiato R, Giacomello M, Carafoli E (2014) The plasma membrane calcium pump: new ways to look at an old enzyme. J Biol Chem 289:10261–10268
16. Strehler EE (2015) Plasma membrane calcium ATPases: from generic Ca^{2+} sump pumps to versatile systems for fine- tuning cellular Ca^{2+}. Biochem Biophys Res Commun 460:26–33
17. Dunham ET, Glynn IM (1961) Adenosine triphosphatase activity and the active movements of alkali metal ions. J Physiol Lond 156:274–293
18. Schatzmann HJ (1966) ATP-dependent Ca^{2+} extrusion from human red cells. Experientia 22:364–368

19. Pederson PL, Carafoli E (1987) Ion motive ATPases. I. Ubiquity, properties, and significance for cell function. Trends Biochem Sci 12:146–150
20. Pederson PL, Carafoli E (1987) Ion motive ATPases. II. Energy coupling and work output. Trends Biochem Sci 12:186–189
21. Palmgren MG, Nissen P (2011) P-type ATPases. Annu Rev Biophys 40:243–266
22. Gopinath RM, Vincenzi FF (1977) Phosphodiesterase protein activator mimics red blood cell cytoplasmic activator of the (Ca^{2+} + Mg^{2+}) ATPase. Biochem Biophys Res Commun 77:1203–1209
23. Jarrett HW, Penniston JT (1977) Partial purification of the (Ca^{2+} + Mg^{2+}) ATPase activator from human erythrocytes. Its similarity to the activator of 3′-5′ cyclic nucleotide phosphodiesterase. Biochem Biophys Res Commun 77:1210–1216
24. Niggli V, Penniston JT, Carafoli E (1979) Purification of the (Ca^{2+}-Mg^{2+})-ATPase from human erythrocytes using a calmodulin affinity column. J Biol Chem 254:9955–9958
25. Niggli V, Adunyah ES, Penniston JT, Carafoli E (1981) Purified (Ca^{2+}-Mg^{2+})-ATPase of the erythrocyte membrane. Reconstitution and effect of calmodulin and phospholipids. J Biol Chem 256:395–401
26. James P, Maeda M, Fischer R, Verma AK, Krebs J, Penniston JT, Carafoli E (1988) Identification and primary structure of a calmodulin binding domain of the Ca^{2+} pump of human erythrocytes. J Biol Chem 263:2905–2910
27. Shull GE, Greeb J (1988) Molecular cloning of two isoforms of the plasma membrane Ca^{2+}-transporting ATPase from rat brain. Structural and functional domains exhibit similarity to Na+, K+− and other cation transport ATPases. J Biol Chem 263:8646–8657
28. Verma AK et al (1988) Complete primary structure of a human plasma membrane Ca^{2+} pump. J Biol Chem 263:14152–14159
29. Baekgaard L, Luoni L, De Michelis MI, Palmgren MG (2006) The plant plasma membrane Ca2+ pump ACA8 contains overlapping as well as physically separated autoinhibitory and calmodulin-binding domains. J Biol Chem 281:1058–1065
30. Strehler EE, Strehler-Page M-A, Vogel G, Carafoli E (1989) mRNAs for plasma membrane calcium pumpisoforms differing in their regulatory domain are generated by alternative splicing that involves two internal donor sites in a single exon. Proc Natl Acad Sci USA 86:6908–6912
31. Strehler EE, Zacharias DA (2001) Role of alternative splicing in generating isoform diversity among plasma membrane calcium pumps. Physiol Rev 81:21–50
32. Krebs J (2015) The plethora of PMCA isoforms: alternative splicing and differential expression. Biochim Biophys Acta 1853:2018–2024
33. Tidow H, Hein KL, Baekgaard L, Palmgren MG, Nissen P (2010) Expression, purification, crystallization and preliminary X-ray analysis of calmodulin in complex with the regulatory domain of the plasma membrane Ca2+−ATPase ACA8. Acta Crystallogr Sect F Struct Biol Cryst Commun 66:361–363
34. Falchetto R, Vorherr T, Brunner J, Carafoli E (1991) The plasma membrane Ca2+ pump contains a site that interacts with its calmodulin-binding domain. J Biol Chem 266:2930–2936
35. Falchetto R, Vorherr T, Carafoli E (1992) The calmodulin binding site of the plasma membrane Ca2+ pump interacts with the transduction domain of the enzyme. Protein Sci 1:1613–1621
36. Dupont Y (1976) Fluorescence studies of the sarcoplasmic reticulum calcium pump. Biochem Biophys Res Commun 71:544–550
37. Krebs J, Vasak M, Scarpa A, Carafoli E (1987) Conformational differences between the E_1 and E_2 states of the calcium adenosinetriphosphatase of the erythrocyte plasma membrane as revealed by circular dichroism and fluorescence spectroscopy. Biochemistry 26:3921–3926
38. Toyoshima C, Nakasako M, Nomura H, Ogawa H (2000) Crystal structure of the calcium pump of sarcoplasmic reticulum at 2.6 A resolution. Nature 405:647–655
39. Toyoshima C (2009) How Ca2+-ATPase pumps ions across the sarcoplasmic reticulum membrane. Biochim Biophys Acta 1793:941–946

40. Niggli V, Sigel E, Carafoli E (1982) The purified Ca2+ pump of human erythrocyte membranes catalyzes an electroneutral Ca2+−H+ exchange in reconstituted liposomal systems. J Biol Chem 257:2350–2356
41. Inesi G, Kurzmack M, Coan C, Lewis DE (1980) Cooperative calcium binding and ATPase activation in sarcoplasmic reticulum vesicles. J Biol Chem 255:3025–3031
42. Kosk-Kosicka D, Bzdega T (1988) Activation of the erythrocyte Ca2+-ATPase by either self-association or interaction with calmodulin. J Biol Chem 263:18184–18189
43. Krebs J, Helms V, Griesinger C, Carafoli E (2003) The regulation of the calcium signal by membrane pumps. Helv Chim Acta 86:3875–3888
44. Schwede T, Kopp J, Guex N, Peitsch MC (2003) SWISS_MODEL: an automated protein homology-modeling server. Nucleic Acids Res 31:3381–3385
45. Kataoka M, Head JF, Vorherr T, Krebs J, Carafoli E (1991) Small-angle X-ray scattering study of calmodulin bound to two peptides corresponding to parts of the calmodulin-binding domain of the plasma membrane Ca2+ pump. Biochemistry 30:6247–6251
46. Elshorst B et al (1999) NMR solution structure of a complex of calmodulin with a binding peptide of the Ca2+ pump. Biochemistry 38:12320–12332
47. Hoeflich KP, Ikura M (2002) Calmodulin in action: diversity in target recognition and activation mechanisms. Cell 108:739–742
48. Guerini D, Krebs J, Carafoli E (1984) Stimulation of the purified erythrocyte Ca2+-ATPase by tryptic fragments of calmodulin. J Biol Chem 259:15172–15177
49. Gao ZH, Krebs J, VanBerkum MF, Tang WJ, Maune JF, Means AR, Stull JT, Beckingham K (1993) Activation of four enzymes by two series of calmodulin mutants with point mutations in individual Ca2+ binding sites. J Biol Chem 268:20096–20104
50. Ikura M, Spera S, Barbato G, Kay LE, Krinks M, Bax A (1991) Secundary structure and side-chain1H and 13C resonance assignments of calmodulin in solution by heteronuclear multidimensional NMR spectroscopy. Biochemistry 30:9216–9228
51. Ikura M, Barbato G, Klee CB, Bax a (1992) Solution structure of calmodulin and its complex with a myosin light chain kinase fragment. Cell Calcium 13:391–400
52. Ikura M, Clore GM, Gronenborn AM, Zhu G, Klee CB, Bax A (1992) Solution structure of a calmodulin-target peptide complex by multidimensional NMR. Science 256:632–638
53. Juranic N et al (2010) Calmodulin wraps around its binding domain in the plasma membrane Ca2+ pump anchored by a novel 18-1 motif. J Biol Chem 285:4015–4024
54. Carafoli E, Krebs J (2016) Calcium and calmodulin signaling. In: Bradshaw RA, Stahl PD (eds) Encyclopedia of cell biology, vol 3. Elsevier, Waltham, MA, pp 161–169
55. Enyedi A et al (1994) The Ca2+ affinity of the plasma membrane Ca2+ pump is controlled by alternative splicing. J Biol Chem 269:41–43
56. Silverstein RS, Tempel BL (2006) Atp2b2 encoding plasma membrane Ca2+-ATPase type 2, (PMCA2) exhibits tissue specific first exon usage in hair cells, neurons and mammary glands of mice. Neuroscience 141:245–257
57. Brini M, Cali T, Ottolini D, Carafoli E (2013) The plasma membrane calcium pump in health and disease. FEBS J 280:5385–5397
58. Prasad V, Okunade GW, Miller ML, Shull GE (2004) Phenotypes of SERCA and PMCA knock out mice. Biochem Biophys Res Commun 322:1192–1203
59. Hilfiker H, Guerini D, Carafoli E (1994) Cloning and expression of isoform 2 of the human plasma membrane Ca2+ ATPase. Functional properties of the enzyme and its splicing products. J Biol Chem 269:26178–26183
60. Furuta H, Luo L, Hepler K, Ryan AF (1998) Evidence for differential regulation of calcium by outer versus inner hair cells: plasma membrane Ca-ATPase gene expression. Hear Res 123:10–26
61. Dumont RA, Lins U, Filoteo AG, Penniston JT, Kachar B, Gillespie PG (2001) Plasma membrane Ca2+-ATPase isoform 2a is the PMCA of hair bundles. J Neurosci 21:5066–5078
62. Eakin TJ, Antonelli MC, Malchiodi EL, Baskin DG, Stahl WL (1995) Localization of the plasma membrane Ca2+-ATPase isoform PMCA3 in rat cerebellum, choroid plexus and hippocampus. Mol Brain Res 29:71–80

63. Stauffer TP, Guerini D, Carafoli E (1995) Tissue distribution of the four gene products of the plasma membrane Ca^{2+} pump. A study using specific antibodies. J Biol Chem 270:12184–12190
64. Greeb J, Shull GE (1989) Molecular cloning of a third isoform of the calmodulin-sensitive plasma membrane Ca2+- transporting ATPase that is expressed predominantly in brain and skeletal muscle. J Biol Chem 264:18569–18576
65. Goellner GM, DeMarco SJ, Strehler EE (2003) Characterization of PISP, a novel single-PDZ protein that binds to all plasma membrane Ca2+-ATPase b-splice variants. Ann NY Acad Sci 986:461–471
66. Kim E, DeMarco SJ, Marfatia SM, Chisti AH, Sheng M, Strehler EE (1998) Plasma membrane Ca2+ ATPase isoform 4b binds to membrane-associated guanylate kinase (MAGUK) proteins via their PDZ (PSD95/Dlg/ZO-1) domains. J Biol Chem 273:1591–1595
67. Fujimoto T (1993) Calcium pump of the plasma membrane is localized in caveolae. J Cell Biol 120:1147–1157
68. Pani B, Singh BB (2009) Lipid rafts/caveolae as microdomains of calcium signaling. Cell Calcium 45:625–633
69. Okunade GW et al (2004) Targeted ablation of plasma membrane Ca2+-ATPase (PMCA) 1 and 4 indicates a major housekeeping function for PMCA1 and a critical role in hyper-activated sperm motility and male fertility for PMCA4. J Biol Chem 279:33742–33750
70. Brandt P, Neve RL (1992) Expression of plasma membrane calcium-pumping ATPase mRNAs in developing rat brain and adult brain subregions: evidence for stage-specific expression. J Neurochem 59:1566–1569
71. Kip SN, Gray NW, Burette A, Canbay A, Weinberg RJ, Strehler EE (2006) Changes in the expression of plasma membrane calcium extrusion systems during the maturation of hippo-campal neurons. Hippocampus 16:20–34
72. Kenyon KA, Bushong EA, Mauer AS, Strehler EE, Weinberg RJ, Burette AC (2010) Cellular and subcellular localization of the neuron-specific plasma membrane calcium ATPase PMCA1a in the rat brain. J Comp Neurol 518:3169–3183
73. Strehler EE, Caride AJ, Filoteo AG, Xiong Y, Penniston JT, Enyedi A (2007) Plasma membrane Ca2+ ATPases as dynamic regulators of cellular calcium handling. Ann NY Acad Sci 1099:226–236
74. Krebs J (1998) Calmodulin-dependent protein kinase IV: regulation of function and expres-sion. Biochim Biophys Acta 1448:183–189
75. Xie J, Black DL (2001) A CaMKIV responsive RNA element mediates depolarization-induced alternative splicing of ion channels. Nature 410:936–939
76. Liu G et al (2012) A conserved serine of heterogeneous nuclear ribonucleoprotein L (hnRNP L) mediates depolarization-regulated alternative splicing of potassium channels. J Biol Chem 287:22709–22716
77. Xie J, Calvin J, Stoilov P, Park J, Black DL (2005) A consensus CaMKIV-responsive RNA sequence mediates regulation of alternative exons in neurons. RNA 11:1825–1834
78. Krebs J, Means RL, Honegger P (1996) Induction of calmodulin kinase IV by the thyroid hormoneduring the development of rat brain. J Biol Chem 271:11055–11058
79. Krebs J (2017) Implications of the thyroid hormone on neuronal development with special emphasis on the calmodulin-kinase IV pathway. Biochim Biophys Acta 1864:877–882
80. Street VA, McKee-Johnson JW, Fonseca RC, Tempel BL, Noben-Trauth K (1998) Mutations in a plasma membrane Ca2+-ATPase gene cause deafness in deafwaddler mice. Nat Genet 19:390–394
81. Kozel PJ et al (1998) Balance and hearing deficits in mice with a null mutation in the gene encoding plasma membrane Ca2+-ATPase isoform 2. J Biol Chem 273:18693–18696
82. Ficarella R et al (2007) A functional study of plasma membrane calcium-pump isoform 2 mutants causing digenic deafness. Proc Natl Acad Sci USA 104:1516–1521
83. Reinhardt TA, Horst RL (1999) Ca2+-ATPases and their expression in the mammary gland of pregnant and lactating rats. Am J Phys 276:C796–C802
84. Jeong J et al (2016) PMCA2 regulates HER2 protein kinase localization and signaling and promotes HER2-mediated breast cancer. Proc Natl Acad Sci USA 113:E282–E290

85. Beuschlein F et al (2013) Somatic mutations in ATP1A1 and ATP2B3 lead to aldosterone-producing adenomas and secondary hypertension. Nat Genet 45:440–445
86. Williams TA et al (2014) Somatic ATP1A1, ATP2B3, and KCNJ5 mutations in aldosterone-producing adenomas. Hypertension 63:188–195
87. Zanni G et al (2012) Mutation of plasma membrane Ca2+ ATPase isoform3 in a family with X-linked congenital cerebellar ataxia impairs Ca2+ homeostasis. Proc Natl Acad Sci USA 109:14514–14519
88. Wang MG, Yi H, Hilfiker H, Carafoli E, Strehler EE, McBride OW (1994) Localization of two genes encoding plasma membrane Ca2+-ATPases isoforms 2 (ATP2B2) and 3 (ATP2B3) to human chromosomes 3p26-25 and Xq28, respectively. Cytogenet Cell Genet 67:41–45
89. Feyma T et al (2016) Dystonia in ATP2B3-associated X-linked spinocerebellar ataxia. Mov Disord 31:1752–1753
90. Tatsuki F et al (2016) Involvement of Ca(2+)-dependent hyperpolarization in sleep duration in mammals. Neuron 90:70–85
91. Wennemuth G, Babcock DF, Hille B (2003) Calcium clearance mechanisms of mouse sperm. J Cell Biol 122:115–128
92. Schuh K et al (2004) Plasma membrane Ca2+ ATPase 4 is required for sperm motility and male fertility. J Biol Chem 279:28220–28226
93. Brandenburger T et al (2011) Switch of PMCA4 splice variants in bovine epididymis results in altered isoform expression during functional sperm maturation. J Biol Chem 286:7938–7946
94. Prasad V et al (2014) Ablation of plasma membrane Ca2+-ATPase isoform 4 prevents development of hypertrophy in a model of hypertrophyc cardiomyopathy. J Mol Cell Cardiol 77:53–63
95. Wu X et al (2009) Plasma membrane Ca2+-ATPase isoform 4 antagonizes cardiac hypertrophy in association with calcineurin inhibition in rodents. J Clin Invest 119:976–985
96. Ho PW, Pang SY, Li M, Tse ZH, Kung MH, Sham PC, Ho SL (2015) PMCA4 (ATP2B4) mutation in familial spastic paraplegia causes delay in intracellular calcium extrusion. Brain Behav 5:e00321
97. Li M, Ho PW, Pang SY, Tse ZH, Kung MH, Sham PC, Ho SL (2014) PMCA4 (ATP2B4) mutation in familial spastic paraplegia. PLoS One 9:e104790
98. Marques-da-Silva D, Gutierrez-Merino C (2014) Caveolin-rich lipid rafts of the plasma membrane of mature cerebellar granule neurons are microcompartments for calcium/reactive oxygen and nitrogen species cross-talk signaling. Cell Calcium 56:108–123
99. Schuh K, Uldrijan S, Telkamp M, Röthlein N, Neyses L (2001) The plasma membrane calmodulin-dependent calcium pump: a major regulator of nitric oxide synthase I. J Cell Biol 155:201–205
100. Oceandy D et al (2007) Neuronal nitric oxide synthase signaling in the heart is regulated by the sarcolemmal calcium pump 4b. Circulation 115:483–492
101. Mohamed TM et al (2011) Plasma membrane calcium pump (PMCA4)-neuronal nitric-oxide synthase complex regulates cardiac contractility through modulation of a compartmentalized cyclic nucleotide microdomain. J Biol Chem 286:41520–41529
102. Bozulik LD, Malik MT, Powell DW, Nanez A, Link AJ, Ramos KS, Dean WL (2007) Plasma membrane Ca(2+)-ATPase associates with CLP36, alpha-actinin, and actin in human platelets. Thromb Haemost 97:587–597
103. Kruger WA, Yun CC, Monteith GR, Poronnik P (2009) Muscarinic-induced recruitment of plasma membrane Ca2+-ATPase involves PSD-95/Dlg/Zo-1-mediated interactions. J Biol Chem 284:1820–1830
104. Gomez-Varela D, Schmidt M, Schoellermann J, Peters EC, Berg DK (2012) PMCA2 via PSD-95 controls calcium signaling by α7-containing nicotinic acetylcholine receptors on aspiny interneurons. J Neurosci 32:6894–6905
105. Carafoli E, Zurini M (1982) The Ca2+-pumping ATPase of plasma membranes: purification, reconstitution and properties. Biochim Biophys Acta 683:279–301

106. Choquette D, Hakim G, Filoteo AG, Plishker GA, Bostwick JR, Penniston JT (1984) Regulation of plasma membrane Ca2+ ATPases by lipids of the phosphatidylinositol cycle. Biochem Biophys Res Commun 125:908–915
107. Ambudkar IS, de Souza LB, Ong HL (2017) TRPC1, Orai 1, and STIM1 in SOCE: friends in tight spaces. Cell Calcium 63:33–39
108. Hogan PG, Rao A (2015) Store-operated calcium entry: mechanisms and modulation. Biochem Biophys Res Commun 460:40–49
109. Maleth J, Choi S, Muallem S, Ahuja M (2015) Translocation of PI(4,5) P2-poor and PI(4,5)P2-rich microdomains during store depletion determines STIM1 conformation and Orai1 gating. Nat Commun 5:5843
110. Liou J, Fivaz M, Inoue T, Meyer T (2007) Live-cell imaging reveals sequential oligomerization and local plasma membrane targeting of stromal interaction molecule 1 after Ca2+ store depletion. Proc Natl Acad Sci USA 104:9301–9306
111. Ong HL, Ambudkar IS (2011) The dynamic complexity of the TRPC1 channelosome. Channels 5:424–431

Chapter 2
Structure-Function Relationship of the Voltage-Gated Calcium Channel $Ca_v1.1$ Complex

Jianping Wu, Nieng Yan, and Zhen Yan

Abstract Voltage-gated calcium (Ca_v) channels are miniature membrane transistors that convert membrane electrical signals to intracellular Ca^{2+} transients that trigger many physiological events. In mammals, there are ten subtypes of Ca_v channel, among which $Ca_v1.1$ is the first $Ca_v\alpha1$ to be cloned. $Ca_v1.1$ is specified for the excitation–contraction coupling of skeletal muscles, and has been a prototype in the structural investigations of Ca_v channels. This article summarized the recent advances in the structural elucidation of $Ca_v1.1$ and the mechanistic insights derived from the 3.6 Å structure obtained using single-particle, electron cryomicroscopy. The structure of the $Ca_v1.1$ complex established the framework for mechanistic understanding of excitation–contraction coupling and provides the template for molecular interpretations of the functions and disease mechanisms of Ca_v and Na_v channels.

Keywords Voltage-gated calcium channel · DHPR · $Ca_v1.1$ · Structure

Abbreviations

Ca_v	Voltage-gated calcium channel
DHPR	Dihydropyridine receptor
E-C coupling	Excitation-contraction coupling
Na_v	Voltage-gated sodium channel
RyR	Ryanodine receptor
TM	Transmembrane
VGIC	Voltage-gated ion channel
VSD	Voltage sensing domain

J. Wu · N. Yan · Z. Yan (✉)
State Key Laboratory of Membrane Biology, Tsinghua-Peking Joint Center for Life Sciences, School of Life Sciences and School of Medicine, Tsinghua University, Beijing, China

Beijing Advanced Innovation Center for Structural Biology, School of Life Sciences, Tsinghua University, Beijing, China
e-mail: zhenyan0920@126.com

J. Krebs (ed.), *Membrane Dynamics and Calcium Signaling*, Advances in Experimental Medicine and Biology 981,
https://doi.org/10.1007/978-3-319-55858-5_2

2.1 Introduction

Voltage-gated calcium (Ca_v) channels are a large family of membrane proteins that are activated upon the change of membrane potentials. The Ca^{2+} ions permeated by the Ca_v channel act as second messengers that trigger a cascade of cellular events involved in a multitude of physiological processes such as muscle contraction, synaptic transmission, hormone secretion, gene expression and cell death (Fig. 2.1) [1, 2].

2.1.1 Classification of Voltage-Gated Calcium Channels

Ca_v channels exhibit tissue specificity. Ten subtypes of Ca_v channels have been identified in mammals through the voltage-clamp measurements of Ca^{2+} currents in distinct tissues and organisms (Table 2.1) [3, 4]. The ten subtypes can be divided into three subfamilies based on their sequence similarity. The Ca_v1 channels activate at high voltage and conduct large and long lasting ion currents, thus designated as the L-type calcium channels [5]. The Ca_v1 channels can be specifically inhibited by dihydropyridine and its derivatives. They are thereby also named as the dihydropyridine receptor (DHPR) [6, 7]. In contrast, the Ca_v3 members are designated as T-type calcium channel for activation at low voltage and conduct tiny single channel current, and the current is transient [4, 8]. The Ca_v2 channels can be further divided to the P/Q-type, the N-type, and the R-type based on their Ca^{2+} current properties and inhibition by specific toxins [4, 9–11].

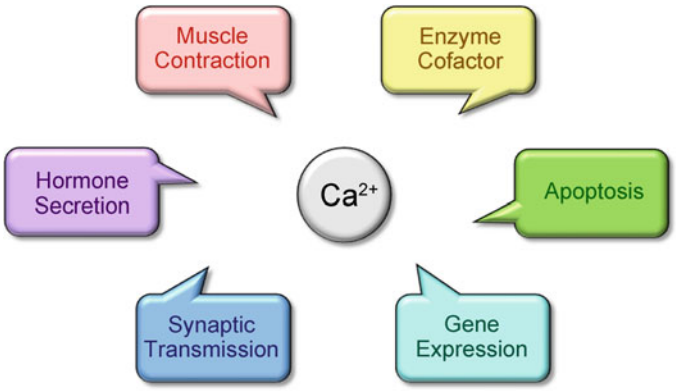

Fig. 2.1 The physiological functions of Ca^{2+} ions. Ca^{2+} ions play an important role in muscle contraction, apoptosis, gene expression, synaptic transmission, hormone secretion, and can also act as enzyme cofactor

Table 2.1 Classification of voltage-gated calcium channels

Ca^{2+} current type	Ca^{2+} channel	Specific blocker	Functions
L	$Ca_v1.1$	DHPs	E-C coupling Gene regulation
	$Ca_v1.2$		E-C coupling Hormone secretion Gene regulation
	$Ca_v1.3$		Hormone secretion Gene regulation
	$Ca_v1.4$		Visual transduction
N	$Ca_v2.1$	ω-CTx-GVIA	Neurotransmitter release Dendritic Ca^{2+} transients
P/Q	$Ca_v2.2$	ω-Agatoxin	Neurotransmitter release Dendritic Ca^{2+} transients
R	$Ca_v2.3$	SNX-482	Neurotransmitter release Dendritic Ca^{2+} transients
T	$Ca_v3.1$	None	Repetitive ring
	$Ca_v3.2$		Repetitive ring
	$Ca_v3.3$		Repetitive ring

2.1.2 Molecular Properties of Ca_v

Ca_v channels belong to the voltage-gated ion channel superfamily, which has a conserved core fold. Unlike their prokaryotic homologues, which are homotetramers, the ion conducting α1 subunit of eukaryotic Ca_v channels is a single peptide chain with four similar repeats linked by intracellular loops [12]. Each repeat contains six transmembrane helices named S1–S6, among which S1–S4 of each repeat form the voltage sensing domain (VSD) and S5–S6 of the four repeats constitute the ion conducing pore (Fig. 2.2) [14].

Ca_v1 and Ca_v2 channels also contain several auxiliary subunits that form a complex with the α1 subunit (Fig. 2.2). The auxiliary subunits include the extracellular α2δ subunit, the cytosolic β subunit and sometimes the transmembrane γ subunit [1]. The auxiliary subunits are not essential for the channel permeation, but they can regulate the membrane trafficking and channel properties of the α1 subunit. For example, the α2δ subunit can facilitate channel translocation to the cell surface, and the β subunit modulates the kinetic properties of the channel [15–17]. In skeletal muscle, the β subunit in $Ca_v1.1$ plays an essential role in the excitation-contraction coupling [18–20]. The γ subunit assists channel inactivation [21, 22].

Not only α subunit has different subtypes, each auxiliary subunit may have distinct subtypes and splicing isoforms. Four genes encoding the β subunit have been identified, and each can yield different isoforms by alternative splicing [16, 23]. The α2 and δ subunits result from proteolytic cleavage of a single gene product. Besides, four genes have been reported encoding the α2δ subunit [24]. Combinations of the distinct α1 subtypes with various auxiliary subunits give rise to the diversity of Ca_v channels.

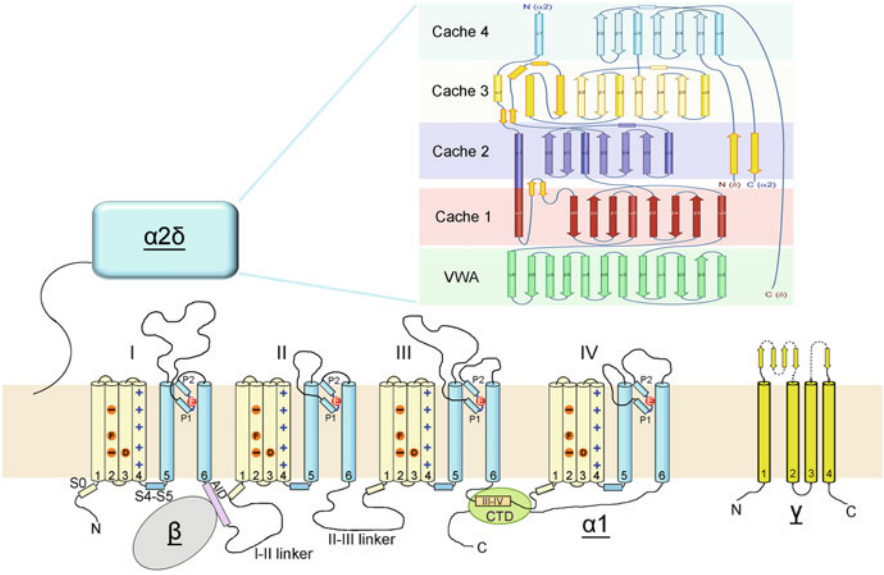

Fig. 2.2 Topology of Ca_v channels. Ca_v channels contain several subunits: the ion permeation subunit α1, the extracellular α2δ subunits, the cytosolic β subunit and sometimes the transmembrane γ subunit. The topology shown here is of $Ca_v1.1$. The upper right pannel is adapted from Wu et al. [13]

2.1.3 Channelopathies

Voltage-gated calcium channels play essential roles in various physiological processes, and their disorders will trigger serious diseases, such as hypokalemic periodic paralysis ($Ca_v1.1$ related), cardiac arrhythmia ($Ca_v1.2$ related), autism spectrum disorder ($Ca_v1.2$ related), stationary night blindness ($Ca_v1.4$), cerebellar ataxia ($Ca_v2.2$) [1, 25].

Ca_v channels represent important drug targets. The α1 subunits are directly targeted by various natural toxins and clinical drugs that treat hypertension, arrhythmia, and angina pectoris. The α2δ-1 subunit is targeted by the gabapentinoid drugs gabapentin and pregabalin [26, 27].

2.2 Structural Studies of Voltage-Gated Calcium Channels

Because of the physiological and pathological importance, the structural studies of Ca_v channels have been pursued for decades. However, the long sequence of the single peptide chain with various intracellular linkers makes the channels resistant to recombinant overexpression, nor to say crystallization. Besides, the existence of the

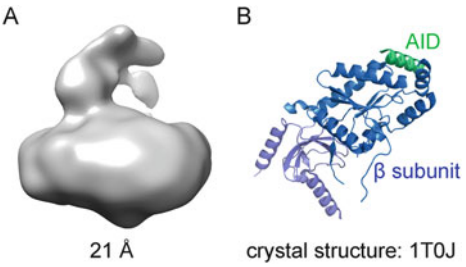

Fig. 2.3 Previous structural studies of Ca_v channels. (**a**) Low resolution cryo-EM map of $Ca_v1.1$. The nominal resolution is 21 Å [28]. (**b**) Crystal structure of the β subunit in complex with AID [29]

auxiliary subunits and various post-translational modifications such as glycosylation add further challenges to obtain a crystal structure of the Ca_v channel complex. Despite extensive efforts, the structural information of eukaryotic Ca_v channels have remained elusive. There were only low resolution cryo-EM maps reported (Fig. 2.3a) [28, 30–32]. High resolution crystal structures were obtained for the β1 subunit alone and in complex with the α1-interacting domain (AID) motif from the α1 subunit (Fig. 2.3b) [29, 33, 34].

Prokaryotic homologues of voltage-gated calcium or sodium channel are homotetramers, hence relatively easier than the eukaryotic ones for structural pursuit using X-ray crystallography. In the past several years, researchers have been focusing on the structural characterizations of the prokaryotic homologues of Ca_v or Na_v channel. A few crystal structures of bacterial Na_v channels were obtained, including Na_vAb [35], Na_vRh [36] and Na_vMs [37] since 2011. Moreover, the crystal structure of a Na_vAb variant that exhibits calcium selectivity, hence named Ca_vAb, was determined [38]. These structures represent imperative steps towards molecular understanding of the Na_v/Ca_v channels. However, there are still many questions remaining to be answered, including the most straightforward questions like how the four repeats of α1 subunit are organized spatially and how the auxiliary subunits interact with the α1 subunit. A high resolution structure of a eukaryotic Ca_v channel is required to address these questions.

The recent technological breakthrough in electron microscopy (EM), including the development of direct electron detector for image acquisition and new algorithms for data processing, provided an unprecedented opportunity to solve structures of challenging targets that were nearly insurmountable by X-ray crystallography. Structural biology by single-particle cryo-EM, used to be nick-named 'blob-ology', has been used to solve macromolecular structures at resolutions that can resolve side chains. Compared to X-ray crystallography, cryo-EM has two obvious advantages: (1) only several microliters of sample solutions are required, and (2) crystallization is spared. Cryo-EM has become a prevailing approach for structural biology of membrane proteins and macromolecular machineries since 2013 [39, 40]. The eukaryotic Ca_v channels have molecular weights beyond 300 kDa with the auxiliary subunits, representing suitable targets for cryo-EM.

$Ca_v1.1$ is the first $Ca_vα1$ to be cloned, and it has been a prototype in the functional, structural, and mechanistic investigations of Ca_v channels [12, 41]. There is only one isoform of β subunit, $β_{1a}$, in skeletal muscle [42], and the $Ca_v1.1$ complex is

exclusively expressed in skeletal muscle with relatively high abundance. It thereby may be easier to purify the $Ca_v1.1$ complex to homogeneity for cryo-EM imaging than for other Ca_v channels from other tissues. Several purification methods for $Ca_v1.1$ from rabbit skeletal muscle have been reported in literature [43–45]. Recently, a revised strategy for purification of $Ca_v1.1$ from rabbit skeletal muscle membrane was developed, using GST-fused β_{1a} subunit to compete with the endogenous β_{1a} subunit to pull down the whole complex [46]. This strategy is simple and more specific. The protein obtained using this protocol is of high purity and well behaved, representing an ideal target for single particle cryo-EM analysis.

In 2015, the cryo-EM structure of rabbit $Ca_v1.1$ was obtained at 4.2 Å resolution [46]. Most of the secondary structure elements of the protein complex were revealed in this structure. All the subunits were identified and the arrangement of the four repeats in α1 subunit has been revealed. In the following year, the resolution of the $Ca_v1.1$ structure was further improved to 3.6 Å resolution, which allowed assignment of most side chains [13]. This is the first near atomic structure of a eukaryotic Ca_v channels. The high resolution structure provides important insights into the understanding of the structure-function relationship of Ca_v and the related Na_v channels.

2.3 Structural Analysis of $Ca_v1.1$

2.3.1 The Overall Architecture of $Ca_v1.1$

The structure of $Ca_v1.1$ is constituted by the ion-permeating core subunit α1, the extracellular α2δ subunit, the intracellular β_{1a} subunit, and the transmembrane γ subunit. The overall structure is approximately 170 Å in height and 100 Å in the longest dimension of the width (Fig. 2.4a).

2.3.2 Structure of the α1 Subunit

The α1 subunit in eukaryotic Ca_v channels is a single peptide chain that folds into four similar repeats. Therefore, an evident and interesting question arose: how are the four homologous repeats arranged? Clockwise, counterclockwise, or intertwined?

Careful examination of the 4.2 Å cryo-EM reconstruction suggested that the four repeats are arranged in a clockwise manner in the extracellular view, which was then unambiguously confirmed by the 3.6 Å cryo-EM map (Fig. 2.4b). This repeat organization principle may be conserved in all eukaryotic Ca_v or Na_v channels.

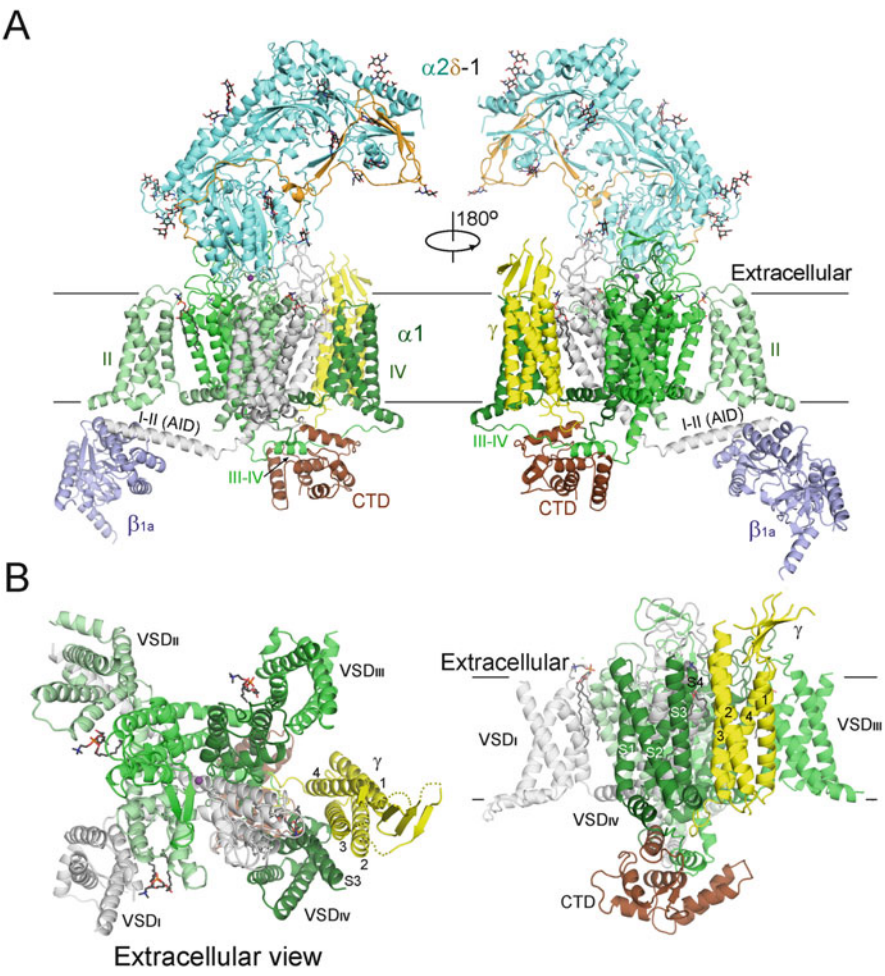

Fig. 2.4 Structure of the $Ca_v1.1$ channel complex from rabbit. (**a**) Overall structure of $Ca_v1.1$. The structure is color-coded for different subunits. The four repeats of the α1 subunit are colored from white to dark green and CTD is colored brown. (**b**) Spatial arrangement of α1 subunit. The four repeats are arranged clockwisely in the extracellular view. Adapted from Wu et al. [13]

2.3.3 The VSDs of $Ca_v1.1$

The VSDs are responsible for voltage sensing. Among the four transmembrane segments S1–S4 in each VSD, S4 contains repetitively aligned basic residues Arg or Lys that occur every three residues. They are named the "gating charges". The four VSDs of $Ca_v1.1$ are similar but non-identical with each other. The S3 segments of prokaryotic homologues Na_vAb and Na_vRh are largely unfolded on the extracellular side, whereas the S3 segments of $Ca_v1.1$ are full transmembrane helices.

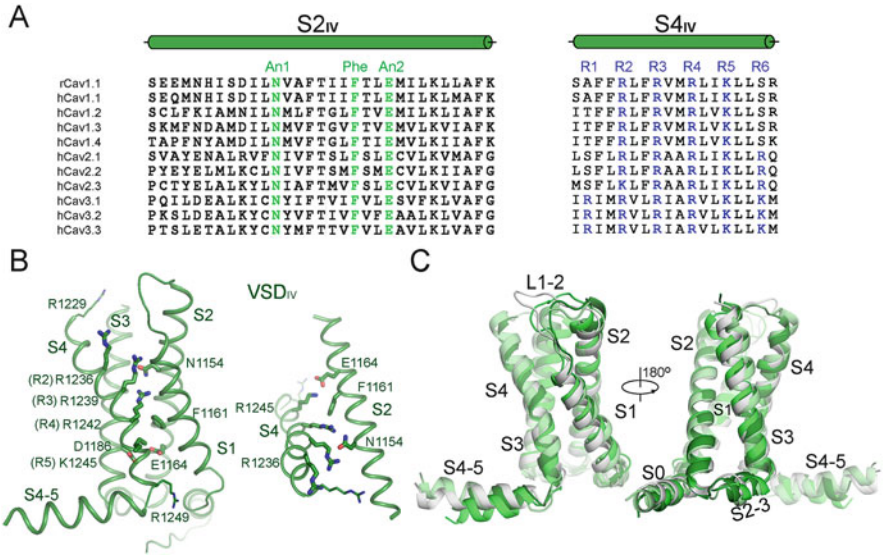

Fig. 2.5 VSD_{IV} of $Ca_v1.1$. (**a**) Sequence alignment of $S4_{IV}$ helix. The conserved R/K highlighted blue. (**b**) Structure of the VSD_{IV} of $Ca_v1.1$. (**c**) Structural superimposition of the four VSDs of $Ca_v1.1$. Adapted from Wu et al. [13]

According to the sequence alignment of $Ca_v1.1$ and ten human Ca_v channels, there are up to six gating charge residues on each S4 segment, defined as R1–R6 (Fig. 2.5a). For the rabbit $Ca_v1.1$, there are R1–R5 on $S4_I$, R2–R6 on $S4_{II}$, R1–R5 on $S4_{III}$, and R2–R5 on $S4_{IV}$.

In each VSD, all the gating charges are aligned on one side of the 3_{10} helix of S4. The R5 residues and $R6_{II}$ are below, whereas the R1–R4 residues are above the conserved occluding Phe in the charge transfer centre, representing the depolarized or 'up' conformation of VSDs (Fig. 2.5b). Considering the closed pore and the 'up' VSDs, the structure of $Ca_v1.1$ shown here may represent a potentially inactivated state. The R1–R4 residues are above the conserved occluding Phe in the charge transfer center, representing the depolarized or up conformation of VSDs. This is consistent with the sample conditions of 0 mV membrane potential (depolarized state).

2.3.4 The Selectivity Filter

The selectivity filter (SF) is responsible for ion selection. In $Ca_v1.1$, the SF is constituted by an outer site comprising the side chains of four essential Glu residues and an inner site formed by the carbonyl oxygen of the two preceding residues.

The SF of different voltage gated ion channels exhibits distinct chemical and structural features. The selectivity filter of K_V channels is constituted by the carbonyl oxygen of the residues. But in Ca_v and Na_v channels, the side chains of the outer site

residues are important for selectivity. In Na_v channels, the key residues are Asp/Glu/Lys/Ala (DEKA).

The SF of $rCa_v1.1$ is constituted by the side groups of Glu292/614/1014/1323 and the two preceding residues in each repeat that contribute the carbonyl oxygen (C=O). A consecutive stretch of density stands along the selectivity filter vestibule that can be deconvoluted to a round disc in the centre of the four Glu residues and a sphere surrounded by the eight C=O groups. Two Ca^{2+} ions are tentatively assigned to the middle disc and the inner sphere. The two maps (3.6 Å and 4.2 Å) were from two different batches of protein which was purified in 10 mM and 0.5 mM Ca^{2+}, respectively. The shape and position of the density in the selectivity filter vestibule in the two maps are different (Fig. 2.6a). The heights of the two Ca^{2+} ions in the 3.6 Å

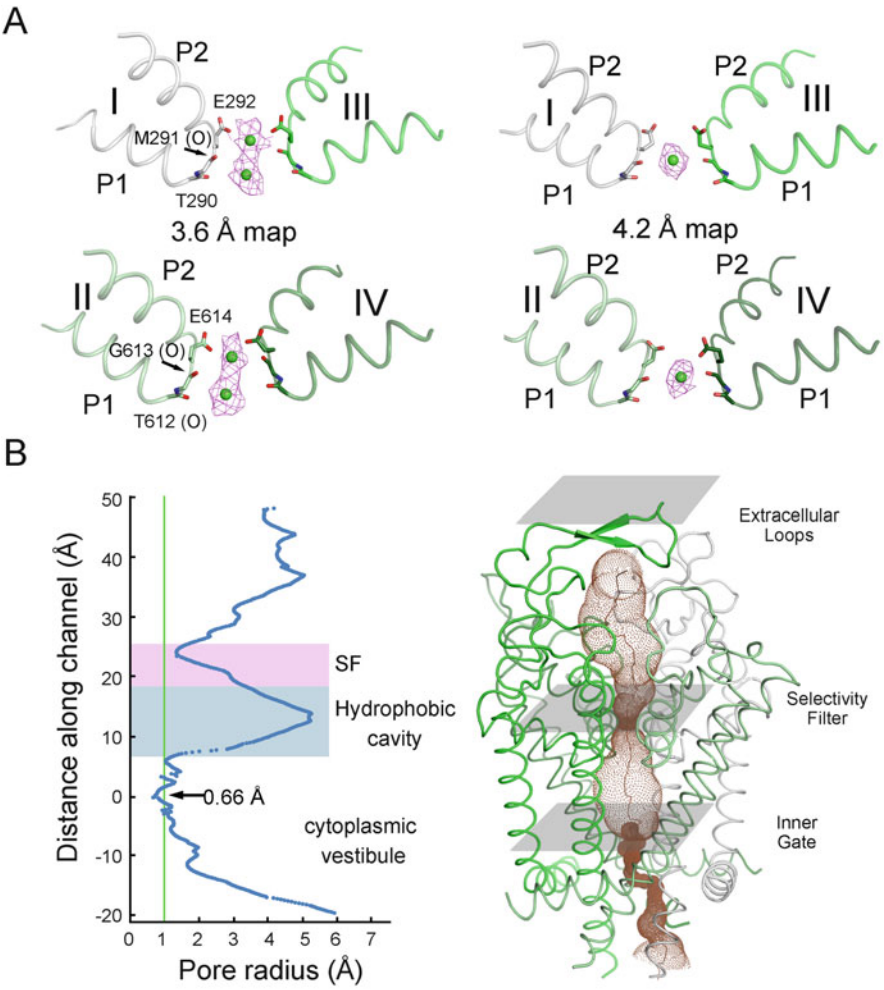

Fig. 2.6 Selectivity filter. (**a**) Structures of the selectivity filter obtained from two different maps. (**b**) The permeation path of the pore domain. Adapted from Wu et al. [13]

map are similar to those in Ca_{vAb} [38], except that the inner one is slightly off the central axis and closer to repeats I and II.

Above the entrance to the Ca^{2+} permeation path, the extended extracellular loops, which are stabilized by many disulfide bonds, form a windowed dome. The window is enriched in negatively charged residues, which may help attract cations. Below the SF is a hydrophobic cavity with fenestrations. The radius in the inner gate is less than 1 Å too narrow to permeate Ca^{2+} ions (Fig. 2.6b). Therefore the structure is in a closed conformation. Considering the closed pore and the 'up' VSDs, the reported structure of $Ca_v1.1$ may represent a potentially inactivated state.

2.3.5 The Auxiliary Subunits

In the structure of the rabbit $Ca_v1.1$ channel complex, four tandem cache domains and one VWA domain are identified in the α2δ subunit. Although these domains are organized separately in space, they involve intertwined sequences. Interestingly, although the δ subunit and α2 subunit are separated in the primary sequence, they co-fold with each other. The δ subunit contributes three β-strands to the fourth Cache domain. Cys1074 in the δ subunit forms a disulfide bond with Cys406 in the VWA domain. The extended conformation of δ is stabilized through multiple intra and inter-subunit disulfide bonds. In total, four disulfide bonds were observed between the α2- and δ-subunits and two within the δ-subunit.

There was a debate on whether the δ subunit is a transmembrane protein or a GPI (glycosylphosphatidylinositol)-anchored protein. In the 3.6 Å resolution EM map, there is no extra density for a TM helix. The density for δ subunit ended after Cys1074, which happened to be the predicted site for GPI modification. Besides, in the related MS result, no peptide can be detected after Cys1074. The structure appeared to support that δ subunit is a membrane anchored protein.

In the $Ca_v1.1$ complex structure, four transmembrane helices (named TM1–4), an extracellular β sheet and the cytosolic amino (N)- and C-terminal loops are resolved for the γ subunit. The transmembrane interface between α1 and γ is mediated by TM2 and TM3 of γ and the S3 and S4 segments in α1-VSD_{IV}. All of the residues constituting the interface are hydrophobic residues, which are unlikely to provide the specificity between γ and VSD_{IV}. On the intracellular side, the C-terminus of γ subunit contains some polar residues that are hydrogen-bonded with the III–IV linker in the α1 subunit, which may provide the interaction specificity with VSD_{IV} but not for other VSDs. The direct contact between γ and VSD_{IV} may affect the conformational changes of the latter during voltage dependent activation or inactivation, thereby providing the molecular basis for the antagonistic modulation of the γ subunit.

Before the determination of the structure of $Ca_v1.1$ complex, the crystal structure of β has been reported. The different cryo-EM maps of $Ca_v1.1$ revealed distinct conformations of the intracellular domains. The AID motif is sandwiched between α1-VSD_{II} and β. Comparison of the different EM 3D reconstructions reveals shifts of

the C terminus of $S6_I$ and the ensuing I–II helix. Meanwhile, the β-subunit undergoes a pronounced displacement between the two reconstructions.

2.3.6 *Structural Mapping of Disease-Associated Mutations*

Ca_v channels and the closely related Na_v channels play a major role in a multitude of physiological and pathological processes. Hundreds of mutations have been identified in these channels. The structure presented here represents the first atomic model of a single-chain eukaryotic Ca_v or Na_v channel. Structural mapping of the disease-associated mutations will greatly foster mechanistic understanding of the related disorders and provide the opportunity for novel drug development targeting these channels (Fig. 2.7).

2.4 Voltage-Gated Calcium Channels in Excitation-Contraction Coupling

Excitation-contraction coupling (E-C coupling) of muscles is an important and fundamental physiological process. Multiple proteins are involved in this signal transduction cascade, among which the ryanodine receptor RyR and Ca_v channels are two key components [47].

RyRs are high-conductance calcium release channels located on the sarco/endoplasmic (SR/ER) membrane. They are responsible for the rapid release of Ca^{2+} from intracellular stores during E-C coupling [48–50]. As the largest known ion channel, the homotetrameric RyR has a molecular mass of more than 2.2 MDa with each protomer containing about 5000 residues [51, 52]. In mammals, there are three isoforms: RyR1 and RyR2 are primarily expressed in skeletal and cardiac muscles, respectively, and RyR3 was originally found in the brain [53–56]. Recently, the near atomic 3D structures of RyR1 and RyR2 in multiple conformations have been reported [57–60]. Details of RyRs are discussed in a later chapter.

Ca_v channels, which are located in the transverse tubule (or T-tubule) are activated upon plasma membrane depolarization, and then induce the activation of the downstream RyRs. The sudden increase of the cytoplasmic Ca^{2+} triggers a cascade of cellular events that eventually result in muscle contraction. Ca^{2+} ions are then pumped back to the SR by the calcium ATPase SERCA, leading to muscle relaxation [47].

$Ca_v1.1$ (in skeletal muscle) and $Ca_v1.2$ (in cardiac muscle) sense the changes of the membrane potential of the plasma membrane and activate RyR1 and RyR2, respectively, but via different mechanisms (Fig. 2.8). In skeletal muscle, $Ca_v1.1$ undergoes conformational changes in response to membrane depolarization, which then activate RyR1 through physical association. It is called the "mechanical

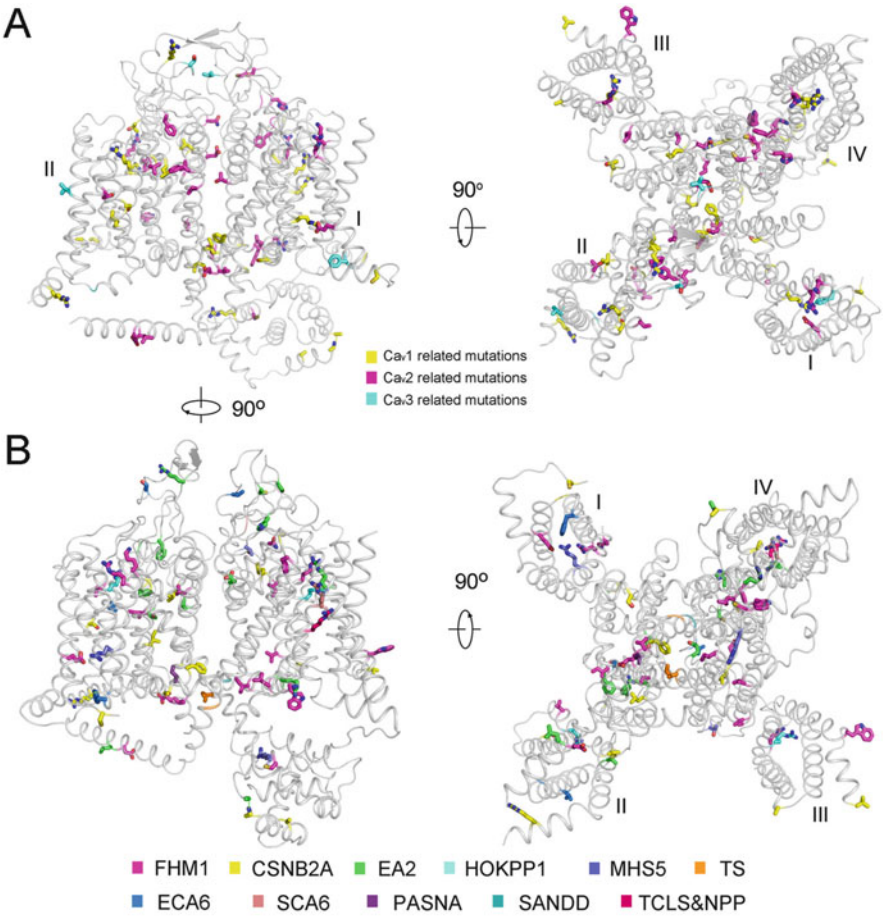

Fig. 2.7 Structural mapping of disease-associated mutations identified in the human Ca_v channels. The disease-related mutations identified in six human Ca_v channels are mapped to the structure of the r$Ca_v1.1\alpha1$ and color coded for different subtypes of Ca_v channels (**a**) or disorders (**b**). HOKPP1: periodic paralysis hypokalemic 1; MHS5: malignant hyperthermia 5; TCLS&NPP: Transient compartment-like syndrome and normokalaemic periodic paralysis; TS: Timothy syndrome; BRGDA3: Brugada syndrome 3; SANDD: sinoatrial node dysfunction and deafness; PASNA: primary aldosteronism, seizures, and neurologic abnormalities; NIDDM: non-insulin-dependent diabetes mellitus; CSNB2A: night blindness, congenital stationary, 2A; AIED: Aaland island eye disease; SCA6: spinocerebellar ataxia 6; FHM1: migraine, familial hemiplegic, 1; EA2: episodic ataxia 2; ECA6: epilepsy, childhood absence 6

coupling" mechanism [61]. In cardiac muscle, it is the Ca^{2+} influx mediated by $Ca_v1.2$ that activates RyR2, a mechanism known as the "calcium induced calcium release" (CICR) [62].

To understand the activation mechanism of RyR1 by $Ca_v1.1$, the accurate interaction between $Ca_v1.1$ and RyR1 is needed. Although the near atomic resolution

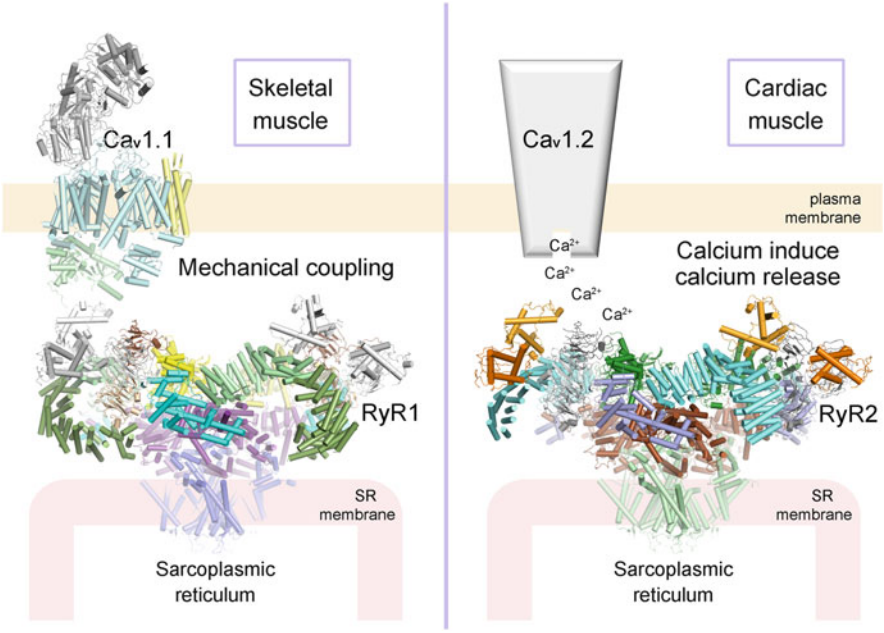

Fig. 2.8 Working models for activation of RyR1/2 by $Ca_v1/2$, respectively. In the skeletal muscle, RyR1 is activated by the membrane depolarization-induced conformational changes of $Ca_v1.1$ through physical interactions. It is called the "mechanical coupling" mechanism. In cardiac muscle, $Ca_v1.2$ permeates Ca^{2+} ions into the cytosol, leading to the activation of RyR2, a mechanism known as the "calcium induced calcium release"

structures of $Ca_v1.1$ and RyR1 have been solved, there is no detailed structural information on the $Ca_v1.1$ and RyR1 supercomplex. According to the structural analysis, a speculative mechanism is proposed [57]. As reported, RyR1 is activated through direct physical contacts with the $Ca_v1.1$ [61, 63–65]. Multiple areas, such as the SPRY3 domain of RyR1 and β-subunit of $Ca_v1.1$, are involved in their coupling [66]. The conformational changes of the VSDs of $Ca_v1.1\alpha1$ may induce shifts of the β-subunit and other cytoplasmic segments of $Ca_v1.1$, subsequently triggering the motion of the adjacent RyR1 cytoplasmic domains. Note that the SPRY3 domain of RyR1 is in direct contact with the N-terminal domain (NTD) within the same protomer. Potential shifts of the SPRY3 domain may be translated to the conformational changes of NTD, and subsequently the Handle domain and the Central domain. So the structural shifts triggered by $Ca_v1.1$ at the periphery of the RyR1 cytoplasmic region are propagated along the superhelical assemblies of the cytoplasmic domains to the Central domain, eventually leading to the opening of the intracellular gate. Nonetheless, the speculative mechanism still awaits experimental evidence.

2.5 Perspective

Voltage-gated calcium channels play essential roles in a multitude of physiological processes. The structure of $Ca_v1.1$ complex provides clues to the gating mechanism and selectivity, which establishes a foundation for mechanistic understanding of E-C coupling and provides a three-dimensional template for molecular interpretations of the functions and disease mechanisms of Ca_v and Na_v channels.

In the past few decades, most high resolution protein structures were obtained from X-ray crystallography. Until a few years ago, we witnessed the breakthrough of cryo-EM. The resolution was improved to near atomic resolution (beyond 4 Å), a "resolution revolution". A number of important protein or protein complex structures were solved. However, regardless of single-particle cryo-EM or X-ray crystallography, purification of the protein is required. Therefore, some proteins or protein complexes that are resistant to in vitro purification cannot yield high resolution structure. To visualize the E-C coupling ultrastructure formed by RyR1 and $Ca_v1.1$, we may eventually have to employ another technology, electron tomography (ET), which can image the samples in situ. The rapid technological development of ET may allow structural resolution the RyR1-$Ca_v1.1$ supercomplex to molecular details in the near future.

References

1. Catterall WA (2011) Voltage-gated calcium channels. Cold Spring Harb Perspect Biol 3: a003947
2. Clapham DE (2007) Calcium signaling. Cell 131:1047–1058
3. Ertel EA, Campbell KP, Harpold MM, Hofmann F, Mori Y, Perez-Reyes E, Schwartz A, Snutch TP, Tanabe T, Birnbaumer L et al (2000) Nomenclature of voltage-gated calcium channels. Neuron 25:533–535
4. Nowycky MC, Fox AP, Tsien RW (1985) Three types of neuronal calcium channel with different calcium agonist sensitivity. Nature 316:440–443
5. Tsien RW, Lipscombe D, Madison DV, Bley KR, Fox AP (1988) Multiple types of neuronal calcium channels and their selective modulation. Trends Neurosci 11:431–438
6. Fleckenstein A (1983) History of calcium antagonists. Circ Res 52:I3–16
7. Kohlhardt M, Fleckenstein A (1977) Inhibition of the slow inward current by nifedipine in mammalian ventricular myocardium. Naunyn Schmiedebergs Arch Pharmacol 298:267–272
8. Carbone E, Lux HD (1984) A low voltage-activated, fully inactivating Ca channel in vertebrate sensory neurones. Nature 310:501–502
9. Llinas R, Yarom Y (1981) Electrophysiology of mammalian inferior olivary neurones in vitro. Different types of voltage-dependent ionic conductances. J Physiol 315:549–567
10. Llinas RR, Sugimori M, Cherksey B (1989) Voltage-dependent calcium conductances in mammalian neurons. The P channel. Ann NY Acad Sci 560:103–111
11. Randall A, Tsien RW (1995) Pharmacological dissection of multiple types of Ca2+ channel currents in rat cerebellar granule neurons. J Neurosci 15:2995–3012
12. Tanabe T, Takeshima H, Mikami A, Flockerzi V, Takahashi H, Kangawa K, Kojima M, Matsuo H, Hirose T, Numa S (1987) Primary structure of the receptor for calcium channel blockers from skeletal muscle. Nature 328:313–318

13. Wu J, Yan Z, Li Z, Qian X, Lu S, Dong M, Zhou Q, Yan N (2016) Structure of the voltage-gated calcium channel Ca(v)1.1 at 3.6 A resolution. Nature 537:191–196
14. Takahashi M, Seagar MJ, Jones JF, Reber BF, Catterall WA (1987) Subunit structure of dihydropyridine-sensitive calcium channels from skeletal muscle. Proc Natl Acad Sci USA 84:5478–5482
15. Davies A, Hendrich J, Van Minh AT, Wratten J, Douglas L, Dolphin AC (2007) Functional biology of the alpha(2)delta subunits of voltage-gated calcium channels. Trends Pharmacol Sci 28:220–228
16. Dolphin AC (2003) Beta subunits of voltage-gated calcium channels. J Bioenerg Biomembr 35:599–620
17. Dolphin AC (2013) The alpha2delta subunits of voltage-gated calcium channels. Biochim Biophys Acta 1828:1541–1549
18. Cheng W, Altafaj X, Ronjat M, Coronado R (2005) Interaction between the dihydropyridine receptor Ca2+ channel beta-subunit and ryanodine receptor type 1 strengthens excitation-contraction coupling. Proc Natl Acad Sci USA 102:19225–19230
19. Gregg RG, Messing A, Strube C, Beurg M, Moss R, Behan M, Sukhareva M, Haynes S, Powell JA, Coronado R et al (1996) Absence of the beta subunit (cchb1) of the skeletal muscle dihydropyridine receptor alters expression of the alpha 1 subunit and eliminates excitation-contraction coupling. Proc Natl Acad Sci USA 93:13961–13966
20. Schredelseker J, Di Biase V, Obermair GJ, Felder ET, Flucher BE, Franzini-Armstrong C, Grabner M (2005) The beta 1a subunit is essential for the assembly of dihydropyridine-receptor arrays in skeletal muscle. Proc Natl Acad Sci USA 102:17219–17224
21. Andronache Z, Ursu D, Lehnert S, Freichel M, Flockerzi V, Melzer W (2007) The auxiliary subunit gamma 1 of the skeletal muscle L-type Ca2+ channel is an endogenous Ca2+ antagonist. Proc Natl Acad Sci USA 104:17885–17890
22. Kang MG, Campbell KP (2003) Gamma subunit of voltage-activated calcium channels. J Biol Chem 278:21315–21318
23. Olivera BM, Miljanich GP, Ramachandran J, Adams ME (1994) Calcium channel diversity and neurotransmitter release: the omega-conotoxins and omega-agatoxins. Annu Rev Biochem 63:823–867
24. Klugbauer N, Lacinova L, Marais E, Hobom M, Hofmann F (1999) Molecular diversity of the calcium channel alpha2delta subunit. J Neurosci 19:684–691
25. Zamponi GW, Striessnig J, Koschak A, Dolphin AC (2015) The physiology, pathology, and pharmacology of voltage-gated calcium channels and their future therapeutic potential. Pharmacol Rev 67:821–870
26. Bian F, Li Z, Offord J, Davis MD, McCormick J, Taylor CP, Walker LC (2006) Calcium channel alpha2-delta type 1 subunit is the major binding protein for pregabalin in neocortex, hippocampus, amygdala, and spinal cord: an ex vivo autoradiographic study in alpha2-delta type 1 genetically modified mice. Brain Res 1075:68–80
27. Li Z, Taylor CP, Weber M, Piechan J, Prior F, Bian F, Cui M, Hoffman D, Donevan S (2011) Pregabalin is a potent and selective ligand for alpha(2)delta-1 and alpha(2)delta-2 calcium channel subunits. Eur J Pharmacol 667:80–90
28. Wolf M, Eberhart A, Glossmann H, Striessnig J, Grigorieff N (2003) Visualization of the domain structure of an L-type Ca2+ channel using electron cryo-microscopy. J Mol Biol 332:171–182
29. Van Petegem F, Clark KA, Chatelain FC, Minor DL (2004) Structure of a complex between a voltage-gated calcium channel beta-subunit and an alpha-subunit domain. Nature 429:671–675
30. Hu HL, Wang Z, Wei RS, Fan GZ, Wang QL, Zhang KM, Yin CC (2015) The molecular architecture of dihydropyrindine receptor/L-type Ca2+ channel complex. Sci Rep 5:8370
31. Murata K, Nishimura S, Kuniyasu A, Nakayama H (2010) Three-dimensional structure of the alpha(1)-beta complex in the skeletal muscle dihydropyridine receptor by single-particle electron microscopy. J Electron Microsc 59:215–226
32. Serysheva II, Ludtke SJ, Baker MR, Chiu W, Hamilton SL (2002) Structure of the voltage-gated L-type Ca2+ channel by electron cryomicroscopy. Proc Natl Acad Sci USA 99:10370–10375

33. Chen YH, Li MH, Zhang Y, He LL, Yamada Y, Fitzmaurice A, Shen Y, Zhang HL, Tong L, Yang J (2004) Structural basis of the alpha(1)-beta subunit interaction of voltage-gated Ca2+ channels. Nature 429:675–680
34. Opatowsky Y, Chen CC, Campbell KP, Hirsch JA (2004) Structural analysis of the voltage-dependent calcium channel beta subunit functional core and its complex with the alpha 1 interaction domain. Neuron 42:387–399
35. Payandeh J, Scheuer T, Zheng N, Catterall WA (2011) The crystal structure of a voltage-gated sodium channel. Nature 475:353–358
36. Zhang X, Ren WL, DeCaen P, Yan CY, Tao X, Tang L, Wang JJ, Hasegawa K, Kumasaka T, He JH et al (2012) Crystal structure of an orthologue of the NaChBac voltage-gated sodium channel. Nature 486:130–U160
37. Sula A, Booker J, Ng LCT, Naylor CE, DeCaen PG, Wallace BA (2017) The complete structure of an activated open sodium channel. Nat Commun 8:14205
38. Tang L, El-Din TMG, Payandeh J, Martinez GQ, Heard TM, Scheuer T, Zheng N, Catterall WA (2014) Structural basis for Ca2+ selectivity of a voltage-gated calcium channel. Nature 505:56–61
39. Liao M, Cao E, Julius D, Cheng Y (2013) Structure of the TRPV1 ion channel determined by electron cryo-microscopy. Nature 504:107–112
40. Yan C, Hang J, Wan R, Huang M, Wong CC, Shi Y (2015a) Structure of a yeast spliceosome at 3.6-angstrom resolution. Science 349:1182–1191
41. Bannister RA, Beam KG (2013) Ca(V)1.1: the atypical prototypical voltage-gated Ca(2)(+) channel. Biochim Biophys Acta 1828:1587–1597
42. Buraei Z, Yang J (2013) Structure and function of the beta subunit of voltage-gated Ca(2)(+) channels. Biochim Biophys Acta 1828:1530–1540
43. Curtis BM, Catterall WA (1984) Purification of the calcium-antagonist receptor of the voltage-sensitive calcium-channel from skeletal-muscle transverse tubules. Biochemistry 23:2113–2118
44. Florio V, Striessnig J, Catterall WA (1992) Purification and reconstitution of skeletal-muscle calcium channels. Methods Enzymol 207:529–546
45. Sharp AH, Imagawa T, Leung AT, Campbell KP (1987) Identification and characterization of the dihydropyridine-binding subunit of the skeletal-muscle dihydropyridine receptor. J Biol Chem 262:12309–12315
46. Wu J, Yan Z, Li Z, Yan C, Lu S, Dong M, Yan N (2015) Structure of the voltage-gated calcium channel Cav1.1 complex. Science 350:aad2395
47. Lanner JT, Georgiou DK, Joshi AD, Hamilton SL (2010) Ryanodine receptors: structure, expression, molecular details, and function in calcium release. Cold Spring Harb Perspect Biol 2:a003996
48. Inui M, Saito A, Fleischer S (1987) Purification of the ryanodine receptor and identity with feet structures of junctional terminal cisternae of sarcoplasmic reticulum from fast skeletal muscle. J Biol Chem 262:1740–1747
49. Lai FA, Erickson HP, Rousseau E, Liu QY, Meissner G (1988) Purification and reconstitution of the calcium release channel from skeletal muscle. Nature 331:315–319
50. Pessah IN, Waterhouse AL, Casida JE (1985) The calcium-ryanodine receptor complex of skeletal and cardiac muscle. Biochem Biophys Res Commun 128:449–456
51. Bhat MB, Zhao J, Takeshima H, Ma J (1997) Functional calcium release channel formed by the carboxyl-terminal portion of ryanodine receptor. Biophys J 73:1329–1336
52. Takeshima H, Nishimura S, Matsumoto T, Ishida H, Kangawa K, Minamino N, Matsuo H, Ueda M, Hanaoka M, Hirose T et al (1989) Primary structure and expression from complementary DNA of skeletal muscle ryanodine receptor. Nature 339:439–445
53. Hakamata Y, Nakai J, Takeshima H, Imoto K (1992) Primary structure and distribution of a novel ryanodine receptor/calcium release channel from rabbit brain. FEBS Lett 312:229–235

54. Nakai J, Imagawa T, Hakamat Y, Shigekawa M, Takeshima H, Numa S (1990) Primary structure and functional expression from cDNA of the cardiac ryanodine receptor/calcium release channel. FEBS Lett 271:169–177
55. Otsu K, Willard HF, Khanna VK, Zorzato F, Green NM, MacLennan DH (1990) Molecular cloning of cDNA encoding the Ca2+ release channel (ryanodine receptor) of rabbit cardiac muscle sarcoplasmic reticulum. J Biol Chem 265:13472–13483
56. Rossi D, Sorrentino V (2002) Molecular genetics of ryanodine receptors Ca2+-release channels. Cell Calcium 32:307–319
57. Bai XC, Yan Z, Wu JP, Li ZQ, Yan N (2016) The central domain of RyR1 is the transducer for long-range allosteric gating of channel opening. Cell Res 26:995–1006
58. des Georges A, Clarke OB, Zalk R, Yuan Q, Condon KJ, Grassucci RA, Hendrickson WA, Marks AR, Frank J (2016) Structural basis for gating and activation of RyR1. Cell 167:145–157
59. Peng W, Shen HZ, Wu JP, Guo WT, Pan XJ, Wang RW, Chen SRW, Yan N (2016) Structural basis for the gating mechanism of the type 2 ryanodine receptor RyR2. Science 354(6310): aah5324
60. Yan Z, Bai XC, Yan C, Wu J, Li Z, Xie T, Peng W, Yin CC, Li X, Scheres SH et al (2015b) Structure of the rabbit ryanodine receptor RyR1 at near-atomic resolution. Nature 517:50–55
61. Rios E, Brum G (1987) Involvement of dihydropyridine receptors in excitation-contraction coupling in skeletal muscle. Nature 325:717–720
62. Endo M (1977) Calcium release from the sarcoplasmic reticulum. Physiol Rev 57:71–108
63. Franzini-Armstrong C, Protasi F, Ramesh V (1999) Shape, size, and distribution of Ca(2+) release units and couplons in skeletal and cardiac muscles. Biophys J 77:1528–1539
64. Protasi F, Franzini-Armstrong C, Flucher BE (1997) Coordinated incorporation of skeletal muscle dihydropyridine receptors and ryanodine receptors in peripheral couplings of BC3H1 cells. J Cell Biol 137:859–870
65. Tanabe T, Beam KG, Adams BA, Niidome T, Numa S (1990) Regions of the skeletal muscle dihydropyridine receptor critical for excitation-contraction coupling. Nature 346:567–569
66. Perez CF, Mukherjee S, Allen PD (2003) Amino acids 1-1,680 of ryanodine receptor type 1 hold critical determinants of skeletal type for excitation-contraction coupling. Role of divergence domain D2. J Biol Chem 278:39644–39652

Chapter 3
Structure-Dynamic Coupling Through Ca^{2+}-Binding Regulatory Domains of Mammalian NCX Isoform/Splice Variants

Daniel Khananshvili

Abstract Mammalian Na^+/Ca^{2+} exchangers (NCX1, NCX2, and NCX3) and their splice variants are expressed in a tissue-specific manner and are regulated by Ca^{2+} binding CBD1 and CBD2 domains. NCX2 does not undergo splicing, whereas in NCX1 and NCX3, the splicing segment (with mutually exclusive and cassette exons) is located in CBD2. Ca^{2+} binding to CBD1 results in Ca^{2+}-dependent tethering of CBDs through the network of interdomain salt-bridges, which is associated with NCX activation, whereas a slow dissociation of "occluded" Ca^{2+} inactivates NCX. Although NCX variants share a common structural basis for Ca^{2+}-dependent tethering of CBDs, the Ca^{2+} off-rates of occluded Ca^{2+} vary up to 50-fold, depending on the exons assembly. The Ca^{2+}-dependent tethering of CBDs rigidifies the interdomain movements of CBDs without any significant changes in the CBDs' alignment; consequently, more constraining conformational states become more populated in the absence of global conformational changes. Although this Ca^{2+}-dependent "population shift" is a common mechanism among NCX variants, the strength and span of backbone rigidification from the C-terminal of CBD1 to the C-terminal of CBD2 is exon dependent. The mutually exclusive exons differentially stabilize/destabilize the backbone dynamics of Ca^{2+}-bound CBDs in NCX1 and NCX3 variants, whereas the cassette exons control the stability of the interdomain linker. The combined effects of mutually exclusive and cassette exons permit a fine adjustment of two different regulatory pathways: the Ca^{2+}-dependent activation (controlled by CBD1) and the Ca^{2+}-dependent alleviation of Na^+-induced inactivation (controlled by CBD2). Exon-controlled dynamic features match with cell-specific regulatory requirements in a given variant.

Keywords NCX · SAXS · HDX-MS · Dynamic coupling · Population shift · Allosteric regulation · Alternative splicing · Exon

D. Khananshvili (✉)
Department of Physiology and Pharmacology, Sackler School of Medicine, Tel-Aviv University, Tel-Aviv, Israel
e-mail: dhanan@post.tau.ac.il

J. Krebs (ed.), *Membrane Dynamics and Calcium Signaling*, Advances in Experimental Medicine and Biology 981,
https://doi.org/10.1007/978-3-319-55858-5_3

3.1 Ca^{2+} Sensing by Isoform/Splice Variants and Multitask Ca^{2+} Signaling

Calcium (Ca^{2+}) controls multitask communicative messages in every living cell, where numerous biochemical reactions, managed by Ca^{2+}, are precisely tuned in time and space [1–3]. Multichannel regulatory passageways are especially complex in multicellular organisms, reaching a culmination of sophistication in excitable tissues [2, 4, 5]. Even relatively "small" alterations in Ca^{2+} homeostasis may lead to functional disorders with life-threating outcomes [1–3, 6]. An evolutionary selection of the Ca^{2+} ion, as a communal and multipurpose regulatory substance, has produced distinct gene isoforms and their splice variants encoding specifically folded motifs of Ca^{2+} binding domains (EF-hand, C_2, and others) [1, 2, 7, 8]. Moreover, similarly folded versions of isoform/splice variants produce structurally similar proteins with distinct coordination chemistry, thereby providing a major toolbox for diversifying the number of Ca^{2+}-binding sites with different affinities for Ca^{2+} binding [1, 2, 6]. Although the major principles of Ca^{2+} coordination chemistry are well understood, it remains unclear how the regulatory specificity and selectivity of Ca^{2+} sensing is achieved when the regulatory massage is decoded upon Ca^{2+} binding, and how the decoded information propagates over a long distance [2, 7, 9]. Recently developed concepts offer an updated view of allosteric regulation in proteins, according to which a greater importance is given to changes in the dynamic distribution of numerous conformational states rather than to ligand-induced global changes in protein conformations [10–12]. Protein rigidity seems to serve as a central feature for regulatory signal decoding, diversification, and common communication between distant sites in multidomain proteins, thereby representing a dynamic mode of regulatory coupling [10, 12]. According to this scenario, more rigid conformational states become more populated upon ligand binding in the absence of any global conformation changes [10, 11]. In dealing with these issues, this review focuses on Ca^{2+} sensing CBD domains of Na^+/Ca^{2+} exchangers (NCX).

3.2 Structural and Regulatory Specificities of NCX Isoform/Splice Variants

NCX extrudes $1Ca^{2+}$ ion from the cytosol or organelle matrix (e.g., nuclei or mitochondria) in exchange with $3Na^+$ ions, while utilizing the electrochemical gradient of Na^+ and thus, control Ca^{2+} homeostasis in many cell types [4, 5, 13–15]. In mammals, NCX1, NCX2, and NCX3 gene isoforms and their splice variants are expressed in a tissue-specific manner [14, 16–18]. NCX1 is universally distributed, practically in every mammalian cell, although several splice variants of NCX1 are exclusively expressed in specific tissue (e.g., NCX1-ACDEF in cardiomyocites). NCX2 is predominantly expressed in the brain and spinal cord, but it can be also found in gastrointestinal and kidney tissues; NCX3 is mainly expressed in the

brain and skeletal muscle [4, 14, 16]. At least seventeen NCX1 and five NCX3 splice variants are produced through alternative splicing, whereas NCX2 has no splice variants [14, 16]. Altered expression and/or regulation of tissue-specific NCX variants is associated with heart failure, arrhythmia, cerebral ischemia, neurodegenerative diseases, and other maladies [4, 5]. Selective pharmacological targeting of NCX variants could be beneficial, although the rational development of drug candidates remains challenging [4]. The gene family of Na^+/Ca^{2+} (NCX) exchangers belongs to the superfamily of Ca^{2+}/Cation (Ca/CA) exchangers, which contain highly conserved α_1 and α_2 repeats, involved in ion transport activities [14, 16, 17, 19]. The crystal structure of full-length mammalian NCX is currently unavailable, although the crystal structure of the archaeal NCX (NCX_Mj) [19, 20] serves as an excellent model system for resolving ion-transport mechanisms [21–24]. Prokaryotic and eukaryotic NCXs entail ten transmembrane helices (TM1-TM10) [15, 19], where only eukaryotic NCXs contain a cytoplasmic f-loop (between TM5 and TM6) with two Ca^{2+}-binding regulatory domains (CBD1 and CBD2), which form a "head-to-tail" tandem (CBD12) through a short linker (Fig. 3.1) [22, 23, 25, 26]. Interestingly, the mitochondrial Na^+/Ca^{2+} exchanger (NCLX) does not contain regulatory CBD domains [4, 5, 27].

3.2.1 *Coordination Chemistry Controls the Number and Affinity of Ca^{2+} Sites in Uniformly Folded CBDs*

High-resolution X-ray and NMR structures of isolated CBD1, CBD2, and CBD12 revealed that both CBDs possess a β-immunoglobulin (Ig)-like folding, where a seven-strand β-sandwich motif is formed by two antiparallel β-sheets entailing A-B-E and D-C-F-G strands (Fig. 3.1) [23, 25, 28–30]. Moreover, the overlay of CBD1 and CBD2 crystal structures revealed nearly identical folding with RMSD = 1.3 Å, where all Ca^{2+} binding sites of CBDs reside at distal loops of C-terminal ends [28–32]. Despite these structural similarities, CBD1 and CBD2 differ in a number of Ca^{2+} binding sites and in their coordination chemistry. The Ig-like folding of CBDs is very similar to proteins belonging to C_2-domains, although the canonical C_2-folding refers to an eight-strand β-sandwich motif (instead of seven in CBDs). CBD1 contains four Ca^{2+} binding sites (Ca1-Ca4), whereas the number of Ca^{2+} binding sites at CBD2 varies from zero to three (CaI-CaIII) in a variant-dependent manner [23, 25, 28, 29, 33]. In CBD1, the cluster of four Ca^{2+} binding sites is compiled in a parallelogram-like configuration (with a 3.9–4.4 Å distance between distinct sites), allowing one to place four divalent cations into proximity. Polydentate coordination allows a ligation of two (D500) or even three (E451) Ca^{2+} ions at once. In CBD1, the Ca^{2+}-coordinating residues are allocated at the C-terminus and three loops: EF, AB, and CD [28–30] (Fig. 3.1). The C3 and C4 sites have a high affinity ($K_d \sim 0.3$ μM) for Ca^{2+}, whereas the affinity of Ca1 and Ca2 is at least 50 times lower [34–36]. In CBD2, the Ca^{2+} binding sites are ~5.5 Å apart, where K585 (which is in a homologous position to E454 in CBD1) forms a salt-bridge with D552 and E648 without Ca^{2+}, thereby stabilizing apo-CBD2 [28]. Thus, without Ca^{2+}, CBD2 is more stable than CBD1.

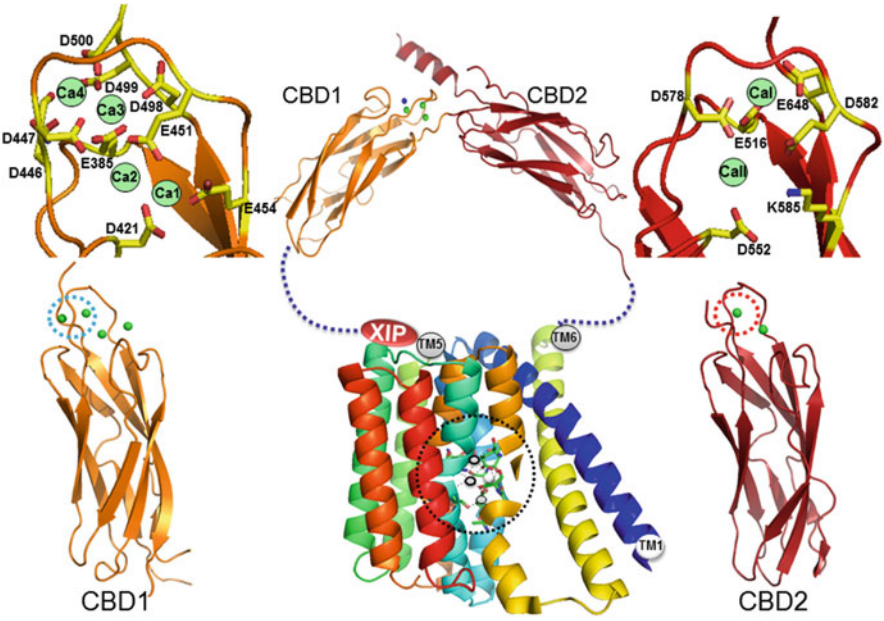

Fig. 3.1 Regulatory CBD domains of eukariotic NCX. Archaeal and eukaryotic NCX contain ten trans-membrane helices (TM1-10), whereas only eukaryotic NCXs contain a regulatory cytosolic f-loop (~500 amino acids) between the TM5 and TM6. The f-loop contains two Ca^{2+}-binding regulatory domains, CBD1 and CBD2, where CBD1 is linked with TM5 and CBD2 with TM6, assigned as structurally unresolved dotted lines. The CBDs are connected through a very short interdomain linker in a head-to-tail conformation, thereby forming a two-domain regulatory tandem (CBD12). The trans-membrane helical structures were reproduced according to the crystal structure of archaeal NCX_Mj (3V5U), whereas the CBD12 tandem is depicted according to the crystal structure of NCX1-CBD12-AD (3US9). The ion binding/transport sites, located on TM2, TM3, TM7 and TM8 helices reproduced according to the crystal structure of NCX_Mj (3V5U). The crystal structures of NCX1-CBD1 (2DPK), NCX1-CBD2-AD (2QVM) and NCX1-CBD12-AD (3US9) were used for the presentation (a black cycle). The Ca^{2+} binding sites are located at the C-terminal tips of CBD1 and CBD2, where green balls represent Ca^{2+} ions. Ca^{2+} binding to the Ca3-Ca4 sites of CBD1 results in Ca^{2+}-dependent activation of mammalian NCX variants (a blue cycle), whereas Ca^{2+} binding to the CaI site of CBD2 refers to Ca^{2+}-dependent alleviation of Na^{+}-induced inactivation (a red cycle)

In CBD2 only a single residue (D578) bridges the CaI and CaII sites via a bidentate ligation. The CaI and CaII sites of CBD2 have a moderate (K_d = 2–10 μM) and low (K_d > 20 μM) affinity, respectively [23, 33–35].

3.2.2 Each CBD Domain Plays a Distinct Regulatory Role

Mammalian NCXs exhibit two major modes of Ca^{2+}-dependent allosteric regulation [26, 37–39]. The first mode refers to Ca^{2+}-dependent activation, whereas the second mode implies the Ca^{2+}-dependent alleviation of Na^{+}-induced inactivation, which

exists in some variants. Notably, the Na^+-induced inhibition is due to Na^+ interaction with the transport domains (not with CBDs) [26, 39, 40]. The absence of Na^+-transients in non-excitable tissues and the presence of Na^+ transients in excitable tissues explains the need for Ca^{2+}-dependent alleviation of Na^+-dependent inactivation in excitable tissues [26, 33].

In mammalian NCX variants, the Ca^{2+} binding to Ca3-Ca4 sites of CBD1 activates ion exchange activities up to 20-fold, whereas the Ca^{2+} binding to the CaI site of CBD2 results in Ca^{2+}-dependent alleviation of Na^+-dependent inactivation [39, 41–43]. Since NCX2 lacks Na^+-dependent inactivation, the Ca^{2+}-dependent alleviation is not required for NCX2. The kidney splice variant (NCX1-BD) does not bind Ca^{2+} at CBD2 (since the CaI site is structurally destabilized in CBD2); thus, it lacks Ca^{2+}-dependent alleviation of Na^+-induced inactivation [25, 33, 34, 44]. Functional assignments of low-affinity Ca^{2+} binding sites of CBD1 (Ca1 and Ca2) and CBD2 (CaII) are less clear, although these sites could serve as the Mg^{2+} rather than the Ca^{2+} sites, which are constitutively occupied by Mg^{2+} under physiological conditions [23, 35, 45]. Interestingly, the occupation of Ca1-Ca2 sites by Mg^{2+} decreases the affinity at nearby Ca3-Ca4 sites of CBD1, whereas the occupation of the CaII site by Mg^{2+} increases the Ca^{2+} affinity at CaI [29, 35, 40]. Eukaryotic NCXs are very sensitive to cytosolic acidification (e.g., under ischemia/acidosis conditions) since protons effectively compete with Ca^{2+} for binding at CBDs [23, 41, 46].

In contrast with mammalian NCX, a *Drosophila* NCX ortholog exhibits an opposite regulatory response to Ca^{2+}. Namely, Ca^{2+} binding to the Ca3-Ca4 sites of the CALX1.1 splice variant inactivates ion exchange activity, whereas in the second variant, CALX1.2, Ca^{2+} has no regulatory effect on exchange activity [31, 32, 37, 47]. CALX1-CBD2 variants do not bind Ca^{2+}, so the Ca^{2+}-dependent alleviation of Na^+-induced inactivation is physiologically irrelevant for CALX variants. CALX1 also undergoes alternative splicing only at CBD2, where the two splice variants differ only by five amino acids [31, 32]. These five residues in CALX1-CBD2 are located within a FG-loop between the H1 α-helix and the β-strand, which matches the cassette exons positions in mammalian NCX1 [25, 31].

3.2.3 *Exon Arrays Differentially Control the Tissue-Specific Regulatory Modes of NCX Variants*

In NCX1 (17 splice variants), NCX3 (5 splice variants), and CALX1 (2 splice variants) the alternative splicing segment is located in CBD2 [25, 26, 31, 32]. Mutually exclusive exons (A or B) control the capacity and/or affinity of Ca^{2+} binding at both CBD1 and CBD2, although they have opposite effects in NCX1 and NCX3. In NCX1, alternative splicing arises from merging six small exons (A, B, C, D, E, and F), where the mutually exclusive exons, A and B, are expressed in excitable and

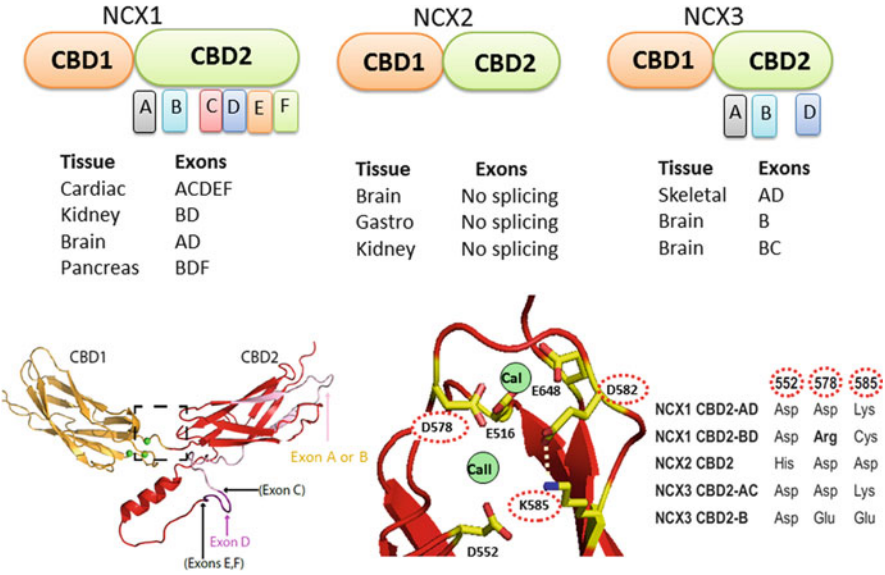

Fig. 3.2 In mammalian NCX1 and NCX3 variants, the splice segment is exclusively located on CBD2. In NCX1, tissue-specific splice variants arise from a combination of six small exons A, B, C, D, E, and F, whereas a mutually exclusive exon (either A or B) shows up in every splice variant. NCX2 does not undergo alternative splicing and NCX3 contains only A, B, and C exons. To show the position of the splice segment and specific exons, the NMR structures of NCX1-CBD1 (2FWS, orange), NCX1-CBD2-AD (2FWU, red), and NCX1-CBD2-BD (2KLT, green) structures were superimposed on the template of the two-domain NCX1-CBD12-AD crystal structure (3US9). Residues in positions 552, 578, and 585 form the CBD2 Ca^{2+}-binding sites between the CD- and EF-loops and thus, determine the number of Ca^{2+} binding sites and their affinity for Ca^{2+} at CBD2. Single-point substitutions at specific positions diversify the roles of exon A and B in NCX1 and NCX3 isoform/splice variants

non-excitable tissues, respectively (Fig. 3.2) [14, 16, 18]. In NCX1, cassette exons (C, D, E, F) merge either with A or B exon to generate the cardiac (ACDEF), brain (AD), and kidney (AC) variants among others [14, 16, 23]. In NCX3, alternative splicing involves only three exons (A, B, and C), whereas both A and B exons are expressed in neuronal tissues [14, 25, 33]. In A-exon-containing NCX1 variants, CBD2 binds two Ca^{2+} ions, whereas in B-exon-containing NCX1 variants, CBD2 does not bind Ca^{2+} [34]. Thus, in NCX1 the Ca^{2+}-dependent alleviation occurs only in A-exon-containing variants, since their CBD2 bind Ca^{2+} [26, 38, 39, 44]. CBD2 of NCX2 binds only one Ca^{2+} with very low affinity, which is functionally invalid under physiologically relevant conditions (probably because the absence of Na^{+}-dependent inactivation in NCX2) [25, 33]. In NCX3, exon A is expressed in skeletal tissues and exon B is expressed in neuronal tissues [14, 16, 25]. The A-exon-containing variant (AC) of NCX3 does not bind Ca^{2+} to CBD2 [33], whereas the exon B variants (B or BC) bind three Ca^{2+} ions at CBD2 [25, 33]. Intriguingly, NCX3-AC (no Ca^{2+}binding to CBD2) exhibits less Na^{+}-dependent inactivation in

comparison with NCX3-B (which binds three Ca^{2+} ions at CBD2). Thus, exons A and B affect inversely the Ca^{2+} binding to CBD2 in NCX1 and NCX3 variants.

The exon-dependent effects on Ca^{2+} binding capacity/affinity strongly correlate with diverse regulatory responses of NCX variants. For example, Ca^{2+} binding to CBD1 activates the brain (AD), cardiac (ACDEF), and kidney (BD) variants of NCX1, although the Ca^{2+}-dependent alleviation of Na^{+}-induced inactivation (controlled by CBD2) occurs only in the cardiac and brain variants (the kidney variant does not bind Ca^{2+}) [25, 34]. The exon A- and B-dependent regulatory differences between NCX1 variants are due to splice-dependent structural editing of E and F strands, which participate in Ca^{2+} binding at CBD2 [25]. Namely, the B-exon variants of NCX1 contain arginine (instead of aspartate or glutamate) and cysteine (instead of lysine) residues at positions 578 and 585, which prevents the Ca^{2+} binding to the CaI site and thus, destabilizes CBD2. NCX1-CBD2-AD retains its structural integrity even in the absence of Ca^{2+} since in the apo state K585 forms salt-bridges with D552 and E648 (the CaI site of CBD2) whereas in the Ca^{2+}-bound state K585 interacts with E582 (Fig. 3.2) [23, 25]. In NCX2-CBD2 (no splice variants), the replacement of D552 by histidine aborts one of the two sole Ca^{2+}-coordinating atoms (which eliminates the CaII site and reduces Ca^{2+} affinity at the CaI site), whereas in NCX3-CBD2-B, the replacement of K585 by glutamate results in three Ca^{2+} ions binding at CBD2 (Fig. 3.2) [25, 33].

3.3 Synergistic Interactions Between CBDs Control the Ca^{2+} Sensing Features

Synergistic interactions between CBDs modify Ca^{2+} sensing properties at both CBDs, where Ca^{2+} binding to Ca3-Ca4 sites of CBD1 results either in activation (mammalian NCXs), inhibition (CALX1.1), or no response (CALX1.2) to regulatory Ca^{2+} [28, 35, 36, 44, 48]. Moreover, mammalian NCXs show considerable differences in Ca^{2+}-dependent activation (controlled by CBD1) and Ca^{2+}-dependent alleviation of Na^{+}-induced inactivation (controlled by CBD2). For example, the Ca3-Ca4 sites of the brain (AD), cardiac (ACDEF), and kidney (BD) splice variants of NCX1-CBD12 show up to 50-fold differences in the Ca^{2+} binding affinity and in the Ca^{2+} off-rates of occluded Ca^{2+} [29, 34]. In contrast with NCX1, NCX2-CBD12 and NCX3-CBD12 share similar affinities for Ca^{2+} at Ca3-C4 sites of CBD1, although the occluded Ca^{2+} dissociates ~10-fold slower in skeletal muscle (AC) than in the brain (BC) variants [23, 33]. Slower dissociation of occluded Ca^{2+} from the skeletal variant matches the physiological needs, since in myocytes NCX must clear up much more cytosolic Ca^{2+} than in neurons [23, 34–36, 49].

Short interdomain linker of CBDs is highly conserved among all known NCX variants and play a critical role in Ca^{2+}-dependent tethering/rigidification of CBDs [29, 33–36, 49]. Deletion or elongation of this linker (501-HAGIFT-506) accelerates (up to ~50-fold) the dissociation of occluded Ca^{2+}, whereas it decreases the Ca^{2+}

binding affinity up to ~10-fold at the Ca3-Ca4 sites [34]. Slow dissociation of Ca^{2+} from the Ca3-Ca4 sites of CBD12 (assigned as an "occluded" Ca^{2+}) was observed for all tested NCX and CALX variants, meaning that interdomain coupling is controlled by the linker [29, 33–36, 49–51]. G503 is the only residue in the linker mutation for which aborts a slow dissociation of occluded Ca^{2+} and interdomain CBDs movements, as reported by stopped-flow and SAXS techniques [36]. Moreover, the crystal structures of NCX1-CBD12 [29] and CALX-CBD12 [31, 32] show that the dihedral φ/ψ angles at position 503 are only allowed for glycine and that any other residue at this position would require rotation around the C_α atom of this residue with resulting steric clashes in the protein structure. Moreover, patch-clamp analysis of full-size NCX revealed that mutations of either G503 in mammalian NCX1 or analogous G555 in CALX1.1 abort the Ca^{2+}-dependent regulation [37, 38, 43]. Thus, the interdomain linker encodes crucial information for the dynamic coupling of regulation in the NCX and CALX variants. Rapidly progressing genetic tools may allow the usage of relevant mutations for investigating the physiological roles of NCX in intact cells, tissues and organs [4, 5, 23]. Even though no mutations of NCX have been discovered yet with disease consequences, it might be worthwhile to mention that specific mutations in the two-domain interface of CBDs may abort the Ca^{2+}-dependent regulation of NCX. Under certain pathophysiological conditions (e.g., an intensive physical load and/or stress conditions) the mutations aborting the Ca^{2+}-dependent regulation could be very dangerous, since the rates of NCX-mediated extrusion would not match to required physiological needs for extruding the cytosolic Ca^{2+} (e.g., during the action potential plateau and/or repolarization period). This may lead to the overload of the intracellular Ca^{2+} stories (e.g., sarcoplasmic reticulum in cardiomyocytes), which may cause life-threating arrhythmias, neuronal disorders (e.g., affecting the synaptic signal transmission), altered hormone secretion, etc. [4, 5, 13].

3.3.1 CBD12 Crystal Structures Highlight the Functional Significance of the Two-Domain Interface

Although the crystal structures of the isolated CBD1 and CBD2 domains [28, 30] have provided detailed information on the Ca^{2+} coordination chemistry, this structural information does not explain the strong synergistic interactions between the CBDs observed in the NCX and CALX variants. Only the discovery of the two-domain tandem (CBD12) crystal structures [29, 31, 32] provided important information that elucidated the structural basis of dynamic coupling associated with Ca^{2+} binding.

The crystal structures of NCX1-CBD12-AD [29], CALX1.1-CBD12, and CALX1.2-CBD12 [31, 32] have identified a relatively small contact area (~360 $Å^2$) between the CBDs, where the two-domain tandem adopts a wide-open (extended) conformation with an interdomain angle of ~117°. These structural similarities are especially interesting in light of striking differences in the NCX and CALX variants

regarding their responses to regulatory Ca^{2+}. Namely, Ca^{2+} interaction with Ca3-Ca4 sites of CBD1 activates NCX1-AD (and the other NCX variants), whereas in CALX variants the Ca^{2+} binding to Ca3-Ca4 sites either inhibits (CALX1.1) or has no effect (CALX1.2) [26, 37–39, 43]. Notably, isolated CBD1, CBD2, and CBD12 exhibit nearly an identical coordination chemistry with a few (but critical) exceptions [29, 31, 32]. Namely, E385 coordinates only Ca3 in isolated CBD1, whereas this residue coordinates Ca2, Ca3, and Ca4 in the CBD12 of NCX1-AD, CALX1.1, or CALX1.2. Most importantly, D499 forms bidentate coordination with Ca4 in CBD12, in contrast with the monodentate coordination in isolated CBD1, which is critical for Ca^{2+}-dependent tethering of CBDs.

More than twenty residues are buried in the two-domain interface of CBDs, which can be split up into three regions: hydrophilic, hydrophobic, and the FG-loop/α-helix array [29, 31, 32]. The hydrophilic region embraces a focal interdomain electrostatic network centered at R532 in CBD2, where R532 forms bifurcated hydrogen-bonded and non-hydrogen bonded salt-bridges with D499 and D500 in CBD1 and D565 in CBD2 (Fig. 3.3). The significance of this Ca^{2+}-dependent tethering is that D499 and D500 also participate in the coordination of the Ca3-Ca4 sites, while concomitantly stabilizing the CBD interface. This interfacial region is highly conserved among NCX and CALX variants. This highly sophisticated interdomain network of salt-bridges clearly acts as the principal linchpin that holds the two CBDs together, thereby representing a structural basis for Ca^{2+} occlusion. This Ca^{2+}-dependent interdomain tethering is a common module among NCX and CALX variants; it underlies dynamic coupling, although the dissociation rates of occluded Ca^{2+} are controlled by the exon assembly [23, 33–36, 49]. The physiological relevance of the exon-dependent kinetic regulation of occluded Ca^{2+} dissociation is that it actually controls NCX inactivation kinetics in diverse tissue-specific variants in order to dynamically control the Ca^{2+} extrusion rates in different cell types [4, 5, 13]. This feature is strikingly prominent when comparing the skeletal (AC) and neuronal (B and BC) NCX3 variants, which exhibit ~10-fold differences in the occluded Ca^{2+} off-rates at comparable K_d values for Ca^{2+} binding [33].

The hydrophobic interfacial region contains residues from the Ca^{2+}-binding EF loop of CBD1, the linker, and the FG loop of CBD2. F450 serves as a core residue, forming van der Waals interactions with H501, I628, A629, M631, and G632; this region may limit linker flexibility through the Ca^{2+}-dependent interaction of F450 with H501 [23, 29, 52]. The interfacial region, formed between the CD and EF loops of CBD1 and the FG-loop (where alternative splicing occurs) and the α-helix of CBD2 (next to the Ca3-Ca4 sites of CBD1), is engaged in a few incredible interactions, although the involved residues are quite inaccessible to the bulk phase (Fig. 3.3). In NCX1-CBD12-AD, most of the FG-loop of CBD2 is unstructured except for a short α-helix region (620–629) in the C-terminal portion of the FG-loop, where the side chains of this α-helix directly contribute to the CBD interface [23, 29]. In contrast, the FG-loop of CALX1-CBD2 forms two-headed short helices (H1 and H2) nearly perpendicular to the plane of β-sheets (Fig. 3.3) [31, 32]. Notably, the α-helix regions of NCX and CALX are very close to the interdomain linker and the Ca3-Ca4 sites of CBD1 (involved in the Ca^{2+}-dependent tethering of CBDs).

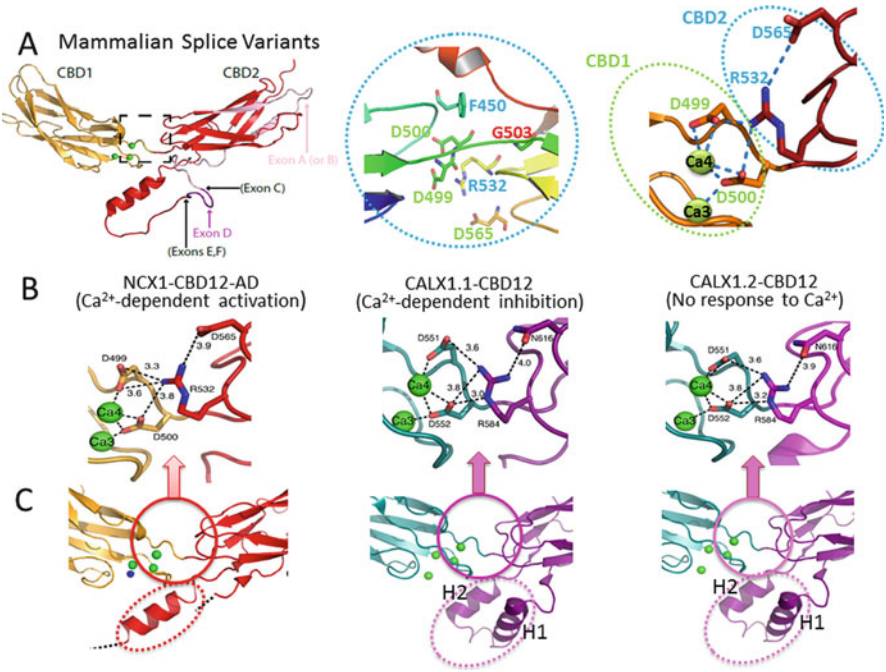

Fig. 3.3 Structure of the two-domain interface in NCX1-CBD12 and CALX1-CBD12. The hydrophilic region of the two-domain interface includes a pivotal interdomain electrostatic network centered at R532 in CBD2, where R532 forms bifurcated hydrogen-bonded and non-hydrogen bonded salt-bridges with D499, D500 in CBD1 and with D565 in CBD2. D499 and D500 also coordinate Ca^{2+} at the Ca3-Ca4 sites, thereby concurrently rigidifying the two-domain interface (the CBD1 and CBD2 residues are in green and blue, respectively). The Ca^{2+}-tethered salt-bridge structure at the two-domain interface is nearly identical in NCX1-CBD12-AD (3US9), CALX1.1-CBD12 (3RB5) and CALX1.2 (3RB7), involving specific interactions of the CBD1 Ca^{2+} binding loops with the interdomain linker, the CBD2 flexible FG loop and the strictly conserved CBD2 BC loop. The interdomain linker owns flexibility (controlled by G503) that adjusts the right track of Ca^{2+}-mediated tethering of CBDs, whereas the relay of CBDs (upon Ca^{2+} binding) stabilizes the stochastic oscillations of the linker to restrict CBD movements. F450 (in the hydrophobic core), prevents the propagation of Ca^{2+}-induced rigidification toward the N-terminal tip of CBD1. In contrast with NCX1-CBD12, the two splice variants of CALX contain a "two-headed" helix H1–H2 (nearby the FG-loop, next to the splicing segment)

In conjunction with HDX-MS analyses, one may posit that the α-helix region of NCX and CALX differentially control the strength and span of backbone rigidification from the C-terminal of CBD1 toward the C-terminal of CBD2, upon the Ca^{2+} binding to the Ca3-Ca4 sites [23, 29, 50, 51]. Recent HDX-MS and SAXS analyses of the CBD12 variants of NCX1, NCX2, NCX3, and CALX strongly support this possibility, suggesting that the Ca^{2+}-dependent propagation of backbone rigidification within the CBD2 domain (but not within the CBD1 domain) may account for regulatory differences among the NCX and CALX variants, exhibiting either positive, negative, or no response to Ca^{2+} [23, 50–52].

3.3.2 *Ca^{2+} Dependent Rigidification Underlies Dynamic Coupling of CBDs*

NMR, SAXS, and HDX-MS studies demonstrated that the Ca^{2+}-induced tethering of CBDs, associated with a slow dissociation of "occluded" Ca^{2+} from CBD12, constrains CBD movements [29, 33, 49, 53, 54]. Extended mutational analyses of isolated CBD12 mutants provided further evidence for a critical role of interfacial structural elements in a slow dissociation of occluded Ca^{2+} and in Ca^{2+}-epended tethering of CBDs [36, 49, 51, 52]. For example, mutation of R532 (in the BC loop of CBD2), which participates in an electrostatic interdomain network (by interacting with D499 and D500 at Ca3-Ca4 on CBD1) aborts the slow dissociation of occluded Ca^{2+}. Thus, in CBD12 (but not in isolated CBD1 or CBD2), R532 controls Ca^{2+} occlusion through an interdomain salt-bridge network, although R532 is not directly involved in Ca^{2+} coordination. Mutation of F540 also abolishes the slow dissociation of occluded Ca^{2+}, thereby revealing the functional importance of an interdomain hydrophobic core in regulatory coupling [52]. On the one hand, the interdomain linker possesses the needed flexibility (controlled by G503) to put on the right track the Ca^{2+}-mediated tethering of CBDs, whereas on the other hand, the relay of CBDs (upon Ca^{2+} binding) stabilizes the stochastic oscillations of the linker to restrict CBD movements [36, 53, 54]. Most probably, the dissociation of the first Ca^{2+} ion, accompanied by the interdomain salt-bridges, prevents the complete unfolding of Ca3-Ca4 sites in CBD1 by electrostatic compensation, thereby enabling occlusion of the remaining ion. Following dissociation of the second Ca^{2+} ion, CBD1 binding sites may undergo further unfolding. Since the CBD interface is highly conserved among NCX variants [29, 31, 32], the covalent linker and the interdomain salt-bridge are ascribed to a two-in-one module for dynamic coupling in NCX and CALX. The splice segment modulates the dynamics of the common interdomain module to modify the Ca^{2+}-dependent regulation of NCX and CALX variants.

3.4 Structure-Dynamic Basis for Ca^{2+} Evoked Decoding of Regulatory Massage

High-resolution X-ray structures of isolated CBD12 from CALX1.1 and CALX1.2 display small differences in the interdomain angle (~8°) between the CBDs, which were suggested as the structural basis for differential regulatory responses to regulatory Ca^{2+} [32]. According to this rationale, the interdomain angle in CBD12 might significantly differ in CALX1.1 (Ca^{2+} binding to Ca3-C4 sites has an inhibitory effect) and in NCX1-AD (Ca^{2+} binding to Ca3-C4 sites has an activating effect), since they exhibit diverse regulatory responses to Ca^{2+}. In disagreement with this proposal, however, the interdomain angle of Ca^{2+}-bound CBD12 is nearly identical for NCX1-CBD12-AD (117.4°) and CALX1.1-CBD12 (117.7°), meaning that the CBD alignment cannot account for regulatory diversity in NCX and CALX

orthologs [29, 32]. SAXS and HDX-MS analyses revealed that the Ca^{2+}-dependent tethering of CBDs rigidifies the CBD interface in all tested variants of NCX1 and CALX, although the strength, expansion, and remoteness of Ca^{2+}-dependent rigidification varies among variants [23, 29, 49–51].

SAXS analyses of isolated NCX1-CBD12 (AD, BD), NCX2-CBD12, and NCX3-CBD12 (B, BC) revealed that whereas the global structural parameters (e.g., the maximal intramolecular distance, the radius of gyration) are largely similar in the apo- and Ca^{2+}-bound forms, the Ca^{2+} binding narrows the conformational distributions [29, 36, 49–52]. Namely, Ca^{2+} binding to the Ca3-Ca4 sites results in a population shift of conformational states, where more constrained conformational states become more populated at a dynamic equilibrium [49]. SAXS analyses showed that Ca^{2+}-bound conformational distributions of CALX1.1-CBD12 and CALX1.2-CBD12 are nearly identical to those of NCX1-CBD12, NCX2-CBD12, and NCX3-CBD12 [23, 29, 36, 49–51]. Consistent with the population shift mechanism, NMR analysis of the NCX1 and CALX variants of CBD12 showed that Ca^{2+} binding to Ca3-Ca4 sites restricts the linkers' flexibility and CBDs motions [53, 54]. Thus, Ca^{2+} occlusion at the Ca3-Ca4 sites of the NCX and CALX variants rigidifies the backbone dynamics through the Ca^{2+}-dependent tethering of CBDs. The strength and extent of Ca^{2+}-dependent rigidification differ in an exon-dependent manner, as has been shown by HDX-MS [50–52]. NMR analyses of apo NCX1-CBD12-AD showed that Ca^{2+} binding restricts the linker's flexibility without altering the CBDs' alignment [54]. Similar NMR data obtained for CALX1.1-CBD12 [53], meaning that a "population shift" is the common mechanism for the NCX and CALX variants. The Ca^{2+}-dependent dynamic coupling may involve numerous conformational transitions with small energetic barriers in the absence of large conformational changes [10, 12, 23]. In all tested variants the Ca^{2+}-induced rigidification propagates from the Ca3-Ca4 sites of CBD1 to CBD2 through the two-domain interface, whereas F450 prevents the signal propagation from the Ca3-Ca4 sites to the N-terminal of CBD1 [49, 50, 52]. Thus, the Ca^{2+} binding to the Ca3-Ca4 sites of CBD1 rigidifies CBD2 (but not CBD1), where the Ca^{2+}-induced signal propagates from the C-terminal of CBD1 to the C-terminal tip of CBD2.

3.5 Exon-Specific Roles in Editing the Regulatory Massage

HDX-MS experiments demonstrated that strength and extent of Ca^{2+}-dependent rigidification strikingly differ in the NCX1-CBD12-AD, CALX1.1-CBD12, and CALX1.2-CBD12 variants which may account for regulatory differences in these variants [23, 50–52]. Namely, in the Ca^{2+}-activated variant (NCX1-CBD12-AD) the backbone rigidification spans from the Ca3-Ca4 sites of CBD1, through the α-helix of CBD2 up to the C-terminal tip of CBD2 over a distance of 30–50 Å, whereas the Ca^{2+}-dependent rigidification stops at the CBD2 α-helix in the Ca^{2+}-inhibited variant (CALX1.1-CBD12) [51]. An intermediate picture is observed for

CALX1.2-CBD12 (exhibiting no response to regulatory Ca^{2+}). Significant differences in the backbone dynamics observed even between the CALX1.1-CBD12 and CALX1.2-CBD12 variants [51], meaning that five additional residues in the splicing segment affect the strength and expansion of Ca^{2+}-dependent rigidification within CBD2).

In general, it is widely accepted that splicing segments contain intrinsically disordered regions [10–12, 55, 56]. Despite their inability to achieve a "discrete" and stable tertiary structure, intrinsically disordered regions adopt a defined conformation upon ligand binding, thereby allowing "dynamic coupling" to occur [10, 12]. Consistent with this, the Ca^{2+} binding to CBDs results in a population shift of preexisting conformational states without undergoing large conformational changes [23, 29, 49, 51, 52]. Systematic analyses of NCX1-CBD12 and NCX3-CBD12 splice variants with stopped-flow, equilibrium binding, along with HDX-MS techniques strongly support the notion that the mutually exclusive exons, A and B, have opposite and reciprocal effects on CBD stability [49, 50, 52]. For example, in NCX1 exon B increases the Ca^{2+} affinity at the Ca3-Ca4 sites of CBD1 with a slower dissociation of occluded Ca^{2+} and prevents Ca^{2+} binding to CBD2 [34–36]. Consistent with this, exon B effectively stabilizes the Ca^{2+}-sites of CBD1, while destabilizing the Ca^{2+} sites of CBD2, as revealed by HDX-MS [51, 52]. Exon A of NCX1 effectively stabilizes the Ca^{2+} sites of CBD2, whereas it destabilizes the Ca^{2+} sites of CBD1 [52]. Notably, the roles of the A and B exons are somewhat different in NCX3 and NCX1 [50–52]. Namely, in NCX3, exon A destabilizes the Ca^{2+} binding sites of CBD2 (no Ca^{2+} binding to CBD2) and stabilizes the Ca^{2+} binding sites of CBD1, whereas exon B enhances the Ca^{2+} binding capacity and affinity at CBD2 (three Ca^{2+} ions bind to CBD2 since K585 is replaced by glutamate) and destabilizes the Ca^{2+} binding at CBD1 [8, 14]. HDX-MS analyses of NCX3-CBD12-AC, NCX3-CBD12-B, and NCX2-CBD12-BC revealed that exons A and B play different roles in stabilizing the CBD1 and CBD2 sites in NCX3 and NCX1 [50].

In contrast with mutually exclusive exons, the cassette exons (C, D, E, F) do not affect the dynamic features of apo CBD1, rather than rigidifying the flexibility of the interdomain linker and of CBD2 upon Ca^{2+} binding [23, 29, 50, 51]. For example, the FG-loop/α-helix region of CBD2 is similarly stabilized in both NCX1-CBD12-BD and NCX1-CBD12-ACDEF, as compared with NCX1-CBD12-AD [51, 52]. Thus, both mutually exclusive and cassette exons control the strength and extent of Ca^{2+}-dependent rigidification within CBD2. Thus, the combined actions of mutually exclusive and cassette exons ensure a fine tuning of Ca^{2+}-dependent activation (controlled by CBD1) and Ca^{2+}-dependent alleviation of Na^{+}-induced inactivation (controlled by CBD2). Notably, the gradual addition of cassette exons to the splicing segment (e.g., in NCX1-CBD12-ACDEF) increasingly stabilizes the Ca^{2+}-bound CBD12 [34, 51, 52]. This is quite intriguing, since the existence of intrinsically disordered segments contradicts with the high entropic cost that the system must acquire upon ligand binding. One possibility is that unfolded linear structures at the splicing segment minimize the entropic cost of ligand binding through enthalpy compensation [10, 12, 55, 56]. Thus, the lengthening of a splicing segment by adding cassette exons may govern the enthalpy-compensated entropy cost that

enables the fine-tuning of regulation. We posit that the exon-controlled balancing between the translational and rotational movements of CBDs distinctively shape the propagation of allosteric massage from the C-terminal of CBD1 (Ca3-Ca4 sites) through the linker toward the C-terminal of CBD2. It remains to be discovered how the allosteric signal propagates from the C-terminal tip of CBD2 to membrane-embedded ion-transport domains (presumably to TM6) [13, 23].

3.6 Conclusions

Multidisciplinary studies reported synergistic interactions between the CBDs that shape the dynamic range and the kinetic features of Ca^{2+}-dependent regulation in NCX variants, thereby providing insights into the mechanisms underlying CBD interactions in isolated CBD12 and full-size NCX1. According to these studies, the isolated preparations of CBD12 largely represent the Ca^{2+} sensitivity and kinetics of Ca^{2+}-dependent regulation in their matching of full-size NCX variants. Thus, isolated CBD12 serves as an ideal model for investigating the structure-dynamic mechanisms underlying the allosteric regulation specificities in NCX variants. The interactions between CBD1 and CBD2 in the context of CBD12 results in increased affinity for Ca^{2+} at CBD1 and slow dissociation of an "occluded" Ca^{2+} ion from CBD1. Alternative splicing at CBD2 not only affects the Ca^{2+} binding affinity and capacity at CBD2—it also affects the Ca^{2+} interactions with CBD1, establishing up to 50-fold differences both in the Ca^{2+} binding affinity and the Ca^{2+} off-rates of occluded Ca^{2+} in NCX1. NCX2 and NCX3 also exhibit synergistic interactions between the CBDs, similarly to NCX1. NCX3 variants exhibit similar Ca^{2+} affinity at CBD1, but the dissociation rate of occluded Ca^{2+} is ~10-fold slower in skeletal muscle than in the brain variants. These differences in Ca^{2+} affinity and off-rates at the Ca3-Ca4 sites may have physiological relevance for diversifying regulatory responses in full-size NCX variants expressed in a tissue-specific manner.

X-ray crystallography and stopped-flow studies revealed that Ca^{2+} binding to CBD1 results in Ca^{2+} occlusion and tethering of CBD1 and CBD2 through the formation of a hydrogen-bonded salt-bridge network at the two-domain interface, which yields a more stable (rigidified) structure upon Ca^{2+} binding. The crystallographic structures of the CBD12 variants of NCX and CALX, exhibiting positive, negative, and no response to regulatory Ca^{2+}, display nearly identical interdomain angles between CBD1 and CBD2, meaning the two-domain alignment does not shape the regulatory specificity. In agreement with this, SAXS studies revealed that Ca^{2+} binding and occlusion at the interface of NCX1-CBD12 splice variants induces a shift towards narrowly distributed, elongated conformations, as predicted by the population shift mechanism. Thus, the Ca^{2+}-dependent tethering and occlusion of Ca^{2+} at the two-domain interface restricts interdomain CBD movements through a population shift, which is a common mechanism for variants exhibiting positive, negative, and no response to regulatory Ca^{2+}. Finally, HDX-MS analyses of NCX1, NCX2, and NCX3 variants of CBD12 have shown that Ca^{2+} binding mainly

rigidifies the backbone dynamics of the interdomain linker and CBD2 (and not CBD1), whereas the alternative splicing of CBD2 secondarily modifies the location, strength, and expansion of rigidification throughout CBD2. Importantly, the Ca^{2+}-induced effects on CBD2 backbone dynamics correlate well with the regulatory specificity found in the matching splice variants of full-size NCX variants. Thus, NCX variants share a common mechanism for the initial decoding of the regulatory signal upon Ca^{2+} occlusion and tethering of CBDs (i.e., through the population shift mechanism), whereas alternative splicing of CBD2 controls the propagation and strength of Ca^{2+}-dependent rigidification and thereby, diversifies the regulatory response. The mutually exclusive exons, A and B, diversely stabilize/destabilize the Ca^{2+}-bound states of CBDs in NCX1 and NCX3, whereas the cassette exons (C, D, E, and F) stabilize the interdomain linker upon Ca^{2+} binding. Jointly merged modes of mutually exclusive and cassette exons can properly balance between the two regulatory pathways—the Ca^{2+}-dependent activation (controlled by CBD1) and the Ca^{2+}-dependent alleviation of Na^{+}-induced inactivation (controlled by CBD2) in a given variant [9, 51].

Acknowledgments This work was supported by the Israel Science Foundation Grant #825/14 to DK. The financial support of the Fields Estate foundation to DK is highly appreciated.

References

1. Carafoli E, Krebs J (2016) Why calcium? How calcium became the best communicator. J Biol Chem 291:20849–20857
2. Krebs J (2009) The influence of calcium signaling on the regulation of alternative splicing. Biochim Biophys Acta 1793:979–984
3. McCue HV, Haynes LP, Burgoyne RD (2010) The diversity of calcium sensor proteins in the regulation of neuronal function. Cold Spring Harb Perspect Biol 2(8):a004085
4. Khananshvili D (2013) The SLC8 gene family of sodium-calcium exchangers (NCX) – structure, function, and regulation in health and disease. Mol Asp Med 34:220–235
5. Khananshvili D (2014) Sodium-calcium exchangers (NCX): molecular hallmarks underlying the tissue-specific and systemic functions. Pflugers Arch 466:43–60
6. Brini M, Calì T, Ottolini D, Carafoli E (2014) The plasma membrane calcium pump in health and disease. FEBS J 280:5385–5397
7. Gifford JL, Walsh MP, Vogel HJ (2007) Structures and metal-ion-binding properties of the Ca^{2+}-binding helix-loop-helix EF-hand motifs. Biochem J 405:199–221
8. Plattner H, Verkhratsky A (2016) Inseparable tandem: evolution chooses ATP and Ca^{2+} to control life, death and cellular signalling. Philos Trans R Soc Lond Ser B Biol Sci 371:1700
9. Williams RJP (1999) Calcium: the developing role of its chemistry in biological evolution. In: Carafoli E, Klee C (eds) Calcium as a cellular regulator. Oxford University Press, New York, pp 3–27
10. Nussinov R, Tsai CJ (2013) Allostery in disease and in drug discovery. Cell 153:293–305
11. Rader AJ, Brown SM (2011) Correlating allostery with rigidity. Mol BioSyst 7:464–471
12. Tsai CJ, Nussinov R (2014) A unified view of "how allostery works". PLoS Comput Biol 10: e1003394

13. Khananshvili D (2016) Regulation of Ca^{2+}-ATPases, V-ATPases and F-ATPases. In: Chakraborti S, Dhalla NS (eds) Advances in biochemistry in health and disease, vol 14. Springer, Cham, pp 93–116
14. Philipson KD, Nicoll DA (2000) Sodium-calcium exchange: a molecular perspective. Annu Rev Physiol 62:111–133
15. Ren X, Philipson KD (2013) The topology of the cardiac Na^+/Ca^{2+} exchanger, NCX1. J Mol Cell Cardiol 57:68–71
16. Lytton J (2007) Na^+/Ca^{2+} exchangers: three mammalian gene families control Ca^{2+} transport. Biochem J 406:365–382
17. Nicoll DA, Longoni S, Philipson KD (1990) Molecular cloning and functional expression of the cardiac sarcolemmal Na^+-Ca^{2+} exchanger. Science 250:562–565
18. Quednau BD, Nicoll DA, Philipson KD (1997) Tissue specificity and alternative splicing of the Na^+/Ca^{2+} exchanger isoforms NCX1, NCX2, and NCX3 in rat. Am J Phys 272:C1250–C1261
19. Liao J, Li H, Zeng W, Sauer DB, Belmares R, Jiang Y (2012) Structural insight into the ion-exchange mechanism of the sodium/calcium exchanger. Science 335:686–690
20. Liao J, Marinelli F, Lee C, Huang Y, Faraldo-Gómez JD, Jiang Y (2016) Mechanism of extracellular ion exchange and binding-site occlusion in a sodium/calcium exchanger. Nat Struct Mol Biol 23:590–599
21. Almagor L, Giladi M, van Dijk L, Buki T, Hiller R, Khananshvili D (2014) Functional asymmetry of bidirectional Ca^{2+}-movements in an archaeal sodium-calcium exchanger (NCX_Mj). Cell Calcium 56:276–284
22. Giladi M, Almagor L, van Dijk L, Hiller R, Man P, Forest E, Khananshvili D (2016) Asymmetric preorganization of inverted pair residues in the sodium–calcium exchanger. Sci Rep 6:20753
23. Giladi M, Tal I, Khananshvili D (2016) Structural features of ion transport and allosteric regulation in sodium-calcium exchanger (NCX) proteins. Front Physiol 7(30):1–13
24. Marinelli F, Almagor L, Hiller R, Giladi M, Khananshvili D, Faraldo-Gomez JD (2014) Sodium recognition by the Na+/Ca2+ exchanger in the outward-facing conformation. Proc Natl Acad Sci USA 111:E5354–E5362
25. Hilge M, Aelen J, Foarce A, Perrakis A, Vuister GW (2009) $Ca2^+$ regulation in the Na^+/Ca^{2+} exchanger features a dual electrostatic switch mechanism. Proc Natl Acad Sci USA 106:14333–14338
26. Hilge M, Aelen J, Vuister GW (2006) Ca^{2+} regulation in the Na^+/Ca^{2+} exchanger involves two markedly different Ca^{2+} sensors. Mol Cell 22:15–25
27. Palty R, Silverman WF, Hershfinkel M, Caporale T, Sensi SL, Parnis J, Nolte C, Fishman D, Shoshan-Barmatz V, Herrmann S, Khananshvili D, Sekler I (2010) NCLX is an essential component of mitochondrial Na^+/Ca^{2+} exchange. Proc Natl Acad Sci USA 107:436–441
28. Besserer GM, Ottolia M, Nicoll DA, Chaptal V, Cascio D, Philipson KD, Abramson J (2007) The second Ca^{2+}-binding domain of the Na^+ Ca^{2+} exchanger is essential for regulation: crystal structures and mutational analysis. Proc Natl Acad Sci USA 104:18467–18472
29. Giladi M, Sasson Y, Fang X, Hiller R, Buki T, Wang YX, Hirsch JA, Khananshvili D (2012c) A common Ca^{2+}-driven interdomain module governs eukaryotic NCX regulation. PLoS One 7: e39985
30. Nicoll DA, Sawaya MR, Kwon S, Cascio D, Philipson KD, Abramson J (2006) The crystal structure of the primary Ca^{2+} sensor of the Na^+/Ca^{2+} exchanger reveals a novel Ca^{2+} binding motif. J Biol Chem 281:21577–21581
31. Wu M, Le HD, Wang M, Yurkov V, Omelchenko A, Hnatowich M, Nix J, Hryshko LV, Zheng L (2010) Crystal structures of progressive Ca^{2+} binding states of the Ca^{2+} sensor Ca^{2+} binding domain 1 (CBD1) from the CALX Na^+/Ca^{2+} exchanger reveal incremental conformational transitions. J Biol Chem 285:2554–2561
32. Wu M, Tong S, Gonzalez J, Jayaraman V, Spudich JL, Zheng L (2011) Structural basis of the Ca^{2+} inhibitory mechanism of Drosophila Na^+/Ca^{2+} exchanger CALX and its modification by alternative splicing. Structure 19:1509–1517

33. Tal I, Kozlovsky T, Brisker D, Giladi M, Khananshvili D (2016) Kinetic and equilibrium properties of regulatory Ca^{2+}-binding domains in sodium-calcium exchangers 2 and 3. Cell Calcium 59:181–188
34. Giladi M, Bohbot H, Buki T, Schulze DH, Hiller R, Khananshvili D (2012) Dynamic features of allosteric Ca^{2+} sensor in tissue-specific NCX variants. Cell Calcium 51:478–485
35. Giladi M, Boyman L, Mikhasenko H, Hiller R, Khananshvili D (2010) Essential role of the CBD1-CBD2 linker in slow dissociation of Ca^{2+} from the regulatory two-domain tandem of NCX1. J Biol Chem 285:28117–28125
36. Giladi M, Friedberg I, Fang X, Hiller R, Wang YX, Khananshvili D (2012) G503 is obligatory for coupling of regulatory domains in NCX proteins. Biochemistry 51:7313–7320
37. Dyck C, Maxwell K, Buchko J, Trac M, Omelchenko A, Hnatowich M, Hryshko LV (1998) Structure-function analysis of CALX1.1, a Na^+-Ca^{2+} exchanger from Drosophila. Mutagenesis of ionic regulatory sites. J Biol Chem 273:12981–12987
38. Dyck C, Omelchenko A, Elias CL, Quednau BD, Philipson KD, Hnatowich M, Hryshko LV (1999) Ionic regulatory properties of brain and kidney splice variants of the NCX1 Na^+-Ca^{2+} exchanger. J Gen Physiol 114:701–711
39. Hilgemann DW, Matsuoka S, Nagel GA, Collins A (1992) Steady-state and dynamic properties of cardiac sodium-calcium exchange. Sodium-dependent inactivation. J Gen Physiol 100:905–932
40. Boyman L, Mikhasenko H, Hiller R, Khananshvili D (2009) Kinetic and equilibrium properties of regulatory calcium sensors of NCX1 protein. J Biol Chem 284:6185–6193
41. Boyman L, Hagen BM, Giladi M, Hiller R, Lederer WJ, Khananshvili D (2011) Proton-sensing Ca^{2+} binding domains regulate the cardiac Na^+/Ca^{2+} exchanger. J Biol Chem 286:28811–28820
42. Hryshko LV, Matsuoka S, Nicoll DA, Weiss JN, Schwarz EM, Benzer S, Philipson KD (1996) Anomalous regulation of the Drosophila Na^+-Ca^{2+} exchanger by Ca^{2+}. J Gen Physiol 108:67–74
43. Matsuoka S, Nicoll DA, Hryshko LV, Levitsky DO, Weiss JN, Philipson KD (1995) Regulation of the cardiac Na^+-Ca^{2+} exchanger by Ca^{2+}. Mutational analysis of the Ca^{2+} binding domain. J Gen Physiol 105:403–420
44. Ottolia M, Nicoll DA, Philipson KD (2009) Roles of two Ca^{2+}-binding domains in regulation of the cardiac Na^+-Ca^{2+} exchanger. J Biol Chem 284:32735–32741
45. Breukels V, Konijnenberg A, Nabuurs SM, Touw WG, Vuister GW (2011) The second Ca^{2+}-binding domain of NCX1 binds Mg^{2+} with high affinity. Biochemistry 50:8804–8812
46. DiPolo R, Beauge L (2006) Sodium/calcium exchanger: influence of metabolic regulation on ion carrier interactions. Physiol Rev 86:155–203
47. Omelchenko A, Dyck C, Hnatowich M, Buchko J, Nicoll DA, Philipson KD, Hryshko LV (1998) Functional differences in ionic regulation between alternatively spliced isoforms of the Na^+-Ca^{2+} exchanger from Drosophila melanogaster. J Gen Physiol 111:691–702
48. John SA, Ribalet B, Weiss JN, Philipson KD, Ottolia M (2011) Ca^{2+}-dependent structural rearrangements within Na^+-Ca^{2+} exchanger dimers. Proc Natl Acad Sci USA 108:1699–1704
49. Giladi M, Hiller R, Hirsch JA, Khananshvili D (2013) Population shift underlies Ca^{2+}-induced regulatory transitions in the sodium-calcium exchanger (NCX). J Biol Chem 288:23141–23149
50. Giladi M, Lee SY, Ariely Y, Teldan Y, Granit R, Strulevich R, Haitin Y, Chung KY, Khananshvili D (2017) Structure-based dynamic arrays in regulatory domains of sodium-calcium exchanger (NCX) isoforms. Sci Rep 7(1):993
51. Giladi M, Lee SY, Hiller R, Chung KY, Khananshvili D (2015) Structure-dynamic determinants governing a mode of regulatory response and propagation of allosteric signal in splice variants of Na^+/Ca^{2+} exchange (NCX) proteins. Biochem J 465:489–501
52. Lee SY, Giladi M, Bohbot H, Hiller R, Chung KY, Khananshvili D (2016) Structure-dynamic basis of splicing dependent regulation in tissue-specific variants of the sodium-calcium exchanger (NCX1). FASEB J 30:1356–1366

53. Abiko LA, Vitale PM, Favaro DC, Hauk P, Li DW, Yuan J, Bruschweiler-Li L, Salinas RK, Brüschweiler R (2016) Model for the allosteric regulation of the Na^+/Ca^{2+} exchanger (NCX). Proteins 84:580–590
54. Salinas RK, Bruschweiler-Li L, Johnson E, Bruschweiler R (2011) Ca^{2+} binding alters the interdomain flexibility between the two cytoplasmic calcium-binding domains in the Na^+/Ca^{2+} exchanger. J Biol Chem 286:32123–32131
55. Buljan M, Chalancon G, Dunker AK, Bateman A, Balaji S, Fuxreiter M, Babu MM (2013) Alternative splicing of intrinsically disordered regions and rewiring of protein interactions. Curr Opin Struct Biol 23:443–450
56. Latysheva NS, Flock T, Weatheritt RJ, Chavali S, Babu MM (2015) How do disordered regions achieve comparable functions to structured domains? Protein Sci 24:909–922

Part II
Endoplasmic/Sarcoplasmic Reticulum

Chapter 4
The Endoplasmic Reticulum and the Cellular Reticular Network

Luis B. Agellon and Marek Michalak

Abstract The endoplasmic reticulum and the other organelles of the eukaryotic cell are membrane-bound structures that carry out specialized functions. In this chapter, we discuss strategies that the cell has adopted to link and coordinate the different activities occurring within its various organelles as the cell carries out its physiological role.

Keywords Calcium signaling · Cell stress · Cellular reticular network · Homeostasis · Membrane contact sites

Abbreviations

ATF6	activating transcription factor 6
BiP	immunoglobulin binding protein
ER	endoplasmic reticulum
ERAD	ER-associated degradation
ERMAS	ER-mitochondria encounter structure
GRP	glucose regulated protein
HSP	heat shock protein
$InsP_3$	inositol-1,4,5-trisphosphate
IRE	serine/threonine-protein kinase/endoribonuclease inositol-requiring enzyme
ORAI	Ca^{2+} release-activated Ca^{2+} channel
PERK	dsRNA-activated protein kinase-like ER kinase
PDI	protein disulfide isomerase

L. B. Agellon (✉)
School of Human Nutrition, McGill University, Ste. Anne de Bellevue, Quebec, Canada
e-mail: luis.agellon@mcgill.ca

M. Michalak (✉)
Department of Biochemistry, University of Alberta, Edmonton, Alberta, Canada
e-mail: marek.michalak@ualberta.ca

J. Krebs (ed.), *Membrane Dynamics and Calcium Signaling*, Advances in Experimental Medicine and Biology 981,
https://doi.org/10.1007/978-3-319-55858-5_4

RER	rough ER
SARAF	SOCE-associated regulatory factor
SCAP	SREBP cleavage activating protein
SER	smooth ER
SERCA	sarcoplasmic/endoplasmic reticulum Ca^{2+}-ATPase
SOCE	store-operated Ca^{2+} entry
SR	sarcoplasmic reticulum
SREBP	sterol-response element-binding protein
STIM	stromal-interacting molecule
RyR	ryanodine receptor
UPR	unfolded protein response
Xbp1	X-box binding protein 1

4.1 Introduction

A defining feature of eukaryotic cells is the compartmentalization of various cellular functions specialized within organelles. These organelles are separated from each other by membranes and provide distinct protected environments where the cell can carry out various specialized functions at greater efficiencies by populating these structures with a unique set of proteins and lipids that can partition the required set of metabolites. On the other hand, segregation of functions poses a problem regarding substrate and metabolite exchange among membrane-bound compartments as well as intracellular communication that is essential for coordination of cellular metabolic activities. Recent developments have provided insights into the strategies employed by the cell to overcome the problem.

4.2 The ER

The ER is an extensive system of membranes arranged as a "net-like" network that in many cases occupies most of the interior of the cell (Fig. 4.1). This organelle houses a variety of critical ATP-requiring functions, such as maintenance of cellular homeostasis, synthesis of membrane-associated, luminal and secreted proteins, correct folding of proteins and glycoproteins, post-translational modification of proteins, lipid and steroid synthesis, Ca^{2+} storage and signaling, to name a few [1–3]. In some cellular systems, the ER provides specialized functions such as support of excitation-contraction in muscle (sarcoplasmic reticulum, SR), detoxification as well as lipid synthesis (smooth ER, SER) such as in hepatic and intestinal cells, support of protein secretory functions such as in pancreatic and liver cells (rough ER, RER), and activation of cells of the immune and nervous systems (Ca^{2+} signaling).

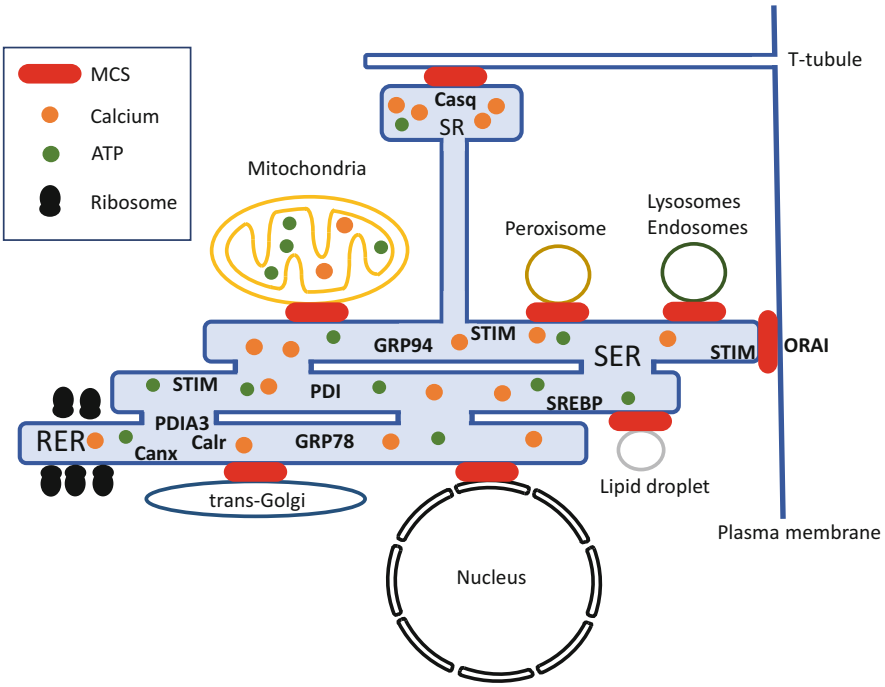

Fig. 4.1 Cellular reticular network and interorganellar membrane contacts sites. The figure depicts the joining of ER membranes to cellular organelles to form the cellular reticular network from the plasma membrane to the nuclear envelope. The membrane contact sites enable rapid distribution and exchange of substrates, metabolites and signalling molecules to support proteostasis and lipidostasis. *Calr* calreticulin, *Casq* calsequestrin, *Canx* calnexin, *PDI* protein disulfide isomerase, *RER* rough endoplasmic reticulum, *SER* smooth endoplasmic reticulum

To perform these diverse functions, the ER engages a wide assortment of multifunctional integral membrane and luminal chaperones, folding enzymes and sensor molecules [4]. Chaperones are specialized proteins that assist in folding of polypeptides and in the assembly of multi-subunit proteins while folding enzymes accelerate folding process by supporting posttranslational modifications of newly synthesized proteins [5, 6]. Folding sensors play a key role in recognition of the properly folded or malfolded proteins [7]. These proteins are not only involved in ensuring the fidelity of protein folding, posttranslational modifications of newly synthesized proteins, but also contribute to storage of Ca^{2+} ions, facilitation of Ca^{2+} signaling, lipid and steroid synthesis and modification, and many other cellular roles beyond those occurring within the ER lumen [1, 8–11]. The ER also contains membrane-associated proteins that support cellular lipid and steroid synthesis [8, 9]. Importantly, ER resident chaperones and folding enzymes are major luminal ER Ca^{2+} binding proteins, and together with the inositol-1,4,5-trisphosphate ($InsP_3$) receptor/Ca^{2+} release channel, the ER Ca^{2+}-ATPase (SERCA) pump and

ER-associated Ca^{2+} sensors stromal interacting molecule (STIM) proteins, are vital for Ca^{2+}-based intracellular communication [2, 12, 13]. The ER membrane also contains an assortment of integral membrane kinases, which together with the ER-resident chaperones and folding enzymes, regulate ER stress responses allowing cellular adaptation to many challenges originating from environmental, metabolic and intrinsic demands [14, 15]. Some organelles, such as mitochondria and nucleus, are also equipped with additional specialized stress coping mechanisms [16–20]. These mechanisms work in concert with ER stress coping strategies to preserve or regain cellular homeostasis and prevent cellular dysfunction.

4.3 ER and Ca^{2+} Homeostasis

The ER is the main site of intracellular Ca^{2+} storage and physiological source of Ca^{2+} for intracellular signaling [2]. Disruption of Ca^{2+} homeostasis within the ER as well as release of Ca^{2+} from ER stores activate transcriptional and translational cascades that produce components involved in key pathways, such as the unfolded protein response (UPR), protein folding, ER-associated degradation (ERAD), expansion of the membrane systems as well as apoptosis [2, 12, 13]. Many of the ER proteins involved in Ca^{2+} binding and signaling also participate in nearly all critical ER functions [4, 21–25]. These proteins collectively make up the luminal ER Ca^{2+} stores, maintaining the total Ca^{2+} concentration in the ER within the μM to mM range, which is critical for the preservation of the integrity and survival of the cell. Among these ER resident Ca^{2+} binding proteins, calreticulin represents the major protein responsible for sequestering approximately 50% of luminal ER Ca^{2+} [26]. Other ER chaperones, GRP94 and GRP78 (also known as immunoglobulin binding protein or BiP) have relatively low capacity for binding Ca^{2+} and contribute approximately 30% of the total luminal ER Ca^{2+} store by virtue of their abundance [27–29]. The remaining balance of the luminal ER Ca^{2+} store is bound to proteins such as ER resident oxidoreductases, a PDI-like family of proteins [30–32]. In some cell types, such as muscle cells, calsequestrin is the major Ca^{2+} binding protein in the lumen of SR [33, 34].

4.4 ER-Plasma Membrane Connection: Store-Operated Calcium Entry

After the release of Ca^{2+} from the ER stores, the cell engages a recovery system to restore cellular Ca^{2+} levels to the initial state and replenish luminal ER Ca^{2+} stores *via* the action of the SERCA pump. Depletion of luminal ER Ca^{2+} stores leads to activation of store-operated Ca^{2+} entry (SOCE) mechanism [13, 35–37], a concept

initially proposed by Putney [38]. SOCE is an excellent example of coordination of Ca^{2+} signaling between the ER lumen, the plasma membrane and the extracellular environment. This process involves the ER-resident Ca^{2+} sensors STIM proteins and plasma membrane Ca^{2+} channels known as Calcium Release-Activated Calcium Modulator (ORAI). STIM senses reductions in luminal ER Ca^{2+} stores, resulting in oligomerization of STIM and complex formation with ORAI [37, 39, 40] bringing plasma membrane Ca^{2+} channels close to ER membrane embedded Ca^{2+} pumps. This ORAI-STIM interaction effectively causes the influx of Ca^{2+} from the extracellular milieu, increasing cytoplasmic Ca^{2+} levels and subsequently refilling of the luminal ER Ca^{2+} stores.

In vertebrates, there are two isoforms of STIM proteins, STIM1 and STIM2 [13]. STIM1 is activated by receptor-mediated ER Ca^{2+} release whereas STIM2 is involved in maintaining resting ER Ca^{2+} concentration [41]. Both isoforms are ubiquitously expressed and share common structural features. STIM1 and STIM2 contain a single transmembrane domain and two EF-hands, a helix-loop-helix structural motif characteristic of Ca^{2+}-binding proteins [42], which are important for the Ca^{2+} sensing activity. In addition to the N-terminal EF-hands, STIM proteins contain the sterile α motif (SAM) domain and three coiled-coil domains (CC1-3) at their C-terminal end, which are exposed to the cytoplasm and important for interaction with ORAI [13]. ORAIs are plasma membrane proteins with four transmembrane domains, which function as a Ca^{2+} channel. The crystal structure of ORAI from *Drosophila melanogaster* revealed that the Ca^{2+} channel is comprised of a hexameric assembly of ORAI subunits arranged around a central ion pore [43]. In mammalian cells, there are three isoforms of ORAI proteins, namely ORAI1, ORAI2 and ORA3. All the ORAI isoforms support functional SOCE [44]. ORAI1 and ORAI3 form multimeric Ca^{2+} channels that are also regulated in a Ca^{2+} store-independent way by lipid messengers arachidonic acid and leukotriene C4 [45–47]. No interaction between STIM and ORAI is apparent at resting ER Ca^{2+} levels, but upon depletion of the luminal ER Ca^{2+}, STIM molecules oligomerize due to conformation changes at the CC1 domain. The STIM multimers then recruit and gate the ORAI channels at ER and plasma membranes junctions. The ER also contains a negative regulator of SOCE, known as SOCE-associated regulatory factor (SARAF), that associates with STIM to facilitate slow Ca^{2+}-dependent inactivation thus protecting cells from Ca^{2+} overfilling. STIM-ORAI signaling requires additional associated proteins including CRACR2A, STIMATE, junctate, POST, and septins [13]. Luminal ER oxidoreductase PDIA3 can also control STIM function, and consequently STIM1-induced SOCE, by binding to two conserved cysteines in the luminal domain of STIM1 [48]. Additionally, PDIA3 can regulate SERCA2b, a non-muscle isoform of SERCA, enabling further dynamic control of ER Ca^{2+} homeostasis [49]. The actions of PDIA3 illustrate how multiple ER activities, such as protein folding and posttranslational modification, are linked with Ca^{2+} transport and maintenance of ER Ca^{2+} homeostasis.

4.5 ER and Protein Quality Control

Considering that over 30% of proteins are synthesized and processed in the ER, it is not surprising that the ER has evolved a sophisticated protein quality control system to preserve proteostasis [1, 3, 10, 11, 50, 51]. Proteostasis (protein homeostasis) refers to optimal folding and function of proteome [51]. Proteostasis is accomplished by an elaborate mechanism that integrates key cellular processes, namely biosynthethic and degradative pathways as well as control of gene transcription. Disrupted proteostasis is detrimental for the survival of the cell and health of the organism. The cell has a wide repertoire of molecular chaperones, which include cytoplasmic heat shock proteins (HSPs) [52], a subset of glucose regulatory proteins (GRP78/BiP and GRP94), the lectin chaperones calreticulin, calnexin, and ER degradation-enhancing α-mannosidase-like protein [53, 54]. These chaperones are specialized with respect to their substrates. For example, calreticulin, calnexin and PDIA3 are the proteins that make up the core machinery responsible for ensuring quality control of newly synthesized glycoproteins [1, 3, 10, 11, 51]. The ER-associated oxidoreductases [protein disulphide isomerases (PDIs) and peptidyl prolyl isomerases (PPIs)], oligosaccharide transferases, glucosidases and mannosidases are responsible for protein modifications such as disulfide bond formation and N-linked glycosylation [1, 50, 55–57]. Depletion of luminal ER Ca^{2+} inhibits chaperone function causing a global ER stress and disrupted proteostasis [22, 58, 59].

4.6 ER and Cellular Stress Coping Response Strategies

Loss of nutrients/energy homeostasis is a universal feature defining the induction of ER stress and impacts on all aspects of cellular function. Ca^{2+} signaling may be the principal mechanism involved in recognizing, communicating the state of cellular reticular homeostasis, and coordinating the activities to multiple corrective strategies. Mitochondria and the nucleus also developed stress responses to prevent cellular dysfunction due to stress challenges, environmental and metabolic demands [16–20, 60]. Activation of the UPR leads to translational attenuation to prevent synthesis of new proteins in the ER, transcriptional induction of genes encoding chaperones, folding enzymes and other proteins involved in ERAD, controlled degradation of misfolded proteins, and activation of apoptosis if the cell is unable to re-establish ER homeostasis [14]. The UPR coping strategy in the ER is thought to be comprised of three separate pathways, each controlled by distinct ER-associated integral membrane sensor proteins: the ER kinase dsRNA-activated protein kinase-like ER kinase (PERK), activating transcription factor 6 (ATF6), and inositol-requiring enzyme 1 (IRE1) embedded in the ER membrane and complexed with GRP78/BiP in the lumen of the ER [14]. Additionally, a controlled self-digestion and degradation process known as autophagy, is stimulated to help promote cell

survival by eliminating damaged cellular components [8, 61, 62]. Autophagy may also provide the cell with a short-term source of raw materials (such as amino acids and fatty acids) and energy substrates [63].

Luminal ER Ca^{2+} binding proteins, such as GRP78/BiP, and the Ca^{2+}-dependent microRNA miR-322 have been identified as bonafide regulators of UPR [64, 65]. Calreticulin, a major ER Ca^{2+} binding protein, associates with ATF6 in a carbohydrate-dependent manner, and together with GRP78/BiP (also an ER Ca^{2+} binding protein), maintains ATF6 in its transcriptionally inactive membrane-bound precursor state [66]. PDIA5, under stress conditions, promotes ATF6α export from the ER and activation of its target genes [67]. PDIA6 is a regulator of IRE1 activity in response to depletion of luminal ER Ca^{2+} stores [64, 68]. The binding of PDIA6 with the luminal domain of IRE1α in a cysteine-dependent manner has been shown to enhance IRE1α activity [64, 68]. This effect is specific for the IRE1α branch since PDIA6 has no influence on the activity of the PERK branch of the UPR pathway [64, 68]. Depletion of luminal ER Ca^{2+} and activation of SOCE reduces the abundance of the microRNA miR-322, which in turn regulates PDIA6 mRNA stability and consequently IRE1α activity [64]. Other microRNAs have been shown to regulate components that maintain ER homeostasis, including channels that control Ca^{2+} fluxes across the ER membrane [69]. The expression of these microRNAs is sensitive to changes in ER Ca^{2+} homeostasis [69]. The luminal ER environment (amount of Ca^{2+}, composition of ER resident proteins) together with non-coding RNAs including microRNAs cooperate to control UPR status and to maintain homeostasis within the entire cellular reticular network [64, 69, 70].

4.7 ER and Lipid Metabolism

Cellular membranes are comprised of proteins as well as lipids, which include phospholipids, glycolipids and sterols [71]. The lipid constituents are not evenly distributed throughout the membrane systems of the cell. The plasma membrane and organellar membranes have characteristic lipid compositions which defines their identity. For instance, unesterified cholesterol is typically abundant in the mammalian plasma membrane and rare in ER membranes. Cardiolipin is enriched in mitochondrial membranes. Membrane leaflets may display lipid asymmetry as observed in the plasma membrane where phosphatidylserine is present in greater abundance in the inner leaflet whereas phosphatidylethanolamine is more highly represented in the outer leaflet. These lipids serve not only a structural role but also as a source of lipid metabolites that act as signaling molecules such as $InsP_3$, diacylglycerols and others [71]. Heterologous membrane systems do not readily mix or merge largely due to the physicochemical properties imparted by their distinct lipid compositions. It is thought that fusion of dissimilar membranes requires the action of specific proteins present at the sites of membrane interactions [71, 72]. The unique lipid composition of the plasma membrane and organellar membranes may also partly determine the characteristic proteome associated with these different

membrane systems by virtue of specific lipid-protein interactions that promote the retention of specific proteins in certain types of membrane environments.

Membrane lipid homeostasis, or lipidostasis, involves regulated synthesis of certain lipid species and lipid quality control to remove damaged lipids [51]. The ER is the major site of membrane lipid synthesis, although other organelles participate in producing biosynthetic intermediates, as in the case of phosphatidylserine synthesis (involves mitochondria) [73] and cholesterol synthesis (involves peroxisomes) [74, 75]. The enzymes responsible for these reactions are either embedded in membranes or located in the lumen of the organelles. Conversion of cholesterol into other bioactive compounds, such as steroid hormones, vitamin D metabolites and bile acids, also occurs in the ER in conjunction with other organelles [76, 77]. Vitamin D is known as a major regulator of systemic Ca^{2+} homeostasis [78] and is also important in the maintenance of cell signaling pathways [12]. The secondary bile acid known as ursodeoxycholic acid is a potent proteostasis promoter [79]. Considering the intimate relationships between specific lipids and proteins that comprise the various membrane systems of the cell, we propose that the coordination of lipidostasis and proteostasis is a key aspect necessary for assembly of functional membrane units to preserve cellular function and viability [51]. A recent study established that specific amino acid residues within the transmembrane domain of SERCA make ordered contacts with membrane phosphatidylcholine residues that surround the transmembrane domain to facilitate Ca^{2+} transport into the cell [80]. Disrupted lipidostasis is likely to curtail SERCA function and thus impair cellular Ca^{2+} homeostasis.

The induction of the UPR has been observed to induce phosphatidylcholine synthesis. This was initially attributed to the activation of the IRE1 branch of the pathway since enforced expression of Xbp1s mRNA could recapitulate the effect of UPR induction [81]. The increase in the synthesis of phosphatidylcholine supports expansion of ER membranes and is likely a part of the response to resolve ER stress. Interestingly, there were no changes in the abundance of mRNA of genes that are known to participate in the synthesis of phosphatidylcholine, suggesting that induction of membrane lipid synthesis is accomplished via posttranscriptional mechanisms. ATF6 was also found capable of stimulating phosphatidylcholine synthesis in an Xbp1s-independent fashion [82]. It is not clear how these transcription factors augment phosphatidylcholine synthesis. Nevertheless, the findings support for the notion that lipidostasis is linked to proteostasis, considering that membrane assembly is a concerted process involving both lipids and proteins.

Deletion of calreticulin dramatically reduces luminal ER Ca^{2+} stores, and causes the extreme elevation of blood lipids in mice and intracellular lipid accumulation in worms [83]. Sterol response element binding proteins (SREBPs) are master regulators of lipid homeostasis by regulating the expression of genes involved in cholesterol and triacylglycerol metabolism [9, 84, 85]. There are three SREBP isoforms known as SREBP-1a, SREBP-1c (both encoded by the SREBP1 gene) and SREBP-2 (encoded by the SREBP2 gene). These transcription factors are synthesized as precursor ER integral membrane proteins. Structurally, the SREBPs are composed of a transcription factor domain located in the N-terminal region of the protein, a

transmembrane domain, and a regulatory domain located in the C-terminal region of the protein that interacts with another ER membrane protein known as SREBP cleavage activating protein (SCAP). SREBP processing is triggered by the reduction of unesterified cholesterol concentration in the ER membrane [86]. When unesterified cholesterol is abundant in the ER membrane, the SREBP-SCAP complex is retained in ER. However, when the ER membrane is depleted of unesterified cholesterol, the SREBP-SCAP complex migrates to the Golgi apparatus where SREBP is sequentially processed by two Golgi resident proteases known as Site-1 and Site-2 proteases, respectively, to release its N-terminal fragment which is the active transcription factor. A recent discovery has added a twist in the complexity of this regulatory framework by elaborating the existence of a link between luminal ER Ca^{2+} homeostasis and cholesterol metabolism [83]. The direct reduction of the luminal ER Ca^{2+} caused the shrinkage of the unesterified cholesterol pool in the ER that triggers SREBP processing without altering the size of the total intracellular unesterified cholesterol pool [83]. This finding suggests that the size of the luminal ER Ca^{2+} pool may be involved in determining the basal sensitivity setpoint of the cholesterol sensing mechanism inherent to the SREBP processing pathway, and thus highlight the importance of luminal ER Ca^{2+} homeostasis in lipid metabolism.

4.8 ER and Membrane Contact Sites

The compartmentalization of specialized functions within discrete membrane bound organelles creates a challenge for efficient transport and exchange of molecules between compartments. Recent studies have documented the promiscuity of ER membranes for forming contacts with the plasma membrane and other organelles (mitochondria, peroxisomes, lysosomes, endosome, trans-Golgi, phagosomes, nuclear envelope) including lipid droplets [87–95]. These membrane contact sites occur between two heterologous membranes that are situated in very close proximity, approximately 10–30 nm, from each other and appear to be highly stable [36, 96, 97] except for STIM-ORAI (ER-plasma membrane) contacts which form transiently in the process of replenishing cellular Ca^{2+} stores. Contacts between other organelles, not involving the ER, have not been observed. It is also noteworthy that membrane contact sites between ER membranes with ribosomes (i.e., RER) and other organellar membranes are observed, implying possible functional heterogeneity in the membranes that make up the ER [93]. The joining of ER membranes to organellar membranes forms the cellular reticular network [14] characterized by interconnected membranes, tubules, vesicles and cisternae spanning the plasma membrane to the nuclear envelope linked together by membrane contacts sites that form portals that facilitates rapid passage of transport of substrates and metabolites (such as nutrients, biosynthetic intermediates, ATP) and signaling molecules (such as lipid messengers, Ca^{2+} ions) (Fig. 4.1) [14, 36, 94, 95, 98].

Recent studies have determined the identity of some of the molecules associated with membrane contacts sites [94, 99–101]. Proteins found at these structures

include Ca^{2+} binding proteins (e.g., STIM, ORAI, SERCA, RyR), chaperones, transporters, and lipid binding and lipid transfer proteins. Membrane contact sites may represent highly specialized sites of function as suggested by studies on phospholipid synthesis [73, 102]. The existence of these structures may account for the rapid non-vesicular transport of various lipid metabolites between organelles, such as during biosynthesis of membrane lipids and cholesterol. Indeed, many of the proteins that have been characterized are lipid transfer proteins, whose substrates include fatty acids, phospholipids, sterols and their metabolites including those that serve as messengers [99, 103, 104]. In yeast, several specialized proteins associated with membrane contact sites between ER and mitochondria have been identified. These proteins form a functional unit referred to as ER-mitochondria encounter structure (ERMES) [96, 103, 105]. The equivalent functional unit in mammalian cells has not been described.

Furthermore, release of luminal ER Ca^{2+} generates areas of Ca^{2+} microdomains characterized by a high Ca^{2+} concentration and occur at the contact region between the ER and plasma membrane where Ca^{2+} channels on the plasma membrane open [37, 39, 40]. The formation of ER-membrane contacts and the complexity of Ca^{2+} signaling proteins in these microdomains accounts for the specific characteristics of discrete Ca^{2+} signals [89]. One of the best characterized membrane contacts are those formed between skeletal and cardiac muscle T (transverse)-tubules (extensions of the plasma membrane) and the SR [106–109]. These membrane contacts are the driving force to support excitation-contraction coupling in the muscle and the mechanisms behind the Ca^{2+}-induced Ca^{2+} release in the cardiac muscle [110]. Membrane contacts between ER and mitochondria and Ca^{2+} microdomains that form between $InsP_3R$ and Ca^{2+} uniporters on the mitochondria support uptake of Ca^{2+} by mitochondria to match energy supply by Ca^{2+}-dependent stimulation of oxidative phosphorylation [95, 111].

This versatile arrangement of contacts between ER and organellar membranes offers the cell an ability to influence and/or support highly specialized functions throughout the cellular reticular network. Impairment of the ER-organellar contact sites might be involved in the pathogenesis of diseases such as neurodegenerative diseases [51]. Understanding how the process involved in the formation, maintenance and function of ER-membrane contact sites are regulated will provide insight into the role of ER Ca^{2+} in coordinating gene expression and cellular function.

4.9 Conclusions

The ER is an extensive network of membranes that occupies a major proportion of the cell interior. The ER and the other organelles are characterized by unique proteome and lipidome which together provide ideal environments that enable specialized functions within the cell. Ca^{2+} homeostasis in general, and ER luminal Ca^{2+} in particular, is essential for the function of the ER and reticular network. Ca^{2+} is a key molecule involved in orchestrating the metabolic pathways occurring in

different compartments of the cell. Internal or external factors that result in the loss of nutrient and energy homeostasis impose stress on cellular functions. Coping response strategies operate to alleviate and eliminate stress in the ER and other organelles to maintain proteostasis and lipidostasis within the entire cellular reticular network. ER membranes can form resilient contacts with the membranes of other organelles forming a complex cellular reticular network. Membrane contact sites enable rapid distribution and exchange of substrates, metabolites and signalling molecules to ensure optimal cellular function and homeostasis.

Acknowledgements Research in our laboratories is supported by grants from the Canadian Institutes of Health Research grants MOP-15291, MOP-15415, MOP-86750 and PS-153325.

Conflict of Interest The authors declare no conflict of interest.

References

1. Hebert DN, Molinari M (2007) In and out of the ER: protein folding, quality control, degradation, and related human diseases. Physiol Rev 87:1377–1408
2. Krebs J, Agellon LB, Michalak M (2015) Ca^{2+} homeostasis and endoplasmic reticulum (ER) stress: an integrated view of calcium signaling. Biochem Biophys Res Commun 460:114–121
3. McCaffrey K, Braakman I (2016) Protein quality control at the endoplasmic reticulum. Essays Biochem 60:227–235
4. Coe H, Michalak M (2009) Calcium binding chaperones of the endoplasmic reticulum. Gen Physiol Biophys 28 Spec No Focus:F96–F103
5. Bose D, Chakrabarti A (2017) Substrate specificity in the context of molecular chaperones. IUBMB Life 69(9):647–659
6. Horowitz S, Koldewey P, Stull F, Bardwell JC (2017) Folding while bound to chaperones. Curr Opin Struct Biol 48:1–5
7. Caramelo JJ, Parodi AJ (2015) A sweet code for glycoprotein folding. FEBS Lett 589:3379–3387
8. Baiceanu A, Mesdom P, Lagouge M, Foufelle F (2016) Endoplasmic reticulum proteostasis in hepatic steatosis. Nat Rev Endocrinol 12:710–722
9. Horton JD, Goldstein JL, Brown MS (2002) SREBPs: activators of the complete program of cholesterol and fatty acid synthesis in the liver. J Clin Invest 109:1125–1131
10. Vincenz-Donnelly L, Hipp MS (2017) The endoplasmic reticulum: a hub of protein quality control in health and disease. Free Radic Biol Med 108:383–393
11. Volpi VG, Touvier T, D'Antonio M (2016) Endoplasmic reticulum protein quality control failure in myelin disorders. Front Mol Neurosci 9:162
12. Berridge MJ (2016) The inositol trisphosphate/calcium signaling pathway in health and disease. Physiol Rev 96:1261–1296
13. Soboloff J, Rothberg BS, Madesh M, Gill DL (2012) STIM proteins: dynamic calcium signal transducers. Nat Rev Mol Cell Biol 13:549–565
14. Groenendyk J, Agellon LB, Michalak M (2013) Coping with endoplasmic reticulum stress in the cardiovascular system. Annu Rev Physiol 75:49–67
15. Hetz C, Chevet E, Oakes SA (2015) Proteostasis control by the unfolded protein response. Nat Cell Biol 17:829–838

16. D'Amico D, Sorrentino V, Auwerx J (2017) Cytosolic proteostasis networks of the mitochondrial stress response. Trends Biochem Sci 42(9):712–725
17. Dicks N, Gutierrez K, Michalak M, Bordignon V, Agellon LB (2015) Endoplasmic reticulum stress, genome damage, and cancer. Front Oncol 5:11
18. Jovaisaite V, Auwerx J (2015) The mitochondrial unfolded protein response-synchronizing genomes. Curr Opin Cell Biol 33:74–81
19. Stepien KM, Heaton R, Rankin S, Murphy A, Bentley J, Sexton D, Hargreaves IP (2017) Evidence of oxidative stress and secondary mitochondrial dysfunction in metabolic and non-metabolic disorders. J Clin Med 6(7):E71
20. Szymanski J, Janikiewicz J, Michalska B, Patalas-Krawczyk P, Perrone M, Ziolkowski W, Duszynski J, Pinton P, Dobrzyn A, Wieckowski MR (2017) Interaction of mitochondria with the endoplasmic reticulum and plasma membrane in calcium homeostasis, lipid trafficking and mitochondrial structure. Int J Mol Sci 18(7):E1576
21. Baumann O, Walz B (2001) Endoplasmic reticulum of animal cells and its organization into structural and functional domains. Int Rev Cytol 205:149–214
22. Corbett EF, Michalak M (2000) Calcium, a signaling molecule in the endoplasmic reticulum? Trends Biochem Sci 25:307–311
23. High S, Lecomte FJ, Russell SJ, Abell BM, Oliver JD (2000) Glycoprotein folding in the endoplasmic reticulum: a tale of three chaperones? FEBS Lett 476:38–41
24. Jakob CA, Chevet E, Thomas DY, Bergeron JJ (2001) Lectins of the ER quality control machinery. Results Probl Cell Differ 33:1–17
25. Molinari M, Helenius A (2000) Chaperone selection during glycoprotein translocation into the endoplasmic reticulum. Science 288:331–333
26. Nakamura K, Zuppini A, Arnaudeau S, Lynch J, Ahsan I, Krause R, Papp S, De Smedt H, Parys JB, Müller-Esterl W, Lew DP, Krause K-H, Demaurex N, Opas M, Michalak M (2001) Functional specialization of calreticulin domains. J Cell Biol 154:961–972
27. Lievremont JP, Rizzuto R, Hendershot L, Meldolesi J (1997) BiP, a major chaperone protein of the endoplasmic reticulum lumen, plays a direct and important role in the storage of the rapidly exchanging pool of Ca^{2+}. J Biol Chem 272:30873–33089
28. Van PN, Peter F, Soling H-D (1989) Four intracisternal calcium-binding glycoproteins from rat liver microsomes with high affinity for calcium. No indication for calsequestrin-like proteins in inositol 1,4,5-trisphosphate-sensitive calcium sequestering rat liver vesicles. J Biol Chem 264:17494–17501
29. Waser M, Mesaeli N, Spencer C, Michalak M (1997) Regulation of calreticulin gene expression by calcium. J Cell Biol 138:547–557
30. Lebeche D, Lucero HA, Kaminer B (1994) Calcium binding properties of rabbit liver protein disulfide isomerase. Biochem Biophys Res Commun 202:556–561
31. Lucero HA, Kaminer B (1999) The role of calcium on the activity of ERcalcistorin/protein-disulfide isomerase and the significance of the C-terminal and its calcium binding. A comparison with mammalian protein-disulfide isomerase. J Biol Chem 274:3243–3251
32. Lucero HA, Lebeche D, Kaminer B (1998) ERcalcistorin/protein-disulfide isomerase acts as a calcium storage protein in the endoplasmic reticulum of a living cell. Comparison with calreticulin and calsequestrin. J Biol Chem 273:9857–9863
33. Faggioni M, Knollmann BC (2012) Calsequestrin 2 and arrhythmias. Am J Physiol Heart Circ Physiol 302:H1250–H1260
34. Lee D, Michalak M (2010) Membrane associated Ca^{2+} buffers in the heart. BMB Rep 43:151–157
35. Bhardwaj R, Hediger MA, Demaurex N (2016) Redox modulation of STIM-ORAI signaling. Cell Calcium 60:142–152
36. Saheki Y, De Camilli P (2017) Endoplasmic reticulum-plasma membrane contact sites. Annu Rev Biochem 86:659–684
37. Zhou Y, Cai X, Nwokonko RM, Loktionova NA, Wang Y, Gill DL (2017) The STIM-Orai coupling interface and gating of the Orai1 channel. Cell Calcium 63:8–13

38. Takemura H, Putney JW Jr (1989) Capacitative calcium entry in parotid acinar cells. Biochem J 258:409–412
39. Delpire E (2016) STIM and Orai proteins in calcium signaling: an AJP-cell physiology series of themed reviews. Am J Physiol Cell Physiol 310:C401
40. Tanwar J, Motiani RK (2017) Role of SOCE architects STIM and Orai proteins in cell death. Cell Calcium https://doi.org/10.1016/j.ceca.2017.06.002
41. Brandman O, Liou J, Park WS, Meyer T (2007) STIM2 is a feedback regulator that stabilizes basal cytosolic and endoplasmic reticulum Ca^{2+} levels. Cell 131:1327–1339
42. Kawasaki H, Kretsinger RH (2017) Structural and functional diversity of EF-hand proteins: Evolutionary perspectives. Protein Sci 26(10):1898–1920
43. Hou X, Pedi L, Diver MM, Long SB (2012) Crystal structure of the calcium release-activated calcium channel Orai. Science 338:1308–1313
44. DeHaven WI, Smyth JT, Boyles RR, Putney JW Jr (2007) Calcium inhibition and calcium potentiation of Orai1, Orai2, and Orai3 calcium release-activated calcium channels. J Biol Chem 282:17548–17556
45. Gonzalez-Cobos JC, Zhang X, Zhang W, Ruhle B, Motiani RK, Schindl R, Muik M, Spinelli AM, Bisaillon JM, Shinde AV, Fahrner M, Singer HA, Matrougui K, Barroso M, Romanin C, Trebak M (2013) Store-independent Orai1/3 channels activated by intracrine leukotriene C4: role in neointimal hyperplasia. Circ Res 112:1013–1025
46. Thompson JL, Shuttleworth TJ (2013) Exploring the unique features of the ARC channel, a store-independent Orai channel. Channels (Austin) 7:364–373
47. Zhang W, Zhang X, Gonzalez-Cobos JC, Stolwijk JA, Matrougui K, Trebak M (2015) Leukotriene-C4 synthase, a critical enzyme in the activation of store-independent Orai1/Orai3 channels, is required for neointimal hyperplasia. J Biol Chem 290:5015–5027
48. Prins D, Groenendyk J, Touret N, Michalak M (2011) Modulation of STIM1 and capacitative Ca^{2+} entry by the endoplasmic reticulum luminal oxidoreductase ERp57. EMBO Rep 12:1182–1188
49. Li Y, Camacho P (2004) Ca^{2+}-dependent redox modulation of SERCA 2b by ERp57. J Cell Biol 164:35–46
50. Ellgaard L, McCaul N, Chatsisvili A, Braakman I (2016) Co- and post-translational protein folding in the ER. Traffic 17:615–638
51. Jung J, Michalak M, Agellon LB (2017) Endoplasmic reticulum malfunction in the nervous system. Front Neurosci 11:220
52. Balchin D, Hayer-Hartl M, Hartl FU (2016) In vivo aspects of protein folding and quality control. Science 353:aac4354
53. Bernasconi R, Molinari M (2011) ERAD and ERAD tuning: disposal of cargo and of ERAD regulators from the mammalian ER. Curr Opin Cell Biol 23:176–183
54. Qi L, Tsai B, Arvan P (2017) New insights into the physiological role of endoplasmic reticulum-associated degradation. Trends Cell Biol 27:430–440
55. Grek C, Townsend DM (2014) Protein disulfide isomerase superfamily in disease and the regulation of apoptosis. Endoplasmic Reticul Stress Dis 1:4–17
56. Parakh S, Atkin JD (2015) Novel roles for protein disulphide isomerase in disease states: a double edged sword? Front Cell Dev Biol 3:30
57. Trombetta ES, Parodi AJ (2003) Quality control and protein folding in the secretory pathway. Annu Rev Cell Dev Biol 19:649–676
58. Carafoli E, Krebs J (2016) Why calcium? How calcium became the best communicator. J Biol Chem 291:20849–20857
59. Gidalevitz T, Prahlad V, Morimoto RI (2011) The stress of protein misfolding: from single cells to multicellular organisms. Cold Spring Harb Perspect Biol 3(6):a009704
60. Wang M, Kaufman RJ (2014) The impact of the endoplasmic reticulum protein-folding environment on cancer development. Nat Rev Cancer 14:581–597

61. Nakka VP, Prakash-babu P, Vemuganti R (2016) Crosstalk between endoplasmic reticulum stress, oxidative stress, and autophagy: potential therapeutic targets for acute CNS injuries. Mol Neurobiol 53:532–544
62. Zhang C, Syed TW, Liu R, Yu J (2017) Role of endoplasmic reticulum stress, autophagy, and inflammation in cardiovascular disease. Front Cardiovasc Med 4:29
63. Kaur J, Debnath J (2015) Autophagy at the crossroads of catabolism and anabolism. Nat Rev Mol Cell Biol 16:461–472
64. Groenendyk J, Peng Z, Dudek E, Fan X, Mizianty MJ, Dufey E, Urra H, Sepulveda D, Rojas-Rivera D, Lim Y, Kim do H, Baretta K, Srikanth S, Gwack Y, Ahnn J, Kaufman RJ, Lee SK, Hetz C, Kurgan L, Michalak M (2014) Interplay between the oxidoreductase PDIA6 and microRNA-322 controls the response to disrupted endoplasmic reticulum calcium homeostasis. Sci Signal 7:ra54
65. Leung AK, Sharp PA (2010) MicroRNA functions in stress responses. Mol Cell 40:205–215
66. Hong M, Luo S, Baumeister P, Huang JM, Gogia RK, Li M, Lee AS (2004) Underglycosylation of ATF6 as a novel sensing mechanism for activation of the unfolded protein response. J Biol Chem 279:11354–11363
67. Higa A, Taouji S, Lhomond S, Jensen D, Fernandez-Zapico ME, Simpson JC, Pasquet JM, Schekman R, Chevet E (2014) Endoplasmic reticulum stress-activated transcription factor ATF6alpha requires the disulfide isomerase PDIA5 to modulate chemoresistance. Mol Cell Biol 34:1839–1849
68. Eletto D, Eletto D, Dersh D, Gidalevitz T, Argon Y (2014) Protein disulfide isomerase A6 controls the decay of IRE1alpha signaling via disulfide-dependent association. Mol Cell 53:562–576
69. Khan S, Greco D, Michailidou K, Milne RL, Muranen TA, Heikkinen T, Aaltonen K, Dennis J, Bolla MK, Liu J, Hall P, Irwanto A, Humphreys K, Li J, Czene K, Chang-Claude J, Hein R, Rudolph A, Seibold P, Flesch-Janys D, Fletcher O, Peto J, dos Santos Silva I, Johnson N, Gibson L, Aitken Z, Hopper JL, Tsimiklis H, Bui M, Makalic E, Schmidt DF, Southey MC, Apicella C, Stone J, Waisfisz Q, Meijers-Heijboer H, Adank MA, van der Luijt RB, Meindl A, Schmutzler RK, Muller-Myhsok B, Lichtner P, Turnbull C, Rahman N, Chanock SJ, Hunter DJ, Cox A, Cross SS, Reed MW, Schmidt MK, Broeks A, Van't Veer LJ, Hogervorst FB, Fasching PA, Schrauder MG, Ekici AB, Beckmann MW, Bojesen SE, Nordestgaard BG, Nielsen SF, Flyger H, Benitez J, Zamora PM, Perez JI, Haiman CA, Henderson BE, Schumacher F, Le Marchand L, Pharoah PD, Dunning AM, Shah M, Luben R, Brown J, Couch FJ, Wang X, Vachon C, Olson JE, Lambrechts D, Moisse M, Paridaens R, Christiaens MR, Guenel P, Truong T, Laurent-Puig P, Mulot C, Marme F, Burwinkel B, Schneeweiss A, Sohn C, Sawyer EJ, Tomlinson I, Kerin MJ, Miller N, Andrulis IL, Knight JA, Tchatchou S, Mulligan AM, Dork T, Bogdanova NV, Antonenkova NN et al (2014) MicroRNA related polymorphisms and breast cancer risk. PLoS One 9:e109973
70. McMahon M, Samali A, Chevet E (2017) Regulation of the unfolded protein response by non-coding RNA. Am J Physiol Cell Physiol 313(3):C243–C254
71. van Meer G, Voelker DR, Feigenson GW (2008) Membrane lipids: where they are and how they behave. Nat Rev Mol Cell Biol 9:112–124
72. Chernomordik LV, Kozlov MM (2008) Mechanics of membrane fusion. Nat Struct Mol Biol 15:675–683
73. Kannan M, Lahiri S, Liu LK, Choudhary V, Prinz WA (2017) Phosphatidylserine synthesis at membrane contact sites promotes its transport out of the ER. J Lipid Res 58:553–562
74. Cerqueira NM, Oliveira EF, Gesto DS, Santos-Martins D, Moreira C, Moorthy HN, Ramos MJ, Fernandes PA (2016) Cholesterol biosynthesis: a mechanistic overview. Biochemistry 55:5483–5506
75. Kovacs WJ, Olivier LM, Krisans SK (2002) Central role of peroxisomes in isoprenoid biosynthesis. Prog Lipid Res 41:369–391
76. Agellon LB (2008) Metabolism and function of bile acids. In: Vance DE, Vance JE (eds) Biochemistry of lipids, lipoproteins and membranes, 5th edn. Elsevier, Amsterdam

77. Miller WL (2013) Steroid hormone synthesis in mitochondria. Mol Cell Endocrinol 379:62–73
78. Fleet JC (2017) The role of vitamin D in the endocrinology controlling calcium homeostasis. Mol Cell Endocrinol 453:36–45
79. Vega H, Agellon LB, Michalak M (2016) The rise of proteostasis promoters. IUBMB Life 68:943–954
80. Norimatsu Y, Hasegawa K, Shimizu N, Toyoshima C (2017) Protein-phospholipid interplay revealed with crystals of a calcium pump. Nature 545:193–198
81. Sriburi R, Jackowski S, Mori K, Brewer JW (2004) XBP1: a link between the unfolded protein response, lipid biosynthesis, and biogenesis of the endoplasmic reticulum. J Cell Biol 167:35–41
82. Bommiasamy H, Back SH, Fagone P, Lee K, Meshinchi S, Vink E, Sriburi R, Frank M, Jackowski S, Kaufman RJ, Brewer JW (2009) ATF6alpha induces XBP1-independent expansion of the endoplasmic reticulum. J Cell Sci 122:1626–1636
83. Wang WA, Liu WX, Durnaoglu S, Lee SK, Lian J, Lehner R, Ahnn J, Agellon LB, Michalak M (2017) Loss of calreticulin uncovers a critical role for calcium in regulating cellular lipid homeostasis. Sci Rep 7:5941
84. Brown MS, Goldstein JL (1997) The SREBP pathway: regulation of cholesterol metabolism by proteolysis of a membrane-bound transcription factor. Cell 89:331–340
85. Shimano H (2001) Sterol regulatory element-binding proteins (SREBPs): transcriptional regulators of lipid synthetic genes. Prog Lipid Res 40:439–452
86. Radhakrishnan A, Goldstein JL, McDonald JG, Brown MS (2008) Switch-like control of SREBP-2 transport triggered by small changes in ER cholesterol: a delicate balance. Cell Metab 8:512–521
87. Barneda D, Christian M (2017) Lipid droplet growth: regulation of a dynamic organelle. Curr Opin Cell Biol 47:9–15
88. Daniele T, Schiaffino MV (2014) Organelle biogenesis and interorganellar connections: Better in contact than in isolation. Commun Integr Biol 7:e29587
89. Filadi R, Pozzan T (2015) Generation and functions of second messengers microdomains. Cell Calcium 58:405–414
90. Joshi AS, Zhang H, Prinz WA (2017) Organelle biogenesis in the endoplasmic reticulum. Nat Cell Biol 19:876–882
91. Nunes-Hasler P, Demaurex N (2017) The ER phagosome connection in the era of membrane contact sites. Biochim Biophys Acta 1864:1513–1524
92. Penny CJ, Kilpatrick BS, Eden ER, Patel S (2015) Coupling acidic organelles with the ER through Ca^{2+} microdomains at membrane contact sites. Cell Calcium 58:387–396
93. Phillips MJ, Voeltz GK (2016) Structure and function of ER membrane contact sites with other organelles. Nat Rev Mol Cell Biol 17:69–82
94. Prinz WA (2014) Bridging the gap: membrane contact sites in signaling, metabolism, and organelle dynamics. J Cell Biol 205:759–769
95. Prudent J, McBride HM (2017) The mitochondria-endoplasmic reticulum contact sites: a signalling platform for cell death. Curr Opin Cell Biol 47:52–63
96. Helle SC, Kanfer G, Kolar K, Lang A, Michel AH, Kornmann B (2013) Organization and function of membrane contact sites. Biochim Biophys Acta 1833:2526–2541
97. Orci L, Ravazzola M, Le Coadic M, Shen WW, Demaurex N, Cosson P (2009) From the Cover: STIM1-induced precortical and cortical subdomains of the endoplasmic reticulum. Proc Natl Acad Sci U S A 106:19358–19362
98. Jain A, Holthuis JCM (2017) Membrane contact sites, ancient and central hubs of cellular lipid logistics. Biochim Biophys Acta 1864:1450–1458
99. Chiapparino A, Maeda K, Turei D, Saez-Rodriguez J, Gavin AC (2016) The orchestra of lipid-transfer proteins at the crossroads between metabolism and signaling. Prog Lipid Res 61:30–39

100. Lang A, John Peter AT, Kornmann B (2015) ER-mitochondria contact sites in yeast: beyond the myths of ERMES. Curr Opin Cell Biol 35:7–12
101. Levine TP, Patel S (2016) Signalling at membrane contact sites: two membranes come together to handle second messengers. Curr Opin Cell Biol 39:77–83
102. Vance JE (1990) Phospholipid synthesis in a membrane fraction associated with mitochondria. J Biol Chem 265:7248–7256
103. Raturi A, Simmen T (2013) Where the endoplasmic reticulum and the mitochondrion tie the knot: the mitochondria-associated membrane (MAM). Biochim Biophys Acta 1833:213–224
104. Wong LH, Levine TP (2016) Lipid transfer proteins do their thing anchored at membrane contact sites... but what is their thing? Biochem Soc Trans 44:517–527
105. Michel AH, Kornmann B (2012) The ERMES complex and ER-mitochondria connections. Biochem Soc Trans 40:445–450
106. Barone V, Randazzo D, Del Re V, Sorrentino V, Rossi D (2015) Organization of junctional sarcoplasmic reticulum proteins in skeletal muscle fibers. J Muscle Res Cell Motil 36:501–515
107. Landstrom AP, Beavers DL, Wehrens XH (2014) The junctophilin family of proteins: from bench to bedside. Trends Mol Med 20:353–362
108. Louch WE, Nattel S (2017) T-tubular collagen: a new player in mechanosensing and disease? Cardiovasc Res 113(8):839–840
109. Manfra O, Frisk M, Louch WE (2017) Regulation of cardiomyocyte T-tubular structure: opportunities for therapy. Curr Heart Fail Rep 14:167–178
110. Eisner DA, Caldwell JL, Kistamas K, Trafford AW (2017) Calcium and excitation-contraction coupling in the heart. Circ Res 121:181–195
111. De Stefani D, Rizzuto R, Pozzan T (2016) Enjoy the trip: calcium in mitochondria back and forth. Annu Rev Biochem 85:161–192

Chapter 5
Structure-Function Relationship of the SERCA Pump and Its Regulation by Phospholamban and Sarcolipin

Przemek A. Gorski, Delaine K. Ceholski, and Howard S. Young

Abstract Calcium is a universal second messenger involved in diverse cellular processes, including excitation-contraction coupling in muscle. The contraction and relaxation of cardiac muscle cells are regulated by the cyclic movement of calcium primarily between the extracellular space, the cytoplasm and the sarcoplasmic reticulum (SR). The rapid removal of calcium from the cytosol is primarily facilitated by the sarco(endo)plasmic reticulum calcium ATPase (SERCA) which pumps calcium back into the SR lumen and thereby controls the amount of calcium in the SR. The most studied member of the P-type ATPase family, SERCA has multiple tissue- and cell-specific isoforms and is primarily regulated by two peptides in muscle, phospholamban and sarcolipin. The multifaceted regulation of SERCA via these peptides is exemplified in the biological fine-tuning of their independent oligomerization and regulation. In this chapter, we overview the structure-function relationship of SERCA and its peptide modulators, detailing the regulation of the complexes and summarizing their physiological and disease relevance.

Keywords Calcium · Sarcoplasmic reticulum · Calcium ATPase · Phospholamban · Sarcolipin

5.1 Calcium Homeostasis

Calcium is a universal second messenger involved in diverse cellular processes such as fertilization, gene transcription, protein synthesis, neurotransmission, apoptosis, and excitation-contraction coupling in muscle tissue [1]. Sustaining calcium homeo-

Przemek A. Gorski and Delaine K. Ceholski contributed equally to this work.

P. A. Gorski · D. K. Ceholski · H. S. Young (✉)
Department of Biochemistry, University of Alberta, Edmonton, AB, Canada
e-mail: hyoung@ualberta.ca

J. Krebs (ed.), *Membrane Dynamics and Calcium Signaling*, Advances in Experimental Medicine and Biology 981,
https://doi.org/10.1007/978-3-319-55858-5_5

stasis in the cell is central in allowing these processes to occur, and it is achieved through movement of calcium across membranes by various transporters and channels. One of the most important roles of calcium is in muscle cells where its intracellular concentration oscillates as a mechanism for controlling muscle contraction and relaxation.

The contraction and relaxation of cardiac muscle cells are regulated by the cyclic movement of calcium primarily between the extracellular space, the cytoplasm and the sarcoplasmic reticulum (SR) [2]. The process of cardiac muscle contraction begins with an action potential that depolarizes the plasma membrane and induces the L-type calcium channel (dihydropyranine receptor, DHPR) to open, allowing a small influx of calcium. In turn, this initiates a massive calcium release from the SR stores through the ryanodine receptor (RyR). The sudden increase in cytosolic calcium results in binding of calcium to troponin-C and initiation of muscle contraction. For muscle relaxation to occur, the calcium concentration in the cytosol needs to be restored to resting levels. The rapid removal of calcium from the cytosol is primarily facilitated by the sarco(endo)plasmic reticulum calcium ATPase (SERCA) which pumps calcium back into the SR lumen and thereby controls the amount of calcium in the SR. To balance the influx of calcium via the DHPR, a small amount of calcium is moved into the extracellular space by the sodium-calcium exchanger (NCX) and plasma membrane calcium ATPase (PMCA). Therefore, SERCA is central in determining the rate of relaxation and the strength of subsequent muscle contractions.

5.2 SERCA Isoforms and Human Disease (P-Type ATPases)

The SERCA pumps are highly conserved membrane proteins that have been identified in both prokaryotes and eukaryotes. In humans, three genes (*ATP2A1-3*) encode for multiple isoforms and splice variants of SERCA (SERCA1a-b, SERCA2a-d, SERCA3a-f), which allow for developmental and tissue-dependent expression patterns and alternative splicing [3]. Due to the high sequence identity, all of the SERCA isoforms are predicted to have the same topology and virtually identical tertiary structure. Despite their high structural homology, these pumps differ significantly in their regulatory and kinetic properties, thereby accommodating cell- or tissue-specific calcium handling requirements.

5.2.1 SERCA1

The SERCA1 gene (*ATP2A1*) can be alternatively spliced to generate the SERCA1a or SERCA1b isoforms, which are predominantly expressed in the adult and fetal

fast-twitch skeletal muscles, respectively. SERCA1a is identical to SERCA1b, except the last C-terminal residue of SERCA1a (994 amino acids) is replaced by eight highly charged amino acids in SERCA1b (1001 amino acids) [3]. Although the physiological role of SERCA1b remains elusive, this isoform was shown to be important for skeletal muscle development as it is expressed in neonatal stages along with SERCA2a but is completely replaced by SERCA1a in adult muscle cells. The SERCA1a variant has been extensively studied in different expression systems and animal models, and much functional and structural information is available. In this regard, SERCA1a has been a paradigm for the family of P-type ATPases. SERCA1a is highly abundant in the skeletal muscle where it is regulated by a single transmembrane peptide, sarcolipin (SLN) [4]. Compared to the cardiac SERCA2a isoform, SERCA1a appears to have the same affinity for calcium but a higher kinetic turnover rate. Because of its higher turnover rate, overexpression of SERCA1a in the cardiomyocytes of mice with ischemia-reperfusion injury was not only able to functionally substitute for SERCA2a, but it also significantly enhanced calcium transport and slowed down disease progression [5–7].

The gene encoding SERCA1 has been implicated in Brody disease, a rare inherited disorder of the skeletal musculature [8]. Several studies have indicated that mutations in the *ATP2A1* gene result in either a loss of function or premature termination codon resulting in a truncated protein [9]. As a result of dysfunctional SERCA1a, calcium is not properly transported back into the SR after its release into the cytoplasm, resulting in impaired muscle relaxation and stiffness. However, defects in genes encoding proteins other than SERCA have been linked to this disease implying that the origin of Brody disease is genetically heterogeneous [8].

5.2.2 SERCA2

The *ATP2A2* gene encodes for four splice variants of SERCA2 (a-d). The muscle-specific isoform, SERCA2a, is expressed in cardiac and slow-twitch skeletal muscle, making it a key determinant of normal cardiac development and function [10]. SERCA2a is 84% identical to SERCA1a, and is reversibly regulated by the single transmembrane proteins phospholamban (PLN) and sarcolipin (SLN) in cardiac muscle [11]. SERCA2b is the most unique splice variant of all of the Ca^{2+}-ATPases, as it has a C-terminal extension that forms an eleventh transmembrane domain that protrudes into the endoplasmic reticulum (ER) lumen [12]. It is referred to as the house-keeping isoform, as it is ubiquitously expressed in the ER of most cell types. Unlike SERCA2a, it is only sensitive to regulation by PLN [13]. SERCA2c is a more recently identified variant which has been found to be expressed at very low levels in monocytes and epithelial and hematopoietic cells [14] and SERCA2d mRNA was found in skeletal muscle but there is no functional evidence for endogenous SERCA2d protein [15].

The SERCA2 splice variants display functional differences that can be attributed to the different C-terminal ends of the proteins. Overexpression studies have clearly

demonstrated that SERCA2b has a twofold higher affinity for calcium and a twofold lower catalytic turnover rate compared to SERCA2a [13]. A more detailed explanation for the observed differences was given by in-depth kinetic analysis of the SERCA2b isoform, which indicated that the C-terminal extension reduces the rate of calcium dissociation, phospho-enzyme intermediate conformational change, and dephosphorylation [16]. SERCA2c was only recently shown to have the lowest apparent calcium affinity of the three SERCA2 variants, suggesting that it might serve its function in an environment with a locally high calcium concentration [14].

Although extremely rare, mutations in the SERCA2 gene have been linked to several human pathologies [17]. Missense mutations in the SERCA2 gene cause Darier's disease, a severe skin disorder characterized by loss of adhesion between epidermal cells, but do not effect cardiac function. More recently, mutations in the SERCA2 gene have been linked to lung and colon cancer. Studies in mice have shown that only one copy of the SERCA2 gene is necessary to maintain proper cardiac function but deletion of both genes is lethal [18]. Heterozygous mice are viable but show a 35% decrease in SERCA levels. Defects in the regulation of SERCA2a as well as low activity or expression levels of this isoform in the heart can lead to hypertrophy, cardiomyopathy, and end-stage heart failure.

5.2.3 SERCA3

SERCA3 is the most recently identified member of the SERCA family. Its primary sequence is ~75% identical to those of SERCA1 and SERCA2. Alternative splicing of the *ATP2A3* gene gives rise to six variants of SERCA3 that have been identified in humans (SERCA3a-f) [17]. However, only three splice variants have so far been detected at the protein level (SERCA3a-c) [3]. The functional properties of this subfamily of calcium pumps are poorly understood. The hallmark of SERCA3 is its low affinity for calcium (fivefold lower than other SERCA isoforms) and its insensitivity to PLN. In addition, it has a significantly higher affinity for vanadate inhibition (vanadate is a transition-state analogue that inhibits ATPases), and a higher pH optimum compared to other SERCA pumps. Just like the other SERCA isoforms, SERCA3 isoforms only vary at their C-termini, suggesting that the C-terminal tail region may contribute to the differences observed in the enzymatic activities.

SERCA3 isoforms are primarily expressed in hematopoietic cell lineages, epithelial cells, and endocrine pancreatic β-cells [19]. Recently, SERCA3 expression was also observed in human cardiomyocytes. The SERCA3 expression profile often overlaps with the ubiquitous SERCA2b, although their relative subcellular locations are significantly different. Unique compartmentalization of the different SERCA isoforms might be crucial to their physiological role in maintaining calcium homeostasis within a cell. The high expression of SERCA3 in pancreatic β-cells and mutations in the *ATP2A3* gene, which have been associated with type II diabetes, have suggested that SERCA3 plays a crucial role in metabolic homeostasis

[20]. Surprisingly, SERCA3 knock-out mice present normal glucose tolerance but display a smooth muscle relaxation defect [21]. In addition, abnormal SERCA3 expression levels have been linked to several types of cancer including lung, breast, gastric, and colon [22–25].

5.3 Catalytic Cycle of Calcium Transport by SERCA

It is well accepted that P-type ATPases undergo large conformational changes to transport ions or lipid molecules across the membrane [26]. These pumps cycle between a high affinity (E1) and low affinity (E2) state, both of which have phosphorylated intermediates (E1-P and E2-P). The E1-E2 model of active transport by P-type ATPase pumps was originally proposed by Post and Albers to describe the ion transport by the Na^+/K^+-ATPase and later adopted for the ion transport by SERCA [27]. In the case of SERCA, the E1 state defines the high calcium affinity (micromolar) and E2 the low calcium affinity (millimolar) conformations of the enzyme. It is well established that calcium transport by SERCA is tightly coupled to ATP hydrolysis. The energy generated from one ATP molecule drives SERCA to pump two calcium ions in exchange for two to three protons. The E1 and E2 states do not indicate that the transporting enzyme is in either the "open" or "closed" conformation but rather represent two distinct SERCA states with high affinity for calcium or protons, respectively [28].

The mechanism of ATP-dependent calcium transport by SERCA is summarized in Fig. 5.1. The cycle begins in the high-affinity E1-ATP state where the two calcium binding sites are exposed to the cytosol. Successive binding of two calcium ions results in a release of two to three protons into the cytosol and formation of the $(Ca^{2+})_2$-E1-ATP intermediate. Calcium binding triggers auto-phosphorylation by the γ-phosphate of ATP at the highly conserved aspartic acid residue, Asp^{351}. This results in the formation of a high-energy phospho-intermediate, $(Ca^{2+})_2$-E1-P-ADP, in which the bound calcium becomes occluded and is inaccessible to the cytosol or lumen [29]. It is important to note that at this point in the transport cycle, high ADP concentrations in the cytosol can reverse the reaction resulting in regeneration of ATP and release of calcium ions into the cytosol. The next step in the transport cycle involves exchange of ADP for ATP and transition into the low-energy $(Ca^{2+})_2$-E2-P-ADP state in which the calcium ions remain occluded. Conversion to the $(H^+)_{2\text{-}3}$-E2-P-ATP state results in the release of calcium ions into the lumen and binding of two to three protons to compensate for the net negative charge of the calcium binding sites. Subsequently, dephosphorylation of the enzyme leads to the formation of the $(H^+)_{2\text{-}3}$-E2-ATP state in which protons are occluded. The final step of the transport cycle is the release of protons into the cytosol and reformation of the E1-ATP state with the ion binding sites primed for the binding of cytosolic calcium in the next reaction cycle [30]. The role of ATP in the calcium transport cycle has traditionally been described as catalytic, where nucleotide molecules were thought to only be associated with the E1 forms of the enzyme. More recently, however, ATP has been

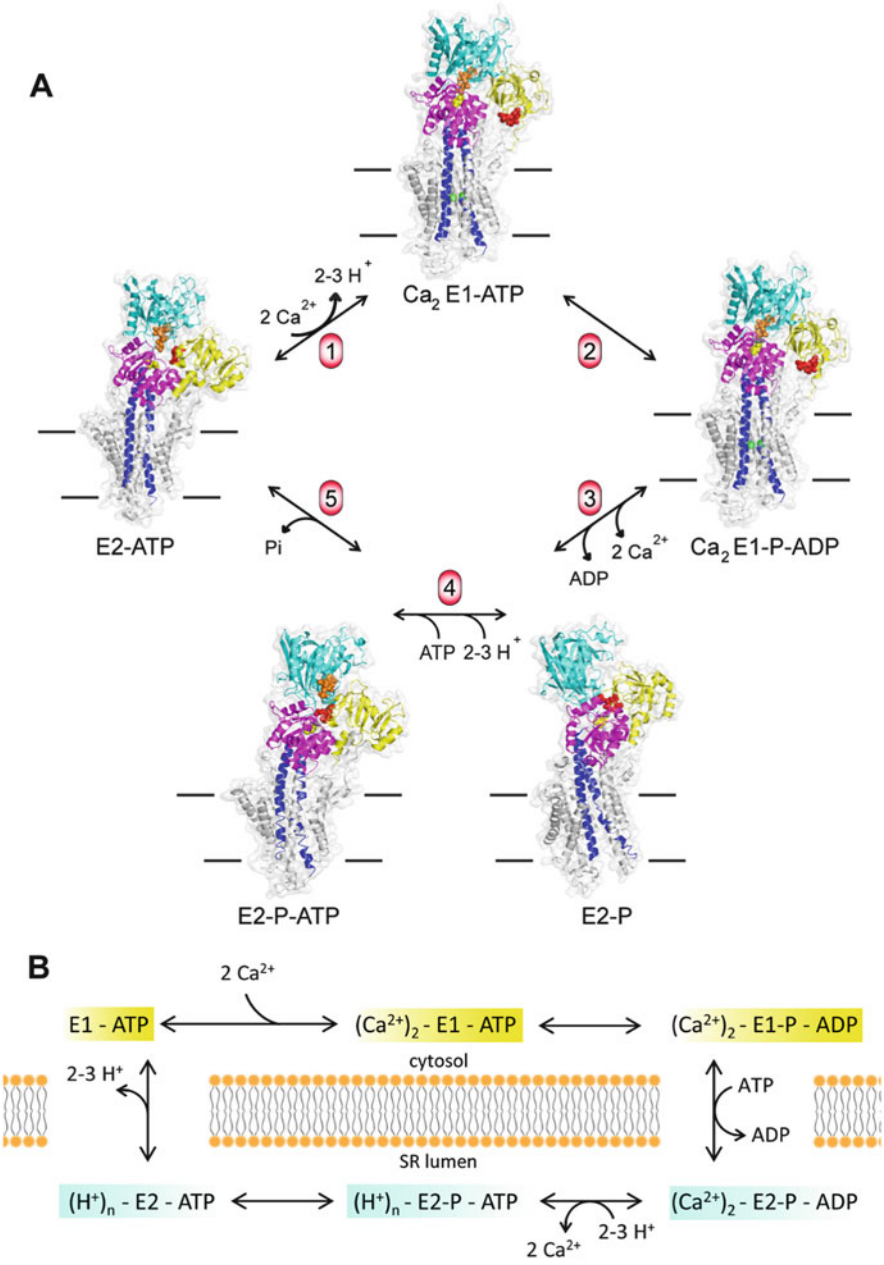

Fig. 5.1 SERCA calcium transport cycle. (**a**) Transparent surface and cartoon representations of key structures of SERCA in the calcium transport cycle. P-domain of SERCA is magenta, N-domain is cyan, A-domain is yellow, and helices TM1–10 are grey except TM4 and TM5 which are blue. Calcium ions are shown as green spheres, nucleotide (ATP or ADP) is shown as orange spheres, and TGES motif residues are shown as red spheres (PDBs: 1T5T, 1T5S, 3B9B, 3B9R, 2C8K). (**b**) Post-Albers scheme for the SERCA reaction cycle. SERCA exists in either an E1

shown to not only play a catalytic but also a modulatory role in the transport cycle [31]. At physiological concentrations, ATP appears to bind to SERCA in various intermediate states and accelerate partial reaction steps involved in calcium binding, calcium translocation, and dephosphorylation of SERCA. Although the details of this stimulatory action of ATP on SERCA are still largely unexplained, some structural studies revealed that the modulatory binding site overlaps with the catalytic one [31–33]. Therefore, it is now accepted that ATP (or ADP) is bound to every intermediate in the pump's transport cycle.

5.4 Structural Studies of SERCA

SERCA is the best studied member of the P-type ATPase family as a result of numerous functional and structural studies carried out in the last few decades. The three dimensional structure of rabbit SERCA1a was the first to be determined and for a long time served as a model for the architecture and molecular mechanism of other P-type ATPases. Despite the difficulties associated with crystallization of membrane proteins, over 60 high-resolution X-ray crystallographic structures have been solved, revealing the pump's structural complexity. These atomic models cover nearly all of the reaction intermediates, which correspond to the different conformations that the enzyme assumes during the calcium transport cycle.

In 1985, MacLennan and coworkers proposed a secondary-structure model of SERCA based on an amino acid sequence of rabbit SERCA1a [34]. This model predicted the SERCA pump to consist of ten membrane spanning helices and three cytoplasmic domains. In the following years, extensive mutagenesis studies identified many important functional features of the pump and the involvement of transmembrane segments in calcium binding [35]. Together with initial electron microscopy data [36], these early studies gave the first clues to the architecture and function of SERCA. In 1993, the first complete three dimensional structure of SERCA was obtained by cryo-electron microscopy [37]. Tubular crystals of SERCA in the presence of vanadate, a key crystallization component which traps P-type ATPases in an E2 conformation, provided three dimensional maps to 14 Å resolution. This early structure revealed a large cytoplasmic domain connected to the transmembrane domain via a short stalk region. A more detailed view of the calcium pump was achieved in 1998 when an improved 8 Å resolution structure of SERCA was obtained [38]. This was mainly accomplished by crystallizing SERCA in the presence of a high-affinity inhibitor thapsigargin (TG), which is known to

Fig. 5.1 (continued) (high affinity for calcium; yellow) or E2 (low affinity for calcium; blue) state. Two cytosolic calcium ions are exchanged for two to three luminal protons. Nucleotide is always bound, either in a catalytic or modulatory mode, and SERCA is auto-phosphorylated at a conserved aspartic acid residue (Asp^{351})

stabilize the transmembrane segments of the enzyme. The new structure of SERCA determined by electron microscopy provided an enhanced view of the transmembrane domain which was observed to be composed of ten transmembrane helices consistent with the previously proposed secondary-structure model [34].

The first high resolution structure of SERCA was obtained by X-ray crystallography in 2000 by Toyoshima and coworkers and represented a great milestone in the field [39]. The structure was solved to 2.6 Å resolution and depicted a calcium bound $(Ca^{2+})_2$-E1 SERCA intermediate. The new SERCA structure largely confirmed previous models but allowed for examination of the calcium pump at an atomic level. The SERCA X-ray structure confirmed that the transmembrane domain of SERCA indeed consists of ten transmembrane (TM) helices, two of which (TM4 and TM5) are long and extend from the membrane into the cytoplasmic domain. It also revealed two high affinity calcium binding sites (site I and II) in the transmembrane domain which are located side-by-side and close to the cytoplasmic surface of the membrane. Experimental evidence suggests a sequential and cooperative mode of calcium binding to SERCA, where binding of the first calcium ion results in a conformational change in the enzyme leading to an increased affinity for the second calcium ion [35]. This has been confirmed by mutagenesis studies which revealed that mutations in site I prevent binding of calcium at both sites, whereas mutation within site II only interfered with calcium binding to that site and not site I [40]. Interestingly, the amino acids involved in calcium binding seen in this structure are in high agreement with previous mutagenesis studies.

The large cytoplasmic headpiece of the pump was visualized as three distinct domains: the nucleotide binding (N), phosphorylation (P), and actuator (A) domains. The N-domain is the largest of the three cytoplasmic domains and is responsible for recruiting and positioning ATP to allow phosphorylation to occur. The nucleotide binding pocket within this domain contains a highly conserved residue, Phe^{487}, which interacts with the adenine ring of the ATP molecule. The N-domain is connected to the highly conserved P-domain via a flexible hinge region. Located in the top region of the P-domain is a conserved DKTGT motif, which includes an aspartate residue (Asp^{351} in SERCA) necessary for formation of the high energy aspartyl-phosphate intermediate. In this first $(Ca^{2+})_2$-E1 crystal structure, the phosphorylation site was located ~30 Å away from the nucleotide binding site, and thus provided little information as to how the phosphorylation event is coupled to calcium transport. Finally, the smallest cytosolic domain is the A-domain and it is well separated from the other cytosolic domains. Its role is to coordinate movements in the cytoplasmic domain that occur during the reaction cycle with movements in the membrane domain, allowing for calcium translocation to occur. The A-domain also controls the dephosphorylation reaction via the signature TGES sequence present in all P-type ATPases [29].

Although the first high resolution structure of SERCA provided a detailed description of the enzyme, it also raised new questions; particularly, the relation of the large conformational changes in the cytoplasmic domains and how they might translate to changes in the transmembrane domain and in turn affect calcium binding and dissociation. Many of these questions were answered in 2002 when Toyoshima

and coworkers released the second high resolution structure of SERCA in the calcium-free state [41]. This X-ray crystal structure was solved to 3.1 Å resolution and represented the E2-TG intermediate. Comparison of the $(Ca^{2+})_2$-E1 SERCA structure with the new E2-TG structure allowed a direct comparison of the enzyme in two distinct conformations at an atomic level. The new E2-TG SERCA structure revealed that in the absence of calcium the cytoplasmic domains drastically change their conformations and form a compact headpiece, consistent with the previous structures in the E2 state solved by electron microscopy. Comparing the $(Ca^{2+})_2$-E1 and the E2-TG structures, the N-domain inclines 60° relative to the P-domain and the P-domain inclines by about 30° with respect to the membrane and assumes a more upright position. The A-domain undergoes a ~110° horizontal rotation between the two states. Despite the large conformational changes, the overall structure of each cytoplasmic domain remains unchanged as SERCA transitions from the $(Ca^{2+})_2$-E1 to the E2-TG state. Therefore, the conformational changes are mainly restricted to the linker regions between the domains, strongly suggesting a critical role of the linker regions between the cytoplasmic and the transmembrane domains in proper SERCA function.

Nucleotide is bound to SERCA throughout the entire reaction cycle, either in a catalytic or modulatory mode. While the purpose of catalytic ATP binding is the autophosphorylation of Asp^{351}, the role of modulatory ATP binding is less obvious. At physiological concentrations of ATP (5–8 mM), SERCA is working at nearly maximum capacity and binding of modulatory ATP could provide a regulatory mechanism to ensure that SERCA can overcome rate-limiting reaction steps [42]. These mechanisms could include quick conversion rates between reaction intermediates, prevention of reversal of the reaction cycle by high ADP levels, or stabilization of reaction intermediates leading to efficient coupling of ATP hydrolysis and calcium transport [28]. While the physiological mechanism of modulatory ATP binding isn't evident, the structural evidence is clear and does not appear to be an artifact of crystallization using inhibitors [32, 33]. While this is contradicted by the publication of structures without nucleotide bound [41], it should be noted that SERCA can proceed through the reaction cycle with ATP concentrations well below physiological levels, where a significant number of SERCA molecules would not have bound modulatory nucleotide [28]. While this results in slower conversion rates between reaction intermediates, it provides an explanation for the absence of nucleotide in some structures of SERCA.

5.4.1 Structural Insights into the SERCA Calcium Transport Cycle

Since 2002, the SERCA field has benefited from dozens of high resolution structures crystallized in the presence of many different inhibitors and nucleotide analogues [28]. To date, we have a near complete understanding of reaction intermediates in the

SERCA transport cycle. While there are many SERCA structures available, only a selected few will be discussed herein to briefly describe the structural changes that accompany calcium transport.

SERCA structures representing the key reaction intermediates of the calcium transport cycle are shown in Fig. 5.1a. The reaction cycle begins with the enzyme in the calcium-free state and bound nucleotide (E2-ATP) depicted by the E2-AMPPCP crystal structure [31]. In the E2-ATP state, the A-domain is oriented in a manner suitable for close interactions with the P- and N-domains. The tight association of the cytoplasmic domains keeps the conserved TGES dephosphorylation motif away from the phosphorylation site and the γ-phosphate of the N-domain-bound ATP molecule away from the phosphorylatable Asp^{351} (~10 Å). In the absence of calcium, SERCA cannot be phosphorylated by ATP and the TGES loop remains withdrawn from the phosphorylation site, thus the E2-ATP conformation represents a resting state. For the γ-phosphate of ATP to come into proximity with Asp^{351}, SERCA needs to change its conformation. This is achieved upon binding of two cytosolic calcium ions in exchange for 2–3 protons, which results in the formation of the $(Ca^{2+})_2$-E1-ATP state represented by the $(Ca^{2+})_2$-E1-AMPPCP structure [43]. Binding of calcium ions leads to stabilization of the enzyme, and translational and rotational changes in transmembrane helices (TM1-4) that are later transmitted to the cytoplasmic domains. In the $(Ca^{2+})_2$-E1-AMPPCP structure, the A-domain is rotated counterclockwise allowing a small movement of the N-domain towards the P-domain and in turn closer approach of ATP to the catalytic Asp^{351}. In the following step, transfer of the γ-phosphate of ATP to Asp^{351} leads to the formation of the $(Ca^{2+})_2$-E1-P-ADP high-energy intermediate represented by the $(Ca^{2+})_2$-E1-ADP-AlF_4^- structure [43]. Although the $(Ca^{2+})_2$-E1-AMPPCP and the $(Ca^{2+})_2$-E1-ADP-AlF_4^- structures are quite similar, subtle rearrangements lead to occlusion of calcium ions in the $(Ca^{2+})_2$-E1-P-ADP state as confirmed by experimental studies. Another important difference between these two complexes is related to the cation coordination of bound nucleotide. Unlike the $(Ca^{2+})_2$-E1-AMPPCP structure where only one magnesium ion coordinates the γ-phosphate of the AMPPCP molecule, the $(Ca^{2+})_2$-E1-ADP-AlF_4^- structure reveals one magnesium coordinating AlF_4^- and a second magnesium coordinating the α- and β-phosphates of ADP. The second magnesium is only present in a transition state and is thought to lower the activation energy required for the phosphate transfer [28]. Once the transfer of the γ-phosphate from ATP to Asp^{351} is complete, the enzyme transitions to the low energy E2-P-ATP state depicted by the E2-BeF_3^- structure. At this time, bound ADP is exchanged with an ATP molecule. Direct comparison of the $(Ca^{2+})_2$-E1-ADP-AlF_4^- and the E2-BeF_3^- structures reveals a 50° rotation of the N-domain relative to the P-domain and a clockwise 108° rotation of the A-domain. This drastic movement of the A-domain causes a lateral movement of the TM1-TM2 and TM3-TM4 pairs relative to the TM5-TM10 complex, which results in the formation of a luminal access channel. This conformational change orients the side chains of the calcium binding residues towards the lumen allowing for the release of calcium ions to take place. It is important to mention that the E1-P to E2-P transition is thought to occur in two steps: formation of the calcium

occluded $(Ca^{2+})_2$-E2-P intermediate followed by the opening of the channel [28]. Unfortunately, the structure of the occluded $(Ca^{2+})_2$-E2-P intermediate has not yet been determined. As the calcium ions leave the luminal channel, 2–3 protons are taken up to partially compensate for the negatively charged carboxylate groups at the ion binding sites. This is followed by closure of the luminal channel and transition into the $(H^+)_{2-3}$-E2-P-ATP proton occluded state represented by the E2-AlF_4^--ATP structure [29]. In this conformation, the conserved TGES motif located on the A-domain docks into the phosphorylation site and coordinates water molecules for a hydrolytic cleavage of the phosphate group. Following dephosphorylation, the enzyme assumes a more relaxed state and the TGES motif is retracted from the phosphorylation site allowing release of the bound phosphate. In the final step of the reaction cycle, SERCA returns to the E2-ATP state and is ready for the next pair of cytosolic calcium ions to bind.

5.5 Regulation of SERCA by Phospholamban

5.5.1 Introduction to Phospholamban

PLN is the predominant regulator of SERCA in cardiac, smooth and slow-twitch skeletal muscle [11]. PLN is a 52-amino acid type I integral membrane protein that contains three distinct domains: a cytoplasmic domain Ia (residues 1–20) with two phosphorylation sites (Ser^{16} and Thr^{17}), a flexible linker domain Ib (residues 21–30), and a hydrophobic transmembrane domain II (residues 31–52) (Fig. 5.2a). PLN exists in a dynamic equilibrium between monomeric and pentameric states. While the monomer is considered the "active" inhibitory species, the pentamer has historically been regarded as an "inactive" storage form of PLN. In its dephosphorylated state, PLN functionally interacts with SERCA and lowers its apparent affinity for calcium. This inhibition is reversed either by elevated cytosolic calcium or by phosphorylation of PLN at Ser^{16} by cAMP-dependent protein kinase A (PKA) or Thr^{17} by calcium/calmodulin-dependent protein kinase II (CaMKII) or protein kinase B (Akt) [11]. Modeling of the NMR structure of PLN onto crystal structure of SERCA, with restraints imposed by mutagenesis and cross-linking studies, revealed a hydrophobic groove in the transmembrane domain of SERCA formed by helices TM2, TM4, TM6 and TM9 to which PLN is thought to bind [44, 45]. This groove is open in the E2 calcium-free state of SERCA and closed in the E1 calcium-bound state. Since PLN binds to the open groove in the E2 conformation of SERCA, this provides a probable mechanism by which PLN inhibits the E2-E1 transition in the catalytic cycle of SERCA. The X-ray crystallography structure of SERCA1a and a gain-of-function PLN mutant revealed the conformation of the PLN transmembrane domain in complex with a cation-free E1-like conformation of SERCA1a [46].

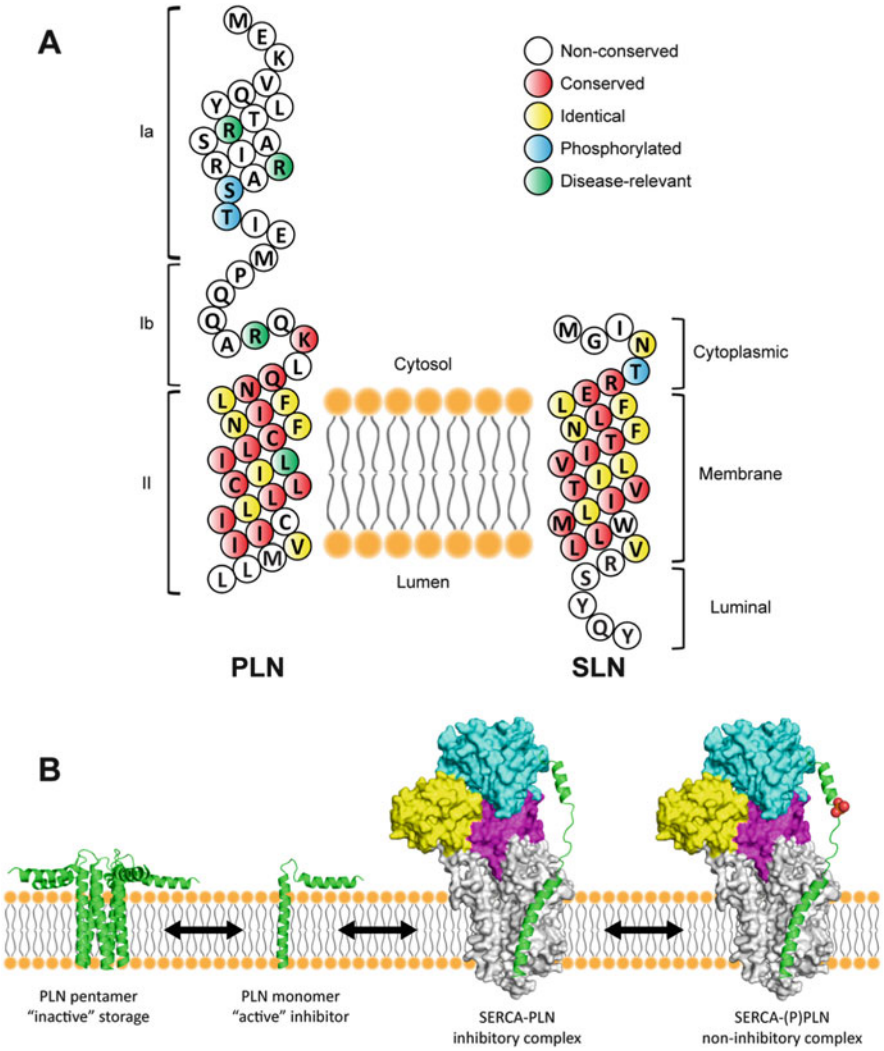

Fig. 5.2 (**a**) Topology models of PLN and SLN. PLN is 52 amino acids and its domain structure is shown on the left. SLN is 31 amino acids and its domain structure is shown on the right. Non-conserved, conserved, identical and phosphorylated residues are coloured according to the legend. Arg9, Arg14, Arg25, and Leu39 in PLN are indicated as residues that are disease-relevant. (**b**) Mass action theory. SERCA is shown in surface representation (P-domain is magenta, N-domain is cyan, A-domain is yellow, and transmembrane domain is grey) and PLN as a cartoon (green) representation. Phosphorylated PLN is shown with orange spheres on the cytoplasmic domain. PLN exists in dynamic equilibrium between pentameric and monomeric states, of which the monomer is the active inhibitory species. Monomeric dephosphorylated PLN functionally interacts with SERCA thereby inhibiting the pump. This inhibition can be relieved upon increased cytosolic calcium or phosphorylation of PLN

5.5.2 *Oligomerization of Phospholamban and the Theory of Mass Action*

Scanning mutagenesis of the transmembrane domain initially identified two helical faces of PLN: one was involved in pentamer formation and the other was involved in SERCA inhibition [47]. This was deduced because mutation of residues on one "face" of the helix resulted in loss of SERCA inhibition and had little effect on PLN pentamer formation, while mutation of residues on the other "face" of the helix resulted in superinhibition of SERCA by way of pentamer destabilization. These observations led to the "mass action" theory and the conclusion that the PLN monomer is the active inhibitory species and, upon dissociation from SERCA, oligomerized to form pentamers, a less active or inactive storage form of PLN [11] (Fig. 5.2b). Mutations that prevent pentamer formation were initially assessed by SDS-PAGE, and fluorescence resonance energy transfer (FRET) studies have shown that many of the mutations initially identified to prevent oligomerization actually do form pentamers (such as Ile^{40}-Ala), although they are more dynamic than wild-type PLN pentamers [48]. In fact, many mutations have been identified that do not abide by the mass action theory: several mutations in the transmembrane domain (Ile^{40}-Leu [49]) and domain Ib (Lys^{27}-Ala, Asn^{30}-Ala [50]) form pentamers normally but are superinhibitory, while another mutation (Cys^{41}-Phe [47]) is monomeric yet retains normal inhibitory function. This more recent work has shown that residues along the entire circumference of the transmembrane helix of PLN contribute to SERCA inhibition [49]. However, despite evidence to the contrary, the mass action theory is still the currently accepted model of PLN inhibition of SERCA, primarily because of the absence of an alternative suitable model.

The PLN pentamer is formed and stabilized by a leucine-isoleucine zipper with equivalent contributions made by all five monomers (Fig. 5.3). However, the role of the transmembrane cysteines (Cys^{36}, Cys^{41} and Cys^{46}) in pentamer formation has been of great interest. The chemistry of the cysteine side chain would allow for disulfide bond formation, which could aid in pentamer formation. However, mutation of the transmembrane cysteines results in normal SERCA inhibition while completely preventing pentamer formation, which appears to contradict the mass action theory [47]. However, it has been shown that while these cysteines are not important for pentamer formation, they are important for pentamer stability and the chemical properties of the sulfhydryl group play only a minor role in the structure of the pentamer [51]. Labelling studies using a thiol-reactive spin label found that Cys^{41} is buried within the PLN pentamer, but Cys^{36} and Cys^{46} are readily accessible to labelling in PLN pentameric states [52]. These studies led to the generation of an AFA PLN mutant (Cys^{36}-Ala, Cys^{41}-Phe, Cys^{46}-Ala), which has been a commonly used tool for studying the structure and function of the PLN monomer.

During muscle contraction and relaxation, inhibition of SERCA by PLN is reversed by either high cytosolic calcium or phosphorylation of PLN. The prevailing dogma suggests that monomeric PLN dissociates from SERCA and reassembles into pentamers. Most studies agree on the PLN monomer as the active inhibitory species

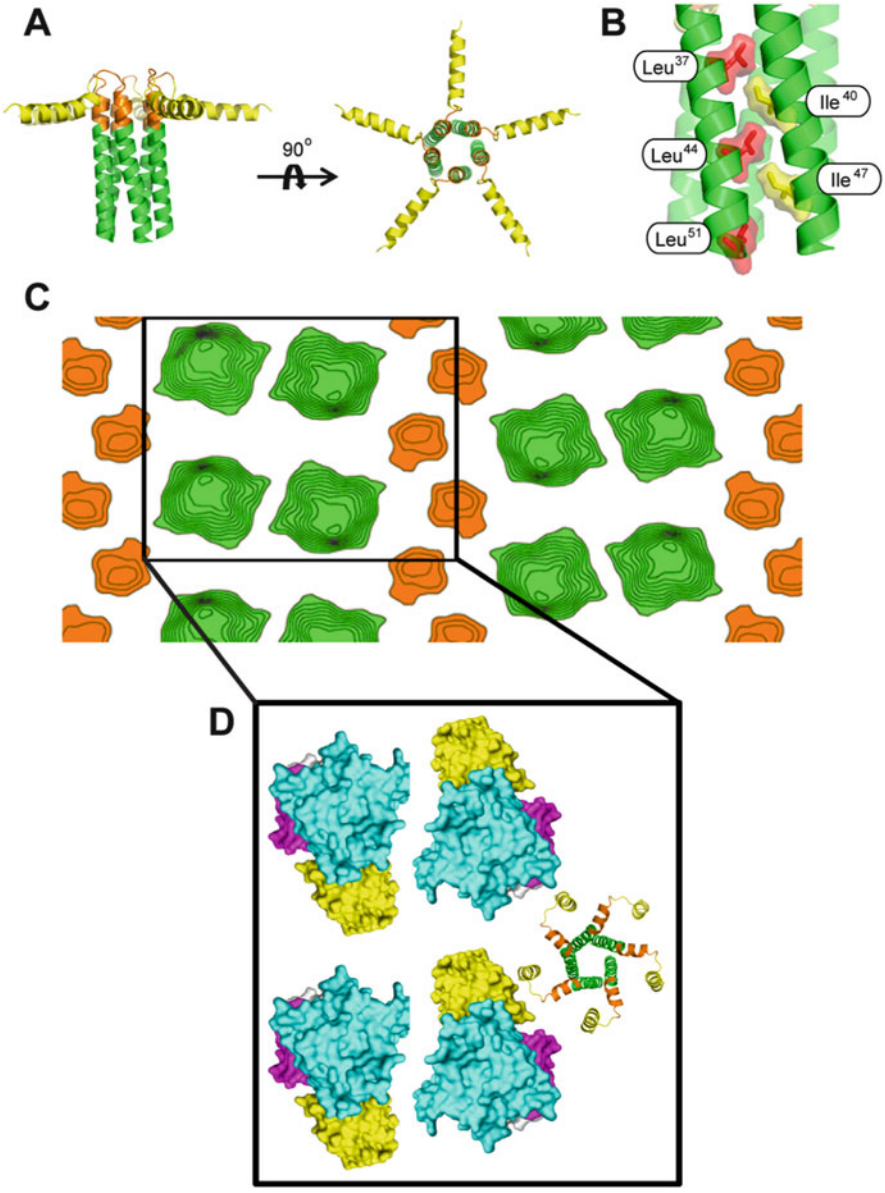

Fig. 5.3 Structure of the PLN pentamer and its interaction with SERCA. (**a**) The "pinwheel" model of the PLN pentamer (left: side view, right: top-down view; PDB 2KYV). (**b**) Domain II leucine-isoleucine motif in the "pinwheel" model. Leucine side chains (shown as stick and space filling representation in red) interact with isoleucine side chains (shown as stick and space filling representation in yellow) of the neighboring PLN monomer. (**c**) Projection map from cryo-electron microscopy of SERCA and PLN co-crystals. Positive contours are colored for the characteristic anti-parallel SERCA dimer ribbons (green) and the associated oligomeric PLN densities (orange). (**d**) Model for the interaction of SERCA (PDB 1KJU) with pentameric PLN (PDB 1ZLL) based on the projection map from 2D co-crystals. SERCA and PLN are in surface and cartoon representations, respectively

of SERCA [49], but the role of the PLN pentamer has remained an anomaly. While some studies disregard it as an inactive storage form of PLN [53], others have determined that the channel-like architecture of the pentamer may enable it to conduct ions, such as calcium [54] or chloride [55]. Electron microscopy studies have found evidence of a physical interaction between the PLN pentamer and SERCA [56]. This interaction was shown to be at an accessory site distinct from the inhibitory interaction of the PLN monomer and required functional PLN for the interaction to occur [57] (Fig. 5.3). In addition, the X-ray crystallography structure of the complex between SERCA and a gain-of-function PLN mutation revealed a second PLN monomer that doesn't come into contact with SERCA [46]. While the physiological role of PLN oligomerization isn't understood, it is clear that it is important. Transgenic mice expressing a monomeric mutant of PLN (Cys^{41}-Phe) revealed a defect in relaxation and depressed cardiac function, despite the fact that SR calcium transport assays were identical for wild-type and Cys^{41}-Phe PLN [58]. While the monomer may be the active inhibitory species of PLN, the pentamer is clearly necessary for optimal regulation of contractility in the heart.

Another convoluting factor is the phosphorylation of PLN and its effect on SERCA and PLN oligomerization. Phosphorylation of PLN causes reversal of SERCA inhibition, which was originally thought to take place by dissociation of the inhibitory complex, resulting in PLN oligomerization. However, most studies agree that phosphorylated PLN remains associated with SERCA [59], implying that PLN can retain non-inhibitory interactions with SERCA. Electron paramagnetic resonance (EPR) studies have shown that phosphorylation of PLN promotes pentamer formation [60] and this was confirmed with a phospho-mimetic mutant (Ser^{16}-Glu) of PLN studied with nuclear magnetic resonance spectroscopy (NMR) [61] and FRET [62]. This is in contrast to what is observed by SDS-PAGE, where there is no difference in the pentamer to monomer ratio upon phosphorylation [63]. Structures of phosphorylated PLN pentamer and SERCA obtained by electron microscopy have confirmed that phosphorylation of PLN causes a selective disordering of the cytoplasmic domain but the transmembrane domain retains interactions with SERCA [57]. Additionally, PLN pentamer interactions with SERCA were at an accessory site (helix TM3 and the C-terminus) versus the inhibitory binding site of the PLN monomer (helices TM2, TM4, TM6 and TM9). This accessory interaction may facilitate directed diffusion of monomeric or phosphorylated PLN to-and-from the inhibitory site of SERCA, thereby offering one explanation for how phosphorylated PLN retains interactions with SERCA in a non-inhibitory state.

5.5.3 SERCA Inhibition by Phospholamban

Mutagenesis has been a powerful tool to study the residues in the transmembrane domain of PLN that are important for SERCA inhibition. Early mutagenesis studies identified two "faces" of the PLN helix: one side formed a leucine-isoleucine zipper

that was important for pentamer formation and one side was important for the inhibitory interaction with SERCA. Alanine mutagenesis of the transmembrane domain of PLN determined that mutation of residues that resulted in gain of inhibition must not interact with SERCA [47]; however, later studies showed that amino acid substitutions other than alanine produced different results [49]. Many residues that were initially thought to only be involved in PLN pentamer formation were now shown to also be involved in the inhibitory interaction with SERCA. This revealed that residues along most of the circumference of the transmembrane domain of PLN were involved in SERCA inhibition, including Leu^{31}, Asn^{34}, Phe^{35}, Ile^{38}, and Leu^{42}. When mutated to alanine, they resulted in severe or complete loss of SERCA inhibition (e.g. Asn^{34}-Ala results in complete loss of function) even when combined with superinhibitory mutations (double mutant Asn^{34}-Ala, Ile^{40}-Ala still results in complete loss of function [47]). PLN is thought to inhibit SERCA through mostly hydrophobic interactions, so is it particularly odd to see a polar asparagine residue embedded in the membrane; however, asparagine residues in transmembrane helices have been found to have important functional roles and contribute to thermodynamic stability [64]. In order to examine the role of each individual residue, SERCA co-reconstitution studies have been done with α-helical peptides mimicking the transmembrane domain of PLN. A peptide consisting of all the native leucine residues in the transmembrane domain of PLN with all other residues mutated to alanine resulted in approximately 80% of wild-type inhibition of SERCA, revealing that a simple hydrophobic surface was enough for partial SERCA inhibition [65]. Addition of the essential asparagine residue of PLN in its native position in this peptide resulted in superinhibition of SERCA, which might be expected considering the severe loss of function with the Asn^{34}-Ala mutant [65]. Moving the asparagine upstream or downstream by one residue or one turn of the helix in the peptide revealed the importance of the correct positioning of an asparagine residue in PLN [66]. These studies further defined the inhibition of SERCA by PLN: not only is a hydrophobic surface necessary for inhibition but an asparagine residue is required for probable hydrogen bonding to SERCA at Thr^{805} and/or Thr^{317} [44, 66]. Furthermore, the PLN binding site on SERCA can accept a variety of simple hydrophobic peptides that lead to at least partial SERCA inhibition, and the functional role of individual PLN residues depends on the surrounding amino acid sequence.

The inhibitory interaction between SERCA and PLN has been well-studied and there is a wealth of information on the role of particular PLN residues in inhibition and oligomerization. Mutagenesis studies have identified important residues in PLN for SERCA inhibition as measured by SERCA-dependent calcium transport [67] or ATP hydrolysis (indirect measurement by coupled-enzyme assays) [68]. Initial studies identified the transmembrane domain of PLN as having a key inhibitory role, as deletion of the cytoplasmic domain of PLN or the cytoplasmic domain by itself had minimal effects on SERCA activity [67]. However, other studies have found that mutation of some residues in the cytoplasmic domain of PLN can cause a slight loss of SERCA inhibition compared to wild-type PLN [69]. Examining the role of the cytoplasmic domain of PLN alone on SERCA activity is challenging, as it is usually anchored to the SR membrane by the transmembrane domain and in close

proximity to SERCA. Experiments done with SERCA in the presence of a cytoplasmic PLN peptide have been conflicting, as some studies have reported an effect [70, 71] and others have not [72]. However, there is an enormous molar excess of cytoplasmic peptide needed in these experiments (300-fold excess) so the physiological relevance of these results is debatable. It is generally agreed upon that the transmembrane domain provides the majority of PLN's inhibitory capacity (~80%), while the cytoplasmic domain provides reversibility and the remaining inhibitory capacity (~20%). However, the discovery of hereditary mutations in the cytoplasmic domain of PLN [73–75] that cause complete loss of SERCA inhibition and heart failure conflict with the generalization that the cytoplasmic domain of PLN plays a small role in inhibition.

5.5.4 *Structural Studies of Phospholamban and SERCA/Phospholamban Complex*

Several structures of PLN have been obtained by NMR spectroscopy, which is an ideal technique for small proteins up to 30 kDa in size. The propensity of PLN to oligomerize has made it difficult to study the structure of monomeric PLN; however, monomeric mutants of PLN, such as Cys^{41}-Phe or AFA (Cys^{36}-Ala, Cys^{41}-Phe, Cys^{46}-Ala) PLN, have facilitated the process. Traaseth et al. determined the structure of a PLN monomer in lipid bilayers and showed that it consists of two α-helices (domains Ia and II) that are connected by a short β-turn [76]. This agreed well with a prior NMR structure in organic solvent, though this latter structure was more helical [77]. Both of these structures were of monomeric PLN and the composition of the lipid bilayer is thought to play a significant role in the structure of PLN and its inhibition of SERCA, with bilayer thickness and the composition and saturation of lipids having effects on SERCA activity [78]. However, most structures of PLN, including models of the PLN pentamer, indicate a flexible region connecting the cytoplasmic and transmembrane helices. This region of PLN performs two essential functions: the positive charges (e.g. Lys^{27}) fine-tune the inhibitory interaction with SERCA and it transmits phosphorylation of the cytoplasmic domain (e.g. Ser^{16} in domain Ia) to relief-of-inhibition in the transmembrane domain (domain II).

The quaternary structure of the PLN pentamer is stabilized by a leucine-isoleucine zipper, which is formed by contributions from all five PLN monomers. There have been many structural studies performed on the PLN pentamer with conflicting results. Two main models emerged for the structure of the pentamer, a pinwheel conformation with the cytoplasmic domains perpendicular to the bilayer normal interacting with the phospholipid headgroups [79], and a bellflower conformation with the cytoplasmic domains perched above the bilayer surface [55] (Fig. 5.3). While the pinwheel conformation has become the consensus model, the inherent flexibility of the cytoplasmic domain, and differing experimental conditions

(detergent micelles, lipid micelles, oriented lipid bilayers) and techniques (solid state NMR, solution state NMR) can all influence the structure obtained. Also, PLN is not alone in the SR membrane and the presence of SERCA and other SR components could alter its structure and dynamics. The pinwheel and bellflower structural models of the PLN pentamer both adhere to the proposed leucine-isoleucine zipper for pentamer formation; though neither model completely explains all experimental observations. It has been shown that the cytoplasmic domain of PLN interacts with phospholipid headgroups [80] and that lipid composition can alter SERCA activity, both in the absence and presence of PLN [78]; these interactions would not be possible with the bellflower model. Although PLN inhibits SERCA primarily through intramembrane interactions, there is sufficient evidence for a physical interaction between the cytoplasmic domains of PLN and SERCA [67, 69]. Most compelling, Lys^{3} in the cytoplasmic domain of PLN was found to cross-link to Lys^{397} and Lys^{400} in the N-domain of SERCA [81]. The pinwheel model of the PLN pentamer implies a lack of a physical association between the cytoplasmic domain of PLN and SERCA, though this domain must undergo a structural transition in the SERCA-PLN inhibitory complex [82, 83].

There were several early models of the inhibitory SERCA-PLN complex derived from X-ray crystal structures of SERCA, NMR structures of the PLN monomer, and cross-linking data [44]. The models of SERCA and PLN identified a groove formed by helices TM2, TM6 and TM9 of SERCA in the E2 state that could accommodate PLN; this groove closes as SERCA transitions into the E1-$(Ca^{2+})_2$-ATP state, such that PLN would impede the conformational transition of SERCA [44]. The solid state NMR structure of a PLN monomer in the presence of SERCA [82] satisfied cross-linking data and was similar to an initial model presented by Toyoshima and coworkers using an NMR structure of a free PLN monomer and an X-ray crystal structure of SERCA [44]. While mutagenesis data has been important for determining a functional interaction between PLN and SERCA, cross-linking has proved the existence of a physical association. The first evidence of a physical interaction between PLN and SERCA was the cross-linking of the ε-amino group of Lys^{3} to Lys^{397} and Lys^{400} of SERCA [81]. The cross-link did not form in the presence of calcium or when PLN was phosphorylated. The close proximity of Lys^{397} and Lys^{400} to Asp^{351} led the authors to speculate that PLN inhibition might affect formation of the SERCA aspartyl-phosphate intermediate. Since this seminal observation, additional attempts to cross-link the cytoplasmic domain of PLN to SERCA have failed [84, 85], though the models show that this interaction is plausible and would require small structural alterations in PLN to occur. In more recent cross-linking studies [59, 84–87], cross-linking of PLN to SERCA was dependent on the presence of nucleotide and abrogated by calcium; additionally, the presence of SERCA inhibitors (e.g. thapsigargin) prevented cross-linking. With this in mind, recall that the structural models of the SERCA-PLN complex have been generated using the nucleotide-free, thapsigargin-inhibited structure of SERCA [44]. Thus, while these models do provide insight into the interaction between SERCA and PLN, they may not represent the physiological inhibitory complex. In addition, the physical interaction between SERCA and PLN does not necessarily correlate with

inhibition, as a cross-link between a loss-of-function form of PLN (Leu^{31}-Cys) and SERCA proved that a non-inhibitory form of PLN could still interact with SERCA [85]. Finally, the structure of a gain-of-function mutant of PLN in complex with SERCA was determined by X-ray crystallography [46]. In this structure, PLN stabilizes a novel calcium-free E1-like conformation of SERCA, which is quite distinct from the expected calcium-free E2 conformation of SERCA upon which the SERCA-PLN molecular models were based.

5.5.5 Regulation of Phospholamban

The inhibitory capacity of PLN can be modified through several different mechanisms. PLN is "capped" at its N-terminal methionine residue by post-translational acetylation. While initial studies with a cytoplasmic peptide reported this acetylation to have an effect on inhibition of SERCA [88], later studies on the full-length protein showed no effect on SERCA inhibition or PLN oligomeric state [51]. Nitric oxide-dependent *S*-nitrosylation of PLN has also been observed and, since this post-translational modification affects cysteine residues, it would modify PLN in the transmembrane domain (Fig. 5.2a). Initial experiments have shown greater *S*-nitrosylation of the PLN pentamer compared to the monomer, which resulted in an increase in SERCA activity independent of PLN phosphorylation [89]. HCLS1-associated protein X-1 (HAX-1), a ubiquitously expressed cytosolic protein that protects cardiomyocytes from cell death, has also been implicated in regulation of the SERCA-PLN complex [90]. It interacts with the cytoplasmic domain of PLN and was found to inhibit SERCA activity, presumably through increasing the monomer to pentamer ratio of PLN in the SR. HAX-1 preferentially localizes to the mitochondria; however, in the presence of PLN, it redistributes to the SR. These findings, along with the observation that SR calcium load is linked to apoptotic sensitivity in the cell, point to a critical role in communication between the SR and mitochondria in determining cell fate. In addition, HAX-1 recruits the small heat shock protein 90 (Hsp90) from the ER to the PLN-SERCA2a complex, implying an association between calcium homeostasis and ER stress signaling. PLN also binds to multiple A-kinase anchoring proteins (AKAP7γ/δ; AKAP15; AKAP18δ), as well as the anchoring subunit of protein phosphatase-1 (PP-1), muscle glycogen-targeting subunit of protein phosphatase 1 (Gm) [90]. These interactions allow for careful modulation of PLN phosphorylation status and SERCA activity. PP-1 interacts with inhibitor-1 and small Hsp20, both of which are regulators of PP-1 activity and calcium cycling, and phosphorylation of inhibitor-1 or Hsp20 by PKA increases PLN phosphorylation and contractility in the heart. The activation of Hsp20 (through phosphorylation) coupled with inactivation of inhibitor-1 (through dephosphorylation) during heart failure exemplify the complex regulation of PLN through its associated proteins.

PLN was initially identified as a major cardiac SR phospho-protein, thus providing the inspiration for its name (phospholamban was derived from *phosphate* and the

Greek word '*to receive*' [91–93]). The primary role of the cytoplasmic domain is reversal of PLN inhibition of SERCA through phosphorylation. Under basal conditions, approximately half of the PLN in the SR is phosphorylated or non-inhibitory [11]. During exercise, stress or disease, the ratio of phosphorylated to non-phosphorylated PLN can change, resulting in altered SERCA activity. PLN is phosphorylated by PKA at Ser^{16} [11] and by protein kinase B (Akt) [94] or CaMKII [11] at Thr^{17}; it was also shown to be phosphorylated in vitro by protein kinase C at Ser^{10} but this has not been confirmed in vivo [95]. The role of dual-site phosphorylation is not entirely understood, since phosphorylation of PLN at either Ser^{16} or Thr^{17} is sufficient for complete reversal of SERCA inhibition. Also, there is some inconsistency in the literature as to whether or not these sites are phosphorylated independently or if phosphorylation of one is dependent upon phosphorylation of the other. In vitro, Ser^{16} and Thr^{17} can be phosphorylated independently; however, phosphorylation of Ser^{16} is a prerequisite for Thr^{17} phosphorylation during β-adrenergic stimulation in vivo [96]. In the absence of β-adrenergic stimulation, phosphorylation of Thr^{17} does occur but is predominant only in pathophysiological conditions, such as acidosis [97]. Using synthetic phosphopeptides, the phosphorylation states of PLN were stoichiometrically quantified and their relative effects on SERCA were determined [98]. Ser^{16}-phosphorylated PLN is the most highly populated state of PLN in cardiac homogenates followed by unphosphorylated PLN then dual phosphorylated PLN, with Thr^{17}-phosphorylated PLN being the least populated state. Of the phosphorylated PLN states, SERCA inhibition is most relieved by Ser^{16} phosphorylation followed by dual phosphorylation and then Thr^{17} phosphorylation of PLN.

While phosphorylation of PLN completely reverses SERCA inhibition, co-immunoprecipitation studies have shown that phosphorylated PLN retains interactions with SERCA [99]. It is noteworthy to point out that it was initially found that treatment of PLN with an anti-PLN antibody (2D11) resulted in reversal of SERCA inhibition [100] and this has been used as a technique to mimic phosphorylation [59]. Spectroscopic and NMR studies have shown that phosphorylation induces an order-to-disorder conformational change in the cytoplasmic domain of PLN [101]. The "ordered" state of PLN has the cytoplasmic domain directly in contact with the membrane while it is detached from the membrane in the "disordered" state. This was attributed to the flexibility of the "hinge" region of domain Ib of PLN. Interestingly, this conformational change is also seen with an increase in magnesium concentration, as it supposedly disrupts interactions between the negatively charged phospholipid headgroups and the positively charged cytoplasmic domain of PLN, but was not influenced by changes in potassium concentration. Changes in calcium concentration did not have an effect on the order-to-disorder equilibrium, suggesting that relief of SERCA inhibition by phosphorylation and micromolar cytosolic calcium concentration occur by different mechanisms [102]. According to the currently accepted model of SERCA inhibition, PLN becomes phosphorylated while bound to SERCA, requiring a tertiary complex to be formed between SERCA, PLN and the kinase. Models of SERCA and PLN reveal that there is space for a kinase to fit although there is no structural information on this complex [44]. Structural and functional studies of PKA and peptide substrates have shown

that PKA requires an unstructured peptide to bind, requiring PLN to unwind between Thr^{8} and Glu^{19} in order for phosphorylation to occur [11]. Solution NMR studies on the structure of AFA PLN showed phosphorylation to cause unwinding of domain Ia [103], while other studies on wild-type PLN using circular dichroism or Fourier transform infrared methods found that phosphorylation resulted in no structural changes at all [104, 105]. More recent solution NMR studies have examined the conformational dynamics of PLN binding to PKA, and a single deletion of an arginine in PLN's recognition sequence for PKA reduces its binding affinity and dramatically reduces phosphorylation kinetics [83, 106]. Molecular dynamics simulations have suggested that phosphorylation causes a salt bridge to form between the phosphorylated serine and Arg^{9}, Arg^{13} and/or Arg^{14} of PLN, and these salt bridges trigger disordering of the cytoplasmic α-helix, resulting in loss of SERCA inhibition [107]. In general, most studies agree that phosphorylation induces disorder in the cytoplasmic domain of PLN, which is responsible for reversal of SERCA inhibition.

5.5.6 Phospholamban in Heart Failure

Since 2003, several mutations in PLN have been identified that lead to familial dilated cardiomyopathy (DCM) in humans by affecting SERCA inhibition by PLN and PKA-mediated phosphorylation of PLN [73–75, 108, 109]. All residues in PLN at which hereditary mutations that cause DCM have been found are shown in Fig. 5.2a and a model of heart disease caused by SERCA dysregulation is shown in Fig. 5.4a–c.

5.5.6.1 Arg^{9}-Cys (R9C)

In 2003, the first human mutation in PLN that causes DCM was identified. A dominant arginine to cysteine missense mutation at residue 9 (R9C) in the cytoplasmic domain of PLN was found in a large family and cosegregated with heart disease [73]. The startling finding was the severity of disease caused by this mutation, with early symptom onset (between 20 and 30 years of age) quickly progressing to heart failure (5–10 years later). In many patients, the severity of the disease necessitated cardiac transplantation and the average age of death of affected individuals is 25. Interestingly, all patients that have been found are heterozygous for R9C PLN and no homozygous individuals have been identified. Transgenic R9C PLN mice also exhibited heart failure leading to early death [73]. Co-transfection of HEK293 cells with SERCA and R9C PLN revealed that R9C PLN does not inhibit SERCA and is not phosphorylated by PKA, implying that it is a complete loss of function mutant. It was concluded that R9C PLN prevents the phosphorylation of wild-type PLN by "trapping" PKA, as immunoprecipitation studies showed that increasing amounts of R9C PLN pulled down increasing amounts of PKA [73]. Further work

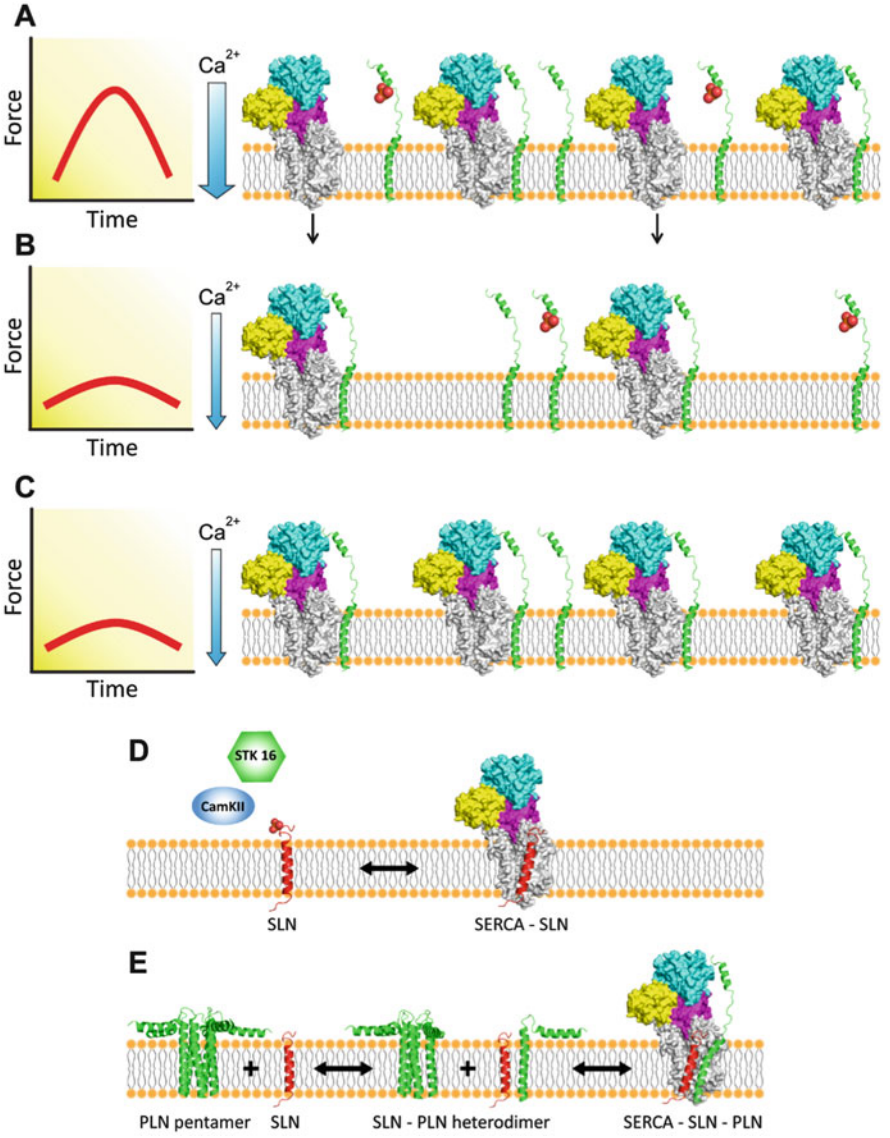

Fig. 5.4 Regulation of SERCA by PLN and SLN in the heart. SERCA is shown as a surface (P-domain is magenta, N-domain is cyan, A-domain is yellow, and transmembrane domain is grey) and PLN as a cartoon (green) representation. Phosphorylated PLN and SLN are shown with orange spheres on the cytoplasmic domains. (**a**) In healthy resting individuals, approximately half of PLN is inhibitory (non-phosphorylated), giving rise to normal calcium transients and pumping capacity of the heart. (**b**) During heart failure, SERCA expression is diminished, giving rise to super-inhibition of SERCA, decreased calcium transients, and decreased pumping capacity of the heart. (**c**) Hereditary mutations in PLN cause decreased calcium transients and pumping capacity of the heart, leading to heart disease. (**d**) SLN exists mainly as a monomer and upon interaction with SERCA it inhibits its activity. This inhibition can be relieved upon increased cytosolic calcium or phosphorylation of SLN by CaMKII or STK16. (**e**) Super-inhibition of SERCA by the SLN-PLN

using transgenic mice with a R9C PLN transgene and 2, 1 or 0 wild-type PLN alleles in mice determined that the disease-causing mechanism for R9C PLN is dependent on the presence of wild-type PLN [110]. It was also shown that R9C PLN increases the stability of the PLN pentameric assembly via disulfide bridge formation, preventing its binding to SERCA2a as well as phosphorylation by PKA [111]. These effects are increased under oxidizing conditions, suggesting that oxidative stress may exacerbate the cardiotoxic effects of R9C PLN. Comparative proteomics study on mice overexpressing R9C PLN identified changes in expression in proteins involved in ER stress, apoptosis and cytoskeletal remodelling, revealing widespread changes in the heart as a result of the R9C mutation in PLN [112]. Experiments performed in adult rabbit cardiomyocytes determined that R9C PLN reduces SERCA2a inhibition by decreasing the amount of inhibitory complex, resulting in acute inotropic and lusitropic effects but producing impaired frequency potentiation and blunted β-adrenergic responsiveness [113]. In purified SERCA-PLN proteoliposomes, it was found that R9C is a complete loss-of-function mutant of PLN. Importantly, in the presence of wild-type PLN to mimic heterozygous conditions, R9C exerts a dominant negative effect on the activity of SERCA [114]. Other hydrophobic substitutions at Arg^{9} (including Leu, Val, and Met) recapitulated the loss of function observed with R9C, identifying hydrophobic imbalance in PLN as a potential determinant for DCM. Additionally, R9C PLN could not be phosphorylated by PKA, which led to the identification of Arg^{9} as an important determinant of efficient phosphorylation by PKA despite the fact that Arg^{9} is not part of the canonical Arg^{13}-Arg-Ala-Ser^{16} PKA recognition motif of PLN [115].

5.5.6.2 Arg^{14}-Deletion (R14del)

In 2006, a second mutation was identified in the cytoplasmic domain of PLN that was linked to DCM in humans. Deletion of Arg^{14} (R14del) in PLN was found in a large Greek family with hereditary heart failure [74]. In the Netherlands, the R14del mutation is thought to be present in 10–15% of DCM patients, and the mutation is thought to have arose in the country 575–825 years ago [116]. While no homozygous individuals have been found, heterozygous individuals develop left ventricular dilation, contractile dysfunction and episodic ventricular arrhythmias by middle age. Transgenic R14del PLN mice recapitulate human cardiomyopathy, both in physiological and histopathological abnormalities [74]. Since Arg^{14} is part of the PKA recognition motif in PLN (Arg^{13}-Arg-Ala-Ser^{16}), it was hypothesized that the disease-causing mechanism is lack of a normal β-adrenergic response. However, it was found that R14del PLN is normally phosphorylated by PKA in HEK293 cells.

Fig. 5.4 (continued) heterodimers. SLN interferes with the PLN pentamer formation by direct interaction with PLN. The SLN-PLN heterodimers bind with higher affinity to SERCA than either SLN or PLN alone

This was a surprising finding, as mutation or deletion of Arg^{13} or Arg^{14} in PLN was previously shown to abolish PKA-mediated phosphorylation [69]. In a co-expression system, homozygous R14del PLN expression results in mild loss of SERCA inhibition and heterozygous R14del PLN expression results in SERCA super-inhibition, which is not fully reversed by PKA phosphorylation. This chronic suppression of SERCA activity was found to be caused by destabilization of mixed wild-type and R14del PLN pentamers, which increases the ratio of PLN monomer to pentamer in the SR. Immunofluorescence studies of HEK293 cells transfected with both wild-type and R14del PLN found that all PLN localizes to the ER. Another study examined the effect of R14del PLN in a PLN-null mouse (homozygous R14del) [117]. R14del PLN was found to be minimally phosphorylated at Ser16 by PKA and CaMKII-mediated phosphorylation of Thr17 was absent. Immunofluorescence studies found that R14del PLN does not co-localize in the SR with SERCA but rather is targeted to the plasma membrane where it interacts with the Na^+,K^+-ATPase. Examination of murine cardiac homogenates revealed that while R14del has no effect on calcium reuptake by SERCA (presumably because there is no PLN present in the SR), R14del PLN activates the Na^+,K^+-ATPase. Further confounding elucidation of the mechanism, examination of R14del PLN from patient cardiac explants and in human induced pluripotent stem cell-derived cardiomyocytes revealed mislocalization and aggregation of R14del PLN and an arrhythmogenic and hypertrophic phenotype [118, 119].

The R14del mutation in PLN was identified in another family with hereditary DCM in 2006 [120]. Strikingly, these two patients exhibited late-onset (60–70 years of age), mild DCM. Neither patient had any complaints related to heart failure although both had mildly impaired left ventricular performance. Notably, one patient was evaluated for muscular dystrophy because of slowly progressive muscle weakness with symptoms of leg pain and difficulty standing yet there were no problems in any other limbs. A skeletal muscle biopsy was normal and the patient tested negative for muscular dystrophy.

5.5.6.3 Arg^9-Leu (R9L) and Arg^9-His (R9H)

R9L and R9H were identified in DCM patients in Brazil in a study where over one thousand patients with a variety of DCM etiologies, including idiopathic, ischemic, Chagas, valvular, and hypertensive, were screened [75]. Of the two patients with R9L, one presented with idiopathic DCM and died at 30 years of age (her mother died of the same cause but no DNA was available for genotyping), and the second presented with Chagas disease and hypertension and she died at 69 years of age because of advanced heart failure. The patient with the R9H mutation died at 43 years of age due to idiopathic DCM. While R9L does appear to cosegregate with disease, clinical data point to the R9H mutation not causing DCM or being a low-penetrant allele because several relatives of this patient also had the R9H mutation and only one had cardiac disease. The potential disease-causing mechanisms of these two mutations were not discussed in this study but they did point out

that Arg^{9} is of paramount importance to proper PLN function and appears to be a "hot spot" for mutations linked to DCM. In purified SERCA-PLN proteoliposomes, it was found that R9L PLN behaves similarly to R9C PLN, resulting in complete loss of SERCA inhibition and lack of phosphorylation by PKA [114, 115]. R9H PLN results in normal SERCA inhibition but is not phosphorylated by PKA.

5.5.6.4 Leu^{39}-Stop (L39stop)

L39stop is the only mutation identified in the transmembrane domain of PLN, and both homozygous and heterozygous individuals have been identified [108]. Heterozygous individuals display hypertrophy without diminished contractile performance, while homozygous individuals develop DCM and heart failure, requiring cardiac transplantation before 30 years of age. Several heterozygous subjects were found to have normal left ventricular systolic function by echocardiographic examination, revealing incomplete penetrance of the L39stop phenotype. In HEK293 cells and adult rat cardiomyocytes, homozygous L39stop PLN had identical calcium uptake rates compared to SERCA alone, while heterozygous L39stop PLN was identical to wild-type PLN, indicating that L39stop PLN does not have a dominant effect on SERCA activity in the presence of wild-type PLN. It was also found that patients harboring the homozygous L39stop mutation have a 50% reduction in SERCA expression in cardiac SR, which likely contributes to disease. While wild-type PLN localizes to the ER in HEK293 cells, L39stop PLN was found on the plasma membrane; however, L39stop was also found in the insoluble fraction of ER microsomes (wild-type PLN was found in the soluble fraction), indicating that L39stop PLN could be a highly unstable or rapidly degraded and inactive form of PLN. It was concluded that homozygous L39stop individuals are effectively "PLN-null", which leads to DCM in humans. This is in stark opposition to what is seen in mouse models, where PLN reduction or ablation results in normal cardiac contractile function and does not lead to heart failure, even in advanced age [121]. Molecular dynamics simulations of L39stop determined that this mutation would be unable to form oligomers and would be translocated out of the bilayer and solubilized [122].

5.5.6.5 Arg^{25}-Cys (R25C)

In 2015, four heterozygous family members were identified as carriers of the R25C mutation [123]. All had implantable cardiac defibrillators and three had developed prominent ventricular arrhythmias. In adult rat cardiomyocytes, R25C PLN acts as a superinhibitor of SERCA, which is relieved by phosphorylation, and is associated with an increased frequency of calcium sparks and waves as well as stress-induced after-contractions. Accompanying this phenotype is an increase in CaMKII activity and hyper-phosphorylation of RyR2 at Ser^{2814}, providing the first evidence that a mutation in PLN can affect both calcium uptake and release in the SR.

5.5.6.6 Mutations in the Promoter and Intronic Regions

The human PLN gene is located on chromosome 6 and, in addition to mutations in the coding region, several mutations have been identified in the promoter region and surrounding introns. Small nucleotide polymorphisms (SNPs) in the promoter region of PLN that have been found include: 77 bases upstream (−77) [124], 42 bases upstream (−42) [125] and 36 bases upstream (−36) [126, 127] of the PLN transcriptional start site. These mutations are found only in the heterozygous form and have been shown to alter expression of PLN; however, they have also been identified in both healthy individuals and patients with cardiac disease [125].

5.6 Regulation of SERCA by Sarcolipin

5.6.1 Introduction to Sarcolipin

SLN was first described as a low molecular-weight protein that co-purified with preparations of SERCA and was named to reflect its origin as a proteolipid of the SR [128]. SLN is the predominant regulator of SERCA and calcium homeostasis in fast-twitch skeletal muscle [129, 130]. However, SLN is also expressed in the atria of the heart, where it can interact with PLN and lead to super-inhibition of SERCA [131–133]. Structural similarities between the SLN and PLN genes, as well as the significant sequence identity clearly suggest that these proteins are homologous members of the same gene family [4, 11]. SLN is a 31-residue type I integral membrane protein with a transmembrane domain and short cytoplasmic and luminal domains (Fig. 5.2a) [128]. Amino acid conservation in the transmembrane domains of SLN and PLN suggests that SLN inhibits SERCA by binding and lowering the apparent calcium affinity of the enzyme in a manner similar to PLN [130]. However, recent data demonstrate that unlike PLN, which primarily binds to SERCA in an E2 calcium-free state, SLN remains associated with SERCA throughout its kinetic transport cycle [134–136].

5.6.2 Regulatory Mechanism of SERCA Inhibition by Sarcolipin

SLN inhibition of SERCA has been less well characterized than PLN, mainly due to the assumption that SLN inhibits SERCA in a similar manner as PLN. However, there are important differences in the way SLN inhibits SERCA. For example, it is well accepted that SLN lowers the apparent calcium affinity of SERCA to a lesser extent than PLN [130, 137]. In addition, some studies have found that SLN decreases the maximum reaction rate (V_{max}) of SERCA at micromolar calcium concentrations,

indicating that SLN inhibition is not relieved by increased cytosolic calcium [138–140]. Furthermore, it is not well established if phosphorylation of SLN is a physiologically relevant mechanism, although two kinases, CaMKII and Serine/Threonine Kinase 16 (STK16), have been reported to target SLN (Fig. 5.4d) [141, 142]. Finally, in contrast to PLN which is known to assemble into stable pentamers, SLN is thought to exist primarily as a monomer [130]. However, evidence indicates that SLN can also form oligomers in detergent and lipid environments [143, 144].

The differences in the amino acid composition between SLN and PLN are responsible for the structural changes that give these peptides their own unique functional properties. The N-terminal cytoplasmic domain of SLN (residues 1–7) is much shorter than that of PLN and lacks the corresponding phosphorylation sites. This region of SLN is poorly conserved among different species except for the highly conserved Thr^5 residue, considered as a putative phosphorylation site (Fig. 5.2a) [4]. The role of Thr^5 in phosphorylation-mediated regulation of SLN was first demonstrated in heterologous co-expression studies with SERCA in which the phospho-mimetic Thr^5-Glu SLN mutant resulted in the expected complete loss of function, whereas Thr^5-Ala SLN was a gain-of-function mutation [130]. In addition, the N-terminal domain of SLN may play a role in uncoupling of SERCA, causing an increase in ATP hydrolysis and heat production [136]. The α-helical transmembrane domain of SLN (residues 8–27) is composed of 19 residues, 8 of which are identical and 8 are highly conserved compared to the corresponding residues in the transmembrane domain of PLN. Despite the high sequence conservation between the transmembrane regions of SLN and PLN, alanine-scanning mutagenesis did not recapitulate the gain of function behavior associated with residues that destabilize the PLN pentamer [130]. Nevertheless, mutation of Leu^8 and Asn^{11} in SLN resulted in the expected loss of function observed for the comparable Leu^{31} and Asn^{34} in PLN, residues critical for proper PLN function. The last five residues of SLN are perfectly conserved among mammals and make up its luminal domain (residues 27–31) which extends into the SR lumen. The C-terminal regions of SLN and PLN represent a striking difference between these proteins, where the polar luminal tail in SLN (Arg^{27}-Ser-Tyr-Gln-Tyr^{31}) is substituted by the more hydrophobic C-terminal end in PLN (Met^{50}-Leu-Leu^{52}). Solid-state NMR studies demonstrated that the two aromatic residues (Tyr^{29} and Tyr^{31}) of SLN are required for interaction with SERCA [138]. Furthermore, functional studies in co-reconstituted proteoliposomes concluded that the luminal domain of SLN is responsible for lowering the maximal activity of SERCA and encodes most of its inhibitory properties [145]. In addition to this functional role, the luminal domain was reported to be important for targeting or retention of SLN in the SR membrane [146].

5.6.3 Structure of Sarcolipin

In contrast to PLN, there have been few structural studies of SLN. Considering its low molecular weight and highly hydrophobic nature, the structure of SLN has been predominantly studied by NMR in detergent and lipid environments. The initial 3D

structure of SLN was determined in detergent (SDS) micelles and revealed that SLN forms a compact α-helical transmembrane domain (residues 9–27) with two short unstructured termini consisting of residues 1–8 in the cytoplasmic N-terminus and residues 27–31 in the luminal C-terminus (Fig. 5.2a) [147]. Additionally, the orientation of SLN was found to be perpendicular to the membrane plane. A subsequent NMR structure of SLN was determined in dodecylphosphocholine (DPC) micelles, conditions that more closely mimic the native membrane environment [148]. The overall structure of SLN was highly similar to the initial SLN structure solved in the presence of detergent, indicating that this protein adopts the same conformation in detergent and lipid environments. However, contrasting what was observed in the initial structural study [147], SLN was determined to adopt a tilted orientation with the helix axis tilted by ~23° with respect to the membrane normal. In addition, spin relaxation measurements revealed four dynamic domains of SLN: an unstructured N-terminus (residues 1–6), a dynamic helix (residues 7–14), a highly rigid helix (residues 15–26), and an unstructured C-terminus (residues 27–31). The more hydrophilic N-terminal portion of the transmembrane domain of SLN is reminiscent of domain Ib of PLN, whereas the more hydrophobic and rigid segment resembles domain II of PLN, suggesting that sequence conservation between these two proteins is reflected in the conservation of both structure and dynamics. This study also indicated that the dynamic peptide backbone of the cytoplasmic and luminal domains of SLN become more structured in the presence of SERCA, suggesting that these regions of SLN might be stabilized through interactions with the pump.

5.6.4 Oligomeric State of Sarcolipin

It is well documented that monomeric PLN can assemble into stable pentamers, which are easily visualized by SDS-PAGE [11], whereas SLN has been found to migrate primarily as a monomer in SDS-PAGE [130]. However, several studies have since shown that SLN can form a mixture of oligomeric species. For example, SLN has been shown to aggregate after purification in non-ionic detergents, as well as self-associate into higher order oligomers stabilized by chemical cross-linking in detergent micelles and liposomes [143]. Recently, a fluorescence study done in insect cells directly demonstrated that SLN monomers associate into dimers and higher order oligomers, whereas mutant Ile^{17}-Ala SLN only formed monomers and dimers [144]. The same study also revealed that the binding affinity of SLN for itself is very similar to that of SLN for SERCA.

Another interesting factor supporting the oligomerization of SLN came from recent studies which reported channel-like activity for SLN reconstituted into tethered bilayer lipid membranes [149, 150]. SLN was reported to form channels selective for chloride and phosphate anions and impermeable to inorganic cations. This ion-channel activity was abolished by the Thr^{18}-Ala mutation in the transmembrane domain of SLN. In addition, the transport of phosphate by the SLN channel

was found to be activated in the presence of ATP and inhibited by ADP. Intriguingly, the SLN channel shares some features with the unidentified phosphate transporter found in the SR, which is thought to enhance the level of accumulation of calcium ions in the SR when SERCA is activated by ATP [151, 152]. Although the physiological role of the SLN channel is still debatable, these studies suggest that SLN must oligomerize in order to exhibit channel-like activity.

5.6.5 *Sarcolipin Physically Interacts with SERCA*

Mutagenesis studies of both SLN and SERCA in combination with functional measurements and co-immunoprecipitation studies provided the first insights into where SLN binds on the SERCA pump [134]. Since residues in the transmembrane domain of PLN responsible for interactions with SERCA are conserved in SLN, the effects of SLN mutations were compared to the previously characterized mutations in PLN [100]. With respect to binding SERCA, mutations in PLN had more dramatic effects on binding than SLN mutations, suggesting that PLN has higher affinity for SERCA than SLN. The most notable differences were that Leu^{8}-Ala SLN had no effect on binding to SERCA (the equivalent Leu^{31}-Ala PLN decreased binding by 73%) and Ile^{17}-Ala SLN decreased binding by 18% (the equivalent Ile^{40}-Ala PLN increased binding by 145%). In addition, mutations in SERCA that reduced regulatory function with PLN had similar effects on SLN binding, further suggesting that SLN binds in the same region of SERCA as PLN. Based on these results, an NMR structure of SLN was modeled onto the calcium-free crystal structure of SERCA. Modeling revealed that the SERCA-SLN complex closely resembles the previously generated SERCA-PLN model [44, 153], with the transmembrane domain of SLN occupying the same grove as the transmembrane of PLN, and the C-terminal luminal domain interacting with aromatic residues in the TM1–TM2 loop of SERCA.

A major breakthrough in understanding the interactions between SERCA and its regulator SLN came about with the recent publication of two high resolution crystal structures of the SERCA-SLN complex (Fig. 5.5) [154, 155]. These structures represent SLN bound to SERCA in a calcium-free state and for the first time provide detailed structural information explaining the mechanism of SERCA regulation by SLN. These structures reveal that SLN traps SERCA in a previously unobserved magnesium-bound state, denoted as E1-Mg^{2+}, with the calcium binding sites exposed to the cytosol and the conformation of the pump being intermediate between the calcium-free (E2) and the calcium bound (E1-Ca^{2+}) states. Two magnesium ions appear to be bound at the second calcium binding site (site II) which is not fully formed in the E1-Mg^{2+} state (Fig. 5.5b). Therefore, it is possible that binding of a calcium ion at site I causes displacement of magnesium ions and complete formation of site II. This hypothesis is supported by functional studies which indicate that magnesium can access calcium binding sites from the cytosol and high magnesium concentrations can inhibit calcium binding to SERCA [156]. Taken together, it is

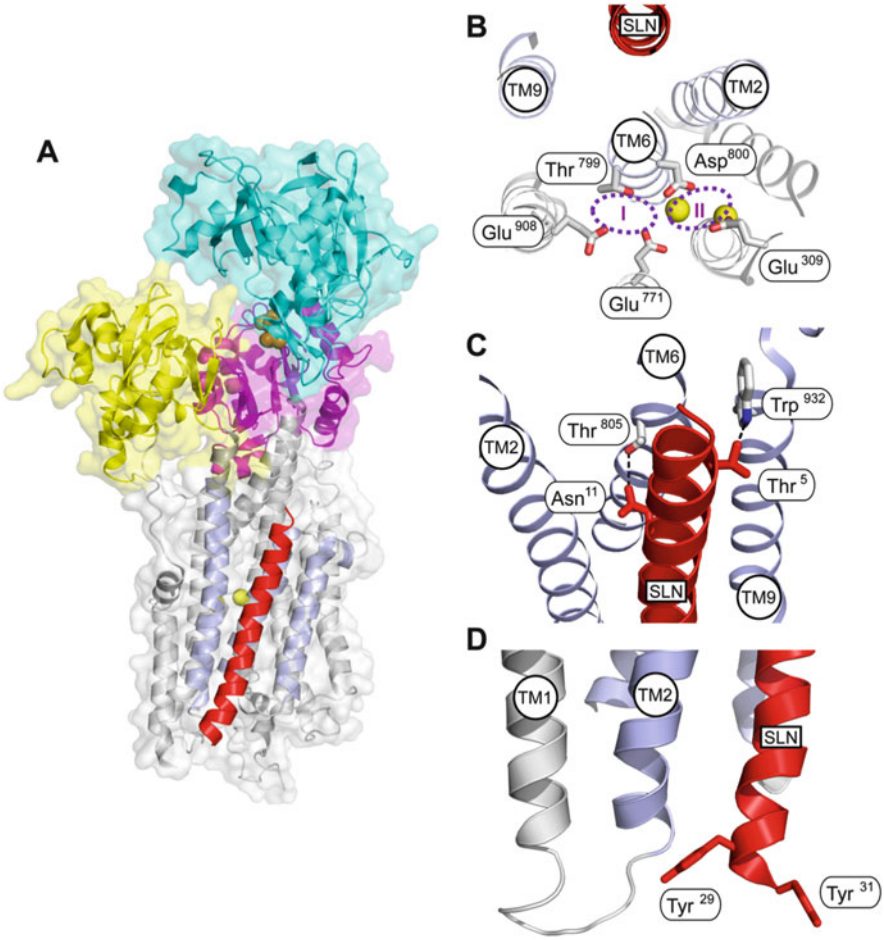

Fig. 5.5 High-resolution structure of SERCA in complex with SLN. (**a**) SERCA is shown in transparent surface and cartoon with the P-domain in magenta, N-domain in cyan, A-domain in yellow, TM2 and TM9 in light purple and the rest of the transmembrane (TM) helices in grey. Magnesium ions are shown as yellow spheres. SLN is shown in red cartoon. (**b**) Close-up view of the calcium binding sites with two magnesium ions occupying site II. Calcium ion coordinating side chains are shown as grey sticks. (**c**) Close-up view of the interactions between the N-terminal part of SLN and TM2, TM6 and TM9 helices of SERCA. Asn^{11} and Thr^{5} (red sticks) of SLN are shown to interact with Thr^{805} and Trp^{932} (grey sticks) of SERCA, respectively. (**d**) Close-up view showing the proximity of Tyr^{29} and Tyr^{31} to the luminal end of TM1–TM2 of SERCA

possible that SERCA utilizes magnesium ions to modulate the efficiency of calcium binding that may delay SERCA activation relative to the contractile filaments.

The structures of the SERCA-SLN complex reveal SLN as a slightly bent α-helix bound in a groove surrounded by TM2, TM6, and TM9 of SERCA, which is highly consistent with previous models, cross-linking and mutagenesis

studies [134, 135]. The SLN binding cleft appears particularly narrow in the cytoplasmic end where the putative SLN phosphorylation site, residue Thr^{5}, makes contacts with the pump (Fig. 5.5c). Thus, phosphorylation at this site would result in steric clash that relieves binding of SLN to SERCA. These structures also directly demonstrate the importance of the highly conserved Asn^{11} (Asn^{34} in PLN) as it clearly forms extensive interactions with Thr^{805} of SERCA, explaining why mutation of this residue to alanine results in loss of inhibitory function and weaker association of SLN with SERCA (Fig. 5.5c). Unfortunately, the amino- and carboxy-termini of SLN are poorly defined in both structures, preventing accurate assignment of the last three C-terminal residues (^{29}Tyr-Gln-Tyr^{31}). Nevertheless, the C-terminal domain of SLN appears to be in proximity to the aromatic residues in the TM1–TM2 loop (Fig. 5.5d). In summary, these structures suggest that by direct binding to the transmembrane domain of SERCA, SLN interferes with transition from the magnesium bound E1-Mg^{2+} state into the calcium bound E1-Ca^{2+} state, and thereby decreases the apparent affinity of SERCA for calcium.

5.6.6 Role of Sarcolipin in the Heart

Aside from being the primary regulator of SERCA1 in skeletal muscle, SLN is known to be an active regulator of cardiac SERCA2a. This was initially demonstrated in studies performed in HEK293 cells, where co-expression of SLN with SERCA2a decreased the apparent calcium affinity of the pump [137]. Indeed, SLN mRNA was then demonstrated to be specifically expressed in the atria of mouse hearts but absent in the ventricles [131]. In the same study, SLN mRNA was also detected in human atria. These findings were later confirmed with detection of SLN at the protein level in the atria of mouse and rat [132]. Furthermore, several studies have shown that expression of SLN in cardiac muscle appears to be differentially regulated under diverse physiological and pathophysiological states. For example, expression of SLN at both mRNA and protein levels has been shown to be down-regulated in the atria of patients with chronic atrial fibrillation [157, 158], which appears to contribute to atrial remodeling [159]. Similarly, down-regulation of SLN mRNA levels was reported in a transgenic mouse model of cardiac hypertrophy [131]. Conversely, a more recent study showed that SLN mRNA is up-regulated approximately 50-fold in hypertrophied ventricles of Nkx2-5 null mice [160]. In addition, one study reported a significant increase of SLN mRNA expression in the mouse atria during development [131].

Compared to PLN, the function of SLN in cardiac calcium homeostasis and contractility is not fully defined. Important insights into the physiological role of SLN in the heart were obtained with the help of transgenic mouse models with alterations in SLN protein levels. The first genetically engineered mice overexpressing SLN in cardiac muscle displayed a decrease in SERCA2a calcium affinity, a decrease in calcium transient amplitude, and slowed muscle relaxation [140, 161]. The inhibitory effect of SLN was reversed by treatment with

isoproterenol (a β-agonist), suggesting that SLN is a reversible inhibitor of SERCA2a. Overall, these mice were very similar to a previously characterized mouse model overexpressing PLN. To investigate the independent role of SLN in the heart, mice overexpressing SLN in a PLN null background were generated [142]. Overexpression of SLN in the absence of PLN caused a decrease in the apparent calcium affinity of SERCA2a, reduced calcium transient amplitude, and impaired contractility as compared to PLN knockout mice. In agreement with previously studied SLN mouse models, isoproterenol treatment relieved SLN inhibition, further demonstrating that SLN can mediate the β-adrenergic response in the heart. These studies also identified Thr^5 as a potential phosphorylation site and directly demonstrated that SLN can be phosphorylated by STK16 (Fig. 5.2a). However, the physiological role of STK16 in the β-adrenergic pathway is yet to be defined.

The functional significance of SLN down-regulation in cardiac muscle was later demonstrated with a SLN knockout mouse [162]. In the atria, ablation of SLN resulted in increased apparent calcium affinity of SERCA2a, increased calcium transient amplitudes, and enhanced cardiac contractility. SLN knockout mice did not exhibit any developmental abnormalities, but were susceptible to arrhythmias and atrial remodeling upon old age, most likely due to enhanced SERCA2a activity [159, 162]. In addition, the absence of SLN in the atria showed blunted responses to isoproterenol, which implies that β-adrenergic stimulation in the atria is largely mediated by SLN. This was further supported by a study overexpressing SLN in rat ventricular myocytes, which provided evidence that SLN can be phosphorylated at Thr^5 by CaMKII (Fig. 5.2a) [141]. Taken together, these studies strongly suggest that SLN is an important regulator of SERCA2a function and cardiac contractility of the atria.

Since SLN and PLN are co-expressed in the heart, it is possible that the two regulators have a synergistic effect on SERCA activity. Interestingly, co-expression of SLN and PLN with SERCA2a in HEK293 cells was shown to induce super-inhibition of SERCA2a activity [137]. Initially, it was proposed that SLN mediates its inhibitory effect through forming a stable binary complex with PLN that results in destabilization of PLN pentamers [134]. This leads to increased concentrations of PLN monomers, considered to be the active form of PLN, thus promoting super-inhibition of the SERCA pump. However, aside from the reduced apparent calcium affinity of SERCA, a reduction in maximal activity was also observed. This suggested that it is not only the increase in PLN monomers that causes super-inhibition of SERCA. On the basis of more recent mutagenesis and co-immunoprecipitation studies, a modified model for the super-inhibition of SERCA was presented according to which the hetero-dimeric interactions between SLN and PLN are stronger than homo-dimeric interactions between PLN monomers [135]. Thus, a stable SLN-PLN hetero-dimer could form first and then fit into the PLN binding groove on SERCA causing super-inhibition (Fig. 5.4e). Indeed, according to a structural model of the SERCA-PLN-SLN ternary complex, the cavity formed by the TM2, TM4, TM6, and TM9 helices of SERCA in the calcium-free E2 state is large enough to accommodate SLN and PLN simultaneously but too narrow to bind two PLN monomers [134, 135]. In addition, a more recent study of PLN-SLN chimeras in co-reconstituted proteoliposomes revealed that PLN combined with the C-terminal

tail of SLN is sufficient for super-inhibition of SERCA, indicating that direct interactions between SERCA and both PLN and SLN are necessary for super-inhibition to occur [145]. It is noteworthy to point out, however, that evidence for a super-inhibitory action of PLN and SLN in atrial muscle under normal physiological settings has never been reported.

5.6.7 Sarcolipin Regulates Thermogenesis in Skeletal Muscle

In addition to regulating SERCA calcium transport activity, SLN has recently emerged as a regulator of thermogenesis in skeletal muscle [163]. Interestingly, SLN was shown to uncouple SERCA calcium transport from ATP hydrolysis, resulting in futile cycling of SERCA and leading to an increase in ATP consumption and heat production. The process of SERCA uncoupling was attributed to the fact that SLN appears to remain associated with the pump even at high calcium concentrations [164]. Moreover, the cytosolic N-terminal domain of SLN was shown to be critical for SERCA uncoupling, as truncation of this domain caused SLN to lose its inhibitory and uncoupling properties [136].

Several animal models have been used to study the role of SLN in skeletal muscle physiology, where a number of striking differences were observed between the wild-type, SLN deficient, and SLN overexpressing mice. Although loss of SLN did not affect skeletal muscle function or growth, SLN knock-out mice were unable to maintain normal body temperature when exposed to low temperatures, leading to hypothermia and eventual death [165]. This phenotype was completely reversed by reintroduction of SLN into SLN knock-out mice, suggesting that SLN is necessary for muscle-based thermogenesis. The same was not observed in skeletal muscle-specific PLN knock-out mice exposed to the low temperatures [164]. Furthermore, skeletal muscle-specific SLN knock-out mice were more susceptible to obesity than their wild-type littermates when fed a high fat diet [165]. In contrast, mice overexpressing SLN were resistant to diet-induced obesity and showed increased oxidative metabolism as compared to wild-type or SLN knock-out mice, further demonstrating that the uncoupling of SERCA by SLN causes higher energy expenditure [166]. Taken together, these in vitro and in vivo studies suggest a dual role of SLN in the skeletal muscle: regulation of intracellular calcium levels and modulation of energy metabolism.

5.7 Targeting SERCA Regulatory Complexes as Therapy for Cardiac Disease

Altered calcium handling is a hallmark of heart disease and many studies have found that mRNA levels or expression of proteins involved in SR calcium handling are altered in failing myocardium. Levels of SERCA2a in cardiac SR are depleted in

human heart failure and the reason for this is not entirely known. The decrease in SERCA2a expression leads to higher ratios of PLN-to-SERCA2a, which can result in SERCA2a superinhibition (Fig. 5.4a–c). It has also been shown in a mouse model that superinhibition of SERCA by PLN leads to heart disease [167]. While it has been shown that there is a decrease in PLN mRNA levels during heart failure [168], this does not appear to lead to decreased PLN protein expression [169] and most studies agree that PLN levels are unchanged between normal and failing hearts [11]. However, the phosphorylation of PLN is also decreased in heart failure, further augmenting superinhibition of SERCA [170]. Interestingly, expression of proteins involved in calcium release (RyR) and calcium binding (calsequestrin, calreticulin) are not affected in failing hearts, although there is often a compensatory increase in expression of the sodium-calcium exchanger (NCX) [169].

Since impaired calcium handling in heart failure is often a result of decreased expression and activity of SERCA2a, restoration of SERCA2a by gene transfer using an adeno-associated virus (AAV) has been studied as a treatment for heart failure [171]. While there are particular setbacks to this treatment, such as some patients' immunity to the virus and the potential degradation of newly expressed SERCA2a, it was shown to improve cardiac contractility and partially reverse remodelling of the left ventricle [172, 173]. While phase II clinical trials were successful, the clinical trial did not pass phase IIb/III trials [174, 175]. Since SUMOylation of SERCA2a is important for stability of the enzyme, and SERCA2a stability and SUMOylation both decrease during heart failure [176], the narrative of SERCA2a in heart failure may not be as simple as previously thought.

Impaired calcium handling can also be the result of reduced SERCA2a activity caused by superinhibition by PLN (Fig. 5.4a–c). Two approaches have been examined to alter SERCA2a-PLN interactions in heart failure—the first is to decrease PLN expression and the second is to increase PLN phosphorylation. PLN knockout studies in mice showed that it leads to normal cardiac performance resulting from an increase in SERCA2a affinity for calcium [11]. In support of this study, PLN overexpression in mice resulted in diminished calcium cycling, which was partially rescued by an elevation in epinephrine and norepinephrine levels, but was maladaptive in the long term, as it led to cardiac remodelling, heart failure and early mortality [177]. These studies have pointed to the use of PLN antisense RNA or non-functional PLN mutants to treat heart failure. The second approach to decrease SERCA2a inhibition by PLN is to increase its phosphorylation by PKA. Rather than attempting to phosphorylate PLN by activation of the β-agonist pathway, the focus has been to prevent dephosphorylation of PLN by PP-1. There is accumulating evidence that PP-1 activity is enhanced in heart failure, resulting in a decrease in PLN phosphorylation and cardiac output [178]. When phosphorylated by PKA, I-1 is a physiological inhibitor of PP-1 and this inhibition is reversed by the dephosphorylation of I-1 by protein phosphatase 2A or 2B. If normal activity of PP-1 can be restored by manipulating I-1, this approach could be used as a novel therapeutic in heart failure. Studies in animal models using a constitutively active I-1 construct (Thr^{35}-Asp) have shown enhanced contractility and PLN phosphorylation and reduced expression of pro-apoptotic proteins such as Bax. More recently, AAV

delivery of constitutively active I-1 has been shown to improve cardiac function in a model of swine ischemic heart failure [179].

5.8 Future Directions for SERCA Regulation

SERCA is expressed in all tissues, yet PLN and SLN are only expressed in muscle tissues. The question of how SERCA is regulated in these other tissues has remained a mystery until recently. In 2015, two micropeptides, previously thought to be long non-coding RNAs, were identified and found to directly interact with SERCA in muscle: myoregulin (MLN) and dwarf open reading frame (DWORF) [180, 181]. MLN, a 46 amino acid peptide, was found to be expressed in fast-twitch skeletal muscle where it inhibits SERCA in a similar mechanism to PLN and SLN. DWORF (35 amino acids) is expressed in cardiac, slow-twitch, and fast-twitch skeletal muscle, where it is proposed to activate SERCA by displacing PLN, SLN and MLN. In non-muscle tissues, two peptides were also identified to inhibit SERCA activity: endoregulin (ELN) and another-regulin (ALN) [182]. ELN and ALN were shown to inhibit SERCA2b and SERCA3a, respectively. ALN is the largest peptide inhibitor of SERCA (65 amino acids) and is expressed in similar tissues to SERCA2b—heart, epidermal epithelium, salivary gland, brown fat, intestinal epithelium, and urothelium of the bladder. ELN is also larger than PLN (54 amino acids) and its tissue distribution is distinctly non-muscle (epithelial cells of the trachea and bronchus, lung, intestine, pancreas, and liver). The mechanisms by which MLN, ELN and ALN inhibit SERCA are predicted to be similar to PLN, given their similar topology. Exciting new work has also identified ER/SR-mitochondria crosstalk as being important in calcium homeostasis, and defects in this relationship have been linked to heart disease and cancer [183]. SERCA has emerged as an important player in mediating SR/ER-mitochondrial calcium flux and mitochondria bioenergetics. Specialized ER/SR microdomains (called mitochondria-associated membranes) are held in close proximity to mitochondria by protein tethers and can affect activity of mitochondrial metabolism and ATP production. Indeed, recent work has identified novel modulators of SERCA2b, including thioredoxin (a disulfide isomerase that consists of a single ER transmembrane domain), in these mitochondria-associated membranes, providing further evidence of the role of SERCA on calcium flux at the ER-mitochondria interface and adding to the complexity of the SERCA regulatory mechanisms [184].

References

1. Carafoli E (2002) Calcium signaling: a tale for all seasons. Proc Natl Acad Sci USA 99:1115–1122
2. Bers DM (2002) Cardiac excitation-contraction coupling. Nature 415:198–205
3. Periasamy M, Kalyanasundaram A (2007) SERCA pump isoforms: their role in calcium transport and disease. Muscle Nerve 35:430–442

4. Bhupathy P, Babu GJ, Periasamy M (2007) Sarcolipin and phospholamban as regulators of cardiac sarcoplasmic reticulum Ca2+ ATPase. J Mol Cell Cardiol 42:903–911
5. Ji Y et al (1999) SERCA1a can functionally substitute for SERCA2a in the heart. Am J Phys 276:H89–H97
6. Loukianov E et al (1998) Enhanced myocardial contractility and increased Ca2+ transport function in transgenic hearts expressing the fast-twitch skeletal muscle sarcoplasmic reticulum Ca2+-ATPase. Circ Res 83:889–897
7. Lalli MJ et al (2001) Sarcoplasmic reticulum Ca(2+) atpase (SERCA) 1a structurally substitutes for SERCA2a in the cardiac sarcoplasmic reticulum and increases cardiac Ca(2+) handling capacity. Circ Res 89:160–167
8. MacLennan DH (2000) Ca2+ signalling and muscle disease. Eur J Biochem 267:5291–5297
9. Odermatt A et al (1996) Mutations in the gene-encoding SERCA1, the fast-twitch skeletal muscle sarcoplasmic reticulum Ca2+ ATPase, are associated with Brody disease. Nat Genet 14:191–194
10. Vangheluwe P et al (2003) Ca2+ transport ATPase isoforms SERCA2a and SERCA2b are targeted to the same sites in the murine heart. Cell Calcium 34:457–464
11. MacLennan DH, Kranias EG (2003) Phospholamban: a crucial regulator of cardiac contractility. Nat Rev Mol Cell Biol 4:566–577
12. Gunteski-Hamblin AM, Greeb J, Shull GE (1988) A novel Ca2+ pump expressed in brain, kidney, and stomach is encoded by an alternative transcript of the slow-twitch muscle sarcoplasmic reticulum Ca-ATPase gene. Identification of cDNAs encoding Ca2+ and other cation-transporting ATPases using an oligonucleotide probe derived from the ATP-binding site. J Biol Chem 263:15032–15040
13. Verboomen H et al (1992) Functional difference between SERCA2a and SERCA2b Ca2+ pumps and their modulation by phospholamban. Biochem J 286(Pt 2):591–595
14. Dally S et al (2006) Ca2+-ATPases in non-failing and failing heart: evidence for a novel cardiac sarco/endoplasmic reticulum Ca2+-ATPase 2 isoform (SERCA2c). Biochem J 395:249–258
15. Kimura T et al (2005) Altered mRNA splicing of the skeletal muscle ryanodine receptor and sarcoplasmic/endoplasmic reticulum Ca2+-ATPase in myotonic dystrophy type 1. Hum Mol Genet 14:2189–2200
16. Clausen JD et al (2012) Distinct roles of the C-terminal 11th transmembrane helix and luminal extension in the partial reactions determining the high Ca2+ affinity of sarco(endo)plasmic reticulum Ca2+-ATPase isoform 2b (SERCA2b). J Biol Chem 287(39):460–469
17. Wuytack F, Raeymaekers L, Missiaen L (2002) Molecular physiology of the SERCA and SPCA pumps. Cell Calcium 32:279–305
18. Periasamy M et al (1999) Impaired cardiac performance in heterozygous mice with a null mutation in the sarco(endo)plasmic reticulum Ca2+-ATPase isoform 2 (SERCA2) gene. J Biol Chem 274:2556–2562
19. Wuytack F et al (1995) The SERCA3-type of organellar Ca2+ pumps. Biosci Rep 15:299–306
20. Varadi A et al (1999) Sequence variants of the sarco(endo)plasmic reticulum Ca(2+)-transport ATPase 3 gene (SERCA3) in Caucasian type II diabetic patients (UK Prospective Diabetes Study 48). Diabetologia 42:1240–1243
21. Liu LH et al (1997) Defective endothelium-dependent relaxation of vascular smooth muscle and endothelial cell Ca2+ signaling in mice lacking sarco(endo)plasmic reticulum Ca2+--ATPase isoform 3. J Biol Chem 272(30):538–545
22. Xu XY et al (2012) Aberrant SERCA3 expression is closely linked to pathogenesis, invasion, metastasis, and prognosis of gastric carcinomas. Tumour Biol 33:1845–1854
23. Arbabian A et al (2013) Modulation of endoplasmic reticulum calcium pump expression during lung cancer cell differentiation. FEBS J 280:5408–5418
24. Gelebart P et al (2002) Expression of endomembrane calcium pumps in colon and gastric cancer cells. Induction of SERCA3 expression during differentiation. J Biol Chem 277:26310–26320

25. Papp B, Brouland JP (2011) Altered endoplasmic reticulum calcium pump expression during breast tumorigenesis. Breast Cancer (Auckl) 5:163–174
26. Kuhlbrandt W (2004) Biology, structure and mechanism of P-type ATPases. Nat Rev Mol Cell Biol 5:282–295
27. Albers RW (1967) Biochemical aspects of active transport. Annu Rev Biochem 36:727–756
28. Moller JV et al (2010) The sarcoplasmic Ca2+-ATPase: design of a perfect chemi-osmotic pump. Q Rev Biophys 43:501–566
29. Olesen C et al (2007) The structural basis of calcium transport by the calcium pump. Nature 450:1036–1042
30. Moller JV et al (2005) Transport mechanism of the sarcoplasmic reticulum Ca2+ -ATPase pump. Curr Opin Struct Biol 15:387–393
31. Jensen AM et al (2006) Modulatory and catalytic modes of ATP binding by the calcium pump. EMBO J 25:2305–2314
32. Moncoq K, Trieber CA, Young HS (2007) The molecular basis for cyclopiazonic acid inhibition of the sarcoplasmic reticulum calcium pump. J Biol Chem 282:9748–9757
33. Laursen M et al (2009) Cyclopiazonic acid is complexed to a divalent metal ion when bound to the sarcoplasmic reticulum Ca2+-ATPase. J Biol Chem 284(13):513–518
34. MacLennan DH et al (1985) Amino-acid sequence of a Ca2+ + Mg2+-dependent ATPase from rabbit muscle sarcoplasmic reticulum, deduced from its complementary DNA sequence. Nature 316:696–700
35. Lee AG, East JM (2001) What the structure of a calcium pump tells us about its mechanism. Biochem J 356:665–683
36. Dux L, Martonosi A (1983) Two-dimensional arrays of proteins in sarcoplasmic reticulum and purified Ca2+-ATPase vesicles treated with vanadate. J Biol Chem 258:2599–2603
37. Toyoshima C, Sasabe H, Stokes DL (1993) Three-dimensional cryo-electron microscopy of the calcium ion pump in the sarcoplasmic reticulum membrane. Nature 362:467–471
38. Zhang P et al (1998) Structure of the calcium pump from sarcoplasmic reticulum at 8-A resolution. Nature 392:835–839
39. Toyoshima C et al (2000) Crystal structure of the calcium pump of sarcoplasmic reticulum at 2.6 A resolution. Nature 405:647–655
40. Zhang Z et al (2000) Detailed characterization of the cooperative mechanism of Ca(2+) binding and catalytic activation in the Ca(2+) transport (SERCA) ATPase. Biochemistry 39:8758–8767
41. Toyoshima C, Nomura H (2002) Structural changes in the calcium pump accompanying the dissociation of calcium. Nature 418:605–611
42. Clausen JD et al (2008) Critical interaction of actuator domain residues arginine 174, isoleucine 188, and lysine 205 with modulatory nucleotide in sarcoplasmic reticulum Ca2+-ATPase. J Biol Chem 283(35):703–714
43. Sorensen TL, Moller JV, Nissen P (2004) Phosphoryl transfer and calcium ion occlusion in the calcium pump. Science 304:1672–1675
44. Toyoshima C et al (2003) Modeling of the inhibitory interaction of phospholamban with the Ca2+ ATPase. Proc Natl Acad Sci USA 100:467–472
45. Drachmann ND et al (2014) Comparing crystal structures of Ca(2+) -ATPase in the presence of different lipids. FEBS J 281:4249–4262
46. Akin BL et al (2013) The structural basis for phospholamban inhibition of the calcium pump in sarcoplasmic reticulum. J Biol Chem 288(30):181–191
47. Kimura Y et al (1997) Phospholamban inhibitory function is activated by depolymerization. J Biol Chem 272(15):61–64
48. Robia SL et al (2007) Forster transfer recovery reveals that phospholamban exchanges slowly from pentamers but rapidly from the SERCA regulatory complex. Circ Res 101:1123–1129
49. Cornea RL et al (2000) Reexamination of the role of the leucine/isoleucine zipper residues of phospholamban in inhibition of the Ca2+ pump of cardiac sarcoplasmic reticulum. J Biol Chem 275(41):487–494

50. Kimura Y et al (1998) Phospholamban domain Ib mutations influence functional interactions with the Ca2+-ATPase isoform of cardiac sarcoplasmic reticulum. J Biol Chem 273 (14):238–241
51. Karim CB et al (2001) Role of cysteine residues in structural stability and function of a transmembrane helix bundle. J Biol Chem 276(38):814–819
52. Karim CB et al (1998) Cysteine reactivity and oligomeric structures of phospholamban and its mutants. Biochemistry 37:12074–12081
53. Becucci L et al (2009) On the function of pentameric phospholamban: ion channel or storage form? Biophys J 96:L60–L62
54. Kovacs RJ et al (1988) Phospholamban forms Ca2+-selective channels in lipid bilayers. J Biol Chem 263(18):364–368
55. Oxenoid K, Chou JJ (2005) The structure of phospholamban pentamer reveals a channel-like architecture in membranes. Proc Natl Acad Sci USA 102(10):870–875
56. Stokes DL et al (2006) Interactions between Ca2+-ATPase and the pentameric form of phospholamban in two-dimensional co-crystals. Biophys J 90:4213–4223
57. Glaves JP et al (2011) Phosphorylation and mutation of phospholamban alter physical interactions with the sarcoplasmic reticulum calcium pump. J Mol Biol 405:707–723
58. Chu G et al (1998) Pentameric assembly of phospholamban facilitates inhibition of cardiac function in vivo. J Biol Chem 273(33):674–680
59. Chen Z, Akin BL, Jones LR (2007) Mechanism of reversal of phospholamban inhibition of the cardiac Ca2+-ATPase by protein kinase A and by anti-phospholamban monoclonal antibody 2D12. J Biol Chem 282(20):968–976
60. Cornea RL et al (1997) Mutation and phosphorylation change the oligomeric structure of phospholamban in lipid bilayers. Biochemistry 36:2960–2967
61. Oxenoid K, Rice AJ, Chou JJ (2007) Comparing the structure and dynamics of phospholamban pentamer in its unphosphorylated and pseudo-phosphorylated states. Protein Sci 16:1977–1983
62. Hou Z, Kelly EM, Robia SL (2008) Phosphomimetic mutations increase phospholamban oligomerization and alter the structure of its regulatory complex. J Biol Chem 283 (28):996–9003
63. Wegener AD et al (1986) Proteolytic cleavage of phospholamban purified from canine cardiac sarcoplasmic reticulum vesicles. Generation of a low resolution model of phospholamban structure. J Biol Chem 261:5154–5159
64. Choma C et al (2000) Asparagine-mediated self-association of a model transmembrane helix. Nat Struct Biol 7:161–166
65. Afara MR et al (2006) Rational design of peptide inhibitors of the sarcoplasmic reticulum calcium pump. Biochemistry 45:8617–8627
66. Afara MR et al (2008) Peptide inhibitors use two related mechanisms to alter the apparent calcium affinity of the sarcoplasmic reticulum calcium pump. Biochemistry 47:9522–9530
67. Kimura Y et al (1996) Phospholamban regulates the Ca2+-ATPase through intramembrane interactions. J Biol Chem 271(21):726–731
68. Trieber CA, Afara M, Young HS (2009) Effects of phospholamban transmembrane mutants on the calcium affinity, maximal activity, and cooperativity of the sarcoplasmic reticulum calcium pump. Biochemistry 48:9287–9296
69. Toyofuku T et al (1994) Amino acids Glu2 to Ile18 in the cytoplasmic domain of phospholamban are essential for functional association with the Ca(2+)-ATPase of sarcoplasmic reticulum. J Biol Chem 269:3088–3094
70. Kim HW et al (1990) Functional reconstitution of the cardiac sarcoplasmic reticulum Ca2(+)-ATPase with phospholamban in phospholipid vesicles. J Biol Chem 265:1702–1709
71. Sasaki T et al (1992) Molecular mechanism of regulation of Ca2+ pump ATPase by phospholamban in cardiac sarcoplasmic reticulum. Effects of synthetic phospholamban peptides on Ca2+ pump ATPase. J Biol Chem 267:1674–1679

72. Jones LR, Field LJ (1993) Residues 2-25 of phospholamban are insufficient to inhibit Ca2+ transport ATPase of cardiac sarcoplasmic reticulum. J Biol Chem 268(11):486–488
73. Schmitt JP et al (2003) Dilated cardiomyopathy and heart failure caused by a mutation in phospholamban. Science 299:1410–1413
74. Haghighi K et al (2006) A mutation in the human phospholamban gene, deleting arginine 14, results in lethal, hereditary cardiomyopathy. Proc Natl Acad Sci USA 103:1388–1393
75. Medeiros A et al (2011) Mutations in the human phospholamban gene in patients with heart failure. Am Heart J 162(1088–1095):e1
76. Traaseth NJ et al (2009) Structure and topology of monomeric phospholamban in lipid membranes determined by a hybrid solution and solid-state NMR approach. Proc Natl Acad Sci USA 106(10):165–170
77. Lamberth S et al (2000) NMR solution structure of phospholamban. Helvetica Chimica Acta 83:2141–2152
78. Gustavsson M, Traaseth NJ, Veglia G (2011) Activating and deactivating roles of lipid bilayers on the Ca(2+)-ATPase/phospholamban complex. Biochemistry 50:10367–10374
79. Traaseth NJ et al (2007) Spectroscopic validation of the pentameric structure of phospholamban. Proc Natl Acad Sci USA 104(14):676–681
80. Hughes E, Clayton JC, Middleton DA (2009) Cytoplasmic residues of phospholamban interact with membrane surfaces in the presence of SERCA: a new role for phospholipids in the regulation of cardiac calcium cycling? Biochim Biophys Acta 1788:559–566
81. James P et al (1989) Nature and site of phospholamban regulation of the Ca2+ pump of sarcoplasmic reticulum. Nature 342:90–92
82. Seidel K et al (2008) Structural characterization of Ca^{2+}-ATPase-bound phospholamban in lipid bilayers by solid-state nuclear magnetic resonance (NMR) spectroscopy. Biochemistry 47:4369–4376
83. Gustavsson M et al (2013) Allosteric regulation of SERCA by phosphorylation-mediated conformational shift of phospholamban. Proc Natl Acad Sci USA 110(17):338–343
84. Chen Z et al (2003) Spatial and dynamic interactions between phospholamban and the canine cardiac Ca2+ pump revealed with use of heterobifunctional cross-linking agents. J Biol Chem 278(48):348–356
85. Chen Z, Stokes DL, Jones LR (2005) Role of leucine 31 of phospholamban in structural and functional interactions with the Ca2+ pump of cardiac sarcoplasmic reticulum. J Biol Chem 280(10):530–539
86. Chen Z et al (2006) Cross-linking of C-terminal residues of phospholamban to the Ca2+ pump of cardiac sarcoplasmic reticulum to probe spatial and functional interactions within the transmembrane domain. J Biol Chem 281(14):163–172
87. Jones LR, Cornea RL, Chen Z (2002) Close proximity between residue 30 of phospholamban and cysteine 318 of the cardiac Ca2+ pump revealed by intermolecular thiol cross-linking. J Biol Chem 277(28):319–329
88. Starling AP et al (1996) The effect of N-terminal acetylation on Ca(2+)-ATPase inhibition by phospholamban. Biochem Biophys Res Commun 226:352–355
89. Filice E et al (2011) Crucial role of phospholamban phosphorylation and S-nitrosylation in the negative lusitropism induced by 17beta-estradiol in the male rat heart. Cell Physiol Biochem 28:41–52
90. Kranias EG, Hajjar RJ (2017) The phospholamban journey 4 decades after setting out for Ithaka. Circ Res 120:781–783
91. Tada M et al (1974) The stimulation of calcium transport in cardiac sarcoplasmic reticulum by adenosine 3′:5′’-monophosphate-dependent protein kinase. J Biol Chem 249:6174–6180
92. Katz AM (1998) Discovery of phospholamban. A personal history. Ann N Y Acad Sci 853:9–19
93. Tada M, Kirchberger MA, Katz AM (1975) Phosphorylation of a 22,000-dalton component of the cardiac sarcoplasmic reticulum by adenosine 3′:5′-monophosphate-dependent protein kinase. J Biol Chem 250:2640–2647

94. Catalucci D et al (2009) Akt increases sarcoplasmic reticulum Ca2+ cycling by direct phosphorylation of phospholamban at Thr17. J Biol Chem 284(28):180–187
95. Edes I, Kranias EG (1990) Phospholamban and troponin I are substrates for protein kinase C in vitro but not in intact beating guinea pig hearts. Circ Res 67:394–400
96. Chu G, Kranias EG (2002) Functional interplay between dual site phospholambam phosphorylation: insights from genetically altered mouse models. Basic Res Cardiol 97(Suppl 1): I43–I48
97. Mattiazzi A et al (2006) The importance of the Thr17 residue of phospholamban as a phosphorylation site under physiological and pathological conditions. Braz J Med Biol Res 39:563–572
98. Ablorh NA et al (2014) Synthetic phosphopeptides enable quantitation of the content and function of the four phosphorylation states of phospholamban in cardiac muscle. J Biol Chem 289(29):397–405
99. Asahi M et al (2000) Physical interactions between phospholamban and sarco(endo)plasmic reticulum Ca2+-ATPases are dissociated by elevated Ca2+, but not by phospholamban phosphorylation, vanadate, or thapsigargin, and are enhanced by ATP. J Biol Chem 275 (15):34–38
100. Asahi M et al (1999) Transmembrane helix M6 in sarco(endo)plasmic reticulum Ca(2+)-ATPase forms a functional interaction site with phospholamban. Evidence for physical interactions at other sites. J Biol Chem 274(32):855–862
101. Karim CB et al (2004) Phospholamban structural dynamics in lipid bilayers probed by a spin label rigidly coupled to the peptide backbone. Proc Natl Acad Sci USA 101(14):437–442
102. Karim CB et al (2006) Phosphorylation-dependent conformational switch in spin-labeled phospholamban bound to SERCA. J Mol Biol 358:1032–1040
103. Metcalfe EE, Traaseth NJ, Veglia G (2005) Serine 16 phosphorylation induces an order-to-disorder transition in monomeric phospholamban. Biochemistry 44:4386–4396
104. Arkin IT et al (1995) Structural model of the phospholamban ion channel complex in phospholipid membranes. J Mol Biol 248:824–834
105. Simmerman HK, Lovelace DE, Jones LR (1989) Secondary structure of detergent-solubilized phospholamban, a phosphorylatable, oligomeric protein of cardiac sarcoplasmic reticulum. Biochim Biophys Acta 997:322–329
106. Kim J et al (2015) Dysfunctional conformational dynamics of protein kinase A induced by a lethal mutant of phospholamban hinder phosphorylation. Proc Natl Acad Sci USA 112:3716–3721
107. Sugita Y et al (2006) Structural changes in the cytoplasmic domain of phospholamban by phosphorylation at Ser16: a molecular dynamics study. Biochemistry 45:11752–11761
108. Haghighi K et al (2003) Human phospholamban null results in lethal dilated cardiomyopathy revealing a critical difference between mouse and human. J Clin Invest 111:869–876
109. Young HS, Ceholski DK, Trieber CA (2015) Deception in simplicity: hereditary phospholamban mutations in dilated cardiomyopathy. Biochem Cell Biol 93:1–7
110. Schmitt JP et al (2009) Alterations of phospholamban function can exhibit cardiotoxic effects independent of excessive sarcoplasmic reticulum Ca2+-ATPase inhibition. Circulation 119:436–444
111. Ha KN et al (2011) Lethal Arg9Cys phospholamban mutation hinders Ca2+-ATPase regulation and phosphorylation by protein kinase A. Proc Natl Acad Sci USA 108:2735–2740
112. Gramolini AO et al (2008) Comparative proteomics profiling of a phospholamban mutant mouse model of dilated cardiomyopathy reveals progressive intracellular stress responses. Mol Cell Proteomics 7:519–533
113. Abrol N, de Tombe PP, Robia SL (2015) Acute inotropic and lusitropic effects of cardiomyopathic R9C mutation of phospholamban. J Biol Chem 290:7130–7140
114. Ceholski DK, Trieber CA, Young HS (2012) Hydrophobic imbalance in the cytoplasmic domain of phospholamban is a determinant for lethal dilated cardiomyopathy. J Biol Chem 287(16):521–529

115. Ceholski DK et al (2012) Lethal, hereditary mutants of phospholamban elude phosphorylation by protein kinase A. J Biol Chem 287(26):596–605
116. van der Zwaag PA et al (2013) Recurrent and founder mutations in the Netherlands-Phospholamban p.Arg14del mutation causes arrhythmogenic cardiomyopathy. Neth Hear J 21:286–293
117. Haghighi K et al (2012) The human phospholamban Arg14-deletion mutant localizes to plasma membrane and interacts with the Na/K-ATPase. J Mol Cell Cardiol 52:773–782
118. Karakikes I et al (2015) Correction of human phospholamban R14del mutation associated with cardiomyopathy using targeted nucleases and combination therapy. Nat Commun 6:6955
119. Te Rijdt WP et al (2016) Phospholamban p.Arg14del cardiomyopathy is characterized by phospholamban aggregates, aggresomes, and autophagic degradation. Histopathology 69:542–550
120. DeWitt MM et al (2006) Phospholamban R14 deletion results in late-onset, mild, hereditary dilated cardiomyopathy. J Am Coll Cardiol 48:1396–1398
121. Luo W et al (1994) Targeted ablation of the phospholamban gene is associated with markedly enhanced myocardial contractility and loss of beta-agonist stimulation. Circ Res 75:401–409
122. Abrol N et al (2014) Phospholamban C-terminal residues are critical determinants of the structure and function of the calcium ATPase regulatory complex. J Biol Chem 289 (25):855–866
123. Liu GS et al (2015) A novel human R25C-phospholamban mutation is associated with super-inhibition of calcium cycling and ventricular arrhythmia. Cardiovasc Res 107:164–174
124. Minamisawa S et al (2003) Mutation of the phospholamban promoter associated with hypertrophic cardiomyopathy. Biochem Biophys Res Commun 304:1–4
125. Medin M et al (2007) Mutational screening of phospholamban gene in hypertrophic and idiopathic dilated cardiomyopathy and functional study of the PLN -42 C>G mutation. Eur J Heart Fail 9:37–43
126. Haghighi K et al (2008) A human phospholamban promoter polymorphism in dilated cardiomyopathy alters transcriptional regulation by glucocorticoids. Hum Mutat 29:640–647
127. Landstrom AP et al (2011) PLN-encoded phospholamban mutation in a large cohort of hypertrophic cardiomyopathy cases: summary of the literature and implications for genetic testing. Am Heart J 161:165–171
128. Wawrzynow A et al (1992) Sarcolipin, the "proteolipid" of skeletal muscle sarcoplasmic reticulum, is a unique, amphipathic, 31-residue peptide. Arch Biochem Biophys 298:620–623
129. Odermatt A et al (1997) Characterization of the gene encoding human sarcolipin (SLN), a proteolipid associated with SERCA1: absence of structural mutations in five patients with Brody disease. Genomics 45:541–553
130. Odermatt A et al (1998) Sarcolipin regulates the activity of SERCA1, the fast-twitch skeletal muscle sarcoplasmic reticulum Ca2+-ATPase. J Biol Chem 273(12):360–369
131. Minamisawa S et al (2003) Atrial chamber-specific expression of sarcolipin is regulated during development and hypertrophic remodeling. J Biol Chem 278:9570–9575
132. Vangheluwe P et al (2005) Sarcolipin and phospholamban mRNA and protein expression in cardiac and skeletal muscle of different species. Biochem J 389:151–159
133. Babu GJ et al (2007) Differential expression of sarcolipin protein during muscle development and cardiac pathophysiology. J Mol Cell Cardiol 43:215–222
134. Asahi M et al (2003) Sarcolipin regulates sarco(endo)plasmic reticulum Ca2+-ATPase (SERCA) by binding to transmembrane helices alone or in association with phospholamban. Proc Natl Acad Sci USA 100:5040–5045
135. Morita T et al (2008) Interaction sites among phospholamban, sarcolipin, and the sarco(endo) plasmic reticulum Ca(2+)-ATPase. Biochem Biophys Res Commun 369:188–194
136. Shaikh SA, Sahoo SK, Periasamy M (2016) Phospholamban and sarcolipin: are they functionally redundant or distinct regulators of the Sarco(Endo)Plasmic Reticulum Calcium ATPase? J Mol Cell Cardiol 91:81–91
137. Asahi M et al (2002) Sarcolipin inhibits polymerization of phospholamban to induce superinhibition of sarco(endo)plasmic reticulum Ca2+-ATPases (SERCAs). J Biol Chem 277(26):725–728

138. Hughes E et al (2007) Solid-state NMR and functional measurements indicate that the conserved tyrosine residues of sarcolipin are involved directly in the inhibition of SERCA1. J Biol Chem 282(26):603–613
139. Tupling AR, Asahi M, MacLennan DH (2002) Sarcolipin overexpression in rat slow twitch muscle inhibits sarcoplasmic reticulum Ca2+ uptake and impairs contractile function. J Biol Chem 277(44):740–746
140. Babu GJ et al (2006) Targeted overexpression of sarcolipin in the mouse heart decreases sarcoplasmic reticulum calcium transport and cardiac contractility. J Biol Chem 281:3972–3979
141. Bhupathy P et al (2009) Threonine-5 at the N-terminus can modulate sarcolipin function in cardiac myocytes. J Mol Cell Cardiol 47:723–729
142. Gramolini AO et al (2006) Cardiac-specific overexpression of sarcolipin in phospholamban null mice impairs myocyte function that is restored by phosphorylation. Proc Natl Acad Sci USA 103:2446–2451
143. Hellstern S et al (2001) Sarcolipin, the shorter homologue of phospholamban, forms oligomeric structures in detergent micelles and in liposomes. J Biol Chem 276(30):845–852
144. Autry JM et al (2011) Oligomeric interactions of sarcolipin and the Ca-ATPase. J Biol Chem 286(31):697–706
145. Gorski PA et al (2013) Sarco(endo)plasmic reticulum calcium ATPase (SERCA) inhibition by sarcolipin is encoded in its luminal tail. J Biol Chem 288:8456–8467
146. Gramolini AO et al (2004) Sarcolipin retention in the endoplasmic reticulum depends on its C-terminal RSYQY sequence and its interaction with sarco(endo)plasmic Ca(2+)-ATPases. Proc Natl Acad Sci USA 101(16):807–812
147. Mascioni A et al (2002) Structure and orientation of sarcolipin in lipid environments. Biochemistry 41:475–482
148. Buffy JJ et al (2006) Two-dimensional solid-state NMR reveals two topologies of sarcolipin in oriented lipid bilayers. Biochemistry 45:10939–10946
149. Becucci L et al (2007) An electrochemical investigation of sarcolipin reconstituted into a mercury-supported lipid bilayer. Biophys J 93:2678–2687
150. Becucci L et al (2009) The role of sarcolipin and ATP in the transport of phosphate ion into the sarcoplasmic reticulum. Biophys J 97:2693–2699
151. Stefanova HI, East JM, Lee AG (1991) Covalent and non-covalent inhibitors of the phosphate transporter of sarcoplasmic reticulum. Biochim Biophys Acta 1064:321–328
152. Stefanova HI et al (1991) Effects of Mg2+ and ATP on the phosphate transporter of sarcoplasmic reticulum. Biochim Biophys Acta 1064:329–334
153. Toyoshima C et al (2003) Modeling of the inhibitory interaction of phospholamban with the Ca^{2+} ATPase. Proc Natl Acad Sci USA 100:467–472
154. Winther AM et al (2013) The sarcolipin-bound calcium pump stabilizes calcium sites exposed to the cytoplasm. Nature 495:265–269
155. Toyoshima C et al (2013) Crystal structures of the calcium pump and sarcolipin in the Mg2+-bound E1 state. Nature 495:260–264
156. Henderson IM et al (1994) Binding of Ca2+ to the (Ca(2+)-Mg2+)-ATPase of sarcoplasmic reticulum: kinetic studies. Biochem J 297(Pt 3):625–636
157. Shanmugam M et al (2011) Decreased sarcolipin protein expression and enhanced sarco(endo) plasmic reticulum Ca2+ uptake in human atrial fibrillation. Biochem Biophys Res Commun 410:97–101
158. Uemura N et al (2004) Down-regulation of sarcolipin mRNA expression in chronic atrial fibrillation. Eur J Clin Investig 34:723–730
159. Xie LH et al (2012) Ablation of sarcolipin results in atrial remodeling. Am J Phys Cell Physiol 302:C1762–C1771
160. Pashmforoush M et al (2004) Nkx2-5 pathways and congenital heart disease; loss of ventricular myocyte lineage specification leads to progressive cardiomyopathy and complete heart block. Cell 117:373–386

161. Asahi M et al (2004) Cardiac-specific overexpression of sarcolipin inhibits sarco(endo)plasmic reticulum Ca2+ ATPase (SERCA2a) activity and impairs cardiac function in mice. Proc Natl Acad Sci USA 101:9199–9204
162. Babu GJ et al (2007) Ablation of sarcolipin enhances sarcoplasmic reticulum calcium transport and atrial contractility. Proc Natl Acad Sci USA 104(17):867–872
163. Pant M, Bal NC, Periasamy M (2016) Sarcolipin: a key thermogenic and metabolic regulator in skeletal muscle. Trends Endocrinol Metab 27:881–892
164. Sahoo SK et al (2013) Sarcolipin protein interaction with sarco(endo)plasmic reticulum Ca2+ ATPase (SERCA) is distinct from phospholamban protein, and only sarcolipin can promote uncoupling of the SERCA pump. J Biol Chem 288:6881–6889
165. Bal NC et al (2012) Sarcolipin is a newly identified regulator of muscle-based thermogenesis in mammals. Nat Med 18:1575–1579
166. Maurya SK et al (2015) Sarcolipin is a key determinant of the basal metabolic rate, and its overexpression enhances energy expenditure and resistance against diet-induced obesity. J Biol Chem 290(10):840–849
167. Zhai J et al (2000) Cardiac-specific overexpression of a superinhibitory pentameric phospholamban mutant enhances inhibition of cardiac function in vivo. J Biol Chem 275 (10):538–544
168. Feldman AM et al (1991) Selective gene expression in failing human heart. Quantification of steady-state levels of messenger RNA in endomyocardial biopsies using the polymerase chain reaction. Circulation 83:1866–1872
169. Meyer M et al (1995) Alterations of sarcoplasmic reticulum proteins in failing human dilated cardiomyopathy. Circulation 92:778–784
170. Dash R et al (2001) Gender influences on sarcoplasmic reticulum Ca2+-handling in failing human myocardium. J Mol Cell Cardiol 33:1345–1353
171. del Monte F et al (1999) Restoration of contractile function in isolated cardiomyocytes from failing human hearts by gene transfer of SERCA2a. Circulation 100:2308–2311
172. Jaski BE et al (2009) Calcium upregulation by percutaneous administration of gene therapy in cardiac disease (CUPID Trial), a first-in-human phase 1/2 clinical trial. J Card Fail 15:171–181
173. Jessup M et al (2011) Calcium Upregulation by Percutaneous Administration of Gene Therapy in Cardiac Disease (CUPID): a phase 2 trial of intracoronary gene therapy of sarcoplasmic reticulum Ca2+-ATPase in patients with advanced heart failure. Circulation 124:304–313
174. Kairouz V et al (2012) Molecular targets in heart failure gene therapy: current controversies and translational perspectives. Ann N Y Acad Sci 1254:42–50
175. Hulot JS, Ishikawa K, Hajjar RJ (2016) Gene therapy for the treatment of heart failure: promise postponed. Eur Heart J 37:1651–1658
176. Kho C et al (2011) SUMO1-dependent modulation of SERCA2a in heart failure. Nature 477:601–605
177. Haghighi K et al (2001) Superinhibition of sarcoplasmic reticulum function by phospholamban induces cardiac contractile failure. J Biol Chem 276(24):145–152
178. Nicolaou P, Kranias EG (2009) Role of PP1 in the regulation of Ca cycling in cardiac physiology and pathophysiology. Front Biosci 14:3571–3585
179. Ishikawa K et al (2014) Cardiac I-1c overexpression with reengineered AAV improves cardiac function in swine ischemic heart failure. Mol Ther 22:2038–2045
180. Nelson BR et al (2016) A peptide encoded by a transcript annotated as long noncoding RNA enhances SERCA activity in muscle. Science 351:271–275
181. Anderson DM et al (2015) A micropeptide encoded by a putative long noncoding RNA regulates muscle performance. Cell 160:595–606
182. Anderson DM et al (2016) Widespread control of calcium signaling by a family of SERCA-inhibiting micropeptides. Sci Signal 9:ra119
183. Gorski PA, Ceholski DK, Hajjar RJ (2015) Altered myocardial calcium cycling and energetics in heart failure--a rational approach for disease treatment. Cell Metab 21:183–194
184. Krols M, Bultynck G, Janssens S (2016) ER-mitochondria contact sites: a new regulator of cellular calcium flux comes into play. J Cell Biol 214:367–370

Chapter 6
Structural Insights into IP_3R Function

Irina I. Serysheva, Mariah R. Baker, and Guizhen Fan

Abstract Inositol 1,4,5-trisphosphate receptors (IP_3Rs) are ubiquitously expressed intracellular ligand-gated Ca^{2+} channels present on the endoplasmic reticulum of virtually all eukaryotic cells. These channels mediate the Ca^{2+} release from intracellular stores in response to activation by the signaling molecule IP_3, which functions to transmit diverse signals received by the cell, *e.g.* from hormones, neurotransmitters, growth factors and hypertrophic stimuli, to various signaling pathways within the cell. Thus, IP_3R channels can be conceptualized as highly dynamic scaffold membrane protein complexes, where binding of ligands can change the scaffold structure leading to cellular Ca^{2+} signals that direct markedly different cellular actions. Although extensively characterized in physiological and biochemical studies, the detailed mechanisms of how IP_3Rs produce highly controlled Ca^{2+} signals in response to diversified extra- and intracellular stimuli remains unknown and requires high-resolution knowledge of channel molecular architecture. Recently, single-particle electron cryomicroscopy (cryo-EM) has yielded a long-awaited near-atomic resolution structure of the entire full-length type 1 IP_3R. This structure provides important insights into the molecular underpinnings of ligand-mediated activation and regulation of IP_3R. In this chapter, we evaluate available information and research progress on the structure of IP_3R channel in an attempt to shed light on its function.

Keywords Inositol 1,4,5-trisphosphate receptor · Ca^{2+} release channel · Near-atomic resolution structure · Single-particle cryo-EM

I. I. Serysheva (✉) · M. R. Baker · G. Fan
Department of Biochemistry and Molecular Biology, Structural Biology Imaging Center, McGovern Medical School at The University of Texas Health Science Center, Houston, TX, USA
e-mail: Irina.I.Serysheva@uth.tmc.edu

J. Krebs (ed.), *Membrane Dynamics and Calcium Signaling*, Advances in Experimental Medicine and Biology 981,
https://doi.org/10.1007/978-3-319-55858-5_6

6.1 Introduction

The Ca^{2+} ion is the most common second messenger in eukaryotic cells and plays a crucial role in cellular responses to a wide variety of extra- and intracellular signals. The precise control of cellular cytosolic Ca^{2+} levels (*i.e.* Ca^{2+} signaling) is pivotal to diverse biological processes, including muscle contraction, learning and memory, synaptic transmission, gene transcription, cell division, cell development and apoptosis. For Ca^{2+} signaling to be effective cells must maintain low levels of cytosolic Ca^{2+} under resting conditions and be able to generate rapid and transient increases of cytosolic free Ca^{2+} upon stimulation. Most Ca^{2+} signals result from the release of Ca^{2+} from intracellular stores, such as the endoplasmic reticulum (ER). These Ca^{2+} signals are mediated by Ca^{2+} release channels present on the ER membranes: inositol 1,4, 5-trisphosphate receptors (IP_3Rs) and ryanodine receptors (RyRs). While the RyRs represent the primary Ca^{2+} release channels in striated muscle cells, IP_3Rs are ubiquitously expressed with their highest densities in Purkinje cells of the cerebellum. In situ, IP_3Rs function in association with an array of regulatory molecules ranging from ions and small chemical compounds to proteins. These interactions contribute to the specificity, duration and shape of Ca^{2+} signals generated by these channels and form the basis of their capacity to integrate information from different signaling pathways [1]. Conceptually, IP_3Rs work as signaling hubs through which diverse cellular inputs like IP_3, Ca^{2+}, ATP, thiol modifications, phosphorylation and interacting proteins are integrated and then emerge as cytosolic Ca^{2+} signals. This complex integration of multiple signals leads to a diversified cell signaling pathway that results in markedly different cell actions. The fact that Ca^{2+} serves multiple roles raises the possibility of crosstalk between processes, which may otherwise appear independent. Malfunction of IP_3Rs leads to aberrant Ca^{2+} signaling that is associated with a multitude of human diseases such as cardiac hypertrophy, heart failure, hereditary ataxias, atherosclerosis, hypertension, some migraines, Alzheimer's and Huntington's diseases [2–5]. Unraveling the molecular mechanisms for Ca^{2+} signaling through the activation of Ca^{2+} release channels is necessary for understanding cell function and detailed atomistic knowledge of the protein structure provides critical mechanistic insights into channel function. Until a few years ago, high-resolution 3D structure information on IP_3R channel was limited to crystal structures of *N*-terminal ligand binding domains [6–9], with only a low-resolution single-particle cryo-EM structure available for the entire tetrameric IP_3R [10, 11]. Here we focus on the latest structural insights into the IP_3R architecture solved to near-atomic resolution by single-particle cryo-EM [12], revealing mechanistic details of the channel function. We also consider future prospects and challenges for structural studies of these channels.

6.2 Historical Perspective on the Structural Studies of IP_3R

The early discoveries of receptor-activated hydrolysis of PIP_2 leading to intracellular Ca^{2+} mobilization [13] and the identification of IP_3 as the second messenger molecule responsible for Ca^{2+} release from intracellular stores [14, 15] opened the door to research aimed at revealing the identity of the IP_3 binding protein and detailing the molecular mechanisms underlying IP_3 induced Ca^{2+} release. Since their discovery in vertebrate systems about three decades ago [16–18] and cloning of the gene encoding an IP_3 receptor protein [19, 20], many studies have sought to elucidate the structure-function properties of IP_3R channels. Initial insights into the IP_3R structure were provided based on biochemical, mutagenesis and functional studies from multiple groups. It was proposed that IP_3R protein can be subdivided into four functional regions: an IP_3-binding region comprising ~600 residues at the *N*-terminus of the receptor protein; a central modulatory region with sites for interaction with regulatory molecules, a *C*-terminal channel-forming region containing six putative transmembrane (TM) domains, and a *C*-terminal tail including the last ~160 residues [21, 22]. Predicted membrane topology of IP_3R suggested that both the *N*- and *C*-termini are intracellular contributing to a large cytoplasmic portion of the IP_3R channel that encompasses ~90% of the protein mass. It has been found that mammalian genes encode three homologous isoforms of the receptor (IP_3R1-3) that share ~70% overall sequence identity, which increases to ~90% within the predicted TM region. Each isoform shows distinct properties in terms of modulation by endogenous and exogenous ligands and tissue distribution. IP_3R diversity is further expanded by alternative gene splicing within the cytoplasmic region as well as by the homo- and hetero-tetrameric assembly of the IP_3R subunits into functional channels. Most structural studies to date have focused primarily on type 1 IP_3R, due to it being the most characterized of the mammalian isoforms and its predominance over other isoforms in the ER of cerebellar Purkinje cells.

The first glimpses of IP_3Rs in the native membrane came from EM studies of negatively stained thin-sections of COS cells overexpressing IP_3R [23] and from quick-freeze deep-etch replica EM of Purkinje cells ([24]; see Fig. 6.1). These studies showed that in the membranes IP_3Rs form 2D arrays of square-shaped, compact particles of ~12 nm in diameter. The next essential step towards 3D structure determination of IP_3R1 was the successful isolation of the detergent-solubilized receptor protein from the cerebellar membranes [34, 35]. Early EM images of IP_3R1 channel using negatively stained purified receptor [25, 27, 36] confirmed its overall shape with fourfold symmetry and similar dimensions as described by EM studies of IP_3R in the native membrane [23, 24]. In further pursuit of understanding the 3D structure of the IP_3R, three major structural techniques have been utilized: X-ray crystallography [6–9, 33], nuclear magnetic resonance (NMR) spectroscopy [32, 37] and single-particle cryo-EM [10–12, 26, 28–31]. Until recent methodological and technical advances in cryo-EM, X-ray crystallography was the predominant technique for producing atomic resolution structures of proteins; however, well performing targets were generally small, soluble proteins. The enormity of

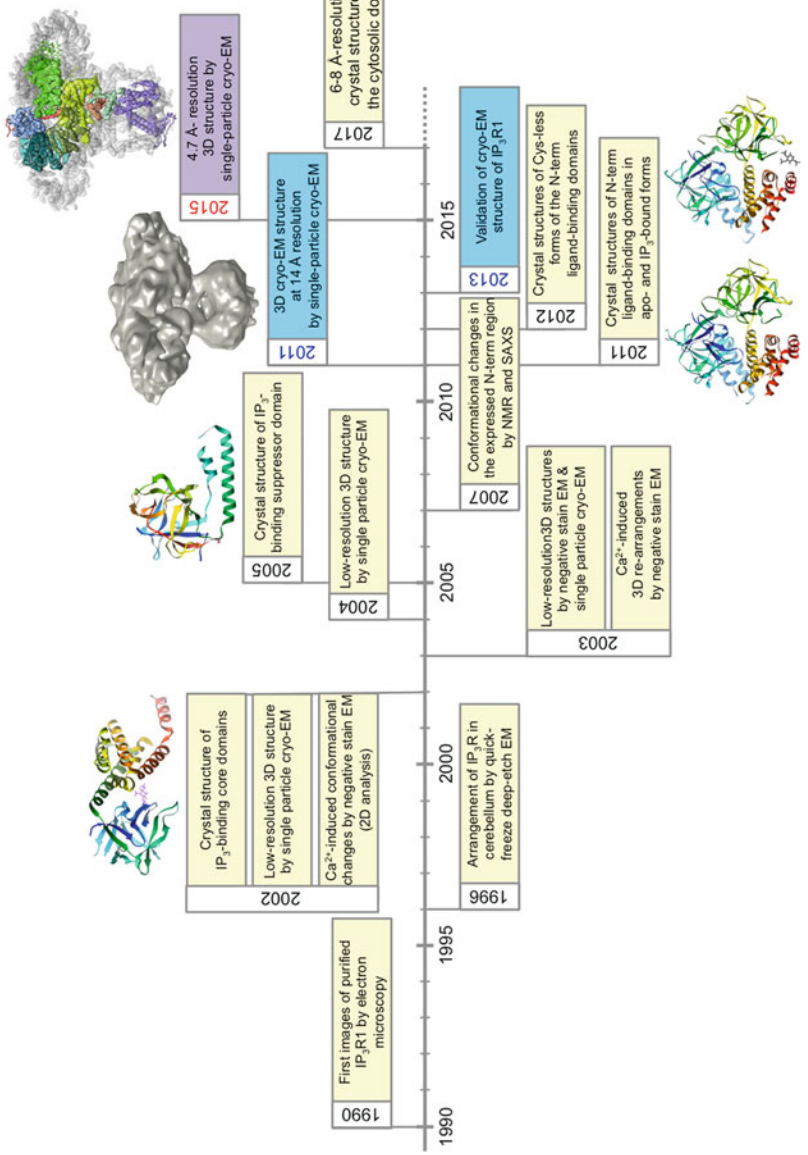

Fig. 6.1 Historical Timeline of IP_3R Structural Studies. In the last three decades, much was learned about the structure of IP_3R which paved the road for intensive research of molecular mechanism: first images of purified IP_3R1 [25]; native arrangement of IP_3R in cerebellum [24]; first 3D map of IP_3R1 by

the IP_3R protein, its functional assembly as a tetramer and the need to extract the channel protein from a lipid bilayer with detergents makes structural studies of IP_3R by X-ray crystallography and NMR largely intractable. Rather, several small pieces of the cytoplasmic *N*-terminal ligand binding domains were expressed and their structures solved by X-ray crystallography [6–9]. These structures, solved at 1.8–3.8 Å resolution in apo- and IP_3-bound states, are in good agreement with one another and describe three discrete domains arranged in a triangular shape: two β-trefoil domains (β-TF1 and β-TF2) followed by an α-helical armadillo repeat (ARM) domain. The IP_3 binding pocket is formed at the interface of β-TF2 and ARM1, and several positively charged residues within the IP_3 binding pocket were identified to be involved in coordinating the phosphate groups of IP_3. In the ligand-bound state, the β-TF2 and ARM1 domains move closer to each other modestly closing the clam-like structure. These observations are consistent with earlier NMR and small-angle X-ray scattering studies [32]. Most recently, low-resolution X-ray structures (6–8 Å) of the mouse IP_3R1 cytosolic domain were obtained [33]. However, the poorly diffracting crystals were not suitable to provide atomic structural details and relied upon the 4.7 Å resolution structure of the full-length, tetrameric IP_3R1 channel solved by cryo-EM [12] to phase the X-ray data in order to build atomic models of the soluble cytosolic domains.

Aforementioned high-resolution X-ray structures of the soluble ligand-binding domains provide important structural details regarding IP_3 binding determinants [6–9], however, interpretations and implications to channel function are largely limited due to the fact that these structures were not solved in the context of a tetrameric channel assembly that likely imposes additional structural constraints underlying the high allostericity of IP_3R channel. Thus, interpretations regarding the structural rearrangements upon ligand binding cannot be unequivocally correlated with functional states of the ion conduction pathway because of a lack of the TM and *C*-terminal domains, that are known to be functionally coupled to ligand-evoked channel activation [38]. Attempts to dock the crystal structures fragments into existing cryo-EM maps [9, 39, 40], assumes that the fragment structures retain an identical conformation as in the full assembly. Therefore, crystallographic and NMR studies failed to answer the fundamental questions on IP_3R activation and gating:

Fig. 6.1 (continued) cryo-EM [26]; Ca^{2+}-induced conformational changes in IP_3R1 [27]; crystal structure of IP_3-binding core domains [6]; 3D structures of IP_3R1 by negative stain EM [28] and by cryo-EM [29]; Ca^{2+}-induced rearrangements of IP_3R1 by EM [30]; another 3D structure of IP_3R1 by cryo-EM [31]; crystal structure of IP_3-binding suppressor domain [7]; ligand-induced conformational changes in the *N*-terminal region by NMR and small-angle X-ray scattering [32]; 3D cryo-EM structure of IP_3R1 in the closed state at subnanometer resolution [10]; crystal structure of *N*-terminal ligand binding domains in Apo- and IP_3-bound forms [8]; Apo and ligand-bound crystal structures of Cys-less forms of the N-terminal ligand-binding domains [9]; validation of IP_3R1 cryo-EM structure [11]; first near-atomic resolution cryo-EM structure of IP_3R1 in its apo-state [12]; 6–8 Å-resolution crystal structures of the cytosolic domains [33]

how the channel detects specific ligand signals and converts them into Ca^{2+} signals; what is a structural basis for functional coupling underlying the ligand-mediated channel gating?

It took over two decades of structural studies to achieve an atomistic model of the full-length, tetrameric IP_3R channel finally solved by using the single-particle cryo-EM technique, which has emerged as the most feasible approach to tackle the structure and evaluate the dynamic aspects of macromolecular assemblies such as Ca^{2+} release channels. However, the journey to a high-resolution structure of IP_3R1 was met with many challenges. In the early 2000s several low-resolution 3D reconstructions (25–40 Å) of the entire IP_3R1 were determined almost simultaneously by single-particle EM, using both negatively stained and vitrified samples [26, 28–31]. These 3D structures while consistent with respect to the basic arrangement of the receptor complex, comprising of large cytoplasmic and TM regions, were strikingly different on a more detailed level. The structures varied in shape, being described as uneven dumbbell, pinwheel, flower-like and hot-air balloon, with each exhibiting vastly different dimensions and putative TM domain configurations. Ultimately, the disparate structures lead to an uncertainty regarding the true 3D structure of IP_3R1 and compromised the credibility for using single-particle cryo-EM as a tool for reliable structure determination. The long-standing controversy about the 3D architecture of entire IP_3R was a critical obstacle substantially slowing progress of research aiming to understand structure-function relationships within the IP_3R channel. To resolve this conundrum, extensive biochemical optimizations and implementation of new single-particle cryo-EM standards were rigorously pursued, finally resulting in a new, unambiguous cryo-EM structure of IP_3R1 solved by our group to intermediate resolution [10]. Ultimately, it was determined that insufficient contrast in early cryo-EM images was the likely culprit for the wide variability exhibited in the previous low-resolution structures of IP_3R1 [10]. To date, the best 3D structure of IP_3R1 in the apo-state is solved to near-atomic resolution by single-particle cryo-EM [12].

6.3 Validation of the 3D Structure of IP_3R

Due to recent technical advances single-particle cryo-EM has emerged as one of the most straightforward and powerful techniques capable of generating reliable near-atomic and atomic-resolution structures of individual proteins and their complexes. However, membranes proteins and complex biological assemblies have been notoriously difficult to prepare for single-particle cryo-EM studies due to their instability outside of their native lipid membrane environment and dynamic nature. Detergents are traditionally used to make membrane proteins soluble and suitable for structural analysis, however the presence of detergent in the buffer leads to producing cryo-EM images, taken at low electron dose, with low signal-to-noise ratio. It is evident that as signal-to-noise ratio is reduced, assignment of particle orientations becomes more susceptible to model bias, leading to the determination of incorrect 3D

reconstruction [41–43]. This was the primary impediment to the early single-particle cryo-EM studies of IP_3R channel that had a number of false-starts [44]. A reliable structure of tetrameric IP_3R1 channel was determined by our group to intermediate resolution (10–15 Å, depending on local flexibility in specific domains) by single-particle cryo-EM in 2011 [10]. Notably, this structure did not bear any resemblance to any of previously published cryo-EM maps (Fig. 6.2) [26, 29, 31]. However, multiple, specific validation methods including tilt validation [45, 46], class-average/map comparisons, independent refinements in multiple software packages and the 'gold standard' resolution evaluation method [47] were applied to clearly prove the veracity of this structure [11]. These key studies [10, 11] laid to rest a critical controversy on the IP_3R1 quaternary structure and highlighted the importance of cryo-EM density map validation at low resolutions. Overall, key to determining a reliable structure of IP_3R1 was an optimized purification procedure combined with biochemical and functional characterization of the purified channel. Choice of the detergent used for the protein solubilization and protein-to-detergent ratio in the sample have been critical factors in achieving optimal vitrification conditions including the protein stability, ice thickness, particle distribution on an EM grid, that together affected the quality of cryo-EM data [41, 42]. Careful consideration of all these factors mentioned above enabled the structure of IP_3R1 to be unambiguously solved initially to nanometer resolution [10] and most recently, to near-atomic resolution, which has provided critical insights into the IP_3R1 gating machinery [12].

6.4 Near-Atomic Resolution Structure of Tetrameric IP_3R Assembly

Structure Determination and Validation Single-particle cryo-EM has recently made impressive strides towards achieving near-atomic (3–5 Å) resolution structures of a wide array of integral membrane proteins [48–57] including the megadalton Ca^{2+} release channels, IP_3Rs and RyRs [12, 58–63]. Moreover, in some favorable cases, the achievable resolution for single particle cryo-EM is now comparable to that produced in atomic-resolution X-ray crystallographic studies (2–3 Å) [48, 64–67]. Two main technical advances in single-particle cryo-EM have had an immediate impact on cryo-EM studies of ion channels and pushed the resolution limit in structural studies of IP_3R1. First, the use of a direct electron detector allowed to produce electron images of ice-embedded channel particles with substantially higher signal-to-noise ratio at both low and high resolution frequencies and to capture multiframe movies that track measurable electron signal throughout a time period. The subsequent alignment of these movie frames eliminates the image blurring that would otherwise happen due to electron beam-induced motion, thus producing higher contrast images of the particles. Second, significant developments in image processing algorithms and methodology for single-particle reconstructions (extensively reviewed in [68–71]) have enhanced our ability to sort out sample

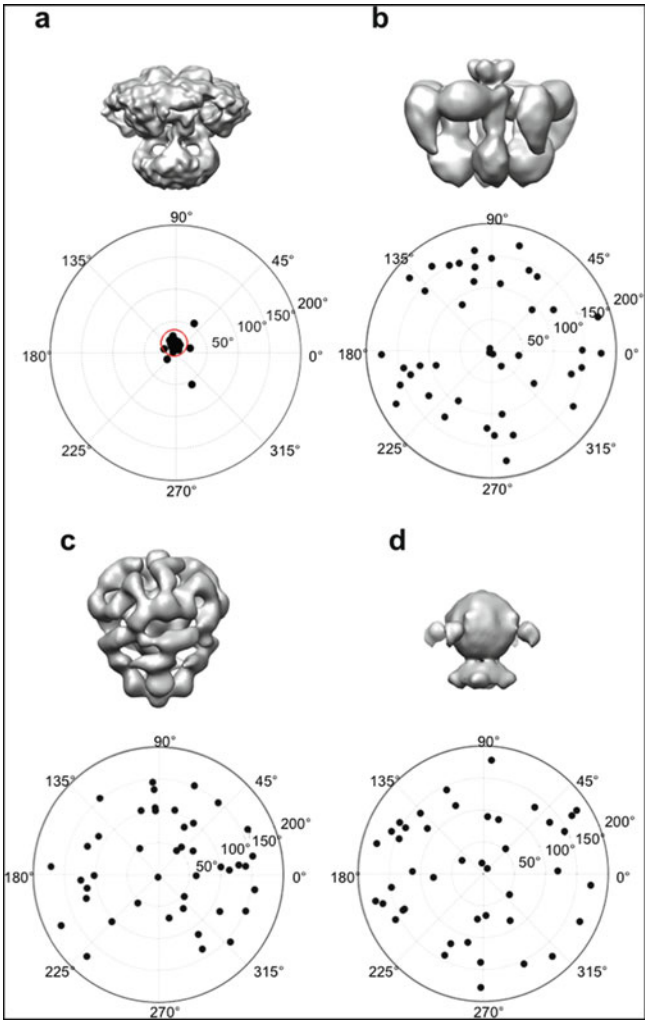

Fig. 6.2 Tilt-pair validation of IP_3R1 structure at intermediate resolution. Validation plots for the tilt-pair images (lower panel) were calculated against four cryo-EM maps (upper panel) [10, 26, 29, 31]. Each point represents a pair of particles with experimentally known relative tilt. The radius indicates the computationally determined amount of tilt, and the azimuth indicates tilt direction. The red circle in (**a**) denotes particle pairs that cluster around the experimental tilt geometry, thus validating IP_3R1 map above (EMDB-5278); note, that maps shown in (**b–d**) produce a completely random distribution with no clustering

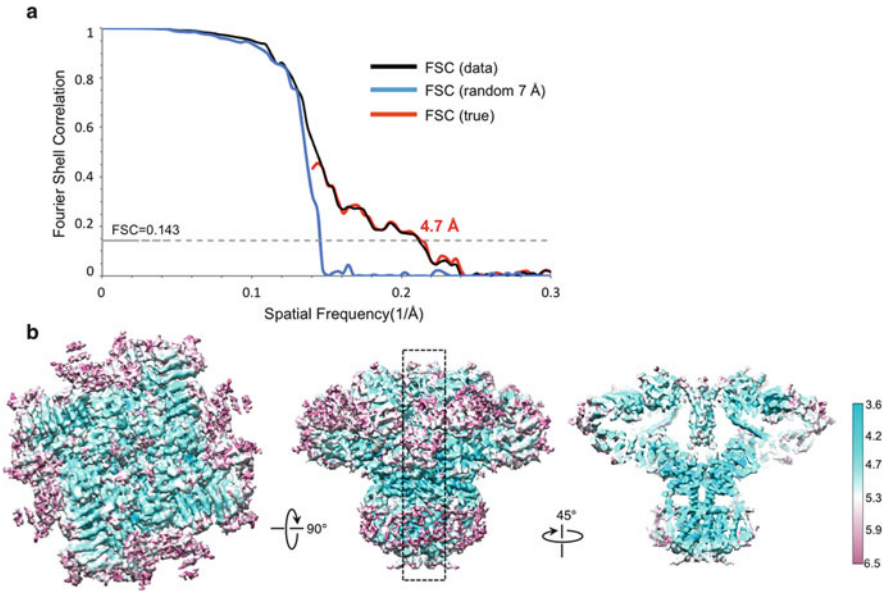

Fig. 6.3 Resolution Evaluation and Validation of 3D reconstruction. (**a**). The gold-standard FSC curve for the final cryo-EM map [12]. The overall resolution is 4.7 Å using the FSC cut-off = 0.143. The blue line shows the FSC curve computed for the data in which the phases were randomized in resolution range from 6 Å to Nyquist; the gold standard FSC curve (black line) is nearly identical to the "true FSC" (red line). (**b**). Estimation of local resolution of 3D reconstruction of IP_3R1: the cryo-EM density map is color-coded according to local resolution estimated by RESMAP [72]. The map is shown in two orthogonal views: a view from cytosol (left) and a side view (middle). A slab density along four-fold channel axis (dashed line in the middle panel) is shown in the right panel. The color scale is shown in the right side of (**b**). As indicated by the local resolution estimation, the central regions are better resolved than the peripheral densities

heterogeneity due to genuine protein flexibility and conformational variability of the IP_3R1 channel. Altogether, this profound progress has led to an exponential growth in the structures solved by single-particle cryo-EM at near-atomic resolutions, including that of IP_3R1.

Overall Channel Architecture The cryo-EM density map of IP_3R1 in the apo-state was determined to 4.7 Å-resolution based on the gold standard FSC criterion [12], and the veracity of the map was addressed by phase randomization tests (Fig. 6.3a) [73] and independent reconstructions using two different software packages (EMAN2.1 and Relion1.3) [74]. The shape and dimensions of the four-fold symmetrical 3D density map of IP_3R1 are in excellent agreement with our intermediate resolution cryo-EM structure: two square-shaped regions with side dimension of ~220 Å and ~120 Å connected via stalk densities to form a mushroom-like assembly of ~190 Å in height [10]. While solved to an overall resolution of 4.7 Å, the resolution and resolvability of structural features in the IP_3R1 density map vary from 3.6 Å to 6.5 Å (Fig. 6.3b). This variability likely arises from the genuine

heterogeneity of channel complexes isolated from native tissue, and from the intrinsically flexible, multi-domain architecture of IP_3R1. Nevertheless, the map was of sufficient quality to trace the backbone topology for 2,327 of 2,750 amino acids and unambiguously identify ten domains that comprise the full-length IP_3R1 protein (Fig. 6.4). Densities in the TM domain were sufficiently resolved to clearly define side-chains of bulky residues along the ion conduction pathway. The individual IP_3R1 subunit is made of ten domains that are arranged in the functional channel assembly around its central four-fold axis to constitute a bulky cytosolic region connected by 'stalk' densities to the TM region (Fig. 6.4).

Solenoid Cytoplasmic Scaffold The majority of cytoplasmic region of the protein structure is built upon multiple α-helical armadillo repeat domains (ARM1–3) with an α-helical domain between ARM1 and ARM2, which constitute many modulator binding sites, and two β-trefoil domains (β-TF1 and β-TF2) comprising the N-terminal domains contribute, with the ARM1 domain, to the IP_3 ligand binding domains (Fig. 6.4). The structure of the ligand binding domains solved by cryo-EM is consistent with structures from X-ray crystallography [12, 74]. After the ARM3, the subunit extends into the 'intervening lateral' domain (ILD), which contains two antiparallel β-strands followed by a helix–turn–helix motif. The *C*-terminus of the ILD connects to TM1 of the TMD, which is comprised of six α-helices (TM1–TM6), a pore (P)-helix and three lumenal loops. The TM6 helix extends beyond the putative lipid bilayer boundaries to cytosol where it is connected to a helical linker domain (LNK) followed by the 80 Å long α-helix of the *C*-terminal domain (CTD).

Transmembrane Domain Structure IP_3R channels are members of the tetrameric cation channel superfamily, where each subunit contains six TM helices (TM1–TM6), whereby the first four TM helices (TM1–TM4) form a peripheral bundle connected to the pore bundle (TM5/TM6) through the lateral TM4–5 linker helix (Figs. 6.6 and 6.7). TM5 and TM6 from each subunit pack in a right-handed bundle creating a single ion-conducting pore in the center of the channel. The pore-forming helices from one subunit interact with the TM1–TM4 helical bundle of the neighboring subunit, described as 'domain swapping'. The swapped architecture of TM domains is a conserved feature of the tetrameric cation channels and helps to stabilize the channel structure.

The Ca^{2+} conduction pathway is lined by four TM6 helices ~55 Å long and, tilted 37° relative to the membrane normal. The TM6 helices closely approach each other curving radially to form a tapering path for ions (Fig. 6.5). A constriction point along the TM6 helices suggests a physical gate for ion permeation. A series of hydrophobic residues, L2582, F2586 and I2590 face the Ca^{2+} permeation pathway with the narrowest point observed at F2586, where it shapes a pore of 5 Å in diameter, suggesting non-conduction Ca^{2+} channel (Fig. 6.6b). R2597, identified closer to the cytosolic vestibule of the ion conduction pathway, likely forms a positively charged constriction region in the tetrameric channel to ensure electrostatic repulsion of positive ions.

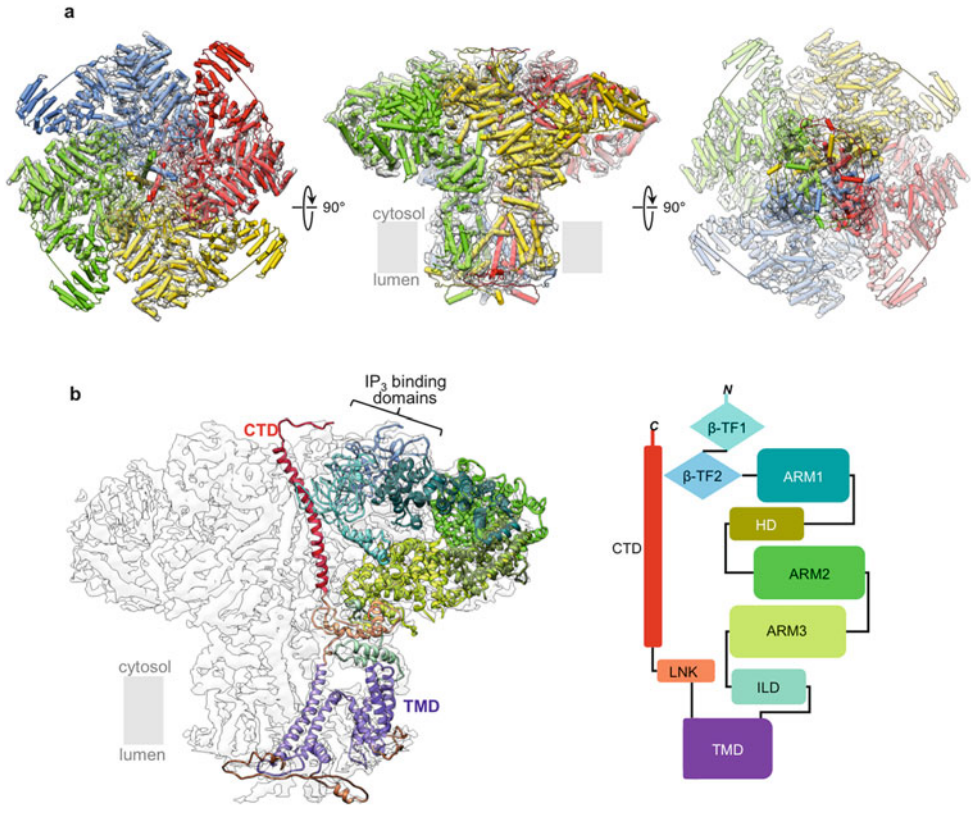

Fig. 6.4 3D Structure of IP_3R1 determined by single-particle cryo-EM at near-atomic resolution. (**a**) Model of IP_3R1 is depicted with each of the four identical subunits color-coded and overlapped with corresponding cryo-EM density map; shown are views from cytosol (left), side view along the membrane (middle)

Structural Coupling in Tetrameric IP_3R1 Particularly unique to the IP_3R1 architecture is that the entire tetrameric channel assembly is built around two four-helix bundles: TM and cytosolic bundle that are connected via the LNK domain to form a central core along the central channel axis (Fig. 6.5). The TM bundle is right-handed and formed by the TM6 helices (one from each subunit) whereas the cytosolic bundle contains the 80 Å long α-helix of the CTD of each subunit packed in a left-handed fashion. This cytoplasmic bundle was described in an earlier cryo-EM study as the 'plug' density [10]. The LNK domain is comprised of two short, nearly orthogonal helices. The *N*-terminal ligand binding domains (LBD) are organized around the CTD bundle and form apical densities in the cryo-EM map of IP_3R1. As a consequence of this structural organization, the CTD bundle connects the LBDs to the TM domains. Moreover, the CTD of one subunit interacts with the β-TF2 domain of the adjacent subunit (Figs. 6.6 and 6.7).

While precise conformational changes associated with IP_3-induced activation of channel gating have yet to be established for the tetrameric channel, several discrete inter- and intra-subunit interfaces identified in the near-atomic cryo-EM structure may be responsible for the propagation of the ligand-binding signal to the TMD, promoting channel opening. Previously, an intra-subunit interface between the β-TF1 and β-TF2 domains was shown to be dynamic, allowing for β-TF1 to twist in response to IP_3 binding [8, 9], however, the context for ligand binding domains arrangement in the tetrameric structure would reveal further interactions important for signal transduction. The β-TF1 domain, termed the suppressor domain due to its role in reducing the channel's affinity for IP_3 [75, 76], contacts the β-TF2 domain of the neighboring subunit via residues within the hotspot loop on β-TF1 (Fig. 6.7). Mutations within the hotspot loop can alter or abolish (Y167A) IP_3-evoked Ca^{2+} release without hindering IP_3 binding to the receptor protein [77]. Removal of the suppressor domain results in a channel that binds IP_3 but fails to open the pore [78, 79]. Furthermore, the β-TF1 domain contains a helix-turn-helix motif that projects into the interior of the cytoplasmic solenoid structure and makes inter-subunit contacts with ARM3 domain of the adjacent subunit. ARM3, which connects to the TMD via ILD, serves an important regulatory domain as it contains the Ca^{2+} sensor region and conserved glutamate residue (E2101) shown to play a role in Ca^{2+} regulation of channel gating. All together, the structural and functional studies point to the importance of the β-TF1 domain in coupling of IP_3 binding to activation of the channel gate.

Therefore, in the tetrameric IP_3R1 the entire cytosolic solenoid scaffold communicates with the TMDs via the ILD and the central CTD helical bundle (Fig. 6.4b, c).

Fig. 6.4 (continued) and from lumen (right). (**b**) Ribbon diagram of a single subunit of IP_3R1 (left panel) with domains color-coded as indicates in the right panel. The model is overlapped with cryo-EM density map of the tetrameric channel. Topological organization of the ten domains identified in one subunit of IP_3R1 (right panel)

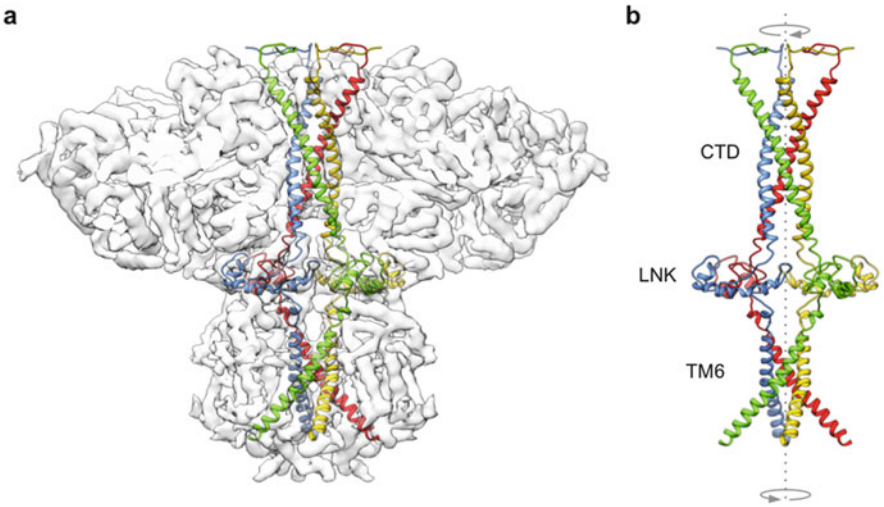

Fig. 6.5 Central core structure of tetrameric IP_3R1. (**a**) Ribbon diagram of α-helical bundle structure is color-coded by subunit and superimposed with cryo-EM density of tetrameric channel. The central bundle structure spans the entire density map of IP_3R1 along its four-fold axis. (**b**) The two alpha-helical bundles are formed by TM6 and CTD -helices from each subunit and connected via four LNK domains (one from each subunit). Of note, the cytosolic bundle of the CTD α-helices is left-handed, while the TM bundle is right-handed Four-fold axis is indicated by the dashed line; arrows indicate the bundle handedness; the central core structure is color-coded by subunit

The near-atomic resolution cryo-EM map of IP_3R1 provides the first direct structural evidence supporting a mechanism whereby IP_3-evoked signals are communicated to the channel gate via long-range allosteric interactions involving the CTD and ARM domains, and the metastable region formed by the ILD and LNK domains at the interface between the CY and TM regions, is responsible for propagation of channel gating signal. This model is consistent with earlier biochemical studies that showed the deletion of last 43 residues from the CTD disrupt channel gating [80]. Noteworthy, the mutations within the 'leaflet' structure [33], corresponding to the first two strands of the ILD observed in the full, tetrameric IP_3R1 channel [12], support the mechanism of signal transduction through the ILD/LNK interface originally proposed by Fan et al. [12]. Moreover, a chimeric channel that essentially lacks the cytosolic C-terminal bundle (via genetic replacement with the highly homologous TMD and CTD from the RyR channel), uncouples IP_3-evoked conformational changes from channel gating [9].

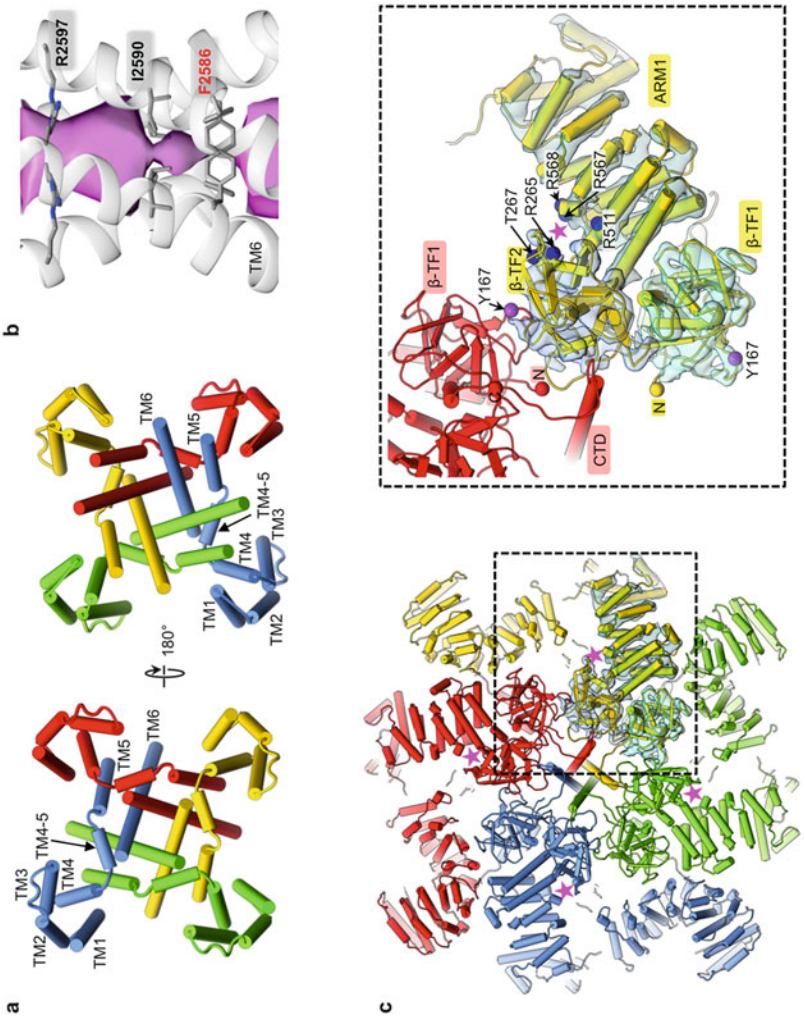

Fig. 6.6 Structural details of IP_3R1. (**a**) Arrangement of TM helices in IP_3R1; subunits are color-coded and viewed from cytosol (left) and lumen (right). (**b**) A bundle of TM6 helices shapes the ion permeation pathway. A series of hydrophobic residues within a constriction region of the channel pore and positively

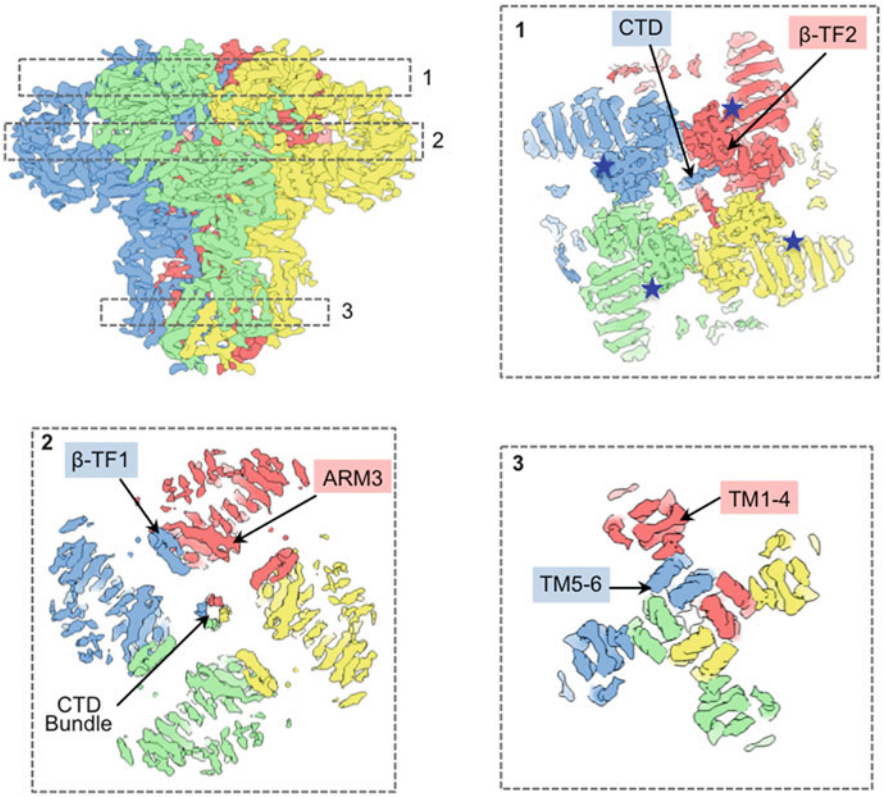

Fig. 6.7 Intra- and inter-subunit interactions. Side view of IP_3R1 density map, slices through the map at indicated positions are shown in (1) structural coupling between the CTD and IP_3-binding domains, blue stars denote IP_3-binding sites; (2) inter-subunit contacts of β-TF1 with ARM3 domains; (3) TM1-TM4 bundle of one subunit interacts with the pore helices (TM5 and TM6) from the neighboring subunit, reflecting the 'domain swapped' architecture

Fig. 6.6 (continued) charged constriction near the cytosolic vestibule of the ion conduction pathway are labeled. (**c**) Structure of IP_3R1 viewed from the cytosol with LBDs and CTDs color-coded by subunit; pink stars denote IP_3-binding sites; zoomed-in panel shows contacts between LBD and CTD of adjacent subunits. Residues involved in IP_3 binding are rendered as blue spheres, purple spheres denote Tyr167

6.5 Structure-Function Conservation in Ca^{2+} Release Channel Family

The ryanodine receptors (RyR) and the inositol 1,4,5-trisphosphate receptors (IP_3R) are two closely related families of intracellular Ca^{2+} release channels. IP_3R and RyR channels principally perform the same intracellular function: to transport Ca^{2+} across the ER/SR membrane. However, they respond to different cellular stimuli, and the intensity, shape and duration of their Ca^{2+} signals are defined by an extensive collection of regulators. IP_3R1s are activated by IP_3 produced in response to cell surface receptor stimulation. Whereas, RyR1 channels respond to small elevations of cytosolic Ca^{2+} or through sensing plasma membrane depolarization by direct coupling with the voltage-gated Ca^{2+} channels in skeletal muscle.

Functional Ca^{2+} release channels form exceptionally large, tetrameric assemblies containing four protomers of about 2,700 amino acid residues for IP_3Rs and about 5,000 amino acid residues for RyRs, accountings for an entire channel molecular mass of over 1.2 MDa and 2.3 MDa, respectively. The channels share 30–40% sequence identity within their *C*-terminal transmembrane domains [19, 20]. Bioinformatic analysis also revealed a shared domain organization in the *N*-terminal regions [81]. However, large sections of the Ca^{2+} release channels have no sequence overlap. Therefore, structural studies of these channels are critical to understanding both their shared and disparate structure-function relationships. Moreover, primary sequence alignments of IP_3R and RyR families have played a major role in the comparative analyses to decipher their structure-function relationship, however, the lack of high-resolution 3D protein structures of IP_3R and RyR substantially restricted the capability to fully rationalize the channels' properties. Quite timely, structures of both IP_3R1 and RyR1 were recently solved to near-atomic resolution by cryo-EM [12, 58–63] and the 3D structural similarities for many domains were more stunning than expected based on primary sequence analysis (Fig. 6.8) [12]. Both structures report an overall α-helical solenoid scaffold structure of a multidomain cytoplasmic region comprising 80–90% of the protein mass, six TM α-helical domains per subunit and cytosolic *N*- and *C*- terminus. However, IP_3R1 exhibits a long α-helical bundle running through the entire cytoplasmic region (Fig. 6.8b), that is not present in RyR1. Furthermore, RyR1 contains several domains that are not found in IP_3R1, doubling the size of its cytoplasmic assembly in comparison to IP_3R1 (Fig. 6.8). It has been recently shown using phylogenetic analyses of the IP_3R and RyR families that the modern RyR genes diverged from an ancient IP_3R gene superfamily [82]. Thus, it is likely that RyR gene acquired the additional domains (SPRY 1–3, Ry1–4, EF-hand) necessary for RyR's specific cell functions on the background of the ancient IP_3R genetic structure. The evolutionary constraints on 3D protein structures are much tighter than those on the primary sequence, and as such protein folds are generally more conserved. Thus, a certain amount of amino acid sequence variation can be tolerated to yield a similar 3D structure, as observed in the high structural conservation but low sequence identity among the shared domains of IP_3R1 and RyR1. Consequently, 3D structural comparisons can give

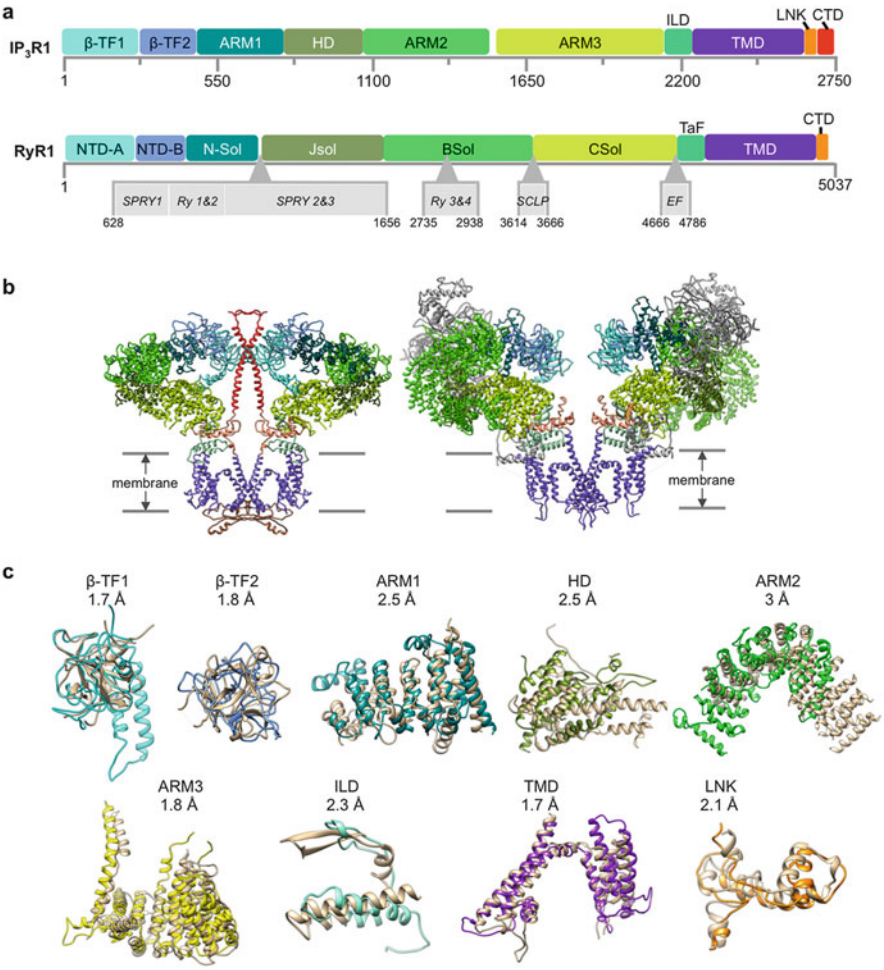

Fig. 6.8 Structural conservation of Ca^{2+} release channels. (**a**) Linear representation of IP_3R1 and RyR1 structural domains based on their structural alignments. RyR1 domains with no structural homology to IP_3R1 are represented as gray insertions below the RyR1 linear representation. (**b**) Structures of IP_3R1 (3JAV), RyR1 (5TB0) viewed along the membrane plane color-coded according to (**a**). (**c**) Correspondence of domains between IP_3R1 and RyR1. Reported are Cα root mean squared deviation for the aligning residue pairs. IP_3R1 domains are color-coded by domain; RyR1 is colored tan

more accurate sequence alignments and be more informative. In the case of IP_3R and RyR, using the entire primary sequence for alignments of such large proteins with low overall sequence homology and many stretches of non-homologous regions results in many misalignments depending on the user's choice of algorithm and options. Recent structural studies of RyR1 clearly demonstrate this point [59, 60].

Cryo-EM studies of IP_3R1 and RyR1 channels reveal a clear structural homology within the *N*-terminal domains: β-TF1, β-TF2 and ARM1 of IP_3R1 and NTD-A, NTD-B and N-Sol of RyR1 (with Cα-RMS deviations of 1.7 Å, 1.8 Å and 2.5 Å, respectively), consistent with previous X-ray crystal structures, yet they share a relatively modest sequence identity (~20–30%) between the channel domains. In IP_3R1 the *N*-terminal domains (β-TF1, β-TF2 and ARM1) are responsible for IP_3 binding and initiating ligand-gated signaling, yet the RyR1 channel does not bind IP_3. However, RyR1 *N*-terminal domains are still relevant to Ca^{2+} channel function as exemplified by mutations within the hotspot loop of RyR1 and RyR2's NTD-A domain correlating with human diseases of malignant hyperthermia, arrhythmia and tachycardia, as well as peptide disruption of hotspot loop interactions resulting in leaky channels [83]. Analogous mutations within β-TF1 of IP_3R1 were found to diminish or ablate IP_3 signaling to the channel pore without affecting IP_3 binding to the channel [77]. Moreover, the β-TF1/NTD-A of IP_3R1 and RyR1, respectively, form an inter-subunit bridge with ARM3/C-solenoid domains, described as the Ca^{2+} sensor, and may relay ligand-evoked signals to the channel. In IP_3R1, the β-TF2/CTD inter-subunit contacts are also proposed to be essential for structure-functional coupling, however, RyR1 lacks an analogous structure indicating that this mode of signal transduction through the CTD bundle is unique to IP_3R1. These structure-function studies support a broadly conserved role for IP_3R1 and RyR1 *N*-terminal domains in relaying important signaling information to the gating machinery.

IP_3R1 and RyR1 are both sensitive to a biphasic Ca^{2+} feedback mechanism, whereby low Ca^{2+} concentrations potentiate channel activation and higher Ca^{2+} concentrations inhibit channel function [84]. However, the locations and physiological impacts of the Ca^{2+} binding sites have yet to be fully resolved. A Ca^{2+} sensor domain in IP_3R1 and RyR1 was first described through efforts to associate conserved residues with their functional role. Mutation of the highly conserved glutamate residues (E4032 in RyR1 and E2101 in IP_3R1) were previously identified to affect Ca^{2+} sensitivity for activation of IP_3R1 and RyR1 channels [85, 86], and therefore the domain was proposed to serve an equivalent Ca^{2+} signaling role in both channel families. However, both Efremov et al. [60] and des Georges et al. [59] claim that the conserved glutamate residues are not equivalent based purely on sequence alignment. In contrast, the structural alignment of the domains containing the E2101 and E4032 (ARM3 of IP_3R1 and *C*-solenoid domain of RyR1) reveal a strongly conserved protein fold (Cα-RMS deviation of 1.8 Å) with the conserved glutamate residues occupying the same spatial location within the domain alignment (Fig. 6.9). The resulting sequence alignment based on the aligned structures showed additional conserved residues (Fig. 6.9), including two residues recently proposed to coordinate Ca^{2+} for RyR1 [59]. Whether these residues play a role in coordinating Ca^{2+} in the IP_3R1 channel remains to be answered by high-resolution structures of the Ca^{2+} bound IP_3R1 channel.

The overall architecture of the TM domains in IP_3R1 is similar to that of RyR1 structure (Fig. 6.8). Both channels are based on the conserved architecture of tetrameric cation channels, in that each subunit has six TM spanning helices in a domain swapped arrangement with one TM6 helix from each subunit comprising the

ion conduction pathway. A physical gate is formed by the large hydrophobic residues on TM6 at F2586 in IP_3R1 and I4937 in RyR1. This structural homology accounts for many functional similarities between IP_3R and RyR channels and suggests a common molecular architecture for the ion-permission pathway. However, important variations (e.g. TM5–6 lumenal and TM2–3 cytosolic loops in IP_3R1 and TMx and S2S3 in RyR1) may explain differences in the gating properties of IP_3R and RyR channels.

Several domains of IP_3R1 have been proposed to form a metastable assembly at the cytosolic and TM interface, whereby the ILD and LNK of the same subunit come together in a highly responsive domain to react to various cellular inputs to control channel gating [12]. Recently, the RyR cryo-EM structure determined in the presence of channel activators, Ca^{2+}, ATP and caffeine, revealed several domain interfaces necessary to coordinate activating ligands, with the CTD playing a major role. ATP binds RyR1 at the interfaces of TM6/CTD/TaF; the Ca^{2+} binding site is

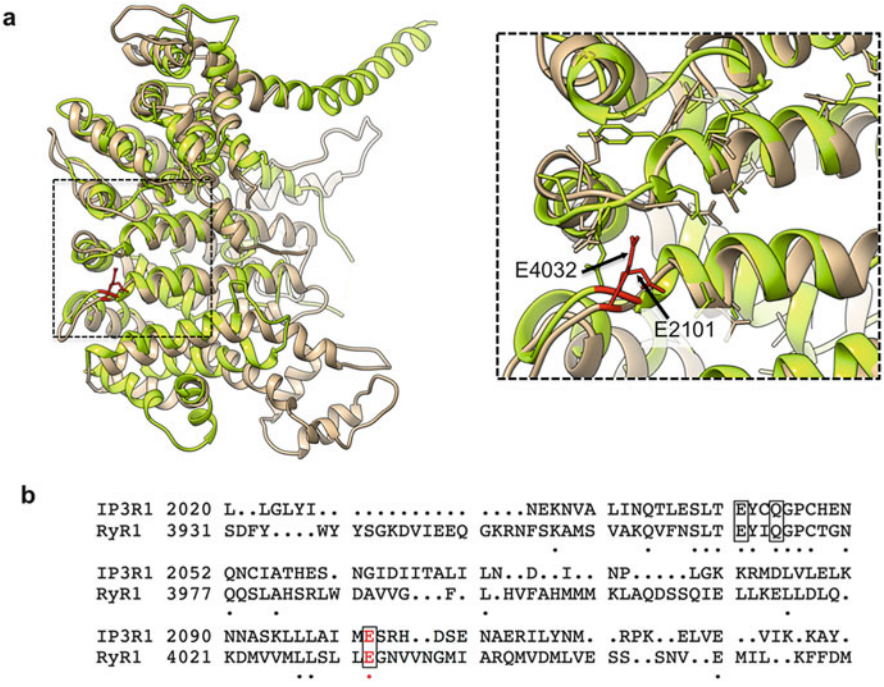

Fig. 6.9 Structural conservation of putative Ca^{2+} sensor region. (**a**) The armadillo repeat domain 3 (ARM3) of IP_3R1 (3JAV) and the C-solenoid of RyR1 (5TB0) share structural and sequence conservation. IP_3R1 is colored chartreuse and RyR1 is colored tan. Cα root mean squared deviation is 1.8 Å. Zoomed-in view shows Ca^{2+} binding pocket identified in RyR1 [59]. The conserved residues E2101 (IP_3R1) and E4032 (RyR1) implicated in channel Ca^{2+} sensitivity are colored red. (**b**) Structure-based sequence alignment for the ARM3 and C-solenoid domain is shown. Structurally equivalent residues in IP_3R1 based on the putatively identified RyR1 Ca^{2+} binding pocket are indicated with a box. E2101 and E4032 are colored red. Identical residues are indicated with a ● below the alignment

comprised of the C-Sol and CTD, while the caffeine binding site is formed by S2S3 domain and the CTD. The RyR1 activators, when bound at the CTD interfaces, are proposed to rearrange the channel by priming the gating machinery to adopt a structural state that that favors a greater open probability [59]. While it is known that IP_3R1 is regulated by ATP and Ca^{2+}, it exhibits a much lower sensitivity to caffeine than RyR1 and fittingly the S2S3 domain which helps to coordinate caffeine in RyR1 is absent in the structure of IP_3R1. Whether the analogous residues play a role in coordinating ATP and Ca^{2+} in the IP_3R1 channel remains to be answered by high-resolution structures of ligand-bound IP_3R1 channel. In IP_3R1 and RyR1 their respective ILD-LNK and TaF-CTD domains form a similar intra-subunit structure, whereby the LNK/CTD domain is sandwiched between the set of β-strands followed and the helix–turn–helix portion of the ILD/TaF domain. We suggest that this points toward a conserved metastable assembly among all Ca^{2+} release channels whereby allosteric modulation of channel gating is funneled through the ILD-LNK of IP_3R or the TaF-CTD of RyR to influence the channel gate (see Fig. 6.10).

6.6 Conclusions and Future Perspective

Understanding structural basis of molecular transport across biological membrane is a challenging frontier in structural biology fascinating researches for many years. Ca^{2+} release channels were among the first ion channels attempted by the single-particle cryo-EM approach. The current cryo-EM studies of IP_3R1 channel provided 4.7 Å-resolution structure of the entire channel in its apo-state that addresses a critical barrier to progress in the IP_3-mediated Ca^{2+} signaling research: understanding the structural basis of the functional coupling between IP_3 binding to the receptor protein and Ca^{2+} translocation via the channel gate. Among tetrameric cation channels with the domain-swapped architecture of the TM assembly, IP_3R1 channel is unique in the respect of the 3D architecture of its *C*-terminal domain forming a left-handed α-helical bundle along the central four-fold axis that spans the entire cytosolic region of the channel. This unexpected arrangement of the CTDs in tetrameric IP_3R suggests a distinctive allosteric mechanism underlying activation of the channel gating that relies on a direct mechanical coupling between the CTD and IP_3-binding domains of adjacent subunits and involves rearrangements of several inter-domain interfaces. Another prominent feature of IP_3R1 channel is the α-helical solenoid architecture of cytoplasmic domains that serve as scaffolds for interaction with multiple auxiliary proteins that associate with IP_3R1 in situ and finely tune its activity (Fig. 6.10). All together, these findings support a mechanism whereby long-range allosteric interactions through the CTD and cytoplasmic domains provide the functional coupling between ligand binding and channel opening. Overall, while the main conclusions reached based on near-atomic resolution cryo-EM structure of IP_3R1 will likely hold, research aimed at the detailed understanding of IP_3R function is now poised to propel structure determination of the entire IP_3R channel at atomic resolution and in different functional states. There is an optimistic

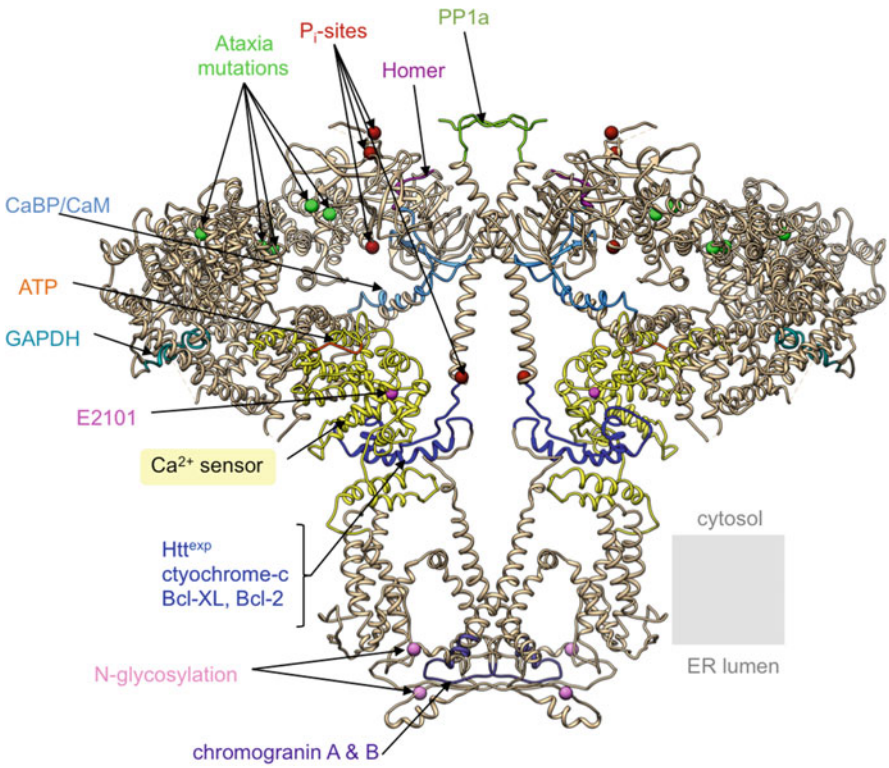

Fig. 6.10 Putative binding sites for several channel-specific ligands are indicated on the IP_3R1 structure; for clarity two opposite subunits are shown. (ATP, ATP-binding; CaM/CaBP, calmodulin/Ca^{2+} binding protein; Htt^{exp}, huntingtin; Bcl-2, B-cell lymphoma-2; Bcl-Xl, B-cell lymphoma-extra-large; PP1a, protein phosphatase 1A; GAPDH, glyceraldehyde-3-phosphate dehydrogenase; magenta sphere denotes E2101) [87]

prospect for further improvement in resolution of IP_3R structure. In general, large proteins proved most amenable for high-resolution single-particle cryo-EM, but they are also prone to large-scale motions in particular domains limiting local-resolutions in the cryo-EM density map. Single-particle cryo-EM is not only a proven alternative to crystallography for 3D structural analysis at atomic level, it is uniquely valuable for probing protein dynamics by capturing 2D images of large particle populations of distinct structural conformations, followed by computationally classifying them and reassembling into a 3D map. Cryo-EM can now efficiently analyze protein structure-function giving rise to many important mechanistic features.

Until now cryo-EM structural studies of IP_3R1 have been conducted on the channel purified from native source, yet the regions for which the IP_3R1 backbone structure that have yet to be resolved overlap with the known locations for alternative splicing and post-translational modifications. This level of heterogeneity cannot be

solved by 'smart' software and has complicated structure-functional studies of IP_3R. In this regard, attempts to reduce the level of structural heterogeneity, with the production of recombinant IP_3R proteins, will be advantageous for achieving higher resolution structures by single-particle cryo-EM. Furthermore, based on numerous functional studies multiple conformations with different lifetimes and stability likely underlie IP_3R's functional states. Approaches to reduce movements of the IP_3R protein include stabilization of the protein conformation by binding of specific ligands, which would promote formation of stable protein complexes suitable for high-resolution structure determination. Thus, success in the structural arena has been, and will continue to be contingent on the development of new technologies including expression of IP_3R proteins, stabilization of specific conformational states and complexes and the ability to collect and process large cryo-EM data sets.

Furthermore, it remains largely unclear to what extent the 3D structures of detergent-solubilized channels represent the structure of the physiologically active channel in biological membrane environment. New approaches are currently being developed to overcome limitations of current single-particle cryo-EM studies of membrane proteins in a detergent-solubilized state. These include substitution of detergents with new surfactants such as 'amphipols' for better structural preservation in the absence of a bilayer, keeping membrane proteins soluble and in their functional form in aqueous solution [41, 88]. Additionally, nano-discs, a disc-shaped lipid bilayer stabilized by encircling amphipathic helical scaffold proteins have been shown to maintain purified membrane proteins in a particularly stable state and allow the protein to be maintained at concentrations suitable for cryo-EM studies [48]. However, one must keep in mind that this approach is prone to a general limitation of single-particle cryo-EM when exploring structure-function of ion channels: both faces of the channel assembly are exposed to the same environment, while in vivo ion channels function in the biological membrane and are exposed to an essentially asymmetric cellular milieu. Structural studies of ion channels reconstituted into lipid vesicles will likely have a high impact on structural analysis as this approach reflects both the presence of lipids, which can affect channel activity and also allows the exploration of the structural basis for gating characteristics in a native-like environment [89–91]. To date, a steadily growing community of researchers is energized with the prospect of using cryo-EM to study ion channels in lipid membrane and to obtain atomic-resolution structure. Overall, the field is now taking advantage of the high-resolution and high-throughput single particle cryo-EM, which together with advanced biochemical and physiological studies, will lead to increased rate of structure-function discoveries in the near future.

Acknowledgments The authors thank Matthew L. Baker for his input on comparative analysis of Ca^{2+} release channels and for critiques on the manuscript. This work was supported by the National Institutes of Health (R01 GM072804), the American Heart Association (16GRNT29720001) and the Muscular Dystrophy Association (295138).

References

1. Foskett JK, White C, Cheung KH, Mak DO (2007) Inositol trisphosphate receptor Ca2+ release channels. Physiol Rev 87:593–658
2. Bezprozvanny I (2007) Inositol 1,4,5-tripshosphate receptor, calcium signalling and Huntington's disease. Subcell Biochem 45:323–335
3. Jacobsen AN, Du XJ, Lambert KA, Dart AM, Woodcock EA (1996) Arrythmogenic action of thrombin during myocardial reperfusion via release of inositol 1,4,5-triphosphate. Circulation 93:23–26
4. Marks AR (1997) Intracellular calcium-release channels: regulators of cell life and death. Am J Phys 272:H597–H605
5. Matsumoto M, Nakagawa T, Innoe T, Nagata E, Tanaka K, Takano H, Minowa O, Kuno J, Sakakibara S, Yamada M, Yoneshima H, Miyawaki A, Fukuuchi Y, Furuichi T, Okano H, Mikoshiba K, Noda T (1996) Ataxia and epileptic seizures in mice lacking type 1 inositol 1,4,5-triphosphate receptor. Nature 379:168–171
6. Bosanac I, Alattia JR, Mal TK, Chan J, Talarico S, Tong FK, Tong KI, Yoshikawa F, Furuichi T, Iwai M, Michikawa T, Mikoshiba K, Ikura M (2002) Structure of the inositol 1,4,5-trisphosphate receptor binding core in complex with its ligand. Nature 420:696–700
7. Bosanac I, Yamazaki H, Matsu-Ura T, Michikawa T, Mikoshiba K, Ikura M (2005) Crystal structure of the ligand binding suppressor domain of type 1 inositol 1,4,5-trisphosphate receptor. Mol Cell 17:193–203
8. Lin CC, Baek K, Lu Z (2011) Apo and InsP-bound crystal structures of the ligand-binding domain of an InsP receptor. Nat Struct Mol Biol 18:1172–1174
9. Seo MD, Velamakanni S, Ishiyama N, Stathopulos PB, Rossi AM, Khan SA, Dale P, Li C, Ames JB, Ikura M, Taylor CW (2012) Structural and functional conservation of key domains in InsP3 and ryanodine receptors. Nature 483:108–112
10. Ludtke SJ, Tran TP, Ngo QT, Moiseenkova-Bell VY, Chiu W, Serysheva II (2011) Flexible architecture of IP3R1 by cryo-EM. Structure 19:1192–1199
11. Murray SC, Flanagan J, Popova OB, Chiu W, Ludtke SJ, Serysheva II (2013) Validation of cryo-EM structure of IP(3)R1 channel. Structure 21:900–909
12. Fan G, Baker ML, Wang Z, Baker MR, Sinyagovskiy PA, Chiu W, Ludtke SJ, Serysheva II (2015) Gating machinery of InsP3R channels revealed by electron cryomicroscopy. Nature 527:336–341
13. Berridge MJ, Fain JN (1979) Inhibition of phosphatidylinositol synthesis and the inactivation of calcium entry after prolonged exposure of the blowfly salivary gland to 5-hydroxytryptamine. Biochem J 178:59–69
14. Berridge MJ (1983) Rapid accumulation of inositol trisphosphate reveals that agonists hydrolyse polyphosphoinositides instead of phosphatidylinositol. Biochem J 212:849–858
15. Streb H, Irvine RF, Berridge MJ, Schulz I (1983) Release of Ca2+ from a nonmitochondrial intracellular store in pancreatic acinar cells by inositol-1,4,5-trisphosphate. Nature 306:67–69
16. Ehrlich BE, Watras J (1988) Inositol 1,4,5-trisphosphate activates a channel from smooth muscle sarcoplasmic reticulum. Nature 336:583–586
17. Ferris CD, Huganir RL, Supattapone S, Snyder SH (1989) Purified inositol 1,4,5-trisphosphate receptor mediates calcium flux in reconstituted lipid vesicles. Nature 342:87–89
18. Iino M (1987) Calcium dependent inositol trisphosphate-induced calcium release in the guinea-pig taenia caeci. Biochem Biophys Res Commun 142:47–52
19. Furuichi T, Yoshikawa S, Miyawaki A, Wada K, Maeda N, Mikoshiba K (1989) Primary structure and functional expression of the inositol 1,4,5- trisphosphate-binding protein P400. Nature 342:32–38
20. Mignery GA, Sudhof TC, Takei K, De Camilli P (1989) Putative receptor for inositol 1,4,5-trisphosphate similar to ryanodine receptor. Nature 342:192–195
21. Mignery GA, Newton CL, Archer BT, Sudhof TC (1990) Structure and expression of the rat inositol 1,4,5-trisphosphate receptor. J Biol Chem 265:12679–12685

22. Yoshikawa S, Tanimura T, Miyawaki A, Nakamura M, Yuzaki M, Furuichi T, Mikoshiba K (1992) Molecular cloning and characterization of the inositol 1,4,5-trisphosphate receptor in Drosophila melanogaster. J Biol Chem 267:16613–16619
23. Takei K, Mignery GA, Mugnaini E, Sudhof TC, De Camilli P (1994) Inositol 1,4,5-trisphosphate receptor causes formation of ER cisternal stacks in transfected fibroblasts and in cerebellar Purkinje cells. Neuron 12:327–342
24. Katayama E, Funahashi H, Michikawa T, Shiraishi T, Ikemoto T, Lino M, Hirosawa K, Mikoshiba K (1996) Native structure and arrangement of inositol-1,4,5-triphosphate receptor molecules in bovine cerebellar Purkinje cells as studied by quick-freeze deep-etch electron microscopy. EMBO J 15:4844–4851
25. Chadwick CC, Saito A, Fleischer S (1990) Isolation and characteriztion of the inositol triphosphate receptor from smooth muscle. Proc Natl Acad Sci 87:2132–2136
26. Jiang QX, Thrower EC, Chester DW, Ehrlich BE, Sigworth FJ (2002) Three-dimensional structure of the type 1 inositol 1,4,5-trisphosphate receptor at 24 A resolution. EMBO J 21:3575–3581
27. Hamada K, Miyata T, Mayanagi K, Hirota J, Mikoshiba K (2002) Two-state conformational changes in inositol 1,4,5-trisphosphate receptor regulated by calcium. J Biol Chem 277:21115–21118
28. Da Fonseca PC, Morris SA, Nerou EP, Taylor CW, Morris EP (2003) Domain organization of the type 1 inositol 1,4,5-trisphosphate receptor as revealed by single-particle analysis. Proc Natl Acad Sci U S A 100:3936–3941
29. Serysheva II, Bare DJ, Ludtke SJ, Kettlun CS, Chiu W, Mignery GA (2003) Structure of the type 1 inositol 1,4,5-trisphosphate receptor revealed by electron cryomicroscopy. J Biol Chem 278:21319–21322
30. Hamada K, Terauchi A, Mikoshiba K (2003) Three-dimensional rearrangements within inositol 1, 4, 5-trisphosphate receptor by calcium. J Biol Chem 278:52881–52889
31. Sato C, Hamada K, Ogura T, Miyazawa A, Iwasaki K, Hiroaki Y, Tani K, Terauchi A, Fujiyoshi Y, Mikoshiba K (2004) Inositol 1,4,5-trisphosphate receptor contains multiple cavities and L-shaped ligand-binding domains. J Mol Biol 336:155–164
32. Chan J, Whitten AE, Jeffries CM, Bosanac I, Mal TK, Ito J, Porumb H, Michikawa T, Mikoshiba K, Trewhella J, Ikura M (2007) Ligand-induced conformational changes via flexible linkers in the amino-terminal region of the inositol 1,4,5-trisphosphate receptor. J Mol Biol 373:1269–1280
33. Hamada K, Miyatake H, Terauchi A, Mikoshiba K (2017) IP3-mediated gating mechanism of the IP3 receptor revealed by mutagenesis and X-ray crystallography. Proc Natl Acad Sci USA 114:4661–4666
34. Maeda N, Niinobe M, Nakahira K, Mikoshiba K (1988) Purification and characterization of P400 protein, a glycoprotein characteristic of Purkinje cell, from mouse cerebellum. J Neurochem 51:1724–1730
35. Supattapone S, Worley PF, Baraban JM, Snyder SH (1988) Solubilization, purification and characteriztion of an inositol triphosphate receptor. J Biol Chem 263:1530–1534
36. Maeda N, Niinobe M, Mikoshiba K (1990) A cerebellar Purkinje cell marker P_{400} protein is an inositol 1,4,5-triphosphate ($insP_3$) receptor protein. Purification and characterization of $InsP_3$ receptor complex. EMBO J 9:61–67
37. Li C, Enomoto M, Rossi AM, Seo MD, Rahman T, Stathopulos PB, Taylor CW, Ikura M, Ames JB (2013) CaBP1, a neuronal Ca^{2+} sensor protein, inhibits inositol trisphosphate receptors by clamping intersubunit interactions. Proc Natl Acad Sci U S A 110:8507–8512
38. Taylor CW, Tovey SC (2010) IP(3) receptors: toward understanding their activation. Cold Spring Harb Perspect Biol 2:a004010
39. Tung CC, Lobo PA, Kimlicka L, Van Petegem F (2010) The amino-terminal disease hotspot of ryanodine receptors forms a cytoplasmic vestibule. Nature 468:585–588
40. Yuchi Z, Lau K, Van Petegem F (2012) Disease mutations in the ryanodine receptor central region: crystal structures of a phosphorylation hot spot domain. Structure 20:1201–1211

41. Baker MR, Fan G, Serysheva II (2015) Single-particle cryo-EM of the ryanodine receptor channel in an aqueous environment. Eur J Transl Myol 25:4803
42. Ludtke SJ, Serysheva II (2013) Single-particle cryo-EM of calcium release channels: structural validation. Curr Opin Struct Biol 23:755–762
43. Stewart A, Grigorieff N (2004) Noise bias in the refinement of structures derived from single particles. Ultramicroscopy 102:67–84
44. Serysheva II, Ludtke SJ (2010) 3D Structure of IP(3) Receptor. Curr Top Membr 66C:171–189
45. Henderson R, Chen S, Chen JZ, Grigorieff N, Passmore LA, Ciccarelli L, Rubinstein JL, Crowther RA, Stewart PL, Rosenthal PB (2011) Tilt-pair analysis of images from a range of different specimens in single-particle electron cryomicroscopy. J Mol Biol 413:1028–1046
46. Rosenthal PB, Henderson R (2003) Optimal determination of particle orientation, absolute hand, and contrast loss in single-particle electron cryomicroscopy. J Mol Biol 333:721–745
47. Scheres SH, Chen S (2012) Prevention of overfitting in cryo-EM structure determination. Nat Methods 9:853–854
48. Gao Y, Cao E, Julius D, Cheng Y (2016) TRPV1 structures in nanodiscs reveal mechanisms of ligand and lipid action. Nature 534:347–351
49. Hite RK, Yuan P, Li Z, Hsuing Y, Walz T, Mackinnon R (2015) Cryo-electron microscopy structure of the Slo2.2 Na(+)-activated K(+) channel. Nature 527:198–203
50. Liao M, Cao E, Julius D, Cheng Y (2013) Structure of the TRPV1 ion channel determined by electron cryo-microscopy. Nature 504:107–112
51. Matthies D, Dalmas O, Borgnia MJ, Dominik PK, Merk A, Rao P, Reddy BG, Islam S, Bartesaghi A, Perozo E, Subramaniam S (2016) Cryo-EM structures of the magnesium channel corA reveal symmetry break upon gating. Cell 164:747–756
52. Paulsen CE, Armache JP, Gao Y, Cheng Y, Julius D (2015) Structure of the TRPA1 ion channel suggests regulatory mechanisms. Nature 520:511–517
53. Shen PS, Yang X, Decaen PG, Liu X, Bulkley D, Clapham DE, Cao E (2016) The structure of the polycystic kidney disease channel PKD2 in lipid nanodiscs. Cell 167:763–773. e11
54. Wang W, Mackinnon R (2017) Cryo-EM structure of the open human ether-a-go-go-related K+ channel hERG. Cell 169:422–430. e10
55. Whicher JR, Mackinnon R (2016) Structure of the voltage-gated K(+) channel Eag1 reveals an alternative voltage sensing mechanism. Science 353:664–669
56. Wu J, Yan Z, Li Z, Qian X, Lu S, Dong M, Zhou Q, Yan N (2016) Structure of the voltage-gated calcium channel Cav1.1 at 3.6 A resolution. Nature 537:191–196
57. Zubcevic L, Herzik MA Jr, Chung BC, Liu Z, Lander GC, Lee SY (2016) Cryo-electron microscopy structure of the TRPV2 ion channel. Nat Struct Mol Biol 23:180–186
58. Bai XC, Yan Z, Wu J, Li Z, Yan N (2016) The central domain of RyR1 is the transducer for long-range allosteric gating of channel opening. Cell Res 26:995–1006
59. Des Georges A, Clarke OB, Zalk R, Yuan Q, Condon KJ, Grassucci RA, Hendrickson WA, Marks AR, Frank J (2016) Structural basis for gating and activation of RyR1. Cell 167:145–157. e17
60. Efremov RG, Leitner A, Aebersold R, Raunser S (2015) Architecture and conformational switch mechanism of the ryanodine receptor. Nature 517:39–43
61. Wei R, Wang X, Zhang Y, Mukherjee S, Zhang L, Chen Q, Huang X, Jing S, Liu C, Li S, Wang G, Xu Y, Zhu S, Williams AJ, Sun F, Yin CC (2016) Structural insights into Ca(2+)-activated long-range allosteric channel gating of RyR1. Cell Res 26:977–994
62. Yan Z, Bai XC, Yan C, Wu J, Li Z, Xie T, Peng W, Yin CC, Li X, Scheres SH, Shi Y, Yan N (2015) Structure of the rabbit ryanodine receptor RyR1 at near-atomic resolution. Nature 517:50–55
63. Zalk R, Clarke OB, Des Georges A, Grassucci RA, Reiken S, Mancia F, Hendrickson WA, Frank J, Marks AR (2015) Structure of a mammalian ryanodine receptor. Nature 517:44–49
64. Bai XC, Yan C, Yang G, Lu P, Ma D, Sun L, Zhou R, Scheres SH, Shi Y (2015) An atomic structure of human gamma-secretase. Nature 525:212–217

65. Bartesaghi A, Merk A, Banerjee S, Matthies D, Wu X, Milne JLS, Subramaniam S (2015) 2.2 Å resolution cryo-EM structure of β-galactosidase in complex with a cell-permeant inhibitor. Science 348:1147–1151
66. Jiang J, Pentelute BL, Collier RJ, Zhou ZH (2015) Atomic structure of anthrax protective antigen pore elucidates toxin translocation. Nature 521:545–549
67. Merk A, Bartesaghi A, Banerjee S, Falconieri V, Rao P, Davis MI, Pragani R, Boxer MB, Earl LA, Milne JL, Subramaniam S (2016) Breaking cryo-EM resolution barriers to facilitate drug discovery. Cell 165:1698–1707
68. Kuhlbrandt W (2014) Cryo-EM enters a new era. elife 3:e03678
69. Liao M, Cao E, Julius D, Cheng Y (2014) Single particle electron cryo-microscopy of a mammalian ion channel. Curr Opin Struct Biol 27:1–7
70. Milne JL, Borgnia MJ, Bartesaghi A, Tran EE, Earl LA, Schauder DM, Lengyel J, Pierson J, Patwardhan A, Subramaniam S (2013) Cryo-electron microscopy—a primer for the non-microscopist. FEBS J 280:28–45
71. Subramaniam S, Earl LA, Falconieri V, Milne JL, Egelman EH (2016) Resolution advances in cryo-EM enable application to drug discovery. Curr Opin Struct Biol 41:194–202
72. Kucukelbir A, Sigworth FJ, Tagare HD (2014) Quantifying the local resolution of cryo-EM density maps. Nat Methods 11:63–65
73. Chen S, Mcmullan G, Faruqi AR, Murshudov GN, Short JM, Scheres SH, Henderson R (2013) High-resolution noise substitution to measure overfitting and validate resolution in 3D structure determination by single particle electron cryomicroscopy. Ultramicroscopy 135:24–35
74. Baker MR, Fan G, Serysheva II (2017) Structure of IP3R channel: high-resolution insights from cryo-EM. Curr Opin Struct Biol 46:38–47
75. Yoshikawa F, Morita M, Monkawa T, Michikawa T, Furuichi T, Mikoshiba K (1996) Mutational analysis of the ligand binding site of the inositol 1,4,5- trisphosphate receptor. J Biol Chem 271:18277–18284
76. Yoshikawa F, Iwasaki H, Michikawa T, Furuichi T, Mikoshiba K (1999) Trypsinized cerebellar inositol 1,4,5-trisphosphate receptor. Structural and functional coupling of cleaved ligand binding and channel domains. J Biol Chem 274:316–327
77. Yamazaki H, Chan J, Ikura M, Michikawa T, Mikoshiba K (2010) Tyr-167/Trp-168 in type 1/3 inositol 1,4,5-trisphosphate receptor mediates functional coupling between ligand binding and channel opening. J Biol Chem 285:36081–36091
78. Szlufcik K, Bultynck G, Callewaert G, Missiaen L, Parys JB, De Smedt H (2006) The suppressor domain of inositol 1,4,5-trisphosphate receptor plays an essential role in the protection against apoptosis. Cell Calcium 39:325–336
79. Uchida K, Miyauchi H, Furuichi T, Michikawa T, Mikoshiba K (2003) Critical regions for activation gating of the inositol 1,4,5-trisphosphate receptor. J Biol Chem 278:16551–16560
80. Schug ZT, Joseph SK (2006) The role of the S4-S5 linker and C-terminal tail in inositol 1,4,5-trisphosphate receptor function. J Biol Chem 281:24431–24440
81. Ponting CP (2000) Novel repeats in ryanodine and IP3 receptors and protein O-mannosyltransferases. Trends Biochem Sci 25:48–50
82. Alzayady K, Sebe-Pedros A, Chandrasekhar R, Wang L, Ruiz-Trillo I, Yule DI (2015) Tracing the evolutionary history of Inositol, 1, 4, 5-Trisphosphate receptor: insights from analyses of capsaspora owczarzaki Ca^{2+} release channel orthologs. Mol Biol Evol 32(9):2236–2253
83. Amador FJ, Liu S, Ishiyama N, Plevin MJ, Wilson A, Maclennan DH, Ikura M (2009) Crystal structure of type I ryanodine receptor amino-terminal beta-trefoil domain reveals a disease-associated mutation "hot spot" loop. Proc Natl Acad Sci U S A 106:11040–11044
84. Bezprozvanny I, Watras J, Ehrlich BE (1991) Bell-shaped calcium-response curves of Ins (1,4,5)P3- and calcium-gated channels from endoplasmic reticulum of cerebellum. Nature 351:751–754
85. Du GG, Maclennan DH (1998) Functional consequences of mutations of conserved, polar amino acids in transmembrane sequences of the Ca^{2+} release channel (ryanodine receptor) of rabbit skeletal muscle sarcoplasmic reticulum. J Biol Chem 273:31867–31872

86. Miyakawa T, Mizushima A, Hirose K, Yamazawa T, Bezprozvanny I, Kurosaki T, Iino M (2001) Ca^{2+}-sensor region of IP(3) receptor controls intracellular Ca^{2+} signaling. EMBO J 20:1674–1680
87. Serysheva II (2014) Toward a high-resolution structure of IP(3)R channel. Cell Calcium 56:125–132
88. Popot JL, Althoff T, Bagnard D, Baneres JL, Bazzacco P, Billon-Denis E, Catoire LJ, Champeil P, Charvolin D, Cocco MJ, Cremel G, Dahmane T, De La Maza LM, Ebel C, Gabel F, Giusti F, Gohon Y, Goormaghtigh E, Guittet E, Kleinschmidt JH, Kuhlbrandt W, Le Bon C, Martinez KL, Picard M, Pucci B, Sachs JN, Tribet C, Van Heijenoort C, Wien F, Zito F, Zoonens M (2011) Amphipols from A to Z. Annu Rev Biophys 40:379–408
89. Jensen KH, Brandt SS, Shigematsu H, Sigworth FJ (2016) Statistical modeling and removal of lipid membrane projections for cryo-EM structure determination of reconstituted membrane proteins. J Struct Biol 194:49–60
90. Liu Y, Sigworth FJ (2014) Automatic cryo-EM particle selection for membrane proteins in spherical liposomes. J Struct Biol 185:295–302
91. Wang L, Sigworth FJ (2009) Structure of the BK potassium channel in a lipid membrane from electron cryomicroscopy. Nature 461:292–295

Chapter 7
IP_3 Receptor Properties and Function at Membrane Contact Sites

Gemma Roest, Rita M. La Rovere, Geert Bultynck, and Jan B. Parys

Abstract The inositol 1,4,5-trisphosphate (IP_3) receptor (IP_3R) is a ubiquitously expressed Ca^{2+}-release channel localized in the endoplasmic reticulum (ER). The intracellular Ca^{2+} signals originating from the activation of the IP_3R regulate multiple cellular processes including the control of cell death versus cell survival via their action on apoptosis and autophagy. The exact role of the IP_3Rs in these two processes does not only depend on their activity, which is modulated by the cytosolic composition (Ca^{2+}, ATP, redox status, ...) and by various types of regulatory proteins, including kinases and phosphatases as well as by a number of oncogenes and tumor suppressors, but also on their intracellular localization, especially at the ER-mitochondrial and ER-lysosomal interfaces. At these interfaces, Ca^{2+} microdomains are formed, in which the Ca^{2+} concentration is finely regulated by the different ER, mitochondrial and lysosomal Ca^{2+}-transport systems and also depends on the functional and structural interactions existing between them. In this review, we therefore discuss the most recent insights in the role of Ca^{2+} signaling in general, and of the IP_3R in particular, in the control of basal mitochondrial bioenergetics, apoptosis, and autophagy at the level of inter-organellar contact sites.

Keywords Apoptosis · Autophagy · Ca^{2+} microdomains · Cell death · Cell survival · Endoplasmic reticulum · IP_3 receptor · Lysosomes · Membrane contact sites · Mitochondria

Gemma Roest and Rita M. La Rovere are Joint first authors.

G. Roest · R. M. La Rovere · G. Bultynck (✉) · J. B. Parys (✉)
Laboratory for Molecular and Cellular Signaling, Department of Cellular and Molecular Medicine & Leuven Kanker Instituut, KU Leuven, Leuven, Belgium
e-mail: geert.bultynck@kuleuven.be; jan.parys@kuleuven.be

J. Krebs (ed.), *Membrane Dynamics and Calcium Signaling*, Advances in Experimental Medicine and Biology 981,
https://doi.org/10.1007/978-3-319-55858-5_7

Abbreviations

ALS	Amyotrophic lateral sclerosis
AMPK	AMP-activated kinase
ATG	Autophagy-related
BIRD-2	Bcl-2/IP_3R disruptor-2 peptide
CICR	Ca^{2+}-induced Ca^{2+} release
CREB	cAMP response element-binding protein
DT40 TKO	DT40 IP_3R triple knock-out
ER	Endoplasmic reticulum
Fis1	Fission 1 homologue
GRP75	Glucose-regulated protein 75
GRP78/BiP	Glucose-regulated protein 78
GSK3β	Glycogen synthase kinase-3β
IMM	Inner mitochondrial membrane
IBC	IP_3-binding core
IP_3	Inositol 1,4,5-trisphosphate
IP_3R	IP_3 receptor
LC3	Microtubule-associated protein light chain 3
LRRK2	Leucine-rich repeat kinase 2
MAM	Mitochondria-associated ER membrane
MCU	Mitochondrial Ca^{2+} uniporter
Mfn	Mitofusin
mPTP	Mitochondrial permeabilization transition pore
mTORC1	Mechanistic target of rapamycin complex 1
OMM	Outer mitochondrial membrane
NAADP	Nicotinic acid adenine dinucleotide phosphate
PACS-2	Phosphofurin acidic cluster sorting protein 2
PERK	Protein kinase RNA-like ER kinase
PIP_3	Phosphatidylinositol 3,4,5-trisphosphate
PKB/Akt	Protein kinase B
PML	Promyelocytic leukemia
PTEN	Phosphatase and tensin homolog
PTPIP51	Protein tyrosine phosphatase-interacting protein-51
ROS	Reactive oxygen species
RyR	Ryanodine receptor
SERCA	Sarco-/endoplasmic reticulum Ca^{2+} ATPase
TCA	Tricarboxylic acid
TFEB	Transcription factor EB
TMX	Thioredoxin-like transmembrane protein
TPC	Two-pore channel
TRPML	Transient receptor potential mucolipin
ULK1/2	Atg1/Unc-51-like kinase 1/2
UPR	Unfolded protein response
VAPB	Vesicle-associated protein B
VDAC	Voltage-dependent anion channel

7.1 The IP_3 Receptor, the Main Ca^{2+}-Release Channel of the Endoplasmic Reticulum

Complex spatio-temporal Ca^{2+} signals regulate many fundamental cellular processes including fertilization, differentiation, proliferation, gene transcription, metabolism, contraction, secretion, etc. [1, 2]. The endoplasmic reticulum (ER) is the main Ca^{2+}-storage organelle and therefore plays a central role in intracellular Ca^{2+} signaling. ER Ca^{2+} handling depends on three major mechanisms, Ca^{2+} uptake via the sarco-/endoplasmic Ca^{2+}-ATPases (SERCA) [3], Ca^{2+} storage by various luminal Ca^{2+}-binding proteins [4] and controlled Ca^{2+} release. Besides passive Ca^{2+} leak through still largely unidentified basal ER Ca^{2+}-leak channels, Ca^{2+} release out of the ER primarily occurs via the inositol 1,4,5-trisphosphate (IP_3) receptor (IP_3R) and the ryanodine receptor (RyR). While the RyR is predominantly expressed in a limited number of tissues, especially muscles and brain [5], the IP_3R is ubiquitously expressed and present in virtually every cell type [6]. IP_3Rs are activated by IP_3 produced by phospholipase C after cell activation, e.g. by extracellular agonists, hormones, growth factors or neurotransmitters, and play a crucial role in the initiation and propagation of intracellular and intercellular Ca^{2+} signals [7–10].

In *Mammalia* and other higher organisms, three different genes encode IP_3Rs (*ITPR1*, *ITPR2* and *ITPR3*) giving rise to three isoforms named IP_3R1, IP_3R2, and IP_3R3 that display at the amino acid level an overall similarity of 75–80% [11]. Each of these isoforms is about 2700 amino acids long and assembles into tetrameric structures with a total molecular mass of 1.2 MDa. Splice isoforms and the possibility to form both homo- and heterotetramers increase the diversity between IP_3Rs. Each monomeric isoform has the same general structure containing five distinct functional domains (Fig. 7.1): the N-terminal coupling domain usually called the suppressor domain (for IP_3R1: a.a. 1–225), the IP_3-binding core (IBC, a.a. 226–578) containing the IP_3-binding site, the central coupling domain or modulatory and transducing domain (a.a. 579–2275), the channel domain containing six transmembrane helices (a.a. 2276–2589) and finally the C-terminal tail also named gatekeeper domain (a.a. 2590–2749) [13, 14].

At the structural level progress has followed two main paths. First, X-ray crystallography permitted to obtain high-resolution structural information of the N-terminal part of the IP_3R, i.e. the suppressor domain and the IBC [15, 16]. The latter contains two domains, a first one containing a β-trefoil fold (IBC-β) and a second one containing an armadillo repeat fold (IBC-α) with the cleft between them forming the IP_3-binding site. Their structure was also resolved at high resolution (3–3.8 Å) both for the apo- and the IP_3-bound form, elucidating changes occurring during IP_3R activation [17, 18]. In the presence of IP_3, a rearrangement of IBC-β and IBC-α occurs, constraining the IP_3-binding cleft. Additionally, the suppressor domain, originally in contact with both IBC-β and IBC-α, re-orients itself, probably to couple to the channel domain for its activation. Recently, Mikoshiba and co-workers succeeded in obtaining the crystal structure for the 2217 a.a. long cytosolic part of IP_3R1 at a resolution of 5.8–7.4 Å [19]. Comparison of the structures of

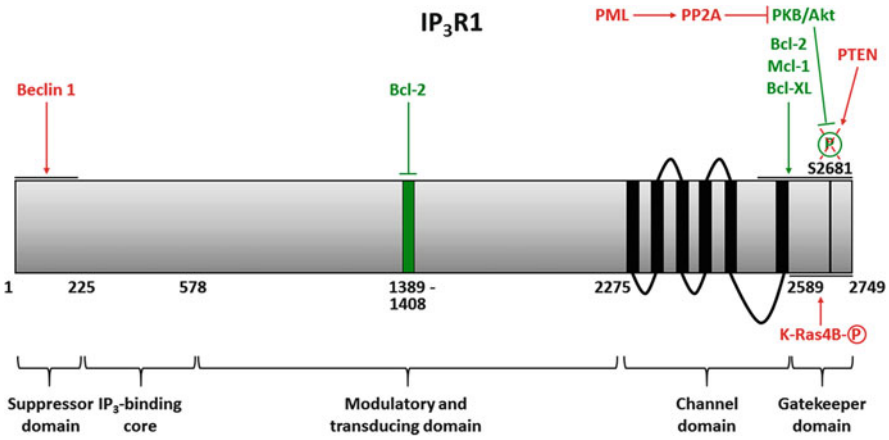

Fig. 7.1 Linear representation of the type 1 IP_3R isoform and its regulation by proteins involved in the control of cell survival and cell death. The five distinct IP_3R1 functional domains are delineated: the suppressor domain, the IP_3-binding core, the modulatory and transducing domain, the channel domain containing the six trans-membrane helices (indicated as black bars) and the gatekeeper domain. Oncogenes are represented in green, while tumor suppressors are indicated in red. Bar-headed lines indicate an inhibitory interaction and arrow-headed lines indicate a stimulatory interaction. For more information, see text. Reproduced with modifications from own previous work ([12], https://doi.org/10.1016/j.bbamcr.2016.01.002)

different truncated variants obtained in the absence and the presence of IP_3 supports a long-range gating mechanism in which the signal is transferred from the IBC via two α-helical domains (HD1, a.a. 605–1009 and HD3, a.a. 1593–2217) to a so-called leaflet (corresponding to a.a. 2195–2215 of HD3) that relays the IP_3R conformational change to the channel pore. Strikingly, the HD3/leaflet region was essential for the IP_3R Ca^{2+}-release activity in intact cells exposed to extracellular agonists.

Second, cryo-electron microscopy allowed gaining an increasingly better view of the full-length IP_3R structure. Serysheva and co-workers obtained by single-particle cryo-electron microscopy about 85% of the structure of rat cerebellar IP_3R1 at a 4.7 Å resolution in the apo-state [20, 21], confirming the close apposition of the N- and C-termini.

This structure enables the binding of four IP_3 molecules to a tetrameric IP_3R, but the exact stoichiometry underlying IP_3R opening by IP_3 remained for a long time elusive. The elegant work of Yule and co-workers, based on the ectopic expression in null-background HEK293 cells of concatenated IP_3Rs of which the IP_3-binding sites could be mutated, indicated that IP_3R-mediated Ca^{2+} release is only triggered when 4 IP_3 molecules are bound to the tetrameric IP_3R [22]. This stringent condition will not only prevent spurious IP_3R opening, but also enables the buffering of a significant amount of IP_3 molecules by the IP_3R channels themselves, ensuring that sufficiently high IP_3 concentrations are reached before IP_3R opening takes place [23].

Besides the physiological agonist IP_3, two metabolites produced by *Penicillium brevicompactum*, the adenophostins A and B, can activate the IP_3R at a much lower concentration than IP_3 itself [24]. Cytosolic Ca^{2+} is considered an important co-agonist of the IP_3R that acts in a bell-shaped dependent manner: a low [Ca^{2+}] (typically $\leq$0.3 μM) enhances IP_3-induced Ca^{2+} release, while a high [Ca^{2+}] (above 0.3 μM) suppresses IP_3-induced Ca^{2+} release [25–28]. ATP [29] and oxidizing conditions as e.g. thimerosal [30, 31] were also shown to stimulate IP_3-induced Ca^{2+} release. Finally, cAMP has been reported to sensitize IP_3Rs [32] independently of any phosphorylation event [33]. Moreover, very recently evidence was presented that when cAMP is produced, IP_3 can induce Ca^{2+} release from a different Ca^{2+} store that is not sensitive to IP_3 alone [34].

Interestingly, each of the IP_3R isoforms acts as a signaling hub, able to integrate various cellular inputs and to deliver a specific output signal that elicits a specific cellular response [9, 10, 35]. It should therefore be emphasized that although all IP_3R isoforms function along the same basic mechanisms, important differences in sensitivity exists between the various IP_3R isoforms, with IP_3R2 being the most atypical one [36]. The sensitivity of the IP_3R isoforms to IP_3 follows the rank-order $IP_3R2 > IP_3R1 > IP_3R3$ [37–41]. In addition, the sensitivity to cytosolic Ca^{2+} varies between the various IP_3R isoforms [42–44]. ATP similarly has a biphasic effect on IP_3R activity with between the IP_3R isoforms different sensitivities as well for the stimulatory [40, 45, 46] as for the inhibitory phase [47]. Moreover, IP_3R2, the isoform that is most sensitive to stimulatory ATP concentrations [45], proved to be dominant in a heterotetrameric receptor [48]. Finally, the oxidizing agent thimerosal has a biphasic action on IP_3R1 but only an inhibitory one on IP_3R3 [46, 49] while cAMP seems to have its main (or only) effect on IP_3R2 [32].

Inhibition of IP_3R activity is generally achieved by one of the following compounds: heparin, 2-APB, xestospongin C (or B) and caffeine. Except for the problem that all those compounds display non-specific effects [50], an additional problem is that they also may display a differential sensitivity between the various IP_3R isoforms [51]. The synthesis of IP_3 derivatives may however provide in the future more specific and/or more potent inhibitors [52].

Further regulation of IP_3R activity can be obtained by various post-translational modifications, including palmitoylation [53], cross-linking by the action of transglutaminase 2 [54] and phosphorylation/dephosphorylation events triggered by multiple protein kinases and protein phosphatases [55, 56]. Finally, the existence of multiple regulatory or scaffolding proteins able to associate with the IP_3R tetramer and to modulate its activity should be emphasized. Over 100 proteins have already been shown to interact with and regulate the IP_3R [57], including IRBIT [58, 59], calmodulin [60–64], neuronal CaBP1 [65–67], the anti-apoptotic Bcl-2 [68–70], Bcl-XL [71] and reticulocalbin 1 [72], the pro-autophagic Beclin 1 [73, 74], the chaperones ERp44 [75], GRP78/BiP [76] and sigma-1 receptor [77] and cytochrome c [78].

Many of these associated proteins, including several oncogenes and tumor suppressors (Fig. 7.1), are involved in the regulation of apoptosis and autophagy [12, 79]. This correlates with the important function of IP_3Rs and IP_3R-mediated Ca^{2+} signals in the control of cell-fate decisions, including processes related to cell death and survival

[80]. More specifically, the role of the IP_3R and of IP_3-induced Ca^{2+} release has been recognized in both apoptosis [81–86] and autophagy [85–90]. These processes depend on the activity of the IP_3R and its regulation by associated proteins and protein kinases, as well as on its intracellular localization, especially at the interface between ER and mitochondria or at the interface between ER and lysosomes.

7.2 Mitochondrial and Lysosomal Ca^{2+} Handling in Cell Death and Survival Processes

7.2.1 Apoptosis and Its Regulation by Ca^{2+}

Apoptosis is the major form of programmed cell death and can be initiated by either an extrinsic or an intrinsic –mitochondrial- pathway that both converge at the level of the activation of the effector caspases (caspase-3, -6 and -7) [91–93].

In the intrinsic pathway, Ca^{2+} overload of the mitochondrial matrix is a well-known factor leading to apoptosis [94]. Interestingly, several links exists between Ca^{2+} and apoptosis. In a first mechanism, mitochondrial Ca^{2+} is thought to bind cardiolipin, which thereby dissociates from mitochondrial complex II. The mitochondrial complex II disintegrates, leading to the release of the succinate dehydrogenase A and B subunits. This results in a massive reactive oxygen species (ROS) production and opening of the mitochondrial permeability transition pore (mPTP) [95]. This mPTP was proposed to arise from dimers of the F-ATP synthase in the inner mitochondrial membrane (IMM) [96, 97], though there still exists some controversy on the exact subunits involved [98]. Recent data indicate that mPTP opening can occur subsequently to Ca^{2+} binding to the β subunit of the catalytic F1 part [99]. This likely results in a conformational change transmitted via the oligomycin-sensitivity conferring protein subunit to the peripheral stalk and the IMM.

The mPTP is a high conductance channel that upon its opening results in the collapse of the electrochemical potential and in a loss of ion and solute distribution, terminating ATP synthesis. Subsequently to mPTP opening, solutes enter the mitochondrial matrix, leading to mitochondrial swelling, rupture of the outer mitochondrial membrane (OMM) and release of the pro-apoptotic factors located in the cristae, including cytochrome c. The release of these factors to the cytoplasm in turn leads to caspase activation and apoptosis [100].

Besides mPTP opening, Ca^{2+} can also indirectly activate mitochondrial apoptosis. Cytosolic Ca^{2+} can activate calcineurin, which dephosphorylates the sensitizer BH3-only protein Bad. This will cause its release from 14-3-3 proteins and allow its interaction with anti-apoptotic Bcl-XL. The latter will then be unable to counteract Bax/Bak activation and the subsequent permeabilization of the OMM will lead to apoptosis [101].

Finally, prolonged, severe depletion of the ER Ca^{2+} store will lead to ER stress and activation of the unfolded protein response (UPR) to re-establish ER

homeostasis. If the latter cannot be achieved, the UPR will eventually promote the expression of pro-apoptotic proteins, including members of the Bcl-2 family like BH3-only proteins, as well as that of GADD34 and of ERO1α, all leading to the cell demise by apoptosis [102, 103].

7.2.2 *Autophagy and Its Regulation by Ca^{2+}*

Autophagy is a highly conserved degradation pathway in which cellular components are targeted to the lysosomes. Basal and stress-induced autophagy act as survival pathways ensuring that protein aggregates, long-lived proteins, lipids, dysfunctional organelles or intracellular pathogens are digested and their constituents recycled, contributing to protein quality control, energy and cellular homeostasis [104]. Yet, excessive autophagy, brought about by the autophagy-inducing Tat-Beclin 1 peptide or by a severe/on-going nutrient starvation stress, can result in autophagic cell death (or so-called "autosis") via a process that is regulated by the Na^+/K^+-ATPase pump [105, 106].

Macroautophagy, generally referred to as autophagy, is the best-studied type of autophagy. It is characterized by the de novo formation of double-membrane vesicles named autophagosomes that engulf cytosolic proteins and/or organelles, the "cargo". These autophagosomes eventually fuse with the lysosome to form autolysosomes in which the cargo is degraded.

Main upstream controllers of autophagy are AMP-activated kinase (AMPK) and mechanistic target of rapamycin complex 1 (mTORC1). AMPK triggers autophagy in two ways, as it can phosphorylate and inhibit mTORC1, while directly activating the Atg1/Unc-51-like kinase 1/2 (ULK1/2) complex. The process downstream of ULK1/2 is further controlled by many proteins including about 30 autophagy-related (Atg) proteins [107, 108].

The initiation of the autophagy can start at various intracellular compartments, though the ER –and the ER-mitochondrial contact sites– seems to form a preferential location [109–111]. The original structure forming on the ER has been named the omegasome, which subsequently expands to form the phagophore [112]. Its subsequent elongation and closure, mediated by the Atg12-Atg5 complex, and the lipidation of microtubule-associated protein light chain 3 (LC3) by Atg4 and Atg8, lead to the formation of the autophagosomes. These will eventually fuse either directly, or indirectly via prior fusion with an endosome, with lysosomes, forming hereby the autolysosomes needed for cargo degradation [107, 113].

The regulation of autophagy by Ca^{2+} appears quite complex as intracellular Ca^{2+} can stimulate or even be essential for autophagy [54, 73, 114–118] while it also can inhibit it [119–122]. Possible explanations to resolve the apparent controversy include the use of various cell types and various autophagy induction methods, and the fact that Ca^{2+} can act on multiple check points upstream of autophagy as well as during the autophagic process [85, 87–89, 123–127]. In that respect, the intracellular localization of the IP_3Rs appears important. Ca^{2+} signals directed to the

mitochondria will e.g. control mitochondrial metabolism and thus impact autophagy differently than Ca^{2+} signals directed to other targets. The importance for cell survival/cell death of IP_3R localization at membrane contact sites will therefore be discussed in the subsequent sections.

7.3 The Role of the IP_3R at ER: Mitochondrial Contact Sites

Ca^{2+} signals originating from the ER critically control cell death and survival by impacting the mitochondria [94, 128, 129]. This is possible through the existence of sites of close apposition between the ER and the mitochondria, covering about 10% of the mitochondrial surface, depending on the metabolic state of the cells [130]. These sites are based on the existence of structural connections between both organelles, resulting in the formation of mitochondria-associated ER membranes (MAMs). In those MAMs, numerous proteins were identified that play a role in Ca^{2+} handling, lipid transfer, inter-organellar tethering, regulation of mitochondrial fission and fusion, cell death control and mitochondrial metabolism [131–136].

The distance between both organelles is an important element in the control of cell death versus cell survival [134]. The contact sites are dynamic structures in which the distance between both membranes as well as the length of these contact sites vary in function of the physiological conditions. In general, the contact sites run over several hundreds of nanometers of length and the distance between smooth ER and mitochondria range between 10 and 50 nm and between rough ER and mitochondria between 50 and 80 nm [130]. By using synthetic linkers, ER-mitochondrial distance could experimentally be fourfold reduced increasing simultaneously fourfold the length of the ER-mitochondrial interface [137]. This resulted in an accelerated mitochondrial Ca^{2+} accumulation and an increased Ca^{2+}-dependent activation of the mPTP. Such tightening of the contact between ER and mitochondria physiologically occurs e.g. in cells undergoing apoptosis.

In physiological conditions, the distance between ER and mitochondria is determined by proteins responsible for tethering both organelles together. Although the molecular identity of the tethers remains less well understood in higher organisms than in yeast, several proteins contributing to ER-mitochondrial tethering have already been identified [133, 134, 138] (Fig. 7.2).

In the first place, one should mention that the ER-localized IP_3Rs are in the MAMs physically coupled to the voltage-dependent anion channels (VDAC) 1 located in the OMM via chaperones like glucose-regulated protein 75 (GRP75) [140] (Fig. 7.2a). This tethering enables an efficient "quasi-synaptic" Ca^{2+} transfer between ER and mitochondria [141]. This structure leads to high local [Ca^{2+}] (in the range of 10–20 μM) in the ER-mitochondrial interspace [142, 143], which overcomes the low-affinity properties of the mitochondrial Ca^{2+} uniporter (MCU) of the IMM [144]. Through the existence of these Ca^{2+} microdomains, the mitochondria

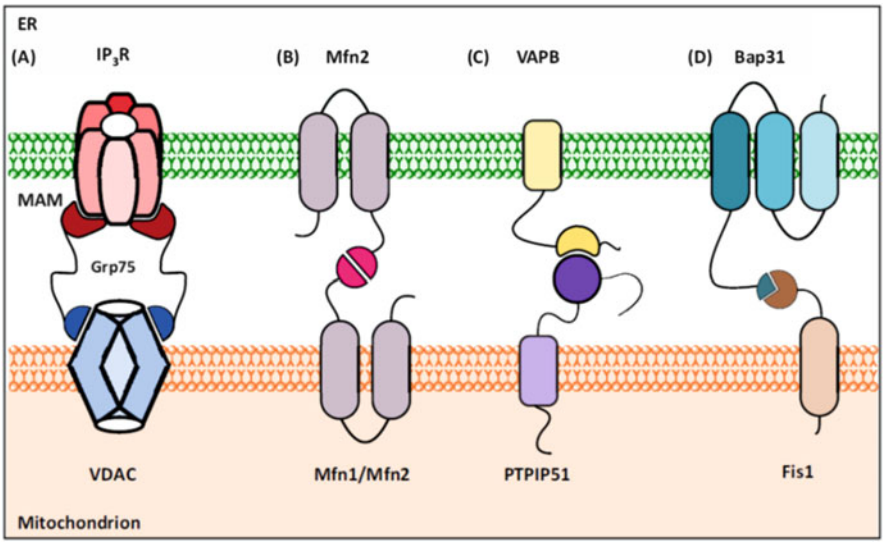

Fig. 7.2 The ER-mitochondrial tethers. Schematic visualization of the most important ER-mitochondrial tethers: (**a**) the IP_3R-GRP75-VDAC tether, (**b**) mitofusin-based tethering, (**c**) the VAPB-PTPIP51 tether and (**d**) the Bap31-Fis1 tether. For more information, see text. Reproduced from ([139], https://doi.org/10.1016/j.tins.2016.01.008) available through https://creativecommons.org/licenses/by/4.0/

can be regulated even by low-level Ca^{2+} signals. Dependently on the Ca^{2+} signal properties either cell survival or cell death can be promoted.

Mitofusin (Mfn) 2, enriched in the MAMs, was proposed to form homo- and heterodimers with mitochondria-localized Mfn2 and Mfn1 respectively (Fig. 7.2b), thereby establishing proper ER-mitochondrial apposition [145, 146]. Mfn2 function can be modulated by various proteins, including trichoplein/mitostatin, which counteracts Mfn2 function [147], and the ubiquitin ligase MITOL, which stimulates Mfn2 degradation [148]. In agreement with the model that Mfn2 has a tethering function, both trichoplein/mitostatin and MITOL impair mitochondrial Ca^{2+} uptake and protect against Ca^{2+}-dependent apoptosis. Other studies however have challenged the concept of Mfn2 as an ER-mitochondrial tether and actually proposed that it functions as an anti-tethering protein. This was based on the observation that cells lacking Mfn2 display an increased ER-mitochondrial tethering and an augmented agonist-induced mitochondrial Ca^{2+} uptake [149–152]. Resolving this controversy will probably depend on obtaining more detailed insights in the molecular composition of the ER-mitochondrial interface [153, 154].

Other proteins endowed with a role as tethers between the ER and the mitochondria are the scaffolds based on (a) vesicle-associated protein B (VAPB) in the ER interacting with protein tyrosine phosphatase-interacting protein-51 (PTPIP51) of the OMM, (b) on Bap31 in the ER and Fission 1 homologue (Fis1) in the OMM and (c) the ER stress sensor protein kinase RNA-like ER kinase (PERK) [133, 134, 138].

VABP is an integral ER membrane protein which mutation occurs in forms of motor neuron diseases including amyotrophic lateral sclerosis (ALS) [155]. Its interaction via its N-terminus with PTPIP51 (Fig. 7.2c) controls ER-mitochondria coupling and Ca^{2+} transfer between both organelles [156]. Moreover, the VAPB P56S mutant, which causes familial type 8 ALS [157], demonstrates both an increased binding to PTPIP51 and an increased Ca^{2+} flux to the mitochondria.

A pro-apoptotic interaction of Bap31 with Fis1 has been demonstrated (Fig. 7.2d), though the role of this interaction under normal physiological conditions is not yet understood [158]. The pro-apoptotic effect is due to the fact that this platform can both recruit pro-caspase-8 and increase Ca^{2+} transfer from the ER to the mitochondria. Moreover, the multifunctional phosphofurin acidic cluster sorting protein 2 (PACS-2) can modulate ER-mitochondria coupling and this has been related to Bap31 cleavage [159, 160].

Finally, PERK contributes to ER-mitochondria tethering independently of its canonical role in the UPR pathway, since in PERK-deficient cells the expression of a kinase-dead PERK was sufficient to re-establish ER-mitochondrial contacts and to re-sensitize them to apoptosis [161].

7.3.1 IP_3R-Mediated Ca^{2+} Signals in Cell Survival

Basal IP_3R-mediated Ca^{2+} signals-usually in the form of Ca^{2+} oscillations- drive mitochondrial bioenergetics (Fig. 7.3a), especially by stimulating the activity of pyruvate dehydrogenase, isocitrate dehydrogenase and α-ketoglutarate dehydrogenase. These enzymes participate in the tricarboxylic acid (TCA) cycle and so control adequate ATP synthesis [162, 163]. In addition to this, mitochondrial Ca^{2+} can also enhance the activity of the ATP synthase complex V and of the adenine nucleotide translocator [164]. Furthermore, IP_3R-driven Ca^{2+} oscillations also sustain the mitochondrial metabolism by driving the transcription of the gene for MCU via regulation of the transcription factor CREB [165].

DT40 cells devoid of all IP_3R isoforms (DT40 TKO, [166]) demonstrated in comparison to their wild-type counterparts a very different basic energy metabolism, with an increased Warburg effect and increased ROS production, explaining their reduced proliferation [167]. These effects may be aggravated by reduced MCU expression in cells lacking IP_3R expression and thus Ca^{2+} oscillations [165]. Inhibition of IP_3Rs in non-tumor cells led to a decreased ATP production, a subsequent activation of AMPK and therefore an increase in pro-survival basal autophagy [168]. The latter effect might depend on growth conditions as the increase in AMPK activity in DT40 TKO cells was observed in one study [168] but not in another [167]. Interestingly, similar results were obtained when ER-mitochondria coupling was impaired by downregulation of VABP or of PTPIP51 [169]. Tightening of the ER-mitochondria connection by a synthetic linker or by overexpression of either VABP or PTPIP51 reversed the effect. However, overexpression of the tether proteins only impaired autophagy induced by mTORC1 inhibition and not nutrient

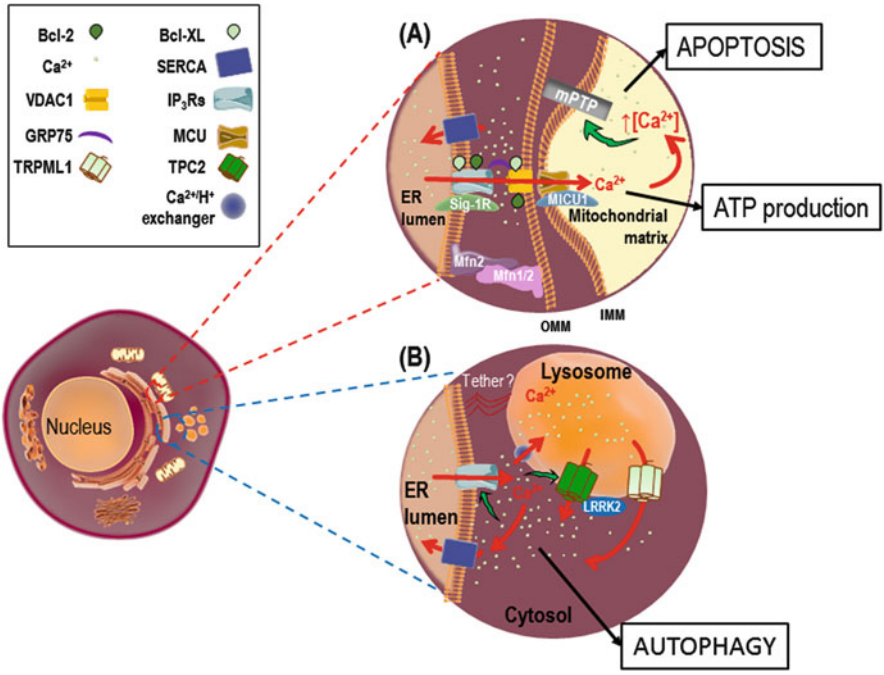

Fig. 7.3 Ca^{2+} transfer between ER and mitochondria and between ER and lysosomes. Schematic representation of Ca^{2+} handling in juxta-ER microdomains. (**a**) Ca^{2+} transfer to the mitochondria is mediated by the close connection between the IP_3R in the ER and VDAC in the outer mitochondrial membrane (OMM). Moreover, additional tethers (the mitofusin tether is depicted) contribute to the close apposition of ER and mitochondria. The Ca^{2+} in the mitochondrial matrix drives mitochondrial bio-energetics via stimulation of the TCA cycle, the ATP synthase complex V and the adenine nucleotide translocator. In case of mitochondrial Ca^{2+} overload, the mPTP is opened, causing mitochondrial swelling and apoptosis. (**b**) Regulation of the Ca^{2+} concentration in the microdomain between ER and lysosomes involves both the IP_3R in the ER membrane and the lysosomal Ca^{2+} channels as TRPML1 and TPC2. Lysosomal Ca^{2+} uptake likely occurs via a Ca^{2+}/H^+ exchanger and molecular identification of ER-lysosomal tethering is presently lacking. The Ca^{2+} in the microdomain between ER and lysosomes can regulate the autophagic process upstream of autophagosome formation, during autophagic flux and via calcineurin-mediated activation of transcription factor EB. Ca^{2+} fluxes are depicted by red arrows. The green arrows indicate stimulatory interactions. For more information, see text

starvation-induced autophagy, uncovering differences between the role of mitochondrial Ca^{2+} handling in different types of autophagy.

In contrast, the survival of tumorigenic cells depends on the IP_3Rs as adequate Ca^{2+} signaling is necessary to sustain mitochondrial metabolism [170, 171]. Although tumor cells proliferate in an uncontrolled way independently of the mitochondrial bioenergetics, they need the TCA cycle for the production of metabolites as nucleotides for cell growth and proliferation. The AMPK activation and the subsequent autophagy occurring after IP_3R inhibition is therefore not sufficient to sustain cell survival, resulting in a mitotic catastrophe.

Of note, the net effect of IP_3Rs on mitochondrial bio-energetics will depend on the local activity of the SERCA pumps at the MAMs (Fig. 7.3a), which, by pumping Ca^{2+} back into the ER, will limit the available Ca^{2+} in this microdomain and thus counteract ER-mitochondrial Ca^{2+} transfer. The local SERCA activity can be dynamically regulated, for instance by associated proteins like thioredoxin-like transmembrane protein (TMX) 1 [172, 173]. This redox-sensitive oxidoreductase is enriched at the MAMs, locally inhibiting SERCA pump activity and thus causing a local increase in $[Ca^{2+}]$ at the ER-mitochondrial interface and enhancing oxidative phosphorylation. In contrast, low levels of TMX1 will enhance SERCA activity, shifting Ca^{2+} away from the mitochondria and from the Ca^{2+}-driven bio-energetic pathway. In fact, loss of TMX1 has been observed in tumor cells, favoring their growth by potentially contributing to the Warburg effect. Nevertheless, a low-level ER-mitochondrial Ca^{2+} transfer must remain present to sustain proper TCA cycling and the production of the mitochondrial intermediates necessary for anabolic processes that ensure cell survival upon cell division [80, 170].

Apart from a regulation of autophagy, mitochondrial Ca^{2+} also impacts mitophagy, the specific elimination of mitochondria via the autophagic process. In fibroblasts expressing a mutation in the electron transport chain leading to a mild phenotype, mitochondrial Ca^{2+} uptake decreased, leading to increased autophagy, increased mitophagy and increased biogenesis of new mitochondria [174]. This adaptive response may account for the limited phenotype observed in these cells. In human RPE1 cells, ER-mitochondrial contacts appeared necessary for starvation-induced autophagy and for mitophagy [175]. The sigma-1 receptor located at the MAMs was crucial for starvation-induced autophagy. Its downregulation, however, did not affect mitophagy, and neither did the downregulation of all the RyR isoforms, of all the SERCA isoforms, or of any of the three IP_3R isoforms. Since the combined knockdown of all three IP_3R isoforms or of the MCU inhibited mitophagy, this specifically indicates the importance of IP_3R-mediated Ca^{2+} transfer from the ER to the mitochondria. Noteworthy, the sigma-1 receptor at the MAMs stabilizes IP_3R3 and so regulates Ca^{2+} transfer between ER and mitochondria [176] (Fig. 7.3a).

The anti-apoptotic proteins Bcl-2, Bcl-XL and Mcl-1, of which at least the first two have been identified in the MAM fraction [136] (Fig. 7.3a), can bind to the gatekeeper domain in the C-terminal region of the IP_3R (Fig. 7.1), which is activated by its interaction with the N-terminal IP_3-binding domain [177]. Their binding leads to a sensitization of the IP_3R, increased transfer of Ca^{2+} to the mitochondria and therefore an increased production of ATP, promoting cell survival [69, 71, 178]. Recent work uncovered the existence of a biphasic action of Bcl-XL on the IP_3R, i.e. a high-affinity activation at low Bcl-XL concentration and a lower affinity inhibition at high Bcl-XL concentrations [179]. Finally, it should be mentioned that Bcl-XL bound to the IP_3R C-terminus in the presence of active K-Ras4B phosphorylated by protein kinase C, forms a trimolecular complex that antagonizes the anti-apoptotic action of Bcl-XL and promotes cell death via excessive autophagy [180].

7.3.2 IP_3R-Mediated Ca^{2+} Signals in Apoptosis

In contrast, excessive IP_3R-mediated Ca^{2+} release directed to the mitochondria will lead to mitochondrial Ca^{2+} overload and eventual apoptosis, as discussed above (Sect. 7.2.1). Especially IP_3R3 [181] and VDAC1 [182] were proposed to play an important role in pro-apoptotic Ca^{2+} signaling, but depending on the cell type, also other IP_3R isoforms can participate in such pro-apoptotic Ca^{2+} signaling [183, 184]. Moreover, besides IP_3Rs, other Ca^{2+}-transport systems that can impact ER-to-mitochondria Ca^{2+} flux can be enriched in the MAMs, including SERCA pumps [185] and S1T, a truncated form of SERCA1, induced upon ER stress and unable to pump Ca^{2+} [186]. By forming an ER Ca^{2+}-leak pathway, S1T expression leads to ER depletion, mitochondrial immobilization and increased ER-mitochondrial contact sites leading to increased mitochondrial Ca^{2+} levels and apoptosis.

At the level of the MAMs, multiple proteins, including oncogenes and tumor suppressors, regulate IP_3R activity and thus ER-mitochondria Ca^{2+} transfer and impact the apoptosis process [12].

Various anti-apoptotic Bcl-2 family members (Fig. 7.3a), including Bcl-2, Bcl-XL and Mcl-1, can modulate IP_3R activity [12, 187–191]. Bcl-2 binds to all three IP_3R isoforms at a conserved stretch of 20 amino acids located in the middle of their modulatory and transducing domain (Fig. 7.1), inhibiting IP_3R-mediated Ca^{2+} release [192]. Bcl-2 in this way prevents pro-apoptotic Ca^{2+} signaling. The BH4 domain of Bcl-2 is hereby sufficient to inhibit IP_3Rs and to protect cells against Ca^{2+}-dependent apoptosis [70]. Of note, the BH4 domain of Bcl-2 appears to be unique compared to the related domain present in Bcl-XL, which was much less effective in binding to and inhibiting IP_3Rs [193]. In contrast, the BH4 domain of Bcl-XL appeared more effective for suppressing VDAC1-mediated pro-apoptotic Ca^{2+} transfer to the mitochondria [194].

Consequently, disrupting the interaction by using a peptide corresponding to the binding site of Bcl-2 on IP_3R1 resulted in increased IP_3R activity and apoptosis [192]. Based on this binding site, the cell-permeable Bcl-2/IP_3R disruptor-2 peptide (BIRD-2) was developed [195]. It elicited spontaneous pro-apoptotic Ca^{2+}-release events in various types of cancer cells, including chronic lymphocytic leukemia [195], diffuse large B-cell lymphoma [183], multiple myeloma and follicular lymphoma [196] and small cell lung cancer [197].

IP_3R activity can also be reduced by phosphorylation by the pro-survival protein kinase B (PKB/Akt) thereby preventing pro-apoptotic Ca^{2+} release [198–200]. The PKB/Akt phosphorylation site is conserved among all three IP_3R isoforms (Fig. 7.1), but a more selective role for PKB/Akt in the regulation of IP_3R3 was proposed, as a study demonstrated that PKB/Akt could only dampen the Ca^{2+} signals in cells expressing that isoform [201]. The phosphatase and tensin homolog (PTEN), a phosphatidylinositol 3,4,5-trisphosphate (PIP_3) phosphatase upstream of PKB/Akt, counteracts the effect of PKB/Akt on IP_3Rs while re-expression of PTEN in PTEN-deficient cancer cells restored their sensitivity to pro-apoptotic Ca^{2+}-dependent stimuli [200]. Further studies indicated a direct role for PTEN on

IP_3R phosphorylation and function at the MAMs, where PTEN functioned as a protein phosphatase counteracting PKB/Akt-mediated phosphorylation of IP_3R3 channels and augmenting ER-mitochondrial Ca^{2+} flux [202]. In addition to this, it was very recently discovered that PTEN promotes Ca^{2+}-induced apoptosis in a phosphatase-independent way [203]. Indeed, PTEN competes with the F-box protein FBXL2, an ubiquitin E3 ligase component belonging to the SCF (SKP1, Cullin 1, F-box protein) E3 ligase family [204] with known tumor suppressor action by arresting the cell cycle [205, 206], for binding to the IP_3R3 channels. FBXL2 is responsible for IP_3R3 ubiquitination and its subsequent proteasomal degradation. As a consequence, PTEN, by competing with FBXL2, stabilizes IP_3R3 and promotes continuous Ca^{2+} transfer to the mitochondria leading to apoptosis. Finally, the negative regulation of IP_3R3 by PKB/Akt is antagonized by the tumor suppressor promyelocytic leukemia (PML) that recruits protein phosphatase PP2A to the MAMs. The latter dephosphorylates PKB/Akt, inhibiting its kinase activity and thus suppressing PKB/Akt-mediated phosphorylation of IP_3Rs (Fig. 7.1). Through this mechanism, PML increases Ca^{2+} release by the IP_3R, supporting mitochondrial Ca^{2+} overload and apoptosis [207].

In the heart, it was demonstrated that cyclophilin D participates to the IP_3R-GRP75-VDAC complex and regulates Ca^{2+} transfer to the mitochondria [208]. Its genetic or pharmacological inhibition attenuated mitochondrial Ca^{2+} overload and protected the cells from the consequences of hypoxia-reoxygenation.

Glycogen synthase kinase-3β (GSK3β) is another regulator of the IP_3R located in the MAMs [209]. GSK3β phosphorylates the IP_3R and increases IP_3-induced Ca^{2+} release. Upon ischemia-reperfusion injury, GSK3β activity is increased in cardiomyocytes, leading to increased pro-apoptotic Ca^{2+} signaling towards the mitochondria and cell death. Conversely, pharmacological inhibition of GSK3β protects the heart against damage subsequent to ischemia-reperfusion injury.

Finally, it should also be mentioned that increased transfer of Ca^{2+} to the mitochondria can also lead to cellular senescence. Adequate Ca^{2+} transfer to the mitochondria via IP_3R2 and the MCU appeared important in oncogene-induced senescence and replicative senescence [210].

7.4 The Role of the IP_3R at ER: Lysosomal Contact Sites

Lysosomes do not only play a fundamental role in the degradation of proteins and organelles, but are also bona fide Ca^{2+} stores [211–213] containing Ca^{2+} at a concentration of about 500 μM while their pH is between 4 and 5 [214]. Ca^{2+} uptake in the lysosomes is usually assumed to be mediated by a Ca^{2+}/H^+ exchanger [215] though other possibilities exist. In contrast to the uncertainty concerning the uptake mechanism, multiple Ca^{2+}-release channels are known to be present in the lysosomes, including transient receptor potential mucolipin (TRPML) 1 and two-pore channel (TPC) 2 [216]. Moreover, the lysosomes were identified as a target for nicotinic acid adenine dinucleotide phosphate (NAADP), a very potent agent eliciting Ca^{2+} release even at nanomolar concentrations (for a recent review, please

see [217]). With respect to the Ca^{2+}-releasing agent NAADP, most evidence point towards channels of the TPC family as their target but other channels, including TRPML1, have also been proposed. Further work is needed to fully understand the function of the various TPC channels, as work by various groups have shown that they can permeate several ions, including Ca^{2+}, Na^+ and H^+, and that their properties can be strongly dependent on experimental conditions and/or the presence of regulatory factors [218, 219].

As the autophagy process is regulated by Ca^{2+} (see above, Sect. 7.2.2) and as the Ca^{2+} ion has only a short range of messenger action [220], it can be assumed that the Ca^{2+} concentration in the microdomain between the ER and the lysosomes plays an important role in the control and/or fine-tuning of the autophagic process. This concentration will depend on the relative activity of the Ca^{2+} transporters in ER and lysosomes, their mutual functional interaction and the relative distance between the two organelles [85] (Fig. 7.3b).

In that respect, it is important to note that the two main Ca^{2+} channels expressed in the lysosomes, i.e. TRPML1 [221–223] and TPC2 [219, 224, 225] have already been implicated in autophagy (see further below).

As is the case for the mitochondria, also a very close association between ER and lysosomes was documented. Extensive contact sites between the two organelles were visualized through electron microscopy, showing in primary human fibroblasts that over 80% of the lysosomes are forming contacts of <20 nm with the ER [226]. This close connection should allow for mutual functional interactions between ER and lysosomes. In rat pulmonary artery smooth muscle cells, the close contacts between lysosomes and the sarcoplasmic reticulum allow for the functional coupling of lysosomes to RyR3 via Ca^{2+}-induced Ca^{2+} release (CICR) [227]. The contact sites involved show a membrane separation of about 15 nm apart, and extend for over 300 nm; increasing the membrane separation to 50 nm leads to a failure in activating RyR3. In contrast to what is known about other contact sites, the molecular mechanisms responsible for ER-lysosomal tethering are still only very partially recognized [228, 229].

Several studies have demonstrated that a small amount of Ca^{2+} released by NAADP can trigger much larger Ca^{2+} signals by activation of IP_3Rs or RyRs located on the ER by CICR or by ER Ca^{2+} store overload [226, 230–232] (Fig. 7.3b). The converse situation is also possible and Ca^{2+} released by the ER can affect lysosomal Ca^{2+} handling by stimulation of either NAADP synthesis or of the NAADP-induced Ca^{2+} release [233]. The Ca^{2+} ions released by the IP_3R can also be taken up in the lysosomes, leading to a dampening of the Ca^{2+} signals [234, 235]. A similar functional interaction also exist between active TRPML1 channel and ER Ca^{2+} release [236].

Taken together, this indicates that Ca^{2+} microdomains exist between the ER and the lysosomes in which the local Ca^{2+} concentration is regulated in a very complex way, whereby the IP_3R plays an important role [85, 213, 237–240] (Fig. 7.3b). These Ca^{2+} microdomains can therefore regulate the autophagy process. Evidence for stimulatory [241, 242] and inhibitory [243, 244] effects of lysosomal Ca^{2+} release on autophagy were presented. These differences in effects can be due to the use of different cellular models and of different mechanisms of autophagy induction differentially affecting the

relation between ER and lysosomes, but can also be an indication that Ca^{2+} can impact in a different way the various stages of the autophagic pathway. Moreover, the various lysosomal Ca^{2+} channels have been linked to different parts of the autophagy process. The absence of TRPML1 led to an upregulation of autophagy induction but an impaired lysosomal fusion resulting in the accumulation of significantly larger vesicles with a higher [Ca^{2+}] [245]. TRPML1 was upregulated during nutrient starvation [246] and is important for the centripetal movement of lysosomes after autophagy induction [247]. In cardiomyocytes, TPCs seem essential for both basal and induced autophagy [248]. Moreover, TPCs can be regulated by the leucine-rich repeat kinase 2 (LRRK2). The latter is a multifunctional protein, of which various mutated species have been implicated in various diseases and Parkinson's disease in particular. In the cell, it participates in the control of various important processes including autophagy [249]. It now appears that LRRK2 stimulates NAADP-induced Ca^{2+} release from the lysosomes [241] (Fig. 7.3b). Furthermore, the aberrant lysosomal morphology observed in fibroblasts from patients harboring the LRRK2 G2019S mutation—the most prominent one in Parkinson's disease- can be rescued by TPC2 inhibition or knockout [250]. The local role of Ca^{2+} in this process is underpinned by the fact that BAPTA-AM, a fast intracellular Ca^{2+} buffer, but not EGTA-AM, a slow intracellular Ca^{2+} buffer, could also rescue the aberrant lysosomal morphology.

Finally, nutrient starvation induced TRPML1-mediated Ca^{2+} release out of the lysosomes, locally activating calcineurin [251]. Calcineurin subsequently dephosphorylated transcription factor EB (TFEB) leading to its nuclear translocation. Importantly, TFEB is a master regulator of many genes of the lysosomal/autophagic pathway [252], including the gene for TRPML1 itself [253, 254]. This demonstrates that TRPML can mediate its own upregulation through Ca^{2+}-dependent activation of TFEB. Moreover, this upregulation appears essential for adapting lysosomes to conditions of nutrient starvation [246].

These results indicate that the IP_3R, together with the lysosomal Ca^{2+} channels, participate in the occurrence of local Ca^{2+} signals in the microdomain between ER and lysosomes and can thus impact autophagy progression at various levels.

7.5 Conclusions

The IP_3R, by evoking intracellular Ca^{2+} signals with a specific spatio-temporal profile, is well known to regulate multiple cellular processes, ranging from fertilization to cell death via control of differentiation/proliferation, metabolism, contraction, secretion and many other processes. The IP_3R, of which three isoforms exist, is finely regulated by a variety of cytosolic factors including Ca^{2+} itself and ATP, as well as by a multitude of regulatory proteins, including cell death and survival proteins and kinases and phosphatases. The intracellular localization of the IP_3R at ER-mitochondrial and at ER-lysosomal contact sites is however also very important for its fundamental role in regulating cellular bioenergetics, autophagy and apoptosis. The existence of Ca^{2+} microdomains at these inter-organellar interfaces and the possibility to locally control [Ca^{2+}] in these microdomains, distinct from the bulk

cytosolic [Ca^{2+}], allows for a versatile role of Ca^{2+} signaling in a cell's decision to engage cell death, cell survival or cell adaptation processes in basal and stress-related conditions.

Acknowledgements GR is recipient of a Ph.D. fellowship of the Research Fund—Flanders (FWO). Work performed in the laboratory of the authors was supported by research grants of the FWO, the Research Council of the KU Leuven and the Interuniversity Attraction Poles Programmes (Belgian Science Policy).

References

1. Berridge MJ, Lipp P, Bootman MD (2000) The versatility and universality of calcium signalling. Nat Rev Mol Cell Biol 1:11–21. https://doi.org/10.1038/35036035
2. Berridge MJ, Bootman MD, Roderick HL (2003) Calcium signalling: dynamics, homeostasis and remodelling. Nat Rev Mol Cell Biol 4:517–529. https://doi.org/10.1038/nrm1155
3. Vandecaetsbeek I, Vangheluwe P, Raeymaekers L et al (2011) The Ca^{2+} pumps of the endoplasmic reticulum and Golgi apparatus. Cold Spring Harb Perspect Biol 3:a004184. https://doi.org/10.1101/cshperspect.a004184
4. Prins D, Michalak M (2011) Organellar calcium buffers. Cold Spring Harb Perspect Biol 3: a004069. https://doi.org/10.1101/cshperspect.a004069
5. Lanner JT (2012) Ryanodine receptor physiology and its role in disease. Adv Exp Med Biol 740:217–234. https://doi.org/10.1007/978-94-007-2888-2_9
6. Vermassen E, Parys JB, Mauger J-P (2004) Subcellular distribution of the inositol 1,4,5-trisphosphate receptors: functional relevance and molecular determinants. Biol Cell 96:3–17. https://doi.org/10.1016/j.biolcel.2003.11.004
7. Fedorenko OA, Popugaeva E, Enomoto M et al (2014) Intracellular calcium channels: inositol-1,4,5-trisphosphate receptors. Eur J Pharmacol 739:39–48. https://doi.org/10.1016/j.ejphar.2013.10.074
8. Foskett JK, White C, Cheung K-H, Mak D-OD (2007) Inositol trisphosphate receptor Ca^{2+} release channels. Physiol Rev 87:593–658. https://doi.org/10.1152/physrev.00035.2006
9. Mikoshiba K (2015) Role of IP_3 receptor signaling in cell functions and diseases. Adv Biol Regul 57:217–227. https://doi.org/10.1016/j.jbior.2014.10.001
10. Parys JB, De Smedt H (2012) Inositol 1,4,5-trisphosphate and its receptors. Adv Exp Med Biol 740:255–279. https://doi.org/10.1007/978-94-007-2888-2_11
11. Taylor CW, Genazzani AA, Morris SA (1999) Expression of inositol trisphosphate receptors. Cell Calcium 26:237–251. https://doi.org/10.1054/ceca.1999.0090
12. Bittremieux M, Parys JB, Pinton P, Bultynck G (2016) ER functions of oncogenes and tumor suppressors: Modulators of intracellular Ca^{2+} signaling. Biochim Biophys Acta 1863:1364–1378. https://doi.org/10.1016/j.bbamcr.2016.01.002
13. Bosanac I, Michikawa T, Mikoshiba K, Ikura M (2004) Structural insights into the regulatory mechanism of IP_3 receptor. Biochim Biophys Acta 1742:89–102. https://doi.org/10.1016/j.bbamcr.2004.09.016
14. Uchida K, Miyauchi H, Furuichi T et al (2003) Critical regions for activation gating of the inositol 1,4,5-trisphosphate receptor. J Biol Chem 278:16551–16560. https://doi.org/10.1074/jbc.M300646200
15. Bosanac I, Alattia J-R, Mal TK et al (2002) Structure of the inositol 1,4,5-trisphosphate receptor binding core in complex with its ligand. Nature 420:696–700. https://doi.org/10.1038/nature01268

16. Bosanac I, Yamazaki H, Matsu-Ura T et al (2005) Crystal structure of the ligand binding suppressor domain of type 1 inositol 1,4,5-trisphosphate receptor. Mol Cell 17:193–203. https://doi.org/10.1016/j.molcel.2004.11.047
17. Lin C-C, Baek K, Lu Z (2011) Apo and $InsP_3$-bound crystal structures of the ligand-binding domain of an $InsP_3$ receptor. Nat Struct Mol Biol 18:1172–1174. https://doi.org/10.1038/nsmb.2112
18. Seo M-D, Velamakanni S, Ishiyama N et al (2012) Structural and functional conservation of key domains in $InsP_3$ and ryanodine receptors. Nature 483:108–112. https://doi.org/10.1038/nature10751
19. Hamada K, Miyatake H, Terauchi A, Mikoshiba K (2017) IP_3-mediated gating mechanism of the IP_3 receptor revealed by mutagenesis and X-ray crystallography. Proc Natl Acad Sci USA 114:4661–4666. https://doi.org/10.1073/pnas.1701420114
20. Fan G, Baker ML, Wang Z et al (2015) Gating machinery of $InsP_3R$ channels revealed by electron cryomicroscopy. Nature 527:336–341. https://doi.org/10.1038/nature15249
21. Serysheva II, Baker M, Fan G (2018) Structural insights into IP_3R function. Adv Exp Med Biol 981
22. Alzayady KJ, Wang L, Chandrasekhar R et al (2016) Defining the stoichiometry of inositol 1,4,5-trisphosphate binding required to initiate Ca^{2+} release. Sci Signal 9:ra35. https://doi.org/10.1126/scisignal.aad6281
23. Taylor CW, Konieczny V (2016) IP_3 receptors: take four IP_3 to open. Sci Signal 9:pe1. https://doi.org/10.1126/scisignal.aaf6029
24. Takahashi M, Kagasaki T, Hosoya T, Takahashi S (1993) Adenophostins A and B: potent agonists of inositol-1,4,5-trisphosphate receptor produced by Penicillium brevicompactum. Taxonomy, fermentation, isolation, physico-chemical and biological properties. J Antibiot (Tokyo) 46:1643–1647
25. Bezprozvanny I, Watras J, Ehrlich BE (1991) Bell-shaped calcium-response curves of Ins(1,4,5)P3- and calcium-gated channels from endoplasmic reticulum of cerebellum. Nature 351:751–754. https://doi.org/10.1038/351751a0
26. Finch EA, Turner TJ, Goldin SM (1991) Calcium as a coagonist of inositol 1,4,5-trisphosphate-induced calcium release. Science 252:443–446
27. Iino M (1990) Biphasic Ca^{2+} dependence of inositol 1,4,5-trisphosphate-induced Ca^{2+} release in smooth muscle cells of the guinea pig taenia caeci. J Gen Physiol 95:1103–1122
28. Parys JB, Sernett SW, DeLisle S et al (1992) Isolation, characterization, and localization of the inositol 1,4,5-trisphosphate receptor protein in Xenopus laevis oocytes. J Biol Chem 267:18776–18782
29. Bezprozvanny I, Ehrlich BE (1993) ATP modulates the function of inositol 1,4,5-trisphosphate-gated channels at two sites. Neuron 10:1175–1184
30. Bootman MD, Taylor CW, Berridge MJ (1992) The thiol reagent, thimerosal, evokes Ca^{2+} spikes in HeLa cells by sensitizing the inositol 1,4,5-trisphosphate receptor. J Biol Chem 267:25113–25119
31. Parys JB, Missiaen L, De Smedt H et al (1993) Bell-shaped activation of inositol-1,4,5-trisphosphate-induced Ca^{2+} release by thimerosal in permeabilized A7r5 smooth-muscle cells. Pflugers Arch 424:516–522
32. Tovey SC, Dedos SG, Taylor EJA et al (2008) Selective coupling of type 6 adenylyl cyclase with type 2 IP_3 receptors mediates direct sensitization of IP_3 receptors by cAMP. J Cell Biol 183:297–311. https://doi.org/10.1083/jcb.200803172
33. Tovey SC, Dedos SG, Rahman T et al (2010) Regulation of inositol 1,4,5-trisphosphate receptors by cAMP independent of cAMP-dependent protein kinase. J Biol Chem 285:12979–12989. https://doi.org/10.1074/jbc.M109.096016
34. Konieczny V, Tovey SC, Mataragka S et al (2017) Cyclic AMP recruits a discrete intracellular Ca^{2+} store by unmasking hypersensitive IP_3 receptors. Cell Rep 18:711–722. https://doi.org/10.1016/j.celrep.2016.12.058

35. Patterson RL, Boehning D, Snyder SH (2004) Inositol 1,4,5-trisphosphate receptors as signal integrators. Annu Rev Biochem 73:437–465
36. Vervloessem T, Yule DI, Bultynck G, Parys JB (2015) The type 2 inositol 1,4,5-trisphosphate receptor, emerging functions for an intriguing Ca^{2+}-release channel. Biochim Biophys Acta 1853:1992–2005. https://doi.org/10.1016/j.bbamcr.2014.12.006
37. Iwai M, Michikawa T, Bosanac I et al (2007) Molecular basis of the isoform-specific ligand-binding affinity of inositol 1,4,5-trisphosphate receptors. J Biol Chem 282:12755–12764. https://doi.org/10.1074/jbc.M609833200
38. Miyakawa T, Maeda A, Yamazawa T et al (1999) Encoding of Ca^{2+} signals by differential expression of IP_3 receptor subtypes. EMBO J 18:1303–1308. https://doi.org/10.1093/emboj/18.5.1303
39. Newton CL, Mignery GA, Südhof TC (1994) Co-expression in vertebrate tissues and cell lines of multiple inositol 1,4,5-trisphosphate ($InsP_3$) receptors with distinct affinities for $InsP_3$. J Biol Chem 269:28613–28619
40. Tu H, Wang Z, Nosyreva E et al (2005) Functional characterization of mammalian inositol 1,4,5-trisphosphate receptor isoforms. Biophys J 88:1046–1055. https://doi.org/10.1529/biophysj.104.049593
41. Vanlingen S, Sipma H, De Smet P et al (2000) Ca^{2+} and calmodulin differentially modulate myo-inositol 1,4, 5-trisphosphate (IP_3)-binding to the recombinant ligand-binding domains of the various IP_3 receptor isoforms. Biochem J 346:275–280
42. Mak DO, McBride S, Foskett JK (2001) Regulation by Ca^{2+} and inositol 1,4,5-trisphosphate ($InsP_3$) of single recombinant type 3 $InsP_3$ receptor channels. Ca^{2+} activation uniquely distinguishes types 1 and 3 $InsP_3$ receptors. J Gen Physiol 117:435–446
43. Mak D-OD, McBride SMJ, Petrenko NB, Foskett JK (2003) Novel regulation of calcium inhibition of the inositol 1,4,5-trisphosphate receptor calcium-release channel. J Gen Physiol 122:569–581. https://doi.org/10.1085/jgp.200308808
44. Tu H, Wang Z, Bezprozvanny I (2005) Modulation of mammalian inositol 1,4,5-trisphosphate receptor isoforms by calcium: a role of calcium sensor region. Biophys J 88:1056–1069. https://doi.org/10.1529/biophysj.104.049601
45. Betzenhauser MJ, Wagner LE, Iwai M et al (2008) ATP modulation of Ca^{2+} release by type-2 and type-3 inositol (1, 4, 5)-triphosphate receptors. Differing ATP sensitivities and molecular determinants of action. J Biol Chem 283:21579–21587. https://doi.org/10.1074/jbc.M801680200
46. Missiaen L, Parys JB, Sienaert I et al (1998) Functional properties of the type-3 $InsP_3$ receptor in 16HBE14o- bronchial mucosal cells. J Biol Chem 273:8983–8986
47. Maes K, Missiaen L, De Smet P et al (2000) Differential modulation of inositol 1,4,5-trisphosphate receptor type 1 and type 3 by ATP. Cell Calcium 27:257–267. https://doi.org/10.1054/ceca.2000.0121
48. Alzayady KJ, Wagner LE, Chandrasekhar R et al (2013) Functional inositol 1,4,5-trisphosphate receptors assembled from concatenated homo- and heteromeric subunits. J Biol Chem 288:29772–29784. https://doi.org/10.1074/jbc.M113.502203
49. Bultynck G, Szlufcik K, Kasri NN et al (2004) Thimerosal stimulates Ca^{2+} flux through inositol 1,4,5-trisphosphate receptor type 1, but not type 3, via modulation of an isoform-specific Ca^{2+}-dependent intramolecular interaction. Biochem J 381:87–96. https://doi.org/10.1042/BJ20040072
50. Bultynck G, Sienaert I, Parys JB et al (2003) Pharmacology of inositol trisphosphate receptors. Pflugers Arch 445:629–642. https://doi.org/10.1007/s00424-002-0971-1
51. Saleem H, Tovey SC, Molinski TF, Taylor CW (2014) Interactions of antagonists with subtypes of inositol 1,4,5-trisphosphate (IP_3) receptor. Br J Pharmacol 171:3298–3312. https://doi.org/10.1111/bph.12685
52. Swarbrick JM, Riley AM, Mills SJ, Potter BVL (2015) Designer small molecules to target calcium signalling. Biochem Soc Trans 43:417–425. https://doi.org/10.1042/BST20140293
53. Fredericks GJ, Hoffmann FW, Rose AH et al (2014) Stable expression and function of the inositol 1,4,5-triphosphate receptor requires palmitoylation by a DHHC6/selenoprotein K

complex. Proc Natl Acad Sci USA 111:16478–16483. https://doi.org/10.1073/pnas.1417176111
54. Hamada K, Terauchi A, Nakamura K et al (2014) Aberrant calcium signaling by transglutaminase-mediated posttranslational modification of inositol 1,4,5-trisphosphate receptors. Proc Natl Acad Sci USA 111:E3966–E3975. https://doi.org/10.1073/pnas.1409730111
55. Bultynck G, Vermassen E, Szlufcik K et al (2003) Calcineurin and intracellular Ca^{2+}-release channels: regulation or association? Biochem Biophys Res Commun 311:1181–1193
56. Vanderheyden V, Devogelaere B, Missiaen L et al (2009) Regulation of inositol 1,4,5-trisphosphate-induced Ca^{2+} release by reversible phosphorylation and dephosphorylation. Biochim Biophys Acta 1793:959–970. https://doi.org/10.1016/j.bbamcr.2008.12.003
57. Prole DL, Taylor CW (2016) Inositol 1,4,5-trisphosphate receptors and their protein partners as signalling hubs. J Physiol 594:2849–2866. https://doi.org/10.1113/JP271139
58. Ando H, Mizutani A, Kiefer H et al (2006) IRBIT suppresses IP_3 receptor activity by competing with IP_3 for the common binding site on the IP_3 receptor. Mol Cell 22:795–806. https://doi.org/10.1016/j.molcel.2006.05.017
59. Devogelaere B, Beullens M, Sammels E et al (2007) Protein phosphatase-1 is a novel regulator of the interaction between IRBIT and the inositol 1,4,5-trisphosphate receptor. Biochem J 407:303–311. https://doi.org/10.1042/BJ20070361
60. Michikawa T, Hirota J, Kawano S et al (1999) Calmodulin mediates calcium-dependent inactivation of the cerebellar type 1 inositol 1,4,5-trisphosphate receptor. Neuron 23:799–808
61. Missiaen L, Parys JB, Weidema AF et al (1999) The bell-shaped Ca^{2+} dependence of the inositol 1,4, 5-trisphosphate-induced Ca^{2+} release is modulated by Ca^{2+}/calmodulin. J Biol Chem 274:13748–13751
62. Patel S, Morris SA, Adkins CE et al (1997) Ca^{2+}-independent inhibition of inositol trisphosphate receptors by calmodulin: redistribution of calmodulin as a possible means of regulating Ca^{2+} mobilization. Proc Natl Acad Sci USA 94:11627–11632
63. Sienaert I, Nadif Kasri N, Vanlingen S et al (2002) Localization and function of a calmodulin-apocalmodulin-binding domain in the N-terminal part of the type 1 inositol 1,4,5-trisphosphate receptor. Biochem J 365:269–277. https://doi.org/10.1042/BJ20020144
64. Yamada M, Miyawaki A, Saito K et al (1995) The calmodulin-binding domain in the mouse type 1 inositol 1,4,5-trisphosphate receptor. Biochem J 308:83–88
65. Haynes LP, Tepikin AV, Burgoyne RD (2004) Calcium-binding protein 1 is an inhibitor of agonist-evoked, inositol 1,4,5-trisphosphate-mediated calcium signaling. J Biol Chem 279:547–555. https://doi.org/10.1074/jbc.M309617200
66. Kasri NN, Holmes AM, Bultynck G et al (2004) Regulation of $InsP_3$ receptor activity by neuronal Ca^{2+}-binding proteins. EMBO J 23:312–321. https://doi.org/10.1038/sj.emboj.7600037
67. Yang J, McBride S, Mak D-OD et al (2002) Identification of a family of calcium sensors as protein ligands of inositol trisphosphate receptor Ca^{2+} release channels. Proc Natl Acad Sci USA 99:7711–7716. https://doi.org/10.1073/pnas.102006299
68. Chen R, Valencia I, Zhong F et al (2004) Bcl-2 functionally interacts with inositol 1,4,5-trisphosphate receptors to regulate calcium release from the ER in response to inositol 1,4,5-trisphosphate. J Cell Biol 166:193–203. https://doi.org/10.1083/jcb.200309146
69. Eckenrode EF, Yang J, Velmurugan GV et al (2010) Apoptosis protection by Mcl-1 and Bcl-2 modulation of inositol 1,4,5-trisphosphate receptor-dependent Ca^{2+} signaling. J Biol Chem 285:13678–13684. https://doi.org/10.1074/jbc.M109.096040
70. Rong Y-P, Bultynck G, Aromolaran AS et al (2009) The BH4 domain of Bcl-2 inhibits ER calcium release and apoptosis by binding the regulatory and coupling domain of the IP_3 receptor. Proc Natl Acad Sci USA 106:14397–14402. https://doi.org/10.1073/pnas.0907555106
71. White C, Li C, Yang J et al (2005) The endoplasmic reticulum gateway to apoptosis by Bcl-X_L modulation of the $InsP_3R$. Nat Cell Biol 7:1021–1028. https://doi.org/10.1038/ncb1302

72. Xu S, Xu Y, Chen L et al (2017) RCN1 suppresses ER stress-induced apoptosis via calcium homeostasis and PERK-CHOP signaling. Oncogenesis 6:e304. https://doi.org/10.1038/oncsis.2017.6
73. Decuypere J-P, Welkenhuyzen K, Luyten T et al (2011) Ins(1,4,5)P_3 receptor-mediated Ca^{2+} signaling and autophagy induction are interrelated. Autophagy 7:1472–1489
74. Vicencio JM, Ortiz C, Criollo A et al (2009) The inositol 1,4,5-trisphosphate receptor regulates autophagy through its interaction with Beclin 1. Cell Death Differ 16:1006–1017. https://doi.org/10.1038/cdd.2009.34
75. Higo T, Hattori M, Nakamura T et al (2005) Subtype-specific and ER lumenal environment-dependent regulation of inositol 1,4,5-trisphosphate receptor type 1 by ERp44. Cell 120:85–98. https://doi.org/10.1016/j.cell.2004.11.048
76. Higo T, Hamada K, Hisatsune C et al (2010) Mechanism of ER stress-induced brain damage by IP_3 receptor. Neuron 68:865–878. https://doi.org/10.1016/j.neuron.2010.11.010
77. Hayashi T, Su TP (2001) Regulating ankyrin dynamics: Roles of sigma-1 receptors. Proc Natl Acad Sci USA 98:491–496. https://doi.org/10.1073/pnas.021413698
78. Boehning D, Patterson RL, Sedaghat L et al (2003) Cytochrome c binds to inositol (1,4,5) trisphosphate receptors, amplifying calcium-dependent apoptosis. Nat Cell Biol 5:1051–1061. https://doi.org/10.1038/ncb1063
79. Akl H, Bultynck G (2013) Altered Ca^{2+} signaling in cancer cells: proto-oncogenes and tumor suppressors targeting IP3 receptors. Biochim Biophys Acta 1835:180–193. https://doi.org/10.1016/j.bbcan.2012.12.001
80. Ivanova H, Kerkhofs M, La Rovere R, Bultynck G (2017) Endoplasmic reticulum–mitochondrial Ca^{2+} fluxes underlying cancer cell survival. Front Oncol 7:Article 70. https://doi.org/10.3389/fonc.2017.00070
81. Decrock E, De Bock M, Wang N et al (2013) IP_3, a small molecule with a powerful message. Biochim Biophys Acta 1833:1772–1786. https://doi.org/10.1016/j.bbamcr.2012.12.016
82. Distelhorst CW, Bootman MD (2011) Bcl-2 interaction with the inositol 1,4,5-trisphosphate receptor: role in Ca^{2+} signaling and disease. Cell Calcium 50:234–241. https://doi.org/10.1016/j.ceca.2011.05.011
83. Ivanova H, Vervliet T, Missiaen L et al (2014) Inositol 1,4,5-trisphosphate receptor-isoform diversity in cell death and survival. Biochim Biophys Acta 1843:2164–2183. https://doi.org/10.1016/j.bbamcr.2014.03.007
84. Joseph SK, Hajnóczky G (2007) IP_3 receptors in cell survival and apoptosis: Ca^{2+} release and beyond. Apoptosis 12:951–968. https://doi.org/10.1007/s10495-007-0719-7
85. La Rovere RML, Roest G, Bultynck G, Parys JB (2016) Intracellular Ca^{2+} signaling and Ca^{2+} microdomains in the control of cell survival, apoptosis and autophagy. Cell Calcium 60:74–87. https://doi.org/10.1016/j.ceca.2016.04.005
86. Smaili SS, Pereira GJS, Costa MM et al (2013) The role of calcium stores in apoptosis and autophagy. Curr Mol Med 13:252–265
87. Bootman MD, Chehab T, Bultynck G, et al (2018) Autophagy and calcium signalling: do we have a consensus? Cell Calcium. https://doi.org/10.1016/j.ceca.2017.08.005.
88. Ghislat G, Knecht E (2013) Ca^{2+}-sensor proteins in the autophagic and endocytic traffic. Curr Protein Pept Sci 14:97–110
89. Parys JB, Decuypere J-P, Bultynck G (2012) Role of the inositol 1,4,5-trisphosphate receptor/Ca^{2+}-release channel in autophagy. Cell Commun Signal CCS 10:17. https://doi.org/10.1186/1478-811X-10-17
90. Sun F, Xu X, Wang X, Zhang B (2016) Regulation of autophagy by Ca^{2+}. Tumour Biol 37 (12):15467–15476. https://doi.org/10.1007/s13277-016-5353-y
91. Czabotar PE, Lessene G, Strasser A, Adams JM (2014) Control of apoptosis by the BCL-2 protein family: implications for physiology and therapy. Nat Rev Mol Cell Biol 15:49–63. https://doi.org/10.1038/nrm3722
92. Letai AG (2008) Diagnosing and exploiting cancer's addiction to blocks in apoptosis. Nat Rev Cancer 8:121–132. https://doi.org/10.1038/nrc2297

93. Tait SWG, Green DR (2013) Mitochondrial regulation of cell death. Cold Spring Harb Perspect Biol 5:a008706. https://doi.org/10.1101/cshperspect.a008706
94. Pinton P, Giorgi C, Siviero R et al (2008) Calcium and apoptosis: ER-mitochondria Ca^{2+} transfer in the control of apoptosis. Oncogene 27:6407–6418. https://doi.org/10.1038/onc.2008.308
95. Hwang M-S, Schwall CT, Pazarentzos E et al (2014) Mitochondrial Ca^{2+} influx targets cardiolipin to disintegrate respiratory chain complex II for cell death induction. Cell Death Differ 21:1733–1745. https://doi.org/10.1038/cdd.2014.84
96. Bonora M, Bononi A, De Marchi E et al (2013) Role of the c subunit of the F_0 ATP synthase in mitochondrial permeability transition. Cell Cycle 12:674–683. https://doi.org/10.4161/cc.23599
97. Giorgio V, von Stockum S, Antoniel M et al (2013) Dimers of mitochondrial ATP synthase form the permeability transition pore. Proc Natl Acad Sci USA 110:5887–5892. https://doi.org/10.1073/pnas.1217823110
98. Giorgio V, Guo L, Bassot C, et al (2018) Calcium and regulation of the mitochondrial permeability transition. Cell Calcium. https://doi.org/10.1016/j.ceca.2017.05.004
99. Giorgio V, Burchell V, Schiavone M et al (2017) Ca^{2+} binding to F-ATP synthase β subunit triggers the mitochondrial permeability transition. EMBO Rep 18(7):1065–1076
100. Bender T, Martinou J-C (2013) Where killers meet--permeabilization of the outer mitochondrial membrane during apoptosis. Cold Spring Harb Perspect Biol 5:a011106. https://doi.org/10.1101/cshperspect.a011106
101. Wang HG, Pathan N, Ethell IM et al (1999) Ca^{2+}-induced apoptosis through calcineurin dephosphorylation of BAD. Science 284:339–343
102. Sano R, Reed JC (2013) ER stress-induced cell death mechanisms. Biochim Biophys Acta 1833:3460–3470. https://doi.org/10.1016/j.bbamcr.2013.06.028
103. Urra H, Dufey E, Lisbona F et al (2013) When ER stress reaches a dead end. Biochim Biophys Acta 1833:3507–3517. https://doi.org/10.1016/j.bbamcr.2013.07.024
104. Ravikumar B, Sarkar S, Davies JE et al (2010) Regulation of mammalian autophagy in physiology and pathophysiology. Physiol Rev 90:1383–1435. https://doi.org/10.1152/physrev.00030.2009
105. Liu Y, Levine B (2015) Autosis and autophagic cell death: the dark side of autophagy. Cell Death Differ 22:367–376. https://doi.org/10.1038/cdd.2014.143
106. Liu Y, Shoji-Kawata S, Sumpter RM et al (2013) Autosis is a Na^+,K^+-ATPase-regulated form of cell death triggered by autophagy-inducing peptides, starvation, and hypoxia-ischemia. Proc Natl Acad Sci USA 110:20364–20371. https://doi.org/10.1073/pnas.1319661110
107. Bento CF, Renna M, Ghislat G et al (2016) Mammalian autophagy: how does it work? Annu Rev Biochem 85:685–713. https://doi.org/10.1146/annurev-biochem-060815-014556
108. Wesselborg S, Stork B (2015) Autophagy signal transduction by ATG proteins: from hierarchies to networks. Cell Mol Life Sci 72:4721–4757. https://doi.org/10.1007/s00018-015-2034-8
109. Hamasaki M, Furuta N, Matsuda A et al (2013) Autophagosomes form at ER-mitochondria contact sites. Nature 495:389–393. https://doi.org/10.1038/nature11910
110. Hayashi-Nishino M, Fujita N, Noda T et al (2009) A subdomain of the endoplasmic reticulum forms a cradle for autophagosome formation. Nat Cell Biol 11:1433–1437. https://doi.org/10.1038/ncb1991
111. Ylä-Anttila P, Vihinen H, Jokitalo E, Eskelinen E-L (2009) 3D tomography reveals connections between the phagophore and endoplasmic reticulum. Autophagy 5:1180–1185
112. Roberts R, Ktistakis NT (2013) Omegasomes: PI3P platforms that manufacture autophagosomes. Essays Biochem 55:17–27. https://doi.org/10.1042/bse0550017
113. Proikas-Cezanne T, Takacs Z, Dönnes P, Kohlbacher O (2015) WIPI proteins: essential PtdIns3P effectors at the nascent autophagosome. J Cell Sci 128:207–217. https://doi.org/10.1242/jcs.146258
114. Decuypere J-P, Kindt D, Luyten T et al (2013) mTOR-controlled autophagy requires intracellular Ca^{2+} signaling. PloS One 8:e61020. https://doi.org/10.1371/journal.pone.0061020

115. Grotemeier A, Alers S, Pfisterer SG et al (2010) AMPK-independent induction of autophagy by cytosolic Ca^{2+} increase. Cell Signal 22:914–925. https://doi.org/10.1016/j.cellsig.2010.01.015
116. Høyer-Hansen M, Bastholm L, Szyniarowski P et al (2007) Control of macroautophagy by calcium, calmodulin-dependent kinase kinase-beta, and Bcl-2. Mol Cell 25:193–205. https://doi.org/10.1016/j.molcel.2006.12.009
117. Luyten T, Welkenhuyzen K, Roest G et al (2017) Resveratrol-induced autophagy is dependent on IP_3Rs and on cytosolic Ca^{2+}. Biochim Biophys Acta 1864:947–956. https://doi.org/10.1016/j.bbamcr.2017.02.013
118. Messai Y, Noman MZ, Hasmim M et al (2014) ITPR1 protects renal cancer cells against natural killer cells by inducing autophagy. Cancer Res 74:6820–6832. https://doi.org/10.1158/0008-5472.CAN-14-0303
119. Engedal N, Torgersen ML, Guldvik IJ et al (2013) Modulation of intracellular calcium homeostasis blocks autophagosome formation. Autophagy 9:1475–1490. https://doi.org/10.4161/auto.25900
120. Gulati P, Gaspers LD, Dann SG et al (2008) Amino acids activate mTOR complex 1 via Ca^{2+}/CaM signaling to hVps34. Cell Metab 7:456–465. https://doi.org/10.1016/j.cmet.2008.03.002
121. Khan MT, Joseph SK (2010) Role of inositol trisphosphate receptors in autophagy in DT40 cells. J Biol Chem 285:16912–16920. https://doi.org/10.1074/jbc.M110.114207
122. Sarkar S, Floto RA, Berger Z et al (2005) Lithium induces autophagy by inhibiting inositol monophosphatase. J Cell Biol 170:1101–1111. https://doi.org/10.1083/jcb.200504035
123. Cárdenas C, Foskett JK (2012) Mitochondrial Ca^{2+}signals in autophagy. Cell Calcium 52:44–51. https://doi.org/10.1016/j.ceca.2012.03.001
124. Decuypere J-P, Bultynck G, Parys JB (2011) A dual role for Ca^{2+} in autophagy regulation. Cell Calcium 50:242–250. https://doi.org/10.1016/j.ceca.2011.04.001
125. East DA, Campanella M (2013) Ca^{2+} in quality control: an unresolved riddle critical to autophagy and mitophagy. Autophagy 9:1710–1719. https://doi.org/10.4161/auto.25367
126. Rimessi A, Bonora M, Marchi S et al (2013) Perturbed mitochondrial Ca^{2+} signals as causes or consequences of mitophagy induction. Autophagy 9:1677–1686. https://doi.org/10.4161/auto.24795
127. Vicencio JM, Lavandero S, Szabadkai G (2010) Ca^{2+}, autophagy and protein degradation: thrown off balance in neurodegenerative disease. Cell Calcium 47:112–121. https://doi.org/10.1016/j.ceca.2009.12.013
128. Decuypere J-P, Monaco G, Bultynck G et al (2011) The IP_3 receptor-mitochondria connection in apoptosis and autophagy. Biochim Biophys Acta 1813:1003–1013. https://doi.org/10.1016/j.bbamcr.2010.11.023
129. Rizzuto R, De Stefani D, Raffaello A, Mammucari C (2012) Mitochondria as sensors and regulators of calcium signalling. Nat Rev Mol Cell Biol 13:566–578. https://doi.org/10.1038/nrm3412
130. Giacomello M, Pellegrini L (2016) The coming of age of the mitochondria-ER contact: a matter of thickness. Cell Death Differ 23:1417–1427. https://doi.org/10.1038/cdd.2016.52
131. Danese A, Patergnani S, Bonora M et al (2017) Calcium regulates cell death in cancer: Roles of the mitochondria and mitochondria-associated membranes (MAMs). Biochim Biophys Acta 1858(8):615–627. https://doi.org/10.1016/j.bbabio.2017.01.003
132. Giorgi C, Missiroli S, Patergnani S et al (2015) Mitochondria-associated membranes: composition, molecular mechanisms, and physiopathological implications. Antioxid Redox Signal 22:995–1019. https://doi.org/10.1089/ars.2014.6223
133. Herrera-Cruz MS, Simmen T (2017) Of yeast, mice and men: MAMs come in two flavors. Biol Direct 12:3. https://doi.org/10.1186/s13062-017-0174-5
134. Naon D, Scorrano L (2014) At the right distance: ER-mitochondria juxtaposition in cell life and death. Biochim Biophys Acta 1843:2184–2194. https://doi.org/10.1016/j.bbamcr.2014.05.011

135. van Vliet AR, Verfaillie T, Agostinis P (2014) New functions of mitochondria associated membranes in cellular signaling. Biochim Biophys Acta 1843:2253–2262. https://doi.org/10.1016/j.bbamcr.2014.03.009
136. Vervliet T, Clerix E, Seitaj B et al (2017) Modulation of Ca^{2+} signaling by anti-apoptotic B-cell lymphoma 2 proteins at the endoplasmic reticulum–mitochondrial interface. Front Oncol 7:Article 75. https://doi.org/10.3389/fonc.2017.00075
137. Csordás G, Renken C, Várnai P et al (2006) Structural and functional features and significance of the physical linkage between ER and mitochondria. J Cell Biol 174:915–921. https://doi.org/10.1083/jcb.200604016
138. Filadi R, Theurey P, Pizzo P (2017) The endoplasmic reticulum-mitochondria coupling in health and disease: Molecules, functions and significance. Cell Calcium 62:1–15. https://doi.org/10.1016/j.ceca.2017.01.003
139. Paillusson S, Stoica R, Gómez-Suaga P et al (2016) There's something wrong with my MAM; the ER-mitochondria axis and neurodegenerative diseases. Trends Neurosci 39:146–157. https://doi.org/10.1016/j.tins.2016.01.008
140. Szabadkai G, Bianchi K, Várnai P et al (2006) Chaperone-mediated coupling of endoplasmic reticulum and mitochondrial Ca^{2+} channels. J Cell Biol 175:901–911. https://doi.org/10.1083/jcb.200608073
141. Csordás G, Thomas AP, Hajnóczky G (1999) Quasi-synaptic calcium signal transmission between endoplasmic reticulum and mitochondria. EMBO J 18:96–108. https://doi.org/10.1093/emboj/18.1.96
142. Csordás G, Várnai P, Golenár T et al (2010) Imaging interorganelle contacts and local calcium dynamics at the ER-mitochondrial interface. Mol Cell 39:121–132. https://doi.org/10.1016/j.molcel.2010.06.029
143. Giacomello M, Drago I, Bortolozzi M et al (2010) Ca^{2+} hot spots on the mitochondrial surface are generated by Ca^{2+} mobilization from stores, but not by activation of store-operated Ca^{2+} channels. Mol Cell 38:280–290. https://doi.org/10.1016/j.molcel.2010.04.003
144. Murgia M, Rizzuto R (2015) Molecular diversity and pleiotropic role of the mitochondrial calcium uniporter. Cell Calcium 58:11–17. https://doi.org/10.1016/j.ceca.2014.11.001
145. de Brito OM, Scorrano L (2008) Mitofusin 2 tethers endoplasmic reticulum to mitochondria. Nature 456:605–610. https://doi.org/10.1038/nature07534
146. Naon D, Zaninello M, Giacomello M et al (2016) Critical reappraisal confirms that Mitofusin 2 is an endoplasmic reticulum-mitochondria tether. Proc Natl Acad Sci USA 113:11249–11254. https://doi.org/10.1073/pnas.1606786113
147. Cerqua C, Anesti V, Pyakurel A et al (2010) Trichoplein/mitostatin regulates endoplasmic reticulum-mitochondria juxtaposition. EMBO Rep 11:854–860. https://doi.org/10.1038/embor.2010.151
148. Sugiura A, Nagashima S, Tokuyama T et al (2013) MITOL regulates endoplasmic reticulum-mitochondria contacts via Mitofusin2. Mol Cell 51:20–34. https://doi.org/10.1016/j.molcel.2013.04.023
149. Cosson P, Marchetti A, Ravazzola M, Orci L (2012) Mitofusin-2 independent juxtaposition of endoplasmic reticulum and mitochondria: an ultrastructural study. PloS One 7:e46293. https://doi.org/10.1371/journal.pone.0046293
150. Filadi R, Greotti E, Turacchio G et al (2015) Mitofusin 2 ablation increases endoplasmic reticulum-mitochondria coupling. Proc Natl Acad Sci USA 112:E2174–E2181. https://doi.org/10.1073/pnas.1504880112
151. Leal NS, Schreiner B, Pinho CM et al (2016) Mitofusin-2 knockdown increases ER-mitochondria contact and decreases amyloid β-peptide production. J Cell Mol Med 20:1686–1695. https://doi.org/10.1111/jcmm.12863
152. Wang PTC, Garcin PO, Fu M et al (2015) Distinct mechanisms controlling rough and smooth endoplasmic reticulum contacts with mitochondria. J Cell Sci 128:2759–2765. https://doi.org/10.1242/jcs.171132

153. Filadi R, Greotti E, Turacchio G et al (2017) On the role of Mitofusin 2 in endoplasmic reticulum-mitochondria tethering. Proc Natl Acad Sci USA 114:E2266–E2267. https://doi.org/10.1073/pnas.1616040114
154. Naon D, Zaninello M, Giacomello M et al (2017) Reply to Filadi et al.: does Mitofusin 2 tether or separate endoplasmic reticulum and mitochondria? Proc Natl Acad Sci USA 114:E2268–E2269. https://doi.org/10.1073/pnas.1618610114
155. Walker AK, Atkin JD (2011) Stress signaling from the endoplasmic reticulum: a central player in the pathogenesis of amyotrophic lateral sclerosis. IUBMB Life 63:754–763. https://doi.org/10.1002/iub.520
156. De Vos KJ, Mórotz GM, Stoica R et al (2012) VAPB interacts with the mitochondrial protein PTPIP51 to regulate calcium homeostasis. Hum Mol Genet 21:1299–1311. https://doi.org/10.1093/hmg/ddr559
157. Nishimura AL, Mitne-Neto M, Silva HC et al (2004) A mutation in the vesicle-trafficking protein VAPB causes late-onset spinal muscular atrophy and amyotrophic lateral sclerosis. Am J Hum Genet 75:822–831
158. Iwasawa R, Mahul-Mellier A-L, Datler C et al (2011) Fis1 and Bap31 bridge the mitochondria-ER interface to establish a platform for apoptosis induction. EMBO J 30:556–568. https://doi.org/10.1038/emboj.2010.346
159. Breckenridge DG, Stojanovic M, Marcellus RC, Shore GC (2003) Caspase cleavage product of BAP31 induces mitochondrial fission through endoplasmic reticulum calcium signals, enhancing cytochrome c release to the cytosol. J Cell Biol 160:1115–1127. https://doi.org/10.1083/jcb.200212059
160. Simmen T, Aslan JE, Blagoveshchenskaya AD et al (2005) PACS-2 controls endoplasmic reticulum-mitochondria communication and Bid-mediated apoptosis. EMBO J 24:717–729. https://doi.org/10.1038/sj.emboj.7600559
161. Verfaillie T, Rubio N, Garg AD et al (2012) PERK is required at the ER-mitochondrial contact sites to convey apoptosis after ROS-based ER stress. Cell Death Differ 19:1880–1891. https://doi.org/10.1038/cdd.2012.74
162. Gellerich FN, Gizatullina Z, Gainutdinov T et al (2013) The control of brain mitochondrial energization by cytosolic calcium: the mitochondrial gas pedal. IUBMB Life 65:180–190. https://doi.org/10.1002/iub.1131
163. McCormack JG, Halestrap AP, Denton RM (1990) Role of calcium ions in regulation of mammalian intramitochondrial metabolism. Physiol Rev 70:391–425
164. Glancy B, Balaban RS (2012) Role of mitochondrial Ca^{2+} in the regulation of cellular energetics. Biochemistry (Mosc) 51:2959–2973. https://doi.org/10.1021/bi2018909
165. Shanmughapriya S, Rajan S, Hoffman NE et al (2015) Ca^{2+} signals regulate mitochondrial metabolism by stimulating CREB-mediated expression of the mitochondrial Ca^{2+} uniporter gene MCU. Sci Signal 8:ra23. https://doi.org/10.1126/scisignal.2005673
166. Sugawara H, Kurosaki M, Takata M, Kurosaki T (1997) Genetic evidence for involvement of type 1, type 2 and type 3 inositol 1,4,5-trisphosphate receptors in signal transduction through the B-cell antigen receptor. EMBO J 16:3078–3088
167. Wen H, Xu WJ, Jin X et al (2015) The roles of IP_3 receptor in energy metabolic pathways and reactive oxygen species homeostasis revealed by metabolomic and biochemical studies. Biochim Biophys Acta 1853:2937–2944. https://doi.org/10.1016/j.bbamcr.2015.07.020
168. Cárdenas C, Miller RA, Smith I et al (2010) Essential regulation of cell bioenergetics by constitutive $InsP_3$ receptor Ca^{2+} transfer to mitochondria. Cell 142:270–283. https://doi.org/10.1016/j.cell.2010.06.007
169. Gómez-Suaga P, Paillusson S, Stoica R et al (2017) The ER-mitochondria tethering complex VAPB-PTPIP51 regulates autophagy. Curr Biol 27:371–385. https://doi.org/10.1016/j.cub.2016.12.038
170. Bultynck G (2016) Onco-IP_3Rs feed cancerous cravings for mitochondrial Ca^{2+}. Trends Biochem Sci 41:390–393. https://doi.org/10.1016/j.tibs.2016.03.006

171. Cárdenas C, Müller M, McNeal A et al (2016) Selective vulnerability of cancer cells by inhibition of Ca^{2+} transfer from endoplasmic reticulum to mitochondria. Cell Rep 15:219–220. https://doi.org/10.1016/j.celrep.2016.03.045
172. Krols M, Bultynck G, Janssens S (2016) ER-Mitochondria contact sites: a new regulator of cellular calcium flux comes into play. J Cell Biol 214:367–370. https://doi.org/10.1083/jcb.201607124
173. Raturi A, Gutiérrez T, Ortiz-Sandoval C et al (2016) TMX1 determines cancer cell metabolism as a thiol-based modulator of ER-mitochondria Ca^{2+} flux. J Cell Biol 214:433–444. https://doi.org/10.1083/jcb.201512077
174. Granatiero V, Giorgio V, Calì T et al (2016) Reduced mitochondrial Ca^{2+} transients stimulate autophagy in human fibroblasts carrying the 13514A>G mutation of the ND5 subunit of NADH dehydrogenase. Cell Death Differ 23:231–241. https://doi.org/10.1038/cdd.2015.84
175. MacVicar TDB, Mannack LVJC, Lees RM, Lane JD (2015) Targeted siRNA screens identify ER-to-mitochondrial calcium exchange in autophagy and mitophagy responses in RPE1 cells. Int J Mol Sci 16:13356–13380. https://doi.org/10.3390/ijms160613356
176. Hayashi T, Su T-P (2007) Sigma-1 receptor chaperones at the ER-mitochondrion interface regulate Ca^{2+} signaling and cell survival. Cell 131:596–610. https://doi.org/10.1016/j.cell.2007.08.036
177. Chan J, Yamazaki H, Ishiyama N et al (2010) Structural studies of inositol 1,4,5-trisphosphate receptor: coupling ligand binding to channel gating. J Biol Chem 285:36092–36099. https://doi.org/10.1074/jbc.M110.140160
178. Williams A, Hayashi T, Wolozny D et al (2016) The non-apoptotic action of Bcl-xL: regulating Ca^{2+} signaling and bioenergetics at the ER-mitochondrion interface. J Bioenerg Biomembr 48:211–225. https://doi.org/10.1007/s10863-016-9664-x
179. Yang J, Vais H, Gu W, Foskett JK (2016) Biphasic regulation of $InsP_3$ receptor gating by dual Ca^{2+} release channel BH3-like domains mediates Bcl-XL control of cell viability. Proc Natl Acad Sci USA 113:E1953–E1962. https://doi.org/10.1073/pnas.1517935113
180. Sung PJ, Tsai FD, Vais H et al (2013) Phosphorylated K-Ras limits cell survival by blocking Bcl-xL sensitization of inositol trisphosphate receptors. Proc Natl Acad Sci USA 110:20593–20598. https://doi.org/10.1073/pnas.1306431110
181. Mendes CCP, Gomes DA, Thompson M et al (2005) The type III inositol 1,4,5-trisphosphate receptor preferentially transmits apoptotic Ca^{2+} signals into mitochondria. J Biol Chem 280:40892–40900. https://doi.org/10.1074/jbc.M506623200
182. De Stefani D, Bononi A, Romagnoli A et al (2012) VDAC1 selectively transfers apoptotic Ca^{2+} signals to mitochondria. Cell Death Differ 19:267–273. https://doi.org/10.1038/cdd.2011.92
183. Akl H, Monaco G, La Rovere R et al (2013) IP_3R2 levels dictate the apoptotic sensitivity of diffuse large B-cell lymphoma cells to an IP_3R-derived peptide targeting the BH4 domain of Bcl-2. Cell Death Dis 4:e632. https://doi.org/10.1038/cddis.2013.140
184. Jayaraman T, Marks AR (1997) T cells deficient in inositol 1,4,5-trisphosphate receptor are resistant to apoptosis. Mol Cell Biol 17:3005–3012
185. Csordás G, Hajnóczky G (2001) Sorting of calcium signals at the junctions of endoplasmic reticulum and mitochondria. Cell Calcium 29:249–262. https://doi.org/10.1054/ceca.2000.0191
186. Chami M, Oulès B, Szabadkai G et al (2008) Role of SERCA1 truncated isoform in the proapoptotic calcium transfer from ER to mitochondria during ER stress. Mol Cell 32:641–651. https://doi.org/10.1016/j.molcel.2008.11.014
187. Akl H, Vervloessem T, Kiviluoto S et al (2014) A dual role for the anti-apoptotic Bcl-2 protein in cancer: mitochondria versus endoplasmic reticulum. Biochim Biophys Acta 1843:2240–2252. https://doi.org/10.1016/j.bbamcr.2014.04.017
188. Greenberg EF, Lavik AR, Distelhorst CW (2014) Bcl-2 regulation of the inositol 1,4,5-trisphosphate receptor and calcium signaling in normal and malignant lymphocytes: potential new target for cancer treatment. Biochim Biophys Acta 1843:2205–2210. https://doi.org/10.1016/j.bbamcr.2014.03.008

189. Lewis A, Hayashi T, Su T-P, Betenbaugh MJ (2014) Bcl-2 family in inter-organelle modulation of calcium signaling; roles in bioenergetics and cell survival. J Bioenerg Biomembr 46:1–15. https://doi.org/10.1007/s10863-013-9527-7
190. Parys JB (2014) The IP_3 receptor as a hub for Bcl-2 family proteins in cell death control and beyond. Sci Signal 7:pe4. https://doi.org/10.1126/scisignal.2005093
191. Vervliet T, Parys JB, Bultynck G (2016) Bcl-2 proteins and calcium signaling: complexity beneath the surface. Oncogene 35:5079–5092. https://doi.org/10.1038/onc.2016.31
192. Rong Y-P, Aromolaran AS, Bultynck G et al (2008) Targeting Bcl-2-IP_3 receptor interaction to reverse Bcl-2's inhibition of apoptotic calcium signals. Mol Cell 31:255–265. https://doi.org/10.1016/j.molcel.2008.06.014
193. Monaco G, Decrock E, Akl H et al (2012) Selective regulation of IP_3-receptor-mediated Ca^{2+} signaling and apoptosis by the BH4 domain of Bcl-2 versus Bcl-XL. Cell Death Differ 19:295–309. https://doi.org/10.1038/cdd.2011.97
194. Monaco G, Decrock E, Arbel N et al (2015) The BH4 domain of anti-apoptotic Bcl-XL, but not that of the related Bcl-2, limits the voltage-dependent anion channel 1 (VDAC1)-mediated transfer of pro-apoptotic $Ca2^{2+}$ signals to mitochondria. J Biol Chem 290:9150–9161. https://doi.org/10.1074/jbc.M114.622514
195. Zhong F, Harr MW, Bultynck G et al (2011) Induction of Ca^{2+}-driven apoptosis in chronic lymphocytic leukemia cells by peptide-mediated disruption of Bcl-2-IP_3 receptor interaction. Blood 117:2924–2934. https://doi.org/10.1182/blood-2010-09-307405
196. Lavik AR, Zhong F, Chang M-J et al (2015) A synthetic peptide targeting the BH4 domain of Bcl-2 induces apoptosis in multiple myeloma and follicular lymphoma cells alone or in combination with agents targeting the BH3-binding pocket of Bcl-2. Oncotarget 6:27388–27402. https://doi.org/10.18632/oncotarget.4489
197. Greenberg EF, McColl KS, Zhong F et al (2015) Synergistic killing of human small cell lung cancer cells by the Bcl-2-inositol 1,4,5-trisphosphate receptor disruptor BIRD-2 and the BH3-mimetic ABT-263. Cell Death Dis 6:e2034. https://doi.org/10.1038/cddis.2015.355
198. Khan MT, Wagner L, Yule DI et al (2006) Akt kinase phosphorylation of inositol 1,4,5-trisphosphate receptors. J Biol Chem 281:3731–3737. https://doi.org/10.1074/jbc.M509262200
199. Marchi S, Rimessi A, Giorgi C et al (2008) Akt kinase reducing endoplasmic reticulum Ca^{2+} release protects cells from Ca^{2+}-dependent apoptotic stimuli. Biochem Biophys Res Commun 375:501–505. https://doi.org/10.1016/j.bbrc.2008.07.153
200. Szado T, Vanderheyden V, Parys JB et al (2008) Phosphorylation of inositol 1,4,5-trisphosphate receptors by protein kinase B/Akt inhibits Ca^{2+} release and apoptosis. Proc Natl Acad Sci USA 105:2427–2432. https://doi.org/10.1073/pnas.0711324105
201. Marchi S, Marinello M, Bononi A et al (2012) Selective modulation of subtype III IP_3R by Akt regulates ER Ca^{2+} release and apoptosis. Cell Death Dis 3:e304. https://doi.org/10.1038/cddis.2012.45
202. Bononi A, Bonora M, Marchi S et al (2013) Identification of PTEN at the ER and MAMs and its regulation of Ca^{2+} signaling and apoptosis in a protein phosphatase-dependent manner. Cell Death Differ 20:1631–1643. https://doi.org/10.1038/cdd.2013.77
203. Kuchay S, Giorgi C, Simoneschi D et al (2017) PTEN counteracts FBXL2 to promote IP_3R3- and Ca^{2+}-mediated apoptosis limiting tumour growth. Nature 546:554–558. https://doi.org/10.1038/nature22965
204. Ilyin GP, Rialland M, Glaise D, Guguen-Guillouzo C (1999) Identification of a novel Skp2-like mammalian protein containing F-box and leucine-rich repeats. FEBS Lett 459:75–79
205. Chen BB, Glasser JR, Coon TA, Mallampalli RK (2011) FBXL2 is a ubiquitin E3 ligase subunit that triggers mitotic arrest. Cell Cycle 10:3487–3494. https://doi.org/10.4161/cc.10.20.17742
206. Chen BB, Glasser JR, Coon TA, Mallampalli RK (2012) F-box protein FBXL2 exerts human lung tumor suppressor-like activity by ubiquitin-mediated degradation of cyclin D3 resulting in cell cycle arrest. Oncogene 31:2566–2579. https://doi.org/10.1038/onc.2011.432

207. Giorgi C, Ito K, Lin H-K et al (2010) PML regulates apoptosis at endoplasmic reticulum by modulating calcium release. Science 330:1247–1251. https://doi.org/10.1126/science.1189157
208. Paillard M, Tubbs E, Thiebaut P-A et al (2013) Depressing mitochondria-reticulum interactions protects cardiomyocytes from lethal hypoxia-reoxygenation injury. Circulation 128:1555–1565. https://doi.org/10.1161/CIRCULATIONAHA.113.001225
209. Gomez L, Thiebaut P-A, Paillard M et al (2016) The SR/ER-mitochondria calcium crosstalk is regulated by GSK3β during reperfusion injury. Cell Death Differ 23:313–322. https://doi.org/10.1038/cdd.2015.101
210. Wiel C, Lallet-Daher H, Gitenay D et al (2014) Endoplasmic reticulum calcium release through ITPR2 channels leads to mitochondrial calcium accumulation and senescence. Nat Commun 5:3792. https://doi.org/10.1038/ncomms4792
211. Morgan AJ (2016) Ca^{2+} dialogue between acidic vesicles and ER. Biochem Soc Trans 44:546–553. https://doi.org/10.1042/BST20150290
212. Morgan AJ, Platt FM, Lloyd-Evans E, Galione A (2011) Molecular mechanisms of endolysosomal Ca^{2+} signalling in health and disease. Biochem J 439:349–374. https://doi.org/10.1042/BJ20110949
213. Penny CJ, Kilpatrick BS, Eden ER, Patel S (2015) Coupling acidic organelles with the ER through Ca^{2+} microdomains at membrane contact sites. Cell Calcium 58:387–396. https://doi.org/10.1016/j.ceca.2015.03.006
214. Xu H, Ren D (2015) Lysosomal physiology. Annu Rev Physiol 77:57–80. https://doi.org/10.1146/annurev-physiol-021014-071649
215. Melchionda M, Pittman JK, Mayor R, Patel S (2016) Ca^{2+}/H^{+} exchange by acidic organelles regulates cell migration in vivo. J Cell Biol 212:803–813. https://doi.org/10.1083/jcb.201510019
216. Patel S, Cai X (2015) Evolution of acidic Ca^{2+} stores and their resident Ca^{2+}-permeable channels. Cell Calcium 57:222–230. https://doi.org/10.1016/j.ceca.2014.12.005
217. Galione A (2015) A primer of NAADP-mediated Ca^{2+} signalling: From sea urchin eggs to mammalian cells. Cell Calcium 58:27–47. https://doi.org/10.1016/j.ceca.2014.09.010
218. Morgan AJ, Davis LC, Ruas M, Galione A (2015) TPC: the NAADP discovery channel? Biochem Soc Trans 43:384–389. https://doi.org/10.1042/BST20140300
219. Patel S (2015) Function and dysfunction of two-pore channels. Sci Signal 8:re7. https://doi.org/10.1126/scisignal.aab3314
220. Allbritton NL, Meyer T, Stryer L (1992) Range of messenger action of calcium ion and inositol 1,4,5-trisphosphate. Science 258:1812–1815
221. Sukumaran P, Schaar A, Sun Y, Singh BB (2016) Functional role of TRP channels in modulating ER stress and autophagy. Cell Calcium 60:123–132. https://doi.org/10.1016/j.ceca.2016.02.012
222. Waller-Evans H, Lloyd-Evans E (2015) Regulation of TRPML1 function. Biochem Soc Trans 43:442–446. https://doi.org/10.1042/BST20140311
223. Wang W, Zhang X, Gao Q, Xu H (2014) TRPML1: an ion channel in the lysosome. Handb Exp Pharmacol 222:631–645. https://doi.org/10.1007/978-3-642-54215-2_24
224. Galione A (2011) NAADP receptors. Cold Spring Harb Perspect Biol 3:a004036. https://doi.org/10.1101/cshperspect.a004036
225. Grimm C, Chen C-C, Wahl-Schott C, Biel M (2017) Two-pore channels: catalyzers of endolysosomal transport and function. Front Pharmacol 8:45. https://doi.org/10.3389/fphar.2017.00045
226. Kilpatrick BS, Eden ER, Schapira AH et al (2013) Direct mobilisation of lysosomal Ca^{2+} triggers complex Ca^{2+} signals. J Cell Sci 126:60–66. https://doi.org/10.1242/jcs.118836
227. Fameli N, Ogunbayo OA, van Breemen C, Evans AM (2014) Cytoplasmic nanojunctions between lysosomes and sarcoplasmic reticulum are required for specific calcium signaling. F1000Research 3:93. https://doi.org/10.12688/f1000research.3720.1

228. Lam AKM, Galione A (2013) The endoplasmic reticulum and junctional membrane communication during calcium signaling. Biochim Biophys Acta 1833:2542–2559. https://doi.org/10.1016/j.bbamcr.2013.06.004
229. Raiborg C, Wenzel EM, Stenmark H (2015) ER-endosome contact sites: molecular compositions and functions. EMBO J 34:1848–1858. https://doi.org/10.15252/embj.201591481
230. Cancela JM, Churchill GC, Galione A (1999) Coordination of agonist-induced Ca^{2+}-signalling patterns by NAADP in pancreatic acinar cells. Nature 398:74–76. https://doi.org/10.1038/18032
231. Churchill GC, Galione A (2001) NAADP induces Ca^{2+} oscillations via a two-pool mechanism by priming IP_3- and cADPR-sensitive Ca^{2+} stores. EMBO J 20:2666–2671. https://doi.org/10.1093/emboj/20.11.2666
232. Gerasimenko JV, Charlesworth RM, Sherwood MW et al (2015) Both RyRs and TPCs are required for NAADP-induced intracellular Ca^{2+} release. Cell Calcium 58:237–245. https://doi.org/10.1016/j.ceca.2015.05.005
233. Morgan AJ, Davis LC, Wagner SKTY et al (2013) Bidirectional Ca^{2+} signaling occurs between the endoplasmic reticulum and acidic organelles. J Cell Biol 200:789–805. https://doi.org/10.1083/jcb.201204078
234. López Sanjurjo CI, Tovey SC, Taylor CW (2014) Rapid recycling of Ca^{2+} between IP_3-sensitive stores and lysosomes. PloS One 9:e111275. https://doi.org/10.1371/journal.pone.0111275
235. López-Sanjurjo CI, Tovey SC, Prole DL, Taylor CW (2013) Lysosomes shape Ins(1,4,5)P3-evoked Ca^{2+} signals by selectively sequestering Ca^{2+} released from the endoplasmic reticulum. J Cell Sci 126:289–300. https://doi.org/10.1242/jcs.116103
236. Kilpatrick BS, Yates E, Grimm C et al (2016) Endo-lysosomal TRP mucolipin-1 channels trigger global ER Ca^{2+} release and Ca^{2+} influx. J Cell Sci 129:3859–3867. https://doi.org/10.1242/jcs.190322
237. Decuypere J-P, Parys JB, Bultynck G (2015) ITPRs/inositol 1,4,5-trisphosphate receptors in autophagy: From enemy to ally. Autophagy 11:1944–1948. https://doi.org/10.1080/15548627.2015.1083666
238. Penny CJ, Kilpatrick BS, Han JM et al (2014) A computational model of lysosome-ER Ca^{2+} microdomains. J Cell Sci 127:2934–2943. https://doi.org/10.1242/jcs.149047
239. Raffaello A, Mammucari C, Gherardi G, Rizzuto R (2016) Calcium at the center of cell signaling: Interplay between endoplasmic reticulum, mitochondria, and lysosomes. Trends Biochem Sci 41:1035–1049. https://doi.org/10.1016/j.tibs.2016.09.001
240. Ronco V, Potenza DM, Denti F et al (2015) A novel Ca^{2+}-mediated cross-talk between endoplasmic reticulum and acidic organelles: implications for NAADP-dependent Ca^{2+} signalling. Cell Calcium 57:89–100. https://doi.org/10.1016/j.ceca.2015.01.001
241. Gómez-Suaga P, Luzón-Toro B, Churamani D et al (2012) Leucine-rich repeat kinase 2 regulates autophagy through a calcium-dependent pathway involving NAADP. Hum Mol Genet 21:511–525. https://doi.org/10.1093/hmg/ddr481
242. Pereira GJS, Hirata H, Fimia GM et al (2011) Nicotinic acid adenine dinucleotide phosphate (NAADP) regulates autophagy in cultured astrocytes. J Biol Chem 286:27875–27881. https://doi.org/10.1074/jbc.C110.216580
243. Lin P-H, Duann P, Komazaki S et al (2015) Lysosomal two-pore channel subtype 2 (TPC2) regulates skeletal muscle autophagic signaling. J Biol Chem 290:3377–3389. https://doi.org/10.1074/jbc.M114.608471
244. Lu Y, Hao B-X, Graeff R et al (2013) Two pore channel 2 (TPC2) inhibits autophagosomal-lysosomal fusion by alkalinizing lysosomal pH. J Biol Chem 288:24247–24263. https://doi.org/10.1074/jbc.M113.484253
245. Wong C-O, Li R, Montell C, Venkatachalam K (2012) Drosophila TRPML is required for TORC1 activation. Curr Biol 22:1616–1621. https://doi.org/10.1016/j.cub.2012.06.055

246. Wang W, Gao Q, Yang M et al (2015) Up-regulation of lysosomal TRPML1 channels is essential for lysosomal adaptation to nutrient starvation. Proc Natl Acad Sci USA 112: E1373–E1381. https://doi.org/10.1073/pnas.1419669112
247. Li X, Rydzewski N, Hider A et al (2016) A molecular mechanism to regulate lysosome motility for lysosome positioning and tubulation. Nat Cell Biol 18:404–417. https://doi.org/10.1038/ncb3324
248. García-Rúa V, Feijóo-Bandín S, Rodríguez-Penas D et al (2016) Endolysosomal two-pore channels regulate autophagy in cardiomyocytes. J Physiol 594:3061–3077. https://doi.org/10.1113/JP271332
249. Manzoni C (2017) The LRRK2-macroautophagy axis and its relevance to Parkinson's disease. Biochem Soc Trans 45:155–162. https://doi.org/10.1042/BST20160265
250. Hockey LN, Kilpatrick BS, Eden ER et al (2015) Dysregulation of lysosomal morphology by pathogenic LRRK2 is corrected by TPC2 inhibition. J Cell Sci 128:232–238. https://doi.org/10.1242/jcs.164152
251. Medina DL, Di Paola S, Peluso I et al (2015) Lysosomal calcium signalling regulates autophagy through calcineurin and TFEB. Nat Cell Biol 17:288–299. https://doi.org/10.1038/ncb3114
252. Settembre C, Di Malta C, Polito VA et al (2011) TFEB links autophagy to lysosomal biogenesis. Science 332:1429–1433. https://doi.org/10.1126/science.1204592
253. Medina DL, Fraldi A, Bouche V et al (2011) Transcriptional activation of lysosomal exocytosis promotes cellular clearance. Dev Cell 21:421–430. https://doi.org/10.1016/j.devcel.2011.07.016
254. Sardiello M, Palmieri M, di Ronza A et al (2009) A gene network regulating lysosomal biogenesis and function. Science 325:473–477. https://doi.org/10.1126/science.1174447

Chapter 8
Structural Details of the Ryanodine Receptor Calcium Release Channel and Its Gating Mechanism

Katrien Willegems and Rouslan G. Efremov

Abstract Ryanodine receptors (RyRs) are large intracellular calcium release channels that play a crucial role in coupling excitation to contraction in both cardiac and skeletal muscle cells. In addition, they are expressed in other cell types where their function is less well understood. Hundreds of mutations in the different isoforms of RyR have been associated with inherited myopathies and cardiac arrhythmia disorders. The structure of these important drug targets remained elusive for a long time, despite decades of intensive research. In the recent years, a technical revolution in the field of single particle cryogenic electron microscopy (SP cryo-EM) allowed solving high-resolution structures of the skeletal and cardiac RyR isoforms. Together with the structures of individual domains solved by X-ray crystallography, this resulted in an unprecedented understanding of the structure, gating and regulation of these largest known ion channels. In this chapter we describe the recently solved high-resolution structures of RyRs, discuss molecular details of the channel gating, regulation and the disease mutations. Additionally, we highlight important questions that require further progress in structural studies of RyRs.

Keywords Calcium signalling · Ryanodine receptor · Ion channel gating · Cryo-EM

8.1 Introduction

Ryanodine receptors (RyRs) are ion channels residing in sarcoplasmic reticulum (SR) or endoplasmic reticulum (ER) membranes. They couple action potential excitation with contraction of muscles, in the process known as excitation–contraction coupling (EC-coupling), by releasing calcium from the intracellular calcium

K. Willegems · R. G. Efremov (✉)
Center for Structural Biology, Vlaams Instituut voor Biotechnologie, Brussels, Belgium

Structural Biology Brussels, Department of Bioengineering Sciences, Vrije Universiteit Brussel, Brussels, Belgium
e-mail: rouslan.efremov@vib-vub.be

J. Krebs (ed.), *Membrane Dynamics and Calcium Signaling*, Advances in Experimental Medicine and Biology 981,
https://doi.org/10.1007/978-3-319-55858-5_8

stores [1]. While the function of RyRs has been primarily characterized in muscle contraction, these receptors are expressed in many cell types including neuronal, smooth muscles, endothelial and pancreatic cells, where exact involvement of RyRs in calcium homeostasis is less well understood [2].

RyRs are high-conductance cation-selective homo-tetrameric ion channels with a molecular mass exceeding 2.2 MDa. This largest known ion channel is named after one of its exogenous ligands ryanodine, an alkaloid plant toxin from *Ryania speciosa*. Known for its insecticidal properties, *Ryania speciosa* was first described in 1796 and ryanodine was identified as the active molecule in 1948 [3]. Later ryanodine was shown to bind with high affinity to a specific receptor [4–7]. Historically in the 1980s it was shown that three properties essential for muscular contraction: sensitivity to ryanodine, fast calcium release from the SR and giant 'foot' structures [8], the high-density regularly-spaced assemblies separating the transverse tubules (T-tubules) and SR membranes, were due to a single protein complex, RyR [9].

Localized to SR/ER membranes, RyR has a large cytoplasmic moiety, consisting of around 4500 amino acids per monomer (Fig. 8.1a), and a relatively small yet functionally important luminal region. RyRs are Ca^{2+} gated cationic ion channels weakly selective for Ca^{2+} over other cations. At nanomolar calcium concentration RyRs are closed. Their open probability rises in submicromolar to micromolar range while millimolar calcium concentrations inhibit the channels [10–12]. The mechanisms of RyR activation in EC-coupling is tissue dependent. In cardiac muscles, an action potential activates L-type voltage gated Ca^{2+} channels ($Ca_v1.2$) inducing an inward flow of calcium that activates RyR2. This coupling mechanism is known as calcium-induced calcium release (CICR). In skeletal muscles the activation of $Ca_v1.1$ triggers opening of RyR1 in the absence of calcium inflow. This still poorly understood mechanism is known as direct coupling [1].

The calcium release by RyR is modulated by many factors ranging from small molecules including Mg^{2+}, ATP, caffeine, toxins, and drugs; to accessory proteins among which are FKBP12/12.6, calmodulin, S100A1 and sorcin; to post translational modifications: phosphorylation, oxidation, and nitrosylation [13]. Thus, RyR can integrate multiple signals to fine-tune responses to cellular stimuli and homeostasis [14].

RyR Isoforms

Three RyR isoforms are found in mammals, RyR1, 2 and 3. They share around 65% sequence identity and have subtle functional differences. The isoforms differ in expression patterns, with RyR1 highly expressed in skeletal muscles and RyR2 in cardiac muscles. RyR3 is ubiquitously expressed at low levels, often overlapping with the expression of one or both of the other isoforms [15, 16]. RyRs are also widely expressed at different levels and specific isoform ratios in several other tissues including neurons, smooth muscles, endothelial cells and pancreatic cells [16]. Two RyR homologues, RyRα and β, have been described in non-mammalian vertebrates [17, 18]. Insects have one RyR homologue that was first described in *Drosophila melanogaster* [19]. The insect RyR is the target of several commercial

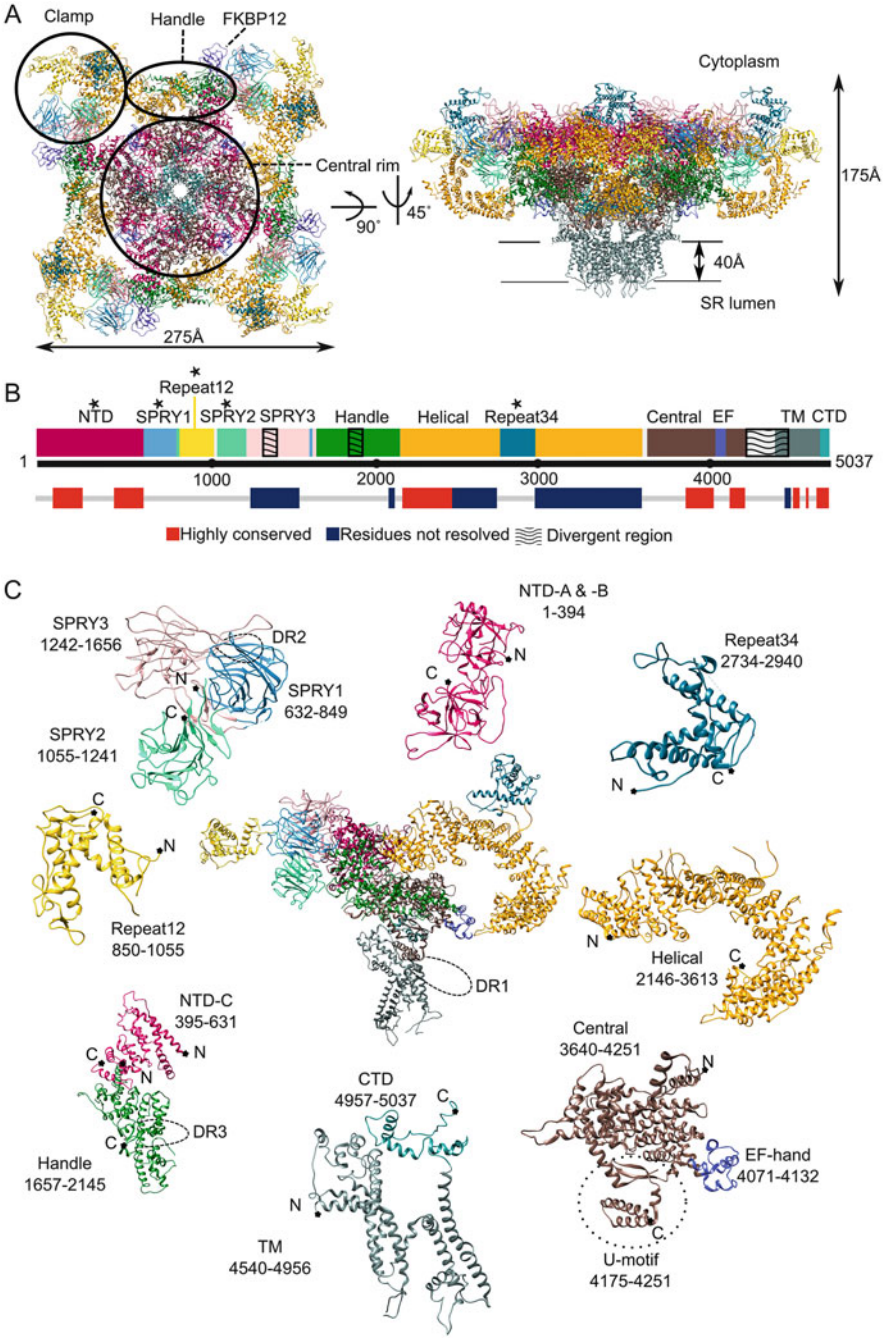

Fig. 8.1 Architecture of RyR1. (**a**). Structure of rabbit RyR1 in complex with FKBP12 (purple) colored by domains. (**b**). Upper bar shows a linear representation of the domain organization within the primary sequence, the color-coding is the same as in (**a**). Divergent regions (DRs) are indicated with wave pattern. Domains for which the X-ray structure was solved are indicated with asterisk.

pesticides belonging to the phthalic acid and anthranilic diamides class [20]. These channel activators are selective for insect RyRs, poorly conserved between vertebrates and invertebrates, making them a suitable target for safe pesticides.

Localization and Organization

Intricacy of RyR function is augmented by the specific protein localization within the cell. In muscle cells some RyRs are localized to terminal cisternae or junctional SR (jSR), a part of the SR in close contact with the T-tubules, invaginations of the sarcolemma. In skeletal muscles two jSRs sandwich one T-tubule forming a triad structure while in cardiac muscles junctions are organized in diads where only one jSR contacts a T-tubule. In the junctions, arrays of around 100 ordered RyR molecules [21, 22] form a functional couplon with 10–25 Ca_v residing in the T-tubular membrane. In skeletal muscles, Ca_v-channels are organized in clusters of four, tetrads, aligned relative to the RyR1 lattice [23]. Within ordered arrays RyRs can allosterically interact with each other to amplify and synchronize Ca^{2+} release [24, 25]. In some cell types RyRs localize to other intracellular nanojunctions [26, 27]. Such nanodomains are found for example at the SR-lysosome junction in smooth muscle cells, where they mediate muscle contraction [27, 28] or at the nucleoplasmic reticulum where RyR1 mediates calcium release into the nucleus [29].

Role of RyR in Diseases

Mutations in RyR have been primarily associated with a range of myopathies and cardiac arrhythmia disorders [30]. The Human Gene Mutation Database (HGMD®, until 2017 [31]) contains 563 mutations in *RyR1* and 287 mutations in *RyR2* that are known to cause inherited diseases. *RyR3* has been much less studied, but at least eight mutations in the gene have been suggested to increase the risk for breast cancer [32, 33].

After more than three decades of intense RyR studies a bulk of functional information has been produced by single channel recordings, calcium imaging and ^{3}[H]-ryanodine binding assays among other methods. This data were complemented by structural methods primarily low to medium resolution single particle electron microscopy (SP EM) maps and by X-ray crystallographic structures of individual domains [34–38]. The last 2 years however have been marked by a significant technological progress in single particle cryo-EM [39], which for the first time allowed solving the high-resolution structure of RyR, building its nearly complete atomic model and gaining insight into the channel gating and regulation mechanisms [40, 41].

In the following sections, we focus on the structure, gating mechanism, regulation and effects of mutations on RyR utilizing the wealth of novel high-resolution structural information.

Fig. 8.1 (continued) Lower bar: highly conserved regions (red) and regions were accurate sequence register has not been determined in cryo-EM models (blue) are indicated. (**c**). Architecture of the RyR1 monomer. Color-coding as in (**a**). The images are made using PDB structure 5T15

8.2 Structure of RyR

Early EM sections on muscle from different species including frog, rabbit and bat [8, 42, 43] later complemented with single particle 3D reconstructions [44] showed that RyR is a very large protein with maximum dimensions exceeding 300 Å. It has a mushroom shape with a cytoplasmic domain constituting 95% of the protein structure and membrane domain the remaining 5%. Encoded by a single polypeptide of around 5000 amino acids long, each RyR monomer can be divided into 13 well-defined domains (Fig. 8.1).

Structural information used to build the currently most complete atomic models of RyR comes from two complementary techniques. High-resolution cryo-EM structures for rabbit skeletal RyR1 and porcine cardiac RyR2 isoforms were recently determined [40, 41, 45–48]. Due to protein flexibility the resolution of the cryo-EM maps on the periphery of the protein is low [46], there the structural models are complemented by high-resolution X-ray structures of individual domains [34–38]. The highest resolution and currently the most complete cryo-EM model of rabbit RyR1 is determined at a resolution of 3.6 Å and includes around 4200 residues [40]. In this model the exact register is not assigned for around 1000 residues (Fig. 8.1b). Taking into account disordered regions and loops, the accurate atomic model currently accounts for around 65% of the RyR1 polypeptide.

There is still no commonly used nomenclature for the RyR domains, to minimize confusion in this chapter we will follow the most traditional naming of domains, where possible, combined with the names introduced in the first atomic structure of RyR1 [41].

Architecture of RyR

The apparent complexity of the RyR structure can be significantly reduced by noticing that the cytoplasmic domain is created by a repetition of only a handful of structural motifs and folds. Thus, around 60% of the cytoplasmic domain is folded into α-solenoid structures created by repeated helical hairpins, another 15% is accounted for by three β-sandwich SPRY domains and another 9% is formed by two α-helical repeat domains. The remaining 16% are shared between two N-terminal β-trefoil domains (9%) and disordered regions (Fig. 8.1). The structure of the TM domain belongs to the voltage-gated ion channel superfamily fold.

The cytoplasmic domain can be divided into the central core moiety and peripheral domains. The central core is composed of two consecutive N-terminal domains (NTD) with a β-trefoil fold (Fig. 8.1c) named NTD-A (residues 1–207) and NTD-B (residues 208–395). NTD-AB is followed by an α-solenoid domain, composed of two separated in sequence stretches of polypeptide, NTD-C (396–632) and Handle domain (1650–2147) (Fig. 8.1c). This α-solenoid domain bends in a horseshoe-like structure composed of ten helical hairpins. On the C-terminal side this domain is continued by the Central domain (3639–4253) positioned underneath the NTD-AB domains of the adjacent RyR protomer. The Central domain is folded into an α-solenoid formed by six helical hairpins complemented with the C-terminal U-motif (Fig. 8.1c).

The central core and TM domain form a compact structure conserved between RyR and its evolutionary homologue inositol-1,4,5-triphosphate receptor, IP_3R. The most conserved regions are found in proximity of the fourfold symmetry axis of the receptor [46].

The central core is 'decorated' by additional, less conserved domains. A large, around 1000 amino acids (residues 632–1650), loop joining helices of the α-solenoid domain (Fig. 8.1b) forms a compact cluster of SPRY domains (SPRY1, SPRY2, SPRY3) with the Repeat12 domain protruding outside to form the characteristic hook-like corners (clamps) of the square-shaped cytoplasmic domain (Fig. 8.1a,c).

Finally, the structure is completed by another large α-solenoid domain, Helical domain (residues 2148–2703 and ~2942–3610), located in the primary sequence between the Handle and Central domain. The Helical domain contains 17 helical hairpins (Fig. 8.1b,c). Its N-terminus contacts the Handle domain and its C-terminus ends under the SPRY cluster of the neighboring protomer. The Repeat34 domain (2734–2939) inserted approximately in the middle of the Helical domain protrudes out of the upper surface of the receptor. Further we describe in more details the structure, function of and interactions between the individual domains.

Central Rim

When assembled into a tetramer, the NTD-AB domains form a ring-like structure also known, from earlier EM studies, as central rim [49] (Fig. 8.1a). This is one of the most conserved domains between RyR and IP_3R (Fig. 8.1b). In IP_3R, NTD-B forms a part of the inositol-triphosphate binding site [50], while in RyR it does not binds any known cofactor. In spite of the significant dimensions of the cytoplasmic domain, the interaction surface between the protomers is relatively small, these interactions are mainly mediated by NTD-AB. NTD-AB interacts with the NTD-AB, Central and Helical domains of the neighboring protomer. These interactions involve hydrogen bonds and numerous salt bridges. Consequently, mutations in NTD-AB can compromise the interaction between the protomers resulting in reduced protein stability and increased flexibility [36] explaining the high concentration of disease mutations within this domain.

Clamps

SPRY are domains with β-sandwich fold named after SplA kinase and RyRs, the proteins in which they were initially identified from sequence alignments [51]. In RyRs, three SPRY domains form a compact cluster in the corner of the cytosolic cap that was traditionally referred to as clamp [49]. The cluster of SPRY domains is located within the region poorly resolved by cryo-EM not allowing reliable ab initio mode building. High-resolution X-ray structures of SPRY1 (633–825, 1622–1649) and SPRY2 (1070–1240) have been solved [34, 38]. The high-resolution structure of SPRY3 (1241–1602) is not known, only the backbone trace for this domain has been built in the cryo-EM model [40]. Interestingly, a polypeptide fragment, remote in sequence, contributes to a β-strand (1622–1649) of the convex β-sheet of SPRY1 [41].

SPRY domains are often involved in protein–protein interactions [52]. In RyR SPRY1, together with the Handle domain, forms a binding site for FKBP12 (12-kDa FK506-binding protein) [41]. SPRY2 is located at the lower side of the SPRY cluster

and interacts with the C-terminal tip of the Helical domain from the neighboring promoter. SPRY3 is positioned on the upper surface of RyR facing the plasma membrane. It was suggested to be involved in the direct coupling mechanism [45, 53]. In addition, the SPRY3 contains a long disordered loop of 133 residues (1297–1430) that corresponds to divergent region 2, DR2 (Fig. 8.1c) [54]. This loop faces the upper surface of the receptor and might be involved in interactions with proteins in the terminal junctions.

Repeat Domains

Two Repeat domains, Repeat12 (861–1054) and Repeat34 (2734–2939) contributed by neighboring protomers, are found relatively close to each other in the clamp domain (Fig. 8.1a). These domains are tandem repeats of around 110 amino acids (Fig. 8.1c) [55]. The crystal structures of both repeat domains are known [35, 37, 38] and they are significantly different despite the similarity expected based on their primary sequence. While the Repeat34 domain has a pseudo symmetrical horseshoe shape formed by repeating two α-helices and one short β-strand, the symmetry in Repeat12 is interrupted by an additional β-sheet and a long structured loop [38]. The resolution of the cryo-EM maps in the regions of Repeat domains is too low to reliably distinguish between two possible docking options. Repeat12 is involved in formation of 2D RyR arrays, thereby it might also be involved in the allosteric coupling between RyRs [14, 56]. Repeat34 is also known as the phosphorylation hot spot of RyRs, the phosphorylation sites are located on the disordered loop linking repeats 3 and 4 [37].

α-Solenoid domains are formed by multiple repeats of helical hairpin motifs, creating extended flat structures common in eukaryotic organisms [57]. α-Solenoid domains often play a role as scaffolds and are involved in protein–protein and protein–ligand interactions. Due to their shape they can be flexible and able to adapt different conformations [58]. Among the α-solenoid domains constituting RyR, the Helical domain is the largest (Fig. 8.1c). It spans around 1200 residues folded into an extended superhelical domain. The Repeat34 domain is inserted approximately in the middle of the Helical domain. Within the tetramer assembly, Helical domains form the edges of the square-like cytoplasmic cap (Fig. 8.1a). Due to the flexibility of the extended RyR cap, the density of a large part of the Helical domain has insufficient resolution to build an accurate model, therefore the polypeptide chain register has been assigned only for 330 N-terminal residues (Fig. 8.1b). The C-terminal end of this domain, formed by an additional seven α-helices, interacts with the SPRY2 domain of an adjacent protomer, stabilizing the tetrameric assembly.

α-Solenoid domain composed of the NTD-C and Handle domain interacts with most other cytoplasmic domains: NDT-AB, SPRY, Helical and Central as well as with FKBP12. The Handle domain has a characteristic protrusion formed by extremely long α-helices (residues 1961–2039) flanked by shorter α-helices (Fig. 8.1c) that harbors one of calmodulin (CaM) binding sites, CaMB1 [40, 59]. The Handle domain also includes a large unresolved loop of 48 (residues 1874–1922) that corresponds to the DR3 region [54] and another long unresolved

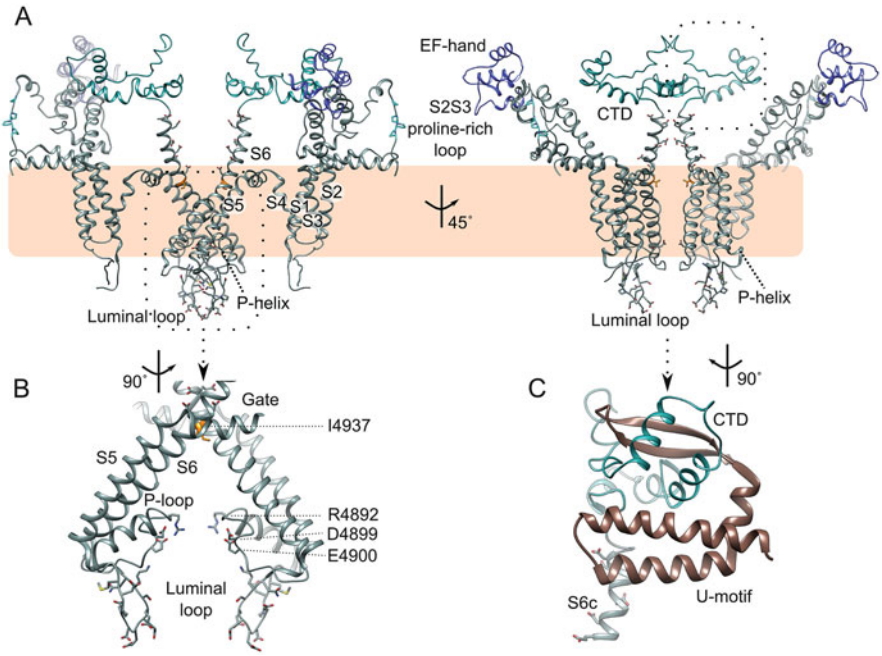

Fig. 8.2 Structure and interactions of the transmembrane domain. (**a**). Side view of a TM domain dimer of rabbit RyR1 in open conformation. The C-terminal domain (CTD) and the EF-hand domain of the adjacent monomer are shown as well, using color-coding as in Fig. 8.1. The proline-rich loop in the S2S3 helical bundle is indicated in cyan. The gate-forming residue I4937 is shown in orange. Side chains for the charged residues in the cytoplasmic S6 helix and in the luminal loop are shown. (**b**). Close-up of the gate and selectivity filter. Side chains of the negatively charged residues on the luminal loop are shown. (**c**). Close-up view of the CTD clamped by the U-motif from the Central domain. The U-motif is omitted on panel (**a**)

loop between the residues 2048 and 2089 (Fig. 8.1b, c). Both loops are found on the outer surface of RyR below the FKBP12-binding site.

Central domain is one of the most conserved domains (Fig. 8.1b) and it is pivotal for allosteric gating of the channel by calcium [40, 45, 47]. Twenty α-helices packed in an armadillo structure build up the domain. It harbors a pair of EF-hands (4071–4132) inserted in a loop connecting two α-helices (Fig. 8.1c). The C-terminus of the Central domain folds in a peculiar structure, coined U-motif [41], critical for the assembly and gating of RyR. The U-motif folded into a β-hairpin and an α-hairpin, separated by a short α-helix is located underneath the Central domain (Figs. 8.1c, 8.2c). The Central domain is linked to the TM domain by an exceptionally long, nearly 400 amino acids, disordered fragment corresponding to DR1 region.

TM domain of RyR belongs to the six transmembrane (TM) helical (S1–6) class of tetrameric ion channels (Figs. 8.1, 8.2) that includes TRP channels and voltage-gated channels. Within this class of channels, the structure of the TM domain is

conserved in spite of poor sequence homology. Helices S1–S4 form a voltage-sensing-like domain (VSD-like domain) (Fig. 8.2). RyRs lack the positive charges on helix S4 responsible for voltage sensing in voltage-gated ion channels. Unique to and conserved between RyRs is a cytoplasmic domain formed between helices S2 and S3 (residues 4666–4787). This S2S3 domain is folded into six short helical segments and an extended proline-reach loop (4756–4765) (Fig. 8.2a) suggested to be a potential SH3-binding site [40]. The S2S3 domain interacts with the EF-hand domain of the neighboring protomer.

The ion pore is formed by S6 helices arranged in a right-handed bundle around fourfold symmetry axis. At the luminal side the architecture of the ion selectivity filter is similar to that of tetrameric potassium channels and TRPV channels. The selectivity filter is formed by the loop connecting S5 and S6 on the luminal side (Fig. 8.2b). It is supported by a half-helix called pore helix (P-helix) and a re-entrant loop with a single helical turn that lines the surface of the selectivity filter. Remarkably, in RyRs the selectivity filter is shorter and wider than in the other known ion channels, which is consistent with high channel conductance and poor selectivity. The carbonyl oxygens of Ala4892, Gly4894, Gly4895 (in rabbit RyR1) form the narrowest constriction of the filter, separated by a distance of ~9 Å versus ~5 Å in other ion channels. On the luminal side Asp4899 and Glu4900 side chains contribute to the wide selectivity filter vestibule. The ion filter in RyR is separated from the gate by a hydrophobic cavity, similar to the other ion channels.

The structures of RyR determined in the absence of free calcium represent the closed channel conformation. The channel gate is located at the cytoplasmic membrane surface, where hydrophobic Ile4937 side chains constrain the pore to a radius of 0.6 Å (Fig. 8.3c, d) making it impermeable to dehydrated charged ions including Ca^{2+}. On the luminal side, the P-helix is linked to the S5 helix with an unusual negatively charged luminal loop (4863–4875) [41] in which six out of seven residues are Asp or Glu (Fig. 8.2). This luminal loop may attract calcium ions and contribute to ion selectivity or might be involved in storage-overload induced calcium release (SOICR) [41]. The ion conduction channel extends over 30 Å into the cytoplasm by unusually long extensions of the S6 helices lined with Glu and Asp residues (Fig. 8.2), which may contribute to ion selectivity as well. The ion conductive pore of RyR does not appear to have a strict, well-defined selectivity filter like most other ion channels. Selection likely happens at several places: cytoplasmic funnel, filter region and luminal loop. Such architecture allows for maintaining high channel conductance without compromising selectivity for positively versus negatively changed ions.

C-terminal domain (CTD, residues 4957–5037) connects the TM domain with the cytoplasmic cap. This domain is very conserved, it folds into five short α-helices positioned under the Central domain where it is tightly clamped by the U-motif (Figs. 8.1c, 8.2c). The S6-CTD connection is rigidified by a zinc ion coordinated by residues Cys4958, Cys4961, His 4978 and His 4983 within a zinc finger motif (Fig. 8.4a). This zinc finger is important for the gating mechanism of RyR and is conserved between RyR and IP_3R.

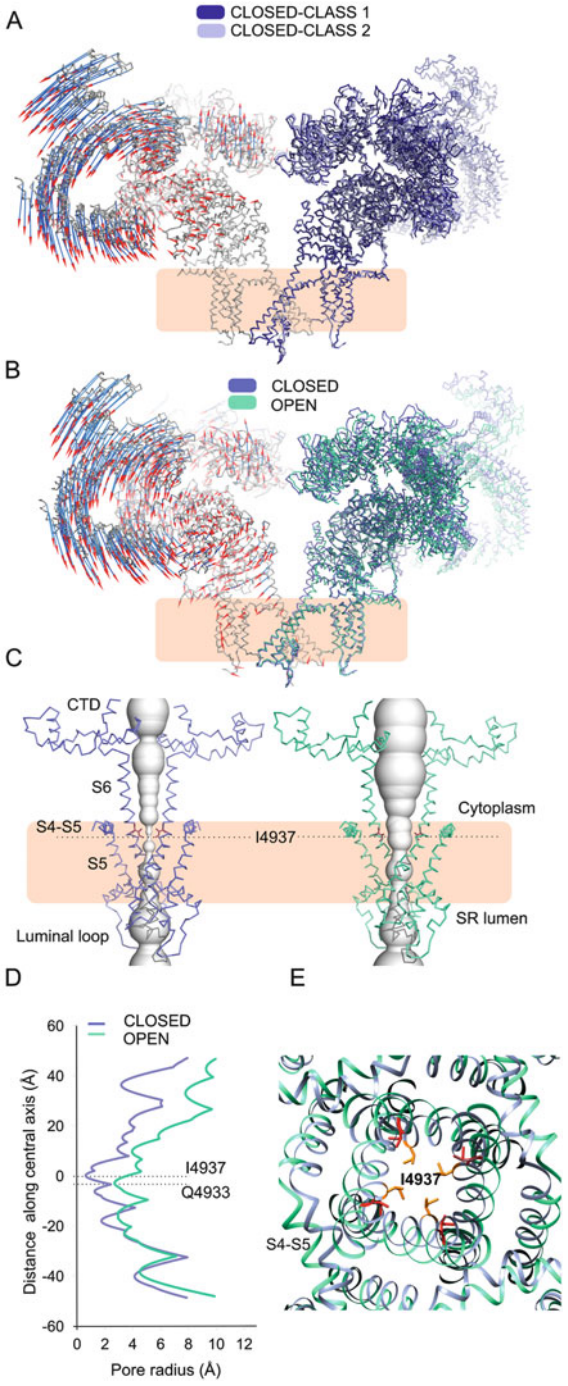

Fig. 8.3 Gating of RyR1. (**a**). Side view of a RyR1 dimer showing the rocking movement of the cytoplasmic cap of RyR1 in closed state. Vector field on the right monomer illustrates the conformational changes upon transition between two conformations observed in closed state of RyR1. The vectors are scaled by a factor of two for clarity. (**b**). Conformational changes upon transition from closed (blue) to open state (green) are similar to the rocking movements between closed states. The vector field shows additional structural changes in the Central and TM domains. Scaling of the vectors as in (**a**). (**c**). Side views of RyR1 dimers in the closed and open state showing the channel pore, color-coding as in (**b**). The surface lining the pore is illustrated in grey and was calculated with HOLE [60]. (**d**). Graph showing the pore radius for the closed and open state along the vertical axis of the channel with the distance shown relative to the gate residue I4937. Color-coding as in (**b**). (**e**). Top view of the gate region showing the opening of the pore-lining helices with the side-chain of the gate-forming residue I4937 moving outward as conformation changes from closed (orange) to open (red) state. (closed state PDB 5TB0, open state PDB 5TAL)

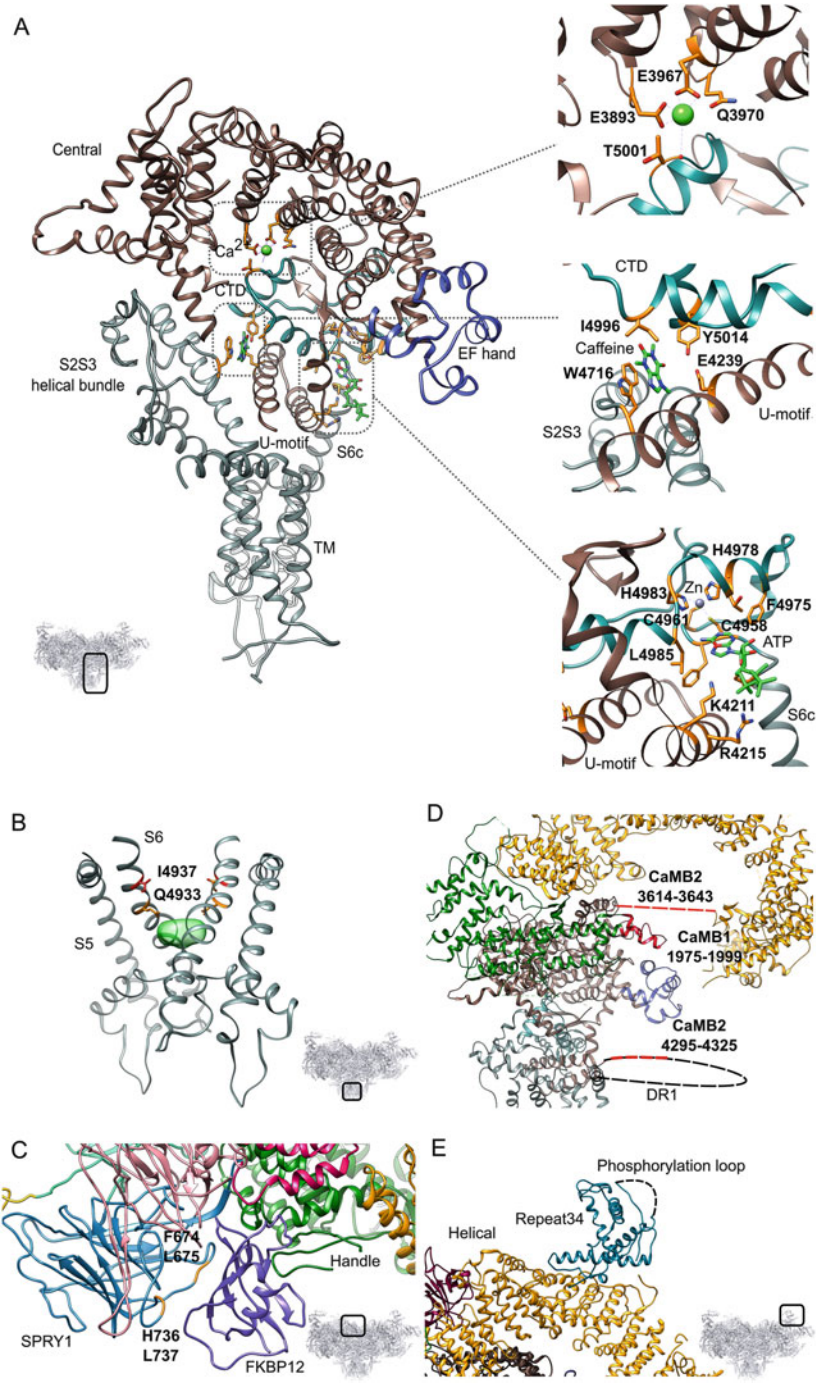

Fig. 8.4 Regulation of RyRs. (**a**). Side view and close-ups of RyR1 monomer showing the Central, TM domain and CTD with bound calcium, caffeine, zinc and ATP at their binding sites. Side chains of residues involved in the binding are shown and colored orange. (**b**). Ryanodine binds inside the

Structural Differences Between RyR Isoforms

At the level of the primary structure there are three major regions of diversity between the mammalian isoforms. These regions are named DR1 (4254–4631), DR2 (1342–1403) and DR3 (1872–1923) (Fig. 8.1c) [54]. As has been described in this section, all these regions are disordered in the structure. While DR2 and DR3 are 50–60 amino acids long, DR1 is exceptionally long and consists of 377 amino acids. The exact role of these regions is not known. A chimera of RyR1 with the DR1 region from RyR2 showed changes in sensitivity to Ca^{2+} and caffeine [61]. In addition, DR1 harbors one of the predicted calmodulin binding sites (CaMB), CaMB3. DR regions are loop-like insertions with their N- and C-termini located close to each other. Therefore they do not play a role of simple linkers between domains but might be involved in mediating interactions of RyR with other proteins or RyR domains [14, 62].

Recently the structure of RyR2 with 65% of sequence identity to RyR1 was determined [47]. As expected the architecture of RyR2 is very similar to that of RyR1 [47]. The functional differences between the channels including mechanisms of EC-coupling, regulation by CaM and other proteins, sensing of luminal Ca^{2+} response to store-overload, as well as difference in affinity for FKBP12 versus FKBP12.6 must be defined by finer structural differences.

8.3 Gating of RyR

Understanding the mechanism of RyR gating by Ca^{2+} is central to understanding RyR function. High-resolution RyR1 structures revealed that the EF-hand domain is located next to the conserved core of the protein and close to S6 gating helices (Fig. 8.2). It was suggested that the EF-hand domain may function as molecular switch triggering calcium-dependent RyR1 gating [46]. Recently it was shown that deletion of the complete EF-hand domain does not affect the activation of RyR by cytosolic calcium [63]. This excludes the role of the EF-hand in calcium-dependent channel activation.

The high-resolution structure of RyR in the open state was required to resolve the molecular mechanism of gating. In particular it was important to visualize the fully opened gate and determine the calcium-binding site. Obtaining the structures of

Fig. 8.4 (continued) pore. Side-chains of the gate residue I4937 (red) and residue Q4933 (orange) involved in the binding are shown. Only the pore-forming helices S5 and S6 are shown for clarity. (**c**). Binding of FKBP12 to SPRY1 and Handle domain. (**d**). Close-up side view of a RyR1 monomer with predicted calmodulin binding sites indicated in red. Only CaMB1 is structured in the most recent 3D models, CaMB2 is indicated with a dashed line between the C-terminus of the Central domain and the N-terminus of the helical domain and CaMB3 is indicated by a red dashed line within the DR1 (black dashed line). (**e**). Repeat34 is a phosphorylation hot spot with five phosphorylation sites located on a disordered loop shown by dashed line

RyR1 in the open state has proven to be a challenge for a number of reasons. The low open probability of RyR1 upon activation by calcium, is one of them. At the optimal concentration of Ca^{2+}, 50 μM, the open probability of RyR1 reaches only around 20% [10, 40]. Therefore, additional ligands like ATP and caffeine, or biphenyl 2,29,3,59,6-pentachlorobiphenyl (PCB95) stabilizing the open state, were required to enrich its population [40, 45]. Another challenge was the flexibility of RyRs [40, 45, 46, 48], which required extensive 3D particle classification [40]. Finally, the choice of detergent was also critical. In Tween-20 for example RyR1 remained in closed conformation under activating condition [45].

High-resolution structures of RyR in open conformation have been reported for: rabbit RyR1 activated by Ca^{2+}, ATP and caffeine determined at resolution of 3.8 Å [40]; rabbit RyR1 activated by combination of calcium and PCB95 determined at resolution of 5.7 Å [45] and porcine RyR2 in presence of calcium and PCB95 at a resolution of 4.2 Å [47].

In the absence of activating ligands, the conformational changes due to flexibility of RyR are not associated with channel gating. They are confined to the crown of the cytoplasmic domain and appear as a rotation of all but the Central, TM and CTD domains around an axis parallel to the membrane plane (Fig. 8.3a) [40, 45]. Between the conformations individual domains move as rigid bodies without significant intra-domain rearrangements [40, 45, 46]. These movements likely represent a continuum of conformations rather than a set of discrete states [40, 45, 46].

In the presence of calcium and activating molecules, specific conformational changes take place in the Central domain and CTD resulting in the gate opening (Fig. 8.3b). Similarly to conformational changes due to channel flexibility, NTD, Handle and Helical domains do not show any intra-domain changes associated with channel opening. They move towards the membrane and twist counter clockwise in the membrane plane by about two degrees.

Interestingly, while the open probability of RyR1 reconstituted into a lipid bilayer under conditions used for cryo-EM is close to unity, in cryo-EM only half of the channels are found in the open conformation [40], suggesting that RyR1 solubilized in CHAPS tends to be stabilized in the closed conformation or remained completely closed when solubilized in Tween-20 [45].

Gate Opening

The conformational changes associated with the transition from closed to open gate involve rotation of the Central domain relative to the S6 helix around the axis parallel to the membrane plane (Fig. 8.3b). In the TM domain, structural changes associated with gate opening include radial outward movement of the S6 helices. This appears as bending of the helix around a hinge located at residue G4934 (G4864 in RyR2), three residues below gate residue I4937 (I4867 in RyR2) (Fig. 8.3c) [40, 47]. This hinge glycine is known to be important for gating in both RyR1 and RyR2 [64, 65]. In the open channel the outward movement of S6 results in dilation of the pore constriction. The Cα-Cα distance between I4937 increases by 6 Å and the distance between the closest atoms of the side chains increases from around 5 to over 12 Å. The pore constriction increases from ~1.2 Å to 7 Å and now occurs at the polar

residues Gln4933 located one helical turn below I4937 (Fig. 8.3d). The remaining parts of the ion pore, including the filter and luminal loops, remain virtually unchanged during gating.

The opening of the cytoplasmic part of the S6 bundle (S6c) is concomitant with an outward shift of the helical hairpin of the U-motif by 3 Å (Fig. 8.3b) and amphipathic helices S4S5 forming a ring around S6 also move outwards by 3 Å (Fig. 8.3e). The VSD-like domain slightly rotates outward as a rigid body away from the channel axis as the gate opens. The opening is likely associated with switching a pattern of salt bridges between the S6 helices and around horizontal S4S5 helix [40, 45]. These networks of salt bridges may stabilize open or closed conformations of the channel minimizing occurrence of the intermediate states.

Calcium-Binding Site

Remarkably, the high-resolution structure of RyR1 in presence of Ca^{2+} reveals a density consistent with a bound Ca^{2+} ion [40]. This putative Ca^{2+} ion is intercalated between the Central domain and the CTD (Fig. 8.4a). It is coordinated by the carboxylate side chains of E3967 and E3893 on the α-solenoid core of the Central domain and the backbone carbonyl of T5001 form the CTD. Residues Q3970 and E5002 are too far away from Ca^{2+} to directly coordinate it but may contribute to ion binding through water molecules [40].

Earlier mutational studies did indicate that the cytosolic calcium-sensing domain is located inside the Central domain: mutating residue E4032 (E3987 in RyR2 and E3885 in RyR3) disrupted CICR in all three isoforms [12, 66]. Interestingly, E4032 is at least 10 Å away from the resolved Ca^{2+} binding site therefore it is not involved in Ca^{2+} binding, but may stabilize the interaction between the CTD and the Central domain. IP_3Rs can also be activated by cytosolic calcium in addition to being sensitive to inositol-1,4,5-trisphosphate [67, 68]. The five residues coordinating the putative Ca^{2+} ion are conserved in all IP_3R isoforms [40].

The Mechanism of Gating

To rationalize how binding of Ca^{2+} leads to the opening of the ion channel, its activation can be considered as a two-step process: first, priming by calcium and second stabilization of the open conformation by ATP and caffeine [40].

Binding of Ca^{2+} results in the nearing of the ion-coordinating residues of the α-solenoid core of the Central domain, E3867 and E3893, towards T5001 on the CTD. The Cα-Cα distances reduce by 1.5–2 Å. As result, the α-solenoid core of the Central domain pivots by about six degrees around the β-hairpin of the U-motif shifting the N-terminus of the Central domain and consequently the rest of the cytoplasmic cap towards the membrane surface resulting in global structural changes. These conformational changes do not result in pore opening, however.

Upon addition of ATP and caffeine, no significant structural changes occur between the Central domain and CTD. The Central domain rotates in the membrane plane and the TM and Central domain are slightly rearranged. The largest structural changes occur locally at S6c (4936–4956) and in the adjacent region of the CTD (4957–4985), accompanied with a shift of the helical hairpin of the U-motif parallel to the membrane. These local structural changes occur exactly next to the ATP and

caffeine binding sites [40]. Since the affinities for both ATP and caffeine are in the millimolar range, their binding energies are relatively small and comparable to the thermal energy. Therefore it appears that in the presence of Ca^{2+} transition from a closed to open channel is associated with bending of S6c and part of the adjacent CTD. This mechanism suggests that the rigid connection between S6 and the CTD, provided by a Zn finger, is critical for the channel gating. To open the channel, the conformational changes need to occur in the context of an assembled tetramer and are dependent on interaction between protomers. Since the interaction of the Central and the CTD domains between protomers is weak, this function is accomplished by NTD-AB making it an important part of the gating mechanism.

8.4 Regulation of Gating

A wide range of endogenous regulators, post-translational modifications and external factors like drugs and pollutants regulate RyRs [13]. Many of these regulators have been thoroughly studied biochemically and now can also be analyzed in the context of high-resolution structural data.

Caffeine and ATP bind RyR with millimolar affinities. Caffeine is a commonly used RyR agonist that decreases the threshold for spontaneous Ca^{2+} release and increases the open probability by changing the sensitivity for luminal Ca^{2+} [69]. ATP and other nucleotides bind RyRs and in presence of Ca^{2+} increase open probability two to threefold [70, 71]. Since ATP concentration in muscle cells is also in the millimolar range, activation of RyR by ATP is physiologically relevant and is important for sustaining EC coupling and avoiding muscle fatigue and metabolic catastrophe when ATP levels in the cell drop [71–73]. Both ATP and caffeine bind at the interface of the CTD with other domains [40]. ATP binds at the interface of S6c with the CTD (residues M4954, E4955, F4959, T4979, L4985) and the U-motif (residues K4211, K4214, R4215) (Fig. 8.4a) [40]. Adenine binds into a hydrophobic pocket formed by the CTD next to the zinc-binding site (C2H2-type, residues C4958, C4961, H4978, H4983), while phosphate groups interact with lysines in a horizontal helix of the U-motif. The caffeine-binding site is located at the interface of the CTD (residues I4996 and Y5014), S2S3 domain (residue W4716) and another helix from the helical hairpin of the U-motif (residue E4239) (Fig. 8.4a) [40]. In line with the important role that the CTD and the U-motif play in the conformational changes during gating, binding of ATP and caffeine in this region stabilize interdomain interactions favoring an open gate.

Ryanodine binds to open RyR with nanomolar affinity and stabilizes a subconductive state [74]. Early studies [75–77] already pointed towards a binding site localized within the pore region and predicted that Q4863 (in RyR2, Q4933 in RyR1) is involved in ryanodine binding [78, 79]. Density corresponding to ryanodine bound to rabbit RyR1 was detected inside the hydrophobic cavity of the pore (Fig. 8.4b) [40]. It is consistent with a single ryanodine molecule bound to Q4933 in agreement with earlier stoichiometric measurements [80]. In contrast to the

other pore-lining residues Q4933 is not conserved in IP_3R, which does not bind ryanodine [5, 6, 40].

When bound in the pore to calcium-activated RyR, ryanodine stabilizes the open conformation of the pore. It partially occludes the ion conductance pathway resulting in a subconductance state. Ruthenium red, a channel blocker, was also visualized inside the pore of a RyR1 [81].

PCB95 is a neurotoxic pollutant selective for RyRs over IP_3Rs in neurons [82, 83]. It binds RyR and stabilizes its open conformation. PCB95 was used to lock RyR1 and RyR2 in the open state for structure determination [45, 47] but its binding site has not been visualized.

Mg^{2+} inhibits RyR at millimolar concentrations [84]. Current structural information does not provide the straightforward explanation of its inhibiting effect. One possibility, discussed by Clarke and Hendrickson [85], is that Mg^{2+} competes with Ca^{2+} for the same binding site but has preference for different ion coordination favoring closed channel conformation.

FKBP

Most of the recently published RyR cryo-EM structures were in complex with the auxiliary protein FKBP12 [40, 41, 45, 47, 48]. FKBP12 and FKBP12.6 are constitutively bound to skeletal and cardiac RyR, respectively. It is suggested that they stabilize the closed state, prevent subconductive states and play a role in allosteric gating [25, 86, 87], which is questioned by other studies [88]. FKBP binds in between the Handle and SPRY1 domain (Figs. 8.1a, 8.4c). Model of SPRY1-FKBP12 interface suggests interaction of FKBP with residues F674, L675, H736 and L737 of SPRY1 [38, 41]. FKBP12 interacts with the surface of the α-solenoid and a downstream loop (residues 1779–1785), over large surface with high shape complementarity (Figs. 8.1a, 8.4c), explaining the high affinity of FKBP.

Calmodulin is one of the best-characterized regulators of RyR. The effect of calmodulin binding is isoform-dependent: RyR1 is activated by apoCaM and inhibited by calcium bound CaM, CaCaM [89], while RyR2 is inhibited by CaM independently of calcium concentrations [90]. Three CaM binding sites (CaMB) were predicted in RyR1: 1975–1999 (1), 3614–3643 (2) and 4295–4325 (3) [91] (Fig. 8.4d). Only CaMB1 is resolved in the structure of RyR [40], the other sites are predicted to be disordered. CaMB1 corresponds to a helical turn in the Handle domain (Fig. 8.4d). Low resolution cryo-EM mapping of CaM binding sites revealed different sites for apoCaM and CaCaM in RyR1 with apoCaM binding ~30 Å higher [92]. These locations and distance are consistent with mapping of CaMB1 and 2 on the highest resolution structure of RyR1 [40]. The CaMB2 is a flexible peptide connecting the C-terminal end of Helical domain with the N-terminus of the Central domain, which is close to CaMB1 in the quaternary structure (Fig. 8.4d). Intriguingly, apoCaM binds to RyR2 at the same location as CaCaM in RyR1, which is consistent with the similar functional effects [91]. A crystal structure of CaCaM bound to a α-helical peptide in CaMB2 region was solved [93]. However, the corresponding peptide is disordered in cryo-EM structures even though its sequence is highly conserved between all RyR isoforms. Given the location of the CaM

binding sites, it likely regulates the open probability of RyR by influencing relative orientations of RyR domains by for example interacting with EF-hand domain [94].

Post-Translational Modifications (PTM)
RyRs are also regulated by post-translational modifications including phosphorylation, oxidation and nitrosylation [95–98]. The effect of PTMs on RyR gating is very complex and it has been a topic of debate and controversy in the field [95]. The importance of phosphorylation in for example heart failure is an accepted phenomenon [95]. Because RyR has over 40 phosphorylation sites, a large number of phosphorylation states can occur complicating the study of the phosphorylation effect [14]. Additionally, comparison of the natively and in vitro dephosphorylated RyR1 did not reveal any significant structural differences [48]. Intriguingly, one of the best characterized phosphorylation hot spots is located within Repeat34 on a disordered loop facing the upper surface of RyR [35, 37], where Ser2808 and Ser2814 (in RyR2) [14] are phosphorylated (Fig. 8.4e). Based on the available structures it can be suggested that the functional significance of this phosphorylation site can only be understood in a context of the in vivo protein assembly around RyR.

8.5 RyR in Diseases

Mutations in RyRs and their accessory proteins have been linked directly and indirectly to a spectrum of human diseases. The largest class of these diseases belongs to a group of channelopathies [99]. More recently, other diseases including Alzheimer's [100] and Huntington's disease [101] have been linked to a distorted calcium homeostasis in neurons, where RyRs and IP_3Rs are thought to play a major role. Abnormalities in post-translational modifications of RyRs can also lead to pathologies among which are muscle fatigue and cardiac arrhythmias [102, 103]. The consequences of disease-causing point mutations on the level of channel function are very diverse, including increased open probability, leakiness of the pore, uncoupling of excitation-contraction or reduced expression [104–112]. Below we give an overview of RyR-associated diseases and analyse them using available structural information.

Diseases Associated with Mutations in RyR1
Malignant hyperthermia (MH) is a pharmacogenetic disease, in which patients with mutations in the *RyR1* gene have a pathological reaction to inhalational anaesthetics (halothane, isoflurane, sevoflurane, desflurane) or depolarizing muscle relaxants (succinylcholine) [113, 114]. Upon exposure, MH will manifest with increased muscle rigidity and an alarming high core body temperature due to excessive hydrolysis of ATP by SERCA (SR/ER calcium ATPases) and PMCA (plasma membrane Ca^{2+} ATPase) reacting to elevated cytoplasmic Ca^{2+} concentration [96]. An MH episode is treated by administration of dantrolene, the molecular mechanism of which is still not understood. Mutations in RyR1 can also lead to congenital myopathies including the most common central core disease (CCD) and

other related myopathies [115]. CCD is characterized by weakness of the muscles, delayed motor development, hypotonia and motor deficiencies. To date physiotherapy to strengthen and maintain the muscles is the only treatment available to the patients [115].

Diseases Associated with Mutations in RyR2

Mutations in the *RyR2* gene are associated with cardiac arrhythmia disorders that often lead to sudden cardiac death (SCD) in young people [116]. Catecholaminergic Polymorphic Ventricular Tachycardia (CPVT) has been associated with mutations in *RyR2* and RyR2-accesory proteins CSQ2 (calsequestrin) [117], triadin [118] and CaM [119]. Sixty percent of all known CPVT mutations are in *RyR2* [120]. CPVT is characterized by severe cardiac arrhythmia in response to emotional or physical stress that can lead to sudden cardiac death in young individuals with a structurally normal heart [121]. No effective treatment for CPTV is available to date.

Arrhythmogenic Right Ventricular Cardiomyopathy 2 (ARVC2) is another rare cardiac arrhythmia disorder caused by mutations in *RyR2* [110, 122]. ARVC covers a diverse spectrum of genotypes with very similar disease phenotypes. The pathological hallmark of ARVC is the progressive substitution of the right ventricle myocardium by fibrofatty tissue [123]. ARVC2 is like CPVT characterized by adrenergic-induced arrhythmias, with no effective treatment available today [124].

Functional Consequences of RyR Mutations

MH mutations in *RyR1* cause an excessive Ca^{2+} leak in response to activators [96, 125]. Two types of RyR1 deregulation have been associated with CCD causing mutations: a constitutively leaky channel [13] and EC-uncoupling [104]. A CCD-causing mutation I4897T (hRyR1) located in the selectivity filter results in dysfunctional EC coupling [104, 126–128]. Therefore only heterozygous carriers are viable [129]. Given the position of the mutation it most likely results in non- or very poorly functioning channels.

CPVT mutations lead to excessive calcium release from the SR during exercise or emotional stress [107]. Several CPVT mutations, spread over the primary sequence, were shown to alter the sensitivity for luminal Ca^{2+} and to lower the threshold for store-overload induced calcium release (SOICR) [108]. Other mutations, mostly located in the N-terminal region, were linked to delayed termination and increased amplitude of Ca^{2+} release [109].

Disease Mutations and RyR Structure

When the disease-causing mutations are plotted onto the linear sequence, four hot spots become evident (Fig. 8.5a) [116, 127]. More recently described mutations in RyR1 are homogeneously distributed over the protein sequence rendering the hot spots less pronounced (Fig. 8.5a). Taken together, around 850 disease-causing mutations have been described for all RyRs (data from HGMD [31]).

Mapping positions of the disease mutations on the RyR structure provides insight on their mechanisms and on the mechanism of RyR. Structurally the hot spots are situated at the NTD, the N-terminal part of the helical domain, the central domain and the TM region (Fig. 8.5b). Interestingly, residues in the Ca^{2+} binding site, the

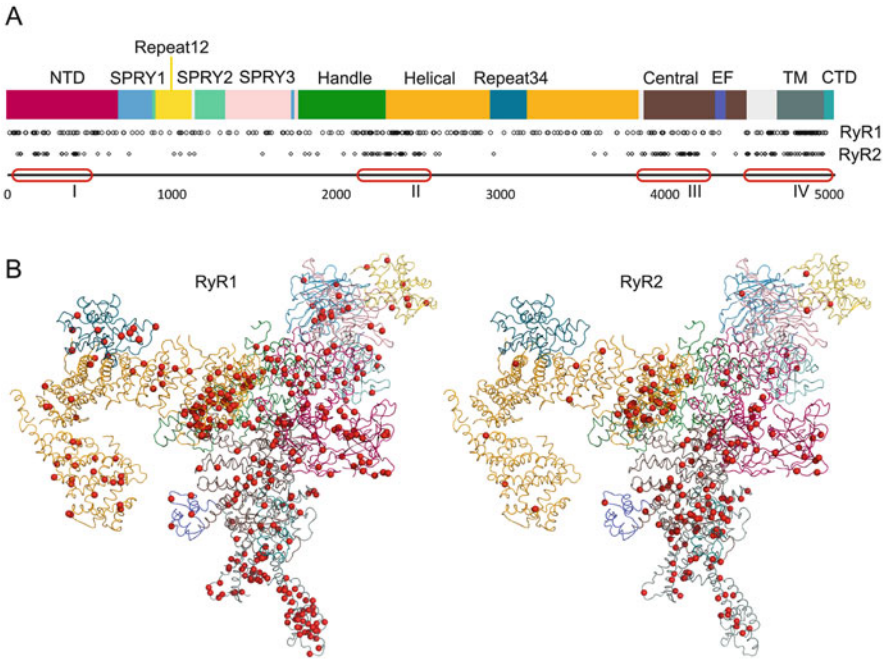

Fig. 8.5 Distribution of disease mutations in RyR1 and RyR2. (**a**). Linear representation of the domain organization (color-coding as in Fig. 8.1) and mutation distribution within the primary sequence, with each circle (RyR1) or diamond (RyR2) representing position of a disease-causing point mutation (The Human Gene Mutation Database, HGMD® [31]). Four mutation hot spots I–IV (red) can be identified. (**b**). Positions of disease-causing mutations (HGMD®) are shown as red spheres for RyR1 (left) and RyR2 (right) monomer. Color-coding of the domains as in Fig. 8.1

zinc finger, or gate-keeper I4937 are not affected by mutations, likely because of their crucial role in RyR functioning, as loss of function mutations would be lethal. Dense clusters of mutations are found at the interfaces of NTD-AB with other domains as well as within NTD-AB. Surprisingly, numerous mutations are found at the interface of NTD-AB with Helical domain (Fig. 8.5b) suggesting important functional role of this interaction. The interface of NTD-AB with Central domain is also often mutated in diseases, as expected from our mechanistic model of gating.

Another important hot spot is found within the TM region. Mutation-induced conformational change of the pore can destabilize the channel to increase or decrease its open probability. An important functional outcome of some mutations in RyR2, located in all mutation hot spots, is an altered threshold for activation by luminal Ca^{2+} [108]. There is no agreement in the field on the location of "luminal Ca^{2+} sensor" [112, 116, 130–133], however.

Interestingly, a noticeable amount of mutations in RyRs are clustered together in the S2S3 helical bundle and the U-motif in close proximity of the recently identified caffeine binding site [40] highlighting a functional role for these structural elements.

A number of mutations are found in the periphery of RyRs (Fig. 8.5b). The functional consequences of these mutations are less evident. They possibly disrupt interaction with accessory proteins including assembly of two-dimensional RyR arrays.

8.6 Conclusions

The last years were marked by a significant progress in the structural studies of RyR. The high-resolution structures revealed detailed organization of this large ion channel and conformational rearrangements associated with the channel gating. In particular, mechanisms of channel permeation by ions and the activation by calcium and small-molecule ligands are now significantly better understood. At the same time many questions related to the regulation of RyR and the functional role of its huge cytoplasmic domain remain unanswered. With the high-resolution structures of RyR at hands it will now be possible to design more accurate experiments to verify the mechanistic hypothesis and accurately interpret results of biophysical and biochemical experiments. Without doubts the coming years will be marked by further progress in revealing the complex function of RyR at atomic level.

Acknowledgements This work was funded by grants from VIB, FWO grant number G.0266.15N and IWT fellowship number 131261 to K.W.

References

1. Rebbeck RT, Karunasekara Y, Board PG et al (2014) Skeletal muscle excitation–contraction coupling: who are the dancing partners? Int J Biochem Cell Biol 48:28–38. https://doi.org/10.1016/j.biocel.2013.12.001
2. Lanner JT, Georgiou DK, Joshi AD, Hamilton SL (2010) Ryanodine receptors: structure, expression, molecular details, and function in calcium release. Cold Spring Harb Perspect Biol 2:a003996
3. Rogers EF, Koniuszy FR (1948) Plant insecticides; ryanodine, a new alkaloid from Ryania speciosa Vahl. J Am Chem Soc 70:3086–3088
4. Fleischer S, Ogunbunmi EM, Dixon MC, Fleer EA (1985) Localization of Ca2+ release channels with ryanodine in junctional terminal cisternae of sarcoplasmic reticulum of fast skeletal muscle. Proc Natl Acad Sci USA 82:7256–7259
5. Imagawa T, Smith JS, Coronado R, Campbell KP (1987) Purified ryanodine receptor from skeletal muscle sarcoplasmic reticulum is the Ca2+-permeable pore of the calcium release channel. J Biol Chem 262:16636–16643
6. Lai FA, Erickson HP, Rousseau E et al (1988b) Purification and reconstitution of the calcium release channel from skeletal muscle. Nature 331:315–319
7. Pessah IN, Francini AO, Scales DJ et al (1986) Calcium-ryanodine receptor complex. Solubilization and partial characterization from skeletal muscle junctional sarcoplasmic reticulum vesicles. J Biol Chem 261:8643–8648

8. Franzini-Armstrong C (1970) Studies of the triad: I. Structure of the junction in frog twitch fibers. J Cell Biol 47:488–499
9. Lai FA, Anderson K, Rousseau E et al (1988a) Evidence for a Ca2+ channel within the ryanodine receptor complex from cardiac sarcoplasmic reticulum. Biochem Biophys Res Commun 151:441–449
10. Chen SR, Leong P, Imredy JP et al (1997a) Single-channel properties of the recombinant skeletal muscle Ca2+ release channel (ryanodine receptor). Biophys J 73:1904–1912
11. Chen SRW, Li X, Ebisawa K, Zhang L (1997b) Functional characterization of the recombinant type 3 Ca2+ release channel (ryanodine receptor) expressed in HEK293 cells. J Biol Chem 272:24234–24246
12. Li P, Chen SR (2001) Molecular basis of Ca(2)+ activation of the mouse cardiac Ca(2)+ release channel (ryanodine receptor). J Gen Physiol 118:33–44
13. Lanner JT (2012) Ryanodine receptor physiology and its role in disease. In: Calcium signaling. Springer, Netherlands, p 217–234
14. Yuchi Z, Van Petegem F (2016) Ryanodine receptors under the magnifying lens: insights and limitations of cryo-electron microscopy and X-ray crystallography studies. Cell Calcium 59:209–227
15. Conti A, Gorza L, Sorrentino V (1996) Differential distribution of ryanodine receptor type 3 (RyR3) gene product in mammalian skeletal muscles. Biochem J 316(Pt 1):19–23
16. Giannini G, Conti A, Mammarella S et al (1995) The ryanodine receptor/calcium channel genes are widely and differentially expressed in murine brain and peripheral tissues. J Cell Biol 128:893–904
17. Ottini L, Marziali G, Conti A et al (1996) Alpha and beta isoforms of ryanodine receptor from chicken skeletal muscle are the homologues of mammalian RyR1 and RyR3. Biochem J 315:207–216
18. Oyamada H, Murayama T, Takagi T et al (1994) Primary structure and distribution of ryanodine-binding protein isoforms of the bullfrog skeletal muscle. J Biol Chem 269:17206–17214
19. Takeshima H, Nishi M, Iwabe N et al (1994) Isolation and characterization of a gene for a ryanodine receptor/calcium release channel in *Drosophila melanogaster*. FEBS Lett 337:81–87
20. Sattelle DB, Cordova D, Cheek TR (2008) Insect ryanodine receptors: molecular targets for novel pest control chemicals. Invert Neurosci 8:107–119
21. Franzini-Armstrong C, Protasi F, Ramesh V (1999) Shape, size, and distribution of Ca(2+) release units and couplons in skeletal and cardiac muscles. Biophys J 77:1528–1539
22. Yin CC, Lai FA (2000) Intrinsic lattice formation by the ryanodine receptor calcium-release channel. Nat Cell Biol 2:669–671
23. Franzini-Armstrong C, Nunzi G (1983) Junctional feet and particles in the triads of a fast-twitch muscle fibre. J Muscle Res Cell Motil 4:233–252
24. Marx SO, Gaburjakova J, Gaburjakova M et al (2001) Coupled gating between cardiac calcium release channels (ryanodine receptors). Circ Res 88:1151–1158
25. Marx SO, Ondrias K, Marks AR (1998) Coupled gating between individual skeletal muscle Ca2+ release channels (ryanodine receptors). Science 281:818–821
26. Evans AM, Fameli N, Ogunbayo OA et al (2016) From contraction to gene expression: nanojunctions of the sarco/endoplasmic reticulum deliver site- and function-specific calcium signals. Sci China Life Sci 59:749–763
27. van Breemen C, Fameli N, Evans AM (2013) Pan-junctional sarcoplasmic reticulum in vascular smooth muscle: nanospace Ca2+ transport for site- and function-specific Ca2+ signalling. J Physiol 591:2043–2054
28. Boittin F-X, Galione A, Evans AM (2002) Nicotinic acid adenine dinucleotide phosphate mediates Ca2+ signals and contraction in arterial smooth muscle via a two-pool mechanism. Circ Res 91:1168–1175

29. Marius P, Guerra MT, Nathanson MH et al (2006) Calcium release from ryanodine receptors in the nucleoplasmic reticulum. Cell Calcium 39:65–73
30. Betzenhauser MJ, Marks AR (2010) Ryanodine receptor channelopathies. Pflugers Arch – Eur J Physiol 460:467–480
31. Stenson PD, Mort M, Ball EV et al (2017) The human gene mutation database: towards a comprehensive repository of inherited mutation data for medical research, genetic diagnosis and next-generation sequencing studies. Hum Genet 526:68–13
32. Abdul M, Ramlal S, Hoosein N (2008) Ryanodine receptor expression correlates with tumor grade in breast cancer. Pathol Oncol Res 14:157–160
33. Zhang L, Liu Y, Song F et al (2011) Functional SNP in the microRNA-367 binding site in the 3'UTR of the calcium channel ryanodine receptor gene 3 (RYR3) affects breast cancer risk and calcification. Proc Natl Acad Sci USA 108:13653–13658
34. Lau K, Van Petegem F (2014) Crystal structures of wild type and disease mutant forms of the ryanodine receptor SPRY2 domain. Nat Comms 5:5397
35. Sharma P, Ishiyama N, Nair U et al (2012) Structural determination of the phosphorylation domain of the ryanodine receptor. FEBS J 279:3952–3964
36. Tung C-C, Lobo PA, Kimlicka L, Van Petegem F (2010) The amino-terminal disease hotspot of ryanodine receptors forms a cytoplasmic vestibule. Nature 468:585–588
37. Yuchi Z, Lau K, Van Petegem F (2012) Disease mutations in the ryanodine receptor central region: crystal structures of a phosphorylation hot spot domain. Structure 20:1201–1211
38. Yuchi Z, Yuen SMWK, Lau K et al (2015) Crystal structures of ryanodine receptor SPRY1 and tandem-repeat domains reveal a critical FKBP12 binding determinant. Nat Commun 6:1–13
39. Kühlbrandt W (2014) Cryo-EM enters a new era. eLife 3:e03678
40. des Georges A, Clarke OB, Zalk R et al (2016) Structural basis for gating and activation of RyR1. Cell 167:145–157.e17
41. Yan Z, Bai X-C, Yan C et al (2015) Structure of the rabbit ryanodine receptor RyR1 at near-atomic resolution. Nature 517:50–55
42. Bonilla E (1977) Staining of transverse tubular system of skeletal muscle by tannic acid-glutaraldehyde fixation. J Ultrastruct Res 2:162–165
43. Revel JP (1962) The sarcoplasmic reticulum of the bat cricothroid muscle. J Cell Biol 12:571–588
44. Wagenknecht T, Grassucci R, Frank J et al (1989) Three-dimensional architecture of the calcium channel/foot structure of sarcoplasmic reticulum. Nature 338:167–170
45. Bai X-C, Yan Z, Wu J et al (2016) The central domain of RyR1 is the transducer for long-range allosteric gating of channel opening. Cell Res 26:995–1006
46. Efremov RG, Leitner A, Aebersold R, Raunser S (2015) Architecture and conformational switch mechanism of the ryanodine receptor. Nature 517:39–43
47. Peng W, Shen H, Wu J et al (2016) Structural basis for the gating mechanism of the type 2 ryanodine receptor RyR2. Science 354:1–17
48. Zalk R, Clarke OB, des Georges A et al (2015) Structure of a mammalian ryanodine receptor. Nature 517:44–49
49. Serysheva II, Schatz M, van Heel M et al (1999) Structure of the skeletal muscle calcium release channel activated with Ca2+ and AMP-PCP. Biophys J 77:1936–1944
50. Seo M-D, Velamakanni S, Ishiyama N et al (2012) Structural and functional conservation of key domains in InsP3 and ryanodine receptors. Nature 483:108–112
51. Ponting C, Schultz J, Bork P (1997) SPRY domains in ryanodine receptors (Ca(2+)-release channels). Trends Biochem Sci 22:193–194
52. Wang D, Li Z, Messing EM, Wu G (2002) Activation of Ras/Erk pathway by a novel MET-interacting protein RanBPM. J Biol Chem 277:36216–36222
53. Perez CF, Mukherjee S, Allen PD (2011) Amino acids 1-1,680 of ryanodine receptor type 1 hold critical determinants of skeletal type for excitation-contraction coupling: role of divergence domain D2. J Biol Chem 278:39644–39652

54. Sorrentino V, Volpe P (1993) Ryanodine receptors: how many, where and why? Trends Pharmacol Sci 14:98–103
55. Zorzato F, Fujii J, Otsu K et al (1990) Molecular cloning of cDNA encoding human and rabbit forms of the Ca2+ release channel (ryanodine receptor) of skeletal muscle sarcoplasmic reticulum. J Biol Chem 265:2244–2256
56. Cabra V, Murayama T, Samsó M (2016) Ultrastructural analysis of self-associated RyR2s. Biophys J 110:2651–2662
57. Marcotte EM, Pellegrini M, Yeates TO, Eisenberg D (1999) A census of protein repeats. J Mol Biol 293:151–160
58. Coates JC (2003) Armadillo repeat proteins: beyond the animal kingdom. Trends Cell Biol 13:463–471
59. Zhang H, Zhang J-Z, Danila CI, Hamilton SL (2003) A noncontiguous, intersubunit binding site for calmodulin on the skeletal muscle Ca2+ release channel. J Biol Chem 278:8348–8355
60. Smart OS, Neduvelil JG, Wang X et al (1996) HOLE: a program for the analysis of the pore dimensions of ion channel structural models. J Mol Graph 14:354–360
61. Du GG, Khanna VK, MacLennan DH (2000) Mutation of divergent region 1 alters caffeine and Ca(2+) sensitivity of the skeletal muscle Ca(2+) release channel (ryanodine receptor). J Biol Chem 275:11778–11783
62. Tompa P, Schad E, Tantos A, Kalmar L (2015) Intrinsically disordered proteins: emerging interaction specialists. Curr Opin Struct Biol 35:49–59
63. Guo W, Sun B, Xiao Z et al (2016) The EF-hand Ca2+ binding domain is not required for cytosolic Ca2+ activation of the cardiac ryanodine receptor. J Biol Chem 291:2150–2160
64. Euden J, Mason SA, Viero C et al (2013) Investigations of the contribution of a putative glycine hinge to ryanodine receptor channel gating. J Biol Chem 288:16671–16679
65. Mei Y, Xu L, Mowrey DD et al (2015) Channel gating dependence on pore lining helix glycine residues in skeletal muscle ryanodine receptor. J Biol Chem 290:17535–17545
66. Chen SR, Ebisawa K, Li X, Zhang L (1998) Molecular identification of the ryanodine receptor Ca2+ sensor. J Biol Chem 273:14675–14678
67. Miyakawa T, Mizushima A, Hirose K et al (2001) Ca(2+)-sensor region of IP(3) receptor controls intracellular Ca(2+) signaling. The EMBO J 20:1674–1680
68. Uchida K, Miyauchi H, Furuichi T et al (2003) Critical regions for activation gating of the inositol 1,4,5-trisphosphate receptor. J Biol Chem 278:16551–16560
69. Kong H, Jones PP, Koop A et al (2008) Caffeine induces Ca2+ release by reducing the threshold for luminal Ca2+ activation of the ryanodine receptor. Biochem J 414:441–452
70. Chan WM, Welch W, Sitsapesan R (2000) Structural factors that determine the ability of adenosine and related compounds to activate the cardiac ryanodine receptor. Br J Pharmacol 130:1618–1626
71. Kermode H, Williams AJ, Sitsapesan R (1998) The interactions of ATP, ADP, and inorganic phosphate with the sheep cardiac ryanodine receptor. Biophys J 74:1296–1304
72. MacIntosh BR, Holash RJ, Renaud JM (2012) Skeletal muscle fatigue – regulation of excitation-contraction coupling to avoid metabolic catastrophe. J Cell Sci 125:2105–2114
73. Smith JS, Coronado R, Meissner G (1985) Sarcoplasmic reticulum contains adenine nucleotide-activated calcium channels. Nature 316:446–449
74. Mukherjee S, Thomas NL, Williams AJ (2014) Insights into the gating mechanism of the ryanodine-modified human cardiac Ca2+-release channel (ryanodine receptor 2). Mol Pharmacol 86:318–329
75. Bhat MB, Zhao J, Takeshima H, Ma J (1997) Functional calcium release channel formed by the carboxyl-terminal portion of ryanodine receptor. Biophys J 73:1329–1336
76. Callaway C, Seryshev A, Wang JP et al (1994) Localization of the high and low affinity [3H] ryanodine binding sites on the skeletal muscle Ca2+ release channel. J Biol Chem 269:15876–15884

77. Witcher DR, McPherson PS, Kahl SD et al (1994) Photoaffinity labeling of the ryanodine receptor/Ca2+ release channel with an azido derivative of ryanodine. J Biol Chem 269:13076–13079
78. Ranatunga KM, Moreno-King TM, Tanna B et al (2005) The Gln4863Ala mutation within a putative, pore-lining trans-membrane helix of the cardiac ryanodine receptor channel alters both the kinetics of ryanoid interaction and the subsequent fractional conductance. Mol Pharmacol 68:840–846
79. Wang R, Zhang L, Bolstad J et al (2003) Residue Gln4863 within a predicted transmembrane sequence of the Ca2+ release channel (ryanodine receptor) is critical for ryanodine interaction. J Biol Chem 278:51557–51565
80. Tanna B, Welch W, Ruest L et al (2003) An anionic ryanoid, 10-O-succinoylryanodol, provides insights into the mechanisms governing the interaction of ryanoids and the subsequent altered function of ryanodine-receptor channels. J Gen Physiol 121:551–561
81. Wei R, Wang X, Zhang Y et al (2016) Structural insights into Ca(2+)-activated long-range allosteric channel gating of RyR1. Cell Res 26:977–994
82. Wong PW, Brackney WR, Pessah IN (1997) Ortho-substituted polychlorinated biphenyls alter microsomal calcium transport by direct interaction with ryanodine receptors of mammalian brain. J Biol Chem 272:15145–15153
83. Wong PW, Pessah IN (1997) Noncoplanar PCB 95 alters microsomal calcium transport by an immunophilin FKBP12-dependent mechanism. Mol Pharmacol 51:693–702
84. Walweel K, Li J, Molenaar P et al (2014) Differences in the regulation of RyR2 from human, sheep, and rat by Ca^{2+} and Mg^{2+} in the cytoplasm and in the lumen of the sarcoplasmic reticulum. J Gen Physiol 144:263–271
85. Clarke OB, Hendrickson WA (2016) Structures of the colossal RyR1 calcium release channel. Curr Opin Struct Biol 39:144–152
86. Brillantes AB, Ondrias K, Scott A et al (1994) Stabilization of calcium release channel (ryanodine receptor) function by FK506-binding protein. Cell 77:513–523
87. Gaburjakova M, Gaburjakova J, Reiken S et al (2001) FKBP12 binding modulates ryanodine receptor channel gating. J Biol Chem 276:16931–16935
88. Xiao J, Tian X, Jones PP et al (2007) Removal of FKBP12.6 does not alter the conductance and activation of the cardiac ryanodine receptor or the susceptibility to stress-induced ventricular arrhythmias. J Biol Chem 282:34828–34838
89. Buratti R, Prestipino G, Menegazzi P et al (1995) Calcium dependent activation of skeletal muscle Ca2+ release channel (ryanodine receptor) by calmodulin. Biochem Biophys Res Commun 213:1082–1090
90. Balshaw DM, Xu L, Yamaguchi N et al (2001) Calmodulin binding and inhibition of cardiac muscle calcium release channel (ryanodine receptor). J Biol Chem 276:20144–20153
91. Huang X, Fruen B, Farrington DT et al (2012) Calmodulin-binding locations on the skeletal and cardiac ryanodine receptors. J Biol Chem 287:30328–30335
92. Samsó M, Wagenknecht T (2002) Apocalmodulin and Ca2+-calmodulin bind to neighboring locations on the ryanodine receptor. J Biol Chem 277:1349–1353. https://doi.org/10.1074/jbc.M109196200
93. Maximciuc AA, Putkey JA, Shamoo Y, Mackenzie KR (2006) Complex of calmodulin with a ryanodine receptor target reveals a novel, flexible binding mode. Structure 14:1547–1556
94. Xiong L, Zhang J-Z, He R, Hamilton SL (2006) A Ca2+-binding domain in RyR1 that interacts with the calmodulin binding site and modulates channel activity. Biophys J 90:173–182
95. Dobrev D, Wehrens XHT (2014) Role of RyR2 phosphorylation in heart failure and arrhythmias: controversies around ryanodine receptor phosphorylation in cardiac disease. Circ Res 114:1311–1319
96. Durham WJ, Aracena-Parks P, Long C et al (2008) RyR1 S-nitrosylation underlies environmental heat stroke and sudden death in Y522S RyR1 knockin mice. Cell 133:53–65

97. Marx SO, Reiken S, Hisamatsu Y et al (2000) PKA phosphorylation dissociates FKBP12.6 from the calcium release channel (ryanodine receptor): defective regulation in failing hearts. Cell 101:365–376
98. Aracena P, Tang W, Hamilton SL, Cecilia Hidalgo PD (2013) Effects of S-glutathionylation and S-nitrosylation on calmodulin binding to triads and FKBP12 binding to type 1 calcium release channels. Antioxid Redox Signal 7:870–881
99. Benkusky NA, Farrell EF, Valdivia HH (2004) Ryanodine receptor channelopathies. Biochem Biophys Res Commun 322:1280–1285
100. Del Prete D, Checler F, Chami M (2014) Ryanodine receptors: physiological function and deregulation in Alzheimer disease. Mol Neurodegener 9:21
101. Raymond LA (2017) Striatal synaptic dysfunction and altered calcium regulation in Huntington disease. Biochem Biophys Res Commun 483:1051–1062. https://doi.org/10.1016/j.bbrc.2016.07.058
102. Bellinger AM, Reiken S, Carlson C et al (2009) Hypernitrosylated ryanodine receptor calcium release channels are leaky in dystrophic muscle. Nat Med 15:325–330
103. Lehnart SE, Mongillo M, Bellinger A et al (2008) Leaky Ca2+ release channel/ryanodine receptor 2 causes seizures and sudden cardiac death in mice. J Clin Invest 118:2230–2245
104. Avila G, O'Brien JJ, Dirksen RT (2001) Excitation–contraction uncoupling by a human central core disease mutation in the ryanodine receptor. Proc Natl Acad Sci USA 98:4215–4220
105. Avila G, Dirksen RT (2001) Functional effects of central core disease mutations in the cytoplasmic region of the skeletal muscle ryanodine receptor. J Gen Physiol 118:277–290
106. George CH, Higgs GV, Lai FA (2003) Ryanodine receptor mutations associated with stress-induced ventricular tachycardia mediate increased calcium release in stimulated cardiomyocytes. Circ Res 93:531–540
107. Jiang D, Xiao B, Zhang L, Chen SRW (2002) Enhanced basal activity of a cardiac Ca2+ release channel (ryanodine receptor) mutant associated with ventricular tachycardia and sudden death. Circ Res 91:218–225
108. Jones PP, Jiang D, Bolstad J et al (2008) Endoplasmic reticulum Ca2+ measurements reveal that the cardiac ryanodine receptor mutations linked to cardiac arrhythmia and sudden death alter the threshold for store-overload-induced Ca2+ release. Biochem J 412:171
109. Tang Y, Tian X, Wang R et al (2012) Abnormal termination of Ca2+ release is a common defect of RyR2 mutations associated with cardiomyopathies. Circ Res 110:968–977
110. Tiso N, Stephan DA, Nava A et al (2001) Identification of mutations in the cardiac ryanodine receptor gene in families affected with arrhythmogenic right ventricular cardiomyopathy type 2 (ARVD2). Hum Mol Genet 10:189–194
111. Xiao Z, Guo W, Sun B et al (2016) Enhanced cytosolic Ca2+ activation underlies a common defect of central domain cardiac ryanodine receptor mutations linked to arrhythmias. J Biol Chem 291:24528–24537
112. Jiang D, Chen W, Wang R et al (2007) Loss of luminal Ca2+ activation in the cardiac ryanodine receptor is associated with ventricular fibrillation and sudden death. Proc Natl Acad Sci USA 104:18309–18314
113. Gonsalves SG, Ng D, Johnston JJ et al (2013) Using exome data to identify malignant hyperthermia susceptibility mutations. Anesthesiology 119:1043–1053
114. Rosenberg H, Pollock N, Schiemann A et al (2015) Malignant hyperthermia: a review. Orphanet J Rare Dis 10:93
115. Jungbluth H (2007) Central core disease. Orphanet J Rare Dis 2:25
116. Priori SG, Chen SRW (2011) Inherited dysfunction of sarcoplasmic reticulum Ca2+ handling and arrhythmogenesis. Circ Res 108:871–883
117. Ackerman MJ, Priori SG, Willems S et al (2011) HRS/EHRA expert consensus statement on the state of genetic testing for the channelopathies and cardiomyopathies this document was developed as a partnership between the Heart Rhythm Society (HRS) and the European Heart Rhythm Association (EHRA). Heart Rhythm 8(8):1308–1339

118. Roux-Buisson N, Cacheux M, Fourest-Lieuvin A et al (2012) Absence of triadin, a protein of the calcium release complex, is responsible for cardiac arrhythmia with sudden death in human. Hum Mol Genet 21:2759–2767
119. Nyegaard M, Overgaard MT, Søndergaard MT et al (2012) Mutations in calmodulin cause ventricular tachycardia and sudden cardiac death. Am J Hum Genet 91:703–712
120. Lieve KV, van der Werf C, Wilde AA (2016) Catecholaminergic polymorphic ventricular tachycardia. Circ J 80:1285–1291
121. Murphy NP, Lubbers ER, Mohler PJ (2017) Advancements in the use of gene therapy for cardiac arrhythmia. Heart Rhythm 14:1061–1062
122. Rampazzo A, Nava A, Erne P et al (1995) A new locus for arrhythmogenic right ventricular cardiomyopathy (ARVD2) maps to chromosome 1q42-q43. Hum Mol Genet 4:2151–2154
123. Corrado D, Link MS, Calkins H (2017) Arrhythmogenic right ventricular cardiomyopathy. N Engl J Med 376:61–72
124. Azaouagh A, Churzidse S, Konorza T, Erbel R (2011) Arrhythmogenic right ventricular cardiomyopathy/dysplasia: a review and update. Clin Res Cardiol 100:383–394
125. Tong J, McCarthy TV, MacLennan DH (1999) Measurement of resting cytosolic Ca2+ concentrations and Ca2+ store size in HEK-293 cells transfected with malignant hyperthermia or central core disease mutant Ca2+ release channels. J Biol Chem 274:693–702
126. Gao L, Balshaw D, Xu L et al (2000) Evidence for a role of the lumenal M3-M4 loop in skeletal muscle Ca(2+) release channel (ryanodine receptor) activity and conductance. Biophys J 79:828–840
127. MacLennan DH, Zvaritch E (2011) Mechanistic models for muscle diseases and disorders originating in the sarcoplasmic reticulum. BBA – Mol Cell Res 1813:948–964
128. Zvaritch E, Depreux F, Kraeva N et al (2007) An Ryr1I4895T mutation abolishes Ca2+ release channel function and delays development in homozygous offspring of a mutant mouse line. Proc Natl Acad Sci USA 104:18537–18542
129. Loy RE, Orynbayev M, Xu L et al (2011) Muscle weakness in Ryr1I4895T/WT knock-in mice as a result of reduced ryanodine receptor Ca2+ ion permeation and release from the sarcoplasmic reticulum. J Gen Physiol 137:43–57
130. Györke I, Gyorke S (1998) Regulation of the cardiac ryanodine receptor channel by luminal Ca2+ involves luminal Ca2+ sensing sites. Biophys J 75:2801–2810
131. Györke S, Terentyev D (2008) Modulation of ryanodine receptor by luminal calcium and accessory proteins in health and cardiac disease. Cardiovasc Res 77:245–255
132. Laver DR (2007) Ca2+ stores regulate ryanodine receptor Ca2+ release channels via luminal and cytosolic Ca2+ sites. Biophys J 92:3541–3555
133. Zhang J, Chen B, Zhong X et al (2014) The cardiac ryanodine receptor luminal Ca 2+sensor governs Ca 2+waves, ventricular tachyarrhythmias and cardiac hypertrophy in calsequestrin-null mice. Biochem J 461:99–106

Chapter 9
Store-Operated Calcium Entry: An Historical Overview

James W. Putney

Abstract Store-operated calcium entry is a mechanism of Ca^{2+} signaling that has evolved from theory to molecules over a period of 30 years. This brief overview summarizes the major milestones that have led to the current concepts regarding the mechanisms and regulation of this most widely encountered of calcium signaling mechanisms.

Keywords Calcium signaling · Calcium channels · Store-operated channels · Intracellular calcium stores · Signaling mechanisms · History

The first appreciation of the function of calcium in tissue responsiveness is generally credited to Sidney Ringer [1], based on his observations of the requirement of extracellular calcium for continued contractility of ex vivo frog hearts. However, the idea that the role of calcium was to trigger events in the cytoplasm came much later, probably in a general sense from Heilbrunn's volumes on *An Outline of General Physiology* [2]. A concise summary of much of the early history of the concept of calcium as a cell signal can be found in a review by Petersen et al. [3].

The field of calcium signaling can be arbitrarily subdivided into mechanisms by which cytoplasmic Ca^{2+} signals are generated, and mechanisms by which Ca^{2+} signals are sensed and interpreted. Muscle led the way with regard to much of the early work on Ca^{2+} signaling, owing largely to the ability to readily observe and measure the response to Ca^{2+} signals, producing muscle contraction or shortening. The basic mechanism of muscle contraction, involving interaction of actin and myosin, was discovered by Albert Szent-Gyorgyi in the 1940s (c.f. [4]), and subsequently a number of studies demonstrated that the direct application of Ca^{2+} to the cytoplasm of skeletal muscle could induce contraction (reviewed in [5]). However the actual Ca^{2+} sensing molecule, troponin, was not found until about

J. W. Putney (✉)
Scientist Emeritus, National Institute of Environmental Health Sciences – NIH, Research Triangle Park, NC, USA
e-mail: putney@niehs.nih.gov

J. Krebs (ed.), *Membrane Dynamics and Calcium Signaling*, Advances in Experimental Medicine and Biology 981,
https://doi.org/10.1007/978-3-319-55858-5_9

20 years later by Ebashi et al. [6]. Remarkably, only about 2 years after the discovery the Ca^{2+} sensing function of troponin, Cheung reported on a Ca^{2+}-dependent activation of cyclic nucleotide phosphodiesterase [7], which turned out to be the most widely encountered intracellular Ca^{2+} sensor, calmodulin [8, 9].

Regarding the mechanism by which Ca^{2+} signals arise, a fundamental question relates to the source of Ca^{2+} entering the cytoplasm. Today we know that Ca^{2+} enters the cytoplasm either across the plasma membrane through Ca^{2+} channels, or from intracellular sites of sequestration, most commonly the endoplasmic (or sarcoplasmic) reticulum. Despite the observations of Ringer of the necessity of external Ca^{2+}, the first suggestion of Ca^{2+} functioning as a signal by Heilbrunn posited a release of Ca^{2+} from stores within the cell [2]. In identifying the source of Ca^{2+} stores, again it was skeletal muscle that led the way. The Ca^{2+} stores in muscle were identified as the sarcoplasmic reticulum, and not as the source of released Ca^{2+}, but rather as the site responsible for removing Ca^{2+} from the cytoplasm, known as "relaxing factor" [10, 11]. Interestingly, despite the clear and accepted view that the source of signaling Ca^{2+} in muscle was the sarcoplasmic reticulum, many held the view that in other cell types, Ca^{2+} was released from mitochondria ([12–14] but see [15]). It was not until the discovery of the Ca^{2+} mobilizing action of inositol 1,4,5-trisphospate (IP_3, [16, 17]) did it become unmistakably clear that the intracellular Ca^{2+} store underlying Ca^{2+} signaling is the endoplasmic (or sarcoplasmic) reticulum.

The first experimental evidence for Ca^{2+} channels in the plasma membrane came from studies of $^{45}Ca^{2+}$ uptake into squid axons [18] and frog Sartorius muscle [19]. At about the same time, the first electrophysiological evidence came from studies in crustaceans [20]. By the 1970s the concept of Ca^{2+} influx as a general contributor to cell activation was gaining general acceptance, and presumptive evidence, based on the effects of adding and removing external Ca^{2+} began to appear [21–24].

A revolution in Ca^{2+} signaling methodology occurred in 1982 with the publication of the first fluorescent Ca^{2+} indicator that could be loaded into the cytoplasm of living cells, Quin2 [25]. Quin2 was shortly thereafter displaced by the technically superior Fura2 [26]. Remarkably, despite the development over the past 30 years of numerous other small molecule indicators, and now the availability of genetically encoded Ca^{2+} indicators, Fura2 still appears to be a favorite in the field as an all-around technically suitable indicator. The ability to measure cytoplasmic Ca^{2+} in real time afforded much better kinetics and not surprisingly the accumulation of considerable information on the relationship between intracellular Ca^{2+} release and Ca^{2+} influx across the plasma membrane.

So, by the 1980s it was clear that Ca^{2+} could enter the cytoplasm by either discharge from the endoplasmic (or sarcoplasmic) reticulum, or by entry across the plasma membrane presumably through Ca^{2+} channels resident there. However, the relationship between the two was not clear. In many excitable cells, the clearest example being the heart, entry of Ca^{2+} through voltage activated channels in the plasma membrane is amplified by a process of Ca^{2+}-induced Ca^{2+} release from the sarcoplasmic reticulum [27]. However, in non-excitable cells (and many excitable cells as well), when Ca^{2+} signals were activated by ligands for surface membrane receptors, the relationship between the two processes was unclear. The majority of

surface receptors that activate Ca^{2+} signals do so by a pathway involving activation of a polyphosphoinositide directed phospholipase C that degrades phosphatidylinositol 4,5-bisphosphate to diacylglycerol and the soluble head group, inositol 1,4,5-trisphosphate (IP_3) [28, 29]. In 1983, Michael Berridge posited that IP_3 could be the signal for release of Ca^{2+} from the endoplasmic reticulum [16], and in a collaboration with other laboratories, provided strong evidence for this idea demonstrating that IP_3 applied to permeabilized pancreatic acinar cells could indeed catalyze rapid release of store Ca^{2+} [17].

Three years after the discovery, I published a hypothesis paper in Cell Calcium proposing a mechanism linking the release of Ca^{2+} by IP_3 to plasma membrane Ca^{2+} entry [30]. The basic idea was that the depletion of Ca^{2+} in the endoplasmic reticulum would by some means signal back to the plasma membrane activating Ca^{2+} permeable channels there. Because I saw this mechanism as providing Ca^{2+} to the intracellular store to be subsequently released by IP_3, I coined the term "capacitative calcium entry" emphasizing the serial arrangement of Ca^{2+} flow and Ca^{2+} storage. The arguments were based on the failure of other investigators to demonstrate direct effects of IP_3 on plasma membrane channels, and earlier work from my laboratory [31] and work from Casteels and Droogmans [32] demonstrating that the refilling of Ca^{2+} pools after discharge did not require an activated receptor. In their 1981 paper, Casteels and Droogmans proposed that refilling occurred through a direct pathway from the extracellular space to the smooth muscle sarcoplasmic reticulum, not traversing the cytoplasm [32].

In 1989, I published two studies carried out by a postdoctoral fellow, Haruo Takemura, that provided strong evidence for the capacitative calcium entry model, and also showed that Ca^{2+} entered the cytoplasm directly, rather than via an obligatory transit through the endoplasmic reticulum. In the first of these, we utilized a protocol by which stores were discharged by a muscarinic agonist in the absence of external Ca^{2+}, the agonist removed by use of a strong blocking agent, and then the stores were reloaded by addition of Ca^{2+} extracellularly [33]. Cytoplasmic Ca^{2+} was monitored by Fura2 fluorescence. This was essentially a repeat of an earlier experiment carried out in my laboratory prior to the advent of fluorescent Ca^{2+} indicators in which $[Ca^{2+}]_i$ was inferred from the rate of $^{86}Rb^+$ efflux (an indicator of Ca^{2+}-activated K^+ channel activity) [31]. As in the previous experiment, Ca^{2+} stores refilled quickly and completely after receptor blockade, confirming the receptor independence of the influx mechanism. However, in the earlier study no indication of a rise in $[Ca^{2+}]_i$ during refilling was seen, while with the fluorescent Ca^{2+} indicator, a clear rapid influx of Ca^{2+} was evident, indicating influx directly into the cytoplasm.

The second study published in 1989 arose from a collaboration between my laboratory and a medicinal chemist in Copenhagen, Ole Thastrup. Thastrup had purified a plant toxin named thapsigargin which he and Michael Hanley had shown was capable of releasing Ca^{2+} from the same pool as agonists, but without increasing IP_3 [34]. Thapsigargin therefore provided a useful test of the capacitative calcium entry model. The results of our experiments, again carried out by Haruo Takemura, showed that thapsigargin activated sustained Ca^{2+} influx in parotid acinar cells, and this entry was not additive with entry activated by a muscarinic

agonist [35]. Additionally, the fact that the apparent rate of entry with thapsigargin was similar to that with a muscarinic agonist further demonstrated that Ca^{2+} entered the cytoplasm by a pathway that did not necessarily traverse the endoplasmic reticulum. With the muscarinic agonist, that increases IP_3, the rate of exit to the cytoplasm should be much faster than with thapsigargin, which does not increase IP_3. Since the rate of entry to the cytoplasm was not greater with IP_3 present, Ca^{2+} must have entered the cytoplasm by a more direct route.

The issue of the route of Ca^{2+} entry was further laid to rest in 1992 when Hoth and Penner published the first report of a store-operated current which they termed I_{crac} [36]. Recordings of this current were published earlier by Lewis and Cahalan [37], but were not recognized as being store-operated. Hoth and Penner [38] extensively characterized I_{crac} which had some interesting and important properties. First, it was slow to develop with a time constant of 20–30 s. This indicated a slow and possibly complex mechanism for activation. The current was very small, of the order of 1 pA/pF at 0 mV. I_{crac} was highly selective for Ca^{2+} over monovalent cations, but would permit permeation of Na^+ in the absence of divalent cations. There was no measurable increase in noise associated with I_{crac}, indicating that the single channel conductance was extremely small. Subsequently, Prakriya and Lewis [39] estimated the single channel conductance of CRAC channels to be of the order of 0.2 pS, based on noise analysis.

The discovery and characterization of I_{crac} clearly established that the basic concept of capacitative or store-operated Ca^{2+} entry was correct. Depletion of Ca^{2+} from the endoplasmic reticulum brings about activation of Ca^{2+} permeable channels in the plasma membrane. Two essential questions remained: what is the signal from the endoplasmic reticulum to the plasma membrane, and what is the molecular nature of the channel?

A number of different laboratories published studies suggesting mechanisms for activating plasma membrane Ca^{2+} channels, including cyclic GMP, an arachidonic acid metabolite, a cytochrome P450 product, a secretion mechanism for channel insertion, inositol tetrakisphosphate, a small G-protein (reviewed in [40]). One interesting approach was to attempt to bioassay a signaling molecule without prior knowledge of its structure. The first such attempt from Randriamampita and Tsien [41] described an activity in extracts of store-depleted cells that activated Ca^{2+} influx. These authors termed this activity calcium influx factor, or CIF. Some properties of CIF were described, including the curious ability to act when applied extracellularly. Subsequently other laboratories carried out studies with similar (although unlikely identical) extracts [42–44]. The Bolotina laboratory carried out a number of studies with partially purified extracts, and demonstrated that its activity depended on the presence of Ca^{2+} independent phospholipase A2 (iPLA2) [45]. The CIF concept has not gained general acceptance, however, owing in part to a frustrating failure to obtain a structure of the active principle, and also owing to alternative discoveries regarding the activation mechanism of CRAC channels, discussed below.

As to the nature of the channel itself, initially much attention was focused on members of the mammalian TRPC subfamily of cation channels. These channels were original

identified [46] by homology with the *Drosophila* photoreceptor TRP channel which was believed to be activated downstream of phospholipase C [47]. Early reports showed activation of *Drosophila* TRP [48] and mammalian TRPC channels [49–52]. However, other studies failed to reproduce these findings [53–55]. This controversy has been discussed in a number of reviews [40, 56–58]. Electrophysiological studies clearly demonstrated that TRPC currents are quite distinct from I_{crac}, being rather non-selective and with much larger single channel openings [49, 59]. Thus, if TRPCs form store-operated channels, it is unlikely they are the canonical CRAC channels originally described by Hoth and Penner [36]. While currently there is still not complete consensus on the roles of TRPCs in store-operated entry, some general points have emerged. First, it is clear that the 7 TRPCs can function as components of non-store-operated channels activated downstream of phospholipase C. TRPC3, 6 and 7 can be activated by the lipid product of phospholipase C, diacylglycerol [54, 60]. TRPC4 and 5 are also activated downstream of phospholipase C, but the precise nature of this regulation is still unknown [55, 61]. The majority of studies suggest that TRPC1 does not function in a homomeric non-store-operated channel [62] but rather as a subunit together with other TRPCs [62, 63]. TRPCs can function as channels regulated by Ca^{2+} store depletion, but as to whether this qualifies them as true store-operated channel is a semantic issue (discussed in more detail below).

The emergence of high-throughput screening techniques eventually led to the identification of both the signaling mechanism and the pore forming subunit of store-operated channels. Roos et al. [64] in a limited screen of potential channel and signaling proteins, identified stromal interacting molecule (STIM) as a critical molecule for activation of I_{crac} in *Drosophila* S2 cells. Shortly thereafter, Liou et al. [65] identified STIM1 and STIM2 in a screen in mammalian cells, and demonstrated that store depletion caused aggregation of STIM molecules at sites close to the plasma membrane. STIM had been previously identified as a plasma membrane protein with a Ca^{2+} binding EF-hand motif [66]. In the plasma membrane, the EF-hand would face the extracellular space, but in the endoplasmic reticulum, it would face the lumen of the endoplasmic reticulum. Thus, Liou et al. [65] demonstrated that mutation of the Ca^{2+} binding EF-hand motif caused constitutive aggregation into near plasma membrane puncta, and constitutive Ca^{2+} influx. Subsequent work by a number of laboratories established that STIM1, and to a lesser extent STIM2, functions as the initial Ca^{2+} sensor in the endoplasmic reticulum (reviewed in [67, 68]). Depletion of Ca^{2+} from the endoplasmic reticulum results in dissociation of Ca^{2+} from STIM1, aggregation of dimers into higher order multimers, and trapping of the multimers in endoplasmic reticulum—plasma membrane junctions where STIM1 interacts with, and directly activates store-operated CRAC channels.

The identification of the pore-forming subunit of the CRAC channel came approximately 1 year after the identification of STIM. Feske et al. [69] utilized a combination of pedigree analysis of a family carrying a mutation resulting in loss of I_{crac}, together with a whole genome screen in *Drosophila* S2 cells and identified a gene encoding a small membrane protein with no previous assigned function. They named this protein Orai, which in Greek mythology were gate keepers. There were three homologs of *Drosophila* Orai in the mammalian database, one of which

corresponded to the mutation responsible for loss of I_{crac}. This was then designated Orai1, and the remaining 2, Orai2 and Orai3. Shortly thereafter two other laboratories confirmed this finding. Vig et al. [70] designated CRACM for CRAC modulator, while Zhang et al. [71] did not propose nomenclature other than the database designation olf186-F. Zhang et al. [71] also provided the important observation that co-expression of Orai with STIM1 results in a many-fold increase in I_{crac}. It is perhaps noteworthy that while all three groups firmly established the necessity of Orai in store-operated Ca^{2+} entry, none went so far as to propose that this molecule was actually a part of the CRAC channel itself. Indeed, Orai has little or no homology to any other known ion channel. Perhaps this is not surprising, given that the properties, especially the single channel conductance of CRAC channels, are so distinct from other known ion channels. The evidence that Orai is indeed a pore forming subunit of the CRAC channel came from studies in which single amino acid mutations resulted in channels with substantially altered ion selectivity [72–74]. Recently the crystal structure of the *Drosophila* Orai channel was published, and surprisingly the channel is a hexamer, formed by three dimers of Orai [75] (but see [76]).

Both STIM and Orai are known to subtend functions other than their roles in store-operated Ca^{2+} entry. STIM1 has been shown to interact with proteins associated with the growing ends of microtubules where it is involved in remodeling of the endoplasmic reticulum [77]. Multiple phosphorylations of the cytoplasmic domain of STIM1 during mitosis prevent this interaction, presumably to allow appropriate segregation of the endoplasmic reticulum from the mitotic spindle [78]. In addition to their role in store-operated CRAC channels, Orai proteins function in other Ca^{2+} permeable channels. Ambudkar's laboratory has shown that Ca^{2+} entering through Orai1 CRAC channels can signal recruitment of TRPC1 channels to the plasma membrane where they interact with STIM1 and open to pass Ca^{2+} [79]. The resulting current, I_{soc} (store-operated Ca^{2+} current), is only modestly Ca^{2+} selective in comparison to I_{crac}. It is not clear whether I_{soc} is a combination of two currents, a CRAC current and a relatively non selective TRPC1 current, or possibly current through a channel formed with both Orai1 and TRPC1 subunits. Orai1 can also function as a pore forming subunit of non-store-operated channels activated by either arachidonic acid [80] or an arachidonic acid metabolite, leukotriene C4 [81]. The current is called I_{arc} (arachidonate regulated Ca^{2+} current) and the ARC channels appear to be pentamers containing both Orai1 and Orai3 subunits [82].

In the 30 years since the proposal of capacitative calcium entry [30] much has been learned about the molecular basis of this widely encountered Ca^{2+} signaling mechanism. Currently, this information is being utilized in the design of animal models to shed light on the systems physiology of store-operated Ca^{2+} entry [83, 84]. And hopefully the next step will see the translation of this information to better understanding of debilitating diseases as well as novel approaches for their amelioration.

References

1. Ringer S (1883) A further contribution regarding the influence of the different constituents of the blood on the contraction of the heart. J Physiol (Lond) 4:29–42
2. Heilbrunn LV (1952) An outline of general physiology, 3rd edn. Saunders, Philadelphia, PA, pp 105–740
3. Petersen OH, Michalak M, Verkhratsky A (2005) Calcium signalling: past, present and future. Cell Calcium 38:161–169
4. Perry SV (2008) Background to the discovery of troponin and Setsuro Ebashi's contribution to our knowledge of the mechanism of relaxation in striated muscle. Biochem Biophys Res Commun 369:43–48
5. Endo M (2006) Calcium ion as a second messenger with special reference to excitation coupling. J Pharmacol Sci 100:519–524
6. Ebashi S, Kodama A, Ebashi F (1968) Troponin. I. Preparation and physiological function. J Biochem 64:465–477
7. Cheung WY (1970) Cyclic 3′,5′-nucleotide phosphodiesterase. Demonstration of an activator. Biochem Biophys Res Comm 38:533–538
8. Klee CB, Newton DL (1985) Calmodulin: an overview. In: Parratt JR (ed) Control and manipulation of calcium movement. Raven Press, New York, pp 131–145
9. Soderling TR (1999) The Ca^{2+}-calmodulin-dependent protein kinase cascade. Trends Biochem Sci 24:232–236
10. Ebashi S, Lipmann F (1962) Adenosine triphosphate-linked concentration of calcium ions in a particulate fraction of rabbit muscle. J Cell Biol 14:389–400
11. Hasselbach W, Makinose M (1962) ATP and active transport. Biochem Biophys Res Commun 7:132–136
12. Blackmore PF, Dehaye JP, Strickland WG, Exton JH (1979) alpha-Adrenergic mobilization of hepatic mitochondrial calcium. Febs Lett 100:117–120
13. Borle AB (1974) Cyclic AMP stimulation of calcium efflux from kidney, liver and heart mitochondria. J Membr Biol 16:221–236
14. Murphy E, Coll K, Rich TL, Williamson JR (1980) Hormonal effects on calcium homeostasis in isolated hepatocytes. J Biol Chem 255:6600–6608
15. Burgess GM, McKinney JS, Fabiato A et al (1983) Calcium pools in saponin-permeabilized guinea-pig hepatocytes. J Biol Chem 258:15336–15345
16. Berridge MJ (1983) Rapid accumulation of inositol trisphosphate reveals that agonists hydrolyse polyphosphoinositides instead of phosphatidylinositol. Biochem J 212:849–858
17. Streb H, Irvine RF, Berridge MJ, Schulz I (1983) Release of Ca^{2+} from a nonmitochondrial store in pancreatic cells by inositol-1,4,5-trisphosphate. Nature 306:67–68
18. Hodgkin AL, Keynes RD (1957) Movements of labelled calcium in squid giant axons. J Physiol 138:253–281
19. Bianchi CP, Shanes AM (1959) Calcium influx in skeletal muscle at rest, during activity, and during potassium contracture. J Gen Physiol 42:803–815
20. Fatt P, Ginsborg BL (1958) The ionic requirements for the production of action potentials in crustacean muscle fibres. J Physiol 142:516–543
21. Bohr DF (1963) Vascular smooth muscle: dual effect of calcium. Science 139:597–599
22. Bohr DF (1973) Vascular smooth muscle updated. Circ Res 32:665–672
23. Putney JW, Poggioli J, Weiss SJ (1981) Receptor regulation of calcium release and calcium permeability in parotid gland cells. Phil Trans R Soc Lond B 296:37–45
24. Van Breemen C, Farinas B, Gerba P, McNaughton ED (1972) Excitation-contraction coupling in rabbit aorta studied by the lanthanum method for measuring cellular calcium influx. Circ Res 30:44–54
25. Tsien RY, Pozzan T, Rink TJ (1982) Calcium homeostasis in intact lymphocytes: cytoplasmic free calcium monitored with a new, intracellularly trapped fluorescent indicator. J Cell Biol 94:325–334

26. Grynkiewicz G, Poenie M, Tsien RY (1986) A new generation of Ca^{2+} indicators with greatly improved fluorescence properties. J Biol Chem 260:3440–3450
27. Fabiato A (1983) Calcium-induced release of calcium from the cardiac sarcoplasmic reticulum. Am J Physiol 245:C1–C4
28. Abdel-Latif AA, Akhtar R, Hawthorne JN (1977) Acetylcholine increases the breakdown of triphosphoinositide of rabbit iris muscle prelabelled with [^{32}P]phosphate. Biochem J 162:61–73
29. Kirk CJ, Creba JA, Downes CP, Michell RH (1981) Hormone-stimulated metabolism of inositol lipids and its relationship to hepatic receptor function. Biochem Soc Trans 9:377–379
30. Putney JW (1986) A model for receptor-regulated calcium entry. Cell Calcium 7:1–12
31. Parod RJ, Putney JW (1978) The role of calcium in the receptor mediated control of potassium permeability in the rat lacrimal gland. J Physiol (Lond) 281:371–381
32. Casteels R, Droogmans G (1981) Exchange characteristics of the noradrenaline-sensitive calcium store in vascular smooth muscle cells of rabbit ear artery. J Physiol (Lond) 317:263–279
33. Takemura H, Putney JW (1989) Capacitative calcium entry in parotid acinar cells. Biochem J 258:409–412
34. Jackson TR, Patterson SI, Thastrup O, Hanley MR (1988) A novel tumour promoter, thapsigargin, transiently increases cytoplasmic free Ca^{2+} without generation of inositol phosphates in NG115-401L neuronal cells. Biochem J 253:81–86
35. Takemura H, Hughes AR, Thastrup O, Putney JW (1989) Activation of calcium entry by the tumor promoter, thapsigargin, in parotid acinar cells. Evidence that an intracellular calcium pool, and not an inositol phosphate, regulates calcium fluxes at the plasma membrane. J Biol Chem 264:12266–12271
36. Hoth M, Penner R (1992) Depletion of intracellular calcium stores activates a calcium current in mast cells. Nature 355:353–355
37. Lewis RS, Cahalan MD (1989) Mitogen-induced oscillations of cytosolic Ca^{2+} and transmembrane Ca^{2+} current. Cell Reg 1:99–112
38. Hoth M, Penner R (1993) Calcium release-activated calcium current in rat mast cells. J Physiol (Lond) 465:359–386
39. Prakriya M, Lewis RS (2002) Separation and characterization of currents through store-operated CRAC channels and Mg^{2+}-inhibited cation (MIC) channels. J Gen Physiol 119:487–507
40. Parekh AB, Putney JW (2005) Store-operated calcium channels. Physiol Rev 85:757–810
41. Randriamampita C, Tsien RY (1993) Emptying of intracellular Ca^{2+} stores releases a novel small messenger that stimulates Ca^{2+} influx. Nature 364:809–814
42. Csutora P, Su Z, Kim HY et al (1999) Calcium influx factor is synthesized by yeast and mammalian cells depleted of organellar calcium stores. Proc Nat Acad Sci USA 96:121–126
43. Thomas D, Hanley MR (1995) Evaluation of calcium influx factors from stimulated Jurkat T-lymphocytes by microinjection into *Xenopus* oocytes. J Biol Chem 270:6429–6432
44. Trepakova ES, Csutora P, Hunton DL et al (2000) Calcium influx factor (CIF) directly activates store-operated cation channels in vascular smooth muscle cells. J Biol Chem 275:26158–26163
45. Smani T, Zakharov SI, Leno E et al (2003) Ca^{2+}-independent phospholipase A2 is a novel determinant of store-operated Ca^{2+} entry. J Biol Chem 278:11909–11915
46. Zhu X, Chu PB, Peyton M, Birnbaumer L (1995) Molecular cloning of a widely expressed human homologue for the *Drosophila trp* gene. FEBS Lett 373:193–198
47. Hardie RC, Minke B (1995) Phosphoinositide-mediated phototransduction in *Drosophila* photoreceptors: the role of Ca^{2+} and *trp*. Cell Calcium 18:256–274
48. Vaca L, Sinkins WG, Hu Y et al (1994) Activation of recombinant *trp* by thapsigargin in Sf9 insect cells. Am J Physiol 267:C1501–C1505
49. Kiselyov K, Xu X, Mozhayeva G et al (1998) Functional interaction between $InsP_3$ receptors and store-operated Htrp3 channels. Nature 396:478–482
50. Liu X, Wang W, Singh BB et al (2000) Trp1, a candidate protein for the store-operated Ca^{2+} influx mechanism in salivary gland cells. J Biol Chem 275:3403–3411

51. Philipp S, Trost C, Warnat J et al (2000) Trp4 (CCE1) protein is part of native calcium release-activated Ca^{2+}-like channels in adrenal cells. J Biol Chem 275:23965–23972
52. Zitt C, Zobel A, Obukhov AG et al (1996) Cloning and functional expression of a human Ca^{2+}-permeable cation channel activated by calcium store depletion. Neuron 16:1189–1196
53. DeHaven WI, Jones BF, Petranka JG et al (2009) TRPC channels function independently of STIM1 and Orai1. J Physiol 587:2275–2298
54. Hofmann T, Obukhov AG, Schaefer M et al (1999) Direct activation of human TRPC6 and TRPC3 channels by diacylglycerol. Nature 397:259–262
55. Schaefer M, Plant TD, Obukhov AG et al (2000) Receptor-mediated regulation of the nonselective cation channels TRPC4 and TRPC5. J Biol Chem 275:17517–17526
56. Abramowitz J, Birnbaumer L (2009) Physiology and pathophysiology of canonical transient receptor potential channels. FASEB J 23:297–328
57. Ambudkar IS, Ong HL (2007) Organization and function of TRPC channelosomes. Pflugers Arch 455:187–200
58. Vazquez G, Wedel BJ, Aziz O et al (2004) The mammalian TRPC cation channels. Biochim Biophys Acta 1742:21–36
59. Hurst RS, Zhu X, Boulay G et al (1998) Ionic currents underlying HTRP3 mediated agonist-dependent Ca^{2+} influx in stably transfected HEK293 cells. FEBS Letters 422:333–338
60. Beck B, Zholos A, Sydorenko V et al (2006) TRPC7 is a receptor-operated DAG-activated channel in human keratinocytes. J Invest Dermatol 126:1982–1993
61. Trebak M, Lemonnier L, DeHaven WI et al (2009) Complex functions of phosphatidylinositol 4,5-bisphosphate in regulation of TRPC5 cation channels. Pflugers Arch 457:757–769
62. Hofmann T, Schaefer M, Schultz G, Gudermann T (2002) Subunit composition of mammalian transient receptor potential channels in living cells. Proc Nat Acad Sci USA 99:7461–7466
63. Strubing C, Krapivinsky G, Krapivinsky L, Clapham DE (2003) Formation of novel TRPC channels by complex subunit interactions in embryonic brain. J Biol Chem 278:39014–39019
64. Roos J, DiGregorio PJ, Yeromin AV et al (2005) STIM1, an essential and conserved component of store-operated Ca^{2+} channel function. J Cell Biol 169:435–445
65. Liou J, Kim ML, Heo WD et al (2005) STIM is a Ca^{2+} sensor essential for Ca^{2+}-store-depletion-triggered Ca^{2+} influx. Curr Biol 15:1235–1241
66. Williams RT, Manji SS, Parker NJ et al (2001) Identification and characterization of the STIM (stromal interaction molecule) gene family: coding for a novel class of transmembrane proteins. Biochem J 357:673–685
67. Johnstone LS, Graham SJ, Dziadek MA (2010) STIM proteins: integrators of signalling pathways in development, differentiation and disease. J Cell Mol Med 14:1890–1903
68. Prakriya M (2009) The molecular physiology of CRAC channels. Immunol Rev 231:88–98
69. Feske S, Gwack Y, Prakriya M et al (2006) A mutation in Orai1 causes immune deficiency by abrogating CRAC channel function. Nature 441:179–185
70. Vig M, Peinelt C, Beck A et al (2006b) CRACM1 is a plasma membrane protein essential for store-operated Ca^{2+} entry. Science 312:1220–1223
71. Zhang SL, Yeromin AV, Zhang XH et al (2006) Genome-wide RNAi screen of Ca^{2+} influx identifies genes that regulate Ca2+ release-activated Ca^{2+} channel activity. Proc Natl Acad Sci USA 103:9357–9362
72. Prakriya M, Feske S, Gwack Y et al (2006) Orai1 is an essential pore subunit of the CRAC channel. Nature 443:230–233
73. Vig M, Beck A, Billingsley JM et al (2006a) CRACM1 multimers form the ion-selective pore of the CRAC channel. Curr Biol 16:2073–2079
74. Yeromin AV, Zhang SL, Jiang W et al (2006) Molecular identification of the CRAC channel by altered ion selectivity in a mutant of Orai. Nature 443:226–229
75. Hou X, Pedi L, Diver MM, Long SB (2012) Crystal structure of the calcium release-activated calcium channel Orai. Science 338:1308–1313
76. Thompson JL, Shuttleworth TJ (2013) How many Orai's does it take to make a CRAC channel? Sci Rep 3:1961

77. Honnappa S, Gouveia SM, Weisbrich A et al (2009) An EB1-binding motif acts as a microtubule tip localization signal. Cell 138:366–376
78. Smyth JT, Petranka JG, Boyles RR et al (2009) Phosphorylation of STIM1 underlies suppression of store-operated calcium entry during mitosis. Nat Cell Biol 11:1465–1472
79. Cheng KT, Liu X, Ong HL et al (2011) Local Ca(2)+ entry via Orai1 regulates plasma membrane recruitment of TRPC1 and controls cytosolic Ca(2)+ signals required for specific cell functions. PLoS Biol 9:e1001025
80. Mignen O, Thompson JL, Shuttleworth TJ (2008) Both Orai1 and Orai3 are essential components of the arachidonate-regulated Ca2+-selective (ARC) channels. J Physiol (Lond) 586:185–195
81. Gonzalez-Cobos JC, Zhang X, Zhang W et al (2013) Store-independent Orai1/3 channels activated by intracrine leukotriene C4: role in neointimal hyperplasia. Circ Res 112:1013–1025
82. Mignen O, Thompson JL, Shuttleworth TJ (2009) The molecular architecture of the arachidonate-regulated Ca2+-selective ARC channel is a pentameric assembly of Orai1 and Orai3 subunits. J Physiol 587:4181–4197
83. Feske S (2009) ORAI1 and STIM1 deficiency in human and mice: roles of store-operated Ca2+ entry in the immune system and beyond. Immunol Rev 231:189–209
84. Putney JW (2011) The physiological function of store-operated calcium entry. Neurochem Res 36:1157–1165

Chapter 10
From Stores to Sinks: Structural Mechanisms of Cytosolic Calcium Regulation

Masahiro Enomoto, Tadateru Nishikawa, Naveed Siddiqui, Steve Chung, Mitsuhiko Ikura, and Peter B. Stathopulos

Abstract All eukaryotic cells have adapted the use of the calcium ion (Ca^{2+}) as a universal signaling element through the evolution of a toolkit of Ca^{2+} sensor, buffer and effector proteins. Among these toolkit components, integral and peripheral proteins decorate biomembranes and coordinate the movement of Ca^{2+} between compartments, sense these concentration changes and elicit physiological signals. These changes in compartmentalized Ca^{2+} levels are not mutually exclusive as signals propagate between compartments. For example, agonist induced surface receptor stimulation can lead to transient increases in cytosolic Ca^{2+} sourced from endoplasmic reticulum (ER) stores; the decrease in ER luminal Ca^{2+} can subsequently signal the opening surface channels which permit the movement of Ca^{2+} from the extracellular space to the cytosol. Remarkably, the minuscule compartments of mitochondria can function as significant cytosolic Ca^{2+} sinks by taking up Ca^{2+} in a coordinated manner. In non-excitable cells, inositol 1,4,5 trisphosphate receptors (IP_3Rs) on the ER respond to surface receptor stimulation; stromal interaction molecules (STIMs) sense the ER luminal Ca^{2+} depletion and activate surface Orai1 channels; surface Orai1 channels selectively permit the movement of Ca^{2+} from the extracellular space to the cytosol; uptake of Ca^{2+} into the matrix through the mitochondrial Ca^{2+} uniporter (MCU) further shapes the cytosolic Ca^{2+} levels. Recent structural elucidations of these key Ca^{2+} toolkit components have improved our understanding of how they function to orchestrate precise cytosolic Ca^{2+} levels for specific physiological responses. This chapter reviews the atomic-resolution structures of IP_3R, STIM1, Orai1 and MCU elucidated by X-ray crystallography,

M. Enomoto · T. Nishikawa · M. Ikura (✉)
Princess Margaret Cancer Center, University Health Network, Toronto, ON, Canada

Department of Medical Biophysics, University of Toronto, Toronto, ON, Canada
e-mail: Mitsu.Ikura@uhnresearch.ca

N. Siddiqui · S. Chung · P. B. Stathopulos (✉)
Department of Physiology and Pharmacology, University of Western Ontario, London, ON, Canada
e-mail: Peter.Stathopulos@schulich.uwo.ca

J. Krebs (ed.), *Membrane Dynamics and Calcium Signaling*, Advances in Experimental Medicine and Biology 981,
https://doi.org/10.1007/978-3-319-55858-5_10

electron microscopy and NMR and discusses the mechanisms underlying their biological functions in their respective compartments within the cell.

Keywords Inositol 1,4,5-trisphosphate receptor (IP_3R) · Stromal interaction molecule-1 (STIM1) · Orai1 · Mitochondrial calcium uniporter (MCU) · Store operated calcium entry (SOCE) · Calcium release activated calcium (CRAC) · X-ray crystallography · Nuclear magnetic resonance (NMR) spectroscopy · Electron microscopy · Calcium signaling

10.1 Calcium Signaling

All eukaryotic cells have adapted changing calcium (Ca^{2+}) ion gradients within and between compartments as primary and secondary cell signaling messages that code and decode myriad processes ranging from fertilization and cell division (i.e. life) to apoptosis and necrosis (i.e. death) in health and disease [1–3]. This universality of Ca^{2+} signaling depends on a toolkit of proteins specifically expressed in the lumens and associated with compartment membranes which facilitate the movement of Ca^{2+} between compartments, buffer free Ca^{2+} concentrations or sense changes in Ca^{2+} levels and effect downstream signaling processes [3–6]. The functions of these protein toolkit components are highly coordinated to precisely regulate Ca^{2+} levels in a temporal and spatial manner, hence the Ca^{2+} concentration levels of intracellular compartments are inter-dependent [4]. In other words, increases in cytosolic Ca^{2+} levels can be driven by changes in endoplasmic reticulum (ER) stored Ca^{2+} levels and locally shaped by sinks such as mitochondria. The plasma membrane (PM) forms a tight, low dielectric barrier which prevents unsolicited passage of ions. Thus, free extracellular Ca^{2+} is basally maintained at approximately mM concentrations, whereas on the other side of the biomembrane, cytosolic Ca^{2+} levels are maintained several orders of magnitude lower at approximately sub-μM concentrations. ER Ca^{2+} levels are in the approximately hundreds of μM, while mitochondrial Ca^{2+} levels are in the approximately μM range [7–10].

While intracellular molecular signaling can be directly initiated by movement of Ca^{2+} down the steep concentration gradient from the extracellular space to the cytosol, a plethora of proteins which decorate the PM can be activated independent of the high extracellular Ca^{2+} levels and lead to cytosolic Ca^{2+} changes solely via movement of compartmentalized Ca^{2+}. For example, G-protein coupled receptors (GPCR)s, receptor tyrosine kinases and T/B-cell receptors are all activated by extracellular ligands which lead to the activation of various phospholipase C isoforms [8, 11]. Phospholipase C catalyzes the hydrolysis of phosphatidylinositol 4,5-bisphosphate (PIP_2) into diacylglycerol (DAG) and inositol 1,4,5-trisphosphate (IP_3) [11]. Both the IP_3 and DAG can subsequently mediate downstream signaling events. DAG can regulate several proteins such as protein kinase C, transient receptor potential (TRP)C and RhoGAP (reviewed in [11]). IP_3 acts as a small diffusible ligand which binds to IP_3 receptors (IP_3R) on the ER with sub-μM affinity

[12]. IP_3Rs are Ca^{2+} channels which have increased open probability with IP_3 bound allowing significant Ca^{2+} to move down the concentration gradient from the ER lumen into the cytosol. Because the ER Ca^{2+} store is finite, the increase in cytosolic Ca^{2+} sourced by the ER lumen is only transient in nature. Sarco/endoplasmic reticulum Ca^{2+} ATPase (SERCA) pumps hydrolyze adenosine triphosphate (ATP) to actively move Ca^{2+} back into the ER lumen against the concentration gradient and restore basal levels of Ca^{2+} [13, 14].

Many cellular processes such as those mediated by transcriptional changes require longer-lived cytosolic Ca^{2+} increases than can be sourced by intracellularly stored Ca^{2+} alone. Consequently, cells have evolved the use of store operated Ca^{2+} entry (SOCE) to couple external cell stimulation and intracellular Ca^{2+} store mobilization with the relatively immense supply of extracellular Ca^{2+}. SOCE is the process whereby ER luminal Ca^{2+} store depletion leads to the activation of Ca^{2+} channels on the PM which facilitate the movement of Ca^{2+} down the steep concentration gradient from the extracellular space to the cytosol [15, 16]. The increase in cytosolic Ca^{2+} is longer lived than the preceding transient release of Ca^{2+} from the internal stores. Physiological SOCE occurs via agonist-induced stimulation of the PM surface receptors and subsequent IP_3 production; however, any means of ER luminal Ca^{2+} depletion will lead to SOCE. For example, pharmacological inhibition of the SERCA using thapsigargin (TG) causes a passive depletion of the ER luminal stores which activates SOCE. TG is a widely used pharmacological research tool to study SOCE [17].

SOCE not only provides Ca^{2+} to the cytosol which refills the ER luminal stores in collaboration with SERCA and promotes sustained cytosolic Ca^{2+} signals for transcriptional changes such as those mediated by the calmodulin/calcineurin/nuclear factor of activated T-cells pathway [18], but also provides Ca^{2+} which can be taken up by other organelles such as mitochondria [19–23]. Mitochondria are known as the powerhouses of cells. This colloquial name stems from the production of large amounts of ATP, a chemical store of energy used by myriad enzymes, structural and transporter proteins. However, the proton pumping by the electron transport chain leads to the generation of a large negative membrane potential across inner mitochondrial membrane which is an enormous driving force for Ca^{2+} uptake into the mitochondrial matrix [24–27]. Unregulated Ca^{2+} uptake into the matrix would be calamitous due to degeneracy of the electrochemical gradient, upregulation of respiratory chain activity and induction of matrix Ca^{2+}-overload linked apoptosis [25, 28]. Thus, cells have evolved the mitochondrial Ca^{2+} uniporter (MCU) to strictly control most of the Ca^{2+} entry across the inner mitochondrial membrane into the matrix. Upon agonist-induced increases in cytosolic Ca^{2+}, through SOCE for example, the MCU is subsequently activated and cytosolic Ca^{2+} is rapidly taken up into the matrix. The Ca^{2+} uptake by MCU shapes the local Ca^{2+} signals in the cytosol and regulates enzyme activity in the matrix [29]. Notably, the increase in matrix Ca^{2+} is only transient as the function of exchanger toolkit components such as the mitochondrial sodium (Na^+)/Ca^{2+} exchanger (NCLX) [30–32] quickly dissipate the Ca^{2+}, preventing the catastrophic chronic disruption of the electrochemical gradient.

The physiological conceptualization of both SOCE and mitochondrial Ca^{2+} uptake preceded the identification of the molecular players mediating these processes by several decades [15, 33]. Using systems biology approaches involving inhibiting and interfering RNA screens, stromal interaction molecule (STIM)-1 and STIM2 were identified as Ca^{2+} sensors of ER luminal Ca^{2+} concentrations and activators of the PM-resident Ca^{2+} channels that drive SOCE [34–36]. Pedigree analyses involving families with severe combined immunodeficiency (SCID) syndromes which are characterized by a lack of Ca^{2+} release-activated Ca^{2+} (CRAC) channel activity in T-cells were used to subsequently identify Orai proteins as the subunits which make up CRAC channels [37–42]. CRAC channels mediate SOCE which underlies the transcriptional changes associated with the immune response [8, 43].

While the SOCE/CRAC components have been well defined over the past decade, the exact molecular identities responsible for mitochondrial Ca^{2+} uptake mechanisms have been elusive until recently. In 2011, computational mining of mitochondria-expressed proteins combined with cell biology approaches led to the identification of the core MCU component which forms the channel pore and a plethora of regulators which collectively function in a higher order complex to mediate Ca^{2+} uptake into the matrix [44, 45]. Some of the prominent MCU regulators include MCUb, a dominant negative channel pore subunit homologue [46], mitochondrial Ca^{2+} uptake (MICU) proteins, gatekeepers and Ca^{2+} threshold regulators of MCU activity [47, 48], MCU regulator-1 (MCUR1), an important scaffold protein which stabilizes the higher order MCU complex [49], essential MCU regulator (EMRE), a single TM protein which is indispensable for mitochondrial Ca^{2+} uptake [50] and SLC25A23, a magnesium (Mg^{2+})-ATP and phosphate transporter which interacts with MCU and MICU1 and enhances mitochondrial Ca^{2+} uptake [51].

Collectively, we are now much closer to illuminating a complete blueprint of the molecular components and signaling networks controlling compartmentalized Ca^{2+} regulation in eukaryotic cells. For example, IP_3Rs, STIMs, Orai1 and MCU complex proteins function in discrete regions of the cells to produce highly coordinated Ca^{2+} signals. IP_3Rs respond to surface agonist-induced IP_3 production by depleting ER luminal Ca^{2+} stores; STIMs sense this ER Ca^{2+} depletion and activate PM Orai1 channels in the activation of SOCE; MCU quickly takes up cytosolic Ca^{2+} to shape the local Ca^{2+} encoded messages. From a structural biology standpoint, tremendous progress has been made in recent years, not only due to the identification of major molecular players mediating SOCE and MCU activity, but also due to technological advancements in structural biology techniques, particularly with respect to IP_3Rs. This chapter reviews important progress made in elucidating the high-resolution structural mechanisms of function of these vital Ca^{2+} signaling toolkit components: IP_3Rs, STIMs, Orai and MCU. Nevertheless, it is important to recognize that IP_3R, STIM, Orai and MCU proteins are only a small fraction of the plethora of proteins involved in the regulation of intracellular Ca^{2+} signaling.

10.2 N-Terminal Domain of IP_3R

Initial structural studies on the IP_3R focused on the N-terminal domain (NTD; residues 1–604), as it contains the binding site of the key IP_3 ligand. High-resolution crystal structures of the NTD determined by X-ray crystallography [52–56] have contributed to our understanding of the molecular mechanism underlying the high ~nM binding affinity of the receptor for IP_3 [57–62]. The NTD of IP_3Rs is composed of two functional domains: the suppressor domain (SD; residues 1–223 of IP_3R1) and the IP_3-binding core (IBC; residues 224–604 of IP_3R1) (Fig. 10.1a). The first high-resolution crystal structure was the IBC of IP_3R1 in complex with IP_3 (PDB code 1N4K) [55]. The IBC forms an L-shaped structure with the two structurally distinct domains: the β-domain (IBC-β) and the α-domain (IBC-α) oriented approximately perpendicular to each other. The IBC-β adopts a β-trefoil fold, whereas IBC-α adopts an armadillo solenoid fold. The basic amino acids located on the cleft of the IBC formed by both domains comprise the IP_3 binding site. The crystal structures of the SD have been determined for IP_3R1 (residues 1–223, PDB code 1XZZ) and IP_3R3 (residues 1–224, PDB code 3JRR) [54, 55]. The SD folds into a hammer-like structure with a β-stranded "head" domain and a helix-turn-helix "arm" domain. The isolated IBC is the minimal region required for IP_3 binding and shows an extremely high affinity for IP_3 in vitro [i.e. equilibrium dissociation constant (K_d) ~2.3 nM] [64]. Intriguingly, the IP_3 binding affinity of the entire NTD encompassing both the SD and IBC is reduced approximately twenty times (i.e. K_d ~45 nM), implying that the SD suppresses IP_3 binding to the IBC [62]. In addition to the suppressive binding role of the SD, it is essential for IP_3-induced channel gating, as a single mutation within the SD (i.e. Tyr167Ala) abolishes IP_3-evoked Ca^{2+} release without affecting the IP_3 binding affinity [65]. Although precisely how the IP_3-binding induced signals are transmitted to the channel domain remained elusive after these seminal structural papers, studies revealed the importance of the Tyr167-containing critical loop of the SD which links IP_3 binding to channel gating [54, 65].

In 2011 and 2012, two research groups independently determined crystal structures of the NTD of IP_3R1. Lin et al. solved both apo- and IP_3-bound NTD structures of rat IP_3R1 at 3.8 Å resolution from a single crystal grown in the presence of IP_3 (PDB code 3T8S) [53]. Subsequently, NTD structures of rat IP_3R1 with all Cys residues mutated to Ala (i.e. the Cys-less form) at higher resolutions were determined. Importantly, the crystals were separately grown in the absence and presence of IP_3, and apo- and IP_3-bound NTD structures were resolved to 3.0 Å for the apo-state (PDB code 3UJ4) and 3.6 Å for the IP_3-bound state (PDB code 3UJ0) (Fig. 10.1a) [52]. The individual structures of the three domains comprising the NTD (i.e. SD, IBC-β and IBC-α) are highly similar to the separately determined structures of SD [54, 55] and IBC [56]. Nonetheless, these NTD structures revealed the arrangement of the SD and IBC domains with respect to one another. The SD, IBC-β and IBC-α in the NTD structure form a triangular architecture with the SD positioned behind the IP_3-binding site. This arrangement suggests that the SD allosterically inhibits IP_3 binding to the IBC. Specifically, the SD interacts with IBC-β and IBC-α, forming

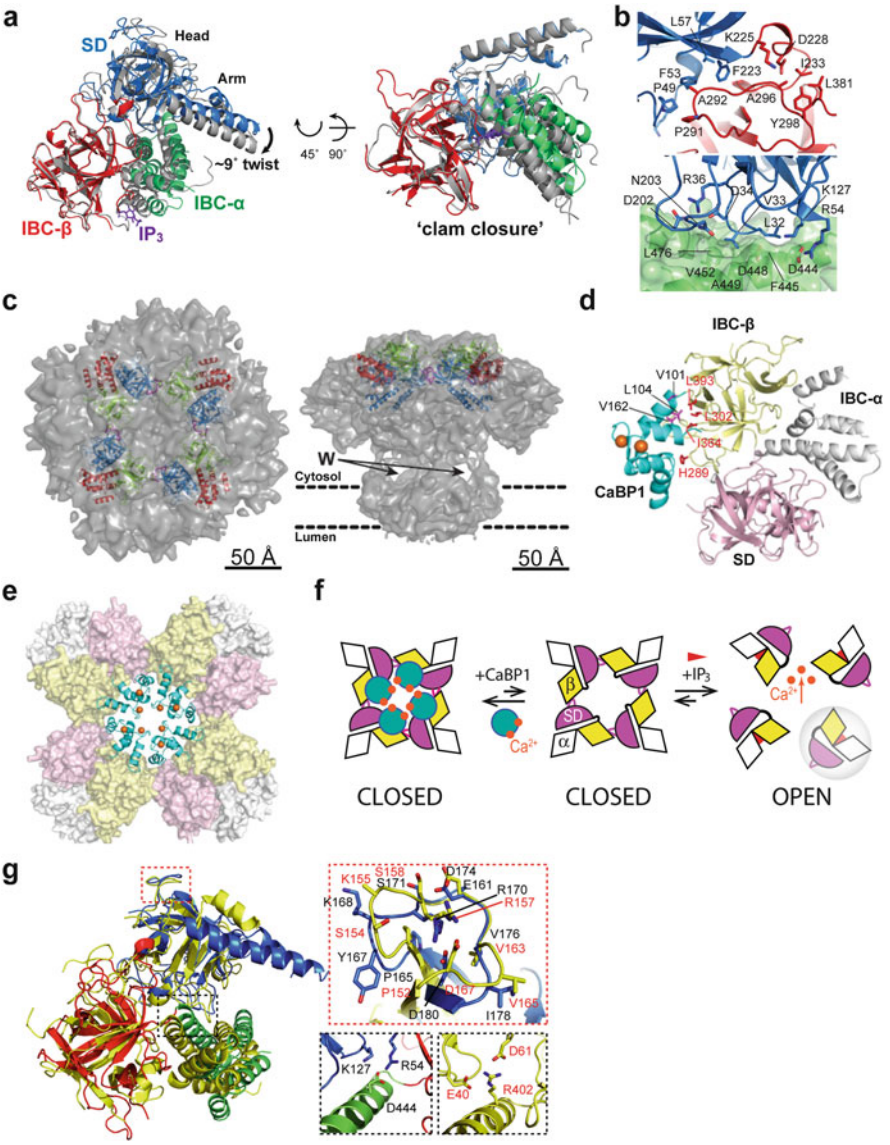

Fig. 10.1 Structural features of IP_3R-NTD region. (**a**). Superimposed apo-NTD and (SD, blue; IBC-β, red; IBC-α, green) and IP_3-bound NTD (gray) structures. The structures are aligned by overlapping the IBC-β. (**b**). The two interfaces between the SD and IBC domains (colored as in *A*). The β-interface (top) and α-interface (bottom) are shown. (**c**). 17.5 Å cyo-EM electron density map of IP_3R1 in the closed state (EMDB code EMD-5278) is shown from top (left) and side (right) views. Docked crystal structures of IP_3R1-NTD (PDB code 3UJ0) are shown as ribbon representation with SD in blue, IBC-β in green and IBC-α in red. The HS-loop in the SD is colored magenta. The windows of IP_3R1 are indicated with arrows. The membrane bilayer boundaries are depicted with broken lines. (**d**). The structure of the C-lobe of CaBP1 (CaBP1-C) bound to IP_3R1-NTD in a 1:1 complex. NMR structural restraints were used to define contacts between IP_3R1-NTD (SD, pink; IBC-β, yellow; IBC-α, gray) and CaBP1-C (cyan, with Ca^{2+} atoms colored orange). Key residues at the binding interface are highlighted in magenta (CaBP1-C) and red (IP_3R1). (**e**). Model

two discrete interfaces (i.e. β-interface and α-interface, respectively) (Fig. 10.1a). The short β-interface (Fig. 10.1b, top) consists predominantly of hydrophobic interactions between Pro49, Phe53 and Phe223 from the SD and Pro291 and Ala292 from the IBC-β, and is supported by a salt bridge between Lys225 and Asp228. The longer α-interface (Fig. 10.1b, bottom) is stabilized by hydrophobic interactions between Val33 in the SD and a pocket formed by Val452, Phe445, Ala449 and Leu476 within the IBC-α. Electrostatic interactions between Arg54 and Lys127 from the SD and Asp444 from the IBC-α also contribute to the stability of the α-interface. The functional importance of residues associated with the α-interface is demonstrated by the Val33Lys mutation, which almost completely abolishes the effects of the SD on IP_3 binding and attenuates the maximal open probability of the full-length channel [55, 66].

10.2.1 IP_3-Induced Receptor Activation

The structural comparison of NTDs in the absence and presence of IP_3 reveals the IP_3 binding-induced conformational changes that are essential for channel activation (Fig. 10.1a). The most significant structural change induced by IP_3 binding is the domain reorientation between IBC-β and IBC-α, resulting in partial closure of the IP_3-binding cleft. Remarkably, the interactions forming the α-interface are completely maintained after IP_3 binding, while the β-interface is disrupted resulting in a slight increase in the distance between the SD and IBC-β. Additionally, the SD rotates towards the IBC, and the direction of swing is nearly perpendicular to the closure of IBC. These studies further refined our understanding of the IP_3-evoked conformational changes which occur within NTD and suggested that the rotational movement of the Tyr167-containing critical loop in SD with respect to IBC-β is an initial step of the key conformational coupling with the channel domain for its activation [52].

Fig. 10.1 (continued) for the tetrameric IP_3R1/CaBP1-C complex (colored as in *D*) generated by superimposing IP_3R1-NTD crystal structure onto the 17.5 Å cyo-EM electron density map of IP_3R1 (EMDB code EMD-5278). (**f**). Interactions between adjacent IP_3R1-NTDs that are mediated by IBC-β (yellow) and the HS-loop of the SD (magenta) hold the tetrameric $InsP_3R1$ in a closed state. IP_3 binding closes the clam-like IBC, disrupting these intersubunit interactions and allowing the channel to open. CaBP1clamps the intersubunit interactions associated with the closed state, thereby inhibiting channel opening. (**g**). Comparison of the IP_3R1-NTD and RyR1-ABC (yellow). The structures are aligned by overlaying IBC-β and the domain B of RyR1. HS-loops in IP_3R1 and RyR1 are highlighted with a red rectangle, and the conserved residues are represented as sticks at top right (IP_3R1, black lettering; RyR1, red lettering). The α-interface of IP_3R1 and the corresponding interface in RyR1 are boxed with a black rectangle, and the preserved salt bridges are depicted in a bottom right. The figures in *A–C* and *G* are reproduced from [52] and *D–F* are reproduced from [63] with permission

Docking the atomic-resolution structures of IP_3R1-NTD into a 17.5 Å resolution full-length cryo-EM structure of IP_3R1 (EMDB code EMD-5278) [67, 68] showed that the NTD forms a tetrameric ring around a fourfold symmetry axis, with the loop containing residues 165–180 of IP_3R1 involved in intersubunit interactions (Fig. 10.1c). Importantly, Li et al. produced covalently linked tetrameric IP_3R1-NTD through site-specific cysteine insertions in the intersubunit interface that was modeled in docking studies and demonstrated that IP_3 inhibits production of cross-linked tetrameric IP_3R1-NTD in a dose-dependent manner [63]. These observations suggest that IP_3-binding closes the clam-like IBC and thereby disrupts these intersubunit interactions, allosterically regulating the ion channel conductance [63].

In 2013, the structure of IP_3R1-NTD in complex with calcium binding protein 1 (CaBP1) [69–72] was determined using nuclear magnetic resonance (NMR) spectroscopy-based chemical shift perturbation mapping and paramagnetic relaxation enhancement (PRE) data [63]. The complex structure showed that exposed hydrophobic residues in Ca^{2+}-bound CaBP1 interact with clustered hydrophobic residues in the IBC-β domain of IP_3R1 (Fig. 10.1d). Superimposition of the IP_3R1-NTD/CaBP1 complex with the tetrameric IP_3R1-NTD revealed that the four molecules of CaBP1 form a ring-like structure around the central cytosolic vestibule (Fig. 10.1e). Further, chemical cross-linking experiments demonstrated that CaBP1 enhances the production of tetrameric IP_3R1-NTD on denaturing gels [63]. The studies suggest that Ca^{2+}-bound CaBP1 clamps the intersubunit interactions and thereby inhibits channel opening (Fig. 10.1f) [63].

Ryanodine receptors (RyRs) are IP_3R-related Ca^{2+} release channels located on the sarcoplasmic reticulum (SR) of excitable cells such as cardiac and skeletal muscle [73–78]. However, instead of being responsive to the IP_3 diffusible messenger, RyRs open in response to local cytoplasmic Ca^{2+} rises or direct coupling to L-type Ca^{2+} channels on the PM in cardiac and skeletal cells, respectively [2–6, 79]. The structure of IP_3R1-NTD can be superimposed on the corresponding N-terminal domain of RyR1, termed the ABC domain where the A, B and C domains are akin to the IP_3R SD-IBC region(PDB code 2XOA) [80] with a relatively low root mean square deviation in the backbone atoms (i.e. <3 Å). The relative orientation of the three domains is almost identical (Fig. 10.1g). The IP_3R1-NTD and RyR1-ABC sequence identity and similarity are low (i.e. 17% and 37%, respectively); however, the sequence and structure of the functionally important loop regions in the two N-terminal regions are conserved [52, 81–86]. Particularly, the backbone and side-chain conformation of the hot-spot (HS)-loop which is essential for IP_3Rs channel gating is homologous to that of RyR (Fig. 10.1g, red box). The HS-loop is so named due to the high frequency of cardiovascular disease-related mutations mapped to this motif in RyRs [80, 82, 87, 88]. The structural conservation between IP_3R1-NTD and RyR1-ABC is readily obvious at the interfaces of the three domains: the salt bridges stabilizing the α-interface of IP_3R1 (i.e. Arg54/Lys127 and Asp444 of IP_3R1) are conserved in the A–C interface of the RyR1-ABC (i.e. Glu40/Asp61 and Arg402 of RyR1), although with a reversal of charges (Fig. 10.1g, black boxes). Remarkably, this high conservation of the key domains between IP_3R and RyR transcends the structure. A chimera in which the SD of IP_3R1 was swapped with the RyR1-A

domain maintains the ability to assemble into a functionally competent tetrameric channel with similar IP_3 sensitivity and magnitude of Ca^{2+} release as wild-type IP_3R1 in live cells [52]. Additionally, a chimera in which the transmembrane channel domain (TMD) and C-terminal domain (CTD) of IP_3R1 were replaced with the counterparts from RyR1 was functionally capable of releasing Ca^{2+} from the ER in response to IP_3 [52]. These studies revealed a remarkably high structural and functional conservation between IP_3R and RyR in the key domains (i.e. ligand-binding NTD and transmembrane domain).

While it has been a challenge to crystallize the full-length IP_3R molecule, cryo-EM technology recently introduced the first near atomic-resolution picture of the enormous IP_3R [89]. In 2015, Serysheva and coworkers determined a ~4.7 Å cryo-EM structure of the full-length IP_3R1 in the closed state (PDB code 3JAV, EMDB code EMD-6369) [89]. At this resolution, the authors were able to trace approximately 85% of the protein backbone and define the domain architecture of the full-length IP_3R1. The structural details of the full-length IP_3R1 elucidated by Serysheva and coworkers are discussed elsewhere in this book. Recently, the crystal structures of the large N-terminal cytoplasmic fragments of IP_3R1 in apo- and IP_3-bound states corresponding to residues 1–1585 and 1–2217 in mouse IP_3R1, respectively, were determined in a monomeric form at 5.8–7.4 Å resolution (PDB code 5GUG, 5X9Z, 5XA0 and 5XA1) [90]. These structures confirmed the domain architecture of the N-terminal cytoplasmic domains proposed by the 4.7 Å cryo-EM structure (Fig. 10.2a), although these crystal structures revealed large differences in relative orientations of the domains compared to those of the tetrameric cryo-EM structure. These differences may be due to the nature of the isolated monomeric form and/or crystal packing. Nevertheless, comparison between apo- and IP_3-bound crystal structures of the large N-terminal cytoplasmic domains uncovered an IP_3-mediated conformational curvature of the α-helical domains (Fig. 10.2b).

10.2.2 Allosteric Regulation of Channel Gating by IP_3

Based on the cryo-EM structure of the intact IP_3R channel in the closed state, what can we speculate about the channel gating mechanism? First, the gating must involve a long-range communication between the ligand binding domain and the TMD. Given the spatial distance between the IP_3-binding domain and the ion-conduction pathway, there must be a coupling mechanism for transmission of ligand-evoked signals to the channel pore to conduct a ligand-binding specific gating. The latest 4.7 Å cryo-EM structure of IP_3R1 suggests allosteric modulation of IP_3R gating by IP_3-binding could occur via discrete intra- and inter-subunit interfaces. Specifically, the helix-turn-helix arm motif of the SD, which is also termed β-trefoil 1 (β-TF1; Fig. 10.2c), likely interacts with the armadillo solenoid repeat 3 (ARM3) within the adjacent subunit; the HS-loop of β-TF1 (i.e. residues 165–180) is positioned to interact with non-contiguous regions of the IBC-β, which is also termed β-trefoil 2 (β-TF2), of the adjacent subunit including residues 246–248, 373–376, 387–389

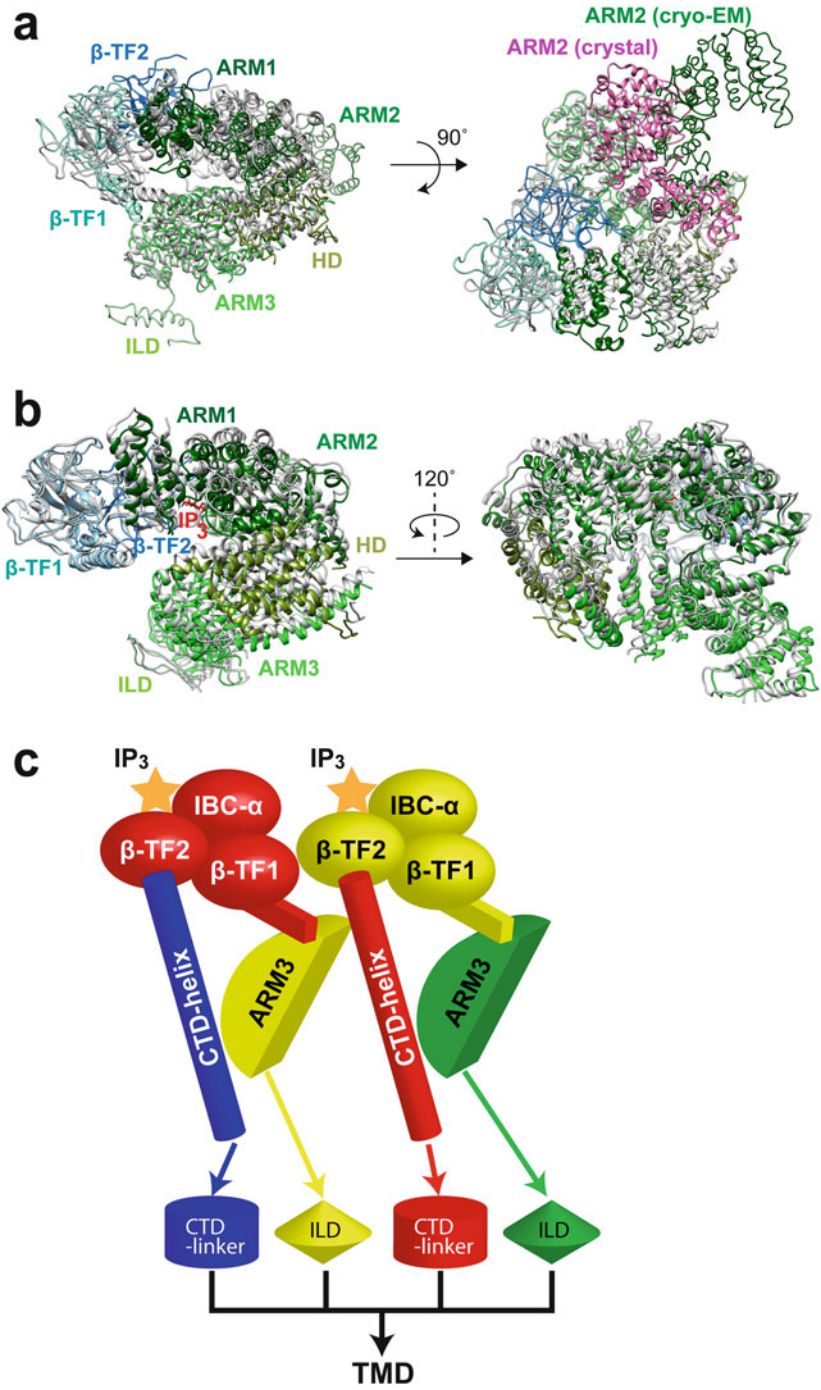

Fig. 10.2 Near high-resolution structures of the large IP_3R1 N-terminal domains in the closed state. (**a**). Superimposition of the 7.3 Å crystal structure of the residues 1–2217 of mouse IP_3R1 (IP_3R1-2217) (PDB code 5X9Z) with the 4.7 Å cryo-EM IP_3R1 structure in the closed state. The structures

and 426–429; the β-TF1 loop (i.e. residues 136–139) forms additional inter-subunit contacts of the ARM2 domain; the CTD of one subunit interacts with the β-TF2 within the adjacent subunit.

The cryo-EM densities comprising these contact sites are not resolved well enough to authenticate these proposed physical interactions; however, a series of previous reports of biochemical data and/or functional consequences of point or deletion mutations support the notion that these interfaces play significant roles for IP_3R channel gating. First, β-TF1 domain deletion mutants of IP_3R1 do not exhibit any measurable IP_3-evoked Ca^{2+} release [91]. Further, a single mutation within the HS-loop (i.e. Tyr167Ala) abrogates IP_3-evoked Ca^{2+} release without affecting the IP_3 binding affinity [65]. Additionally, production of covalently linked tetrameric IP_3R1-NTD by introducing cysteine substitutions at Leu169 within the HS-loop and Thr373 within β-TF2 is attenuated by IP_3 [63]. Deletion of 43 residues or more from the CTD-helix disrupts IP_3-evoked Ca^{2+} release [92]. Remarkably, a chimeric channel in which the CTD-linker and CTD-helix domains of IP_3R1 are swapped with the CTD of RyR1 lacking CTD-helix, exhibits significantly decreased IP_3 efficacy [52]. Collectively, a model for allosteric regulation of IP_3R channel gating by IP_3 is proposed (Fig. 10.2c). One propagation pathway is from the β-TF2 to the CTD-helix/CTD-linker domains of the adjacent subunit via the β-TF2:CTD-helix interface. Another pathway is from the β-TF1 to the ARM3/intervening lateral domain (ILD) via the β-TF1:ARM3 interface. Both transmissions further propagate to the TMD via direct connection between the CTD-linker/TMD and the ILD/TMD. In this scenario, binding of a single IP_3 molecule to one subunit can trigger a cascade of conformational change in two neighboring subunits to propagate the IP_3-evoked activating signal to the ion-conducting pore [93–96]. Elucidating the precise atomic-resolution gating mechanism of IP_3R requires higher-resolution structure determination of both closed and open states of the full-length IP_3R. Further, the crystal and cryo-EM structures provide only static snapshots of these structural states, while molecular motions underlie all regulatory mechanisms. Thus, conformational dynamics studies will also be key to increasing our understanding of the structural mechanisms of IP_3R function [97].

Fig. 10.2 (continued) are aligned by minimizing the backbone atom root mean square deviation of the ARM3 domain. The TMD, CTD-linker and CTD-helix domains in the 4.7 Å cryo-EM IP_3R1 structure are not shown. (**b**). Comparison of IP_3R1-2217 structures in the apo (colored; 7.3 Å, PDB code 5X9Z) and IP_3-bound (gray; 7.4 Å, PDB code 5GUG) states. The structures are aligned by superposing the N-terminal β-TF1/SD and β-TF2/IBC-β domains (residues 7–430). (**c**). Schematic representation of the proposed inter-subunit interactions involved in propagation of IP_3-binding signal to the ion-conducting pore (color-coded by subunit): from β-TF2 to CTD-helix/linker domains and from β-TF1 to ARM3/ILD domains of adjacent subunits. Panels *a–b* and *c* are reproduced with permission from [89, 90], respectively

10.3 STIM1/2 EF-SAM Structure and Function

The ER/SR-resident STIMs and the PM Ca^{2+} channel Orai proteins are the two major players of SOCE [34–36, 39, 40, 42, 98]. STIMs are single-pass transmembrane protein that sense the changes of ER luminal Ca^{2+} levels (Fig. 10.3a) [34, 35, 98, 103–105]. Upon Ca^{2+} store-depletion, STIM proteins undergo oligomerization and translocation to ER-PM junctions (i.e. known as puncta formation), which concomitantly attracts the PM resident Orai to the same junction and allows the two proteins to directly interact, leading to channel activation [98, 106–108]. The entire activation process initiated by the ER Ca^{2+} store-depletion involves multi-step, sequential structural transitions in those proteins that traverse over two membrane layers as a complex [99, 100, 109–112]. High resolution tertiary structures from NMR and X-ray crystallography and the concerted molecular and cellular level studies of those proteins have provided the mechanistic insights to build the current molecular model of SOCE.

The first structural contribution towards elucidating the molecular machinery of SOCE was brought by an NMR structure of the luminal EF-SAM domain of human STIM1 in Ca^{2+} bound form (i.e. quiescent state) [113]. It revealed that the luminal Ca^{2+} sensing domain is made up by a unique packing of two well-characterized ubiquitous structural motifs: EF-hand and sterile α motif (SAM) domains. However, the manner of packing between the EF-hand and SAM domains was the first such example found in nature, where the EF-hand pair consisting of a Ca^{2+} binding canonical EF-hand (cEF) and a non-canonical EF-hand (ncEF), which does not bind Ca^{2+}, form an extensive hydrophobic cleft which interacts with the 5th helix of the SAM domain (i.e. α10 of EF-SAM) (Fig. 10.3b). This α10 helix is centered in the EF-hand cleft with Leu199 and Leu203 hydrophobic side chains acting as anchor residues protruding into the cleft (Fig. 10.3b). Earlier, it had been shown that Ca^{2+} chelation (i.e. Ca^{2+} depletion) causes the isolated EF-SAM to undergo partial unfolding coupled dimerization/oligomerization and also that each isolated domain (i.e. cEF-ncEF and SAM) fails to form stable monomers [99, 113, 114]. Thus, the structure provided atomic level insights of how STIM1 is protected from activation. Indeed, mutations that destabilize the EF-hands or EF-hand:SAM domain interactions suggested by the structure promote di/oligomerization of EF-SAM [113]. Incorporating those mutations in the full length STIM1 expressed in cells resulted in puncta formation, independent of ER Ca^{2+} levels and constitutive SOCE activation [113]. Collectively, these data revealed the vital importance of EF-SAM stability mediated by the EF-hand:SAM domain intramolecular interaction in SOCE regulation.

Vertebrates express a second STIM homologue (i.e. STIM2) [115]. Although STIM1 and STIM2 both detect decreases of ER luminal Ca^{2+} via their luminal domain and activate Orai with the cytosolic domain machinery, the sensitivities to the luminal Ca^{2+} levels and the consequent CRAC activation is distinct [34, 35, 98, 116, 117]. STIM2 is highly sensitive to small changes in luminal Ca^{2+} levels due to a lower Ca^{2+} affinity, but only mediate relatively small CRAC currents [118] which leads to a smaller amount of Ca^{2+} influx into the cytosol [117, 119]. Thus, STIM2 is

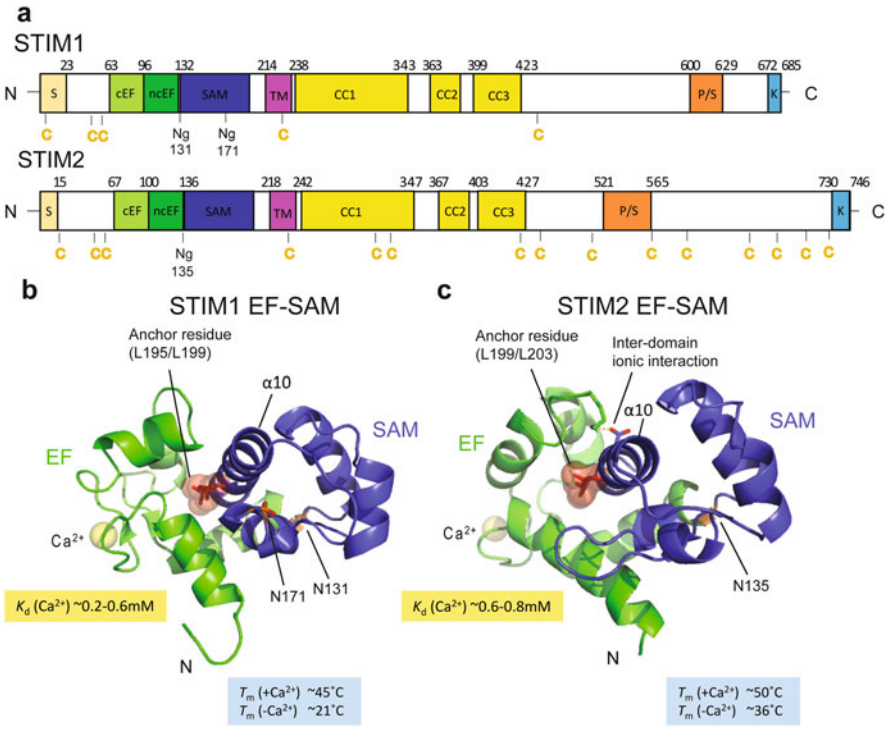

Fig. 10.3 Domain architecture and tertiary structure of the luminal domain of human STIM1 and STIM2. (**a**). Domain architecture of human STIM1 and STIM2. Abbreviation for the domains are as follows: S, signaling peptide sequence; cEF, canonical EF-hand; ncEF, non-canonical EF-hand; SAM, sterile α-motif; TM, trans-membrane region; CC1–CC3, coiled-coil regions 1, 2 and 3, respectively; P/S, Pro/Ser rich region; K, Lys-rich (poly-K) region. *N*-glycosylation sites (Ng) are shown with residue number. Cys residues (C) that are potentially oxidized under oxidative stresses are also shown. (**b**). NMR structure of Ca^{2+}-bound human STIM1 EF-SAM domain (PDB: code 2K60). The mutual folding of the two domains is centered on the anchor residues (L195/L199 shown in red spheres) of the SAM domain (blue). These anchor residues reside in the hydrophobic cleft formed by the EF-hands (green). *N*-glycosylation sites (N131 and N171) that destabilize the EF-SAM domain are shown in orange sticks. (**c**). NMR structure of the Ca^{2+}-bound form of human STIM2 EF-SAM domain (PDB code 2L5Y). The domain packing between EF-hands and SAM domains is maintained by an extended hydrophobic (centered around L199/L203 shown in red spheres) and ionic interactions (K103/D200 shown with stick representations). A putative *N*-glycosylation site (N135) is shown with an orange stick. In *B* and *C*, the estimated Ca^{2+} equilibrium dissociation constants (K_d) and apparent midpoints of temperature denaturation (T_m) are from [99–102]. The Ca^{2+} ion is shown as a yellow sphere

considered a feedback regulator that functions to maintain basal Ca^{2+} levels by regulating small Ca^{2+} fluctuations [117], while STIM1 is a robust ON/OFF regulator of SOCE [34, 35]. In vitro studies of STIM2 EF-SAM have also demonstrated a higher thermostability than the corresponding STIM1 domain monitored by far-UV circular dichroism; consistent with this enhanced stability of STIM2 EF-SAM

compared to STIM1, the STIM2 homologue demonstrates slower oligomerization kinetics induced by the Ca^{2+} chelation, as monitored by static light scattering [101]. Although the higher structural stability of STIM2 EF-SAM was initially somewhat puzzling due to the contradictory lower Ca^{2+} affinity, the tertiary structure of STIM2 EF-SAM provided a structural rationalization for these observations [102]. The structure revealed that STIM2 EF-SAM is formed by extended hydrophobic and ionic interactions compared to STIM1 EF-SAM, thus endowing more tolerance to external perturbations. The hypothesis that linked EF-SAM stability to STIM function was tested further with the engineering of chimeras.STIM1/STIM2 EF-SAM fusions were created by the segmental shuffling of the first and second EF-hands (i.e. EF1 and EF2) and the SAM domains [102]. Thermostability analyses revealed the creation of hyperstable (i.e. super-stable) and the unstable (i.e. super-unstable) species compared to the wild-type homologues using this chimeric approach. A combination of EF1 of STIM1 with EF2 and SAM of STIM2 (i.e. referred as ES122) and EF1 of STIM2 with EF2 and SAM of STIM1 (ES211) resulted in the super-stable and unstable sensors, respectively. When these chimeric EF-SAM domains were incorporated in the full-length STIM1, the mutant with the super-unstable EF-SAM (i.e. ES211) induced constant Ca^{2+} influx irrespective of ER luminal Ca^{2+}, whereas the mutant with the super stable EF-SAM caused a significant delay in the generation of maximal CRAC currents after ER Ca^{2+} depletion [102]. These data unequivocally linked structural stability of the luminal EF-SAM domain with the regulation of SOCE. Post-translation modification of STIM1 can influence the stability of EF-SAM. Specifically, STIM1 can undergo *N*-glycosylation at Asn131 and Asn171 of the SAM domain [103, 105]. Mimicking this glycosylation in vitro was found to reduce Ca^{2+} affinity and thermal stability compared to wild-type, thereby enhancing oligomerization propensity of the domain [120]. Consistent with these in vitro results using isolated EF-SAM domains, expression of an *N*-glycosylation blocking mutant (i.e. Asn131Gln/Asn171Gln) version of full-length STIM1 diminished SOCE Ca^{2+} influx compared to wild-type [120, 121].

The EF-SAM domains are well conserved between STIM1 and STIM2 with ~60% sequence identity. In contrast, the preceding N-terminal regions are quite variable. Although no structural motif is predicted based on sequence, inclusion of the N-terminal sequences (i.e. 40 and 52 additional residues for STIM1 and 2, respectively) stabilizes the luminal domain compared to EF-SAM alone, as indicated by enhanced melting temperatures for both Ca^{2+} bound and unbound forms by ~+15 °C [101]. A pair of Cys residues in this otherwise highly variable N-terminal region are highly conserved among vertebrates. These Cys (i.e. Cys49 and Cys56 in STIM1) are two of the few residues that are conserved between STIM1 and 2 in this N-terminal region. In STIM1, Cys56 was reported to undergo *S*-glutathionylation [122], and Cys49:Cys56 were shown to form an intramolecular disulfide bridge [123] under oxidative stress introduced by hydrogen peroxide or buthionine sulfoximine (BSO). Both these modifications were shown to promote SOCE activation [122, 123]. Although the structural mechanism of the enhanced stability introduced by the non-conserved N-terminal residues has yet to be elucidated, it is likely that Cys oxidation affects the interaction between the N-terminal residues and the

EF-SAM core, which modulates the Ca^{2+} affinity and/or domain stability, thereby modulating SOCE activity.

Initiation of SOCE is facilitated by dimerization and/or oligomerization of STIM proteins in the luminal domains [99, 107, 124]. Furthermore, the overall Ca^{2+} influx (the outcome of the SOCE activation) correlates with the structural stability of the same luminal EF-SAM domain [102]. It should be noted that the structural stability of EF-SAM will also influence the homomeric assembly/disassembly rates which dictates SOCE activation. Vertebrates use the two distinct architectures of STIM1 and STIM2 EF-SAM to sense a wider range of Ca^{2+} depletion and to affect distinct Ca^{2+} signaling outputs. This fine-tuned Ca^{2+} depletion response is achieved by combining EF-hands [125–127] and SAM domains [128–133] with opposing properties within each of the protein: STIM1 has a higher affinity EF-hand domain combined with a low stability SAM domain; STIM2 has a lower affinity EF-hand domain combined with a high stability SAM domain. Additionally, recent studies show that cells further tune SOCE regulation by natural chemical post-translational modifications such as glycosylation [105, 120, 121, 134–136] or Cys thiol oxidation [122, 123] at the luminal domain of STIM proteins.

10.3.1 STIM1 Coiled-Coil Domain Structure and Function

STIM1 contains three coiled-coil domains (i.e. CC1-CC2-CC3) in the cytosolic region of the protein (Fig. 10.3a), which each play different roles in regulating SOCE. While the luminal STIM domains sense the changes in Ca^{2+}, the cytosolic coiled-coil domains are the effector machinery which transduce the sensing into Orai1 activation. CC1, the first of the three conserved domains, encompasses residues 238–337 and has an elongated α-helical structure spanning ~13 nm in length [137]. This extended conformation bridges the bulk of the distance between the ER membrane and the PM, effectively allowing STIM1 to interact with Orai1 channels on the opposite membrane [138–140]. Isolated CC1 fragments tend to dimerize, and structural analysis has highlighted several intermolecular forces which promote this self-association [137]. CC1 homodimerizes in an antiparallel manner with hydrophobic interactions occurring between Leu335, Leu328, Val324 and Ala317 of one subunit and Leu286, Ile290, Ala293 and Leu300 of the corresponding partner subunit. Furthermore, H-bonding occurs between Leu303, Arg304 and Thr307 of one subunit and Glu310 and Gln314 of a parallel subunit, while an ionic bond occurs between Arg304 and Glu318 (Fig. 10.4a).

CC2 and CC3 encompass residues ~363–423 which are within the STIM-Orai activating region (SOAR) [141] also known as the CRAC activating domain (CAD) [142] or coiled-coil boundary 9 (ccb9) [142], the minimal region of STIM1 capable of coupling to and activating Orai channels. An atomic-resolution structure of vital STIM1 region has been determined using a Leu374Met/Val419Ala/Cys436Thr triple mutant SOAR construct [143]. This mutant SOAR also forms a dimer with each monomer resembling an upper case "R"-like structure containing four

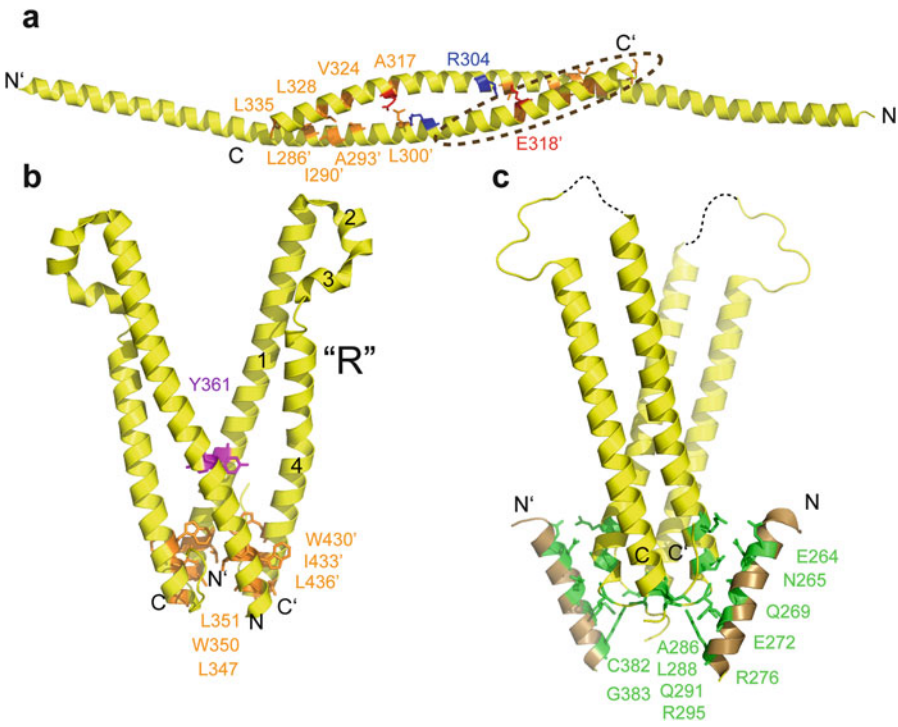

Fig. 10.4 STIM coiled-coil structures in the absence of Orai. (**a**). X-ray crystal structure of human STIM1 CC1 residues ~247–336 (PDB code 4O9B). This human CC1 structure consists of an elongated α-helix which spans ~13 nm. The residues involved in hydrophobic interactions between the C-terminal regions are indicated (orange sticks). Similarly, an intermolecular ionic interaction between the helices is shown between R304 (blue stick representation) and E318 (red stick representation). Note that the precise physiological significance of these intermolecular interactions are not known; however, the tendency for antiparallel interaction between the C-terminal region of CC1 was also revealed in the NMR structure of $CC1_{[TM\text{-}distal]}$–CC2 (see Fig. 10.5). The C-terminal region of CC1 shown to be modulatory in STIM1 function is indicated with a brown dashed ellipse. (**b**). X-ray crystal structure of human SOAR domain (PDB code 3TEQ). This human CC2–CC3 structure is composed of two "R" shaped monomers. The hydrophobic interactions (orange stick representation) and Tyr stacking (magenta stick representation) identified in the crystal structure is shown. The four helices which make up the "R" shaped architecture are labeled on CC2 (1) and CC2 (2, 3, 4). (**c**). X-ray crystal structure of *C. elegans* SOAR extended to include the C-terminal CC1 region (brown) (PDB code 3TER). The residues that make up the H-bond network which pack the CC1 helix (brown) against the core SOAR domain (yellow) are shown (green stick representations). In *A–C* only the most prominent forces which mediate the protein–protein interactions are shown. The location of the amino and carboxyl termini are indicated by (N) and (C), respectively

α-helices: two α-helices located adjacent to the N- and C-terminus, respectively, and two shorter α-helices running antiparallel relative to each other and positioned between the terminal helices (Fig. 10.4b). The dimerized SOAR monomers form a V-shape quaternary structure with several complementary intermolecular interactions stabilizing the dimer state. First, residues Leu347, Trp350 and Leu351 of a

single subunit hydrophobically interact with Leu436, Ile433, and Trp430 of the partner subunit. Furthermore, Arg429 of one subunit forms an H-bond with Thr354 of the second subunit, and Tyr361 residues form stacking interactions between each monomer (Fig. 10.4b).

A *Caenorhabditis elegans* version of SOAR which was extended to include a C-terminal portion of the CC1 domain was also solved by X-ray crystallography. This C-terminal CC1 region, corresponding to residues 310–337 on human STIM1, has been termed the inhibitory helix (IH) since studies suggest it plays a role in keeping STIM1 in a compact, dormant state at rest [143, 144] (Fig. 10.4c). The *C. elegans* crystal structure of this extended version of SOAR shows that the IH CC1 helix interacts with the core SOAR domain via Glu264, Asn265, Gln269, Glu272 and Arg276 H-bonding with Ala286, Leu288, Gln291, Arg295, Gly383 and Cys382 of *C. elegans* SOAR. Additionally, hydrophobic interactions between Val286 of the IH and Pro385 of the core SOAR domain contribute to the interaction stability. Interestingly, deleting the corresponding IH region of the human homologue constitutively activates STIM1, independent of ER Ca^{2+} store depletion [143], and several mutations have been identified which both promote and inhibit this inhibitory function [109, 143–145]. Given that sequence variations of this CC1 region can facilitate both activation and inhibition of SOCE, a "modulatory domain" nomenclature is better suited to the demonstrated functional role.

10.3.2 Drosophila melanogaster *Orai Crystal Structure and Function*

In cellular Ca^{2+} regulation, Orai1 is the subunit component which assembles into CRAC channels and mediates SOCE. While high resolution structural information of any human Orai homologue at the level of the assembled channel remains elusive, X-ray crystallography was used to solve the crystal structure of the *D. melanogaster* Orai homologue which shares >70% sequence similarity with human Orai1 within the transmembrane (TM) regions [146]. Intriguingly, the crystal structure revealed that a single *D. melanogaster* Orai channel exhibits a hexameric quaternary structure which is contrary to several previous studies which suggested human Orai1 assembles as a tetramer [138, 147–149]. The TM helices (i.e. M1–M4) in this crystal structure are arranged in concentric rings such that the innermost core is formed exclusively by M1 of each of the six subunits. M2 and M3 directly surround M1, with the M1 helix extending beyond the lipid bilayer into the cytosol (Fig. 10.5a) [150]. Interestingly, the M2 and M3 positioning around M1 suggests a role in promoting subunit structural integrity for the M2 and M3 helices. The M4 helix also extends into the cytosol and is kinked such that the extension runs parallel to the plane of the inner leaflet. Furthermore, this M4 extension interacts antiparallelly with an adjacent M4 helix which adopts a kink in the opposite direction. Thus, the central pore exhibits a sixfold symmetry, while the peripheral region of the channel shows a threefold symmetry due to pairwise M4 coiled-coil interactions (Fig. 10.5b).

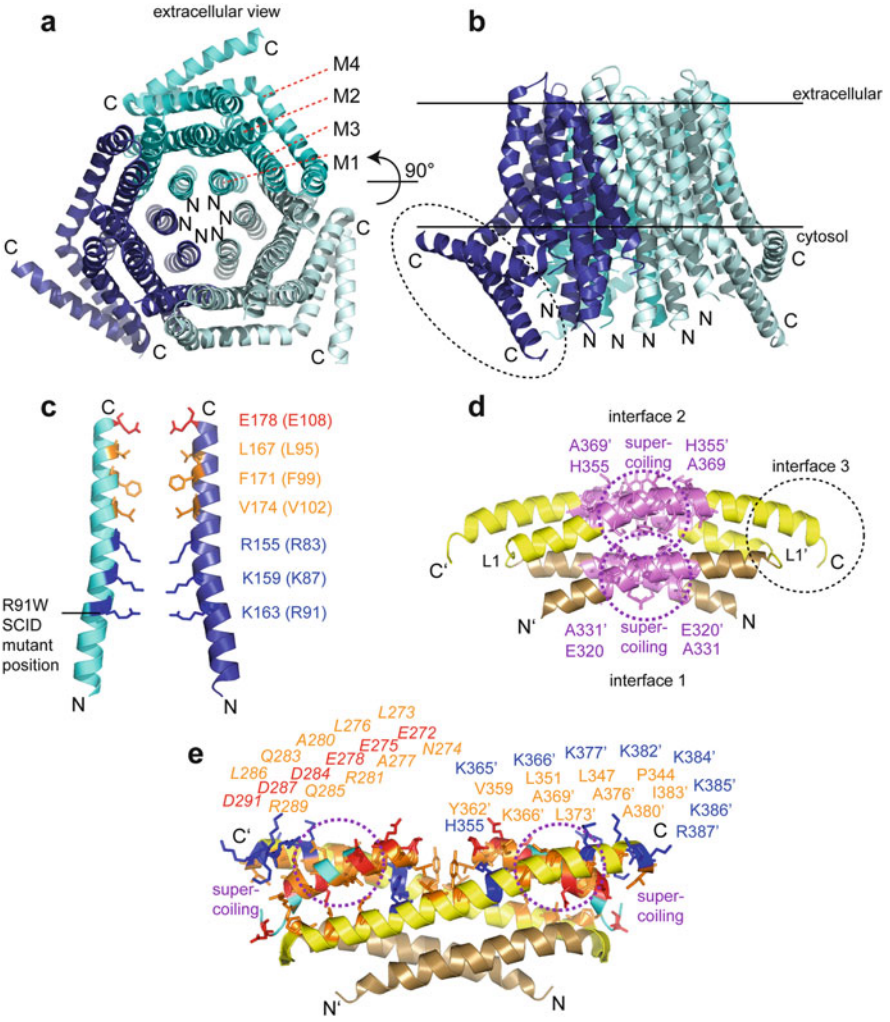

Fig. 10.5 Orai structures alone and in complex with the STIM1 coiled-coil domains. (**a**). Hexameric architecture of *D. melanogaster* Orai (PDB code 4HKR). Each dimer unit within the hexamer is coloured a different shade of blue. The crystal structure shows a sixfold symmetry through the center of the channel made of transmembrane 1 (M1) helices and a threefold symmetry around the outside due to antiparallel interactions of the transmembrane 4 (M4) helices in two different conformations. The packing of transmembrane 2 (M2) and transmembrane 3 (M3) helices relative to M1 and M4 within the monomer is indicated. (**b**). The side view of the channel through the plane of the membrane reveals the extent of the M1 and M4 extensions into the cytosol. The antiparallel C-terminal helix interactions are also evident. (**c**). The pore architecture of *D. melanogaster* Orai consists of an anionic, hydrophobic and basic hierarchy. Only two of the six M1 helices making up the pore (from the six subunits) are shown with the anionic, hydrophobic, basic side chains linking the pore represented as red, orange and blue sticks, respectively. The corresponding human amino acid numbers are given in parentheses beside the fly numbering. (**d**). Human $CC1_{[TM\text{-}distal]}$–CC2 solution NMR structure (PDB code 2MAJ) corresponding to residues 312–387. The three interfaces which stabilize the dimer structure are indicated as the CC1 (brown) supercoiled, CC2 supercoiled region (yellow) and CC2:L1' interface. The residue ranges involved

The pore made up of the six assembled M1 α-helices consists of four major sections based on physical characteristics of the lining residues (Fig. 10.5c). At the extracellular surface lies a glutamate ring that consist of Glu178 (i.e. Glu108 of human Orai1) integral to both Ca^{2+} binding and ion selectivity. Next, a hydrophobic section made up of residues Leu167, Phe171 and Val174 which correspond to Leu95, Phe99, Val102 found in human Orai1 populate the central portion of the pore. The cytosolic/intracellular side of the pore surface has surprisingly basic properties made up of Arg155, Lys159 and Lys163 (i.e. Arg83, Lys87 and Arg91 of human Orai1). Finally, the cytosolic extension of M1 is lined by Gln152 and Trp148 corresponding to Tyr80 and Trp76 of human Orai1. Interestingly, a heritable Arg91Trp mutation in human Orai1 is associated with SCID disease; moreover, the X-ray crystal structure of *D. melanogaster* Orai harboring the Lys163Trp mutation which corresponds to the human Arg91Trp revealed the six introduced Trp residues tightly pack in the M1 cytosolic extension (Fig. 10.5c) [150]. This non-native hydrophobic plug prevents Ca^{2+} ions from traversing into the intracellular side of the channel, and provides a structural mechanism for the loss of function endowed by this mutation and inability for patients with SCID to mount an immune response which dependent on functioning SOCE [37].

10.3.3 STIM1 Coupling to Orai1

One of the reasons STIM1 and SOCE constitute a particularly amenable system to investigate is the remarkable cellular localization and distribution changes which occur after Ca^{2+} depletion. With replete ER Ca^{2+} stores, STIM1 is pervasively distributed in the ER; however, upon ER Ca^{2+} store depletion STIM1 oligomerizes and translocates to sites in close apposition to the PM [107, 124, 139, 140, 151]. The oligomerization initiated by the luminal EF-SAM domain results in a conformational extension of the cytosolic coiled-coil regions, promoting further cytosolic domain homomeric association, culminating in trapping of oligomerized STIM1 at ER-PM junctions [107, 110, 152, 153]. Localization of STIM1 at the PM is the result of

Fig. 10.5 (continued) in the supercoiling are shown as magenta sticks and are labeled. (**e**). Human $CC1_{[TM\text{-}distal]}$–CC2 in complex with the human Orai1 C-terminal peptides corresponding to residues 272–292 (PDB code 2MAK). The CC2 residues which make up the SOAP are indicated in orange and blue stick representations for the hydrophobic and basic residues, respectively. The Orai1 C-terminal peptides (cyan) exhibit acidic (red) and other residues (orange) which complementary pack into the SOAP. The residues which make up the SOAP and the Orai1 residues which pack into the SOAP are labeled only on the right (regular text) and left (italicized text) sides of the structure, respectively. The STIM1 $CC1_{[TM\text{-}distal]}$ and CC2 regions are coloured brown and yellow, respectively, for consistency with Fig. 10.4. The new regions of supercoiling between the Orai1 C-terminal peptides and the CC2 helices are shown with dashed magenta ellipses. In *A*–*E* only the most prominent forces which mediate the protein–protein interactions are shown. The location of the amino and carboxyl termini are indicated by (N) and (C), respectively

interactions of the STIM1 far C-terminal polybasic motif with PM phosphoinositides [154–158] and direct coupling of the STIM1 SOAR region with Orai protein subunits [141, 153, 159]. In fact, studies suggest that STIM1 couples with Orai1 via both the Orai1 M1 and M4 extensions (i.e. C-terminal extension) [141, 153, 159–162]. While the structural basis for STIM1:phosphoinositide interactions remains to be determined, a solution NMR study has provided some atomic-resolution insights into the coupling of STIM1 with the human Orai1 C-terminal extension [144].

Interestingly, the STIM1 fragment used in the complex structure determination was not the CC2–CC3 region which makes up the SOAR/CAD/ccb9 domain, but rather a fragment corresponding to human residues 312–387 which overlaps with the CC1 and CC2 region (i.e. $CC1_{[TM\text{-}distal]}$–CC2, where $CC1_{[TM\text{-}distal]}$ includes the 312–340 stretch and CC2 includes the 341–387 stretch). In the absence of the Orai1 C-terminal peptide, $CC1_{[TM\text{-}distal]}$–CC2 forms a U-shaped dimer structure with each monomer orienting two extended α-helices [i.e. $CC1_{[TM\text{-}distal]}$ (α1)-helix corresponding to residues 312–340 and CC2 (α2)-helix corresponding to residues 345–384] antiparallelly (2MAJ.pdb; Fig. 10.5d). The CC1 and CC2 helices are linked by a short loop (i.e. L1 corresponding to residues 341–343). The symmetric dimers of the $CC1_{[TM\text{-}distal]}$-CC2 segments are formed via CC1: CC1', CC2: CC2' and a C-terminal CC2: L1' interacting interfaces. The CC1:CC1' interface is formed by supercoiling between residues 320–331; similarly, the CC2:CC2' interface is stabilized by supercoiling between residues 355–369. The CC2:L1' interface is made up primarily of hydrophobic packing between residues Ala376, Ala380 and Ile383 on the C-terminal CC2 with Tyr342' and Ala343' of L1' (Fig. 10.5d).

To form active CRAC channels, STIM1 must bind to the Orai1 C-terminal region [141, 153, 159]. A solution structure of human $CC1_{[TM\text{-}distal]}$–CC2 in complex with the human Orai1 C-terminal extension involved in CRAC channel activation consisting of residues 272–292 has been elucidated (2MAK.pdb) [144]. The $CC1_{[TM\text{-}distal]}$–CC2 dimer undergoes three major conformational changes in the formation of a STIM-Orai association pocket (SOAP) which accommodates the $Orai1_{272–292}$ region. First, the $CC1_{[TM\text{-}distal]}$ helices undergo a registry shift; second, the CC2 helices move away from one another to shape an Orai1 binding pocket; third, the C-terminal ends of the CC2 helices erects away from the L1' region through a loss of curvature, allowing access into the CC2-comprised SOAP (Fig. 10.5e). Both polar and non-polar interactions stabilize binding of the $Orai1_{272–292}$ region with $CC1_{[TM\text{-}distal]}$–CC2. Hydrophobic residues on the STIM1 fragment involved in the interaction include Pro344, Leu347, Leu351 and Val359 on the N-terminal side of CC2 in conjunction with Tyr362', Lys366', Ala369', Leu373', Ala376', Ala380' and Ile383' on the C-terminal end of CC2. Orai1 Asn274, Ala277, Arg281, Gln285 and Arg289 residues interact with the N-terminal CC2 region and Leu273, Leu276, Ala280, Gln283 and Leu286 residues interact with the C-terminal CC2'. A basic rim surrounds these hydrophobic residues in the SOAP made up of His355, Lys365' Lys366', Lys377', Lys382', Lys384', Lys385', Lys386' and Arg387'; these basic residues complement the acidic charges of the $Orai1_{272–292}$ region made up of Glu272, Glu275, Glu278, Asp284, Asp287 and Asp291, thereby stabilizing the STIM1:Orai1 association via charge complementarity (Fig. 10.5e).

To gain insight into the precise significance of the interfaces resolved in the STIM1 fragment engineered with the N-terminal boundary outside the vital CAD/SOAR/ccb9 region, a series of mutations were engineered into both the structural construct and full-length STIM1 protein for in vitro biophysical and live cell assessments. A Glu318Gln/Glu319Gln/Glu320Gln/Glu322Gln (4EQ) $CC1_{[TM\text{-}distal]}$ mutant which neutralized the negative Glu charges enhanced both the α-helicity and dimerization propensity of the $CC1_{[TM\text{-}distal]}$–CC2 fragment; moreover, this 4EQ mutant induced spontaneous inward rectifying currents in live cells when engineered into full-length STIM1 and co-expressed with Orai1. Conversely, the Val324Pro CC1 α-helix breaking mutant decreased stability of the $CC1_{[TM\text{-}distal]}$–CC2 fragment, hindered dimerization and suppressed maximal inward rectifying currents [144, 163]. Other $CC1_{[TM\text{-}distal]}$–CC2 dimer destabilizing and basic rim perturbing mutations [i.e. Ile383Arg, Tyr361Lys/Tyr362Lys and Lys382Glu/Lys384Glu/Lys385Glu/Lys386Glu (4KE)] suppressed maximal inward currents. Similarly, charge neutralizing and hydrophobicity perturbing mutations in the $Orai1_{272–292}$ region inhibited CRAC. Ultimately, these mutational studies reinforce the importance of the interfaces resolved in the $CC1_{[TM\text{-}distal]}$–CC2 structures and reveal an important modulatory role for the $CC1_{[TM\text{-}distal]}$ helix overlapping with the previously defined IH (see above) [144, 163].

10.4 MCU Structure and Function

The calcium uniporter holocomplex (uniplex) core protein component, MCU, is an inner mitochondrial dual transmembrane protein connected by a short linker region, with both its N- and C-terminal domains facing the matrix [44, 164]. MCU is the pore forming subunit that mediates Ca^{2+} entry into the mitochondrial matrix [26, 165–167] after assembly into a higher order complex [45, 46]. However, high resolution structural elucidation of this membrane protein remains rather challenging due to its large heteromeric oligomeric state.

Bioinformatic analyses and molecular dynamics modelling predicted a tetrameric organization and a fourfold symmetry for MCU oligomerization [46]. Recent work utilizing a combination of EM and solution NMR has experimentally provided the first structural insights into the pore-forming domains at high resolution (Fig. 10.6a). The hybrid EM/NMR model suggests a pentameric organization for the MCU core [169]. Specifically, negative-stain EM micrographs of *C. elegans* MCU with deleted N-terminal domain (i.e. MCU-ΔNTD) revealed a cylindrical shape with a fivefold symmetry at a resolution of ~18 Å. NMR provided a higher resolution detail of the MCU-ΔNTD oligomer architecture using ~2200 intramonomer and 220 intermonomer distance restraints obtained from nuclear-Overhauser effect measurements [169]. The EM/NMR model was constructed by imposing a fivefold symmetry revealed by the EM. Interestingly, a deep pore-like opening is visible on one end of the cylindrical structure whereas the other end is solid, possibly

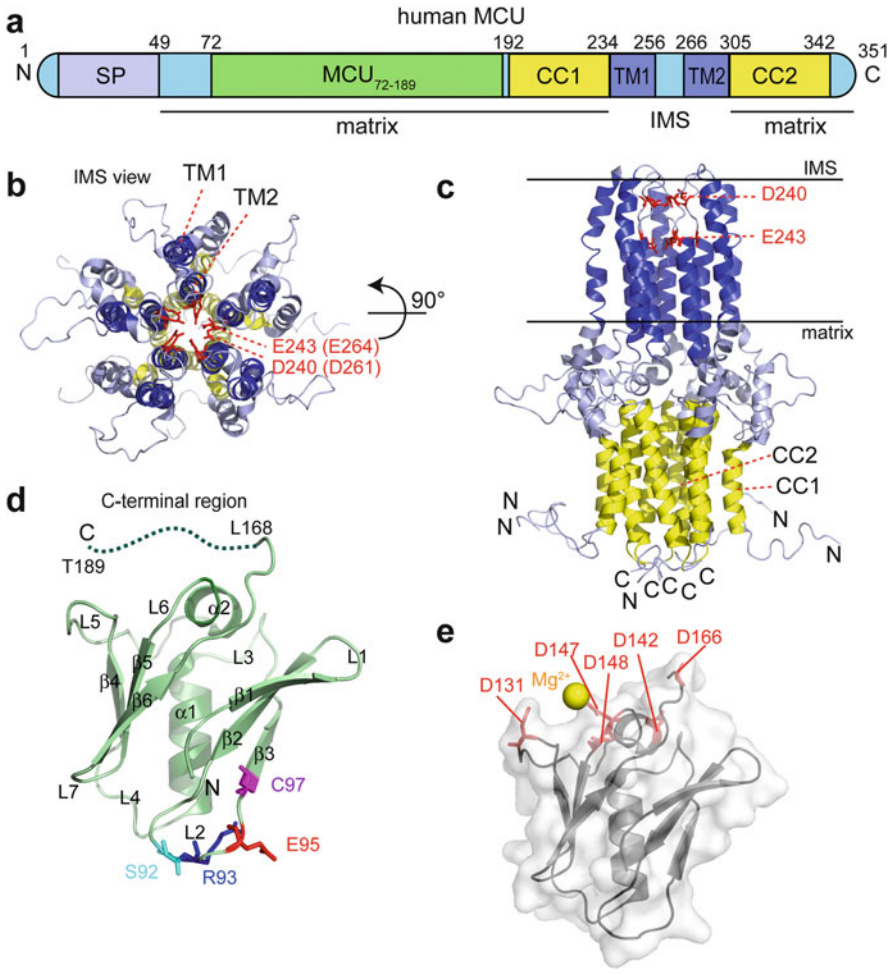

Fig. 10.6 Available high resolution MCU structural data. (**a**). Domain architecture of human MCU (NCBI accession Q8NE86.1). The location of the mitochondrial signal peptide (SP), conserved matrix domain ($MCU_{72–189}$), coiled-coil 1 (CC1), coiled-coil 2 (CC2), transmembrane domain 1 (TM1) and transmembrane domain 2 (TM2) are shown relative to sequence space. The regions of the protein which reside in the matrix and intermembrane space (IMS) are shown below and the residue boundaries for each domain are shown above the architecture diagram. (**b**). Pentameric architecture of an EM:NMR driven hybrid model of the *C. elegans* MCU channel together with the coiled-coil regions (PDB code 5ID3). The relative positions of the TM2 (blue) which lines the pore and TM1 (blue) which packs around the outside of the pore are indicated. The coiled-coil domains (yellow) reside below the TMs in the matrix. The vital D240 and E243 which constitute the DXXE motif at the IMS side of the pore are represented by red sticks. The corresponding human residue numbers are labeled in parentheses. (**c**). The side view of the MCU channel and coiled-coil region through the plane of the inner mitochondrial membrane. The CC2 helices form an interior cluster surrounded by CC1 helices on the matrix side of the membrane. CC1 and CC2 (yellow) are separated from the TMs (dark blue) by juxtamembrane helices (light blue). The location of D240 and E243 are indicated relative to the top and bottom of the inner-mitochondrial membrane. (**d**). X-ray crystal structure of the conserved human MCU matrix domain (PDB code 5KUJ). The $MCU_{72–189}$ region adopts a β-grasp like fold with two, three-stranded β-sheets packing on either

corresponding to the transmembrane domains forming the channel and the CC domains at the C-terminus forming an occlusion, respectively.

At higher resolution, the EM/NMR model showed the second transmembrane helix (i.e. TM2; residues 244–260) forms a hydrophilic inner pore of the channel and is surrounded by the first transmembrane helix (i.e. TM1; residues 215–234) (PDB code 5ID3; Fig. 10.6b). Extending into the matrix is the second coiled-coil helix (i.e. CC2; residues 293–316) that forms a hydrophobic CC bundle just outside the membrane. This CC2 is surrounded by the first CC helix (i.e. CC1; residues 180–193) located in the N-terminal region of MCU-ΔNTD (Fig. 10.6c). The transmembrane domains are not continuous with the CC regions and contain an inner juxtamembrane helix (i.e. IJMH; residues 262–271) and outer juxtamembrane helix (i.e. OJMH; residues 195–213) after TM2 and before TM1, respectively. The EM/NMR model structure also reveals two unstructured loops, one before the CC1 domain (i.e. L1; residues 166–179) and another after the IMJH (i.e. L2; residues 272–292) (Fig. 10.6c). Both the IMJH and OMJH exhibit weak NMR signals due to exchange broadening, suggesting dynamic and/or unstable conformations. The instability may be due to the absence of the NTD. A critical DXXE motif [44, 170] containing two acidic residues links the two TM domains on the inter membrane space-facing side of the membrane. The Asp240 and Glu243 residues of the DXXE have their carboxylic side chains facing the entrance of the pore formed by TMH2. Generation of Asp240Glu or Glu243Asp mutant versions of MCU caused a reduction or complete abrogation of mitochondrial Ca^{2+} uptake in HEK293 cells [169].

The continuous hydrophilic nature of the MCU pore is in contrast to other ion channels like CorA [171] and Orai [150] that consists of several hydrophobic helical turns. This feature may be conducive to the rapid uptake of Ca^{2+} observed by MCU [166, 169].

10.4.1 MCU N-Terminal Domain Structure and Function

Sequence alignment of MCU among eukaryotes reveals a highly conserved region within the matrix-oriented N-terminal domain between residues 75 and 190. This region is omitted in the MCU-ΔNTD studied in the EM/NMR model [169]. The

Fig. 10.6 (continued) side of a central α-helix (α1). The unresolved C-terminal region (i.e. residues 168–189) is shown as a dashed green line. The L2 residues involved in salt bridge formation (R93: E95), susceptible to oxidative modification (C97) and which may undergo phosphorylation (S92) are shown as blue:red, magenta and cyan stick representations, respectively. (**e**). The location of the five Asp residues which confer the formation of the MRAP via the generation of acidic electrostatic surface potential are indicated as red sticks under the transparent surface representation of $MCU_{72–189}$. The Mg^{2+} ion resolved in the high resolution crystal structure is represented by a yellow sphere centrally located around the acidic side chains of D131, D142, D147, D148 and D166. In *A–E* the location of the amino and carboxyl termini are indicated by (N) and (C), respectively. The images in Figs. 10.1, 10.2, 10.3, 10.4, 10.5 and 10.6 were generated using the PyMOL Molecular Graphics System, Schrödinger, LLC and UCSF Chimera [168]

N-terminal domain forms the major soluble region of MCU (Fig. 10.6a). The X-ray crystal structure (1.6 Å) of a human MCU construct corresponding to residues 72–189 has provided high resolution structural insights regarding the role of this highly conserved MCU region in the regulation of mitochondrial Ca^{2+} uptake [172]. Far-UV CD of this $MCU_{72–189}$ construct revealed a mixture of α-helix and β-sheet; accordingly, the crystal structure revealed two central α-helices sitting between two, triple stranded β-sheets, forming an overall β-grasp-like fold (PDB code 5KUJ) (Fig. 10.6d). Arranged in an antiparallel manner, the three β-strands, β1 (i.e. residues 76–80), β2 (i.e. residues 83–88), and β3 (i.e. residues 97–100) form the first of two β-sheets. One long and one short loop, L1 (i.e. residues 81–82) and L2 (i.e. residues 89–96), respectively, connect the three β-strands. The presence of a salt bridge between side chains of Arg93 and Glu95 stabilizes the conformation of L2. Additionally, the close proximity of the salt bridge to the single Cys97 and Ser92, known sites of *S*-glutathionylation and phosphorylation [173, 174], respectively, indicates that this ionic interaction may also play a role in regulating these post-translational modifications. The β3 strand is connected to the central α-helix (i.e. α1; residues 108–118) through loop 3 (i.e. L3; residues 101–107). Similar to the first β-sheet, the second β-sheet also consist of three β-strands, β4 (i.e. residues 125–128), β5 (i.e. residues 149–153), and β6 (i.e. residues 156–160) arranged in an antiparallel manner (Fig. 10.6d). The second β-sheet is located on the C-terminal end of α1 and is connected via loop 4 (i.e. L4; residues 119–124). A short, centrally located α-helix (i.e. α2; residues 141–146) perpendicular to the central α1 connects the β4 and β5 strands. There are long and short loops on either side of α2 (i.e. L5, residues 129–140 and L6, residues 147–148, respectively), linking the helix to the β-strands. A short loop (i.e. L7, residues 154–155) links β5 to β6. The C-terminal region (i.e. residues 168–189) of $MCU_{72–189}$ is dynamic and not resolved in the same crystal structure (Fig. 10.6d) [172]. However, a portion of the C-terminal tail may be stabilized in the presence of lipid-like molecules [174].

The electrostatic surface map reveals a large degree of charge polarity with two distinct negative and two distinct positive regions. A large negative patch near the C-terminal tail is composed of Asp131, Asp142, Asp147, Asp148 and Asp166 [i.e. MCU-regulating acidic patch (MRAP); see below], whereas residues Glu117, Glu118, Asp119, Asp124 and Asp155 makeup the second negative patch closer to the N-terminal region of $MCU_{72–189}$ (Fig. 10.6e). The two patches of basic residues are composed of Arg89, Arg93, Arg94, and Arg96 as well as Arg113, Arg124 and Arg134. The electrostatic surface polarity formed by these patches may assist in higher order assembly of the MCU N-terminal domain [172].

The N-terminal domain has been shown via glutaraldehyde crosslinking, size exclusion chromatography with in-line multi-angle light scattering and analytical ultracentrifugation to independently oligomerize into higher order complexes [172, 174], but the role this oligomerization plays in the regulation of full-length MCU function is yet to be completely understood. Co-immunoprecipitation studies conducted using flag-tagged MCU with a deleted N-terminal domain showed no change in the uniplex assembly [174]. In contrast, using an immuno-enrichment strategy, data for a series of both N- and C-terminal deletions in MCU led to

destabilization of higher order MCU oligomers in HEK293T cells [172]. The N-terminal domain of MCU has also been shown to interact with MCUR1, the scaffolding factor for MCU complex formation [172], suggesting a role for the N-terminal domain in stabilizing and clustering of MCU. Indeed, the spectrophotometric recordings carried out using genetically encoded Ca^{2+} indicators have shown lower Ca^{2+} uptake by mitochondria and reduced Ca^{2+} clearance rates from the cytosol with overexpression of MCU mutants lacking the N-terminal domain as compared to the full length MCU construct [174].

Based on the presence of a magnesium ion (Mg^{2+}) centrally located in the MRAP of the the $MCU_{72–189}$ crystal structure, it has been demonstrated that this acidic patch plays a key role in sensing divalent cations like Ca^{2+} and Mg^{2+} [166, 172, 175–178]. In solution, $MCU_{72–189}$ exhibits reduced stability with increasing levels of divalent cations concomitant with a suppressed self-association. Furthermore, Asp131Arg or Asp147Arg mutations not only show a reduction in Ca^{2+} uptake by mitochondria in mutant overexpressing Hela cells, but also show reduced stability and a monomeric conformation of $MCU_{72–189}$, similar to the properties characterized in the presence of high Ca^{2+} or Mg^{2+} concentrations [172]. In other functional assays, increasing Ca^{2+}concentrations inside the matrix by pharmacologically blocking the efflux of Ca^{2+} in HEK293T cells or high mitochondrial Mg^{2+} significantly reduces MCU Ca^{2+} uptake, consistent with the divalent cation-mediated destabilization of the $MCU_{72–189}$ region [172].

Another crystal structure of the MCU N-terminal domain (i.e. residues 75–165) harboring a Ser92Ala mutation which blocks phosphorylation at this Ser residue position revealed L2 and L4 structural perturbations (PDB code 5BZ6) [174]. The Ser92Ala mutation abrogated the H-bonding between Ser92 (L2) and Asp119 (L4) and consequently, impaired mitochondrial Ca^{2+} uptake activity. Thus, it is conceivable that phosphorylation at the Ser92 site [179] also modulates the H-bonding network between L2 and L4 in the regulation of MCU activity.

Collectively, the identification of MRAP and the role that divalent cations and post-translational modifications play in modulating the structural, biophysical and biochemical properties of this domain reinforce the vital significance of this conserved region in regulating MCU function. While divalent cation binding to MRAP inhibits MCU activity via promoting monomer formation of the N-terminal domain disassembly of full-length MCU [172], recently, it has been shown that *S*-glutathionylation of Cys97 enhances both MCU oligomerization and persistently activates MCU [173]. Thus, the N-terminal domain appears to be a critical sensory hub for environmental and post-translational modification queues which subsequently affects MCU activity.

10.5 Concluding Remarks

Ca^{2+} is a substrate for the aforementioned key Ca^{2+} signaling toolkit components [1–6, 79, 125, 180, 181], essentially 'self-catalyzing' the movement and localization of itself within the cell, as nature often uses metabolites to control the metabolic

enzyme machinery in both positive and negative manners. As such, Ca^{2+} can induce positive or negative feedback on each of the Ca^{2+} signaling machinery to facilitate dynamic initiation and shaping of Ca^{2+} signals at different subcellular locations. In the case of IP_3R, not only do Ca^{2+} concentrations regulate channel open probability with a bell-shaped Ca^{2+} concentration dependence and maximal channel opening at ~0.2 μM [9, 182, 183], but Ca^{2+} levels also activate the Ca^{2+} sensor CaBP1 binding to IP_3Rs which in turn negatively regulates IP_3R channel activity [63, 69, 70, 72, 184]. The NMR-driven complex structure between CaBP1 and IP_3R1 revealed interactions with the IBC-β domain of IP_3R1, clamping the channel in a closed conformation [63]. In the case of STIM1, Ca^{2+} concentrations in the ER regulate the stability of the luminal domain; when Ca^{2+} levels are low and Ca^{2+} is not coordinated in the canonical EF-hand loop, STIM1 undergoes a destabilization-coupled oligomerization event [16, 99, 113, 126, 163, 185–187] which culminates in relocalization of the protein and opening of Orai1-composed PM Ca^{2+} channels. However, high levels of Ca^{2+} in the cytosol may also inhibit STIM1/Orai1 activity through two mechanisms which both involve calmodulin: first, Ca^{2+}-CaM can bind to the polybasic C-terminus of STIM1 and inhibit translocation of STIM1 to the PM [188]; second, Ca^{2+}-CaM can bind to the Orai1 N- and C-termini, thus promoting Ca^{2+}-dependent inactivation [189, 190]. In the case of MCU, the MRAP region has been identified on the conserved matrix domain of the channel protein which interacts with divalent cations including Ca^{2+} and Mg^{2+}, thus, resulting in suppressed self-association of the domain and inhibited channel activity [172]. Therefore, eukaryotic cells have evolved the ability for a remarkable crosstalk between IP_3Rs, STIMs and MCUs where IP_3Rs regulate ER luminal Ca^{2+} levels and STIM1 activation state, STIM/Orai mediate Ca^{2+} entry into the cytosol which can regulate IP_3Rs, STIM1 as well as Orai1 at high local Ca^{2+} concentrations and provide Ca^{2+} for uptake into the mitochondria through MCU. Mitochondrial matrix Ca^{2+} levels can also regulate MCU activity and can influence the level of Ca^{2+} in the cytosol [166, 172, 175–178]. The complexity of Ca^{2+} signaling crosstalk is not limited to these three signaling entities and involves an extensive toolkit of hundreds of Ca^{2+} signaling proteins [2, 3, 191–194]. Additionally, local changes in the cellular environment which may include oxidative stress and pH can also regulate the structure and function of the multitude of Ca^{2+} signaling toolkit component proteins [122, 123, 173, 195–197].

Further research is required to appreciate the full extent of the crosstalk and the underlying molecular mechanisms of these feedback signals. Similarly, given the progress made on elucidating the structural mechanisms of IP_3R, STIM/Orai and MCU function, several structural biology questions have come to the forefront of the respective fields. In the IP_3R field, while cryo-EM has provided unprecedented insights into relative domain organization and potential domain coupling which occurs between IP_3 binding and channel gating, high resolution structural information of many portions of the receptor is lacking, particularly in the most dynamic regions. Further, the precise location of the Ca^{2+} binding sites responsible for the bell-shaped regulation is not known, and along the same lines, the high resolution structural basis for regulatory protein binding is relatively limited. In the STIM/Orai

field, the structure of the full-length cytosolic domain of STIM proteins in complex with full-length Orai1 is unknown; similarly, the stoichiometry of the coupling has yet to be demonstrated definitively. Importantly, the high resolution structure of Orai1 channels in the open state has not been determined. MCU and associated regulators was the last of these three signaling systems to be identified at the genetic level, and thus, many critical structural questions remain outstanding. The structure of the full-length MCU pore is unknown in either the open or closed states. No high resolution structure of MCU in complex with any of the principal regulators (i.e. MCUb, MICUs, MCUR1, EMRE) exists, and most of the regulators themselves are structurally unresolved at high resolution. Post-translational modifications add another layer of regulation to all of these Ca^{2+} signaling proteins, and the effects of these modifications on structure and dynamics are poorly characterized. For example, we have recently shown that *N*-glycosylation and *S*-glutathionylation can have profound effects on the structure and activity of STIM1 and MCU, respectively [120, 173]. Answering these aforementioned structural biology questions is paramount to understanding the underlying atomic-basis for the function of these proteins while paving new avenues to the development of small molecule modulators of these signaling systems with potential to treat disease and for use as research tools. Importantly, these answers will lead to a better comprehension of the molecular mechanisms underlying the function of myriad Ca^{2+} signaling toolkit components beyond IP_3R, STIM, Orai and MCU.

Acknowledgments This work was supported by Natural Sciences and Engineering Research Council of Canada (NSERC) 05239 (to P.B.S.), Canadian Institutes of Health Research (CIHR) MOP-13552 (to M.I.), NSERC UT393093 (to M.I.) and an Ontario Graduate Scholarship (to N.S.). M.I. holds the Canada Research Chair in Cancer Structural Biology.

References

1. Berridge MJ (2009) Cell signalling biology. Portland, London
2. Berridge MJ, Bootman MD, Roderick HL (2003) Calcium signalling: dynamics, homeostasis and remodelling. Nat Rev Mol Cell Biol 4:517–529
3. Berridge MJ, Lipp P, Bootman MD (2000) The versatility and universality of calcium signalling. Nat Rev Mol Cell Biol 1:11–21
4. Bootman MD, Collins TJ, Peppiatt CM, Prothero LS, MacKenzie L, De Smet P, Travers M, Tovey SC, Seo JT, Berridge MJ, Ciccolini F, Lipp P (2001) Calcium signalling – an overview. Semin Cell Dev Biol 12:3–10
5. Bootman MD, Lipp P (2001) Calcium signalling and regulation of cell function. In: Encyclopedia of Life Sciences. p 1–7
6. Bootman MD, Lipp P, Berridge MJ (2001) The organisation and functions of local Ca^{2+} signals. J Cell Sci 114:2213–2222
7. Balshaw D, Gao L, Meissner G (1999) Luminal loop of the ryanodine receptor: a pore-forming segment? Proc Natl Acad Sci USA 96:3345–3347
8. Feske S (2007) Calcium signalling in lymphocyte activation and disease. Nat Rev Immunol 7:690–702

9. Tu H, Nosyreva E, Miyakawa T, Wang Z, Mizushima A, Iino M, Bezprozvanny I (2003) Functional and biochemical analysis of the type 1 inositol (1,4,5)-trisphosphate receptor calcium sensor. Biophys J 85:290–299
10. Alonso MT, Villalobos C, Chamero P, Alvarez J, Garcia-Sancho J (2006) Calcium microdomains in mitochondria and nucleus. Cell Calcium 40:513–525
11. Kadamur G, Ross EM (2013) Mammalian phospholipase C. Annu Rev Physiol 75:127–154
12. Fedorenko OA, Popugaeva E, Enomoto M, Stathopulos PB, Ikura M, Bezprozvanny I (2014) Intracellular calcium channels: inositol-1,4,5-trisphosphate receptors. Eur J Pharmacol 739:39–48
13. Brini M, Carafoli E (2009) Calcium pumps in health and disease. Physiol Rev 89:1341–1378
14. MacLennan DH (2000) Ca^{2+} signalling and muscle disease. Eur J Biochem 267:5291–5297
15. Putney JW Jr (1986) A model for receptor-regulated calcium entry. Cell Calcium 7:1–12
16. Stathopulos PB, Ikura M (2016) Store operated calcium entry: from concept to structural mechanisms. Cell Calcium 63:3–7
17. Andersen TB, Lopez CQ, Manczak T, Martinez K, Simonsen HT (2015) Thapsigargin – from Thapsia L. to mipsagargin. Molecules 20:6113–6127
18. Hogan PG (2017) Calcium-NFAT transcriptional signalling in T cell activation and T cell exhaustion. Cell Calcium 63:66–69
19. Deak AT, Blass S, Khan MJ, Groschner LN, Waldeck-Weiermair M, Hallstrom S, Graier WF, Malli R (2014) IP3-mediated STIM1 oligomerization requires intact mitochondrial Ca^{2+} uptake. J Cell Sci 127:2944–2955
20. Fonteriz R, Matesanz-Isabel J, Arias-Del-Val J, Alvarez-Illera P, Montero M, Alvarez J (2016) Modulation of calcium entry by mitochondria. Adv Exp Med Biol 898:405–421
21. Kopach O, Kruglikov I, Pivneva T, Voitenko N, Verkhratsky A, Fedirko N (2011) Mitochondria adjust Ca(2+) signaling regime to a pattern of stimulation in salivary acinar cells. Biochim Biophys Acta 1813:1740–1748
22. Ma T, Gong K, Yan Y, Song B, Zhang X, Gong Y (2012) Mitochondrial modulation of store-operated Ca(2+) entry in model cells of Alzheimer's disease. Biochem Biophys Res Commun 426:196–202
23. Tang S, Wang X, Shen Q, Yang X, Yu C, Cai C, Cai G, Meng X, Zou F (2015) Mitochondrial Ca^{2+} uniporter is critical for store-operated Ca^{2+} entry-dependent breast cancer cell migration. Biochem Biophys Res Commun 458:186–193
24. Marchi S, Pinton P (2014) The mitochondrial calcium uniporter complex: molecular components, structure and physiopathological implications. J Physiol 592:829–839
25. Patron M, Raffaello A, Granatiero V, Tosatto A, Merli G, De Stefani D, Wright L, Pallafacchina G, Terrin A, Mammucari C, Rizzuto R (2013) The mitochondrial calcium uniporter (MCU): molecular identity and physiological roles. J Biol Chem 288:10750–10758
26. Carafoli E (2003) Historical review: mitochondria and calcium: ups and downs of an unusual relationship. Trends Biochem Sci 28:175–181
27. Raffaello A, De Stefani D, Rizzuto R (2012) The mitochondrial Ca(2+) uniporter. Cell Calcium 52:16–21
28. Orrenius S, Gogvadze V, Zhivotovsky B (2015) Calcium and mitochondria in the regulation of cell death. Biochem Biophys Res Commun 460:72–81
29. Drago I, Pizzo P, Pozzan T (2011) After half a century mitochondrial calcium in- and efflux machineries reveal themselves. EMBO J 30:4119–4125
30. Brini M, Carafoli E (2000) Calcium signalling: a historical account, recent developments and future perspectives. Cell Mol Life Sci 57:354–370
31. De Stefani D, Rizzuto R, Pozzan T (2016) Enjoy the trip: calcium in mitochondria back and forth. Annu Rev Biochem 85:161–192
32. Nita LI, Hershfinkel M, Sekler I (2015) Life after the birth of the mitochondrial Na+/Ca^{2+} exchanger, NCLX. Sci China Life Sci 58:59–65
33. Carafoli E, Balcavage WX, Lehninger AL, Mattoon JR (1970) Ca^{2+} metabolism in yeast cells and mitochondria. Biochim Biophys Acta 205:18–26

34. Liou J, Kim ML, Heo WD, Jones JT, Myers JW, Ferrell JE Jr, Meyer T (2005) STIM is a Ca^{2+} sensor essential for Ca^{2+}-store-depletion-triggered Ca^{2+} influx. Curr Biol 15:1235–1241
35. Roos J, DiGregorio PJ, Yeromin AV, Ohlsen K, Lioudyno M, Zhang S, Safrina O, Kozak JA, Wagner SL, Cahalan MD, Velicelebi G, Stauderman KA (2005) STIM1, an essential and conserved component of store-operated Ca^{2+} channel function. J Cell Biol 169:435–445
36. Zhang SL, Yeromin AV, Zhang XH, Yu Y, Safrina O, Penna A, Roos J, Stauderman KA, Cahalan MD (2006) Genome-wide RNAi screen of Ca^{2+} influx identifies genes that regulate Ca^{2+} release-activated Ca^{2+} channel activity. Proc Natl Acad Sci USA 103:9357–9362
37. Feske S, Gwack Y, Prakriya M, Srikanth S, Puppel SH, Tanasa B, Hogan PG, Lewis RS, Daly M, Rao A (2006) A mutation in Orai1 causes immune deficiency by abrogating CRAC channel function. Nature 441:179–185
38. Mercer JC, Dehaven WI, Smyth JT, Wedel B, Boyles RR, Bird GS, Putney JW Jr (2006) Large store-operated calcium-selective currents due to co-expression of Orai1 or Orai2 with the intracellular calcium sensor, Stim1. J Biol Chem 281:24979–24990
39. Prakriya M, Feske S, Gwack Y, Srikanth S, Rao A, Hogan PG (2006) Orai1 is an essential pore subunit of the CRAC channel. Nature 443:230–233
40. Vig M, Beck A, Billingsley JM, Lis A, Parvez S, Peinelt C, Koomoa DL, Soboloff J, Gill DL, Fleig A, Kinet JP, Penner R (2006) CRACM1 multimers form the ion-selective pore of the CRAC channel. Curr Biol 16:2073–2079
41. Vig M, Peinelt C, Beck A, Koomoa DL, Rabah D, Koblan-Huberson M, Kraft S, Turner H, Fleig A, Penner R, Kinet JP (2006) CRACM1 is a plasma membrane protein essential for store-operated Ca^{2+} entry. Science 312:1220–1223
42. Yeromin AV, Zhang SL, Jiang W, Yu Y, Safrina O, Cahalan MD (2006) Molecular identification of the CRAC channel by altered ion selectivity in a mutant of Orai. Nature 443:226–229
43. Feske S (2012) Immunodeficiency due to defects in store-operated calcium entry. Ann N Y Acad Sci 1238:74–90
44. Baughman JM, Perocchi F, Girgis HS, Plovanich M, Belcher-Timme CA, Sancak Y, Bao XR, Strittmatter L, Goldberger O, Bogorad RL, Koteliansky V, Mootha VK (2011) Integrative genomics identifies MCU as an essential component of the mitochondrial calcium uniporter. Nature 476:341–345
45. De Stefani D, Raffaello A, Teardo E, Szabo I, Rizzuto R (2011) A forty-kilodalton protein of the inner membrane is the mitochondrial calcium uniporter. Nature 476:336–340
46. Raffaello A, De Stefani D, Sabbadin D, Teardo E, Merli G, Picard A, Checchetto V, Moro S, Szabo I, Rizzuto R (2013) The mitochondrial calcium uniporter is a multimer that can include a dominant-negative pore-forming subunit. EMBO J 32:2362–2376
47. Perocchi F, Gohil VM, Girgis HS, Bao XR, McCombs JE, Palmer AE, Mootha VK (2010) MICU1 encodes a mitochondrial EF hand protein required for Ca(2+) uptake. Nature 467:291–296
48. Plovanich M, Bogorad RL, Sancak Y, Kamer KJ, Strittmatter L, Li AA, Girgis HS, Kuchimanchi S, De Groot J, Speciner L, Taneja N, Oshea J, Koteliansky V, Mootha VK (2013) MICU2, a paralog of MICU1, resides within the mitochondrial uniporter complex to regulate calcium handling. PLoS One 8:e55785
49. Mallilankaraman K, Cardenas C, Doonan PJ, Chandramoorthy HC, Irrinki KM, Golenar T, Csordas G, Madireddi P, Yang J, Muller M, Miller R, Kolesar JE, Molgo J, Kaufman B, Hajnoczky G, Foskett JK, Madesh M (2012) MCUR1 is an essential component of mitochondrial Ca^{2+} uptake that regulates cellular metabolism. Nat Cell Biol 14:1336–1343
50. Sancak Y, Markhard AL, Kitami T, Kovacs-Bogdan E, Kamer KJ, Udeshi ND, Carr SA, Chaudhuri D, Clapham DE, Li AA, Calvo SE, Goldberger O, Mootha VK (2013) EMRE is an essential component of the mitochondrial calcium uniporter complex. Science 342:1379–1382
51. Hoffman NE, Chandramoorthy HC, Shanmughapriya S, Zhang XQ, Vallem S, Doonan PJ, Malliankaraman K, Guo S, Rajan S, Elrod JW, Koch WJ, Cheung JY, Madesh M (2014) SLC25A23 augments mitochondrial Ca^{2+} uptake, interacts with MCU, and induces oxidative stress-mediated cell death. Mol Biol Cell 25:936–947

52. Seo MD, Velamakanni S, Ishiyama N, Stathopulos PB, Rossi AM, Khan SA, Dale P, Li C, Ames JB, Ikura M, Taylor CW (2012) Structural and functional conservation of key domains in InsP3 and ryanodine receptors. Nature 483:108–112
53. Lin CC, Baek K, Lu Z (2011) Apo and InsP(3)-bound crystal structures of the ligand-binding domain of an InsP(3) receptor. Nat Struct Mol Biol 18:1172–1174
54. Chan J, Yamazaki H, Ishiyama N, Seo MD, Mal TK, Michikawa T, Mikoshiba K, Ikura M (2010) Structural studies of inositol 1,4,5-trisphosphate receptor: coupling ligand binding to channel gating. J Biol Chem 285:36092–36099
55. Bosanac I, Yamazaki H, Matsu-Ura T, Michikawa T, Mikoshiba K, Ikura M (2005) Crystal structure of the ligand binding suppressor domain of type 1 inositol 1,4,5-trisphosphate receptor. Mol Cell 17:193–203
56. Bosanac I, Alattia JR, Mal TK, Chan J, Talarico S, Tong FK, Tong KI, Yoshikawa F, Furuichi T, Iwai M, Michikawa T, Mikoshiba K, Ikura M (2002) Structure of the inositol 1,4,5-trisphosphate receptor binding core in complex with its ligand. Nature 420:696–700
57. Ding Z, Rossi AM, Riley AM, Rahman T, Potter BV, Taylor CW (2010) Binding of inositol 1,4,5-trisphosphate (IP3) and adenophostin A to the N-terminal region of the IP3 receptor: thermodynamic analysis using fluorescence polarization with a novel IP3 receptor ligand. Mol Pharmacol 77:995–1004
58. Rossi AM, Taylor CW (2013) High-throughput fluorescence polarization assay of ligand binding to IP3 receptors. Cold Spring Harb Protoc 2013:938–946
59. Sipma H, De Smet P, Sienaert I, Vanlingen S, Missiaen L, Parys JB, De Smedt H (1999) Modulation of inositol 1,4,5-trisphosphate binding to the recombinant ligand-binding site of the type-1 inositol 1,4, 5-trisphosphate receptor by Ca^{2+} and calmodulin. J Biol Chem 274:12157–12162
60. Vanlingen S, Sipma H, De Smet P, Callewaert G, Missiaen L, De Smedt H, Parys JB (2001) Modulation of inositol 1,4,5-trisphosphate binding to the various inositol 1,4,5-trisphosphate receptor isoforms by thimerosal and cyclic ADP-ribose. Biochem Pharmacol 61:803–809
61. Yoshikawa F, Iwasaki H, Michikawa T, Furuichi T, Mikoshiba K (1999) Cooperative formation of the ligand-binding site of the inositol 1,4, 5-trisphosphate receptor by two separable domains. J Biol Chem 274:328–334
62. Yoshikawa F, Uchiyama T, Iwasaki H, Tomomori-Satoh C, Tanaka T, Furuichi T, Mikoshiba K (1999) High efficient expression of the functional ligand binding site of the inositol 1,4,5-triphosphate receptor in *Escherichia coli*. Biochem Biophys Res Commun 257:792–797
63. Li C, Enomoto M, Rossi AM, Seo MD, Rahman T, Stathopulos PB, Taylor CW, Ikura M, Ames JB (2013) CaBP1, a neuronal Ca^{2+} sensor protein, inhibits inositol trisphosphate receptors by clamping intersubunit interactions. Proc Natl Acad Sci USA 110:8507–8512
64. Yoshikawa F, Morita M, Monkawa T, Michikawa T, Furuichi T, Mikoshiba K (1996) Mutational analysis of the ligand binding site of the inositol 1,4,5-trisphosphate receptor. J Biol Chem 271:18277–18284
65. Yamazaki H, Chan J, Ikura M, Michikawa T, Mikoshiba K (2010) Tyr-167/Trp-168 in type 1/3 inositol 1,4,5-trisphosphate receptor mediates functional coupling between ligand binding and channel opening. J Biol Chem 285:36081–36091
66. Rossi AM, Riley AM, Tovey SC, Rahman T, Dellis O, Taylor EJ, Veresov VG, Potter BV, Taylor CW (2009) Synthetic partial agonists reveal key steps in IP3 receptor activation. Nature Chem Biol 5:631–639
67. Murray SC, Flanagan J, Popova OB, Chiu W, Ludtke SJ, Serysheva II (2013) Validation of cryo-EM structure of IP(3)R1 channel. Structure 21:900–909
68. Ludtke SJ, Tran TP, Ngo QT, Moiseenkova-Bell VY, Chiu W, Serysheva II (2011) Flexible architecture of IP3R1 by Cryo-EM. Structure 19:1192–1199
69. Haynes LP, Tepikin AV, Burgoyne RD (2004) Calcium-binding protein 1 is an inhibitor of agonist-evoked, inositol 1,4,5-trisphosphate-mediated calcium signaling. J Biol Chem 279:547–555

70. Li C, Chan J, Haeseleer F, Mikoshiba K, Palczewski K, Ikura M, Ames JB (2009) Structural insights into Ca^{2+}-dependent regulation of inositol 1,4,5-trisphosphate receptors by CaBP1. J Biol Chem 284:2472–2481
71. Park S, Li C, Ames JB (2010) 1H, 15N, and 13C chemical shift assignments of calcium-binding protein 1 with Ca^{2+} bound at EF1, EF3 and EF4. Biomol NMR Assign 4:159–161
72. Yang J, McBride S, Mak DO, Vardi N, Palczewski K, Haeseleer F, Foskett JK (2002) Identification of a family of calcium sensors as protein ligands of inositol trisphosphate receptor Ca(2+) release channels. Proc Natl Acad Sci USA 99:7711–7716
73. Clarke OB, Hendrickson WA (2016) Structures of the colossal RyR1 calcium release channel. Curr Opin Struct Biol 39:144–152
74. Hernandez-Ochoa EO, Pratt SJ, Lovering RM, Schneider MF (2015) Critical role of intracellular RyR1 calcium release channels in skeletal muscle function and disease. Front Physiol 6:420
75. Landstrom AP, Dobrev D, Wehrens XHT (2017) Calcium signaling and cardiac arrhythmias. Circ Res 120:1969–1993
76. Leong P, MacLennan DH (1998) Complex interactions between skeletal muscle ryanodine receptor and dihydropyridine receptor proteins. Biochem Cell Biol 76:681–694
77. Van Petegem F (2015) Ryanodine receptors: allosteric ion channel giants. J Mol Biol 427:31–53
78. Yuchi Z, Van Petegem F (2016) Ryanodine receptors under the magnifying lens: insights and limitations of cryo-electron microscopy and X-ray crystallography studies. Cell Calcium 59:209–227
79. Berridge MJ (2002) The endoplasmic reticulum: a multifunctional signaling organelle. Cell Calcium 32:235–249
80. Tung CC, Lobo PA, Kimlicka L, Van Petegem F (2010) The amino-terminal disease hotspot of ryanodine receptors forms a cytoplasmic vestibule. Nature 468:585–588
81. Amador FJ, Liu S, Ishiyama N, Plevin MJ, Wilson A, MacLennan DH, Ikura M (2009) Crystal structure of type I ryanodine receptor amino-terminal beta-trefoil domain reveals a disease-associated mutation "hot spot" loop. Proc Natl Acad Sci USA 106:11040–11044
82. Amador FJ, Stathopulos PB, Enomoto M, Ikura M (2013) Ryanodine receptor calcium release channels: lessons from structure-function studies. Febs J 280:5456–5470
83. Bultynck G, Rossi D, Callewaert G, Missiaen L, Sorrentino V, Parys JB, De Smedt H (2001) The conserved sites for the FK506-binding proteins in ryanodine receptors and inositol 1,4,5-trisphosphate receptors are structurally and functionally different. J Biol Chem 276:47715–47724
84. Seo MD, Enomoto M, Ishiyama N, Stathopulos PB, Ikura M (2014) Structural insights into endoplasmic reticulum stored calcium regulation by inositol 1,4,5-trisphosphate and ryanodine receptors. Biochim Biophys Acta 1853(9):1980–1991
85. Straub SV, Giovannucci DR, Yule DI (2000) Calcium wave propagation in pancreatic acinar cells: functional interaction of inositol 1,4,5-trisphosphate receptors, ryanodine receptors, and mitochondria. J Gen Physiol 116:547–560
86. Yuchi Z, Van Petegem F (2011) Common allosteric mechanisms between ryanodine and inositol-1,4,5-trisphosphate receptors. Channels (Austin) 5:120–123
87. Amador FJ, Kimlicka L, Stathopulos PB, Gasmi-Seabrook GM, Maclennan DH, Van Petegem F, Ikura M (2013) Type 2 ryanodine receptor domain A contains a unique and dynamic alpha-helix that transitions to a beta-strand in a mutant linked with a heritable cardiomyopathy. J Mol Biol 425:4034–4046
88. Stathopulos PB, Seo MD, Enomoto M, Amador FJ, Ishiyama N, Ikura M (2012) Themes and variations in ER/SR calcium release channels: structure and function. Physiology 27:331–342
89. Fan G, Baker ML, Wang Z, Baker MR, Sinyagovskiy PA, Chiu W, Ludtke SJ, Serysheva II (2015) Gating machinery of InsP3R channels revealed by electron cryomicroscopy. Nature 527:336–341

90. Hamada K, Miyatake H, Terauchi A, Mikoshiba K (2017) IP3-mediated gating mechanism of the IP3 receptor revealed by mutagenesis and X-ray crystallography. Proc Natl Acad Sci USA 114(18):4661–4666
91. Uchida K, Miyauchi H, Furuichi T, Michikawa T, Mikoshiba K (2003) Critical regions for activation gating of the inositol 1,4,5-trisphosphate receptor. J Biol Chem 278:16551–16560
92. Schug ZT, Joseph SK (2006) The role of the S4-S5 linker and C-terminal tail in inositol 1,4,5-trisphosphate receptor function. J Biol Chem 281:24431–24440
93. Alzayady KJ, Wagner LE 2nd, Chandrasekhar R, Monteagudo A, Godiska R, Tall GG, Joseph SK, Yule DI (2013) Functional inositol 1,4,5-trisphosphate receptors assembled from concatenated homo- and heteromeric subunits. J Biol Chem 288:29772–29784
94. Alzayady KJ, Wang L, Chandrasekhar R, Wagner LE 2nd, Van Petegem F, Yule DI (2016) Defining the stoichiometry of inositol 1,4,5-trisphosphate binding required to initiate Ca^{2+} release. Sci Signal 9:ra35
95. Chandrasekhar R, Alzayady KJ, Wagner LE 2nd, Yule DI (2016) Unique regulatory properties of heterotetrameric inositol 1,4,5-trisphosphate receptors revealed by studying concatenated receptor constructs. J Biol Chem 291:4846–4860
96. Chandrasekhar R, Alzayady KJ, Yule DI (2015) Using concatenated subunits to investigate the functional consequences of heterotetrameric inositol 1,4,5-trisphosphate receptors. Biochem Soc Trans 43:364–370
97. Berridge MJ (2009) Inositol trisphosphate and calcium signalling mechanisms. Biochim Biophys Acta 1793:933–940
98. Zhang SL, Yu Y, Roos J, Kozak JA, Deerinck TJ, Ellisman MH, Stauderman KA, Cahalan MD (2005) STIM1 is a Ca^{2+} sensor that activates CRAC channels and migrates from the Ca^{2+} store to the plasma membrane. Nature 437:902–905
99. Stathopulos PB, Li GY, Plevin MJ, Ames JB, Ikura M (2006) Stored Ca^{2+} depletion-induced oligomerization of stromal interaction molecule 1 (STIM1) via the EF-SAM region: an initiation mechanism for capacitive Ca^{2+} entry. J Biol Chem 281:35855–35862
100. Zheng L, Stathopulos PB, Li GY, Ikura M (2008) Biophysical characterization of the EF-hand and SAM domain containing Ca^{2+} sensory region of STIM1 and STIM2. Biochem Biophys Res Commun 369:240–246
101. Stathopulos PB, Zheng L, Ikura M (2009) Stromal interaction molecule (STIM) 1 and STIM2 calcium sensing regions exhibit distinct unfolding and oligomerization kinetics. J Biol Chem 284:728–732
102. Zheng L, Stathopulos PB, Schindl R, Li GY, Romanin C, Ikura M (2011) Auto-inhibitory role of the EF-SAM domain of STIM proteins in store-operated calcium entry. Proc Natl Acad Sci USA 108:1337–1342
103. Manji SS, Parker NJ, Williams RT, van Stekelenburg L, Pearson RB, Dziadek M, Smith PJ (2000) STIM1: a novel phosphoprotein located at the cell surface. Biochim Biophys Acta 1481:147–155
104. Williams RT, Manji SS, Parker NJ, Hancock MS, Van Stekelenburg L, Eid JP, Senior PV, Kazenwadel JS, Shandala T, Saint R, Smith PJ, Dziadek MA (2001) Identification and characterization of the STIM (stromal interaction molecule) gene family: coding for a novel class of transmembrane proteins. Biochem J 357:673–685
105. Williams RT, Senior PV, Van Stekelenburg L, Layton JE, Smith PJ, Dziadek MA (2002) Stromal interaction molecule 1 (STIM1), a transmembrane protein with growth suppressor activity, contains an extracellular SAM domain modified by N-linked glycosylation. Biochim Biophys Acta 1596:131–137
106. Baba Y, Hayashi K, Fujii Y, Mizushima A, Watarai H, Wakamori M, Numaga T, Mori Y, Iino M, Hikida M, Kurosaki T (2006) Coupling of STIM1 to store-operated Ca^{2+} entry through its constitutive and inducible movement in the endoplasmic reticulum. Proc Natl Acad Sci USA 103:16704–16709
107. Luik RM, Wang B, Prakriya M, Wu MM, Lewis RS (2008) Oligomerization of STIM1 couples ER calcium depletion to CRAC channel activation. Nature 454:538–542

108. Navarro-Borelly L, Somasundaram A, Yamashita M, Ren D, Miller RJ, Prakriya M (2008) STIM1-Orai1 interactions and Orai1 conformational changes revealed by live-cell FRET microscopy. J Physiol 586:5383–5401
109. Korzeniowski MK, Manjarres IM, Varnai P, Balla T (2010) Activation of STIM1-Orai1 involves an intramolecular switching mechanism. Sci Signal 3:ra82
110. Muik M, Fahrner M, Schindl R, Stathopulos P, Frischauf I, Derler I, Plenk P, Lackner B, Groschner K, Ikura M, Romanin C (2011) STIM1 couples to ORAI1 via an intramolecular transition into an extended conformation. EMBO J 30:1678–1689
111. Yu F, Sun L, Hubrack S, Selvaraj S, Machaca K (2013) Intramolecular shielding maintains the ER Ca^{2+} sensor STIM1 in an inactive conformation. J Cell Sci 126:2401–2410
112. Zheng H, Zhou MH, Hu C, Kuo E, Peng X, Hu J, Kuo L, Zhang SL (2013) Differential roles of the C and N termini of Orai1 protein in interacting with stromal interaction molecule 1 (STIM1) for Ca^{2+} release-activated Ca^{2+} (CRAC) channel activation. J Biol Chem 288:11263–11272
113. Stathopulos PB, Zheng L, Li GY, Plevin MJ, Ikura M (2008) Structural and mechanistic insights into STIM1-mediated initiation of store-operated calcium entry. Cell 135:110–122
114. Huang Y, Zhou Y, Wong HC, Chen Y, Wang S, Castiblanco A, Liu A, Yang JJ (2009) A single EF-hand isolated from STIM1 forms dimer in the absence and presence of Ca^{2+}. Febs J 276:5589–5597
115. Cai X (2007) Molecular evolution and functional divergence of the Ca^{2+} sensor protein in store-operated Ca^{2+} entry: stromal interaction molecule. PLoS One 2:e609
116. Bird GS, Hwang SY, Smyth JT, Fukushima M, Boyles RR, Putney JW Jr (2009) STIM1 is a calcium sensor specialized for digital signaling. Curr Biol 19:1724–1729
117. Brandman O, Liou J, Park WS, Meyer T (2007) STIM2 is a feedback regulator that stabilizes basal cytosolic and endoplasmic reticulum Ca^{2+} levels. Cell 131:1327–1339
118. Zhou Y, Mancarella S, Wang Y, Yue C, Ritchie M, Gill DL, Soboloff J (2009) The short N-terminal domains of STIM1 and STIM2 control the activation kinetics of Orai1 channels. J Biol Chem 284:19164–19168
119. Gruszczynska-Biegala J, Pomorski P, Wisniewska MB, Kuznicki J (2011) Differential roles for STIM1 and STIM2 in store-operated calcium entry in rat neurons. PLoS One 6:e19285
120. Choi YJ, Zhao Y, Bhattacharya M, Stathopulos PB (2017) Structural perturbations induced by Asn131 and Asn171 glycosylation converge within the EFSAM core and enhance stromal interaction molecule-1 mediated store operated calcium entry. Biochim Biophys Acta 1864:1054–1063
121. Kilch T, Alansary D, Peglow M, Dorr K, Rychkov G, Rieger H, Peinelt C, Niemeyer BA (2013) Mutations of the Ca^{2+}-sensing stromal interaction molecule STIM1 regulate Ca^{2+} influx by altered oligomerization of STIM1 and by destabilization of the Ca^{2+} channel Orai1. J Biol Chem 288:1653–1664
122. Hawkins BJ, Irrinki KM, Mallilankaraman K, Lien YC, Wang Y, Bhanumathy CD, Subbiah R, Ritchie MF, Soboloff J, Baba Y, Kurosaki T, Joseph SK, Gill DL, Madesh M (2010) S-glutathionylation activates STIM1 and alters mitochondrial homeostasis. J Cell Biol 190:391–405
123. Prins D, Groenendyk J, Touret N, Michalak M (2011) Modulation of STIM1 and capacitative Ca^{2+} entry by the endoplasmic reticulum luminal oxidoreductase ERp57. EMBO Rep 12:1182–1188
124. Liou J, Fivaz M, Inoue T, Meyer T (2007) Live-cell imaging reveals sequential oligomerization and local plasma membrane targeting of stromal interaction molecule 1 after Ca^{2+} store depletion. Proc Natl Acad Sci USA 104:9301–9306
125. Carafoli E, Krebs J (2016) Why calcium? How calcium became the best communicator. J Biol Chem 291:20849–20857
126. Marshall CB, Nishikawa T, Osawa M, Stathopulos PB, Ikura M (2015) Calmodulin and STIM proteins: two major calcium sensors in the cytoplasm and endoplasmic reticulum. Biochem Biophys Res Commun 460:5–21

127. Nakayama S, Kretsinger RH (1994) Evolution of the EF-hand family of proteins. Annu Rev Biophys Biomol Struct 23:473–507
128. Kim CA, Bowie JU (2003) SAM domains: uniform structure, diversity of function. Trends Biochem Sci 28:625–628
129. Kim CA, Phillips ML, Kim W, Gingery M, Tran HH, Robinson MA, Faham S, Bowie JU (2001) Polymerization of the SAM domain of TEL in leukemogenesis and transcriptional repression. EMBO J 20:4173–4182
130. Mercurio FA, Leone M (2016) The Sam domain of EphA2 receptor and its relevance to cancer: a novel challenge for drug discovery? Curr Med Chem 23:4718–4734
131. Stapleton D, Balan I, Pawson T, Sicheri F (1999) The crystal structure of an Eph receptor SAM domain reveals a mechanism for modular dimerization. Nat Struct Biol 6:44–49
132. Thanos CD, Goodwill KE, Bowie JU (1999) Oligomeric structure of the human EphB2 receptor SAM domain. Science 283:833–836
133. Qiao F, Bowie JU (2005) The many faces of SAM. Sci STKE 2005:re7
134. Csutora P, Peter K, Kilic H, Park KM, Zarayskiy V, Gwozdz T, Bolotina VM (2008) Novel role for STIM1 as a trigger for calcium influx factor production. J Biol Chem 283:14524–14531
135. Czyz A, Brutkowski W, Fronk J, Duszynski J, Zablocki K (2009) Tunicamycin desensitizes store-operated Ca^{2+} entry to ATP and mitochondrial potential. Biochem Biophys Res Commun 381:176–180
136. Mignen O, Thompson JL, Shuttleworth TJ (2007) STIM1 regulates Ca^{2+} entry via arachidonate-regulated Ca^{2+}-selective (ARC) channels without store depletion or translocation to the plasma membrane. J Physiol 579:703–715
137. Cui B, Yang X, Li S, Lin Z, Wang Z, Dong C, Shen Y (2013) The inhibitory helix controls the intramolecular conformational switching of the C-terminus of STIM1. PLoS One 8:e74735
138. Maruyama Y, Ogura T, Mio K, Kato K, Kaneko T, Kiyonaka S, Mori Y, Sato C (2009) Tetrameric Orai1 is a teardrop-shaped molecule with a long, tapered cytoplasmic domain. J Biol Chem 284:13676–13685
139. Luik RM, Wu MM, Buchanan J, Lewis RS (2006) The elementary unit of store-operated Ca^{2+} entry: local activation of CRAC channels by STIM1 at ER-plasma membrane junctions. J Cell Biol 174:815–825
140. Wu MM, Buchanan J, Luik RM, Lewis RS (2006) Ca^{2+} store depletion causes STIM1 to accumulate in ER regions closely associated with the plasma membrane. J Cell Biol 174:803–813
141. Yuan JP, Zeng W, Dorwart MR, Choi YJ, Worley PF, Muallem S (2009) SOAR and the polybasic STIM1 domains gate and regulate Orai channels. Nat Cell Biol 11:337–343
142. Kawasaki T, Lange I, Feske S (2009) A minimal regulatory domain in the C terminus of STIM1 binds to and activates ORAI1 CRAC channels. Biochem Biophys Res Commun 385:49–54
143. Yang X, Jin H, Cai X, Li S, Shen Y (2012) Structural and mechanistic insights into the activation of Stromal interaction molecule 1 (STIM1). Proc Natl Acad Sci USA 109:5657–5662
144. Stathopulos PB, Schindl R, Fahrner M, Zheng L, Gasmi-Seabrook GM, Muik M, Romanin C, Ikura M (2013) STIM1/Orai1 coiled-coil interplay in the regulation of store-operated calcium entry. Nat Commun 4:2963
145. Zhou Y, Srinivasan P, Razavi S, Seymour S, Meraner P, Gudlur A, Stathopulos PB, Ikura M, Rao A, Hogan PG (2013) Initial activation of STIM1, the regulator of store-operated calcium entry. Nat Struct Mol Biol 20:973–981
146. Cai X (2007) Molecular evolution and structural analysis of the Ca(2+) release-activated Ca(2+) channel subunit, Orai. J Mol Biol 368:1284–1291
147. Penna A, Demuro A, Yeromin AV, Zhang SL, Safrina O, Parker I, Cahalan MD (2008) The CRAC channel consists of a tetramer formed by Stim-induced dimerization of Orai dimers. Nature 456:116–120

148. Thompson JL, Shuttleworth TJ (2013) How many Orai's does it take to make a CRAC channel? Sci Rep 3:1961
149. Ji W, Xu P, Li Z, Lu J, Liu L, Zhan Y, Chen Y, Hille B, Xu T, Chen L (2008) Functional stoichiometry of the unitary calcium-release-activated calcium channel. Proc Natl Acad Sci USA 105:13668–13673
150. Hou X, Pedi L, Diver MM, Long SB (2012) Crystal structure of the calcium release-activated calcium channel Orai. Science 338:1308–1313
151. Covington ED, Wu MM, Lewis RS (2010) Essential role for the CRAC activation domain in store-dependent oligomerization of STIM1. Mol Biol Cell 21:1897–1907
152. Muik M, Fahrner M, Derler I, Schindl R, Bergsmann J, Frischauf I, Groschner K, Romanin C (2009) A cytosolic homomerization and a modulatory domain within STIM1 C terminus determine coupling to ORAI1 channels. J Biol Chem 284:8421–8426
153. Muik M, Frischauf I, Derler I, Fahrner M, Bergsmann J, Eder P, Schindl R, Hesch C, Polzinger B, Fritsch R, Kahr H, Madl J, Gruber H, Groschner K, Romanin C (2008) Dynamic coupling of the putative coiled-coil domain of ORAI1 with STIM1 mediates ORAI1 channel activation. J Biol Chem 283:8014–8022
154. Bhardwaj R, Muller HM, Nickel W, Seedorf M (2013) Oligomerization and Ca^{2+}/calmodulin control binding of the ER Ca^{2+}-sensors STIM1 and STIM2 to plasma membrane lipids. Biosci Rep 33(5). https://doi.org/10.1042/BSR20130089
155. Maleth J, Choi S, Muallem S, Ahuja M (2014) Translocation between PI(4,5)P2-poor and PI(4,5)P2-rich microdomains during store depletion determines STIM1 conformation and Orai1 gating. Nat Commun 5:5843
156. Calloway N, Owens T, Corwith K, Rodgers W, Holowka D, Baird B (2011) Stimulated association of STIM1 and Orai1 is regulated by the balance of PtdIns(4,5)P(2) between distinct membrane pools. J Cell Sci 124:2602–2610
157. Korzeniowski MK, Popovic MA, Szentpetery Z, Varnai P, Stojilkovic SS, Balla T (2009) Dependence of STIM1/Orai1-mediated calcium entry on plasma membrane phosphoinositides. J Biol Chem 284:21027–21035
158. Walsh CM, Chvanov M, Haynes LP, Petersen OH, Tepikin AV, Burgoyne RD (2009) Role of phosphoinositides in STIM1 dynamics and store-operated calcium entry. Biochem J 425:159–168
159. Park CY, Hoover PJ, Mullins FM, Bachhawat P, Covington ED, Raunser S, Walz T, Garcia KC, Dolmetsch RE, Lewis RS (2009) STIM1 clusters and activates CRAC channels via direct binding of a cytosolic domain to Orai1. Cell 136:876–890
160. Frischauf I, Muik M, Derler I, Bergsmann J, Fahrner M, Schindl R, Groschner K, Romanin C (2009) Molecular determinants of the coupling between STIM1 and Orai channels: differential activation of Orai1-3 channels by a STIM1 coiled-coil mutant. J Biol Chem 284:21696–21706
161. Lis A, Zierler S, Peinelt C, Fleig A, Penner R (2010) A single lysine in the N-terminal region of store-operated channels is critical for STIM1-mediated gating. J Gen Physiol 136:673–686
162. Zhou Y, Meraner P, Kwon HT, Machnes D, Oh-hora M, Zimmer J, Huang Y, Stura A, Rao A, Hogan PG (2010) STIM1 gates the store-operated calcium channel ORAI1 in vitro. Nat Struct Mol Biol 17:112–116
163. Stathopulos PB, Ikura M (2013) Structural aspects of calcium-release activated calcium channel function. Channels (Austin) 7:344–353
164. Martell JD, Deerinck TJ, Sancak Y, Poulos TL, Mootha VK, Sosinsky GE, Ellisman MH, Ting AY (2012) Engineered ascorbate peroxidase as a genetically encoded reporter for electron microscopy. Nat Biotechnol 30:1143–1148
165. Deluca HF, Engstrom GW (1961) Calcium uptake by rat kidney mitochondria. Proc Natl Acad Sci USA 47:1744–1750
166. Kirichok Y, Krapivinsky G, Clapham DE (2004) The mitochondrial calcium uniporter is a highly selective ion channel. Nature 427:360–364
167. Prentki M, Janjic D, Wollheim CB (1983) The regulation of extramitochondrial steady state free Ca^{2+} concentration by rat insulinoma mitochondria. J Biol Chem 258:7597–7602

168. Pettersen EF, Goddard TD, Huang CC, Couch GS, Greenblatt DM, Meng EC, Ferrin TE (2004) UCSF Chimera – a visualization system for exploratory research and analysis. J Comput Chem 25:1605–1612
169. Oxenoid K, Dong Y, Cao C, Cui T, Sancak Y, Markhard AL, Grabarek Z, Kong L, Liu Z, Ouyang B, Cong Y, Mootha VK, Chou JJ (2016) Architecture of the mitochondrial calcium uniporter. Nature 533:269–273
170. Cao C, Wang S, Cui T, Su XC, Chou JJ (2017) Ion and inhibitor binding of the double-ring ion selectivity filter of the mitochondrial calcium uniporter. Proc Natl Acad Sci USA 114:E2846–E2851
171. Lunin VV, Dobrovetsky E, Khutoreskaya G, Zhang R, Joachimiak A, Doyle DA, Bochkarev A, Maguire ME, Edwards AM, Koth CM (2006) Crystal structure of the CorA Mg^{2+} transporter. Nature 440:833–837
172. Lee SK, Shanmughapriya S, Mok MC, Dong Z, Tomar D, Carvalho E, Rajan S, Junop MS, Madesh M, Stathopulos PB (2016) Structural insights into mitochondrial calcium uniporter regulation by divalent cations. Cell Chem Biol 23:1157–1169
173. Dong Z, Shanmughapriya S, Tomar D, Siddiqui N, Lynch S, Nemani N, Breves SL, Zhang X, Tripathi A, Palaniappan P, Riitano MF, Worth AM, Seelam A, Carvalho E, Subbiah R, Jana F, Soboloff J, Peng Y, Cheung JY, Joseph SK, Caplan J, Rajan S, Stathopulos PB, Madesh M (2017) Mitochondrial Ca^{2+} uniporter is a mitochondrial luminal redox sensor that augments MCU channel activity. Mol Cell 65:1014–1028
174. Lee Y, Min CK, Kim TG, Song HK, Lim Y, Kim D, Shin K, Kang M, Kang JY, Youn HS, Lee JG, An JY, Park KR, Lim JJ, Kim JH, Kim JH, Park ZY, Kim YS, Wang J, Kim do H, Eom SH (2015) Structure and function of the N-terminal domain of the human mitochondrial calcium uniporter. EMBO Rep 16:1318–1333
175. Favaron M, Bernardi P (1985) Tissue-specific modulation of the mitochondrial calcium uniporter by magnesium ions. FEBS Lett 183:260–264
176. Jung DW, Apel L, Brierley GP (1990) Matrix free Mg^{2+} changes with metabolic state in isolated heart mitochondria. Biochemistry 29:4121–4128
177. Moreau B, Parekh AB (2008) Ca^{2+} -dependent inactivation of the mitochondrial Ca^{2+} uniporter involves proton flux through the ATP synthase. Curr Biol 18:855–859
178. Szanda G, Rajki A, Gallego-Sandin S, Garcia-Sancho J, Spat A (2009) Effect of cytosolic Mg^{2+} on mitochondrial Ca^{2+} signaling. Pflugers Arch 457:941–954
179. Joiner ML, Koval OM, Li J, He BJ, Allamargot C, Gao Z, Luczak ED, Hall DD, Fink BD, Chen B, Yang J, Moore SA, Scholz TD, Strack S, Mohler PJ, Sivitz WI, Song LS, Anderson ME (2012) CaMKII determines mitochondrial stress responses in heart. Nature 491:269–273
180. Bootman MD (2012) Calcium signaling. Cold Spring Harb Perspect Biol 4:a011171
181. Bootman MD, Berridge MJ (1995) The elemental principles of calcium signaling. Cell 83:675–678
182. Bezprozvanny I, Watras J, Ehrlich BE (1991) Bell-shaped calcium-response curves of Ins(1,4,5)P3- and calcium-gated channels from endoplasmic reticulum of cerebellum. Nature 351:751–754
183. Tu H, Wang Z, Bezprozvanny I (2005) Modulation of mammalian inositol 1,4,5-trisphosphate receptor isoforms by calcium: a role of calcium sensor region. Biophys J 88:1056–1069
184. Wingard JN, Chan J, Bosanac I, Haeseleer F, Palczewski K, Ikura M, Ames JB (2005) Structural analysis of Mg^{2+} and Ca^{2+} binding to CaBP1, a neuron-specific regulator of calcium channels. J Biol Chem 280:37461–37470
185. Stathopulos PB, Ikura M (2009) Structurally delineating stromal interaction molecules as the endoplasmic reticulum calcium sensors and regulators of calcium release-activated calcium entry. Immunol Rev 231:113–131
186. Stathopulos PB, Ikura M (2010) Partial unfolding and oligomerization of stromal interaction molecules as an initiation mechanism of store operated calcium entry. Biochem Cell Biol 88:175–183

187. Stathopulos PB, Ikura M (2013) Structure and function of endoplasmic reticulum STIM calcium sensors. Curr Top Membr 71:59–93
188. Bauer MC, O'Connell D, Cahill DJ, Linse S (2008) Calmodulin binding to the polybasic C-termini of STIM proteins involved in store-operated calcium entry. Biochemistry 47:6089–6091
189. Liu Y, Zheng X, Mueller GA, Sobhany M, DeRose EF, Zhang Y, London RE, Birnbaumer L (2012) Crystal structure of calmodulin binding domain of orai1 in complex with Ca^{2+} calmodulin displays a unique binding mode. J Biol Chem 287:43030–43041
190. Mullins FM, Park CY, Dolmetsch RE, Lewis RS (2009) STIM1 and calmodulin interact with Orai1 to induce Ca^{2+}-dependent inactivation of CRAC channels. Proc Natl Acad Sci USA 106:15495–15500
191. Dubois C, Prevarskaya N, Vanden Abeele F (2016) The calcium-signaling toolkit: updates needed. Biochim Biophys Acta 1863:1337–1343
192. Marchadier E, Oates ME, Fang H, Donoghue PC, Hetherington AM, Gough J (2016) Evolution of the calcium-based intracellular signaling system. Genome Biol Evol 8:2118–2132
193. Schwaller B (2012) The regulation of a cell's Ca^{2+} signaling toolkit: the Ca^{2+} homeostasome. Adv Exp Med Biol 740:1–25
194. Zampese E, Pizzo P (2012) Intracellular organelles in the saga of Ca^{2+} homeostasis: different molecules for different purposes? Cell Mol Life Sci 69:1077–1104
195. Glitsch M (2011) Protons and Ca^{2+}: ionic allies in tumor progression? Physiology 26:252–265
196. Huang WC, Swietach P, Vaughan-Jones RD, Ansorge O, Glitsch MD (2008) Extracellular acidification elicits spatially and temporally distinct Ca^{2+} signals. Curr Biol 18:781–785
197. Wei WC, Jacobs B, Becker EB, Glitsch MD (2015) Reciprocal regulation of two G protein-coupled receptors sensing extracellular concentrations of Ca^{2+} and H. Proc Natl Acad Sci USA 112:10738–10743

Chapter 11
Assembly of ER-PM Junctions: A Critical Determinant in the Regulation of SOCE and TRPC1

Krishna P. Subedi, Hwei Ling Ong, and Indu S. Ambudkar

Abstract Store-operated calcium entry (SOCE), a unique plasma membrane Ca^{2+} entry mechanism, is activated when ER-[Ca^{2+}] is decreased. SOCE is mediated via the primary channel, Orai1, as well as others such as TRPC1. STIM1 and STIM2 are ER-Ca^{2+} sensor proteins that regulate Orai1 and TRPC1. SOCE requires assembly of STIM proteins with the plasma membrane channels which occurs within distinct regions in the cell that have been termed as endoplasmic reticulum (ER)-plasma membrane (PM) junctions. The PM and ER are in close proximity to each other within this region, which allows STIM1 in the ER to interact with and activate either Orai1 or TRPC1 in the plasma membrane. Activation and regulation of SOCE involves dynamic assembly of various components that are involved in mediating Ca^{2+} entry as well as those that determine the formation and stabilization of the junctions. These components include proteins in the cytosol, ER and PM, as well as lipids in the PM. Recent studies have also suggested that SOCE and its components are compartmentalized within ER-PM junctions and that this process might require remodeling of the plasma membrane lipids and reorganization of structural and scaffolding proteins. Such compartmentalization leads to the generation of spatially- and temporally-controlled Ca^{2+}signals that are critical for regulating many downstream cellular functions.

Keywords ER-PM junctions · SOCE · TRPC1 · Orai1 · STIM1 · STIM2

K. P. Subedi · H. L. Ong · I. S. Ambudkar (✉)
Secretory Physiology Section, Molecular Physiology and Therapeutics Branch, NIDCR, NIH, Bethesda, MD, USA
e-mail: indu.ambudkar@nih.gov

J. Krebs (ed.), *Membrane Dynamics and Calcium Signaling*, Advances in Experimental Medicine and Biology 981,
https://doi.org/10.1007/978-3-319-55858-5_11

11.1 Introduction

Intracellular [Ca^{2+}] ([$Ca^{2+}]_i$) regulates a plethora of critical cellular functions and is tightly controlled by mechanisms that mediate increase, or decrease, in [$Ca^{2+}]_i$. Increase in [$Ca^{2+}]_i$ can result from entry of Ca^{2+} into the cell via plasma membrane Ca^{2+} channels or release of Ca^{2+} from intracellular organelles, such as the endoplasmic reticulum (ER) which is the major intracellular Ca^{2+} store. Physiologically, Ca^{2+} release from the ER is controlled by neurotransmitter activation of plasma membrane receptors that are coupled to the hydrolysis of phosphatidylinositol 4,5-bisphosphate (PIP_2) and generation of inositol 1,4,5-trisphosphate (IP_3), which binds to and activates the IP_3 receptor (IP_3R), a Ca^{2+} channel on the ER membrane. A major consequence of IP_3-induced decrease in ER-[Ca^{2+}] is the activation of store-operated calcium entry (SOCE), a ubiquitous Ca^{2+} entry mechanism which is mediated by plasma membrane channels. SOCE provides [$Ca^{2+}]_i$ signals essential for regulating a variety of cell functions, including gene expression, exocrine secretion, T cell activation and cell migration [1–4]. The main trigger for activation of SOCE, which is a decrease in [Ca^{2+}] within the ER lumen, is sensed by the ER-resident proteins, stromal interaction molecules (STIM1 and STIM2), that function as Ca^{2+} sensors. These proteins multimerize and undergo intramolecular conformational changes that facilitate their clustering in peripheral ER, which lies in close proximity with the plasma membrane, where they are anchored to the plasma membrane via their C-terminal polybasic domains [5, 6]. Importantly, clustering of STIM proteins within the ER-plasma membrane (ER-PM) junctions causes recruitment of channels, such as Orai1 and TRPC1, into these junctions where they are activated by STIM1 and mediate SOCE [7, 8]. Ca^{2+} entry via each channel is utilized by cells for distinct functions. For example, in a salivary gland cell line, Orai1-mediated Ca^{2+} influx results in sustained [$Ca^{2+}]_i$ oscillations and activates NFAT-dependent gene expression, while TRPC1-mediated Ca^{2+} entry contributes to [$Ca^{2+}]_i$ increase and regulates Ca^{2+}-dependent K^+ channels and NFκB [9, 10].

SOCE occurs within spatially segregated Ca^{2+} signaling microdomains where the juxtaposition of ER membrane and the plasma membrane facilitates functional and physical interactions between the proteins in both membranes. Further, these microdomains support dynamic regulation of the channels as well as recruitment and assembly of various accessory proteins that mediate remodeling of ER and plasma membrane to stabilize and modify the spatial and structural architecture of the domain. These changes determine the specificity and optimal rate of protein-protein interactions required for the activation and regulation of SOCE [11, 12]. In addition, recent studies have revealed that other functions, such as lipid transfer between membranes, are also mediated in this cellular region. ER proteins involved in ER-PM lipid exchange are also localized within the ER-PM junctions and these, like STIM1, traverse the space between the two membranes and are anchored to the plasma membrane. The spatial constraints of such microdomains also compartmentalize the Ca^{2+} signals generated by SOCE. Ca^{2+}-dependent signaling proteins such as calmodulin are localized close to the site of Ca^{2+} entry and "sense" local [Ca^{2+}]

near the channel [13]. Several studies have been directed towards identifying the role of plasma membrane lipids associated with this microdomain, mainly because STIM1 and STIM2 have been demonstrated to interact with PIP_2 [14, 15]. Lipid raft domains (LRDs) are biochemically distinct domains in the plasma membrane that are formed by high concentrations and specific organization of lipids, such as cholesterol, PIP_2 and sphingolipids (further discussed below). LRDs serve as a platform for the assembly of various signaling complexes, including calcium signaling complexes. It has been proposed that LRDs facilitate the enrichment of key Ca^{2+} signaling proteins and control functional interactions between proteins that are critically required for generating, modulating and regulating $[Ca^{2+}]_i$ signals [16–18]. Recent studies suggest that LRDs are not rigid structures but are dynamically remodeled both in terms of the composition as well as size and architecture [19].

Another important component in the assembly of SOCE-Ca^{2+} signaling domains is the cortical cytoskeleton underlying the plasma membrane. Reminiscent of vesicle fusion during secretion, interactions between proteins in the ER and plasma membrane will also require disruption of the cortical actin layer. In fact, a number of recent findings demonstrate that remodeling of the cytoskeletal layer probably occurs during regulation of SOCE. Several proteins involved in actin remodeling have been identified (further discussed below) within the ER-PM junctions and the effects of their knockdown or overexpression have been reported, although the exact changes in the cytoskeleton have not yet been revealed. What is important to note is that several cytoskeletal remodeling proteins are controlled via plasma membrane PIP_2. Further, changes in cytoskeleton can remodel the plasma membrane PIP_2. Calcium itself might also regulate actin depolymerization and localize actin remodeling proteins, such as WAVE2, which define a domain for the stable assembly of the STIM1/Orai complex [20]. This reciprocal regulation between plasma membrane lipids and the cortical actin can be very important in the dynamic regulation, stabilization, and compartmentalization of the SOCE microdomain as well as transducing the local Ca^{2+} signal generated within the microdomain [21]. In this chapter, we will discuss current concepts regarding the cellular components that determine the assembly of SOCE channels in ER-PM junctions with primary focus on Orai1 and TRPC1 channels.

11.2 The Molecular Components of SOCE

SOCE, originally termed capacitative calcium entry, was first described by Putney [22], However, the molecular components of this important Ca^{2+} entry pathway were not identified until several decades later. Search for the SOCE channel first led to the identification of the mammalian transient receptor potential canonical (TRPC) channels that were cloned based on the *Drosophila* TRP channel, which is activated by light-induced phospholipase C hydrolysis [23–25]. The TRPC subfamily consists of seven members (TRPCs 1–7) that are all activated following receptor-stimulated PIP_2 hydrolysis. These channels have six transmembrane domains, and a suggested

pore-domain localized between the fifth and sixth membrane-spanning domains [25, 26]. Multiple domains for protein-protein interactions are present both on the N and C terminal regions of the channels. While the discovery of TRPC channels initiated a large number of studies, none of the TRPC family of Ca^{2+}-permeable cation channels generated currents that resembled I_{CRAC} (Ca^{2+} release activated Ca^{2+} current), the first SOCE-associated current to be described in T lymphocytes and mast cells. I_{CRAC} is a highly Ca^{2+}-selective current that is inwardly rectifying with a reversal potential >+40 mV [27–30]. Intensive search for the components of the CRAC channel finally led to the identification of the ER-[Ca^{2+}] sensing proteins, STIM1 and STIM2. Of the two, STIM1 has been more extensively studied and is now well established as the critical and indispensable regulatory component of SOCE [5, 6, 31]. The discovery of STIM1 was followed shortly by the finding of Orai1 and studies showing that it is the pore-forming component of the CRAC channel. Two other Orai proteins, Orai2 and Orai3, have also been identified and although they are reported to have some similarity with Orai1, their physiological function is not clear [32–34]. Together the identification of STIM1 and Orai1 represent the most important advancements in the field of Ca^{2+} signaling. This was further substantiated by data showing that STIM1 and Orai1 are sufficient for the generation of I_{CRAC}.

Loss of either STIM1 or Orai1 in mouse results in embryonic lethality, while in patients, mutations in either gene cause immune defects and deficiencies, diminished skeletal muscle development and ectodermal dysplasia (reviewed in [31, 35]). Mice lacking Orai1 tend to be deficient in both innate and acquired immunity [31, 36, 37], have impaired skeletal muscle and bone development [38–40], and reduced bone density [38, 40]. Mast cells from Orai1 knockout mice showed diminished SOCE, loss of I_{CRAC}, which is accompanied by defective degranulation and cytokine secretion [37]. Acinar cells isolated from the lacrimal glands of Orai1 knockout mice have no detectable SOCE in response to either thapsigargin or muscarinic receptor activation and the secretory response is also severely reduced [41]. Histological examination shows that gland development and structure are normal. Interestingly, it was reported that while female Orai1 knockout mice are fertile, and give birth to pups, they fail to lactate adequately. Mammary glands of Orai1 knockout female mice had normal milk generation but impaired secretion, likely due to failure of Ca^{2+} signaling in myoepithelial cells that are critical in the secretory process within the gland [42]. Loss of Orai1 in pancreatic acinar cells caused secretory defects that lead to changes in the intestinal microbiome and systemic infections that ultimately resulted in morbidity and death [43].

STIM2 is a second ER-localized Ca^{2+}-sensor protein that has been associated with SOCE and Ca^{2+} signaling. It is ubiquitously expressed with STIM1 in human and mouse tissues as well as cell lines (see reviews [44, 45]), although it has not been studied as extensively as STIM1. Like STIM1, STIM2 is also mobilized in response to ER-Ca^{2+} store depletion. It multimerizes and translocates to form puncta in ER-PM junctions, where it clusters with Orai1 and STIM1 [46–50]. The domain architecture of these two proteins are quite similar, with both having the Ca^{2+}-binding EF hand domain, Sterile Alpha Motif (SAM) domain, Coiled-Coiled (CC) domains, STIM1 Orai1 Activating Region (SOAR), and polybasic (K) domain. However, STIM2 is a

poor activator of Orai1 and SOCE when compared to STIM1. The difference in efficiency of gating of Orai1 by the two STIM proteins has been narrowed down to Phe^{394} in STIM1-SOAR domain, the equivalent of which is Leu^{485} in STIM2-SOAR. Further, the interaction between STIM2-SOAR and Orai1 is relatively weaker than that of STIM1-SOAR and Orai1 [49]. Another major difference between STIM2 and STIM1 is in their polybasic C-terminal region, which in STIM2 binds stronger with plasma membrane PIP_2. Data reported by Seedorf and colleagues [14] demonstrated that while a dimer of STIM2 is sufficient to achieve strong binding, a tetramer of STIM1 is required. Notably, while Orai1 can bind to the SOAR domain of a STIM1 mutant lacking its polybasic domain (STIM1ΔK) and induce recovery of its clustering in ER-PM junctions, it cannot do so with STIM2ΔK5 [48]. One possible reason for this might be the weaker binding of STIM2-SOAR to Orai1. This suggests that in STIM2, the polybasic domain is critical for targeting the protein to the SOCE domain. A critical difference between the two proteins is in the Ca^{2+} affinity of their EF-hand domains [46, 51], which determines their response to different ER-$[Ca^{2+}]$. The relatively lower Ca^{2+} affinity of the STIM2 EF-hand domain and the higher affinity of its polybasic domain for plasma membrane PIP_2, enables STIM2 to cluster at ER-PM junctions in response to minimal depletion of ER-Ca^{2+} stores [14, 15, 46, 52–54]. Thus, STIM2 has been proposed to regulate Ca^{2+} entry in unstimulated cells for maintenance of cytosolic Ca^{2+} or to gate Orai1 at low concentrations of agonist stimulation [46, 55, 56].

In a recent study, Ong et al. [48] revealed a novel role for STIM2 in the regulation of SOCE. STIM2 was found to promote STIM1 clustering in ER-PM junctions under conditions when there is less depletion of ER-Ca^{2+} and STIM1 is not mobilized on its own. Thus, STIM2 facilitates assembly of the Orai1-STIM1 complex and activation of SOCE in cells stimulated at low stimulus intensities. They reported that STIM2 associated with and promoted puncta formation of STIM1 in cells stimulated by low [agonist] and when expressed together, Orai1, STIM1, and STIM2 co-clustered under these low stimulation conditions. Importantly, while loss of STIM1 eliminated SOCE at all [agonist], knockdown of STIM2 altered the pattern of SOCE-dependent $[Ca^{2+}]_i$ increases. A sustained elevation in $[Ca^{2+}]_i$ commonly seen in cells stimulated at high [agonist] was converted to a more oscillatory pattern of response, which is typically associated with lower stimulus intensity. Together these data demonstrated that STIM2 enhances STIM1-mediated activation of Orai1 at relatively high ER-$[Ca^{2+}]$ and thus is a key determinant of the SOCE response in cells [48]. The critical contribution of STIM2 to SOCE is provided by studies with mouse T cells and fibroblasts lacking STIM2, which display a decrease in SOCE, cytokine production, and nuclear translocation of the transcription factor, NFAT [57]. Reduced expression of STIM2 leads to impairment of SOCE and Ca^{2+}-dependent gene expression, contributing to neuronal disease in mutant presenilin mice [58]. Further, knockdown of STIM2 in mouse submandibular glands resulted in decreased SOCE together with attenuation of salivary gland fluid secretion stimulated by low [agonist] [48].

All seven members of the TRPC channel family were at some point suggested to be involved in SOCE. However, the data are the strongest for the contribution of

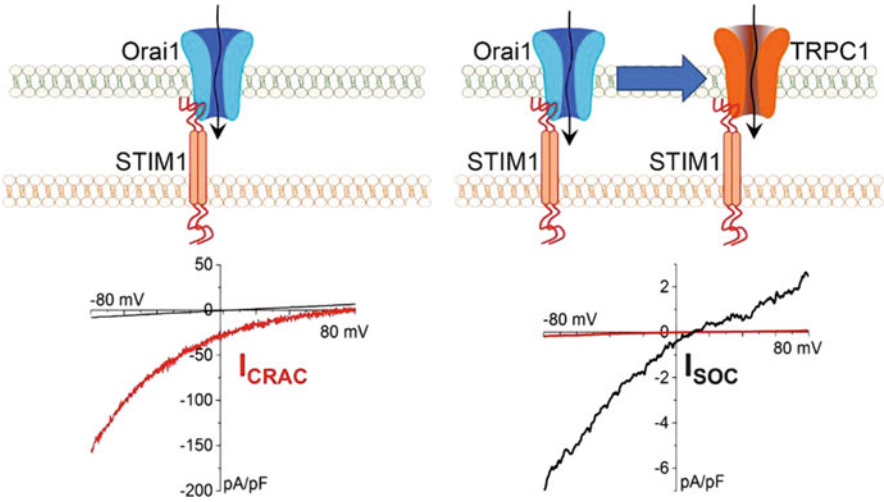

Fig. 11.1 Characteristics of currents generated by Orai1 and TRPC1. STIM1-activated Orai1 channels mediated a highly calcium selective current known as I_{CRAC}. Orai1-mediated Ca^{2+} entry triggers insertion of TRPC1 into the plasma membrane following which the latter is activated by STIM1. Activation of TRPC1 changes the characteristics of the current from I_{CRAC} to a relatively non-selective cation current, I_{SOC}, which is a combination of the individual currents induced by Orai1 and TRPC1

TRPC1 to SOCE. Overexpression of the channel increased, while knockdown of the protein decreased SOCE. Further, the function of TRPC1 was activated by stimulating cells with either agonist or thapsigargin, and inhibited by 1–5 μM Gd^{3+} and 10–20 μM 2APB, which are classical conditions for SOCE. Importantly, whole cell patch clamp measurements under conditions used for CRAC channel measurements resulted in the generation of a cation current that was relatively Ca^{2+}-selective [59–61], completely blocked by low [Gd^{3+}] and 2APB, and decreased by knockdown of TRPC1. As this current does not resemble I_{CRAC}, it has been called store-operated calcium current (I_{SOC}) to distinguish it from I_{CRAC} [62] (Fig. 11.1). Importantly, knockdown of TRPC1 did not affect I_{CRAC}, conclusively demonstrating that it is not a component of the CRAC channel. Additional studies demonstrated that TRPC1 contributes to SOCE in a wide range of cells, including platelets, smooth muscle and endothelial cells [62–68], as well as salivary gland and pancreatic acinar cells [69–71]. Studies with $TRPC1^{-/-}$ mice show that it is a vital Ca^{2+} entry component in several tissues, although the mice display normal viability, development and behavior. TRPC1-mediated Ca^{2+} entry is required for regulating the physiological function of intestinal epithelial cells [72, 73], human malignant gliomas [74], hippocampal neural progenitor cells [75–77]. TRPC1 contributes to maintenance of endothelial cell barrier, wound healing in the intestinal epithelial layer, attenuation of cytotoxicity, contraction of glomerular mesangial cells, and osteoclast formation and function [78–82]. Acinar cells from salivary glands and pancreas and aortic endothelial cells obtained from $TRPC1^{-/-}$

mice exhibit dramatically attenuated SOCE with corresponding reduction in Ca^{2+}-dependent processes such as the activation of K_{Ca} and Ca^{2+}-activated Cl^- channels. Importantly, agonist-stimulated fluid and protein secretion from the salivary glands and pancreas, respectively, as well as vasorelaxation of the aorta were impacted [69–71, 83–85]. It is worth noting that the residual Orai1 cannot compensate for the loss of TRPC1 function in these cells, which clearly establishes the non-redundancy of TRPC1.

11.3 Regulation of TRPC1 Following ER-Ca^{2+} Depletion

The steps initiated by ER-Ca^{2+} depletion culminating in Orai1 activation have now been mapped out in detail. The currently accepted model proposes that a decrease in ER-[Ca^{2+}] cause release of Ca^{2+} from the STIM1-EF hand domain, which then triggers extensive intramolecular and intermolecular rearrangements of STIM1. In resting cells, the protein tracks along microtubules but after store depletion, it oligomerizes and translocates to the cell periphery, aggregating within ER-PM junctions. These junctions are formed by close apposition of the ER membrane with the plasma membrane, which is promoted when the ER-residing STIM1 anchors to the plasma membrane PIP_2, a process that brings ER closer to the PM. Orai1 is recruited by STIM1 into these junctions, where it is subsequently activated by STIM1 to generate SOCE within these junctions. Activation of Orai1 is elicited by interaction of the channel with the SOAR domain in the C-terminal region of STIM1 [33, 34, 86–90]. Importantly, TRPC1 also aggregates with Orai1 and STIM1 within the same ER-PM junctions where STIM1 activates both channels. As mentioned earlier, distinct domains in STIM1 are involved in gating the two channels. Intriguingly, TRPC1 function is not only dependent on STIM1 but also requires Orai1.

Evidence for the regulation of TRPC1 by STIM1 was provided by studies showing that knockdown of STIM1 reduced TRPC1-mediated SOCE and Ca^{2+} current, while co-expression of STIM1+TRPC1 increased SOCE [9, 91, 92]. TRPC1 co-localized and interacted with STIM1 following store depletion while refilling of the ER-Ca^{2+} stores caused dissociation of STIM1 from TRPC1 and inactivation of TRPC1 function [92–97]. A key finding reported by Muallem and colleagues identified the amino acid residues in STIM1 that are involved in gating of TRPC1. These investigators showed that electrostatic interactions between the negatively charged aspartate residues in TRPC1 (^{639}DD^{640}) with the positively charged lysines in the STIM1 polybasic domain (^{684}KK^{685}) triggers gating of TRPC1 [98]. It is interesting that Caveolin-1 (Cav-1), which has been shown to serve as a scaffold for retention of inactive TRPC1 in the plasma membrane region, is displaced from TRPC1 when STIM1 binds to the channel. Further, Cav-1 reassociates with the TRPC1 following refill of ER-Ca^{2+} stores and dissociation of STIM1 [99].

As noted above, activation of TRPC1 requires the presence of functional Orai1. This was first reported by Ambudkar and colleagues in HSG cells [9, 91, 94] and subsequently by other groups in various cell types [100, 101]. These studies demonstrated that knockdown of TRPC1 reduced SOCE by about 60% while loss of Orai1 or STIM1 eliminated SOCE, suggesting that TRPC1-dependent component of SOCE was dependent on Orai1 and STIM1. Overexpression of STIM1 and TRPC1 failed to induce SOCE in the absence of endogenous Orai1 and TRPC1 function was not supported by a pore-deficient mutant of Orai1 (E106Q). These data conclusively established that Orai1 plays an essential role in the activation of TRPC1 by store depletion. It was shown that the Orai1/TRPC1/STIM1 are assembled in a complex within ER-PM junctions after ER-Ca^{2+} depletion and that recruitment of the two channels into the complex requires STIM1 clustering. This was shown in HSG cells [94], human parathyroid cells [102], human liver cells [103], human colon cancer cells [104], mouse pulmonary arterial smooth muscle cells [105, 106], rat kidney fibroblasts [107], rat insulinoma cells [108] and mouse acinar cells from the pancreas and salivary glands [69, 109]. The mechanism underlying TRPC1 activation was provided by Cheng et al. [9] who showed that Ca^{2+} entry mediated by Orai1 triggers recruitment of TRPC1 into the plasma membrane where it is activated by STIM1; non-functional Orai1 mutants, Orai1E106Q or Orai1R91W, do not support the regulated surface expression of TRPC1 [91, 94, 101]. Together these findings reveal that TRPC1/STIM1 and Orai1/STIM1 form distinct channel complexes. While Orai1 is the primary channel to be activated after ER-Ca^{2+} depletion, once activated TRPC1 can modify the Ca^{2+} signal generated by Orai1. Acquisition of TRPC1 function is detected by a change in the characteristics of the current stimulated by ER-Ca^{2+} store depletion from I_{CRAC} to I_{SOC}. Conversely, expression of shTRPC1 or STIM1-EE mutant, a STIM1 mutant that cannot gate TRPC1, converts I_{SOC} into I_{CRAC} ([9]; see Fig. 11.1). While the two channels are localized in close proximity to each other in cells, Ca^{2+} entry mediated by them is utilized by cells to regulate very different cellular functions. Further, the two channels have distinct contributions to the global Ca^{2+} increase in cells that is caused by SOCE [9, 10]. Briefly, Orai1-mediated Ca^{2+} influx regulates the activation of NFAT independently of TRPC1 [110, 111]. However, TRPC1-mediated Ca^{2+} influx is the main source for Ca^{2+} in the regulation of NFκB [9, 10] and K_{Ca} channel in salivary glands [70], as well as Ca^{2+}-dependent Cl^- channel in pancreatic ducts [69].

Targeting of TRPC1 to regions in the cell periphery, near ER-PM junctions, where it can be regulated by STIM1 and Orai1 is a critical determinant in the regulation of its function. TRPC1-containing vesicles can be detected in the sub-plasma membrane region [9]. This localization is essential for TRPC1-containing vesicles to detect the local Ca^{2+}-signal generated by Orai1, and be inserted into the plasma membrane. Since STIM1 also co-clustered with Orai1, TRPC1-STIM1 association is facilitated for channel activation. Internalization of TRPC1 from the plasma membrane, and its transport to this region, is determined by endocytic and exocytic vesicular trafficking pathways, respectively. A recent study reported by de Souza et al. [112] identified the essential vesicular compartments and Rab proteins involved in regulating intracellular trafficking of TRPC1 [112]. This

study demonstrated that TRPC1 is trafficked via a fast-endocytic recycling pathway which involves Rab5 and Rab4. Importantly, this recycling achieves clustering of TRPC1 within ER-PM junctions where STIM1 clusters in response to ER-Ca^{2+} store depletion. The authors reported that expression of Rab5 increased the retention of TRPC1 in early endosomes, leading to reduction of surface expression of TRPC1 and decrease in SOCE. Co-expression of Rab4 with Rab5, but not STIM1 or Rab11, rescued routing of TRPC1 to the plasma membrane. Notably, while STIM1 is required for recruitment of TRPC1 into the plasma membrane and activation after cell stimulation, it is not involved in intracellular trafficking of the channel [112]. This study also showed that internalization of TRPC1 occurs via an endocytic pathway mediated by Arf6 that is independent of clathrin and Cav-1. More importantly, the effects of Rab5 and Arf6 were highly specific for TRPC1, leaving Orai1 and STIM1 unaffected. Thus, mechanisms that regulate/affect plasma membrane expression of TRPC1 also control the modulation of SOCE-generated Ca^{2+}-signals in cells where TRPC1 is present and contributes to Ca^{2+} entry. Further studies are required to determine the exact mechanisms involved in Ca^{2+}-dependent exocytosis of TRPC1-vesicles within the ER-PM junctions.

Other than the important finding that it is triggered by local $[Ca^{2+}]_i$ elevations mediated by Orai1, there are no data to conclusively demonstrate that it is a Ca^{2+}-dependent process. Ca^{2+} sensors or other proteins involved in driving the fusion, such as v-SNAREs and t-SNAREs, that are involved in TRPC1-trafficking have not been identified [9]. The study reported by Cheng et al. [9] argues against a "kiss and run" mechanism for TRPC1 insertion as removal of external Ca^{2+} after channel insertion did not alter plasma membrane levels of TRPC1. Some possible insights into the final step in TRPC1 trafficking comes from studies which show that treatment of human platelets with botulinum toxin significantly decreased SOCE by causing the cleavage and inactivation of SNAP-25 [113]. In endothelial cells, stimulation with thrombin induced assembly of TRPC1 with RhoA and IP_3R, and subsequent translocation of the channel to the plasma membrane. Inhibition of RhoA reduced expression of TRPC1 in the plasma membrane and also adversely affected TRPC1-IP_3R association and attenuated SOCE [66].

11.4 Plasma Membrane Domains in Regulation of SOCE

A number of recent studies suggest that several factors contribute to the assembly of the ER-PM junctions where the regulation of SOCE takes place. There is general agreement that rapid and specific rearrangement of critical proteins within ER/PM junctions control regulation of Ca^{2+} entry, transduction of intracellular Ca^{2+} signals, as well as contribute to the stability of the domain and channel complexes. It has been reported that the membrane environment surrounding the Orai1–channel complex is remodeled or changed after channel activation. Specific regulatory proteins required for modulating SOCE, such as the SOCE-associated regulatory factor (SARAF) which mediates Ca^{2+}-dependent inactivation of Orai1, bind to STIM1

and are recruited to the channel complex [114]. Other proteins like STIMATE interact with STIM1 to enhance its interaction with Orai1 within the junctions. STIMATE requirement for TRPC1/STIM1 interaction has not been reported. It is increasingly clear that lipid components within the plasma membrane also play a critical role in the assembly as well as regulation of the proteins involved in SOCE. For example, a PIP_2 binding protein, Septin, has been recently shown to be required for SOCE [115]. Septin is recruited to ER-PM junctional domains and is required for PIP_2 remodeling which appears to mediate assembly of Orai1/STIM1 channels. Other proteins associated with ER-PM junctions containing STIM1/Orai1 are E-Syt1 and Nir2 [116]. E-Syt1 functions as an ER-to-PM tether and recruits Nir2 to ER-PM junctions where it mediates PIP_2 replenishment after cell stimulation. Both E-Syt1 and Nir2 are co-localized with STIM1 within these junctions. Interaction of SARAF with STIM1 is dependent on E-Syt1-dependent remodeling of PIP_2 in ER-PM junctions, as is the stabilization of STIM1 clusters and assembly of STIM1/Orai1 complex [117]. Most notably, the STIM1-Orai1 complex is initially assembled within a relatively PIP_2-poor domain within ER-PM junctions and SARAF does not bind to STIM1 under this condition, allowing maximal Ca^{2+} influx. The STIM1-Orai1 complex subsequently translocates to a relatively PIP_2-rich domain, which allows SARAF to interact with STIM1 and limit Orai1 function [117]. Alternately, remodeling of PIP_2 around the channel could cause the same effect on SARAF recruitment and channel function. Hence, relatively rapid remodeling of PIP_2 might be required for regulation of Orai1/STIM1 channel. Changes in PIP_2 status in the plasma membrane could be mediated through direct PIP_2 remodeling or by remodeling of the underlying cortical cytoskeleton.

Relatively high amounts of PIP_2 are associated with biochemically distinct lipid domains in the plasma membrane called lipid raft domains (LRDs) (Fig. 11.2). These domains are also enriched in cholesterol and sphingolipids. These membrane regions can be identified based on their relative insolubility in certain detergents at 4°C and their buoyancy on sucrose gradients. Two major types of LRDs have been identified in the plasma membrane, those that contain the cholesterol binding protein, caveolin-1 (Cav-1), and those that do not. The former, known as caveolae, form smooth cholesterol-sensitive and flask-shaped invaginations (50–100 nm) that are found in the plasma membrane of many cell types. In addition to Cav-1, other caveolins (Cav-2, Cav-3) and cavins (Cavin-1 to -4) are also present in the caveolae. Caveolae are predicted to contain between 100 and 200 Cav-1 molecules each, but the minimal Cav-1 oligomer, ~15 Cav-1 molecules, can form oligomerized Cav-1 microdomains that are referred to as the Cav-1 scaffold domain. These non-caveolar Cav-1 microdomains represent raft structures that can recruit signaling proteins and present it to the larger stable caveolar structures [118, 119]. Importantly, Cav-1 has a scaffolding region (aa 82–101) that mediates its binding to multiple signaling proteins [120]. Interaction with Cav-1 facilitates the assembly of its interacting proteins in LRDs. Depending on the type of cell and the location of the LRD, these complexes could carry out a diverse range of cellular signaling. It has also been proposed that caveolar invaginations could facilitate interactions between proteins localized in caveolae with those in intracellular organelles, such as the ER [121]. Thus, caveolae

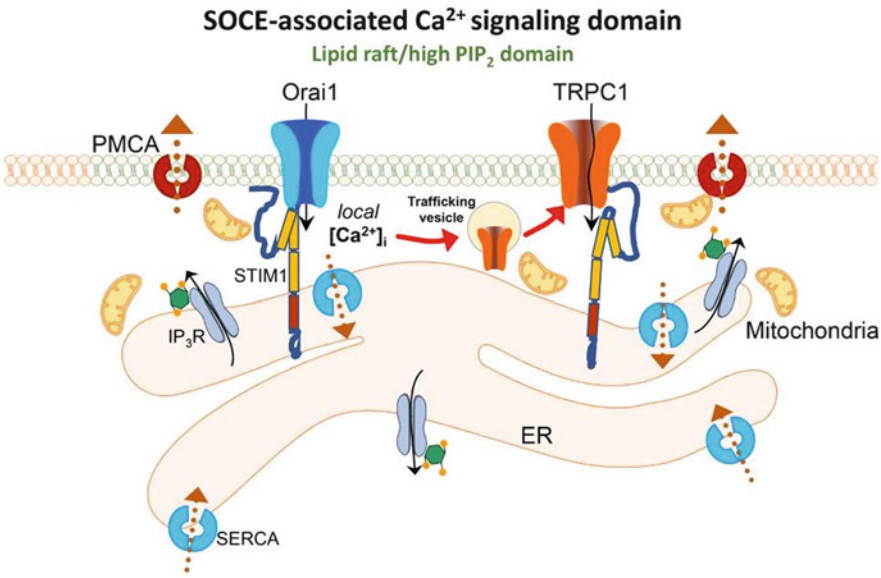

Fig. 11.2 The SOCE-associated Ca^{2+} signaling microdomain. See text for description

have been suggested to be the microdomains for the assembly of Ca^{2+} signaling machinery and regulation of SOCE [18, 122–125].

It was previously believed that all LRDs are stable domains that provide platforms for the assembly of signaling complexes and for mediating processes such as endocytosis. However, new models depict LRDs as much more diverse as well as dynamic structures that vary in size (recently reviewed by Ong and Ambudkar [21]). LRDs are small dynamic domains (<200 nm) where proteins are transiently anchored under resting conditions and in response to stimulation of signaling events, these domains can fuse to create larger and more stable signal transduction platforms or fuse into existing larger signaling complexes [126–128]. Stability of the larger LRD is conferred by protein–protein and/or protein-lipid interactions. Such a process also results in stable accumulation of proteins at sufficiently large concentrations within specific cellular domains which promotes interactions with regulatory components or target proteins. Together, these findings suggest that lipid rafts can form an efficient platform for the compartmentalization of signaling machinery. Scaffolding proteins might be recruited into LRDs and serve as an anchor by binding to the underlying cytoskeleton. Interactions between LRD and cytoskeletal components can contribute to the regulation of its assembly/clustering as well as cytoskeletal dynamics [129, 130]. These cytoskeletal components include actin, tubulin, vinculin, filamin, and tau [131, 132]. Moreover, LRDs themselves can cluster and this clustering may depend upon tethering between cholesterol and actin [133]. It is suggested that remodeling of actin cytoskeleton can control the lateral diffusion of membrane proteins and lipids that are recruited within the LRD [134, 135]. For

example, if Orai1, which is thought to undergo lateral diffusion in the plasma membrane, were recruited into lipid rafts, this type of "fence" might limit its diffusion. Similarly, STIM1 and other SOCE-associated proteins which are mobile in the resting state could get "trapped" within this domain (Fig. 11.2). The presence of STIM1 clusters within ER-PM junctions would facilitate retention of Orai1 and TRPC1 within the same domain. The combination of lateral membrane movement and interaction between membrane proteins within LRD, as well as between the LRD and membrane proteins, with the cytoskeletal and tethering components can control the rate and specificity as well as spatial characteristics of physiologically important responses [21].

11.5 PMCA, SERCA and Ca^{2+} Signaling Microdomains

Key proteins that contribute to regulation of cellular Ca^{2+} homeostasis and associated with SOCE and TRPC channel microdomains are the SERCA, sarco-endoplasmic reticulum calcium pump, and PMCA, plasma membrane calcium pump [136, 137] (Fig. 11.2). Both of these Ca^{2+} pumps affect SOCE as they pump Ca^{2+} out of the cytosol, thereby reducing feedback inhibition of Orai1 and TRPC channels by an increase in $[Ca^{2+}]_i$. While SERCA's primary role is to refill the ER-Ca^{2+} store, PMCA pumps Ca^{2+} across the plasma membrane to prevent cellular overload [138, 139]. Importantly, PMCA has been reported to associate with TRPC1/STIM1 complexes and Orai1/STIM1 complexes in co-immunoprecipitation studies [140, 141]. Interestingly, PIP_2 which has emerged to be critical for regulating SOCE, also regulates PMCA. It was proposed that PIP_2 is a physiological activator of the PMCA pumps [142]. A similar proposal was made for plasma membrane Na^+/Ca^{2+} exchangers [143], although the latter has not been studied in detail in tissues other than cardiac muscle and neurons. The main regulator of PMCA activity is calmodulin, which on binding Ca^{2+}, stimulates Ca^{2+} efflux both by increasing V_{max} and decreasing the K_m for Ca^{2+}. The lipid environment has also been shown to be an important regulator of PMCA activity which is stimulated by acidic phospholipids and long-chain polyunsaturated fatty acids [144]. Cationic domains on the cytoplasmic side of PMCA bind PIP_2. It has been proposed that once agonist stimulation triggers hydrolysis of PIP_2, the pump should immediately become less active. However, it will be activated again by Ca^{2+}, via calmodulin. Caveolae have also been shown to concentrate the PMCA pumps [145]. Some data suggest that PIP_2 is generated and maintained within LRD [146, 147], which are also sites where Orai1/STIM1 and TRPC1/STIM1 are regulated [18]. PMCA has been demonstrated to co-immunoprecipitate with TRPC channels, TRPC1 and TRPC3 [148–150]. Interestingly, PMCA has been shown to be regulated by STIM1 [151]. Thus $[Ca^{2+}]_i$ increases due to SOCE are regulated by STIM1 by activating Orai1 and inhibiting PMCA [152]. The main role PMCA has in SOCE is most likely the regulation of $[Ca^{2+}]$ so as to decrease Ca^{2+}-dependent feedback of the SOCE channels and maintain optimal $[Ca^{2+}]_i$ for activation of downstream effectors. It is

interesting that the "b" isoforms of PMCA contain PDZ-binding domains ([153]; see Fig. 11.2) and can thus interact with a number of proteins, such as MAGUKs, PSD95, NOS-1, etc., that have PDZ domains. Such interactions helps to compartmentalize PMCA into signaling complexes where the Ca^{2+} pump can regulate local $[Ca^{2+}]_i$, so as to regulate proteins that reside in or are recruited to the microdomain. PIP_2 regulation of the pump might also be mediated locally within the micro-domain ([142, 144, 154]). This will allow the PMCA to fine tune local $[Ca^{2+}]$ within ER-PM junctions where Orai1/STIM1 complexes are assembled.

The SERCA is the third component in the regulation of SOCE and Ca^{2+}-microdomains. It colocalizes with STIM1 and Orai1 at puncta which allows efficient filling of the ER-Ca^{2+} stores with minimal diffusion of Ca^{2+} within the cell [155]. The proximity of SERCA to the site of Ca^{2+} entry allows it to detect local [Ca^{2+}] which can be relatively high [155]. The loading of ER-Ca^{2+} depends on the extent of Ca^{2+} leak in the ER, amount of Ca^{2+} entry, and uptake into ER. The spatial architecture of the ER-PM junctions involved in SOCE may also initiate the coupling between SOCE and Ca^{2+} uptake into the ER via SERCA. Some reports show localization of SERCA near STIM1/Orai1 [140, 156]. Of course, the stoichiometry of Orai1, STIM1 and SERCA, would be a critical determinant in the maintenance of Ca^{2+} homeostasis.

11.6 The Role of Lipid Raft Domains in the Regulation of TRPC1

LRDs have been previously proposed to facilitate the enrichment of key Ca^{2+} signaling proteins and control functional interactions between proteins that are required for generating, modulating and regulating $[Ca^{2+}]_i$ signals [16–18, 125]. The polybasic tail region of STIM1 contains a consensus PIP_2-interacting sequence [157, 158]. Deletion of this domain in STIM1 or STIM2 disrupts clustering of the proteins in ER-PM junctions. Overexpression of Orai1 rescues STIM1ΔK clustering, which in turn can gate the channel via SOAR-domain interactions. Thus, PIP_2-rich plasma membrane domains, which include LRDs, are likely to be critical in the regulation of SOCE by STIM1. Consistent with this, several studies have now shown that disruption of lipid rafts alter the interactions of STIM1 with plasma membrane channels, Orai1 and TRPC1, and consequently attenuate SOCE [18, 95, 159].

Early studies with TRPC1 demonstrated that TRPC1 associates with LRDs upon stimulation of cells and that disruption of LRD by treatment with the cholesterol depleting reagents, such as methyl-β-cyclodexrin attenuates SOCE and inhibits TRPC1 partitioning, without affecting intracellular Ca^{2+} release. There are several examples of signaling proteins that partition into membrane raft regions under specific conditions. For example, Ras is known to associate with LRD only in its

inactive GDP-bound state [160]. In contrast, the muscarinic receptor is reported to move into these domains upon binding to an agonist [161]. Caveolar LRD have been proposed to act as scaffolds for pre-assembled signaling complexes, including those involved in Ca^{2+} signaling, which allows the proteins in the complex to be activated following stimulation of cells [16, 18, 123]. Data first reported by Lockwich et al. [162] demonstrated that key Ca^{2+} signaling proteins, including $G\alpha_{q/11}$ and IP_3R, are assembled in a complex with TRPC1 and Cav-1. This study identified two putative caveolin-binding domains in TRPC1 in the N- and C-terminal regions, amino acid residues 281–307 and 626–635, respectively. Subsequently, others reported that mutations in the N-terminal caveolin-binding domain caused loss of plasma membrane scaffolding of TRPC1 together with decrease in SOCE [161]. Thus, these data indicated that TRPC1/SOCE localized to specialized, spatially restricted plasma membrane microenvironment and suggested that the integrity of the LRD is critical for the regulation of SOCE. Several TRPC-SOCE channels have been reported to be localized within the lipid rafts and perturbing the integrity of LRDs (i.e. by depletion of cholesterol) impacts Ca^{2+} entry in all these cases. All mammalian TRPC proteins have putative Cav-1 binding domains in their N- and C-termini and all TRPC proteins have been associated with LRDs [18, 163]. Examples of TRPC1/SOCE association with LRD are as follows: TRPC1 in human salivary gland cells [95, 162, 163], C2C12 skeletal myoblasts [164], striated muscle (as recently reviewed by Sabourin et al. [165]), polymorphonuclear neutrophils [166], endothelial cells [167], human platelets [168], THP-1 monocytic cells [169] and mouse spermatogenic cells and sperm [170].

Importantly, these early studies demonstrated that the ER is located within this microdomain as IP_3R and SERCA, both ER proteins, were immunoprecipitated with TRPC1. The hypothesis proposed at the time was that protein-protein interactions facilitated by the molecular architecture of the domain determine the activation and inactivation of TRPC1/SOCE. However, it was not clear whether LRD disruption interfered with the channel function directly or with the mechanism regulating its activation. Recent studies establish and confirm that critical components and mechanisms associated with SOCE are dependent on LRD and plasma membrane PIP_2. Most importantly, STIM1 was shown to associate with LRD which increased upon stimulation [95, 159]. The polybasic PIP_2-binding domain of STIM1 is likely to be critical in this STIM1-LRD interaction. Disruption of LRD attenuates STIM1 association with LRD and its interaction with TRPC1, which is accompanied by a reduction in SOCE [95]. It is interesting to note that while LRD disruption causes decrease in SOCE by impacting both Orai1/STIM1 and TRPC1/STIM1, loss of Cav-1 affects only TRPC1. Although it has not yet been established, based on the available data with STIM1, we can hypothesize that STIM2 is also partitioned into LRD. Its higher affinity for PIP_2 and lower affinity for Ca^{2+} in the ER-lumen likely determine its partitioning under resting and stimulated conditions. Orai1 has also been shown to have a caveolin binding domain [171]. Moreover, as noted above, regulation of Orai1/STIM1 function is altered by the status of plasma membrane PIP_2. Thus, future studies are required to determine the dynamic nature of plasma membrane lipids within SOCE-associated ER-PM junctions and to identify changes

in Orai1 and TRPC1 activation and regulation that are triggered by lipid dynamics. The STIM1-dependent gating site in TRPC1-C-terminus (aa 639–640; DD) lies very close to the putative Cav-1 binding site (aa 626–635). Although it is unclear whether both the N- and C-terminal Cav-1 binding domains contribute to Cav-1 binding, it is interesting to speculate that displacement of Cav-1 binding from this region could lead to TRPC1 activation. This speculation is based on the dissociation of TRPC1 and caveolin after store depletion which is associated with TRPC1-STIM1 association.

11.7 Conclusions

Localization of the calcium channels (e.g. TRPC1, Orai1) that are involved in SOCE, as well as their regulatory proteins (e.g. STIM1, STIM2), within the narrow confines of the ER-PM junctions facilitates the interactions between them and determines the rate and specificity of these interactions. Increasing evidence supports the concept that the amplitude and temporal pattern of $[Ca^{2+}]$ increase near the channel pore can be quite different from that measured globally. Local and global $[Ca^{2+}]$ are utilized by cells for regulation of distinct cellular functions. Although recent studies have provided knowledge of new proteins and mechanisms that are involved in assembly and stabilization of the ER-PM junctions, further studies are required to determine the exact mechanisms involved in the dynamic remodeling of these junctions. Importantly, a large number of studies have been carried out using exogenously expressed proteins and cell lines. Thus, the status of these junctions in native cells and their physiological relevance remain largely unknown. Another major area where there is a knowledge gap is whether all ER-PM junctions involved in SOCE are similar; i.e. is the regulation of SOCE or architecture of the ER-PM junction different depending on cell type and/or region of the cell. For example, we know that SOCE complexes can include Orai1/STIM1 or TRPC1/Orai1/STIM1 and that these are involved in regulation of distinct cellular functions. So, the question then arises as to whether the architecture and composition of the ER-PM junctions, where these two channel complexes are assembled, are different from each other. Future studies should be focused towards elucidating these aspects of ER-PM junctions and molecular components involved in SOCE.

References

1. Ambudkar IS (2014) Ca^{2+} signaling and regulation of fluid secretion in salivary gland acinar cells. Cell Calcium 55:297–305
2. Berridge MJ (2012) Calcium signalling remodelling and disease. Biochem Soc Trans 40:297–309
3. Berridge MJ (2016) The inositol trisphosphate/calcium signaling pathway in health and disease. Physiol Rev 96:1261–1296

4. Putney JW, Steinckwich-Besancon N, Numaga-Tomita T, Davis FM, Desai PN, D'Agostin DM, Wu S, Bird GS (2017) The functions of store-operated calcium channels. Biochim Biophys Acta 1864:900–906
5. Gudlur A, Zhou Y, Hogan PG (2013) STIM-ORAI interactions that control the CRAC channel. Curr Top Membr 71:33–58
6. Prakriya M, Lewis RS (2015) Store-operated calcium channels. Physiol Rev 95:1383–1436
7. Ong HL, de Souza LB, Ambudkar IS (2016) Role of TRPC channels in store-operated calcium entry. Adv Exp Med Biol 898:87–109
8. Ong HL, de Souza LB, Cheng KT, Ambudkar IS (2014) Physiological functions and regulation of TRPC channels. Handb Exp Pharmacol 223:1005–1034
9. Cheng KT, Liu X, Ong HL, Swaim W, Ambudkar IS (2011) Local Ca^{2+} entry via Orai1 regulates plasma membrane recruitment of TRPC1 and controls cytosolic Ca^{2+} signals required for specific cell functions. PLoS Biol 9:e1001025
10. Ong HL, Jang SI, Ambudkar IS (2012) Distinct contributions of Orai1 and TRPC1 to agonist-induced $[Ca^{2+}]_i$ signals determine specificity of Ca^{2+} -dependent gene expression. PLoS One 7:e47146
11. Chang CL, Chen YJ, Liou J (2017) ER-plasma membrane junctions: why and how do we study them? Biochim Biophys Acta 1864(9):1494–1506
12. Shin DM, Son A, Park S, Kim MS, Ahuja M, Muallem S (2016) The TRPCs, Orais and STIMs in ER/PM junctions. Adv Exp Med Biol 898:47–66
13. Parekh AB (2008) Ca^{2+} microdomains near plasma membrane Ca^{2+} channels: impact on cell function. J Physiol 586:3043–3054
14. Bhardwaj R, Muller HM, Nickel W, Seedorf M (2013) Oligomerization and Ca^{2+}/calmodulin control binding of the ER Ca^{2+}-sensors STIM1 and STIM2 to plasma membrane lipids. Biosci Rep 33:e00077
15. Ercan E, Momburg F, Engel U, Temmerman K, Nickel W, Seedorf M (2009) A conserved, lipid-mediated sorting mechanism of yeast Ist2 and mammalian STIM proteins to the peripheral ER. Traffic 10:1802–1818
16. Ambudkar IS, Ong HL, Singh BB (2010) Molecular and functional determinants of Ca^{2+} signaling microdomains. In: Sitaramayya A (ed) Signal transduction: pathways, mechanisms and diseases. Springer, Heidelberg
17. Jacobson K, Mouritsen OG, Anderson RG (2007) Lipid rafts: at a crossroad between cell biology and physics. Nat Cell Biol 9:7–14
18. Pani B, Singh BB (2009) Lipid rafts/caveolae as microdomains of calcium signaling. Cell Calcium 45:625–633
19. Lingwood D, Simons K (2010) Lipid rafts as a membrane-organizing principle. Science 327:46–50
20. Hartzell CA, Jankowska KI, Burkhardt JK, Lewis RS (2016) Calcium influx through CRAC channels controls actin organization and dynamics at the immune synapse. elife 5:e14850
21. Ong HL, Ambudkar IS (2015) Molecular determinants of TRPC1 regulation within ER-PM junctions. Cell Calcium 58:376–386
22. Putney JW Jr (1990) Capacitative calcium entry revisited. Cell Calcium 11:611–624
23. Birnbaumer L, Zhu X, Jiang M, Boulay G, Peyton M, Vannier B, Brown D, Platano D, Sadeghi H, Stefani E, Birnbaumer M (1996) On the molecular basis and regulation of cellular capacitative calcium entry: roles for Trp proteins. Proc Natl Acad Sci USA 93:15195–15202
24. Montell C, Birnbaumer L, Flockerzi V (2002) The TRP channels, a remarkably functional family. Cell 108:595–598
25. Venkatachalam K, Montell C (2007) TRP channels. Annu Rev Biochem 76:387–417
26. Owsianik G, Talavera K, Voets T, Nilius B (2006) Permeation and selectivity of TRP channels. Annu Rev Physiol 68:685–717
27. Fanger CM, Hoth M, Crabtree GR, Lewis RS (1995) Characterization of T cell mutants with defects in capacitative calcium entry: genetic evidence for the physiological roles of CRAC channels. J Cell Biol 131:655–667

28. Hoth M, Penner R (1992) Depletion of intracellular calcium stores activates a calcium current in mast cells. Nature 355:353–356
29. Hoth M, Penner R (1993) Calcium release-activated calcium current in rat mast cells. J Physiol 465:359–386
30. Lewis RS, Cahalan MD (1989) Mitogen-induced oscillations of cytosolic Ca^{2+} and transmembrane Ca^{2+} current in human leukemic T cells. Cell Regul 1:99–112
31. Feske S (2009) ORAI1 and STIM1 deficiency in human and mice: roles of store-operated Ca^{2+} entry in the immune system and beyond. Immunol Rev 231:189–209
32. Dehaven WI, Smyth JT, Boyles RR, Putney JW Jr (2007) Calcium inhibition and calcium potentiation of Orai1, Orai2, and Orai3 calcium release-activated calcium channels. J Biol Chem 282:17548–17556
33. Feske S, Gwack Y, Prakriya M, Srikanth S, Puppel SH, Tanasa B, Hogan PG, Lewis RS, Daly M, Rao A (2006) A mutation in Orai1 causes immune deficiency by abrogating CRAC channel function. Nature 441:179–185
34. Vig M, Beck A, Billingsley JM, Lis A, Parvez S, Peinelt C, Koomoa DL, Soboloff J, Gill DL, Fleig A, Kinet JP, Penner R (2006) CRACM1 multimers form the ion-selective pore of the CRAC channel. Curr Biol 16:2073–2079
35. Feske S (2010) CRAC channelopathies. Pflugers Arch 460:417–435
36. Gwack Y, Srikanth S, Oh-Hora M, Hogan PG, Lamperti ED, Yamashita M, Gelinas C, Neems DS, Sasaki Y, Feske S, Prakriya M, Rajewsky K, Rao A (2008) Hair loss and defective T- and B-cell function in mice lacking ORAI1. Mol Cell Biol 28:5209–5222
37. Vig M, Dehaven WI, Bird GS, Billingsley JM, Wang H, Rao PE, Hutchings AB, Jouvin MH, Putney JW, Kinet JP (2008) Defective mast cell effector functions in mice lacking the CRACM1 pore subunit of store-operated calcium release-activated calcium channels. Nat Immunol 9:89–96
38. Hwang SY, Foley J, Numaga-Tomita T, Petranka JG, Bird GS, Putney JW Jr (2012) Deletion of Orai1 alters expression of multiple genes during osteoclast and osteoblast maturation. Cell Calcium 52:488–500
39. Lyfenko AD, Dirksen RT (2008) Differential dependence of store-operated and excitation-coupled Ca^{2+} entry in skeletal muscle on STIM1 and Orai1. J Physiol 586:4815–4824
40. Robinson LJ, Mancarella S, Songsawad D, Tourkova IL, Barnett JB, Gill DL, Soboloff J, Blair HC (2012) Gene disruption of the calcium channel Orai1 results in inhibition of osteoclast and osteoblast differentiation and impairs skeletal development. Lab Investig 92:1071–1083
41. Xing J, Petranka JG, Davis FM, Desai PN, Putney JW, Bird GS (2014) Role of Orai1 and store-operated calcium entry in mouse lacrimal gland signalling and function. J Physiol 592:927–939
42. Davis FM, Janoshazi A, Janardhan KS, Steinckwich N, D'Agostin DM, Petranka JG, Desai PN, Roberts-Thomson SJ, Bird GS, Tucker DK, Fenton SE, Feske S, Monteith GR, Putney JW, JR. (2015) Essential role of Orai1 store-operated calcium channels in lactation. Proc Natl Acad Sci USA 112:5827–5832
43. Ahuja M, Schwartz DM, Tandon M, Son A, Zeng M, Swaim W, Eckhaus M, Hoffman V, Cui Y, Xiao B, Worley PF, Muallem S (2017) Orai1-mediated antimicrobial secretion from pancreatic acini shapes the gut microbiome and regulates gut innate immunity. Cell Metab 25:635–646
44. Berna-Erro A, Jardin I, Salido GM, Rosado JA (2017) Role of STIM2 in cell function and physiopathology. J Physiol 595(10):3111–3128
45. Lopez E, Salido GM, Rosado JA, Berna-Erro A (2012) Unraveling STIM2 function. J Physiol Biochem 68:619–633
46. Brandman O, Liou J, Park WS, Meyer T (2007) STIM2 is a feedback regulator that stabilizes basal cytosolic and endoplasmic reticulum Ca2+ levels. Cell 131:1327–1339
47. Darbellay B, Arnaudeau S, Ceroni D, Bader CR, Konig S, Bernheim L (2010) Human muscle economy myoblast differentiation and excitation-contraction coupling use the same molecular partners, STIM1 and STIM2. J Biol Chem 285:22437–22447

48. Ong HL, de Souza LB, Zheng C, Cheng KT, Liu X, Goldsmith CM, Feske S, Ambudkar IS (2015) STIM2 enhances receptor-stimulated Ca^{2+} signaling by promoting recruitment of STIM1 to the endoplasmic reticulum-plasma membrane junctions. Sci Signal 8:ra3
49. Wang X, Wang Y, Zhou Y, Hendron E, Mancarella S, Andrake MD, Rothberg BS, Soboloff J, Gill DL (2014) Distinct Orai-coupling domains in STIM1 and STIM2 define the Orai-activating site. Nat Commun 5:3183–3193
50. Wang Y, Deng X, Zhou Y, Hendron E, Mancarella S, Ritchie MF, Tang XD, Baba Y, Kurosaki T, Mori Y, Soboloff J, Gill DL (2009) STIM protein coupling in the activation of Orai channels. Proc Natl Acad Sci USA 106:7391–7396
51. Stathopulos PB, Ikura M (2013) Structural aspects of calcium-release activated calcium channel function. Channels (Austin) 7:344–353
52. Stathopulos PB, Zheng L, Ikura M (2009) Stromal interaction molecule (STIM) 1 and STIM2 calcium sensing regions exhibit distinct unfolding and oligomerization kinetics. J Biol Chem 284:728–732
53. Zheng L, Stathopulos PB, Li GY, Ikura M (2008) Biophysical characterization of the EF-hand and SAM domain containing Ca^{2+} sensory region of STIM1 and STIM2. Biochem Biophys Res Commun 369:240–246
54. Zheng L, Stathopulos PB, Schindl R, Li GY, Romanin C, Ikura M (2011) Auto-inhibitory role of the EF-SAM domain of STIM proteins in store-operated calcium entry. Proc Natl Acad Sci USA 108:1337–1342
55. Kar P, Bakowski D, Di Capite J, Nelson C, Parekh AB (2012) Different agonists recruit different stromal interaction molecule proteins to support cytoplasmic Ca^{2+} oscillations and gene expression. Proc Natl Acad Sci USA 109:6969–6974
56. Thiel M, Lis A, Penner R (2013) STIM2 drives Ca^{2+} oscillations through store-operated Ca^{2+} entry caused by mild store depletion. J Physiol 591:1433–1445
57. Oh-Hora M, Yamashita M, Hogan PG, Sharma S, Lamperti E, Chung W, Prakriya M, Feske S, Rao A (2008) Dual functions for the endoplasmic reticulum calcium sensors STIM1 and STIM2 in T cell activation and tolerance. Nat Immunol 9:432–443
58. Sun S, Zhang H, Liu J, Popugaeva E, Xu NJ, Feske S, White CL 3rd, Bezprozvanny I (2014) Reduced synaptic STIM2 expression and impaired store-operated calcium entry cause destabilization of mature spines in mutant presenilin mice. Neuron 82:79–93
59. Brueggemann LI, Markun DR, Henderson KK, Cribbs LL, Byron KL (2006) Pharmacological and electrophysiological characterization of store-operated currents and capacitative Ca^{2+} entry in vascular smooth muscle cells. J Pharmacol Exp Ther 317:488–499
60. Liu X, Bandyopadhyay BC, Singh BB, Groschner K, Ambudkar IS (2005) Molecular analysis of a store-operated and 2-acetyl-sn-glycerol-sensitive non-selective cation channel. Heteromeric assembly of TRPC1-TRPC3. J Biol Chem 280:21600–21606
61. Liu X, Groschner K, Ambudkar IS (2004) Distinct Ca^{2+} -permeable cation currents are activated by internal Ca^{2+} -store depletion in RBL-2H3 cells and human salivary gland cells, HSG and HSY. J Membr Biol 200:93–104
62. Liu X, Singh BB, Ambudkar IS (2003) TRPC1 is required for functional store-operated Ca^{2+} channels. Role of acidic amino acid residues in the S5-S6 region. J Biol Chem 278:11337–11343
63. Brownlow SL, Harper AG, Harper MT, Sage SO (2004) A role for hTRPC1 and lipid raft domains in store-mediated calcium entry in human platelets. Cell Calcium 35:107–113
64. Dietrich A, Chubanov V, Kalwa H, Rost BR, Gudermann T (2006) Cation channels of the transient receptor potential superfamily: their role in physiological and pathophysiological processes of smooth muscle cells. Pharmacol Ther 112:744–760
65. Liu X, Wang W, Singh BB, Lockwich T, Jadlowiec J, O'Connell B, Wellner R, Zhu MX, Ambudkar IS (2000) Trp1, a candidate protein for the store-operated Ca^{2+} influx mechanism in salivary gland cells. J Biol Chem 275:3403–3411

66. Mehta D, Ahmmed GU, Paria BC, Holinstat M, Voyno-Yasenetskaya T, Tiruppathi C, Minshall RD, Malik AB (2003) RhoA interaction with inositol 1,4,5-triphosphate receptor and transient receptor potential channel-1 regulates Ca^{2+} entry. J Biol Chem 278:33492–33500
67. Rosado JA, Brownlow SL, Sage SO (2002) Endogenously expressed Trp1 is involved in store-mediated Ca^{2+} entry by conformational coupling in human platelets. J Biol Chem 277:42157–42163
68. Tiruppathi C, Ahmmed GU, Vogel SM, Malik AB (2006) Ca^{2+} signaling, TRP channels, and endothelial permeability. Microcirculation 13:693–708
69. Hong JH, Li Q, Kim MS, Shin DM, Feske S, Birnbaumer L, Cheng KT, Ambudkar IS, Muallem S (2011) Polarized but differential localization and recruitment of STIM1, Orai1 and TRPC channels in secretory cells. Traffic 12:232–245
70. Liu X, Cheng KT, Bandyopadhyay BC, Pani B, Dietrich A, Paria BC, Swaim WD, Beech D, Yildrim E, Singh BB, Birnbaumer L, Ambudkar IS (2007) Attenuation of store-operated Ca^{2+} current impairs salivary gland fluid secretion in $TRPC1^{-/-}$ mice. Proc Natl Acad Sci USA 104:17542–17547
71. Ma X, Cheng KT, Wong CO, O'Neil RG, Birnbaumer L, Ambudkar IS, Yao X (2011) Heteromeric TRPV4-C1 channels contribute to storeoperated Ca^{2+} entry in vascular endothelial cells. Cell Calcium 50:502–509
72. Bomben VC, Turner KL, Barclay TT, Sontheimer H (2011) Transient receptor potential canonical channels are essential for chemotactic migration of human malignant gliomas. J Cell Physiol 226:1879–1888
73. Rao JN, Platoshyn O, Golovina VA, Liu L, Zou T, Marasa BS, Turner DJ, Yuan JX, Wang JY (2006) TRPC1 functions as a store-operated Ca^{2+} channel in intestinal epithelial cells and regulates early mucosal restitution after wounding. Am J Physiol Gastrointest Liver Physiol 290:G782–G792
74. Cuddapah VA, Turner KL, Seifert S, Sontheimer H (2013) Bradykinin-induced chemotaxis of human gliomas requires the activation of $K_{Ca}3.1$ and ClC-3. J Neurosci 33:1427–1440
75. Fiorio Pla A, Maric D, Brazer SC, Giacobini P, Liu X, Chang YH, Ambudkar IS, Barker JL (2005) Canonical transient receptor potential 1 plays a role in basic fibroblast growth factor (bFGF)/FGF receptor-1-induced Ca^{2+} entry and embryonic rat neural stem cell proliferation. J Neurosci 25:2687–2701
76. Li M, Chen C, Zhou Z, Xu S, Yu Z (2012) A TRPC1-mediated increase in store-operated Ca^{2+} entry is required for the proliferation of adult hippocampal neural progenitor cells. Cell Calcium 51:486–496
77. Mcgurk JS, Shim S, Kim JY, Wen Z, Song H, Ming GL (2011) Postsynaptic TRPC1 function contributes to BDNF-induced synaptic potentiation at the developing neuromuscular junction. J Neurosci 31:14754–14762
78. Bollimuntha S, Singh BB, Shavali S, Sharma SK, Ebadi M (2005) TRPC1-mediated inhibition of 1-methyl-4-phenylpyridinium ion neurotoxicity in human SH-SY5Y neuroblastoma cells. J Biol Chem 280:2132–2140
79. Du J, Sours-Brothers S, Coleman R, Ding M, Graham S, Kong DH, Ma R (2007) Canonical transient receptor potential 1 channel is involved in contractile function of glomerular mesangial cells. J Am Soc Nephrol 18:1437–1445
80. Ong EC, Nesin V, Long CL, Bai CX, Guz JL, Ivanov IP, Abramowitz J, Birnbaumer L, Humphrey MB, Tsiokas L (2013) A TRPC1-dependent pathway regulates osteoclast formation and function. J Biol Chem 288:22219–22231
81. Paria BC, Vogel SM, Ahmmed GU, Alamgir S, Shroff J, Malik AB, Tiruppathi C (2004) Tumor necrosis factor-α-induced TRPC1 expression amplifies store-operated Ca^{2+} influx and endothelial permeability. Am J Phys Lung Cell Mol Phys 287:L1303–L1313
82. Sours S, Du J, Chu S, Ding M, Zhou XJ, Ma R (2006) Expression of canonical transient receptor potential (TRPC) proteins in human glomerular mesangial cells. Am J Physiol Ren Physiol 290:F1507–F1515

83. Dietrich A, Fahlbusch M, Gudermann T (2014) Classical transient receptor potential 1 (TRPC1): channel or channel regulator? Cell 3:939–962
84. Pani B, Bollimuntha S, Singh BB (2012) The TR (i)P to Ca^{2+} signaling just got STIMy: an update on STIM1 activated TRPC channels. Front Biosci 17:805–823
85. Sun Y, Birnbaumer L, Singh BB (2015) TRPC1 regulates calcium-activated chloride channels in salivary gland cells. J Cell Physiol 230(11):2848–2856
86. Gwack Y, Srikanth S, Feske S, Cruz-Guilloty F, Oh-Hora M, Neems DS, Hogan PG, Rao A (2007) Biochemical and functional characterization of Orai proteins. J Biol Chem 282:16232–16243
87. Hogan PG, Lewis RS, Rao A (2010) Molecular basis of calcium signaling in lymphocytes: STIM and ORAI. Annu Rev Immunol 28:491–533
88. Liou J, Kim ML, Heo WD, Jones JT, Myers JW, Ferrell JE Jr, Meyer T (2005) STIM is a Ca^{2+} sensor essential for Ca^{2+} -store-depletion-triggered Ca^{2+} influx. Curr Biol 15:1235–1241
89. Prakriya M, Feske S, Gwack Y, Srikanth S, Rao A, Hogan PG (2006) Orai1 is an essential pore subunit of the CRAC channel. Nature 443:230–233
90. Roos J, Digregorio PJ, Yeromin AV, Ohlsen K, Lioudyno M, Zhang S, Safrina O, Kozak JA, Wagner SL, Cahalan MD, Velicelebi G, Stauderman KA (2005) STIM1, an essential and conserved component of store-operated Ca^{2+} channel function. J Cell Biol 169:435–445
91. Cheng KT, Liu X, Ong HL, Ambudkar IS (2008) Functional requirement for Orai1 in store-operated TRPC1-STIM1 channels. J Biol Chem 283:12935–12940
92. Huang GN, Zeng W, Kim JY, Yuan JP, Han L, Muallem S, Worley PF (2006) STIM1 carboxyl-terminus activates native SOC, Icrac and TRPC1 channels. Nat Cell Biol 8:1003–1010
93. Lopez JJ, Salido GM, Pariente JA, Rosado JA (2006) Interaction of STIM1 with endogenously expressed human canonical TRP1 upon depletion of intracellular Ca^{2+} stores. J Biol Chem 281:28254–28264
94. Ong HL, Cheng KT, Liu X, Bandyopadhyay BC, Paria BC, Soboloff J, Pani B, Gwack Y, Srikanth S, Singh BB, Gill DL, Ambudkar IS (2007) Dynamic assembly of TRPC1-STIM1-Orai1 ternary complex is involved in store-operated calcium influx. Evidence for similarities in store-operated and calcium release-activated calcium channel components. J Biol Chem 282:9105–9116
95. Pani B, Ong HL, Liu X, Rauser K, Ambudkar IS, Singh BB (2008) Lipid rafts determine clustering of STIM1 in endoplasmic reticulum-plasma membrane junctions and regulation of store-operated Ca^{2+} entry (SOCE). J Biol Chem 283:17333–17340
96. Yuan JP, Zeng W, Huang GN, Worley PF, Muallem S (2007) STIM1 heteromultimerizes TRPC channels to determine their function as store-operated channels. Nat Cell Biol 9:636–645
97. Zeng W, Yuan JP, Kim MS, Choi YJ, Huang GN, Worley PF, Muallem S (2008) STIM1 gates TRPC channels, but not Orai1, by electrostatic interaction. Mol Cell 32:439–448
98. Yuan JP, Zeng W, Dorwart MR, Choi YJ, Worley PF, Muallem S (2009) SOAR and the polybasic STIM1 domains gate and regulate Orai channels. Nat Cell Biol 11:337–343
99. Pani B, Ong HL, Brazer SC, Liu X, Rauser K, Singh BB, Ambudkar IS (2009) Activation of TRPC1 by STIM1 in ER-PM microdomains involves release of the channel from its scaffold caveolin-1. Proc Natl Acad Sci USA 106:20087–20092
100. Jardin I, Lopez JJ, Salido GM, Rosado JA (2008) Orai1 mediates the interaction between STIM1 and hTRPC1 and regulates the mode of activation of hTRPC1-forming Ca^{2+} channels. J Biol Chem 283:25296–25304
101. Kim MS, Zeng W, Yuan JP, Shin DM, Worley PF, Muallem S (2009) Native store-operated Ca^{2+} influx requires the channel function of Orai1 and TRPC1. J Biol Chem 284:9733–9741
102. Lu M, Branstrom R, Berglund E, Hoog A, Bjorklund P, Westin G, Larsson C, Farnebo LO, Forsberg L (2010) Expression and association of TRPC subtypes with Orai1 and STIM1 in human parathyroid. J Mol Endocrinol 44:285–294

103. Zhang ZY, Pan LJ, Zhang ZM (2010) Functional interactions among STIM1, Orai1 and TRPC1 on the activation of SOCs in HL-7702 cells. Amino Acids 39:195–204
104. Gueguinou M, Harnois T, Crottes D, Uguen A, Deliot N, Gambade A, Chantome A, Haelters JP, Jaffres PA, Jourdan ML, Weber G, Soriani O, Bougnoux P, Mignen O, Bourmeyster N, Constantin B, Lecomte T, Vandier C, Potier-Cartereau M (2016) SK3/TRPC1/Orai1 complex regulates SOCE-dependent colon cancer cell migration: a novel opportunity to modulate anti-EGFR mAb action by the alkyl-lipid Ohmline. Oncotarget 7:36168–36184
105. Ng LC, Mccormack MD, Airey JA, Singer CA, Keller PS, Shen XM, Hume JR (2009) TRPC1 and STIM1 mediate capacitative Ca^{2+} entry in mouse pulmonary arterial smooth muscle cells. J Physiol 587:2429–2442
106. Ng LC, O'Neill KG, French D, Airey JA, Singer CA, Tian H, Shen XM, Hume JR (2012) TRPC1 and Orai1 interact with STIM1 and mediate capacitative Ca^{2+} entry caused by acute hypoxia in mouse pulmonary arterial smooth muscle cells. Am J Phys Cell Phys 303:C1156–C1172
107. Almirza WH, Peters PH, Van Zoelen EJ, Theuvenet AP (2012) Role of Trpc channels, Stim1 and Orai1 in PGF2α-induced calcium signaling in NRK fibroblasts. Cell Calcium 51:12–21
108. Sabourin J, Le Gal L, Saurwein L, Haefliger JA, Raddatz E, Allagnat F (2015) Store-operated Ca^{2+} entry mediated by Orai1 and TRPC1 participates to insulin secretion in rat β -cells. J Biol Chem 290:30530–30539
109. Pani B, Liu X, Bollimuntha S, Cheng KT, Niesman IR, Zheng C, Achen VR, Patel HH, Ambudkar IS, Singh BB (2013) Impairment of TRPC1-STIM1 channel assembly and AQP5 translocation compromise agonist-stimulated fluid secretion in mice lacking caveolin1. J Cell Sci 126:667–675
110. Cheng KT, Ong HL, Liu X, Ambudkar IS (2013) Contribution and regulation of TRPC channels in store-operated Ca^{2+} entry. Curr Top Membr 71:149–179
111. Parekh AB (2011) Decoding cytosolic Ca^{2+} oscillations. Trends Biochem Sci 36:78–87
112. de Souza LB, Ong HL, Liu X, Ambudkar IS (2015) Fast endocytic recycling determines TRPC1-STIM1 clustering in ER-PM junctions and plasma membrane function of the channel. Biochim Biophys Acta 1853:2709–2721
113. Rosado JA, Redondo PC, Salido GM, Sage SO, Pariente JA (2005) Cleavage of SNAP-25 and VAMP-2 impairs store-operated Ca^{2+} entry in mouse pancreatic acinar cells. Am J Phys Cell Phys 288:C214–C221
114. Palty R, Raveh A, Kaminsky I, Meller R, Reuveny E (2012) SARAF inactivates the store operated calcium entry machinery to prevent excess calcium refilling. Cell 149:425–438
115. Sharma S, Quintana A, Findlay GM, Mettlen M, Baust B, Jain M, Nilsson R, Rao A, Hogan PG (2013) An siRNA screen for NFAT activation identifies septins as coordinators of store-operated Ca^{2+} entry. Nature 499:238–242
116. Chang CL, Hsieh TS, Yang TT, Rothberg KG, Azizoglu DB, Volk E, Liao JC, Liou J (2013) Feedback regulation of receptor-induced Ca^{2+} signaling mediated by E-Syt1 and Nir2 at endoplasmic reticulum-plasma membrane junctions. Cell Rep 5:813–825
117. Maleth J, Choi S, Muallem S, Ahuja M (2014) Translocation between PI(4,5)P_2-poor and PI(4,5)P_2-rich microdomains during store depletion determines STIM1 conformation and Orai1 gating. Nat Commun 5:5843
118. Parton RG, Hanzal-Bayer M, Hancock JF (2006) Biogenesis of caveolae: a structural model for caveolin-induced domain formation. J Cell Sci 119:787–796
119. Parton RG, Simons K (2007) The multiple faces of caveolae. Nat Rev Mol Cell Biol 8:185–194
120. Thomas CM, Smart EJ (2008) Caveolae structure and function. J Cell Mol Med 12:796–809
121. Duchen MR, Verkhratsky A, Muallem S (2008) Mitochondria and calcium in health and disease. Cell Calcium 44:1–5
122. Ambudkar IS, Bandyopadhyay BC, Liu X, Lockwich TP, Paria B, Ong HL (2006) Functional organization of TRPC-Ca^{2+} channels and regulation of calcium microdomains. Cell Calcium 40:495–504

123. Hansen CG, Nichols BJ (2010) Exploring the caves: cavins, caveolins and caveolae. Trends Cell Biol 20(4):177–186
124. Isshiki M, Ying Y, Fujita T, Anderson RGW (2002) A molecular sensor detects signal transduction from caveolae in living cells. J Biol Chem 277:23389–23398
125. Ong HL, Ambudkar IS (2012) Role of lipid rafts in the regulation of store-operated Ca^{2+} channels. Cholesterol regulation of ion channels and receptors. Wiley, Hoboken
126. Chen TY, Liu PH, Ruan CT, Chiu L, Kung FL (2006) The intracellular domain of amyloid precursor protein interacts with flotillin-1, a lipid raft protein. Biochem Biophys Res Commun 342:266–272
127. Eggeling C, Ringemann C, Medda R, Schwarzmann G, Sandhoff K, Polyakova S, Belov VN, Hein B, Von Middendorff C, Schonle A, Hell SW (2009) Direct observation of the nanoscale dynamics of membrane lipids in a living cell. Nature 457:1159–1162
128. Simons K, Toomre D (2000) Lipid rafts and signal transduction. Nat Rev Mol Cell Biol 1:31–39
129. Head BP, Patel HH, Roth DM, Murray F, Swaney JS, Niesman IR, Farquhar MG, Insel PA (2006) Microtubules and actin microfilaments regulate lipid raft/caveolae localization of adenylyl cyclase signaling components. J Biol Chem 281:26391–26399
130. Suzuki T, Zhang J, Miyazawa S, Liu Q, Farzan MR, Yao WD (2011) Association of membrane rafts and postsynaptic density: proteomics, biochemical, and ultrastructural analyses. J Neurochem 119:64–77
131. Goudenege S, Dargelos E, Claverol S, Bonneu M, Cottin P, Poussard S (2007) Comparative proteomic analysis of myotube caveolae after milli-calpain deregulation. Proteomics 7:3289–3298
132. Whitehead SN, Gangaraju S, Aylsworth A, Hou ST (2012) Membrane raft disruption results in neuritic retraction prior to neuronal death in cortical neurons. Biosci Trends 6:183–191
133. Goswami D, Gowrishankar K, Bilgrami S, Ghosh S, Raghupathy R, Chadda R, Vishwakarma R, Rao M, Mayor S (2008) Nanoclusters of GPI-anchored proteins are formed by cortical actin-driven activity. Cell 135:1085–1097
134. Kusumi A, Koyama-Honda I, Suzuki K (2004) Molecular dynamics and interactions for creation of stimulation-induced stabilized rafts from small unstable steady-state rafts. Traffic 5:213–230
135. Ritchie K, Iino R, Fujiwara T, Murase K, Kusumi A (2003) The fence and picket structure of the plasma membrane of live cells as revealed by single molecule techniques (review). Mol Membr Biol 20:13–18
136. Lopreiato R, Giacomello M, Carafoli E (2014) The plasma membrane calcium pump: new ways to look at an old enzyme. J Biol Chem 289:10261–10268
137. Ong HL, Ambudkar IS (2011) The dynamic complexity of the TRPC1 channelosome. Channels (Austin) 5:424–431
138. Krebs J (2015) The plethora of PMCA isoforms: alternative splicing and differential expression. Biochim Biophys Acta 1853:2018–2024
139. Krebs J, Agellon LB, Michalak M (2015) Ca^{2+} homeostasis and endoplasmic reticulum (ER) stress: an integrated view of calcium signaling. Biochem Biophys Res Commun 460:114–121
140. Alonso MT, Manjarres IM, Garcia-Sancho J (2012) Privileged coupling between Ca^{2+} entry through plasma membrane store-operated Ca^{2+} channels and the endoplasmic reticulum Ca^{2+} pump. Mol Cell Endocrinol 353:37–44
141. Elaib Z, Saller F, Bobe R (2016) The calcium entry-calcium refilling coupling. Adv Exp Med Biol 898:333–352
142. Choquette D, Hakim G, Filoteo AG, Plishker GA, Bostwick JR, Penniston JT (1984) Regulation of plasma membrane Ca^{2+} ATPases by lipids of the phosphatidylinositol cycle. Biochem Biophys Res Commun 125:908–915

143. Luciani S, Antolini M, Bova S, Cargnelli G, Cusinato F, Debetto P, Trevisi L, Varotto R (1995) Inhibition of cardiac sarcolemmal sodium-calcium exchanger by glycerophosphoinositol 4-phosphate and glycerophosphoinositol 4-5-bisphosphate. Biochem Biophys Res Commun 206:674–680
144. Niggli V, Adunyah ES, Carafoli E (1981) Acidic phospholipids, unsaturated fatty acids, and limited proteolysis mimic the effect of calmodulin on the purified erythrocyte Ca^{2+} - ATPase. J Biol Chem 256:8588–8592
145. Hilgemann DW, Feng S, Nasuhoglu C (2001) The complex and intriguing lives of PIP_2 with ion channels and transporters. Sci STKE 2001:re19
146. Hope HR, Pike LJ (1996) Phosphoinositides and phosphoinositide-utilizing enzymes in detergent-insoluble lipid domains. Mol Biol Cell 7:843–851
147. Pike LJ, Casey L (1996) Localization and turnover of phosphatidylinositol 4,5-bisphosphate in caveolin-enriched membrane domains. J Biol Chem 271:26453–26456
148. Kim JY, Zeng W, Kiselyov K, Yuan JP, Dehoff MH, Mikoshiba K, Worley PF, Muallem S (2006) Homer 1 mediates store- and inositol 1,4,5-trisphosphate receptor-dependent translocation and retrieval of TRPC3 to the plasma membrane. J Biol Chem 281:32540–32549
149. Lockwich T, Pant J, Makusky A, Jankowska-Stephens E, Kowalak JA, Markey SP, Ambudkar IS (2008) Analysis of TRPC3-interacting proteins by tandem mass spectrometry. J Proteome Res 7:979–989
150. Singh BB, Liu X, Tang J, Zhu MX, Ambudkar IS (2002) Calmodulin regulates Ca^{2+} - dependent feedback inhibition of store-operated Ca^{2+} influx by interaction with a site in the C terminus of TrpC1. Mol Cell 9:739–750
151. Ritchie MF, Samakai E, Soboloff J (2012) STIM1 is required for attenuation of PMCA-mediated Ca^{2+} clearance during T-cell activation. EMBO J 31:1123–1133
152. Srikanth S, Gwack Y (2012) Orai1, STIM1, and their associating partners. J Physiol 590:4169–4177
153. Kim E, DeMarco SJ, Marfatia SM, Chishti AH, Sheng M, Strehler EE (1998) Plasma membrane Ca^{2+} ATPase isoform 4b binds to membrane-associated guanylate kinase (MAGUK) proteins via their PDZ (PSD-95/Dlg/ZO-1) domains. J Biol Chem 273:1591–1595
154. Carafoli E, Zurini M (1982) The Ca^{2+}-pumping ATPase of plasma membranes. Purification, reconstitution and properties. Biochim Biophys Acta 683:279–301
155. Manjarres IM, Rodriguez-Garcia A, Alonso MT, Garcia-Sancho J (2010) The sarco/endoplasmic reticulum Ca^{2+} ATPase (SERCA) is the third element in capacitative calcium entry. Cell Calcium 47:412–418
156. Sampieri A, Zepeda A, Asanov A, Vaca L (2009) Visualizing the store-operated channel complex assembly in real time: identification of SERCA2 as a new member. Cell Calcium 45:439–446
157. Heo WD, Inoue T, Park WS, Kim ML, Park BO, Wandless TJ, Meyer T (2006) $PI(3,4,5)P_3$ and $PI(4,5)P_2$ lipids target proteins with polybasic clusters to the plasma membrane. Science 314:1458–1461
158. Liou J, Fivaz M, Inoue T, Meyer T (2007) Live-cell imaging reveals sequential oligomerization and local plasma membrane targeting of stromal interaction molecule 1 after Ca^{2+} store depletion. Proc Natl Acad Sci USA 104:9301–9306
159. Alicia S, Angelica Z, Carlos S, Alfonso S, Vaca L (2008) STIM1 converts TRPC1 from a receptor-operated to a store-operated channel: moving TRPC1 in and out of lipid rafts. Cell Calcium 44:479–491
160. Hancock JF, Parton RG (2005) Ras plasma membrane signalling platforms. Biochem J 389:1–11
161. Feron O, Smith TW, Michel T, Kelly RA (1997) Dynamic targeting of the agonist-stimulated m2 muscarinic acetylcholine receptor to caveolae in cardiac myocytes. J Biol Chem 272:17744–17748

162. Lockwich TP, Liu X, Singh BB, Jadlowiec J, Weiland S, Ambudkar IS (2000) Assembly of Trp1 in a signaling complex associated with caveolin-scaffolding lipid raft domains. J Biol Chem 275:11934–11942
163. Brazer SC, Singh BB, Liu X, Swaim W, Ambudkar IS (2003) Caveolin-1 contributes to assembly of store-operated Ca^{2+} influx channels by regulating plasma membrane localization of TRPC1. J Biol Chem 278:27208–27215
164. Formigli L, Sassoli C, Squecco R, Bini F, Martinesi M, Chellini F, Luciani G, Sbrana F, Zecchi-Orlandini S, Francini F, Meacci E (2009) Regulation of transient receptor potential canonical channel 1 (TRPC1) by sphingosine 1-phosphate in C2C12 myoblasts and its relevance for a role of mechanotransduction in skeletal muscle differentiation. J Cell Sci 122:1322–1333
165. Sabourin J, Cognard C, Constantin B (2009) Regulation by scaffolding proteins of canonical transient receptor potential channels in striated muscle. J Muscle Res Cell Motil 30:289–297
166. Kannan KB, Barlos D, Hauser CJ (2007) Free cholesterol alters lipid raft structure and function regulating neutrophil Ca^{2+} entry and respiratory burst: correlations with calcium channel raft trafficking. J Immunol 178:5253–5261
167. Murata T, Lin MI, Stan RV, Bauer PM, Yu J, Sessa WC (2007) Genetic evidence supporting caveolae microdomain regulation of calcium entry in endothelial cells. J Biol Chem 282:16631–16643
168. Brownlow SL, Sage SO (2005) Transient receptor potential protein subunit assembly and membrane distribution in human platelets. Thromb Haemost 94:839–845
169. Berthier A, Lemaire-Ewing S, Prunet C, Monier S, Athias A, Bessede G, Pais de Barros JP, Laubriet A, Gambert P, Lizard G, Neel D (2004) Involvement of a calcium-dependent dephosphorylation of BAD associated with the localization of Trpc-1 within lipid rafts in 7-ketocholesterol-induced THP-1 cell apoptosis. Cell Death Differ 11:897–905
170. Trevino CL, Serrano CJ, Beltran C, Felix R, Darszon A (2001) Identification of mouse trp homologs and lipid rafts from spermatogenic cells and sperm. FEBS Lett 509:119–125
171. Yu F, Sun L, MachaCa2+ K (2010) Constitutive recycling of the store-operated Ca^{2+} channel Orai1 and its internalization during meiosis. J Cell Biol 191:523–535

Part III
Mitochondria

Chapter 12
Beyond Intracellular Signaling: The Ins and Outs of Second Messengers Microdomains

Riccardo Filadi, Emy Basso, Konstantinos Lefkimmiatis, and Tullio Pozzan

Abstract A typical characteristic of eukaryotic cells compared to prokaryotes is represented by the spatial heterogeneity of the different structural and functional components: for example, most of the genetic material is surrounded by a highly specific membrane structure (the nuclear membrane), continuous with, yet largely different from, the endoplasmic reticulum (ER); oxidative phosphorylation is carried out by organelles enclosed by a double membrane, the mitochondria; in addition, distinct domains, enriched in specific proteins, are present in the plasma membrane (PM) of most cells. Less obvious, but now generally accepted, is the notion that even the concentration of small molecules such as second messengers (Ca^{2+} and cAMP in particular) can be highly heterogeneous within cells. In the case of most organelles, the differences in the luminal levels of second messengers depend either on the existence on their membrane of proteins that allow the accumulation/release of the second messenger (e.g., in the case of Ca^{2+}, pumps, exchangers or channels), or on the synthesis and degradation of the specific molecule within the lumen (the autonomous intramitochondrial cAMP system). It needs stressing that the existence of a surrounding membrane does not necessarily imply the existence of a gradient

Riccardo Filadi and Emy Basso have contributed equally.

R. Filadi
Department of Biomedical Sciences, University of Padova, Padova, Italy

E. Basso
Institute of Neuroscience, Padova Section, National Research Council, Padova, Italy

K. Lefkimmiatis
Institute of Neuroscience, Padova Section, National Research Council, Padova, Italy

Venetian Institute of Molecular Medicine, Padova, Italy

T. Pozzan (✉)
Department of Biomedical Sciences, University of Padova, Padova, Italy

Institute of Neuroscience, Padova Section, National Research Council, Padova, Italy

Venetian Institute of Molecular Medicine, Padova, Italy
e-mail: tullio.pozzan@unipd.it

J. Krebs (ed.), *Membrane Dynamics and Calcium Signaling*, Advances in Experimental Medicine and Biology 981,
https://doi.org/10.1007/978-3-319-55858-5_12

between the cytosol and the organelle lumen. For example, the nuclear membrane is highly permeable to both Ca^{2+} and cAMP (nuclear pores are permeable to solutes up to 50 kDa) and differences in [Ca^{2+}] or [cAMP] between cytoplasm and nucleoplasm are not seen in steady state and only very transiently during cell activation. A similar situation has been observed, as far as Ca^{2+} is concerned, in peroxisomes.

Keywords Ca^{2+} signaling · cAMP · ATP · Second messengers · Microdomains · cAMP sensors · Ca^{2+} sensors · ER · Mitochondria · PKA · PDE

12.1 Introduction

A typical characteristic of eukaryotic cells compared to prokaryotes is represented by the spatial heterogeneity of the different structural and functional components: for example, most of the genetic material is surrounded by a highly specific membrane structure (the nuclear membrane), continuous with, yet largely different from, the endoplasmic reticulum (ER); oxidative phosphorylation is carried out by organelles enclosed by a double membrane, the mitochondria; in addition, distinct domains, enriched in specific proteins, are present in the plasma membrane (PM) of most cells. Less obvious, but now generally accepted, is the notion that even the concentration of small molecules such as second messengers (Ca^{2+} and cAMP in particular) can be highly heterogeneous within cells. In the case of most organelles, the differences in the luminal levels of second messengers depend either on the existence on their membrane of proteins that allow the accumulation/release of the second messenger (e.g., in the case of Ca^{2+}, pumps, exchangers or channels), or on the synthesis and degradation of the specific molecule within the lumen (the autonomous intramitochondrial cAMP system). It needs stressing that the existence of a surrounding membrane does not necessarily imply the existence of a gradient between the cytosol and the organelle lumen. For example, the nuclear membrane is highly permeable to both Ca^{2+} and cAMP (nuclear pores are permeable to solutes up to 50 kDa) and differences in [Ca^{2+}] or [cAMP] between cytoplasm and nucleoplasm are not seen in steady state and only very transiently during cell activation. A similar situation has been observed, as far as Ca^{2+} is concerned, in peroxisomes.

A substantial heterogeneity in both protein and small molecule levels are also observed in the cytosol at rest and more dramatically during stimulation. Thus proteins are differentially enriched in specific regions, e.g., synapses, lipid rafts or caveolins, or can move from cytoplasm to membranes (and vice versa) upon receptor stimulation or channel opening, e.g., protein kinase C, phospholipase C etc. The existence of cell subdomains, macro-, micro- or nano-domains, has thus become a familiar concept for cell biologists, often invoked to explain unexpected results (sometimes with no direct evidence supporting their existence). It is obviously beyond the purpose of the present contribution to discuss how heterogeneities of different proteins, lipids or metabolites are generated and their importance in cell pathophysiology. Here we will concentrate primarily on the dynamic spatial heterogeneity in the concentration of the two most abundant second messengers, Ca^{2+} and cAMP. We will focus not on the different mechanisms that lead to the existence of

gradients between the lumen of organelles and the cytosol, but rather on the generation and role of local micro- or nano-domains during cell activation. We will also briefly discuss the heterogeneity and microdomain functional importance of other small molecules, such as ATP.

12.2 The Microdomain Concept

The term "microdomain" refers to subcellular regions chemically and/or physically different from the close environment. Usually, a microdomain is defined as a zone in which the concentration of a given molecule is distinguishable from that in the surrounding areas. From a spatial point of view, these regions range from few nm (nanodomains) up to few μm; for some metabolites/signaling molecules the existence of concentration gradients, involving a substantial portion of the cell that extends for several μm (macrodomains), have also been reported [1, 2] (and see below). Given that an exact spatial definition of nano- micro- and macrodomains is not available, we will use the term "microdomains" for a general definition of spatial heterogeneities within the cell, independently of their size. Only in a few cases, where the spatial domain is clearly defined in terms of size, we will refer specifically to nano-, micro- or macro-domains.

Microdomains are highly dynamic and their size varies over time, according to the specific type of microdomain and cellular context. Importantly, often their confinement is not rigid and only in few cases they are delimited by membranes. In particular, the concept of heterogeneity in the subcellular molecular composition, and its importance in cell physiology, is immediately clear when referred to the presence of membrane-enclosed organelles, endowed with specific luminal proteins and ions concentrations, distinct from those in the cytosol. Organelles are not usually included among classical microdomains, though the delimiting membranes clearly distinguish and isolate their luminal content from the rest of the cytosol. Accordingly, the heterogeneities in ion concentrations among different luminal regions of the same organelle will be briefly discussed below. On the other hand, more elusive is the notion of microdomain referred to the generation, in restricted regions, not limited by a membrane, of appreciable increases (or decreases) in the concentration of a certain molecule. For example, upon the opening of specific Ca^{2+} channels, the rapid rise in $[Ca^{2+}]$ near their mouths is classically associated with the generation of spatially confined Ca^{2+} microdomains within the cytosol, whose extension (both spatial and temporal) depends on a number of factors, including the nature of the channels, their location, the gradient of $[Ca^{2+}]$ between the two sides of the channels, the presence of different Ca^{2+} buffers able to bind the cation and to shape the microdomain (see below). As a general concept, the essential condition for the generation of microdomains is the presence, within a specific region, or in its immediate surroundings, of a reservoir and/or a source of the involved molecules. This reservoir is typically represented by a discrete compartment/organelle, in which the molecules are stored/accumulated, endowed with the ability to quickly release

part of them in specific conditions. In other cases, a spatially restricted accumulation of enzymatically active proteins is responsible for a localized production of the metabolite resulting from the reaction they catalyze and, of course, for the overlapping depletion of their substrate. This local enrichment of certain enzymes is usually obtained by limiting their diffusion through membrane anchorage or binding to fixed partners/structures. However, in its broad meaning, the term microdomain denotes not only a transient increase in the concentration of a molecule, but also a decrease. In this case, a localized sink-like activity must be present. This activity can be represented by a pump (capable of capturing molecules and accumulating them in a separate compartment), an enzymatic activity (responsible for their clearance/transformation), the presence of buffers (that sequester them), or a favorable chemical and/or electrical gradient (capable of generating a net flux that subtracts the molecules from a region and accumulates them in another). While evidence for microdomains with a concentration of a given molecule higher than that in their immediate surroundings is firmly established and intensively investigated, the nature and existence of microdomains with lower concentrations has been only marginally addressed (see below).

It is important to stress that microdomains are not only dynamic in terms of spatial distribution, but also of temporal duration (from a few μs to minutes). As a typical example, the modulation of the opening time of a channel, or its oscillatory activity alternating closed and open states with variable frequency, is responsible for the generation of extremely short or more long-lasting microdomains. The combination of these two (spatial and temporal) qualitatively distinct, but often strictly interdependent, levels of dynamism, further increases the complexity at the basis of microdomain generation and dissolution. This endows microdomains with the ability to regulate and finely tune many diverse intracellular processes. Last but not least, the generation of microdomains largely depends on the diffusion rate of the molecule. Thus microdomains of the slowly diffusing Ca^{2+} ion are an accepted concept whereas microdomains of very rapidly diffusing ions such as K^+, Na^+ or Cl^-, though theoretically possible, are expected to be of extremely small size and short duration.

12.3 Ca^{2+} Microdomains

The rise in cytosolic Ca^{2+} concentration [Ca^{2+}] can modulate a number of key cellular responses, ranging from cell proliferation to neurotransmitter release all the way to cell death. This remarkable flexibility of Ca^{2+} poses the problem of how the signal can achieve the necessary specificity. In fact, most Ca^{2+} signals are delivered as brief transients that can be organized into regular oscillations, and it has been demonstrated that both the frequency and the amplitude of the signals [3, 4] contain the necessary information, which is specifically decoded by the target(s). In addition, a third layer of control is given by the specific location and spatial constraint of the Ca^{2+} signal through the generation of [Ca^{2+}] microdomains: discrete regions of the cytoplasm that experience a transient [Ca^{2+}] gradient with respect to the rest of the compartment. In

the majority of eukaryotic cells, the bulk cytosolic free calcium concentration is maintained approximately at 100 nM, against an extracellular [Ca^{2+}] of over 1 mM; this concentration difference creates a steep gradient that largely favors Ca^{2+} entry into the cell. The existence of a negative potential across the PM further increases the tendency of Ca^{2+} to enter the cell. Ca^{2+} levels higher than in the cytosol are found within the lumen of most organelles. Various pumps and exchangers contribute to maintaining the resting level of [Ca^{2+}] and ensuring the proper loading of the internal stores: Ca^{2+}-ATPases (PMCA), Na^+/Ca^{2+} (NCX), and Na^+/Ca^{2+}-K^+ exchangers (NCKX) on the PM, the sarco/endoplasmic reticulum Ca^{2+}-ATPase (SERCA) in the ER/SR, the Ca^{2+} uniporter (MCU) in the mitochondrial inner membrane, and the secretory pathway Ca^{2+}-ATPase (SPCA) in the membranes of the Golgi apparatus and of acidic organelles. These Ca^{2+} accumulation systems have different activity/thresholds: PMCA, SPCA and SERCA have low transport rates, but high affinity, so they can respond to modest Ca^{2+} elevations and set basal Ca^{2+} levels, while the NCX, NCKX and MCU have large transport rates but lower affinities and can curb Ca^{2+} transients over a wider dynamic range. Ca^{2+} influx from the extracellular medium is catalyzed by a variety of PM channels, while release of Ca^{2+} from organelles depends on other mechanisms, IP3 and ryanodine receptors (IP3Rs and RyRs) in the ER/SR, a Na^+/Ca^{2+} exchanger (NCLX) in the mitochondria and less well characterized channels such as the two pores channels in acidic organelles [5]. While transient changes in [Ca^{2+}] in the cytosol can be triggered by either PM or organelle Ca^{2+} channel opening, the long-term steady state [Ca^{2+}] in the cytoplasm is solely dependent on the equilibrium between the rate of influx and efflux mechanism across the PM (for a detailed discussion see [6]).

The opening of a Ca^{2+} channel in the PM or in the membrane of a Ca^{2+} storing organelle produces a local increase in $[Ca^{2+}]_{cyt}$ which can be orders of magnitude higher than bulk cytosolic [Ca^{2+}]. Pioneering work that compared the rate and extent of activation of exocytosis in neurons [7, 8], in chromaffin cells, or at the level of neuromuscular junction [9–11] estimated that [Ca^{2+}] at the channel mouth could increase to over $\geq$100 μM. This large increase in local [Ca^{2+}], coupled to the presence of target molecules close to the channel, ensures a rapid and focal activation of specific cell functions. Theoretical calculations and experimental evidence support the notion that the local Ca^{2+} levels depend on the extracellular (or luminal) [Ca^{2+}], the conductivity of the channel, its ionic specificity and opening time, the distance from the channel mouth and the Ca^{2+} buffering capacity of the cytosol [12].

Within the cytosol, Ca^{2+} interacts with Ca^{2+} binding proteins, that are either effectors or simply buffers [13] and of which there are about 200 encoded by the human genome [14]. Negatively charged phospholipids also represent potential Ca^{2+} binding sites, though their role (both quantitatively and qualitatively) has not been extensively investigated. The majority of Ca^{2+} that enters the cytosol binds to the buffers/effectors: fixed and diffusible Ca^{2+} buffers shape the spatial and temporal distribution of Ca^{2+} microdomains. Endogenous Ca^{2+} buffers can reach very high concentrations in the cytoplasm: calibrated immunohistochemistry experiments have shown that parvalbumin in cerebellar basket cells reaches a concentration of 0.6 mM [15]. Experiments with recombinant L-Type Ca^{2+} channels fused to single

calmodulin molecule allowed to estimate the concentration of calmodulin near the channel at values as high as 2.5 mM [16]. The various Ca^{2+} buffers have different properties (as indicated above, they can be fixed or mobile, with high or low affinity) and different expression patterns in different cells; in this way, the spatial and temporal properties of Ca^{2+} signals can substantially vary in any specific cell type even upon opening of the same Ca^{2+} channel. Several studies indicate that most endogenous soluble cytoplasmic buffers have rapid Ca^{2+}-binding rate (k_{on}), in the range of $7.6 \times 10^8\ M^{-1}s^{-1}$ [17–19]. These fast endogenous buffers may reduce the amplitude of Ca^{2+} transients, and the regulation of buffer expression levels could be a method to control the efficacy of the signal. In addition, also fixed endogenous buffers (proteins bound to cytoskeletal elements or to the membrane of local organelles) slow Ca^{2+} equilibration in the cytosol but, being immobile, they are more rapidly saturated. Finally, organelles such as ER or mitochondria, equipped with highly efficient Ca^{2+} uptake mechanisms, can contribute to local buffering by transporting Ca^{2+} into their lumen. Due to the intrinsic relatively slow rate of the Ca^{2+} uptake process, the organelles are expected to play a major role in shaping the local Ca^{2+} gradient only at later times, compared to classical buffers. Fast buffers can become easily saturated in the vicinity of the Ca^{2+} entry site, but would remain largely unsaturated in the surroundings, creating a gradient of free buffer that sharply focuses the microdomain in space [20]. On the other hand, mobile buffers contribute to increasing the diffusion range of Ca^{2+}, spreading it deeply into the cytosol. In this respect, it should be borne in mind that fluorescent indicators used to image Ca^{2+} signals also act as Ca^{2+} buffers, which can significantly increase Ca^{2+} buffering capacity, both local and bulk, and can therefore distort the amplitude and time course of the signal itself [21]. Moreover, mobile buffers contribute to Ca^{2+} redistribution. If the Ca^{2+} indicator is more mobile than endogenous buffers (e.g., Fura-2 whose mobility is estimated to be $2 \times 10^{-6}\ cm^2/s$ [22]) it can greatly increase the rate of spreading of the Ca^{2+} signal in the cytosol [23, 24] and contribute in the dissipation of naturally occurring Ca^{2+} microdomains. The more common way to correct for this last artifact is to microinject Ca^{2+} dyes bound to large latex particles or to express protein based Ca^{2+} indicators.

Given the importance of Ca^{2+} for cell pathophysiology and its multifaceted signaling functions, it is no surprise that cells express more than one type of Ca^{2+} channel on the PM, such as the already mentioned Voltage Operated Channels VOCs, Receptor Operated channels ROCs, Transient Receptor Potential (TRPs), or store operated channels (such as Orai1). Ca^{2+} flux through a channel depends on the electrochemical gradient for Ca^{2+} and upon the intrinsic physicochemical properties of the channels in terms of conductance, opening probability and ionic selectivity; moreover, the heterogeneous distribution of the different channels along the PM also contributes to the characteristics of the signal and its subcellular heterogeneity.

The opening of Ca^{2+} channels on the PM or on the membrane of intracellular Ca^{2+} stores causes the transient, localized increase of Ca^{2+} within discrete areas of the cytoplasm. Depending on the distances traveled by Ca^{2+} ions before reaching the sensor, these areas can be roughly categorized into nano- micro- and macro- Ca^{2+} domains.

Nanodomains have been described in the presynaptic terminals of neurons where the influx of Ca^{2+} from a single Ca^{2+} channel reaches its sensor located within <100 nm from the channel itself. The measurement of Ca^{2+} nanodomains poses several challenges. First, the small dimensions are beyond the spatial resolution of conventional fluorescence microscopy. Moreover, although [Ca^{2+}] can reach high levels (in the order of hundreds of μM), the total amount of Ca^{2+} ions is very small; for example, a nanodomain associated with the opening of a single channel is formed by the flux of approximately 1000 Ca^{2+} ions [25].

To overcome the limitations imposed by the size of the nanodomain on their exploration via conventional microscopy, often indirect approaches have been taken, exploiting the characteristics of two Ca^{2+} chelators, BAPTA and EGTA, with comparable affinities for Ca^{2+}, (220 nM and 70 nM respectively [12, 17]), but very different Ca^{2+}-binding rates (4×10^8 M^{-1} s^{-1} and 1×10^7 M^{-1} s^{-1}, respectively) [17, 26]. Being so fast, BAPTA can potentially buffer all sorts of Ca^{2+} signals, while, even high mM EGTA is ineffective in abolishing events occurring very close to a channel. One of the first and best-studied examples of Ca^{2+} nanodomain comes from the studies of neurotransmitter release at the squid giant synapse where low mM BAPTA completely prevents neurotransmitter release [27] while EGTA is highly inefficient. The alternative use of the two chelators allowed the demonstration that also the inactivation of L-type Ca^{2+} channels on the membrane of excitable cells depends on [Ca^{2+}] near the mouth of the channel itself [28] since the presence of mM EGTA in the cytosol could not prevent channel inhibition (unlike the much faster chelator BAPTA). More recently, the development of a genetically encoded Ca^{2+} sensor (TN-XL) fused to the carboxyl tail of $Ca_v2.2$ Ca^{2+} channel, coupled with TIRF (Total Internal Reflection Fluorescence) microscopy, allowed the visualization of Ca^{2+} nanodomains in HEK293 cells [29].

Discrete clusters of $Ca2^{+}$ channels acting together can produce a microdomain; this arrangement requires the sensor to be placed within <1 μm from the channels to allow the detection of the summed signals. The difference in distance between a nanodomain and a microdomain generate local signals that differ about tenfold in magnitude: 100 μM versus 10 μM; and approximately 1000-fold in speed (microseconds vs. millisecond) [25]. A functionally especially relevant form of Ca^{2+} microdomain in the sub PM level is that occurring in heart cells. Ca^{2+} rises in the bulk cytosolic compartment governs the contraction of the cardiomyocytes, varying its concentration by about 50-fold between each heartbeat, from 0.1 μM in diastole to about 3–5 μM in systole. Initiation of the Ca^{2+} release from cardiac SR, however, depends on the generation of a highly localized Ca^{2+} microdomain at the interface between the T-tubule and the SR membrane where ryanodine receptors (RyRs) (type 2) are localized. T-tubules are deep, highly branched, invaginations of the PM in close contact (15 nm) with the cisternae of the SR. At each heartbeat, in response to the action potential, the generation of an inward Na^{+} current causes the depolarization of the membrane and the activation of L-type Ca^{2+} channels (LTCC). Ca^{2+} influx through LTCCs into the dyadic cleft generates a local, high [Ca^{2+}] microdomain that in turn triggers the opening of the RyRs and the subsequent release of Ca^{2+} from the SR, by a mechanism known as calcium-induced Ca^{2+}

release (CICR) [30]. High-resolution imaging has shown that T-tubule invaginations are not smooth, but host extensive membrane micro folds that generate a diffusion barrier for ion flow [31]. The loss of T-tubule folding in fact causes a faster diffusion of Ca^{2+} and K^+ ions prolonging the action potentials and increasing susceptibility to arrhythmias [31–33]. Due to their small volume (average 4.39×10^5 nm^3), dyadic clefts can experience Ca^{2+} increase of hundreds of μM during systole [34].

It has been shown that a significant number of LTCC are not found in dyads and do not seem to contribute directly to excitation-contraction coupling; nevertheless they are not randomly distributed throughout the sarcolemma, but rather they cluster and associate with signaling molecules within distinct membrane subdomains, and this distinctive distribution with the consequent generation of discrete Ca^{2+} domains might imply their role in controling different cellular functions [35–37]

On the opposite spectrum of domain dimensions, a Ca^{2+} "macro"-domain could be considered the large and sustained increase in Ca^{2+} that occurs for example in pancreatic acinar cells (see below) and in T-lymphocytes upon activation. In the latter case, after a T-cell establishes a stable contact with the membrane of an antigen-presenting cell, the immunological synapse (IS), the subsequent formation of IP3 elicits the release of Ca^{2+} from the ER and, in turn, Ca^{2+}-store depletion produces the activation of Orai channels. The high intracellular [Ca^{2+}] that follows the opening of Orai channels can last from a few minutes up to several hours and is limited to only part of the cytoplasm, opposite to the IS. This unexpected localization of the macrodomain has been proposed to be due to the action of mitochondria that, upon activation, redistribute close to the PM, in the proximity of the open channels [38, 39]. The mitochondrial contribution to lowering Ca^{2+} microdomain in proximity of the IS, also results in a reduction, at least in part, of the Ca^{2+}-dependent Orai1 inactivation [40]. It has also been proposed that PMCA pumps too concentrate at the level of IS [39], where they compete for Ca^{2+} with mitochondria, and this PMCA displacement could participate in maintaining high [Ca^{2+}] in the cytosolic region opposite to the site of receptor activation. A similar Ca^{2+} macrodomain has been observed in neutrophils exposed to a chemotactic gradient [41].

Other characteristic membrane subdomains (present in several cell types), the caveolae, are flask-shaped membrane invaginations [42]. In heart cells, caveolae cluster at the neck of T-tubules and contribute not only to increasing the total PM surface, but also augment the spatial complexity of the T-tubule lumen [43] [44]. Caveolae are enriched with a subset of LTCC [45] and also with β2 adrenergic receptor (β_2-AR) [46], allowing the β-adrenergic system to efficiently regulate Ca^{2+} signaling [47]. The clusterization of specific Ca^{2+} channels with different regulators and different signaling molecules could produce microdomains with distinct regulation and functions [48–50].

Ca^{2+} governs the rhythmic beat-to-beat contraction of individual cardiomyocytes, but it controls also signaling events that regulate gene expression. Given the remarkable, regular concentration fluctuation, it is still debated how Ca^{2+}-activated signaling-proteins can discriminate between contractile Ca^{2+} and signaling Ca^{2+}. It has been proposed that Ca^{2+}-control of gene transcription in cardiomyocytes occurs via the propagation of the cytosolic Ca^{2+} oscillation into the nucleus, and in particular

of high frequency oscillations. Specifically, it has been shown that an increase in the frequency of the Ca^{2+} transients could affect hypertrophic signaling via the activation of calcineurin (CaN) and the consequent nuclear translocation of the nuclear factor of activated T-cells (NFAT) transcription factor [51]. The proposal was that an NFAT integrates the brief Ca^{2+} signals of each contraction-relaxation cycle, resulting in a net translocation of the transcription factor as a function of the frequency of the $[Ca^{2+}]_{cyt}$ oscillations. Moreover, an increase in the frequency of Ca^{2+} transients can result in an increase in diastolic Ca^{2+}, and this could represent a sustained Ca^{2+} signal known to activate CaN [52]. Several animal models of enhanced diastolic Ca^{2+} have been produced through mutations of ER Ca^{2+} channels or Ca^{2+} pumps [53, 54], or modifying specifically the cardiac expression of Na^{+} exchangers [55], and they all show a significant activation of the CaN-NFAT and Ca^{2+}/calmodulin-dependent protein kinase II (CaMKII) signaling resulting in cardiac hypertrophy [56]. In recent years, it has been proposed that also Ca^{2+} segregation within subcellular microdomains could regulate gene transcription. The generation of nuclear Ca^{2+} signals could arise from Ca^{2+} released through rough ER membranes closely associated with the nuclear envelope [57]. In addition, given its continuity with the ER, the nuclear envelope itself can function as a perinuclear Ca^{2+} store capable of releasing Ca^{2+} into the nucleus in response to specific signals [58]; in fact, FRAP experiments using Fluo-5 have shown in adult cardiomyocytes that the lumen of the SR and the perinuclear space are highly interconnected, and this can enable the rapid diffusion of intraluminal Ca^{2+} into the nucleus [59]. Invaginations of the outer and inner nuclear membrane deep into the nuclear matrix can provide a further compartmentalization of the Ca^{2+} signal [60]. These structures are enriched in Ca^{2+} channels (primarily IP3Rs) and their strategic localization could provide the gating for nuclear Ca^{2+} signals [61, 62]. For a detailed description of the current data and models explaining the interplay between contractile and signaling Ca^{2+} in cardiomyocytes the interested reader is referred to two comprehensive reviews [63, 64].

12.4 Ca^{2+} Microdomains at the ER-Mitochondria Interface: Generation and Functional Significance

Mitochondrial Ca^{2+} uptake was first described in the 60s in isolated mitochondria [65]. Ultimately, the uptake depends on the activity of the respiratory chain and the generation, across the inner mitochondrial membrane (IMM), of an electrochemical gradient, negative on the side of the matrix ($\Delta\psi$, ~ -180 mV). The process of mitochondrial Ca^{2+} uptake is controlled and shaped by specialized transport mechanisms, whose molecular identity has been clarified only in the last few years [66, 67], revealing a previously unexpected complexity. An overview of the identity/activity of the proteins that form and regulate the so called "mitochondrial Ca^{2+} uniporter" (MCU) complex (MCUC), as well as of other transporters that allow Ca^{2+} efflux from mitochondrial matrix after its uptake, is beyond the scope of the present contribution

and interested readers are referred to recent reviews [68–71]. Here, we limit ourselves to some aspects of the process that are modulated by the generation of high-concentration Ca^{2+} microdomains (Ca^{2+} hot-spots) on the outer mitochondrial membrane (OMM). In particular, the relatively low affinity of MCU for Ca^{2+} ($K_d \sim 15$ μM) has been believed for long time not to be compatible with an appreciable uptake of the cation from the cytosol, not only at rest ($[Ca^{2+}]_{cyt} \sim 100$ nM), but also upon cell stimulation (peaks $[Ca^{2+}]_{cyt} \sim 2–3$ μM). Thus, in the 1990s, the clear demonstration, by different genetically encoded Ca^{2+} indicators targeted to the mitochondrial matrix [72] (see [73, 74] for reviews on mitochondrial Ca^{2+} probes), that, after IP3-dependent Ca^{2+} mobilization, mitochondria take up Ca^{2+} with a speed and an amplitude much higher than the predicted ones, was initially unexpected. To explain this paradox, it was hypothesized that, in regions where mitochondria are closely juxtaposed to the ER, Ca^{2+} hot spots are generated near the mouths of ER Ca^{2+} channels and experienced by closely located mitochondria [75, 76]. In this way, MCU is exposed transiently to a local high $[Ca^{2+}]$ microdomain and a prompt uptake of the cation takes place. Importantly, the existence of such Ca^{2+} microdomains was initially postulated on the basis of indirect evidence and only more recently has it been formally demonstrated by employing FRET-based Ca^{2+} probes targeted to the OMM [77, 78]. These topics, as well as the significance of ER-mitochondria contacts beyond Ca^{2+} transfer and the molecular identity of the proteins keeping the two organelles at the right distance, have been extensively reviewed and we refer the readers to a couple of recent contributions [79, 80]. Below, we add further considerations on the generation and propagation of Ca^{2+} microdomains in this specific subcellular region, focusing on the different outcomes of the phenomenon, depending on the cellular context.

Upon maximal IP3-linked cell stimulation and ER-Ca^{2+} release, it has been demonstrated that, at the level of the OMM Ca^{2+} hot-spots, $[Ca^{2+}]$ in the 10–30 μM range can be reached; i.e., an order of magnitude higher than that in the bulk cytoplasm [77, 78]. This $[Ca^{2+}]$ is fully compatible with the low affinity for Ca^{2+} of the MCUC, allowing its prompt activation and Ca^{2+} entry into the matrix. However, before bumping into MCU, Ca^{2+} has to cross the OMM. This first barrier is largely permeable to Ca^{2+} and to small molecules <5 kDa. Thus, compared to the tightly impermeable IMM, that requires specialized transporters, the passage of Ca^{2+} through the OMM has received less attention. This passage is believed to occur thanks to the presence of the voltage-dependent-anion-channels (VDACs), characterized by large conductance and poor selectivity. In mammals, three different VDAC isoforms exist (VDAC1, VDAC2, VDAC3) [81] and are among the most abundant OMM proteins. In transgenic mice, only VDAC2 knockout is embryonically lethal, while VDAC1 and VDAC3 absence is compatible with postnatal life, suggesting that the three isoforms are only partially redundant. VDAC1 overexpression has been demonstrated to increase the amplitude of IP3-mediated mitochondrial Ca^{2+} rises and to reduce the delay between cytosolic and mitochondrial Ca^{2+} transients, suggesting that this channel is particularly efficient in allowing Ca^{2+} transfer from ER to mitochondria [82]. Accordingly, in HeLa cells, the separate downregulation of all the three VDAC isoforms has been shown to slightly decrease histamine-evoked

mitochondrial Ca^{2+} uptake, while their overexpression increases it [83]. The relatively modest effects observed upon downregulation of VDACs, as well as the fact that in VDAC1/3$^{-/-}$ MEFs robust IP3-mediated mitochondrial Ca^{2+} rises have been observed [84], suggest that the abundance of these channels, as well as their conductance, are so high that the partial reduction in their concentration is not enough to severely compromise the process. A certain grade of specificity between the different VDAC isoforms, however, has been reported, with VDAC1 specifically involved in the transfer of low-level, pro-apoptotic Ca^{2+} transients from ER to mitochondria [83]. Moreover, VDAC1 has been demonstrated to be physically and functionally connected to the IP3Rs on the side of the ER, through the cytosolic fraction of the molecular chaperone glucose-regulated protein 75 (grp75) [85] (Fig. 12.1). The formation of the IP3R-grp75-VDAC1 complex positively correlates with the process of mitochondrial Ca^{2+} uptake, especially at low extra-mitochondrial [Ca^{2+}] [85]. Interestingly, the assembly of this complex is enhanced by specific apoptotic stimuli [83]. Thus, the recruitment of the IP3Rs (responsible for ER Ca^{2+} release) in very close apposition to VDAC (likely the channel that allows Ca^{2+} to overcome the OMM), is employed by the cells to modulate the efficiency of the cation shuttling from the source (the ER) to the MCU, located in the IMM. On top of that, the very close apposition (10–30 nm) between ER and OMM in specific regions represents a side-by-side obstacle, that limits the lateral Ca^{2+} diffusion and sustains the generation of the microdomains, further favoring the process of Ca^{2+} transfer across the OMM. In addition, SERCA activity has been demonstrated to directly take advantage of the close apposition with mitochondria, that fuel the pump with ATP [86] (see also below). Finally, these localized and spatially restricted rises in [Ca^{2+}] are able to modulate in a bidirectional manner the activity of the IP3Rs per se [87]. Indeed, IP3Rs activity is known to be modulated by a number of factors, including cytosolic ATP and Ca^{2+} levels [88]. Recently, it has been suggested that luminal ER [Ca^{2+}] can indirectly control the temporal extension of IP3Rs opening [89]. In particular, the amplitude of the Ca^{2+} microdomain generated near the mouth of IP3Rs, that depends on the amount of Ca^{2+} present within the lumen, can modulate the opening probability of IP3Rs and induce their closure, switching off the same microdomain fueling. Interestingly, all three IP3Rs isoforms, differently expressed among tissues, are regulated in a biphasic way by the $[Ca^{2+}]_{cyt}$, with low concentrations potentiating their opening and higher concentrations inhibiting it. Noteworthy, the shape of this $[Ca^{2+}]_{cyt}$-dependence is IP3R isoform-specific and a similar specificity has been observed for their modulation by ATP (reviewed in [90]). Thus, while all these players add further complexity to the process of Ca^{2+} microdomains generation/shaping at the ER-mitochondria interface, at the same time they endow it with a finely tuneable and extremely sophisticated flexibility.

Once Ca^{2+} has overcome the OMM, it has to cross the mitochondrial intermembrane space (IMS) before reaching the MCUC, while maintaining a relatively sustained concentration to allow its activation. Although this process has not been studied in detail, a series of considerations can be extrapolated from the available data. The fact that, upon an IP3-dependent stimulation, Ca^{2+} reaches the IMM with a concentration higher than that observed in the bulk cytosol, has been

demonstrated by targeting an aequorin Ca^{2+} probe to the IMS-side of the IMM [75]. Importantly, the distance between the OMM and the IMM is very short (~10 nm) [91], limiting the drop in [Ca^{2+}] induced by the distance from the source, as would be inevitably imposed by Fick's laws of diffusion (see [79] for a review). Moreover, the IMS is relatively poor of soluble Ca^{2+} buffers (that, on the contrary, are abundant in the cytosol), further favoring a rapid diffusion of the cation within this compartment. In the IMS, the only known Ca^{2+} binding sites are immobile and bound to the IMM, such as the EF-hand domains of the MICU1/2/3 (for a review see [68]) or those of specific metabolites transporters [92, 93], with the exception of ATP (particularly abundant in this compartment), whose Ca^{2+} buffering capacity, however, is low, as largely complexed with Mg^{2+}. Finally, it has been recently suggested that, in cardiac muscle, MCU complexes are not homogeneously distributed within the IMM, but are strategically enriched at the level of specific regions where the IMM is in very close apposition with the OMM, the so-called contact points [94]. Interestingly, these IMM-OMM contact points have been demonstrated to be frequently aligned to the sites in which mitochondria are juxtaposed to the junctional SR (jSR) [95]. Thus, it is tempting to speculate that, in addition to the above described intimate relationship between ER (or SR) and OMM Ca^{2+}-handling proteins, a bias MCU complex positioning towards these juxtaposition areas, further enhanced by a closer vicinity between OMM and IMM, may be functional for a more efficient detection of Ca^{2+} microdomains and a prompt MCU activation. Whether this specific MCU submitochondrial distribution is typical only of cardiac cells, or is conserved between different cell types, is currently not known. Finally, it has been recently suggested that, upon propagation of Ca^{2+} signals from ER to mitochondria, mitochondrial cristae compression induces an H_2O_2 nanodomain at the ER-mitochondria interface, capable to impact on Ca^{2+} microdomains generation/transmission [96]. Indeed, the activity of several Ca^{2+}-handling proteins present in mitochondria-associated membranes (MAMs) can be modulated by their oxidative state [97].

The impact of Ca^{2+} microdomains on the activity of MCU may be different, depending on the cell type, as the composition of the MCU complex is variable among tissues. In particular, not only the relative proportion of MCU and MCUb (the dominant negative, inhibitory subunit) is different, with a particularly high MCUb expression in heart, lung and brain [98], but also the expression profile of the MCU regulators MICU1/MICU2/MICU3 is variable (for reviews, see [68, 69]). While MICU1 and MICU2 distribution is relatively homogeneous among tissues, MICU3 expression is restricted to the central nervous system and skeletal muscles [99]. Since MICU1, MICU2 and MICU3, by forming hetero- or homo-dimers, differentially regulate the MCU sigmoidal response to extra-mitochondrial [Ca^{2+}], changing its apparent K_d for the cation, the outcome of mitochondria exposure to Ca^{2+} microdomains may be different according to the specific MCU complex composition.

12.5 Heterogeneity of Ca^{2+} Levels Within Organelles

12.5.1 ER/SR

In eukaryotic cells, ER is composed of a single, continuous membrane system that forms a network of tubules and sheets, starting from the nuclear envelope and ending with the cortical ER, which is closely associated or tethered to the PM. The relative proportion of sheets and tubules is extremely variable among different cell types and is strictly connected to their function. For instance, cells specialized in the secretion of large amounts of proteins, such as pancreatic acinar cells, display predominantly ribosome-studded sheets, while other cell types, for example epithelial cells, are endowed with an abundant tubular network (reviewed in [100]). Importantly, the shape of ER is finely regulated by a number of different proteins, further suggesting that the organelle morphology is strictly connected to its functions (reviewed in [101] [100]). For example, sheets are believed to better accommodate ribosomes and store proteins, thus being mainly involved in protein synthesis, while the curvature of tubules is believed to be ideal for generating vesicles exiting the ER [101]. Although there is now a general consensus that in the majority of the ER the luminal $[Ca^{2+}]$ is homogeneous and in rapid equilibrium within the network, evidence has been provided supporting the existence of ER subcompartments where, either transiently or in steady state, the $[Ca^{2+}]$ may substantially differ from the rest of the organelle (see below). To the best of our knowledge, a detailed study on the relationship between ER morphology and Ca^{2+} handling has never been done, but the continuity of the ER lumen between rough and smooth ER, as well as the presence of luminal mobile Ca^{2+} buffers (such as calreticulin) argue against the presence of a major heterogeneity. Some heterogeneity, however, has been suggested to exist within the ER based on data obtained with selectively-targeted low Ca^{2+} affinity recombinant aequorins [102]. Using this tool, the authors suggested the existence of an ER compartment (that included the majority of the organelle) with mM $[Ca^{2+}]$ and one (or more) compartment(s) (comprising 5–10% of the total) with a much lower $[Ca^{2+}]$. Similar results were more recently obtained by employing a different, lower affinity aequorin mutant [103]. In this study, the authors confirmed the presence of an ER portion (~5% of total ER, assuming homogeneous distribution of the probe within the organelle) with a very low $[Ca^{2+}]$; they also found that another ~5% of total aequorin resides in an ER subcompartment where $[Ca^{2+}]$ is high (in the mM range), but insensitive to SERCA inhibition by thapsigargin/BHQ and to IP3 stimulation.

As to the mechanisms responsible for heterogeneous steady state ER $[Ca^{2+}]$, the most obvious explanation appears to be the heterogeneity in the relative amount/isoform distribution of the SERCAs, of the Ca^{2+} releasing channels, or to the existence of some barriers that hinder the diffusion of the cation in an otherwise luminally continuous organelle. For example, two distinct pools of ER Ca^{2+} were observed in HEK-293T, but not in HeLa cells, due to the expression in the former cell type of relatively high levels of SERCA-3d (which is not fully blocked by the

SERCA inhibitor TBH) [104]. As to heterogeneity of Ca^{2+} releasing channels, they are known to exist (especially in the terminal cisternae of striated muscle SR, but also in MAMs where, for instance, IP3R3 is enriched [105]), but it is unlikely that this, in itself, could cause a significant steady state difference of [Ca^{2+}] between ER/SR domains. It is our biased opinion that the observed heterogeneities in steady state *free* [Ca^{2+}] within the ER/SR are either an artefact of the probe distribution (e.g., part of the probe is localized in non-ER structures) or due to interruptions in the luminal continuity (e.g., ER vesicles budding from the luminally continuous network).

On the contrary, strong evidence supports the conclusion that the *total* Ca^{2+} content can be highly heterogeneous within ER/SR subdomains. For example one of the main Ca^{2+} buffers of the SR, calsequestrin, is selectively concentrated in the terminal cisternae [106]. The local Ca^{2+} content in this SR subcompartment is thus much higher than in the longitudinal SR, although the ER free [Ca^{2+}] is the same. A similar situation applies to Purkinje neurons of the chicken cerebellum where calsequestrin is expressed in the ER lumen and concentrated in some parts of the organelle [107] (reviewed in [108]). Some additional Ca^{2+}-binding proteins, such as the chaperones calnexin and GRP78, have been suggested to be enriched in discrete ER regions, particularly at MAMs [105, 109, 110]. The contribution of these proteins to Ca^{2+} buffering in the ER is, however, much lower than that of the most abundant calreticulin and calsequestrin, and thus the impact of their non-random distribution on ER Ca^{2+} content is likely modest. It is worth mentioning here that changes in the expression levels of luminal Ca^{2+} buffers affect the amount of ER Ca^{2+} content and of Ca^{2+} released after stimulation [111, 112] without modifying the free Ca^{2+} levels. Along the same lines, it should be also stressed that, as revealed by FRAP (or FLIP) experiments of ER-targeted fluorescent proteins [113, 114], organelle morphology can affect the diffusion process of luminal ER proteins and thus changes in ER shape are potentially capable of affecting the speed of Ca^{2+} redistribution.

Finally, transient local microdomains of Ca^{2+} within the ER/SR can be generated during cell stimulation. Indeed, the presence of clusters of high-conductance Ca^{2+} channels, such as RyRs or, to a lesser extent, IP3Rs, can potentially deplete, upon their opening, the local pool of Ca^{2+} in the luminal layer underlying these clusters (Ca^{2+} blinks). Ca^{2+} blinks have been observed in cardiac cells and proposed to be responsible for local RyR2 inactivation [115, 116]. Another example of a local, transient Ca^{2+} microdomain in the ER lumen is that occuring during ER Ca^{2+} refilling after its release due to IP3R activation. After ER Ca^{2+} depletion and store-dependent Ca^{2+} entry (SOCE) activation, ER Ca^{2+} refilling is severely dampened by the presence of BAPTA-AM and, to a much lesser extent, of EGTA-AM [103]. The more potent effect of BAPTA-AM suggests that the process of SOCE, at least in HeLa cells, involves the formation of Ca^{2+} microdomains at the PM-ER junction, that allows a localized Ca^{2+} uptake by SERCA. A similar conclusion was reached by another group that compared SOCE in HeLa and Jurkat T cells, by simultaneously employing an ER-targeted fluorescent probe (CEPIA) and Fura-2 in the cytosol [117]. They found that, during SOCE, while in HeLa cells the process of ER refilling was not accompanied by a significant, parallel increase in cytosolic [Ca^{2+}], in Jurkat cells such an increase was observed. These results suggest that during SOCE, in

some cell types, Ca^{2+} influx from the extracellular milieu through Orai1 channels generates a Ca^{2+} microdomain close to the mouth of the channel, that is almost completely taken up by SERCA of the juxtaposed ER, without spreading of Ca^{2+} into the deep cytosol and thus with minimal bulk cytosolic Ca^{2+} rises (Fig. 12.1). However, the fact that a localized event is capable of triggering, over time, the refilling of $[Ca^{2+}]$ in all the ER, further suggests that the lumen of the organelle is continuous. A similar conclusion was reached by Petersen and co-workers in the pancreatic acinar cells where it was demonstrated that full refilling of the ER Ca^{2+} could be obtained without significant increases in cytosolic $[Ca^{2+}]$ by a cell attached

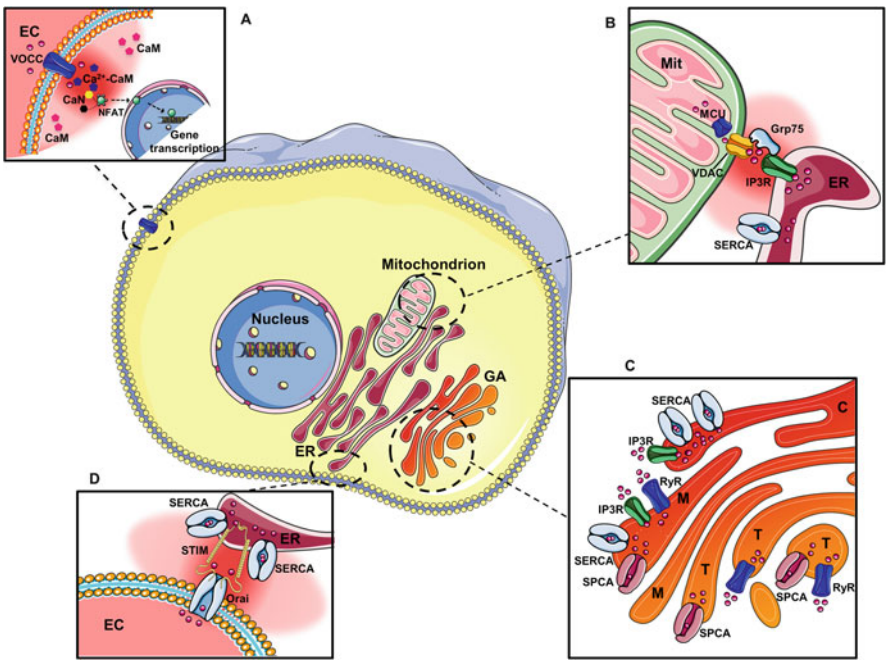

Fig. 12.1 The cartoon represents sites of Ca^{2+}-microdomains generation within a cell, as detailed in the text. (**a**) Opening of Voltage Operated Calcium Channels produces a localized $[Ca^{2+}]$ increase, which can activate calmodulin (CaM); activated calmodulin interacts with and activates calcineurin (CaN). Activated calcineurin dephosphorilates NFAT allowing its nuclear translocation, and subsequent gene transcription. Moreover, Ca^{2+}-bound calmodulin can bind on different sites on the Ca^{2+} channel providing dual feedback modulation of the channel itself. (**b**) Generation of a Ca^{2+}-microdomain at ER-mitochondria interface upon IP3-linked cell stimulation and release of ER-Ca^{2+} content through IP3Rs. Note the drop in ER $[Ca^{2+}]$ after IP3Rs opening and how the process of mitochondrial Ca^{2+} uptake takes advantage of the close apposition between the two organelles (see text for details). (**c**) Heterogeneity of Ca^{2+} content and presence of different pools of Ca^{2+}-handling proteins along the Golgi apparatus (GA). Note in particular the gradient of $[Ca^{2+}]$ between the *cis* (C), the *medial* (M) and the *trans* (T) Golgi network. (**d**) The scheme represents the generation of Ca^{2+}-microdomain at ER-PM contact points after STIM-mediated opening of Orai channels and Ca^{2+} entry through the PM. In certain cell types, the abundant presence of SERCA is capable to limit the diffusion of Ca^{2+} outside these regions

patch pipette containing 1 mM $CaCl_2$, while the rest of the cell was bathed in a Ca^{2+}-free medium [118].

Transient heterogeneities in ER luminal [Ca^{2+}] can be demonstrated also during IP3-linked Ca^{2+} release. For example, it is well known that under physiological concentrations of cholecystokinin (CCK) in pancreatic acinar cells, the Ca^{2+} increase remains restricted to a small region close to the granular pole of the cell, presumably because of the high concentration of IP3Rs in that ER subcompartment [119]. Along the same line, by imaging at a high frame rate ER-GCEPIA in HeLa cells, different kinetics in the release of ER Ca^{2+} at subcellular level were recently observed [117]. In this case, Ca^{2+} release starts at the tip of the cell and then propagates to the perinuclear region, with a wave speed of ~60 μm/s. The observation that local changes in ER [Ca^{2+}] can occur seems to have great physiological importance. For instance, in neurons, it has been recently observed that presynaptic ER [Ca^{2+}] controls STIM1 activation in presynaptic terminals, locally impacting on the activity-driven Ca^{2+} entry, and on the neurotransmitters release probability [120].

12.5.2 Golgi Apparatus

Recently, a diversified expression of Ca^{2+} channels and pumps among the different sub-Golgi compartments has been suggested to be responsible for the existence of a cis- to trans-Golgi [Ca^{2+}] gradient [121, 122]. In particular, while SERCA pumps and IP3Rs are abundant in the cis-Golgi (closer to the ER), they are both excluded from the trans-Golgi network, where SPCA1 totally controls Ca^{2+} uptake. Interestingly, in the intermediate compartment (medial-Golgi), SERCA and SPCA1 co-exist, and IP3Rs are present. As to RyRs, in the cells that express them, they appear to be equally present throughout the whole Golgi apparatus (Fig. 12.1). Thus, this compartmentalized expression of different Ca^{2+} handling proteins endows the Golgi sub-compartments with specific Ca^{2+}-handling identities, capable of overcoming the continuous mixing of membranes and luminal contents among vesicles [122].

12.5.3 Mitochondria

At rest, the [Ca^{2+}] in the matrix of mitochondria is similar to that of the cytosol but during transient increases in $[Ca^{2+}]_{cyt}$, significant heterogeneities in the Ca^{2+} peaks of individual organelles have been observed. For instance, exploiting the property of aequorin to be consumed during the Ca^{2+}-dependent reaction, it was demonstrated that a sub-group of mitochondria (likely those in close apposition with the ER) quickly depletes its pool of aequorin upon the first of a series of Ca^{2+} rises [82, 123, 124]. Moreover, DRP1 overexpression, by fragmenting mitochondrial network, has been shown to increase the variability in mitochondrial Ca^{2+} rises among the different organelles, [125]. Importantly, the fragmented mitochondrial morphology,

by hindering Ca^{2+} diffusion within the mitochondrial network, was shown to be protective against Ca^{2+}-mediated apoptosis. Recently, a heterogeneous sub-cellular mitochondrial response was confirmed by the simultaneous measurements of cytosolic, ER and mitochondrial Ca^{2+} dynamics [117]. Interestingly, cytosolic and ER Ca^{2+} oscillations were similar in the selected regions, while mitochondrial Ca^{2+} rises were different. Given that differences in mitochondrial pH or $\Delta\Psi$ were ruled out by additional experiments, the authors suggested that a different ER-mitochondrial coupling or a heterogeneous distribution of mitochondrial Ca^{2+} handling proteins could be responsible for the observed phenomenon (Fig. 12.1).

12.6 cAMP Microdomains

Similarly to Ca^{2+}, also the other major second messenger, cyclic AMP (cAMP), organizes its signaling cascade in microdomains [74, 126]. In the case of cAMP, microdomains can either depend on a spatial heterogeneity of the second messenger itself and/or be functional due to spatially distinct domains of termination signaling (phosphatases) (Fig. 12.2).

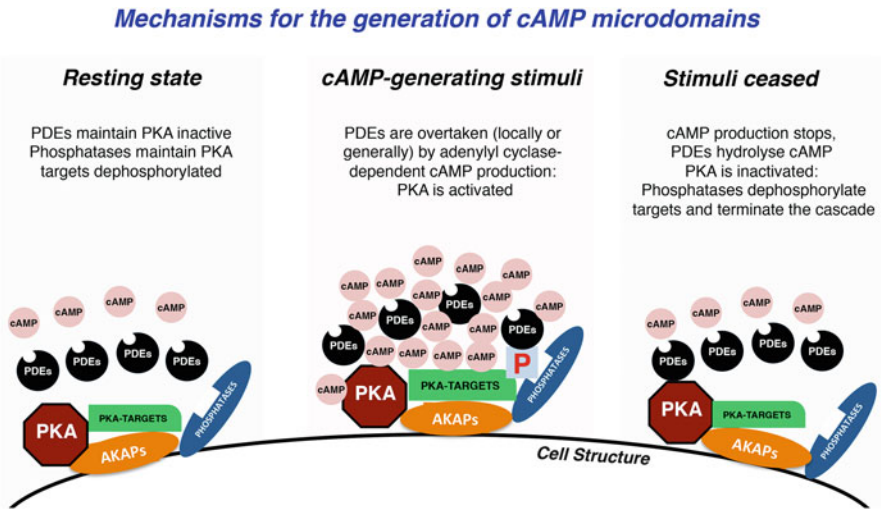

Fig. 12.2 Elements of the cAMP microdomain machinery. AKAP proteins are responsible for localizing PKA in specific subcellular sites and near to its targets. Within these domains PKA remains inactive thanks to the actions of PDEs, strategically located in order to shield PKA from the resting levels of the messenger. During cAMP-generating stimuli, adenylyl cyclases are activated and the resulting increase in cAMP levels may overcome the PDE shield and activate PKA. Once activated, PKA is free to phosphorylate its local targets translating the cAMP signal in functional outcomes. In response to subsiding stimuli, adenylyl cyclases cease to produce cAMP and PDEs rapidly degrade the messenger bringing its levels under the PKA activation threshold. With PKA inactive unopposed phosphatases dephosphorylate the PKA targets effectively terminating the cascade and bringing the whole system to an activation-ready state

The first evidence pointing to a role of compartmentalization in determining the functional pleiotropy of cAMP signaling, dates back to the seminal studies by Hayes and Buxton in cardiac tissue and isolated cells [127, 128]. The authors showed that while both prostaglandin E1 (PGE1) and the β_1- and β_2-adrenergic receptor (β_1-AR/β_2-AR) agonist isoproterenol (Iso) caused similar cAMP elevations, only Iso had the expected effect on contractility (e.g., positive inotropy). These findings prompted the authors to formulate the hypothesis that the components of the cAMP cascade are organized in such a way that intracellular spots with different cAMP concentrations are generated by the two agonists [127]. This model challenged the dogma that, at that time, considered cAMP evenly distributed within the cell. Evidence supporting this hypothesis was obtained by electrophysiological recordings both in frog cardiac myocytes [129] and mammalian cell lines [130], but it was the development of advanced imaging techniques (that enabled direct real-time visualization of cAMP in living cells) that directly supported the existence of cAMP microdomains [131–133]. Since these seminal studies, and thanks to an ever-evolving array of imaging tools [74] [134], the notion of cAMP compartmentalization has been consolidated and it is now widely accepted. However, the mechanisms underlying the generation of cAMP microdomains are only partially understood and are the subject of intense research.

12.6.1 The Generation of cAMP Microdomains

Because of its hydrophilic nature and the relatively small number of specific binding sites, cAMP was believed to be highly diffusible within the cellular cytosol, with some studies calculating diffusion coefficients around 500 $\mu m^2 s^{-1}$ [135, 136]. Such a fast diffusion rate would result, upon cAMP production, in a very rapid and global homogeneous distribution of the molecule in the cell cytosol with the simultaneous activation of all cAMP effectors within the cell [137, 138]. Recently, two independent studies using different approaches demonstrated that the diffusion rate of cAMP in adult cardiac myocytes is much slower than previously measured (i.e., ~35 $\mu m^2 s^{-1}$) [139]; and (~10 $\mu m^2 s^{-1}$) [140]. Albeit reaching to the same conclusions, Agarwal and collaborators propose that cAMP buffering at the level of mitochondria is the primary reason for slow cAMP diffusion, while Richards and colleagues provide evidence that intracellular tortuosity is the main cause for this slow diffusion. Although the relatively slow diffusion rate of cAMP is a prerequisite for the generation of cAMP microdomains, even a cAMP diffusivity at the minimum value calculated (~10 $\mu m^2 s^{-1}$) is not sufficient to create per se a cAMP microdomain and other factors are thus necessary for generating heterogeneities in the second messenger level [141, 142].

In general terms, the generation of heterogeneous cAMP domains within the cell is believed to depend on: (i) the relatively slow rate of cAMP diffusion in the cytosol; (ii) the different subcellular localization of the cAMP synthetizing enzymes, adenylate cyclases (AC); and (iii) the existence of cAMP degrading enzymes with

different cellular localizations and local concentrations. In addition, a functional type of cAMP microdomain can be generated even under conditions of homogeneous cAMP levels, by the differential localization/activity of phosphatases, i.e., the enzymes that effectively terminate the cAMP effect mediated by PKA-dependent phosphorylation [137, 143] [141]. Below, we briefly summarize the characteristics of the different molecules that regulate cAMP production, degradation and transduction, focusing on their relative role in generating and terminating cAMP microdomains.

12.6.2 cAMP Effectors

Contrary to Ca^{2+} (that can regulate protein function by directly binding to a large number of targets), cAMP exerts its actions thanks to a limited array of effectors: the cyclic-nucleotide-gated channels (CNG) [144], the guanine-nucleotide exchange proteins activated by cAMP (EPACs) [145], protein kinase A (PKA)[126, 146] and, the newest addition, the Popeye-domain containing family (POPDC2) [147, 148].

PKA, the most abundant cAMP sensor is a tetramer made by two catalytic (PKA-Cs) and two regulatory (PKA-Rs) subunits. In the human genome there are three genes encoding PKA-C (Cα, Cβ and Cγ) and four genes encoding PKA-Rs (RIα, RIβ, RIIα and RIIβ) [126, 149]. The regulatory subunits are present as dimers thanks to an N-terminal peptide called dimerization/docking domain (D/D). This region is also the site of interaction between PKA-Rs and A-Kinase Anchoring Proteins (AKAPs), a multimember family of tethers responsible for the subcellular localization of the PKA holoenzyme [150]. Most AKAPs bind PKA-RII subunits, but a number of dual (e.g., binding PKA-RI and PKA-RII) [150, 151] or PKA-RI specific AKAPs [152, 153] have been identified. In addition to a characteristic amphipathic domain that aids the interaction with PKA-Rs, each AKAP contains targeting signals that allow its localization to specific subcellular sites. Once on site, the AKAP tethers PKA in a complex that acts as the molecular platform around which the microdomain is built.

Anchoring of PKA-holoenzymes containing different regulatory subunits (known to bind cAMP with different affinities [149]) could determine the cAMP threshold that must be reached within a specific domain in order for local PKA to be activated. Indeed, Di Benedetto and colleagues used FRET-based cAMP sensors in cardiac cells and provided strong evidence that both PKA-RI and PKA-RII are predominantly anchored to distinct subcellular sites and can produce unique phosphorylation patterns [133]. Importantly, when cells were stimulated with Iso the cAMP response was selectively confined to PKA-RII microdomains. In contrast, the domains defined by PKA-RI enzymes responded to prostaglandin 1 and glucagon stimulation [133]. In addition to the type of PKA-Rs, AKAPs determine the physical location of microdomains, a parameter crucial for the function and, importantly, the regulation of local cAMP signals. For instance, a PKA tetramer anchored in the proximity

of a cAMP source (e.g., PM) will be exposed to higher cAMP concentrations when compared to a PKA localized deep in the cell, far from adenylyl cyclases (ACs) [143, 154].

12.6.3 cAMP Generation

There are ten distinct genes that encode ACs. Nine of these proteins are localized at the PM (tmAC1 to tmAC9) while one is unbound, the soluble adenylyl cyclase (sAC or AC10) [155, 156]. Both types of ACs, trans membrane-bound (tm-bound) and soluble, participate in the generation of cAMP microdomains. The role of tm-ACs is more complex and goes beyond cAMP production. Indeed, tm-ACs can act as scaffolds able to form complexes with a number of proteins among which several AKAPs [157]. Interestingly, thanks to this characteristic, AKAPs bring the main cAMP effector (PKA) in close proximity to the main sources of this messenger, the tm-ACs, thus orchestrating the creation of sub-PM cAMP microdomains, bound to respond to activation of the local tm-AC pool. A well-established example is the AKAP79/150. This protein binds tmAC5 and tmAC6 and brings PKA in the vicinity of these enzymes and also to a PKA target, the L-type Ca^{2+} channels [158]. PKA-dependent phosphorylation of L-type Ca^{2+} channels is important for several physiological processes such as hippocampal long-term potentiation [159] and motor coordination [160], just to cite two. It is tempting to speculate that the interaction of AKAP79/150 with AC5 and AC6 brings the source of cAMP near its effector and its local targets creating a close circuit representing a truly independent cAMP microdomain.

The main regulators of tm-AC activity are the G protein-coupled receptors (GPCRs). In this class of proteins, a large number is coupled to cAMP signaling. In particular, cAMP-linked GPCRs respond to extracellular ligands with activation and release of their associated heterotrimeric guanosine-binding proteins (G proteins) that, depending on the type of their associated Gα subunit, can activate (Gαs) or inhibit (Gαi) cAMP production [161]. While the large number of this subgroup of GPCRs confers a significant level of diversity and specificity to cAMP signaling, their specific localization at the PM may have a relevant effect on the creation of microdomains. Strong evidence in support of this hypothesis was provided by Nikolaev et al. in an elegant study where they combined cAMP-sensitive FRET sensors to scanning ion conductance microscopy. They found that, in adult cardiac myocytes, β_1ARs are evenly distributed on the PM. On the contrary, β_2ARs are located mainly on the T-tubules and are absent from non-tubular areas. In line with their wide distribution, β_1AR generate a diffuse cAMP signal whereas signals produced by β_2ARs activation were locally confined [162].

The GPCR-tm-AC axis until recently was believed to generate cAMP only at the PM, but several recent studies provided strong evidence suggesting that some GPCRs generate cAMP also after their internalization [163–167]. These studies opened the exciting possibility that, contrary to the canonical model that

internalization of GPCRs is part of their desensitization process [168], internalized GPCRs maintain their ability to trigger cAMP production [163, 164, 167]. The possible generation of cAMP microdomains by internalized GPCR appears particularly attractive as it provides an intracellular source of cAMP able to "fuel" and selectively activate PKA pools localized deep inside the cell.

The other intracellular source of cAMP is the soluble adenylyl cyclase (sAC). This enzyme is regulated by bicarbonate, Ca^{2+} [156] and ATP [169]. Soluble adenylyl cyclase is found diffused in the cytosol, but in a seminal study Zippin and colleagues found that sAC can also localize to specific subcellular sites, including the nucleus, the midbody, the centrioles and mitochondria [170]. These findings opened the possibility that sAC may regulate the activity of cAMP microdomains deep in the cell, independently of extracellular signals and in response to metabolic stimuli [156]. While the possibility of "feeding" microdomains from intracellular cAMP sources is exciting, it is largely accepted that functional processes activated by extracellular stimuli, that activate tm-ACs, are often dependent on cAMP microdomains [133, 162]. Microdomains of cAMP activated in response to tm-ACs may be located right at the PM or deeper in the cell. Rich and colleagues [130] used CNG channels as cAMP sensors in a whole-cell patch clamp approach and found that near the CNG the concentrations of cAMP elicited by receptor activation are significantly higher than in the bulk cytosol. Microdomains in the sub PM regions are characterized by cAMP concentrations higher than would be expected only based on the vicinity to tm-ACs. As an explanation, the authors put forward the possibility that hindered diffusion of cAMP, thanks to 3D-barriers most likely involving intracellular structures (such as the ER), accounts for the very high sub-PM cAMP concentrations observed in their study [130].

12.6.4 cAMP Degradation

Independently of its source, in order to reach and activate localized PKA moieties cAMP must surpass a barrier created by the most important microdomain-shaping enzymes, the cAMP-hydrolysing phosphodiesterases (PDEs) [171, 172]. There are only two known mechanisms responsible for decreasing intracellular cAMP concentrations. One is the export of cAMP from the cell via members of the ATP binding cassette (ABC) proteins, such as the multi-drug resistance proteins (MRP) 4 and 5 [173]. The quantitative importance of this mechanism is probably minor. The other is PDE-dependent hydrolysis, undisputedly the most important regulator of the cAMP signal. Thus, it is not a surprise that PDEs are critical components of the signaling cascade and crucial regulators of cAMP compartmentalization. There are 11 families of PDEs, eight of which have the ability to hydrolyse cAMP (each comprises several isoforms) [126, 172]. The first evidence of PDE involvement in the generation of compartmentalized cAMP signals was provided in cardiac myocytes, where it was observed that nearly half of the cAMP generated in response to Iso was present in the particulate fraction of the cell extracts. On the contrary, when

Iso treatment was performed in the presence of PDE inhibitors, despite a clear increase in total cAMP, the levels of messenger found in the particulate fraction reduced from 45% to about 20% of the total [174]. The first direct evidence for the key role of PDEs in shaping cAMP microdomains was achieved thanks to the development of cAMP-sensitive FRET-based sensors [175]. Using these tools, Zaccolo and Pozzan visualized the existence of cAMP gradients in living rat neonatal cardiomyocytes stimulated with Iso that depended on PDE activity [131]. This seminal work was followed by a number of subsequent studies that investigated the involvement of specific PDE isoforms in the generation of cAMP microdomains in living cardiac myocytes [176] and in human cells [177].

Shaping localized cAMP signals is not the only important function executed by PDEs. Indeed, these enzymes are responsible for one of the most important characteristics of cAMP microdomains (and the cAMP signaling pathway at large): their termination [126]. Cyclic AMP microdomains are activated in response to transient extracellular signals (such as hormones) [133, 162] or to intracellular cues (e.g., metabolically activated sAC) [178]. Once these signals dissipate, cAMP production is ceased and the PDEs present in the proximity of cAMP microdomains rapidly hydrolyse the remaining messenger, "switching off" the cascade.

12.6.5 Termination of cAMP Signaling

In the case of PKA-centred microdomains, PDEs lower cAMP levels below the levels necessary to maintain PKA activity and efficiently end the activity of the cAMP microdomain. However, the *actions* of this local pathway cannot be terminated by simply eliminating the messenger and inactivating PKA. PKA-based cAMP microdomains transduce cAMP signals via reversible phosphorylation of local targets, and to end the functional effect of PKA on these proteins the action of another class of enzymes, the phosphatases, is required [179]. Phosphatases dephosphorylate the targets, thus effectively terminating the effects of the cAMP rise. While the importance of phosphatases in the termination of cAMP microdomains is intuitive, their involvement in shaping the dynamics of these signaling units has been grossly underestimated. Experimental evidence supporting the possibility that phosphatase activity plays a key role for the temporal definition of the effects of a cAMP rise was recently provided (Lefkimmiatis and colleagues): using FRET-based cAMP and PKA-activity sensors targeted to the OMM, it was demonstrated that PKA dependent phosphorylation at the OMM persisted longer than in the cytosol without any detectable difference in the termination of the cAMP signals in the two compartments [180]. This heterogeneity in the duration of the functional effects of the cAMP increase is due to a different local phosphatase activity.

Based on the findings of over 15 years of intense research on cAMP microdomains, using live cell imaging and advanced biochemical techniques, it can be concluded that compartmentalization of the cAMP cascade is a

multiparametric process. Indeed, a tipical cAMP microdomain requires both the strict localization of the cAMP pathway components (ACs, PDEs, AKAPs, PKA and phosphatases) and the coordinated actions of cellular structures, such as organelles (e.g., mitochondria) [139, 140]. These factors, combined with cAMP buffering [181] and cytosolic viscosity [182]-that drastically restrict cAMP diffusion- enable the PDEs to shape cAMP microdomains [141].

An exemplary cAMP domain fitting virtually all the requirements was described by Maiellaro and colleagues. These authors combined in vivo cAMP imaging to locally applied stimuli by iontophoresis in *Drosophila* motor neurons and were able to show that cAMP signals in response to the invertebrate noradrenaline-like hormone octopamine [183] were confined to single synaptic boutons, while a rise in cAMP levels was undetectable in the axons of the same cell [184]. Immunofluorescence confirmed that octopamine receptors are mostly expressed on the bouton membrane while the PDEs are strategically located in structures reminiscent of fences, most likely to inhibit cAMP diffusion and to increase the confinement of the signal [184]. Taken together these findings point to the possibility that single boutons contain independent cAMP signaling microdomains, produced by the combined actions of locally confined GPCRs, tm-ACs and PDEs [184].

In the aforementioned example PDEs had also the crucial role of blocking the messenger (signal) from diffusing to other compartments and this can be generalised to all the known cAMP microdomains, except for the cAMP microdomain present in the mitochondrial matrix. The innermost mitochondrial compartment cannot be reached by cytosolic cAMP thanks to the impermeability of the IMM. The matrix located autonomous cAMP cascade is fuelled by a resident isoform of sAC, which can be activated by locally produced bicarbonate and by increases of matrix [Ca^{2+}] [178, 180, 185, 186]. The cAMP signaling cascade present in the mitochondrial matrix represents the minimalistic expression of a cAMP microdomain. Indeed, this pathway, thanks to its strict confinement by a double membrane barrier, can be regulated by a single source and potentially a single PDE isoform [178, 185, 187]. Much remains to be understood about the autonomous mitochondrial cAMP signaling cascade, in particular the molecular identification of the specific sAC and PDE expressed in the matrix and the intramitochondrial cAMP targets. Contradictory evidence, in fact, has been obtained about the localization and role of canonical PKA in the organelle matrix [178, 186].

12.7 Ca^{2+} and cAMP Crosstalk

It is now clear that the functional repertoire of signaling pathways controlled by the two main second messengers, cAMP and Ca^{2+}, are not isolated but rather integrated cascades that intermingle at multiple levels, creating a larger signaling network (Fig. 12.3). Indeed the concept of crosstalk between cAMP and Ca^{2+} is known since a long time and supported by a large body of experimental results. Each of these two molecules can reciprocally regulate the intracellular levels of its

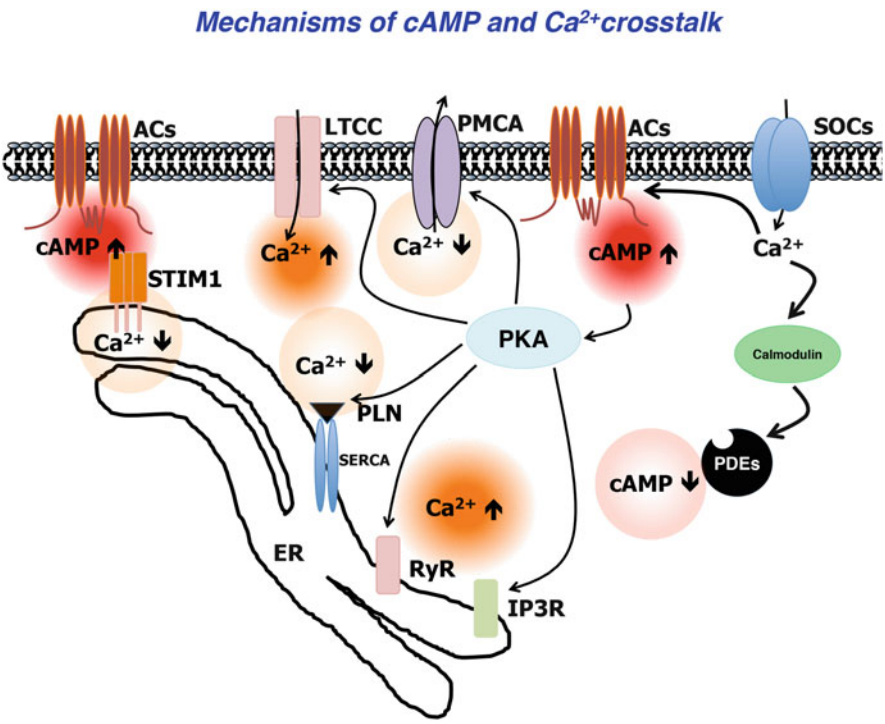

Fig. 12.3 cAMP and Ca^{2+} crosstalk. Ca^{2+} can increase or decrease cAMP levels through direct and indirect pathways. For instance, cytosolic (and localized) Ca^{2+} increases can activate or inhibit adenylyl cyclases increasing or reducing cAMP levels. Increases in Ca^{2+}-calmodulin may result in increased PDE activity and thus more efficient cAMP hydrolysis. cAMP levels can also increase thanks to a mechanism connecting the Ca^{2+} level in the ER lumen to cAMP production. The cAMP/PKA axis contributes to the regulation of cellular Ca^{2+} levels. For example PKA dependent phosphorylation of Ca^{2+} channels, PMCA or phospholamban result in drastic variations of local and bulk Ca^{2+} levels. Abbreviations in the Figure are defined in the text

partner messenger hence regulating the functional outcome of its cascade. An historical example, made over 40 years ago, is the discovery of calmodulin as the protein regulating, in the presence of Ca^{2+}, the activity of a phosphodiesterase (PDE1), one of the enzymes that degrade cAMP [188, 189]. Below we discuss a few examples of the crosstalk between Ca^{2+} and cAMP.

Ca^{2+} can regulate cAMP levels both by direct and indirect mechanisms. Six of the ten known adenylyl cyclase enzymes are, to some extent, regulated by Ca^{2+}. The soluble adenylyl cyclase (sAC) [169] and the transmembrane adenylyl cyclases (tmAC) I, III and VIII are stimulated by Ca^{2+}, while the tmAC V and VI are inhibited by the cation [155, 190]. With the exception of sAC, all the other Ca^{2+}-sensitive adenylyl cyclases are localized at the PM where, thanks to the aid of AKAPs, are in close proximity to Ca^{2+} transport proteins [157]. An interesting exception is represented by tmAC VIII, which was proposed to complex directly with Orai1,

the pore-forming protein of the store operated calcium channels (SOC) [191, 192]. Evidence has been provided that the close apposition of at least some isoforms of tmAC to Ca^{2+} channels (e.g., L-type calcium channels (LTCC) [193]) is strategic to sense the local Ca^{2+} microdomain (see [193]). A novel Ca^{2+}-related mechanism that results in cAMP increases without the requirement of changes in the levels of cytosolic Ca^{2+} was recently reported. This mechanism named store-operated cAMP signaling (SOcAMPs) [194] is triggered by the clustering of the ER-Ca^{2+} sensor stromal interaction molecule 1 (STIM1) which occurs in response to decrease in the ER Ca^{2+} levels and results in the activation of at least two ACs, AC3 [195] and AC6 [196]. Ca^{2+}-dependent activation of sAC is unique as it offers the possibility to generate cAMP in intracellular sites away from the PM where all the other cAMP producing enzymes are located. A classic example of this possibility is the generation of cAMP within mitochondria, a phenomenon dependent on a matrix located sAC and driven by mitochondrial Ca^{2+} uptake [185, 197, 198]. In addition to influencing the function of ACs Ca^{2+} can affect the function of the other regulatory branch of cAMP signaling, the PDEs. A classic example, as mentioned above, is PDE1. Indeed, different isoforms of PDE1 contain at their N terminus Ca^{2+}/calmodulin binding domains. Calmodulin-dependent activation increases the Vmax of PDE1 several fold, resulting in more efficient cAMP hydrolysis [199, 200]. Last, but not least, termination of PKA dependent pathways requires the dephosphorylation of the substrate. Noteworthy one of the most abundant and potent phosphatases is calcineurin, a classical example of Ca^{2+}-calmodulin activated enzymes.

As Ca^{2+} is able to modulate cAMP levels, similarly the cAMP/PKA axis can shape Ca^{2+} signals. Indeed the function of several Ca^{2+} transporting proteins located at the ER and at the PM can be regulated by cAMP-triggered PKA-dependent phosphorylation.

IP3R, RyRs and the SERCA regulator phospholamban (PLN) are three proteins through which the cAMP/PKA axis regulates the uptake and release of Ca^{2+} from its intracellular stores. PKA dependent phosphorylation of IP3Rs (in S1589 and S1755 for IP3R1 or S937 of IP3R2) augments the receptor affinity for IP3, increasing the probability of Ca^{2+} release from the ER in response to IP3 [201, 202]. Similarly cAMP-induced phosphorylation of RyR1 at S2843 and RyR2 at S2030 and S2809 increases the Ca^{2+}-permeability of these channels and results in increased Ca^{2+} leak [203, 204]. One of the best known synergistic effects between Ca^{2+} and cAMP is found in the cardiac tissue in response to β-adrenergic stimulation: on one hand, the rise in cAMP caused by receptor activation is known to up-regulate, via PKA-dependent phosphorylation, the activity of L type, voltage gated, Ca^{2+} channels localized in the T tubules [205, 206]. This in turn results in an increase in the amount of Ca^{2+} flowing through the PM during each contraction-relaxation cycle and a more efficient release of Ca^{2+} from RyRs (also phosphorylated by PKA) through Ca^{2+} induced Ca^{2+} release; on the other hand, PKA activation causes the phosphorylation of phospholamban, PLN, followed by an increase of SERCA activity and thus a more efficient Ca^{2+} uptake into the SR [126, 207]. Of interest, evidence suggests that these two events (occurring at the PM and SR levels) are

modulated by different cAMP microdomains and thus can be independently controlled.

cAMP dependent phosphorylation modulates also the other mechanisms controling Ca^{2+} clearance from the cytosol, i.e., the PM Ca^{2+} ATPase (PMCA) and the Na^{+}/Ca^{2+} exchanger (NCX). While PKA-dependent phosphorylation of NCX is still a matter of debate [208, 209], the effects of phosphorylation of PMCA are well established. Indeed PKA dependent phosphorylation of PMCA (in particular of PMCA1) increases the activity of the pump and thus a more efficient extrusion of Ca^{2+} from the cytosol [210, 211]. Finally, Sekler [212] and co-workers have suggested that the activity of the mitochondrial Na^{+}/Ca^{2+} exchanger NCLX is also modulated by matrix levels of cAMP, though the nature of the effector system within mitochondria is still to be clarified.

In conclusion, there are many examples of synergistic or antagonistic roles of these two second messengers. Noteworthy, in many cases the synergic or antagonistic roles of Ca^{2+} and cAMP occur in spatially restricted cellular regions where the levels of the two signaling molecules substantially differ from those found in the bulk cytoplasm.

12.8 ATP Microdomains

In living cells, the gradient of [ATP] between the intracellular (~2–10 mM) and the extracellular environment (~10 nM) is one of the steepest, with a difference of $\sim 10^6$ fold. For this reason, in addition to its main role as the most abundant intracellular energy-storing molecule, ATP is also used as an extracellular signaling molecule (and in certain cases, as an autocrine signal). Notably, and differently from Ca^{2+}, the [ATP] is higher within the cell, favoring its exit upon opening of specific channels/pores, PM damage or exocytosis (see below). The generation of ATP microdomains in the extracellular compartment has been the subject of intense investigation in the last years. The high ATP diffusion coefficient, the intrinsic instability/reactivity of the molecule and the constant presence of a pool of extracellular ectonucleotidases that degrade ATP [213–215] are all factors that should contribute to rapidly dissipate extracellular ATP microdomains, limiting their role to very short-range signaling events (paracrine or autocrine signaling). However, it has been suggested that [ATP] in the very thin layer close to cell surface can be much higher than in the bulk extracellular environment, reaching, under certain conditions and in specific points, the hundred micromolar level [216]. The purinergic signaling is mediated by two classes of PM purinergic receptors activated by ATP and/or other adenine nucleotides binding: the ionotropic P2X and the metabotropic G-protein coupled receptors (among which the P2Y nucleotide receptors). These receptors are involved in the control of a variety of cellular events, ranging from the activation of Ca^{2+} fluxes to the modulation of the immune response [217–221]. The basal, physiological blood [ATP] (~20 nM, [222] is usually not enough to sustain the activation of purinergic receptors, in particular of those endowed with the lowest affinity, such as P2X7. By

targeting luciferase to the external side of the PM, [ATP] of ~ 100 μM has been measured upon P2X7R activation in recombinant P2X7R-expressing HEK293 cells [223]. Similarly, by a two-enzymes-based method, exploiting NADPH generation starting from glucose and ATP, an [ATP] up to 80 μM has been reported in the peri-PM layer of stimulated Jurkat cells [224].

As to the mechanisms responsible for ATP release, they are not completely characterized and can be divided into three main pathways. The first is the passive efflux through PM ATP-permeable channels. For instance, VDACL (volume and voltage dependent ATP-conductive large-conductance anion channel) (set of channels distinc form the mitochondrial VDACs) has been proposed to be important for a swelling-induced ATP release [225]. Connexins hemichannels have been associated to ATP release and have been proposed to be essential in intercellular waves in choclear epithelial cells (mechanically induced, [226–228]), as well as pannexins [229]. Interestingly, a strong, ATP-mediated activation of the P2X7 receptor has been suggested to induce the same receptor to form a large conductance, non-selective pore, through which ATP itself can efflux towards the extracellular milieu. This efflux in turn generates an ATP microdomain near its mouth and establishes a positive feedback, capable to recruit additional receptors, leading to a massive Ca^{2+} entry and eventually to cell death [230]. The second mechanism for ATP extrusion is active transport, based on poorly characterized ABC transporters, expressed already in protists [231]. Finally, ATP can be released by exocytosis of vesicles in platelets, mast cells, astrocytes and neurons [226, 232, 233]. Evidence that ATP is co-stored with neurotransmitters in specific vesicles has been provided, as well as the existence of nucleotide transporters capable of accumulating ATP in these vesicles (reviewed in [234]). Last, but not least, it must be stressed that, at synaptic level, the pre- and post- synaptic membranes are very closely associated. This creates a restricted environment, in which not only the neurotransmitter-based signaling is favored, but also the diffusion of ATP (or other released molecules) is limited, sustaining the existence of spatially confined microdomains. In addition to exocytosis, also PM damage (such as in necrotic cells) can trigger ATP release, and this can be important for the induction of an inflammatory response [235]. In this respect, extracellular ATP is considered among the most potent damage-associated molecular pattern (DAMPs).

Above, we discussed the mechanisms that lead to the generation of ATP microdomains in the extracellular environment, as well as their importance for purinergic signaling. While the steep [ATP] gradient between the two sides of the PM immediately provides the physical/chemical basis for the onset of such microdomains, the generation of intracellular heterogeneities in [ATP] is much less intuitive. Indeed, on the one hand, the very high cytosolic [ATP], its high diffusion coefficient and the lack of specialized ATP buffers (such as those for Ca^{2+}) argue against the presence of physiologically relevant local differences in intracellular [ATP]. On the other hand, a number of indirect observations suggests that these localized variations in intracellular [ATP] actually exist and play some relevant functional role. To the best of our knowledge, the existence of such intracellular ATP microdomains is presently based on only indirect evidence and intracellular

ATP gradients have not been directly visualized by imaging techniques. Below, we provide a few examples.

A first consideration that can be helpful to explain the occurrence of intracellular [ATP] gradients is that, in the majority of cells, a substantial proportion of ATP is synthesized within mitochondria and then extruded into the cytosol. Thus, it appears immediately clear that a bias positioning of mitochondria within the cells can create the conditions for a localized rise in [ATP]. For instance, in highly polarized cells such as neurons, it has been suggested that the transport of mitochondria toward high-energy demanding regions (i.e., synapses) is necessary to provide a highly efficient local ATP supply [236] (and see also below). Similarly, mitochondria in adult cardiomyocytes are in a highly ordered and stationary positioning [237] close to the sarcomeres, the SR and the T-tubules, forming the so-called intracellular energetic unit (ICEU) [238–241]. At this level, the four structures are so closely packed that, during contraction, Ca^{2+} and ATP are released and taken up/consumed in the ICEU before they diffuse outside it (reviewed in [242]). In particular, during each contraction/relaxation cycle, Ca^{2+} is released from SR through RyRs in the dyadic cleft, formed by the close apposition of SR with the T-tubules. In turn, Ca^{2+} promptly diffuses outside the dyadic cleft to allow sarcomeres contraction and is pumped back into the SR by SERCA. A local and prompt ATP fueling to the Ca^{2+} pump, provided by nearby mitochondria, represents a highly advantageous spatial arrangement. Indeed, alterations of the cytoarchitecture in mice hearts have a deep impact on ATP transfer from mitochondria to the SR [243].

Oscillations in the intracellular ATP levels, and in particular in the ATP/ADP ratio, are known to be potent modulator of K_{ATP} channel activity. K_{ATP} channels control a plethora of physiological processes, but are particularly important in the regulation of insulin secretion from pancreatic β cells. Briefly, ATP binding to the pore-forming subunits induces channel closure, while interaction of intracellular Mg^{2+}ADP with the regulatory SUR1 subunits stimulates channel opening (reviewed in [244, 245]). In β-cells, when [glucose] is low, the low cytosolic [ATP]/[ADP] ratio keeps the K_{ATP} channels open and maintains the membrane hyperpolarized, preventing electrical activity and insulin secretion. At higher [glucose], on the contrary, the increased glucose metabolism augments the [ATP]/[ADP] ratio, inhibiting K_{ATP} current and depolarizing the membrane. In turn, Ca^{2+} influx is activated and insulin secreted. Interestingly, the increased intracellular [Ca^{2+}] activates Ca^{2+} ATP-ases, inducing ATP consumption particularly at sub-PM level that may contribute to partial K_{ATP} reopening and termination of the signal [246, 247]. Recently, it has been proposed that, during glucose stimulation, at least part of the increased ATP production is due to mitochondrial activity, and a complex interplay between ATP increase, cytosolic Ca^{2+} oscillations, mitochondrial Ca^{2+} uptake and Ca^{2+}-induced stimulation of mitochondrial dehydrogenases has been suggested [248–250].

While mitochondrial ATP synthesis can be responsible for local [ATP] increases, the opposite, i.e., localized [ATP] drops, can be hypothesized close to sites of high ATP consumption. Although, in contrast to Ca^{2+}, specialized ATP buffers are not known, all the enzymes/pumps that use ATP to exert their energy-consuming

activities can be considered an ATP sink. Importantly, differently from buffers, these proteins do not simply bind ATP, i.e. they are not saturable, but continuously consume ATP. In other words, their potential to locally deplete the pool of ATP is even higher than that of hypothetical buffers. Of course, the enrichment of these ATP-consuming enzymes into clusters or spatially confined regions enhances the local ATP utilization. For instance, the PM Na^+/K^+ ATPase is the most abundant ion pump within the cell, capable of consuming considerable amounts of ATP to maintain the Na^+/K^+ gradient across the PM. Thus, it is not surprising that, near these pumps, a locally lower [ATP] could be observed. This may be particularly relevant in excitable cells, such as neurons. Indeed, upon an action potential, the massive fluxes of Na^+ and K^+ between the extracellular milieu and the sub-PM layer need to be actively rescued by the intense activity of the Na^+/K^+ ATPase. Thus, a local need for ATP is present at synapses, during intense electrical activity, and it is believed to be fulfilled by the regional recruitment of energetically active mitochondria, as discussed above [236]. Moreover, in addition to the necessity to restore the Na^+/K^+ balance, it must be mentioned that, during action potentials, sub-PM [Ca^{2+}] also increases (see above). Ca^{2+} levels must turn back to basal, and this is obtained, at least in part, through the activity of PM Ca^{2+} ATPases. Although PM Ca^{2+} ATPases are less abundant than Na^+/K^+ ATPase (arguing against their capacity to significantly locally deplete ATP), their activity has been proposed to be modulated by the presence of sub-PM mitochondria [251]. Again, the presence of mitochondria in the vicinity of the pumps could be important for local ATP supply or, as it has been proposed, for local Ca^{2+} buffering due to mitochondrial Ca^{2+} uptake, being Ca^{2+} itself a regulator of the pump activity [251]. Finally, it has been suggested that the activity of hexokinase 1 (HK1), the first enzyme of glycolysis responsible for the ATP-driven conversion of glucose into glucose-6-P, is modulated by its dynamic association with the OMM, because of its preferential utilization of mitochondria-derived ATP [252–254]. Although the reasons of this preference are presently not completely clear, it has been proposed that the attachment of HK1 to VDAC (the channel through which mitochondrial ATP is exported into the cytosol and cytosolic ADP imported into mitochondria), provides a spatial advantage to directly fuel the activity of the enzyme with ATP [255]. Conformational changes in the HK1 ATP-binding domain, following attachment to mitochondria, have been also suggested to be responsible for this substrate specificity [254]. Recently, it has been demonstrated that a specific drop in mitochondria-produced ATP activates the cytosolic energy sensor AMPK, promptly inducing the phosphorylation of the mitochondrial fission factor (Mff). In turn, this induces Drp1 recruitment to the OMM and triggers mitochondrial fission [256]. The fact that a mitochondrial defect is capable to activate a cytosolic pathway further highlights the capacity of certain signaling events to discriminate between the source of ATP. However, whether (and how) a pool of AMPK is capable of specifically detecting changes in mitochondria-derived ATP, is currently not clear.

12.9 Other Microdomains

Above, we have discussed how the combination of different players generates microdomains of Ca^{2+}, cAMP and ATP. Microdomains of ions such as Na^+ and K^+, on the other hand, have been proposed to be transiently formed close to the mouth of their PM-located channels, but their existence is temporally and spatially shortened by their extremely high diffusion coefficient. Nevertheless, evidence for the existence of Na^+ microdomains in the subsarcolemmal space of cardiomyocytes ("fuzzy space") has been provided, and the interested readers are referred to a recent review [257]. Similarly, the high diffusion constant of IP3 (283 $\mu m^2/s$ [258]), generated by the PLC-mediated hydrolysis of PM-localized PIP2, has been classically considered as an argument against the generation of physiologically relevant heterogeneities in [IP3] within the cells. However, a confined PLC recruitment to specific PM regions, as well as a biased distribution of GPRCs, have been suggested to be responsible for localized IP3 production [259]. Moreover, the IP3 diffusion has recently been re-calculated in intact neuroblastoma cells, by photoreleasing a poorly metabolized IP3 analog. Interestingly, using this method, the diffusion coefficient was found to be ~30-fold lower (~10 $\mu m^2/s$) than before, due to the presence of a large number of IP3Rs in these cells, that can act as immobile IP3 buffers [260]. Clearly, a lower diffusion coefficient is compatible with a local rather than a global signaling of this second messenger. In addition, IP3 has been demonstrated to diffuse between cells through the gap junctions, composed of connexins (reviewed in [261], but see also [262]). Thus, an [IP3] gradient between adjacent cells is formed and is part of the mechanism responsible for the spread of intercellular Ca^{2+} waves [227, 263].

12.10 Conclusions

Above, we have discussed how cells exploit microdomains to decipher the more diverse stimuli. The possibility to control both the temporal and spatial extension of these elementary events, as well as the continuous cross-talk between microdomains involving different molecules, represents an extremely powerful tool that allows the cells to orchestrate and finely tune a plethora of signaling cascades, employing only few messengers. The development of novel probes, capable of reliably and quickly reporting changes in the concentration of the molecules under investigation (while interfering minimally with the dynamics of these changes), will offer the opportunity to more accurately visualize the generation of microdomains at sub-organellar level. Surely, a parallel rapid improvement on the speed and spatial resolution of different imaging techniques appears of fundamental importance to follow over time these events, allowing a precise and detailed evaluation of their physiological (or pathological) significance.

Acknowledgments The original work by the Authors has been supported by grants from the Italian Ministry of University and Research (MIUR), by Telethon Foundation, by Cariparo Foundation, by the National Research Council (CNR) and by the University of Padova to TP. We are grateful to Dr. P. Magalhaes for critically reading the manuscript.

References

1. Petersen OH (2012) Specific mitochondrial functions in separate sub-cellular domains of pancreatic acinar cells. Pflugers Arch 464(1):77–87. https://doi.org/10.1007/s00424-012-1099-6
2. Lioudyno MI, Kozak JA, Penna A et al (2008) Orai1 and STIM1 move to the immunological synapse and are up-regulated during T cell activation. Proc Natl Acad Sci USA 105 (6):2011–2016. https://doi.org/10.1073/pnas.0706122105
3. Berridge MJ (2006) Calcium microdomains: organization and function. Cell Calcium 40 (5–6):405–412
4. Samanta K, Parekh AB (2016) Spatial Ca^{2+} profiling: decrypting the universal cytosolic Ca^{2+} oscillation. J Physiol 595(10):3053–3062. https://doi.org/10.1113/JP272860
5. Calcraft PJ, Ruas M, Pan Z et al (2009) NAADP mobilizes calcium from acidic organelles through two-pore channels. Nature 459(7246):596–600
6. Rizzuto R, Pozzan T (2006) Microdomains of intracellular Ca^{2+}: molecular determinants and functional consequences. Physiol Rev 86(1):369–408
7. Heidelberger R, Heinemann C, Neher E et al (1994) Calcium dependence of the rate of exocytosis in a synaptic terminal. Nature 371(6497):513–515
8. Beutner D, Voets T, Neher E et al (2001) Calcium dependence of exocytosis and endocytosis at the cochlear inner hair cell afferent synapse. Neuron 29(3):681–690
9. Roberts WM, Jacobs RA, Hudspeth AJ (1990) Colocalization of ion channels involved in frequency selectivity and synaptic transmission at presynaptic active zones of hair cells. J Neurosci 10(11):3664–3684
10. Robitaille R, Adler EM, Charlton MP (1990) Strategic location of calcium channels at transmitter release sites of frog neuromuscular synapses. Neuron 5(6):773–779
11. Prakriya M, Solaro CR, Lingle CJ (1996) $[Ca^{2+}]$i elevations detected by BK channels during Ca^{2+} influx and muscarine-mediated release of Ca^{2+} from intracellular stores in rat chromaffin cells. J Neurosci 16(14):4344–4359
12. Naraghi M, Neher E (1997) Linearized buffered Ca^{2+} diffusion in microdomains and its implications for calculation of $[Ca^{2+}]$ at the mouth of a calcium channel. J Neurosci 17 (18):6961–6973
13. Carafoli E, Santella L, Branca D et al (2001) Generation, control, and processing of cellular calcium signals. Crit Rev Biochem Mol Biol 36(2):107–260
14. Berridge MJ, Bootman MD, Roderick HL (2003) Calcium signalling: dynamics, homeostasis and remodelling. Nat Rev Mol Cell Biol 4(7):517–529
15. Eggermann E, Jonas P (2011) How the 'slow' Ca(2+) buffer parvalbumin affects transmitter release in nanodomain-coupling regimes. Nat Neurosci 15(1):20–22. https://doi.org/10.1038/nn.3002
16. Mori MX, Erickson MG, Yue DT (2004) Functional stoichiometry and local enrichment of calmodulin interacting with Ca^{2+} channels. Science 304(5669):432–435. https://doi.org/10.1126/science.1093490
17. Nagerl UV, Novo D, Mody I et al (2000) Binding kinetics of calbindin-D(28k) determined by flash photolysis of caged Ca(2+). Biophys J 79(6):3009–3018. https://doi.org/10.1016/S0006-3495(00)76537-4

18. Faas GC, Schwaller B, Vergara JL et al (2007) Resolving the fast kinetics of cooperative binding: Ca^{2+} buffering by calretinin. PLoS Biol 5(11):e311. https://doi.org/10.1371/journal.pbio.0050311
19. Faas GC, Raghavachari S, Lisman JE et al (2011) Calmodulin as a direct detector of Ca^{2+} signals. Nat Neurosci 14(3):301–304. https://doi.org/10.1038/nn.2746
20. Nowycky MC, Pinter MJ (1993) Time courses of calcium and calcium-bound buffers following calcium influx in a model cell. Biophys J 64(1):77–91. https://doi.org/10.1016/S0006-3495(93)81342-0
21. Augustine GJ, Neher E (1992) Neuronal Ca^{2+} signalling takes the local route. Curr Opin Neurobiol 2(3):302–307
22. Strautman AF, Cork RJ, Robinson KR (1990) The distribution of free calcium in transected spinal axons and its modulation by applied electrical fields. J Neurosci 10(11):3564–3575
23. Gabso M, Neher E, Spira ME (1997) Low mobility of the Ca^{2+} buffers in axons of cultured Aplysia neurons. Neuron 18(3):473–481
24. Sabatini BL, Oertner TG, Svoboda K (2002) The life cycle of Ca^{2+} ions in dendritic spines. Neuron 33(3):439–452
25. Augustine GJ, Santamaria F, Tanaka K (2003) Local calcium signaling in neurons. Neuron 40(2):331–346
26. Naraghi M (1997) T-jump study of calcium binding kinetics of calcium chelators. Cell Calcium 22(4):255–268
27. Adler EM, Augustine GJ, Duffy SN et al (1991) Alien intracellular calcium chelators attenuate neurotransmitter release at the squid giant synapse. J Neurosci 11(6):1496–1507
28. Plant TD, Standen NB, Ward TA (1983) The effects of injection of calcium ions and calcium chelators on calcium channel inactivation in Helix neurones. J Physiol 334:189–212
29. Tay LH, Dick IE, Yang W et al (2012) Nanodomain Ca(2)(+) of Ca(2)(+) channels detected by a tethered genetically encoded Ca(2)(+) sensor. Nat Commun 3:778. https://doi.org/10.1038/ncomms1777
30. Bers DM (2002) Cardiac excitation-contraction coupling. Nature 415(6868):198–205. https://doi.org/10.1038/415198a
31. Hong T, Yang H, Zhang SS et al (2014) Cardiac BIN1 folds T-tubule membrane, controlling ion flux and limiting arrhythmia. Nat Med 20(6):624–632. https://doi.org/10.1038/nm.3543
32. Fu Y, Shaw SA, Naami R et al (2016) Isoproterenol promotes rapid ryanodine receptor movement to bridging integrator 1 (BIN1)-organized dyads. Circulation 133(4):388–397. https://doi.org/10.1161/CIRCULATIONAHA.115.018535
33. Sacconi L, Ferrantini C, Lotti J et al (2012) Action potential propagation in transverse-axial tubular system is impaired in heart failure. Proc Natl Acad Sci USA 109(15):5815–5819. https://doi.org/10.1073/pnas.1120188109
34. Hayashi T, Martone ME, Yu Z et al (2009) Three-dimensional electron microscopy reveals new details of membrane systems for Ca^{2+} signaling in the heart. J Cell Sci 122(Pt 7):1005–1013. https://doi.org/10.1242/jcs.028175
35. Takagishi Y, Rothery S, Issberner J et al (1997) Spatial distribution of dihydropyridine receptors in the plasma membrane of guinea pig cardiac myocytes investigated by correlative confocal microscopy and label-fracture electron microscopy. J Electron Microsc (Tokyo) 46(2):165–170
36. Takagishi Y, Yasui K, Severs NJ et al (2000) Species-specific difference in distribution of voltage-gated L-type Ca(2+) channels of cardiac myocytes. Am J Physiol Cell Physiol 279(6):C1963–C1969
37. Glukhov AV, Balycheva M, Sanchez-Alonso JL et al (2015) Direct evidence for microdomain-specific localization and remodeling of functional L-type calcium channels in rat and human atrial myocytes. Circulation 132(25):2372–2384. https://doi.org/10.1161/CIRCULATIONAHA.115.018131

38. Quintana A, Schwindling C, Wenning AS et al (2007) T cell activation requires mitochondrial translocation to the immunological synapse. Proc Natl Acad Sci USA 104(36):14418–14423. https://doi.org/10.1073/pnas.0703126104
39. Quintana A, Pasche M, Junker C et al (2011) Calcium microdomains at the immunological synapse: how ORAI channels, mitochondria and calcium pumps generate local calcium signals for efficient T-cell activation. EMBO J 30(19):3895–3912. https://doi.org/10.1038/emboj.2011.289
40. Hoth M, Fanger CM, Lewis RS (1997) Mitochondrial regulation of store-operated calcium signaling in T lymphocytes. J Cell Biol 137:633–648
41. Tarlowe MH, Kannan KB, Itagaki K et al (2003) Inflammatory chemoreceptor cross-talk suppresses leukotriene B4 receptor 1-mediated neutrophil calcium mobilization and chemotaxis after trauma. J Immunol 171(4):2066–2073
42. Levin KR, Page E (1980) Quantitative studies on plasmalemmal folds and caveolae of rabbit ventricular myocardial cells. Circ Res 46(2):244–255
43. Murphy RM, Mollica JP, Lamb GD (2009) Plasma membrane removal in rat skeletal muscle fibers reveals caveolin-3 hot-spots at the necks of transverse tubules. Exp Cell Res 315 (6):1015–1028. https://doi.org/10.1016/j.yexcr.2008.11.022
44. Zampighi G, Vergara J, Ramon F (1975) On the connection between the transverse tubules and the plasma membrane in frog semitendinosus skeletal muscle. Are caveolae the mouths of the transverse tubule system? J Cell Biol 64(3):734–740
45. Balijepalli RC, Foell JD, Hall DD et al (2006) Localization of cardiac L-type Ca(2+) channels to a caveolar macromolecular signaling complex is required for beta(2)-adrenergic regulation. Proc Natl Acad Sci USA 103(19):7500–7505. https://doi.org/10.1073/pnas.0503465103
46. Wright PT, Nikolaev VO, O'Hara T et al (2014) Caveolin-3 regulates compartmentation of cardiomyocyte beta2-adrenergic receptor-mediated cAMP signaling. J Mol Cell Cardiol 67:38–48. https://doi.org/10.1016/j.yjmcc.2013.12.003
47. Balijepalli RC, Kamp TJ (2008) Caveolae, ion channels and cardiac arrhythmias. Prog Biophys Mol Biol 98(2–3):149–160. https://doi.org/10.1016/j.pbiomolbio.2009.01.012
48. Makarewich CA, Correll RN, Gao H et al (2012) A caveolae-targeted L-type Ca(2)+ channel antagonist inhibits hypertrophic signaling without reducing cardiac contractility. Circ Res 110 (5):669–674. https://doi.org/10.1161/CIRCRESAHA.111.264028
49. Best JM, Kamp TJ (2012) Different subcellular populations of L-type Ca^{2+} channels exhibit unique regulation and functional roles in cardiomyocytes. J Mol Cell Cardiol 52(2):376–387. https://doi.org/10.1016/j.yjmcc.2011.08.014
50. Hong T, Shaw RM (2017) Cardiac T-tubule microanatomy and function. Physiol Rev 97 (1):227–252. https://doi.org/10.1152/physrev.00037.2015
51. Colella M, Grisan F, Robert V et al (2008) Ca^{2+} oscillation frequency decoding in cardiac cell hypertrophy: role of calcineurin/NFAT as Ca^{2+} signal integrators. Proc Natl Acad Sci USA 105(8):2859–2864. https://doi.org/10.1073/pnas.0712316105
52. Dolmetsch RE, Lewis RS, Goodnow CC et al (1997) Differential activation of transcription factors induced by Ca^{2+} response amplitude and duration. Nature 386:855–858
53. Shan J, Betzenhauser MJ, Kushnir A et al (2010) Role of chronic ryanodine receptor phosphorylation in heart failure and beta-adrenergic receptor blockade in mice. J Clin Invest 120(12):4375–4387. https://doi.org/10.1172/JCI37649
54. Zhao W, Yuan Q, Qian J et al (2006) The presence of Lys27 instead of Asn27 in human phospholamban promotes sarcoplasmic reticulum Ca^{2+}-ATPase superinhibition and cardiac remodeling. Circulation 113(7):995–1004. https://doi.org/10.1161/CIRCULATIONAHA.105.583351
55. Jordan MC, Henderson SA, Han T et al (2010) Myocardial function with reduced expression of the sodium-calcium exchanger. J Card Fail 16(9):786–796. https://doi.org/10.1016/j.cardfail.2010.03.012

56. Nakamura TY, Iwata Y, Arai Y et al (2008) Activation of Na+/H+ exchanger 1 is sufficient to generate Ca^{2+} signals that induce cardiac hypertrophy and heart failure. Circ Res 103 (8):891–899. https://doi.org/10.1161/CIRCRESAHA.108.175141
57. Guo A, Cala SE, Song LS (2012) Calsequestrin accumulation in rough endoplasmic reticulum promotes perinuclear Ca^{2+} release. J Biol Chem 287(20):16670–16680. https://doi.org/10.1074/jbc.M112.340927
58. Petersen OH, Gerasimenko OV, Gerasimenko JV et al (1998) The calcium store in the nuclear envelope. Cell Calcium 23(2-3):87–90
59. Wu X, Bers DM (2006) Sarcoplasmic reticulum and nuclear envelope are one highly interconnected Ca^{2+} store throughout cardiac myocyte. Circ Res 99(3):283–291. https://doi.org/10.1161/01.RES.0000233386.02708.72
60. Guatimosim S, Amaya MJ, Guerra MT et al (2008) Nuclear Ca^{2+} regulates cardiomyocyte function. Cell Calcium 44(2):230–242. https://doi.org/10.1016/j.ceca.2007.11.016
61. Wu X, Zhang T, Bossuyt J et al (2006) Local $InsP_3$-dependent perinuclear Ca^{2+} signaling in cardiac myocyte excitation-transcription coupling. J Clin Investig 116(3):675–682
62. Zima AV, Bare DJ, Mignery GA et al (2007) IP_3-dependent nuclear Ca^{2+} signalling in the mammalian heart. J Physiol 584(Pt 2):601–611
63. Goonasekera SA, Molkentin JD (2012) Unraveling the secrets of a double life: contractile versus signaling Ca^{2+} in a cardiac myocyte. J Mol Cell Cardiol 52(2):317–322. https://doi.org/10.1016/j.yjmcc.2011.05.001
64. Ibarra C, Vicencio JM, Varas-Godoy M et al (2014) An integrated mechanism of cardiomyocyte nuclear Ca(2+) signaling. J Mol Cell Cardiol 75:40–48. https://doi.org/10.1016/j.yjmcc.2014.06.015
65. Deluca HF, Engstrom GW (1961) Calcium uptake by rat kidney mitochondria. Proc Natl Acad Sci USA 47:1744–1750
66. De Stefani D, Raffaello A, Teardo E et al (2011a) A forty-kilodalton protein of the inner membrane is the mitochondrial calcium uniporter. Nature 476(7360):336–340. https://doi.org/10.1038/nature10230
67. Baughman JM, Perocchi F, Girgis HS et al (2011) Integrative genomics identifies MCU as an essential component of the mitochondrial calcium uniporter. Nature 476(7360):341–345
68. De Stefani D, Rizzuto R, Pozzan T (2016) Enjoy the trip: calcium in mitochondria back and forth. Annu Rev Biochem 85:161–192. https://doi.org/10.1146/annurev-biochem-060614-034216
69. Mammucari C, Raffaello A, Vecellio Reane D et al (2016) Molecular structure and pathophysiological roles of the mitochondrial calcium uniporter. Biochim Biophys Acta 1863 (10):2457–2464. https://doi.org/10.1016/j.bbamcr.2016.03.006
70. Kamer KJ, Mootha VK (2015) The molecular era of the mitochondrial calcium uniporter. Nat Rev Mol Cell Biol 16(9):545–553. https://doi.org/10.1038/nrm4039
71. Pendin D, Greotti E, Pozzan T (2014a) The elusive importance of being a mitochondrial Ca^{2+} uniporter. Cell Calcium 55(3):139–145. https://doi.org/10.1016/j.ceca.2014.02.008
72. Rizzuto R, Simpson AW, Brini M et al (1992) Rapid changes of mitochondrial Ca^{2+} revealed by specifically targeted recombinant aequorin. Nature 358(6384):325–327
73. Pendin D, Greotti E, Filadi R et al (2014b) Spying on organelle Ca^{2+} in living cells: the mitochondrial point of view. J Endocrinol Invest 38(1):39–45. https://doi.org/10.1007/s40618-014-0178-2
74. Pendin D, Greotti E, Lefkimmiatis K et al (2017) Exploring cells with targeted biosensors. J Gen Physiol 149(1):1–36. https://doi.org/10.1085/jgp.201611654
75. Rizzuto R, Pinton P, Carrington W et al (1998) Close contacts with the endoplasmic reticulum as determinants of mitochondrial Ca^{2+} responses. Science 280(5370):1763–1766
76. Csordás G, Thomas AP, Hajnoczky G (1999) Quasi-synaptic calcium signal transmission between endoplasmic reticulum and mitochondria. EMBO J 18:96–108

77. Giacomello M, Drago I, Bortolozzi M et al (2010) Ca^{2+} hot spots on the mitochondrial surface are generated by Ca^{2+} mobilization from stores, but not by activation of store-operated Ca^{2+} channels. Mol Cell 38(2):280–290. https://doi.org/10.1016/j.molcel.2010.04.003
78. Csordas G, Varnai P, Golenar T et al (2010) Imaging interorganelle contacts and local calcium dynamics at the ER-mitochondrial interface. Mol Cell 39(1):121–132
79. Filadi R, Pozzan T (2015) Generation and functions of second messengers microdomains. Cell Calcium 58(4):405–414. https://doi.org/10.1016/j.ceca.2015.03.007
80. Filadi R, Theurey P, Pizzo P (2017) The endoplasmic reticulum-mitochondria coupling in health and disease: molecules, functions and significance. Cell Calcium 62:1–15. https://doi.org/10.1016/j.ceca.2017.01.003
81. Messina A, Reina S, Guarino F et al (2012) VDAC isoforms in mammals. Biochim Biophys Acta 1818(6):1466–1476. https://doi.org/10.1016/j.bbamem.2011.10.005
82. Rapizzi E, Pinton P, Szabadkai G et al (2002) Recombinant expression of the voltage-dependent anion channel enhances the transfer of Ca^{2+} microdomains to mitochondria. J Cell Biol 159(4):613–624
83. De Stefani D, Bononi A, Romagnoli A et al (2011b) VDAC1 selectively transfers apoptotic Ca^{2+} signals to mitochondria. Cell Death Differ 19(2):267–273. https://doi.org/10.1038/cdd.2011.92
84. Filadi R, Greotti E, Turacchio G et al (2016) Presenilin 2 modulates endoplasmic reticulum-mitochondria coupling by tuning the antagonistic effect of mitofusin 2. Cell Rep 15(10):2226–2238
85. Szabadkai G, Bianchi K, Varnai P et al (2006) Chaperone-mediated coupling of endoplasmic reticulum and mitochondrial Ca^{2+} channels. J Cell Biol 175(6):901–911
86. De Marchi U, Castelbou C, Demaurex N (2011) Uncoupling protein 3 (UCP3) modulates the activity of Sarco/endoplasmic reticulum Ca^{2+}-ATPase (SERCA) by decreasing mitochondrial ATP production. J Biol Chem 286(37):32533–32541
87. Landolfi B, Curci S, Debellis L et al (1998) Ca^{2+} homeostasis in the agonist-sensitive internal store: functional interactions between mitochondria and the ER measured in situ in intact cells. J Cell Biol 142:1235–1243
88. Foskett JK, White C, Cheung KH et al (2007) Inositol trisphosphate receptor Ca^{2+} release channels. Physiol Rev 87(2):593–658
89. Vais H, Foskett JK, Ullah G et al (2012) Permeant calcium ion feed-through regulation of single inositol 1,4,5-trisphosphate receptor channel gating. J Gen Physiol 140(6):697–716. https://doi.org/10.1085/jgp.201210804
90. Ivanova H, Vervliet T, Missiaen L et al (2014) Inositol 1,4,5-trisphosphate receptor-isoform diversity in cell death and survival. Biochim Biophys Acta 1843(10):2164–2183. https://doi.org/10.1016/j.bbamcr.2014.03.007
91. Perkins G, Renken C, Martone ME et al (1997) Electron tomography of neuronal mitochondria: three-dimensional structure and organization of cristae and membrane contacts. J Struct Biol 119(3):260–272
92. del Arco A, Satrustegui J (2004) Identification of a novel human subfamily of mitochondrial carriers with calcium-binding domains. J Biol Chem 279(23):24701–24713. https://doi.org/10.1074/jbc.M401417200
93. Satrustegui J, Pardo B, Del Arco A (2007) Mitochondrial transporters as novel targets for intracellular calcium signaling. Physiol Rev 87(1):29–67
94. De La Fuente S, Fernandez-Sanz C, Vail C et al (2016) Strategic positioning and biased activity of the mitochondrial calcium uniporter in cardiac muscle. J Biol Chem 291(44):23343–23362. https://doi.org/10.1074/jbc.M116.755496
95. Garcia-Perez C, Schneider TG, Hajnoczky G et al (2011) Alignment of sarcoplasmic reticulum-mitochondrial junctions with mitochondrial contact points. Am J Physiol Heart Circ Physiol 301(5):H1907–H1915. https://doi.org/10.1152/ajpheart.00397.2011
96. Booth DM, Enyedi B, Geiszt M et al (2016) Redox nanodomains are induced by and control calcium signaling at the ER-mitochondrial interface. Mol Cell 63(2):240–248

97. Giorgi C, Bonora M, Sorrentino G et al (2015) p53 at the endoplasmic reticulum regulates apoptosis in a Ca^{2+}-dependent manner. Proc Natl Acad Sci USA 112(6):1779–1784. https://doi.org/10.1073/pnas.1410723112
98. Raffaello A, De Stefani D, Sabbadin D et al (2013) The mitochondrial calcium uniporter is a multimer that can include a dominant-negative pore-forming subunit. EMBO J 32 (17):2362–2376. https://doi.org/10.1038/emboj.2013.157
99. Plovanich M, Bogorad RL, Sancak Y et al (2013) MICU2, a paralog of MICU1, resides within the mitochondrial uniporter complex to regulate calcium handling. PLoS One 8(2):e55785. https://doi.org/10.1371/journal.pone.0055785 PONE-D-12-28515
100. Westrate LM, Lee JE, Prinz WA et al (2015) Form follows function: the importance of endoplasmic reticulum shape. Annu Rev Biochem 84:791–811. https://doi.org/10.1146/annurev-biochem-072711-163501
101. Zhang H, Hu J (2016) Shaping the endoplasmic reticulum into a social network. Trends Cell Biol 26(12):934–943. https://doi.org/10.1016/j.tcb.2016.06.002
102. Montero M, Alvarez J, Scheenen WJJ et al (1997) Ca^{2+} homeostasis in the endoplasmic reticulum: coexistence of high and low [Ca^{2+}] subcompartments in intact HeLa cells. J Cell Biol 139:601–611
103. de la Fuente S, Fonteriz RI, Montero M et al (2013) Ca^{2+} homeostasis in the endoplasmic reticulum measured with a new low-Ca^{2+}-affinity targeted aequorin. Cell Calcium 54 (1):37–45. https://doi.org/10.1016/j.ceca.2013.04.001
104. Aulestia FJ, Redondo PC, Rodriguez-Garcia A et al (2011) Two distinct calcium pools in the endoplasmic reticulum of HEK-293T cells. Biochem J 435(1):227–235
105. Hayashi T, Su TP (2007) Sigma-1 receptor chaperones at the ER-mitochondrion interface regulate Ca(2+) signaling and cell survival. Cell 131(3):596–610. https://doi.org/10.1016/j.cell.2007.08.036
106. Villa A, Podini P, Panzeri MC et al (1993) The endoplasmic-sarcoplasmic reticulum of smooth muscle: immunocytochemistry of vas deferens fibers reveals specialized subcompartments differently equipped for the control of Ca^{2+} homeostasis. J Cell Biol 121(5):1041–1051
107. Villa A, Podini P, Clegg DO et al (1991) Intracellular Ca^{2+} stores in chicken Purkinje neurons: differential distribution of the low affinity-high capacity Ca^{2+} binding protein, calsequestrin, of Ca^{2+} ATPase and of the ER lumenal protein, Bip. J Cell Biol 113(4):779–791
108. Meldolesi J, Pozzan T (1998) The heterogeneity of ER Ca^{2+} stores has a key role in nonmuscle cell signaling and function. J Cell Biol 142(6):1395–1398
109. Myhill N, Lynes EM, Nanji JA et al (2008) The subcellular distribution of calnexin is mediated by PACS-2. Mol Biol Cell 19(7):2777–2788
110. Lynes EM, Bui M, Yap MC et al (2012) Palmitoylated TMX and calnexin target to the mitochondria-associated membrane. EMBO J 31(2):457–470
111. Bastianutto C, Clementi E, Codazzi F et al (1995) Overexpression of calreticulin increases the Ca^{2+} capacity of rapidly exchanging Ca^{2+} stores and reveals aspects of their lumenal microenvironment and function. J Cell Biol 130:847–855
112. Mery L, Mesaeli N, Michalak M et al (1996) Overexpression of calreticulin increases intracellular Ca^{2+} storage and decreases store-operated Ca^{2+} influx. J Biol Chem 271:9332–9339
113. de Brito OM, Scorrano L (2008) Mitofusin 2 tethers endoplasmic reticulum to mitochondria. Nature 456(7222):605–610
114. Orso G, Pendin D, Liu S et al (2009) Homotypic fusion of ER membranes requires the dynamin-like GTPase atlastin. Nature 460(7258):978–983. https://doi.org/10.1038/nature08280
115. Sobie EA, Dilly KW, dos Santos CJ et al (2002) Termination of cardiac Ca^{2+} sparks: an investigative mathematical model of calcium-induced calcium release. Biophys J 83(1):59–78
116. Brochet DX, Yang D, Di Maio A et al (2005) Ca^{2+} blinks: rapid nanoscopic store calcium signaling. Proc Natl Acad Sci USA 102(8):3099–3104. https://doi.org/10.1073/pnas.0500059102
117. Suzuki J, Kanemaru K, Ishii K et al (2014) Imaging intraorganellar Ca^{2+} at subcellular resolution using CEPIA. Nat Commun 5:4153. https://doi.org/10.1038/ncomms5153

118. Mogami H, Nakano K, Tepikin AV et al (1997) Ca^{2+} flow via tunnels in polarized cells: recharging of apical Ca^{2+} stores by focal Ca^{2+} entry through basal membrane patch. Cell 88 (1):49–55
119. Thorn P, Lawrie AM, Smith PM et al (1993) Local and global cytosolic Ca^{2+} oscillations in exocrine cells evoked by agonists and inositol trisphosphate. Cell 74(4):661–668
120. de Juan-Sanz J, Holt GT, Schreiter ER et al (2017) Axonal endoplasmic reticulum Ca^{2+} content controls release probability in CNS nerve terminals. Neuron 93(4):867–881 e866. https://doi.org/10.1016/j.neuron.2017.01.010
121. Lissandron V, Podini P, Pizzo P et al (2010) Unique characteristics of Ca^{2+} homeostasis of the trans-Golgi compartment. Proc Natl Acad Sci USA 107(20):9198–9203. https://doi.org/10.1073/pnas.1004702107
122. Wong AK, Capitanio P, Lissandron V et al (2013) Heterogeneity of Ca^{2+} handling among and within Golgi compartments. J Mol Cell Biol 5(4):266–276. https://doi.org/10.1093/jmcb/mjt024
123. Filippin L, Magalhães PJ, Di Benedetto G et al (2003) Stable interactions between mitochondria and endoplasmic reticulum allow rapid accumulation of calcium in a subpopulation of mitochondria. J Biol Chem 278:39224–39234
124. Montero M, Alonso MT, Carnicero E et al (2000) Chromaffin-cell stimulation triggers fast millimolar mitochondrial Ca^{2+} transients that modulate secretion. Nat Cell Biol 2(2):57–61
125. Szabadkai G, Simoni AM, Chami M et al (2004) Drp-1-dependent division of the mitochondrial network blocks intraorganellar Ca^{2+} waves and protects against Ca^{2+}-mediated apoptosis. Mol Cell 16(1):59–68
126. Lefkimmiatis K, Zaccolo M (2014) cAMP signaling in subcellular compartments. Pharmacol Ther 143(3):295–304. https://doi.org/10.1016/j.pharmthera.2014.03.008
127. Hayes JS, Brunton LL, Mayer SE (1980) Selective activation of particulate cAMP-dependent protein kinase by isoproterenol and prostaglandin E1. J Biol Chem 255(11):5113–5119
128. Buxton IL, Brunton LL (1983) Compartments of cyclic AMP and protein kinase in mammalian cardiomyocytes. J Biol Chem 258(17):10233–10239
129. Jurevicius J, Fischmeister R (1996) cAMP compartmentation is responsible for a local activation of cardiac Ca^{2+} channels by beta-adrenergic agonists. Proc Natl Acad Sci USA 93:295–299
130. Rich TC, Fagan KA, Nakata H et al (2000) Cyclic nucleotide-gated channels colocalize with adenylyl cyclase in regions of restricted cAMP diffusion. J Gen Physiol 116(2):147–161
131. Zaccolo M, Pozzan T (2002) Discrete microdomains with high concentration of cAMP in stimulated rat neonatal cardiac myocytes. Science 295(5560):1711–1715
132. Nikolaev VO, Bunemann M, Schmitteckert E et al (2006) Cyclic AMP imaging in adult cardiac myocytes reveals far-reaching beta1-adrenergic but locally confined beta2-adrenergic receptor-mediated signaling. Circ Res 99(10):1084–1091. https://doi.org/10.1161/01.RES.0000250046.69918.d5
133. Di Benedetto G, Zoccarato A, Lissandron V et al (2008) Protein kinase A type I and type II define distinct intracellular signaling compartments. Circ Res 103(8):836–844
134. Jiang JY, Falcone JL, Curci S et al (2017) Interrogating cyclic AMP signaling using optical approaches. Cell Calcium 64:47–56. https://doi.org/10.1016/j.ceca.2017.02.010
135. Dworkin M, Keller KH (1977) Solubility and diffusion coefficient of adenosine 3′:5′-monophosphate. J Biol Chem 252(3):864–865
136. Nikolaev VO, Gambaryan S, Engelhardt S et al (2005) Real-time monitoring of the PDE2 activity of live cells: hormone-stimulated cAMP hydrolysis is faster than hormone-stimulated cAMP synthesis. J Biol Chem 280(3):1716–1719. https://doi.org/10.1074/jbc.C400505200
137. Saucerman JJ, Greenwald EC, Polanowska-Grabowska R (2014) Mechanisms of cyclic AMP compartmentation revealed by computational models. J Gen Physiol 143(1):39–48. https://doi.org/10.1085/jgp.201311044

138. Houslay MD (2010) Underpinning compartmentalised cAMP signalling through targeted cAMP breakdown. Trends Biochem Sci 35(2):91–100. https://doi.org/10.1016/j.tibs.2009.09.007
139. Richards M, Lomas O, Jalink K et al (2016) Intracellular tortuosity underlies slow cAMP diffusion in adult ventricular myocytes. Cardiovasc Res 110(3):395–407. https://doi.org/10.1093/cvr/cvw080
140. Agarwal SR, Clancy CE, Harvey RD (2016) Mechanisms restricting diffusion of intracellular cAMP. Sci Rep 6:19577. https://doi.org/10.1038/srep19577
141. Lohse C, Bock A, Maiellaro I et al (2017) Experimental and mathematical analysis of cAMP nanodomains. PLoS One 12(4):e0174856. https://doi.org/10.1371/journal.pone.0174856 PONE-D-16-39245
142. Yang PC, Boras BW, Jeng MT et al (2016) A computational modeling and simulation approach to investigate mechanisms of subcellular cAMP compartmentation. PLoS Comput Biol 12(7):e1005005. https://doi.org/10.1371/journal.pcbi.1005005 PCOMPBIOL-D-16-00287
143. Calebiro D, Maiellaro I (2014) cAMP signaling microdomains and their observation by optical methods. Front Cell Neurosci 8:350. https://doi.org/10.3389/fncel.2014.00350
144. Matulef K, Zagotta WN (2003) Cyclic nucleotide-gated ion channels. Annu Rev Cell Dev Biol 19:23–44. https://doi.org/10.1146/annurev.cellbio.19.110701.154854
145. Kawasaki H, Springett GM, Mochizuki N et al (1998) A family of cAMP-binding proteins that directly activate Rap1. Science 282(5397):2275–2279
146. Beavo JA, Brunton LL (2002) Cyclic nucleotide research – still expanding after half a century. Nat Rev Mol Cell Biol 3(9):710–718. https://doi.org/10.1038/nrm911
147. Schindler RF, Scotton C, Zhang J et al (2016) POPDC1(S201F) causes muscular dystrophy and arrhythmia by affecting protein trafficking. J Clin Invest 126(1):239–253. https://doi.org/10.1172/JCI79562
148. Schindler RF, Brand T (2016) The Popeye domain containing protein family – a novel class of cAMP effectors with important functions in multiple tissues. Prog Biophys Mol Biol 120(1-3):28–36. https://doi.org/10.1016/j.pbiomolbio.2016.01.001
149. Taylor SS, Zhang P, Steichen JM et al (2013) PKA: lessons learned after twenty years. Biochim Biophys Acta 1834(7):1271–1278. https://doi.org/10.1016/j.bbapap.2013.03.007
150. Langeberg LK, Scott JD (2015) Signalling scaffolds and local organization of cellular behaviour. Nat Rev Mol Cell Biol 16(4):232–244. https://doi.org/10.1038/nrm3966
151. Jarnaess E, Ruppelt A, Stokka AJ et al (2008) Dual specificity A-kinase anchoring proteins (AKAPs) contain an additional binding region that enhances targeting of protein kinase A type I. J Biol Chem 283(48):33708–33718. https://doi.org/10.1074/jbc.M804807200
152. Means CK, Lygren B, Langeberg LK et al (2011) An entirely specific type I A-kinase anchoring protein that can sequester two molecules of protein kinase A at mitochondria. Proc Natl Acad Sci USA 108(48):E1227–E1235. https://doi.org/10.1073/pnas.1107182108
153. Bachmann VA, Mayrhofer JE, Ilouz R et al (2016) Gpr161 anchoring of PKA consolidates GPCR and cAMP signaling. Proc Natl Acad Sci USA 113(28):7786–7791. https://doi.org/10.1073/pnas.1608061113
154. Cooper DM, Crossthwaite AJ (2006) Higher-order organization and regulation of adenylyl cyclases. Trends Pharmacol Sci 27(8):426–431. https://doi.org/10.1016/j.tips.2006.06.002
155. Halls ML, Cooper DM (2017) Adenylyl cyclase signalling complexes – pharmacological challenges and opportunities. Pharmacol Ther 172:171–180. https://doi.org/10.1016/j.pharmthera.2017.01.001
156. Tresguerres M, Levin LR, Buck J (2011) Intracellular cAMP signaling by soluble adenylyl cyclase. Kidney Int 79(12):1277–1288. https://doi.org/10.1038/ki.2011.95
157. Dessauer CW (2009) Adenylyl cyclase – A-kinase anchoring protein complexes: the next dimension in cAMP signaling. Mol Pharmacol 76(5):935–941. https://doi.org/10.1124/mol.109.059345

158. Lu Y, Allen M, Halt AR et al (2007) Age-dependent requirement of AKAP150-anchored PKA and GluR2-lacking AMPA receptors in LTP. EMBO J 26(23):4879–4890. https://doi.org/10.1038/sj.emboj.7601884
159. Lu Y, Zhang M, Lim IA et al (2008) AKAP150-anchored PKA activity is important for LTD during its induction phase. J Physiol 586(17):4155–4164. https://doi.org/10.1113/jphysiol.2008.151662
160. Tunquist BJ, Hoshi N, Guire ES et al (2008) Loss of AKAP150 perturbs distinct neuronal processes in mice. Proc Natl Acad Sci USA 105(34):12557–12562. https://doi.org/10.1073/pnas.0805922105
161. Dorsam RT, Gutkind JS (2007) G-protein-coupled receptors and cancer. Nat Rev Cancer 7 (2):79–94. https://doi.org/10.1038/nrc2069
162. Nikolaev VO, Moshkov A, Lyon AR et al (2010) b2-adrenergic receptor redistribution in heart failure changes cAMP compartmentation. Science 327(5973):1653–1657. https://doi.org/10.1126/science.1185988
163. Calebiro D, Nikolaev VO, Gagliani MC et al (2009) Persistent cAMP-signals triggered by internalized G-protein-coupled receptors. PLoS Biol 7(8):e1000172. https://doi.org/10.1371/journal.pbio.1000172
164. Irannejad R, Tomshine JC, Tomshine JR et al (2013) Conformational biosensors reveal GPCR signalling from endosomes. Nature 495(7442):534–538. https://doi.org/10.1038/nature12000
165. Irannejad R, von Zastrow M (2014) GPCR signaling along the endocytic pathway. Curr Opin Cell Biol 27:109–116. https://doi.org/10.1016/j.ceb.2013.10.003
166. Tsvetanova NG, Trester-Zedlitz M, Newton BW et al (2017) G protein-coupled receptor endocytosis confers uniformity in responses to chemically distinct ligands. Mol Pharmacol 91(2):145–156. https://doi.org/10.1124/mol.116.106369
167. Tsvetanova NG, von Zastrow M (2014) Spatial encoding of cyclic AMP signaling specificity by GPCR endocytosis. Nat Chem Biol 10(12):1061–1065. https://doi.org/10.1038/nchembio.1665
168. Kamal FA, Travers JG, Blaxall BC (2012) G protein-coupled receptor kinases in cardiovascular disease: why "where" matters. Trends Cardiovasc Med 22(8):213–219. https://doi.org/10.1016/j.tcm.2012.07.023
169. Zippin JH, Chen Y, Straub SG et al (2013) CO2/HCO3(−)- and calcium-regulated soluble adenylyl cyclase as a physiological ATP sensor. J Biol Chem 288(46):33283–33291. https://doi.org/10.1074/jbc.M113.510073
170. Zippin JH, Chen Y, Nahirney P et al (2003) Compartmentalization of bicarbonate-sensitive adenylyl cyclase in distinct signaling microdomains. FASEB J 17(1):82–84. https://doi.org/10.1096/fj.02-0598fje
171. Omori K, Kotera J (2007) Overview of PDEs and their regulation. Circ Res 100(3):309–327. https://doi.org/10.1161/01.RES.0000256354.95791.f1
172. Kokkonen K, Kass DA (2017) Nanodomain regulation of cardiac cyclic nucleotide signaling by phosphodiesterases. Annu Rev Pharmacol Toxicol 57:455–479. https://doi.org/10.1146/annurev-pharmtox-010716-104756
173. Hofer AM, Lefkimmiatis K (2007) Extracellular calcium and cAMP: second messengers as "third messengers"? Physiology (Bethesda) 22:320–327. https://doi.org/10.1152/physiol.00019.2007
174. Hohl CM, Li QA (1991) Compartmentation of cAMP in adult canine ventricular myocytes. Relation to single-cell free Ca^{2+} transients. Circ Res 69(5):1369–1379
175. Zaccolo M, De Giorgi F, Cho CY et al (2000) A genetically encoded, fluorescent indicator for cyclic AMP in living cells. Nat Cell Biol 2:25–29
176. Mongillo M, McSorley T, Evellin S et al (2004) Fluorescence resonance energy transfer-based analysis of cAMP dynamics in live neonatal rat cardiac myocytes reveals distinct functions of compartmentalized phosphodiesterases. Circ Res 95(1):67–75. https://doi.org/10.1161/01.RES.0000134629.84732.11

177. Terrin A, Di Benedetto G, Pertegato V et al (2006) PGE(1) stimulation of HEK293 cells generates multiple contiguous domains with different [cAMP]: role of compartmentalized phosphodiesterases. J Cell Biol 175(3):441–451
178. Acin-Perez R, Salazar E, Kamenetsky M et al (2009) Cyclic AMP produced inside mitochondria regulates oxidative phosphorylation. Cell Metab 9(3):265–276
179. Hunter T (1995) Protein kinases and phosphatases: the yin and yang of protein phosphorylation and signaling. Cell 80(2):225–236
180. Lefkimmiatis K, Leronni D, Hofer AM (2013) The inner and outer compartments of mitochondria are sites of distinct cAMP/PKA signaling dynamics. J Cell Biol 202(3):453–462. https://doi.org/10.1083/jcb.201303159
181. Chen C, Nakamura T, Koutalos Y (1999) Cyclic AMP diffusion coefficient in frog olfactory cilia. Biophys J 76(5):2861–2867. https://doi.org/10.1016/S0006-3495(99)77440-0
182. Feinstein WP, Zhu B, Leavesley SJ et al (2012) Assessment of cellular mechanisms contributing to cAMP compartmentalization in pulmonary microvascular endothelial cells. Am J Physiol Cell Physiol 302(6):C839–C852. https://doi.org/10.1152/ajpcell.00361.2011
183. Roeder T (1999) Octopamine in invertebrates. Prog Neurobiol 59(5):533–561
184. Maiellaro I, Lohse MJ, Kittel RJ et al (2016) cAMP signals in drosophila motor neurons are confined to single synaptic boutons. Cell Rep 17(5):1238–1246. https://doi.org/10.1016/j.celrep.2016.09.090
185. Di Benedetto G, Scalzotto E, Mongillo M et al (2013) Mitochondrial Ca^{2+} uptake induces cyclic AMP generation in the matrix and modulates organelle ATP levels. Cell Metab 17(6):965–975. https://doi.org/10.1016/j.cmet.2013.05.003
186. Lefkimmiatis K (2014) cAMP signalling meets mitochondrial compartments. Biochem Soc Trans 42(2):265–269. https://doi.org/10.1042/BST20130281
187. Acin-Perez R, Russwurm M, Gunnewig K et al (2011) A phosphodiesterase 2A isoform localized to mitochondria regulates respiration. J Biol Chem 286(35):30423–30432
188. Cheung WY (1970) Cyclic 3′,5′-nucleotide phosphodiesterase. Demonstration of an activator. Biochem Biophys Res Commun 38(3):533–538
189. Kakiuchi S, Yamazaki R (1970) Calcium dependent phosphodiesterase activity and its activating factor (PAF) from brain studies on cyclic 3′,5′-nucleotide phosphodiesterase (3). Biochem Biophys Res Commun 41(5):1104–1110
190. Mons N, Decorte L, Jaffard R et al (1998) Ca^{2+}-sensitive adenylyl cyclases, key integrators of cellular signalling. Life Sci 62(17-18):1647–1652
191. Willoughby D, Everett KL, Halls ML et al (2012) Direct binding between Orai1 and AC8 mediates dynamic interplay between Ca^{2+} and cAMP signaling. Sci Signal 5(219):ra29. https://doi.org/10.1126/scisignal.2002299
192. Martin AC, Willoughby D, Ciruela A et al (2009) Capacitative Ca^{2+} entry via Orai1 and stromal interacting molecule 1 (STIM1) regulates adenylyl cyclase type 8. Mol Pharmacol 75(4):830–842. https://doi.org/10.1124/mol.108.051748
193. Efendiev R, Dessauer CW (2011) A kinase-anchoring proteins and adenylyl cyclase in cardiovascular physiology and pathology. J Cardiovasc Pharmacol 58(4):339–344. https://doi.org/10.1097/FJC.0b013e31821bc3f000005344-201110000-00002
194. Lefkimmiatis K, Srikanthan M, Maiellaro I et al (2009) Store-operated cyclic AMP signalling mediated by STIM1. Nat Cell Biol 11(4):433–442. https://doi.org/10.1038/ncb1850
195. Maiellaro I, Lefkimmiatis K, Moyer MP et al (2012) Termination and activation of store-operated cyclic AMP production. J Cell Mol Med 16(11):2715–2725. https://doi.org/10.1111/j.1582-4934.2012.01592.x
196. Spirli C, Locatelli L, Fiorotto R et al (2012) Altered store operated calcium entry increases cyclic 3′,5′-adenosine monophosphate production and extracellular signal-regulated kinases 1 and 2 phosphorylation in polycystin-2-defective cholangiocytes. Hepatology 55(3):856–868. https://doi.org/10.1002/hep.24723
197. Di Benedetto G, Pendin D, Greotti E et al (2014) Ca^{2+} and cAMP cross-talk in mitochondria. J Physiol 592(Pt 2):305–312. https://doi.org/10.1113/jphysiol.2013.259135

198. Katona D, Rajki A, Di Benedetto G et al (2015) Calcium-dependent mitochondrial cAMP production enhances aldosterone secretion. Mol Cell Endocrinol 412:196–204. https://doi.org/10.1016/j.mce.2015.05.002
199. Jeon KI, Jono H, Miller CL et al (2010) Ca^{2+}/calmodulin-stimulated PDE1 regulates the beta-catenin/TCF signaling through PP2A B56 gamma subunit in proliferating vascular smooth muscle cells. FEBS J 277(24):5026–5039. https://doi.org/10.1111/j.1742-4658.2010.07908.x
200. Goraya TA, Masada N, Ciruela A et al (2004) Sustained entry of Ca^{2+} is required to activate Ca^{2+}-calmodulin-dependent phosphodiesterase 1A. J Biol Chem 279(39):40494–40504. https://doi.org/10.1074/jbc.M313441200
201. Wagner LE 2nd, Joseph SK, Yule DI (2008) Regulation of single inositol 1,4,5-trisphosphate receptor channel activity by protein kinase A phosphorylation. J Physiol 586(15):3577–3596. https://doi.org/10.1113/jphysiol.2008.152314
202. Betzenhauser MJ, Fike JL, Wagner LE 2nd et al (2009) Protein kinase A increases type-2 inositol 1,4,5-trisphosphate receptor activity by phosphorylation of serine 937. J Biol Chem 284(37):25116–25125. https://doi.org/10.1074/jbc.M109.010132
203. Lanner JT, Georgiou DK, Joshi AD et al (2010) Ryanodine receptors: structure, expression, molecular details, and function in calcium release. Cold Spring Harb Perspect Biol 2(11): a003996
204. Marks AR (2013) Calcium cycling proteins and heart failure: mechanisms and therapeutics. J Clin Invest 123(1):46–52. https://doi.org/10.1172/JCI62834
205. Kamp TJ, Hell JW (2000) Regulation of cardiac L-type calcium channels by protein kinase A and protein kinase C. Circ Res 87(12):1095–1102
206. Haase H, Karczewski P, Beckert R et al (1993) Phosphorylation of the L-type calcium channel beta subunit is involved in beta-adrenergic signal transduction in canine myocardium. FEBS Lett 335(2):217–222
207. Cerra MC, Imbrogno S (2012) Phospholamban and cardiac function: a comparative perspective in vertebrates. Acta Physiol (Oxf) 205(1):9–25. https://doi.org/10.1111/j.1748-1716.2012.02389.x
208. Wei SK, Ruknudin A, Hanlon SU et al (2003) Protein kinase A hyperphosphorylation increases basal current but decreases beta-adrenergic responsiveness of the sarcolemmal Na+-Ca^{2+} exchanger in failing pig myocytes. Circ Res 92(8):897–903. https://doi.org/10.1161/01.RES.0000069701.19660.1401.RES.0000069701.19660.14
209. Wanichawan P, Louch WE, Hortemo KH et al (2011) Full-length cardiac Na^{+}/Ca^{2+} exchanger 1 protein is not phosphorylated by protein kinase A. Am J Physiol Cell Physiol 300(5):C989–C997. https://doi.org/10.1152/ajpcell.00196.2010
210. Guerini D, Pan B, Carafoli E (2003) Expression, purification, and characterization of isoform 1 of the plasma membrane Ca^{2+} pump: focus on calpain sensitivity. J Biol Chem 278 (40):38141–38148. https://doi.org/10.1074/jbc.M302400200
211. Bruce JI, Yule DI, Shuttleworth TJ (2002) Ca^{2+}-dependent protein kinase--a modulation of the plasma membrane Ca^{2+}-ATPase in parotid acinar cells. J Biol Chem 277(50):48172–48181. https://doi.org/10.1074/jbc.M208393200
212. Palty R, Silverman WF, Hershfinkel M et al (2010) NCLX is an essential component of mitochondrial Na+/Ca^{2+} exchange. Proc Natl Acad Sci USA 107(1):436–441
213. Zimmermann H, Zebisch M, Strater N (2012) Cellular function and molecular structure of ecto-nucleotidases. Purinergic Signal 8(3):437–502. https://doi.org/10.1007/s11302-012-9309-4
214. Verkhratsky A, Burnstock G (2014) Biology of purinergic signalling: its ancient evolutionary roots, its omnipresence and its multiple functional significance. Bioessays 36(7):697–705. https://doi.org/10.1002/bies.201400024
215. Plattner H, Verkhratsky A (2016) Inseparable tandem: evolution chooses ATP and Ca^{2+} to control life, death and cellular signalling. Philos Trans R Soc Lond B Biol Sci 371(1700). https://doi.org/10.1098/rstb.2015.0419

216. Falzoni S, Donvito G, Di Virgilio F (2013) Detecting adenosine triphosphate in the pericellular space. Interface Focus 3(3):20120101. https://doi.org/10.1098/rsfs.2012.0101rsfs20120101
217. Burnstock G, Boeynaems JM (2014) Purinergic signalling and immune cells. Purinergic Signal 10(4):529–564. https://doi.org/10.1007/s11302-014-9427-2
218. Burnstock G, Verkhratsky A (2010) Long-term (trophic) purinergic signalling: purinoceptors control cell proliferation, differentiation and death. Cell Death Dis 1:e9. https://doi.org/10.1038/cddis.2009.11
219. Di Virgilio F, Adinolfi E (2017) Extracellular purines, purinergic receptors and tumor growth. Oncogene 36(3):293–303. https://doi.org/10.1038/onc.2016.206
220. Di Virgilio F, Vuerich M (2015) Purinergic signaling in the immune system. Auton Neurosci 191:117–123. https://doi.org/10.1016/j.autneu.2015.04.011
221. Surprenant A, North RA (2009) Signaling at purinergic P2X receptors. Annu Rev Physiol 71:333–359. https://doi.org/10.1146/annurev.physiol.70.113006.100630
222. Coade SB, Pearson JD (1989) Metabolism of adenine nucleotides in human blood. Circ Res 65 (3):531–537
223. Pellegatti P, Falzoni S, Pinton P et al (2005) A novel recombinant plasma membrane-targeted luciferase reveals a new pathway for ATP secretion. Mol Biol Cell 16(8):3659–3665. https://doi.org/10.1091/mbc.E05-03-0222
224. Corriden R, Insel PA, Junger WG (2007) A novel method using fluorescence microscopy for real-time assessment of ATP release from individual cells. Am J Physiol Cell Physiol 293(4): C1420–C1425. https://doi.org/10.1152/ajpcell.00271.2007
225. Sabirov RZ, Dutta AK, Okada Y (2001) Volume-dependent ATP-conductive large-conductance anion channel as a pathway for swelling-induced ATP release. J Gen Physiol 118(3):251–266
226. Bodin P, Burnstock G (2001) Purinergic signalling: ATP release. Neurochem Res 26 (8-9):959–969
227. Ceriani F, Pozzan T, Mammano F (2016) Critical role of ATP-induced ATP release for Ca^{2+} signaling in nonsensory cell networks of the developing cochlea. Proc Natl Acad Sci USA 113 (46):E7194–E7201. https://doi.org/10.1073/pnas.1616061113
228. Romanello M, Pani B, Bicego M et al (2001) Mechanically induced ATP release from human osteoblastic cells. Biochem Biophys Res Commun 289(5):1275–1281. https://doi.org/10.1006/bbrc.2001.6124S0006-291X(01)96124-8
229. D'Hondt C, Ponsaerts R, De Smedt H et al (2011) Pannexin channels in ATP release and beyond: an unexpected rendezvous at the endoplasmic reticulum. Cell Signal 23(2):305–316
230. Adinolfi E, Callegari MG, Ferrari D et al (2005) Basal activation of the P2X7 ATP receptor elevates mitochondrial calcium and potential, increases cellular ATP levels, and promotes serum-independent growth. Mol Biol Cell 16(7):3260–3272. https://doi.org/10.1091/mbc.E04-11-1025
231. Sauvage V, Aubert D, Escotte-Binet S et al (2009) The role of ATP-binding cassette (ABC) proteins in protozoan parasites. Mol Biochem Parasitol 167(2):81–94. https://doi.org/10.1016/j.molbiopara.2009.05.005
232. Pankratov Y, Lalo U, Verkhratsky A et al (2007) Quantal release of ATP in mouse cortex. J Gen Physiol 129(3):257–265
233. Pankratov Y, Lalo U, Verkhratsky A et al (2006) Vesicular release of ATP at central synapses. Pflugers Arch 452(5):589–597. https://doi.org/10.1007/s00424-006-0061-x
234. Bonora M, Patergnani S, Rimessi A et al (2012) ATP synthesis and storage. Purinergic Signal 8(3):343–357. https://doi.org/10.1007/s11302-012-9305-8
235. Russo MV, McGavern DB (2015) Immune Surveillance of the CNS following Infection and Injury. Trends Immunol 36(10):637–650. https://doi.org/10.1016/j.it.2015.08.002
236. Sheng ZH (2017) The interplay of axonal energy homeostasis and mitochondrial trafficking and anchoring. Trends Cell Biol 27(6):403–416. https://doi.org/10.1016/j.tcb.2017.01.005

237. Beraud N, Pelloux S, Usson Y et al (2009) Mitochondrial dynamics in heart cells: very low amplitude high frequency fluctuations in adult cardiomyocytes and flow motion in non beating Hl-1 cells. J Bioenerg Biomembr 41(2):195–214. https://doi.org/10.1007/s10863-009-9214-x
238. Boncompagni S, Rossi AE, Micaroni M et al (2009) Mitochondria are linked to calcium stores in striated muscle by developmentally regulated tethering structures. Mol Biol Cell 20 (3):1058–1067. https://doi.org/10.1091/mbc.E08-07-0783
239. Franzini-Armstrong C (2007) ER-mitochondria communication. How privileged? Physiology (Bethesda) 22:261–268
240. Kohlhaas M, Maack C (2013) Calcium release microdomains and mitochondria. Cardiovasc Res 98(2):259–268. https://doi.org/10.1093/cvr/cvt032
241. Anmann T, Varikmaa M, Timohhina N et al (2014) Formation of highly organized intracellular structure and energy metabolism in cardiac muscle cells during postnatal development of rat heart. Biochim Biophys Acta 1837(8):1350–1361. https://doi.org/10.1016/j.bbabio.2014.03.015
242. Pasqualini FS, Nesmith AP, Horton RE et al (2016) Mechanotransduction and metabolism in cardiomyocyte microdomains. Biomed Res Int 2016:4081638. https://doi.org/10.1155/2016/4081638
243. Wilding JR, Joubert F, de Araujo C et al (2006) Altered energy transfer from mitochondria to sarcoplasmic reticulum after cytoarchitectural perturbations in mice hearts. J Physiol 575 (Pt 1):191–200. https://doi.org/10.1113/jphysiol.2006.114116
244. Ashcroft FM, Rorsman P (2013) K(ATP) channels and islet hormone secretion: new insights and controversies. Nat Rev Endocrinol 9(11):660–669. https://doi.org/10.1038/nrendo.2013.166
245. Rorsman P, Ramracheya R, Rorsman NJ et al (2014) ATP-regulated potassium channels and voltage-gated calcium channels in pancreatic alpha and beta cells: similar functions but reciprocal effects on secretion. Diabetologia 57(9):1749–1761. https://doi.org/10.1007/s00125-014-3279-8
246. Detimary P, Gilon P, Henquin JC (1998) Interplay between cytoplasmic Ca^{2+} and the ATP/ADP ratio: a feedback control mechanism in mouse pancreatic islets. Biochem J 333 (Pt 2):269–274
247. Rolland JF, Henquin JC, Gilon P (2002) Feedback control of the ATP-sensitive K(+) current by cytosolic Ca(2+) contributes to oscillations of the membrane potential in pancreatic beta-cells. Diabetes 51(2):376–384
248. Tanaka T, Nagashima K, Inagaki N et al (2014) Glucose-stimulated single pancreatic islets sustain increased cytosolic ATP levels during initial Ca^{2+} influx and subsequent Ca^{2+} oscillations. J Biol Chem 289(4):2205–2216. https://doi.org/10.1074/jbc.M113.499111
249. Tarasov AI, Semplici F, Li D et al (2013) Frequency-dependent mitochondrial Ca(2+) accumulation regulates ATP synthesis in pancreatic beta cells. Pflugers Arch 465 (4):543–554. https://doi.org/10.1007/s00424-012-1177-9
250. Tarasov AI, Semplici F, Ravier MA et al (2012) The mitochondrial Ca^{2+} uniporter MCU is essential for glucose-induced ATP increases in pancreatic beta-cells. PLoS One 7(7):e39722. https://doi.org/10.1371/journal.pone.0039722PONE-D-12-06521
251. Frieden M, Arnaudeau S, Castelbou C et al (2005) Subplasmalemmal mitochondria modulate the activity of plasma membrane Ca^{2+}-ATPases. J Biol Chem 280(52):43198–43208. https://doi.org/10.1074/jbc.M510279200
252. Arora KK, Pedersen PL (1988) Functional significance of mitochondrial bound hexokinase in tumor cell metabolism. Evidence for preferential phosphorylation of glucose by intramitochondrially generated ATP. J Biol Chem 263(33):17422–17428
253. Shinohara Y, Sagawa I, Ichihara J et al (1997) Source of ATP for hexokinase-catalyzed glucose phosphorylation in tumor cells: dependence on the rate of oxidative phosphorylation relative to that of extramitochondrial ATP generation. Biochim Biophys Acta 1319 (2–3):319–330

254. Cesar Mde C, Wilson JE (1998) Further studies on the coupling of mitochondrially bound hexokinase to intramitochondrially compartmented ATP, generated by oxidative phosphorylation. Arch Biochem Biophys 350(1):109–117
255. Wilson JE (2003) Isozymes of mammalian hexokinase: structure, subcellular localization and metabolic function. J Exp Biol 206(Pt 12):2049–2057
256. Toyama EQ, Herzig S, Courchet J et al (2016) Metabolism. AMP-activated protein kinase mediates mitochondrial fission in response to energy stress. Science 351(6270):275–281. https://doi.org/10.1126/science.aab4138
257. Aronsen JM, Swift F, Sejersted OM (2013) Cardiac sodium transport and excitation-contraction coupling. J Mol Cell Cardiol 61:11–19. https://doi.org/10.1016/j.yjmcc.2013.06.003
258. Allbritton NL, Meyer T, Stryer L (1992) Range of messenger action of calcium ion and inositol 1,4,5-trisphosphate. Science 258(5089):1812–1815
259. Suzuki KG, Fujiwara TK, Edidin M et al (2007) Dynamic recruitment of phospholipase C gamma at transiently immobilized GPI-anchored receptor clusters induces IP3-Ca^{2+} signaling: single-molecule tracking study 2. J Cell Biol 177(4):731–742. https://doi.org/10.1083/jcb.200609175
260. Dickinson GD, Ellefsen KL, Dawson SP et al (2016) Hindered cytoplasmic diffusion of inositol trisphosphate restricts its cellular range of action. Sci Signal 9(453):ra108. https://doi.org/10.1126/scisignal.aag1625
261. Decrock E, De Bock M, Wang N et al (2013) IP3, a small molecule with a powerful message. Biochim Biophys Acta 1833(7):1772–1786. https://doi.org/10.1016/j.bbamcr.2012.12.016
262. Hernandez VH, Bortolozzi M, Pertegato V et al (2007) Unitary permeability of gap junction channels to second messengers measured by FRET microscopy. Nat Methods 4(4):353–358. https://doi.org/10.1038/nmeth1031
263. Sneyd J, Wilkins M, Strahonja A et al (1998) Calcium waves and oscillations driven by an intercellular gradient of inositol (1,4,5)-trisphosphate. Biophys Chem 72(1–2):101–109

Chapter 13
Mitochondrial VDAC, the Na^+/Ca^{2+} Exchanger, and the Ca^{2+} Uniporter in Ca^{2+} Dynamics and Signaling

Varda Shoshan-Barmatz and Soumasree De

Abstract Mitochondrial Ca^{2+} uptake and release play pivotal roles in cellular physiology by regulating intracellular Ca^{2+} signaling, energy metabolism, and cell death. Ca^{2+} transport across the inner and outer mitochondrial membranes (IMM, OMM, respectively), is mediated by several proteins, including the voltage-dependent anion channel 1 (VDAC1) in the OMM, and the mitochondrial Ca^{2+} uniporter (MCU) and Na^+-dependent mitochondrial Ca^{2+} efflux transporter, (the NCLX), both in the IMM. By transporting Ca^{2+} across the OMM to the mitochondrial inner-membrane space (IMS), VDAC1 allows Ca^{2+} access to the MCU, facilitating transport of Ca^{2+} to the matrix, and also from the IMS to the cytosol. Intra-mitochondrial Ca^{2+} controls energy production and metabolism by modulating critical enzymes in the tricarboxylic acid (TCA) cycle and fatty acid oxidation. Thus, by transporting Ca^{2+}, VDAC1 plays a fundamental role in regulating mitochondrial Ca^{2+} homeostasis, oxidative phosphorylation, and Ca^{2+} crosstalk among mitochondria, cytoplasm, and the endoplasmic reticulum (ER). VDAC1 has also been recognized as a key protein in mitochondria-mediated apoptosis, and apoptosis stimuli induce overexpression of the protein in a Ca^{2+}-dependent manner. The overexpressed VDAC1 undergoes oligomerization leading to the formation of a channel, through which apoptogenic agents can be released. Here, we review the roles of VDAC1 in mitochondrial Ca^{2+} homeostasis, in apoptosis, and in diseases associated with mitochondria dysfunction.

Keywords VDAC · Mitochondria · Ca^{2+} transport · MCU · NCLX · Ca^{2+} homeostasis · ER-mitochondria crosstalk

V. Shoshan-Barmatz (✉) · S. De
Department of Life Sciences and the National Institute for Biotechnology in the Negev, Ben-Gurion University of the Negev, Beer-Sheva, Israel
e-mail: vardasb@bgu.ac.il

J. Krebs (ed.), *Membrane Dynamics and Calcium Signaling*, Advances in Experimental Medicine and Biology 981,
https://doi.org/10.1007/978-3-319-55858-5_13

13.1 Overview

The intracellular Ca^{2+} concentration ($[Ca^{2+}]i$) serves as a ubiquitous signaling mechanism, which is then integrated with other signal-transduction cascades to control a variety of cellular processes. These include muscle contraction, neuronal processing and transmission, gene expression, proliferation, and apoptosis [1]. Tight regulation of $[Ca^{2+}]i$ is essential, since dysregulation of Ca^{2+} fluxes may lead to a Ca^{2+} overload and cytotoxicity and is associated with several human disorders [2–4]. This is accomplished by a variety of Ca^{2+} transport systems, located in the plasma membrane, in intracellular organelles such as mitochondria and the ER, as well as in other membrane compartments. Within a given compartment Ca^{2+} may be buffered by binding to proteins and other molecules or may exist in a free form, distributed differentially across compartments [5].

13.2 Mitochondria and Ca^{2+} Dynamics

Mitochondria serve as a major hub of cellular Ca^{2+} homeostasis, able to sequester large, sudden increases in $[Ca^{2+}]i$, by using the membrane potential gradient ($\Delta\Psi$) across the IMM [6]. Mitochondrial Ca^{2+} is a fundamental requirement for a wide range of cellular activities, such as the control of oxidative phosphorylation [7, 8], modulation of cytosolic Ca^{2+}signals [9, 10], cell death [11], secretion [12, 13], and the production of reactive oxygen species (ROS) [14].

Mitochondrial Ca^{2+} transporters in the OMM and IMM transport Ca^{2+} to the IMS and the matrix, respectively [4]. The mitochondrial matrix is one of the stores or buffers, used by the cell to control Ca^{2+} concentration and dynamics. In mammalian heart cells, the mitochondria represent about one third of the total cell volume, which allows them to contribute to Ca^{2+} buffering [15]. Within the mitochondrial matrix Ca^{2+} is precipitated as an insoluble salt, $CaPO_4$, which exists in equilibrium with the free, readily available $[Ca^{2+}]i$ [16, 17].

13.3 Ca^{2+} Transporters in the Mitochondria

Mitochondrial Ca^{2+} is regulated via a number of transporters. While the movement of Ca^{2+} across the IMM is mediated via several proteins, including the MCU [18, 19], and the Na^+/Ca^{2+} exchanger NCLX [20, 21], in the OMM, it is VDAC1 that is responsible for Ca^{2+} transport [22–25].

13.3.1 VDAC1: The Ca^{2+} Transporter in the OMM

13.3.1.1 VDAC1 Structure, Channel Conductance, Properties, and Regulation

Three different VDAC isoforms, VDAC1, VDAC2, and VDAC3 have been identified. While these molecules share several structural and functional properties, they appear to assume different physiological roles [26–28]. While limited information is available regarding the functions of VDAC2 and VDAC3 [26, 29, 30], VDAC1 is highly expressed in most cells [31–33], and as the most prevalent and best studied isoform is the focus of this review.

VDAC1 has been purified from mitochondria isolated from liver, brain, and other tissues [34]. Channel activity analyzed following reconstitution of the purified protein into a planar lipid bilayer (PLB), showed a symmetrical bell-shaped voltage-dependent conductance with a maximum (4 nS at 1 M KCl) at −20 to +20 mV and decreased at higher negative and positive potentials [28, 35]. VDAC1 is permeable to small ions (e.g. Cl^-, K^+, Na^+), to large anions, such as glutamate [35] and ATP [36], and to large cations, such as acetylcholine, dopamine [35], where the ionic selectivity is voltage dependent [35, 37, 38].

The structure of VDAC1 comprises 19 transmembrane β-strands connected by flexible loops to form a β-barrel, and a 26-residue-long N-terminal region that usually lies inside the pore, but can translocate outwards [31, 39, 40] (Fig. 13.1). This N-terminal region mobility is important for channel gating, interaction with the anti-apoptotic proteins, Bax, Bcl2, and Bcl-xL [41–45], as well as association with hexokinase (HK) [41, 46], and VDAC1 dimer formation [45].

VDAC1 is able to form oligomers, specifically dimers to hexamers, and higher-order moieties [47–56]. Following induction of apoptosis, monomeric or dimeric

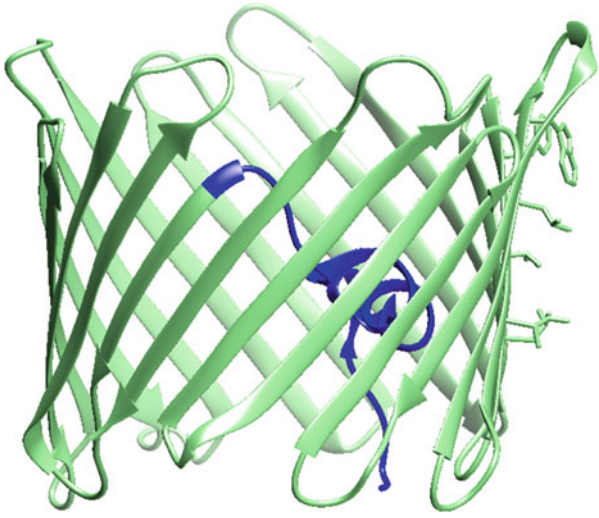

Fig. 13.1 Proposed three-dimensional structure of VDAC1. The X-ray crystal structure of VDAC1 in a ribbon representation is shown. The β-barrel is formed by19 β-strands and the N-terminal helix (colored blue) is folded into the pore interior. (PDB code: 3EMN)

VDAC1 undergoes conformational changes to assemble into the higher oligomeric states required to facilitate cytochrome c (Cyto *c*) release and subsequent apoptosis [41, 47, 48].

13.3.1.2 VDAC1, a Multifunctional Channel Controlling Cell Metabolism

Located in the OMM, VDAC1 is well positioned to serve as a mitochondrial gatekeeper, controlling the metabolic and energy cross-talk between the mitochondria and the rest of the cell [28, 57, 58]. VDAC1 transports solutes of up to 5 kDa in and out of the mitochondria and mediates the fluxes of ions including Ca^{2+}, nucleotides, and metabolites (pyruvate, malate, succinate, NADH/NAD), hemes, and cholesterol across the OMM [28, 57, 59] (Fig. 13. 2). VDAC1 thus serves as a shuttle for respiratory chain substrates [36, 57]. VDAC1 in the OMM is considered to be a hub protein interacting with over 200 proteins [60] that regulate the integration of mitochondrial functions with other cellular activities. Thus, VDAC1 appears to be a convergence point for a variety of cell survival and death signals, which act through association with ligands and proteins.

13.3.1.3 VDAC1 a Ca^{2+} Channel in the OMM

VDAC1 was shown to control the OMM Ca^{2+} permeability [22–25]. Voltage clamp of bilayer-reconstituted VDAC1 in the presence of $CaCl_2$ concentration gradients across the bilayer demonstrated a well-defined voltage-dependent channel conductance with either NaCl or KCl solution [22, 24] Bilayer-reconstituted VDAC1 showed a higher permeability to Ca^{2+} in the low conductance state [24]. The permeability ratio of VDAC1 for Ca^{2+} over Cl^- (PCa^{2+}/PCl^-) is 0.02–0.38 [22, 24] and both cationic and anionic conductance states are blocked by ruthenium red (RuR) and lanthanides [61, 62]. The Ca^{2+} permeability of VDAC1 reconstituted into liposomes was also demonstrated [22].

There are a number of studies that support the proposed function of VDAC1 in the transport of Ca^{2+} and in cellular Ca^{2+} homeostasis. These showed that over-expression of VDAC1 increased mitochondrial Ca^{2+} concentration in HeLa cells and skeletal myotubes [63], while siRNA against VDAC1 attenuated mitochondrial Ca^{2+} uptake and cell apoptosis as induced by H_2O_2 or ceramide. Interestingly, VDAC2 silencing had the opposite effect [64]. In addition, the interaction of Bcl-xL with VDAC1 or VDAC3, could enhance Ca^{2+} transfer across the OMM and thus the magnitude of Ca^{2+} transfer into the mitochondrial matrix [65]. Several VDAC1-interacting molecules, including 4,4′-diisothiocyanostilbene-2,2′-disulfonic acid (DIDS), 4-acetamido-4′-isothiocyanatostilbene-2,2′-disulfonic acid (SITS), and dinitrostilbene-2,2′-disulfonic acid (DNDS), were shown to inhibit the rise in $[Ca^{2+}]i$ levels associated with apoptosis induction and prevent cell death [62, 66]. In yet another example, 5-aminolevulinic precluded Ca^{2+}-mediated oxidative stress and apoptosis through VDAC1 inhibition [67, 68].

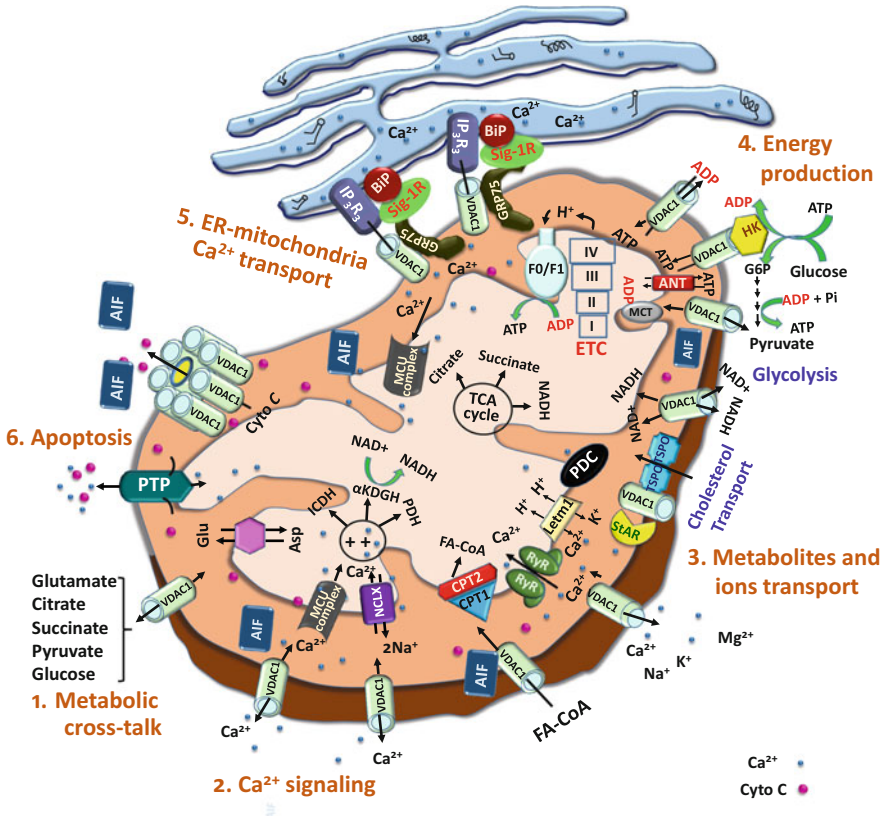

Fig. 13.2 Schematic representation of VDAC1 as a multi-functional protein involved in Ca^{2+} and metabolite transport, energy production and the structural-functional association of mitochondria with the ER. The various functions of VDAC1 in cell and mitochondria functions are presented. These include: **1**. Control of metabolic cross-talk between the mitochondria and the rest of the cell; **2**. As a Ca^{2+} channel transports Ca^{2+} to the IMS and functions in Ca^{2+} signaling by; **3**. Metabolites, cholestrol and ions transport; **4**. Mediating cellular energy production by transporting ATP/ADP and NAD^+/NADH and acyl-CoA from the cytosol to the IMS, and regulating glycolysis via the association with HK; **5**. Involvement in structural and functional association with the ER, mediating Ca^{2+} transport from the ER to mitochondria; **6**. Participation in apoptosis via its oligomerization to form a protein-conducting channel within a VDAC1 homo-oligomer, allowing Cyto *c* release and apoptotic cell death. Ca^{2+} influx and efflux transport systems in the IMM are shown. Ca^{2+} uptake into the matrix is mediated by a Ca^{2+}-selective transporter, the mitochondrial Ca^{2+} uniporter (MCU), regulated by a calcium-sensing accessory subunit (MCU1). Ryanodine receptor (RyR) in the IMM mediates Ca^{2+} influx. Ca^{2+} efflux is mediated by NCLX, a Na^+/Ca^{2+} exchanger. High levels of matrix Ca^{2+} accumulation trigger the opening of the PTP, a fast Ca^{2+} release channel. The function of Ca^{2+} in regulation of energy production is mediated via TCA cycle regulation. This includes activation of pyruvate dehydrogenase (PDH), isocitrate dehydrogenase (ICDH) and α-ketoglutarate dehydrogenase (α KGDH) by intra-mitochondrial Ca^{2+}, leading to enhanced activity of the TCA cycle. The electron transport chain (ETC) and the ATP synthase (F_0F_1) are also presented. VDAC1 mediates the transfer of fatty acid acyl-CoAs across the OMM to the IMS, where they are converted into acylcarnitine by CPT1a for further processing by β-oxidation. Molecular fluxes are indicated by arrows. VDAC1 is involved in cholesterol transport by being

The intracellular concentration of Ca^{2+} can regulate VDAC1 gating by prolonging a fully open state of the channel, thereby promoting metabolite exchange [25]. Evidence that this effect may be mediated by Ca^{2+} binding site(s) in the VDAC1 protein comes from the observations that reagents known to interact with Ca^{2+} binding sites, such as RuR and derivatives, or $La^{3+}$and Tb^{3+}, can inhibit the conductance [62]. Significantly, RuR did not reduce the conductance of E72Q or E202Q mutated VDAC1 [62]. Thus, it has become apparent that VDAC1 both mediates Ca^{2+} transport and is also regulated by Ca^{2+} binding.

13.3.2 Ca^{2+} Transporters and Their Regulation in the IMM

Mitochondrial matrix Ca^{2+} levels are determined by a whole variety of IMM transporters and their associated regulators. These include the MCU [18, 19], mitochondrial calcium uptake one protein (MICU1) [69, 70], MCU regulator 1 (MCUR1) [71] , MICU2 [72], MCUb [73], EMRE [74], the Na^+/Ca^{2+} exchanger (NCLX) [20], SLC25A23 [75], and the permeability transition pore (PTP) [76, 77]. Mitochondrial Ca^{2+} influx is driven by the electrical potential across the IMM ($\Delta\Psi_m$) [68, 78] (Fig. 13.2).

13.3.2.1 MCU and Its Regulatory Proteins

In the IMM, calcium accumulation in the matrix is dependent on the transport of Ca^{2+} from the IMS into the matrix as mediated by a complex composed of the MCU [18, 19], its paralog MCUb [73], MICU1 [70] and MICU2 [72]. The last two of these are both regulated by Ca^{2+} through their EF-hand domains, and the recently identified transmembrane protein EMRE [9, 18, 19, 74, 79, 80]. The MCU consists of two transmembrane and N-terminal domains and forms a complex in the IMM, with several protein regulators, which have an effect on the gating [3, 81, 82]. MICU1, MICU2, and MCUb are most likely negative regulators, while MCUR1, EMRE, and SLC25A23 are essential for MCU activity [69, 72, 74, 75, 83]. MCUR1 however, may have additional functions, such as in cytochrome c oxidase (COX) assembly [80, 82, 84], as a cytosolic Ca^{2+} buffering agent [85], or in ROS generation [86].

Fig. 13.2 (continued) constituent of a multi-protein complex, the transduceosome, containing Star/TSPO/VDAC1. The ER associated with the mitochondria is presented with key proteins indicated. These include the inositol 3 phosphate receptor type 3 (IP3R3), the sigma1 receptor (Sig1R) (a reticular chaperone), binding immunoglobulin protein (BiP), the ER heat shock protein(HSP70 (chaperone and glucose-regulated protein 75 (GRP75). IP3 activates the IP3R in the ER to release Ca^{2+} that is directly transferred to the mitochondrion via VDAC1

The functional role of MCU under physiological conditions was extensively studied using several silencing techniques [84, 87–91]. Interestingly, MCU deletion was found to be embryonic lethal for C57BL/6 mice, whereas knockout mice on an outbred CD1 background were viable, albeit with reduced numbers [92]. Mitochondria derived from MCU−/− mice do not display a capacity to rapidly uptake calcium or calcium-induced PTP opening with no protection against cell death [89]. In cardiac-specific conditional MCU-deficient mice, the heart displayed increased resistance to ischaemia-reperfusion injury [93, 94]. However, unexpectedly, MCU knockout mice did not exhibit obvious defects in any physiological functions [89, 95].

13.3.2.2 Other Ca^{2+} Influx Pathways

The leucine zipper-EF-hand-containing transmembrane protein 1 (*Letm1*), encodes a putative mitochondrial Ca^{2+}/H^+ antiporter that drives the uptake of Ca^{2+} into mitochondria at nanomolar cytosolic Ca^{2+} concentrations [96]. This transport is not affected by RuR [97]. Cellular Letm1 knockdown reduced $Ca^{2+}{}_{mito}$ uptake, $H^+{}_{mito}$ extrusion, impaired mitochondrial ATP generation capacity, disrupted early embryonic development, altered glucose metabolism, and increased susceptibility to seizures [98]. Similarly, silencing of LETM1 impaired basal mitochondrial oxygen consumption, and ATP production, increased ROS production, and promoted AMPK activation, autophagy, and cell cycle arrest [99]. These wide-ranging effects suggest that the LETM1-dependent mitochondrial Ca^{2+} flux is very important in shaping cellular bioenergetics.

Another proposed pathway for Ca^{2+} uptake is the mitochondrial ryanodine receptor (mRyR). The use of [^{3}H]ryanodine binding, immunogold labeling and Western blot techniques, mRyR was identified in the IMM of isolated heart mitochondria where it is thought to mediate ryanodine-sensitive, rapid mitochondrial Ca^{2+} uptake [100]. The mRyR was found to be related to the skeletal muscle type 1 RyR isoform [101] and single mRyR channel activity was recorded following its reconstitution into a PLB [102]. It has been suggested that under certain situations (e.g. mitochondrial Ca^{2+}overload), mRyR channels may also mediate Ca^{2+} efflux [103].

13.3.3 Ca^{2+} Efflux Out of Mitochondria

In order to maintain resting levels of Ca^{2+}, it may be necessary to expel Ca^{2+} from the mitochondria across the IMM, a process mediated by NCLX, a Na^+/Ca^{2+} exchanger and possibly by Letm1, since this protein functions as a Ca^{2+}/H^+ antiporter under certain conditions [96], although it has also been characterized as a H^+/K^+ antiporter.

13.3.3.1 NCLX Mediating Ca^{2+} Efflux

The Na/Ca/Li exchanger (NCLX) is located in the IMM and is the major transporter of mitochondrial matrix Ca^{2+} to the IMS [20, 104–107]. Thus, mitochondrial Ca^{2+} concentration is mainly determined by the balance between influx through the MCU and efflux via NCLX [108]. NCLX is active primarily in excitable cells and in contrast to the plasma membrane Na^+/Ca^{2+} exchanger, it can also transport Li^+ ions [109]. In ischemia, NCLX acts as a key regulator of mitochondrial Ca^{2+} accumulation [110] and in diabetic cardiac myocytes NCLX is more susceptive to the change in the outside (cytosolic) Na^+ concentration compared with controls [111].

Mitochondrial metabolism is likely to be affected by the activity of NCLX because Ca^{2+} activates several enzymes of the Krebs cycle. This association has been demonstrated in endothelial cells where NCLX, was upregulated under conditions of high glucose. In addition, knockdown of NCLX induced ROS generation and increased activation of the PYD domains-containing protein 3 (NLRP3) inflammasome, by mediating the efflux of mitochondrial [Ca^{2+}]. These findings indicate that NCLX may protect against oxidative stress and inflammasome activation in high glucose conditions at an early stage [112].

13.3.3.2 Other Proteins That have been Proposed to Mediate Ca^{2+} Efflux from Mitochondria

The transient opening of the mitochondrial permeability transition pore (MPTP or PTP) represents another mechanism for Ca^{2+} release from mitochondria. PTP is a high-conductance non-specific pore activated by ROS, Ca^{2+} overload, and other agents, leading to mitochondrial swelling and the release of Cyto *c* into the cytosol. Thus, its function in Ca^{2+} efflux is probably a response to a non-physiological Ca^{2+} overload, which would depolarize mitochondria by an irreversible opening of IMM channel, leading to apoptotic and necrotic cell death associated with disease pathogenesis [113, 114]. The exact molecular composition of this pathological channel has not yet been conclusively defined. Initially, PTP was proposed to comprise VDAC1 in the OMM, ANT in the IMM, and cyclophilin D (CypD), a resident of the matrix [113, 115, 116]. Recent studies presented the option that the F0/F1 ATPase is a constituent of the mPTP and other additional candidates have also been suggested (for review see [117]). The concentration of Ca^{2+} directly regulates the opening of the PTP pore to allow rapid Ca^{2+} efflux, and also participates in the integration of downstream processes that may include mitochondrial energetics, ROS production, protein mediated signaling, and the proteolysis of regulatory proteins, that affect its opening [118].

As mentioned above LETM1, not only imports Ca^{2+} through the IMM, but can also extrude Ca^{2+} from the matrix when the mitochondrial Ca^{2+} concentration is high [96].

13.4 Mitochondria Ca^{2+}, VDAC1 and Regulation of Metabolism

Mitochondria play a major role in in the regulation of cellular energetics and metabolism [6]. Ca^{2+} in the mitochondrial matrix controls energy metabolism by enhancing the rate of NADH production via modulating critical enzymes, such as those of the tricarboxylic acid (TCA) cycle and fatty acid oxidation [119, 120], thereby linking glycolysis to the TCA cycle [121]. The Ca^{2+} in the mitochondrial matrix is an essential cofactor for several rate-limiting TCA enzymes including pyruvate dehydrogenase, isocitrate dehydrogenase, and α-ketoglutarate dehydrogenase [4]. Stimulation of such Ca^{2+}-sensitive dehydrogenases in the mitochondrial matrix, increases NADH availability and hence the flow of electrons down the respiratory chain, which enhances a rate-limiting step for rapid ATP synthesis in stimulated cells [122]. An increase in Ca^{2+} also leads to activation of complex V, and the F1F0 ATPase [123]. In addition, Ca^{2+} can also influence the activity of mitochondrial enzymes located on the outer surface of the inner IMM, such as glycerophosphate dehydrogenase, and influence the malate-aspartate shuttle and glutamate/malate dependent respiration through activation of the aspartate-glutamate carriers [124, 125].

A tight link exists between mitochondrial Ca^{2+} transport and the electrochemical potential ($\Delta\Psi m$) across the IMM. Ca^{2+} entry through the MCU is driven by $\Delta\Psi m$ (negative inside) generated by the electron transfer chain. Indeed, Ca^{2+} uptake by mitochondria also depolarizes the $\Delta\Psi m$ to limit ATP production [126]. In the mitochondria of hippocampal neurons, activation of energy metabolism by cytosolic Ca^{2+}, hyperpolarized $\Delta\Psi$ after an initial depolarization caused by increased ATP demand [127]. However, in CD4 immune cells, IL-6 facilitated mitochondrial hyperpolarization accompanied by an increase in mitochondrial Ca^{2+} levels, which is uncoupled from the production of ATP by oxidative phosphorylation, and membrane potential, is sustained late during activation. This effect represents an alternative pathway by which IL-6 regulates the effector function of CD4 cells and contributes to the pathogenesis of inflammatory diseases [128]. In astroglial cells, mitochondrial Ca^{2+} levels and mitochondrial membrane potential mirror the cellular H_2O_2 levels, in a manner that depends on the form and pattern of H_2O_2 stimulation [129].

The observation that intra-mitochondrial Ca^{2+} controls energy metabolism by enhancing the rate of NADH production through modulation of critical enzymes, in the TCA cycle and enzymes responsible for fatty acid oxidation [119], makes VDAC1 Ca^{2+} transport activity, essential for cellular energy production. The importance of VDAC1 in cell energy and metabolism homeostasis is reflected in the findings that closure of VDAC1 [73], or down-regulation of VDAC1 expression decreased metabolite exchange between mitochondria and the cytosol and inhibited cell growth [130, 131]. Thus VDAC1 controls metabolism not only by mediating the transport of metabolites, including pyruvate, malate, succinate, ATP and ADP, and NAD^+/NADH, into and out of mitochondria [28], but also via its Ca^{2+} transport activity.

13.5 Mitochondrial Ca^{2+}, VDAC1 and Regulation of Apoptosis

The induction of apoptosis is associated with a disruption of cell Ca^{2+} homeostasis and energy production [132, 133]. Indeed, many anti-cancer drugs and other cytotoxic agents, such as thapsigargin, staurosporine, As_2O_3, and selenite, induce apoptotic cell death, as well as disrupt cell Ca^{2+} homeostasis [134, 135]. VDAC1, as an important Ca^{2+} transporter can contribute to the mitochondrial Ca^{2+} overload, which is a hallmark of cell apoptosis. There is accumulated evidence to show that a mitochondrial Ca^{2+} overload can induce the release of mitochondrial apoptotic factors into the cytosol probably via activation of PTP and/or perturbation or rupture of the OMM [136]. The observation that pro-apoptotic stimuli reduced mitochondrial Ca^{2+} overload [137], supports the suggestion that the release of the overloaded Ca^{2+} subsequent to PTP opening.

All the three human VDAC isoforms have the same effect on Ca^{2+} influx into mitochondria as assessed by both selective silencing and over-expression of each forms [64]. This is despite the observations that while VDAC1 possesses pro-apoptotic activity [130], and VDAC2 may possess anti-apoptotic activity [27], VDAC3 has no significant effect on apoptosis [64]. Recent studies suggest that apoptotic signals upregulate VDAC1 in a Ca^{2+}-dependent manner, leading to over expression and consequent oligomerization to form a channel through which Cyto *c*- is released, leading to cell death [134, 135]. The results suggests that a common mechanism for a variety of apoptosis-inducing agents may involve an increase in $[Ca^{2+}]i$ and that this in turn leads to an up-regulation of VDAC1 expression [135].

Evidence for the important function of increased levels of VDAC1 in apoptosis induction comes from mouse coronary vascular endothelial cells (MCECs) isolated from diabetic mice where the upregulation of VDAC1 was associated with increased mitochondrial Ca^{2+} concentration, mitochondrial O_2 production, and mPTP opening activity [138]. In contrast, a downregulation of VDAC1 in diabetic MCECs decreased mitochondrial Ca^{2+} concentration and subsequently normalized the levels of mPTP activity and mitochondrial ROS [139].

Further support for the link between increase $[Ca^{2+}]i$ and apoptosis comes from the newly developed VDAC1 inhibitors, AKOS-022 and VBIT-4, which interact directly with VDAC1 to reduce channel conductance and prevent VDAC1 oligomerization, and thereby inhibit the release of Cyto *c* and apoptosis as induced by various means and in various cell lines [140]. The compounds also protect against apoptosis-associated mitochondria dysfunction, restoring dissipated $m\Delta\psi$ and thus cell energy and metabolism, and decreasing ROS production, as well as preventing disruption of intracellular Ca^{2+} levels [140]. In addition, VDAC1-based peptides were shown to have the ability to limit Ca^{2+} uptake into the mitochondrial matrix and inhibit ROS generation in lung cancer cells [141].

A number of proteins have been shown to interact with VDAC1 in a Ca^{2+}-dependent manner and/or affect apoptosis and $[Ca^{2+}]i$ levels. Bcl-XL, a member of an anti-apoptotic Bcl2 family of proteins, interacts with VDAC1 and VDAC3 to

promote mitochondrial Ca^{2+} uptake in response to cellular Ca^{2+} elevation and therefore participates in the Ca^{2+} gating mechanism of VDAC channels [65]. In addition this interaction can promotes cell migration [142].

Gelsolin (Gsn), is a Ca^{2+}-dependent actin-regulatory protein that modulates actin assembly and disassembly [143]. Human (h)Gsn has both pro-apoptotic or anti-apoptotic activity, depending on the cell type [144]. hGsn reduces VDAC1 channel activity and Cyto *c* release from liposomes through direct binding to VDAC1 in a Ca^{2+}-dependent manner [144, 145].

Binding of endothelial NO synthase eNOS to VDAC1 amplified eNOS activity in a Ca^{2+}-mediated manner [146] and EBV (Epstein-Barr virus) infection, one of the causes of nasopharyngeal carcinoma was shown to involve VDAC1 regulation to alter the release of Ca^{2+} and Cyto *c* from the mitochondria [147].

13.6 VDAC1 Function in ER/Mitochondria-Ca^{2+} Cross-Talk

Ca^{2+} flux from ER to mitochondria and its accumulation in the matrix triggers other reactions and regulates several mitochondrial processes, as the activities of several enzymes, to regulation of $[Ca^{2+}]i$ and activation of cell apoptotic pathways [148, 149]. The regulation of Ca^{2+} flow from the ER to the mitochondria is achieved by a combination of a local modulation of Ca^{2+} transport systems, the tightness of the physical association between the ER and mitochondrial membranes [150, 151], and the ER Ca^{2+} load [152]. Several studies point to the existence of a small number of proteins in Mitochondrial Associated Membranes (MAM), which may be important for this process [153–156]. Electron tomography results initially suggested that the strict apposition of ER and mitochondria is mediated by a tethering structure [23]. Later, such tethering was shown to involve a complex between the IP3 receptor in the ER and VDAC1 in the OMM, linked by a chaperone called grp75 [150, 151], together with mitofusin-2, a protein expressed in the ER and on mitochondrial surfaces that forms homodimers or heterodimers with mitofusin-1 [153, 157].

The contact sites between the ER and mitochondria play central roles in cellular homeostasis and processes, including $[Ca^{2+}]i$ signaling [158], lipid synthesis [159], cellular metabolism [121], autophagy [160], the control of ER redox [161], apoptosis progression [162], and mitochondrial fission and recycling processes [153, 163]. ER–mitochondrial Ca^{2+} transfer plays a central role in oncogenesis and in the response of cancer cells to chemotherapy [164].

The dynamics of Ca^{2+} transfer between the ER and mitochondria appear to be modulated by the apoptosis-regulating Bcl-2 family of proteins. ER-to-mitochondrion communication has been shown to be regulated by BH3-only proteins [165, 166] while p53, has been proposed to influence ER-mitochondrion contact site formation and Ca^{2+} transfer at the MAMs [167]. Since both p53 [168] and members of the Bcl2 family of proteins [169, 170] have been shown to interact with

VDAC1, their effects on Ca^{2+} flux at the MAMs may be attributable to such interactions.

13.7 microRNA Mediated Regulation of Mitochondrial Ca^{2+} Transporters and Channels

MicroRNAs (miRNAs), a group of small noncoding RNAs have been characterized as novel regulators of post-transcriptional gene expressions of several cellular processes, including cell proliferation, differentiation, and apoptosis. Recently, a number of miRNAs related to mitochondrial Ca^{2+} channels and transporters, like VDAC and the MCU complex have been identified [171–174].

13.7.1 miRNAs Regulate VDAC1

The miR-29a moiety was identified as able to reduce the expression of VDAC1 [171]. There was a reduction in miR-29a expression in patients and animal models of several neurodegenerative disorders, including Alzheimer's disease (AD), Huntington's disease, and spinocerebellar ataxias [175]. Since miR-29a was also shown to regulate cell survival of astrocytes differentially by targeting VDAC1 [176], these observations suggest that VDAC1 down-regulation by miR-29 is an important aspect of neuronal cell survival in the brain [175]. This in agreement with the finding that high-levels of VDAC1 were demonstrated in AD post-mortem brains and in Amyloid Precursor Protein (APP) transgenic mice [177]. As VDAC1 over-expression triggers apoptosis [178–180], its over-expression in AD may be associated with neuronal cell death.

Another molecule, miR-320a was also reported to down-regulate VDAC1 expression. As a result, the miRNA promoted mitophagy in serum starved cervical cancer cells [172], and ectopic overexpression of miR320a blocked tumor cell proliferation and invasion in non-small cell lung cancer (NSCLC), both in vitro and in vivo [181]. miR-320a was also revealed as a novel therapeutic target for astroglia-mediated HIV-1 neuropathogenesis, as a consequence of the effect of down-regulating VDAC1 [182]. Yet, another miRNA species, miR-7, was shown to be able to inhibit VDAC1 expression and thereby prevent proliferation and metastasis in hepatocellular carcinoma [174], possibly by affecting the PTP [183]. A very recent study demonstrated that the lncRNA-H19/miR-675 axis may regulate high glucose-induced apoptosis by targeting VDAC1, which may provide a novel therapeutic strategy for the treatment of diabetic cardiomyopathy [184]. The therapeutic potential of a number of miRNAs able to regulate VDAC1 expression level is clear in view of the observations that VDAC1 overexpression is associated with a variety of pathological conditions including AD [177, 185, 186], and

cardiovascular diseases [187]. In addition, hyperglycemia has been shown to increase VDAC1 expression in β cells [188] and in the kidney [189].

13.7.2 miRNAs Regulate the MCU Complex

miRNA species may also affect $Ca2^+$ homeostasis by targeting the MCU. Overexpression of miR-25 in HeLa cells drastically reduces MCU levels and mitochondrial Ca^{2+} uptake [173], while, in cardiomyocytes, miR-25-mediates down-regulation of the MCU protected the cells against oxidative damage [190]. Down-regulation of the MCU complex by miR-138 and miR-25 was found to prevent the Pulmonary Arterial Hypertension (PAH) cancer phenotype [191].

The effects of miRNA targeting of VDAC1 or MCU in pathological conditions indicate the importance of these proteins in normal cell and tissue physiology.

13.8 Defects of Other Mitochondrial Proteins in Ca^{2+} Homeostasis and Diseases

The importance of a tight regulation of mitochondrial Ca^{2+} has been noted in several human disorders [2, 4, 173, 192]. Indeed, the role of mitochondrial Ca^{2+} in several diseases is well demonstrated.

13.8.1 Diabetes

Ca^{2+} uptake into mitochondria is important for metabolism-secretion coupling in pancreatic β-cells [193], where it activates glucose-stimulated insulin secretion [194]. Interference with mitochondrial Ca^{2+} uptake have been proposed is thought to contribute to the pathogenesis of type 2 diabetes (T2D) mellitus [195]. Knock-down of MICU1 and MCU reduced mitochondrial Ca^{2+} uptake, ATP production, and D-glucose-stimulated insulin secretion in β-cells [87] and defects in the function of the MAMs in an animal model of T2D (Cisd2 knockout mice) resulted in a deficiency in Ca^{2+} uptake and in insulin insensitivity of adipocytes [196].

13.8.2 Cancer

Malfunctions in several cellular mechanisms, including cell proliferation, mitochondrial metabolism, and cell death are common in cancers, and Ca^{2+} uptake into or

release from the mitochondria are central to all these processes. Hence, the mitochondria are important in inducing pivotal "cancer hallmarks", and mitochondrial Ca^{2+} remodeling plays a pivotal role in providing the required processes for tumorigenesis and survival [197].

13.8.3 Other Diseases

It was recently demonstrated that LETM1 protein expression is significantly decreased in white adipose tissue from HF mice and ob/ob mice compared to relevant control mice [198]. In addition, certain mitochondrial and endoplasmic reticulum homeostasis regulating genes are over-expressed in several hereditary neurodegenerative disorders, like Alzheimer's dementia, ALS and FTD-ALS, Parkinson's disease, Inherited Peripheral Neuropathies, and Hereditary Spastic Paraplegia [2].

In summary, the physiological roles of mitochondrial Ca^{2+} are important in regulating both bioenergetics and cell death. Since the correct level of mitochondrial Ca^{2+} is essential to fine-tune cellular energetics, while mitochondrial overload causes cell death, regulation of the process is critical for normal cell function. This regulation of mitochondrial Ca^{2+} involves transporters such as VDAC1 in the OMM, and MCU and the NCLX in the IMM. The importance of VDAC1 as a key protein in Ca^{2+} transport across the OMM was initially underestimated with the focus placed on the IMM transporters. However, it has recently, become clear that in order for the Ca^{2+} to become accessible to the IMM Ca^{2+} transporters, it must first cross the OMM into the IMS with VDAC1 being the only known Ca^{2+} transporter in the OMM. Dysregulation of Ca^{2+} homeostasis leads to pathophysiology with alterations in mitochondrial Ca^{2+} handling associated with many pathology including cancer and Alzheimer's disease.

References

1. Berridge MJ, Lipp P, Bootman MD (2000) The versatility and universality of calcium signalling. Nat Rev Mol Cell Biol 1(1):11–21
2. Krols M, van Isterdael G, Asselbergh B, Kremer A, Lippens S, Timmerman V, Janssens S (2016) Mitochondria-associated membranes as hubs for neurodegeneration. Acta Neuropathol 131(4):505–523
3. Marchi S, Pinton P (2014) The mitochondrial calcium uniporter complex: molecular components, structure and physiopathological implications. J Physiol 592(5):829–839
4. Rizzuto R, De Stefani D, Raffaello A, Mammucari C (2012) Mitochondria as sensors and regulators of calcium signalling. Nat Rev Mol Cell Biol 13(9):566–578
5. Berridge MJ, Bootman MD, Roderick HL (2003) Calcium signalling: dynamics, homeostasis and remodelling. Nat Rev Mol Cell Biol 4:517–529
6. Glancy B, Balaban RS (2012) Role of mitochondrial Ca2+ in the regulation of cellular energetics. Biochemistry 51(14):2959–2973

7. Cox DA, Matlib MA (1993) A role for the mitochondrial Na(+)-Ca2+ exchanger in the regulation of oxidative phosphorylation in isolated heart mitochondria. J Biol Chem 268 (2):938–947
8. Maack C, Cortassa S, Aon MA, Ganesan AN, Liu T, O'Rourke B (2006) Elevated cytosolic Na+ decreases mitochondrial Ca2+ uptake during excitation-contraction coupling and impairs energetic adaptation in cardiac myocytes. Circ Res 99(2):172–182
9. Gunter TE, Buntinas L, Sparagna G, Eliseev R, Gunter K (2000) Mitochondrial calcium transport: mechanisms and functions. Cell Calcium 28(5-6):285–296
10. Xia HM, Eliason SL, Harper SQ, Martins IH, Orr HT, Paulson HL, Yang L, Kotin RM, Davidson BL (2004) RNAi suppresses polyglutamineinduced neurodegeneration in a model of spinocerebellar ataxia. Nat Med 10:816–820
11. Giacomello M, Drago I, Pizzo P, Pozzan T (2007) Mitochondrial Ca2+ as a key regulator of cell life and death. Cell Death Differ 14(7):1267–1274
12. Maechler P, Kennedy ED, Pozzan T, Wollheim CB (1997) Mitochondrial activation directly triggers the exocytosis of insulin in permeabilized pancreatic beta-cells. EMBO J 16 (13):3833–3841
13. Lee B, Miles PD, Vargas L, Luan P, Glasco S, Kushnareva Y, Kornbrust ES, Grako KA, Wollheim CB, Maechler P, Olefsky JM, Anderson CM (2003) Inhibition of mitochondrial Na+-Ca2+ exchanger increases mitochondrial metabolism and potentiates glucose-stimulated insulin secretion in rat pancreatic islets. Diabetes 52(4):965–973
14. Martinovich GG, Golubeva EN, Martinovich IV, Cherenkevich SN (2012) Redox regulation of calcium signaling in cancer cells by ascorbic acid involving the mitochondrial electron transport chain. J Biophys 2012:1–6
15. Williams GSB, Boyman L, Chikando AC, Khairallah RJ, Lederer WJ (2013) Mitochondrial calcium uptake. Proc Nat Acad Sci 110(26):10479–10486
16. Prins D, Michalak M (2011) Organellar calcium buffers. Cold Spring Harb Perspect Biol 3 (3):1–16
17. Nicholls DG (2005) Mitochondria and calcium signaling. Cell Calcium 38(3–4):311–317
18. Baughman JM, Perocchi F, Girgis HS, Plovanich M, Belcher-Timme CA, Sancak Y, Bao XR, Strittmatter L, Goldberger O, Bogorad RL, Koteliansky V, Mootha VK (2011) Integrative genomics identifies MCU as an essential component of the mitochondrial calcium uniporter. Nature 476(7360):341–345
19. De Stefani D, Raffaello A, Teardo E, Szabo I, Rizzuto R (2011) A forty-kilodalton protein of the inner membrane is the mitochondrial calcium uniporter. Nature 476(7360):336–340
20. Palty R, Silverman WF, Hershfinkel M, Caporale T, Sensi SL, Parnis J, Nolte C, Fishman D, Shoshan-Barmatz V, Herrmann S, Khananshvili D, Sekler I (2010) NCLX is an essential component of mitochondrial Na+/Ca2+ exchange. Proc Natl Acad Sci U S A 107(1):436–441
21. Boyman L, Williams GS, Khananshvili D, Sekler I, Lederer WJ (2013) NCLX: the mitochondrial sodium calcium exchanger. J Mol Cell Cardiol 59:205–213
22. Gincel D, Zaid H, Shoshan-Barmatz V (2001) Calcium binding and translocation by the voltage-dependent anion channel: a possible regulatory mechanism in mitochondrial function. Biochem J 358(Pt 1):147–155
23. Rapizzi E, Pinton P, Szabadkai G, Wieckowski MR, Vandecasteele G, Baird G, Tuft RA, Fogarty KE, Rizzuto R (2002) Recombinant expression of the voltage-dependent anion channel enhances the transfer of Ca2+ microdomains to mitochondria. J Cell Biol 159 (4):613–624
24. Tan W, Colombini M (2007) VDAC closure increases calcium ion flux. Biochim Biophys Acta 1768(10):2510–2515
25. Bathori G, Csordas G, Garcia-Perez C, Davies E, Hajnoczky G (2006) Ca2+-dependent control of the permeability properties of the mitochondrial outer membrane and voltage-dependent anion-selective channel (VDAC). J Biol Chem 281(25):17347–17358

26. De Pinto V, Guarino F, Guarnera A, Messina A, Reina S, Tomasello FM, Palermo V, Mazzoni C (2010) Characterization of human VDAC isoforms: a peculiar function for VDAC3? Biochim Biophys Acta 1797(6-7):1268–1275
27. Cheng EH, Sheiko TV, Fisher JK, Craigen WJ, Korsmeyer SJ (2003) VDAC2 inhibits BAK activation and mitochondrial apoptosis. Science 301(5632):513–517
28. Shoshan-Barmatz V, De Pinto V, Zweckstetter M, Raviv Z, Keinan N, Arbel N (2010) VDAC, a multi-functional mitochondrial protein regulating cell life and death. Mol Asp Med 31 (3):227–285
29. Menzel Viviana A, Cassará MC, Benz R, De Pinto V, Messina A, Cunsolo V, Saletti R, Hinsch K-D, Hinsch E (2009) Molecular and functional characterization of VDAC2 purified from mammal spermatozoa. Biosci Rep 29(6):351–362
30. Xu X, Decker W, Sampson MJ, Craigen WJ, Colombini M (1999) Mouse VDAC isoforms expressed in yeast: channel properties and their roles in mitochondrial outer membrane permeability. J Membr Biol 170(2):89–102
31. Bayrhuber M, Meins T, Habeck M, Becker S, Giller K, Villinger S, Vonrhein C, Griesinger C, Zweckstetter M, Zeth K (2008) Structure of the human voltage-dependent anion channel. Proc Natl Acad Sci U S A 105(40):15370–15375
32. Messina A, Reina S, Guarino F, De Pinto V (2012) VDAC isoforms in mammals. Biochim Biophys Acta 1818(6):1466–1476
33. Shoshan-Barmatz V, Golan M (2012) Mitochondrial VDAC1: function in cell life and death and a target for cancer therapy. Curr Med Chem 19(5):714–735
34. Ben-Hail D, Shoshan-Barmatz V (2014) Purification of VDAC1 from rat liver mitochondria. Cold Spring Harb Protoc 2014(1):94–99
35. Gincel D, Silberberg SD, Shoshan-Barmatz V (2000) Modulation of the voltage-dependent anion channel (VDAC) by glutamate1. J Bioenerg Biomembr 32(6):571–583
36. Rostovtseva T, Colombini M (1997) VDAC channels mediate and gate the flow of ATP: implications for the regulation of mitochondrial function. Biophys J 72(5):1954–1962
37. Colombini M (1980) Structure and mode of action of a voltage dependent anion-selective channel (VDAC) located in the outer mitochondrial membrane. Ann N Y Acad Sci 341:552–563
38. Benz R (1994) Permeation of hydrophilic solutes through mitochondrial outer membranes: review on mitochondrial porins. Biochim Biophys Acta 1197(2):167–196
39. Hiller S, Garces RG, Malia TJ, Orekhov VY, Colombini M, Wagner G (2008) Solution structure of the integral human membrane protein VDAC-1 in detergent micelles. Science 321(5893):1206–1210
40. Ujwal R, Cascio D, Colletier JP, Faham S, Zhang J, Toro L, Ping P, Abramson J (2008) The crystal structure of mouse VDAC1 at 2.3 A resolution reveals mechanistic insights into metabolite gating. Proc Natl Acad Sci U S A 105(46):17742–17747
41. Abu-Hamad S, Arbel N, Calo D, Arzoine L, Israelson A, Keinan N, Ben-Romano R, Friedman O, Shoshan-Barmatz V (2009) The VDAC1 N-terminus is essential both for apoptosis and the protective effect of anti-apoptotic proteins. J Cell Sci 122(Pt 11):1906–1916
42. Shi Y, Chen J, Weng C, Chen R, Zheng Y, Chen Q, Tang H (2003) Identification of the protein-protein contact site and interaction mode of human VDAC1 with Bcl-2 family proteins. Biochem Biophys Res Commun 305(4):989–996
43. Arbel N, Ben-Hail D, Shoshan-Barmatz V (2012) Mediation of the antiapoptotic activity of Bcl-xL protein upon interaction with VDAC1 protein. J Biol Chem 287(27):23152–23161
44. Arbel N, Shoshan-Barmatz V (2010) Voltage-dependent anion channel 1-based peptides interact with Bcl-2 to prevent antiapoptotic activity. J Biol Chem 285(9):6053–6062
45. Geula S, Ben-Hail D, Shoshan-Barmatz V (2012) Structure-based analysis of VDAC1: N-terminus location, translocation, channel gating and association with anti-apoptotic proteins. Biochem J 444(3):475–485

46. Arzoine L, Zilberberg N, Ben-Romano R, Shoshan-Barmatz V (2009) Voltage-dependent anion channel 1-based peptides interact with hexokinase to prevent its anti-apoptotic activity. J Biol Chem 284(6):3946–3955
47. Zalk R, Israelson A, Garty ES, Azoulay-Zohar H, Shoshan-Barmatz V (2005) Oligomeric states of the voltage-dependent anion channel and cytochrome c release from mitochondria. Biochem J 386(Pt 1):73–83
48. Keinan N, Tyomkin D, Shoshan-Barmatz V (2010) Oligomerization of the mitochondrial protein voltage-dependent anion channel is coupled to the induction of apoptosis. Mol Cell Biol 30(24):5698–5709
49. Zeth K, Meins T, Vonrhein C (2008) Approaching the structure of human VDAC1, a key molecule in mitochondrial cross-talk. J Bioenerg Biomembr 40(3):127–132
50. Goncalves RP, Buzhynskyy N, Prima V, Sturgis JN, Scheuring S (2007) Supramolecular assembly of VDAC in native mitochondrial outer membranes. J Mol Biol 369(2):413–418
51. Hoogenboom BW, Suda K, Engel A, Fotiadis D (2007) The supramolecular assemblies of voltage-dependent anion channels in the native membrane. J Mol Biol 370(2):246–255
52. Malia TJ, Wagner G (2007) NMR structural investigation of the mitochondrial outer membrane protein VDAC and its interaction with antiapoptotic Bcl-xL. Biochemistry 46 (2):514–525
53. Shoshan-Barmatz V, Keinan N, Zaid H (2008) Uncovering the role of VDAC in the regulation of cell life and death. J Bioenerg Biomembr 40(3):183–191
54. Azoulay-Zohar H, Israelson A, Abu-Hamad S, Shoshan-Barmatz V (2004) In self-defence: hexokinase promotes voltage-dependent anion channel closure and prevents mitochondria-mediated apoptotic cell death. Biochem J 377(Pt 2):347–355
55. Ujwal R, Cascio D, Chaptal V, Ping P, Abramson J (2009) Crystal packing analysis of murine VDAC1 crystals in a lipidic environment reveals novel insights on oligomerization and orientation. Channels (Austin) 3(3):167–170
56. Raschle T, Hiller S, TY Y, Rice AJ, Walz T, Wagner G (2009) Structural and functional characterization of the integral membrane protein VDAC-1 in lipid bilayer nanodiscs. J Am Chem Soc 131(49):17777–17779
57. Shoshan-Barmatz V, Ben-Hail D (2012) VDAC, a multi-functional mitochondrial protein as a pharmacological target. Mitochondrion 12(1):24–34
58. Shoshan-Barmatz V, Ben-Hail D, Admoni L, Krelin Y, Tripathi SS (2015) The mitochondrial voltage-dependent anion channel 1 in tumor cells. Biochim Biophys Acta 1848(10 Pt B):2547–2575
59. Kholmukhamedov EL, Czerny C, Lovelace G, Beeson KC, Baker T, Johnson CB, Pediaditakis P, Teplova VV, Tikunov A, MacDonald J, Lemasters JJ (2010) The role of the voltage-dependent anion channels in the outer membrane of mitochondria in the regulation of cellular metabolism. Biofizika 55(5):822–833
60. Ko JH, Gu W, Lim I, Zhou T, Bang H (2014) Expression profiling of mitochondrial voltage-dependent anion channel-1 associated genes predicts recurrence-free survival in human carcinomas. PLoS One 9(10):e110094
61. Gincel D, Vardi N, Shoshan-Barmatz V (2002) Retinal voltage-dependent anion channel: characterization and cellular localization. Invest Ophthalmol Vis Sci 43(7):2097–2104
62. Israelson A, Abu-Hamad S, Zaid H, Nahon E, Shoshan-Barmatz V (2007) Localization of the voltage-dependent anion channel-1 Ca2+-binding sites. Cell Calcium 41(3):235–244
63. Madesh M, Hajnoczky G (2001) VDAC-dependent permeabilization of the outer mitochondrial membrane by superoxide induces rapid and massive cytochrome c release. J Cell Biol 155(6):1003–1015
64. De Stefani D, Bononi A, Romagnoli A, Messina A, De Pinto V, Pinton P, Rizzuto R (2012) VDAC1 selectively transfers apoptotic Ca2+ signals to mitochondria. Cell Death Differ 19 (2):267–273

65. Huang H, Hu X, Eno CO, Zhao G, Li C, White C (2013) An interaction between Bcl-xL and the voltage-dependent anion channel (VDAC) promotes mitochondrial Ca2+ uptake. J Biol Chem 288(27):19870–19881
66. Ben-Hail D, Shoshan-Barmatz V (2016) VDAC1-interacting anion transport inhibitors inhibit VDAC1 oligomerization and apoptosis. Biochim Biophys Acta 1863(7 Pt A):1612–1623
67. Chen H, Gao W, Yang Y, Guo S, Wang H, Wang W, Zhang S, Zhou Q, Xu H, Yao J, Tian Z, Li B, Cao W, Zhang Z, Tian Y (2014) Inhibition of VDAC1 prevents Ca(2)(+)-mediated oxidative stress and apoptosis induced by 5-aminolevulinic acid mediated sonodynamic therapy in THP-1 macrophages. Apoptosis 19(12):1712–1726
68. De Stefani D, Rizzuto R, Pozzan T (2016) Enjoy the trip: calcium in mitochondria back and forth. Ann Rev Biochem 85:161–192
69. Mallilankaraman K, Doonan P, Cárdenas C, Chandramoorthy Harish C, Müller M, Miller R, Hoffman Nicholas E, Gandhirajan RK, Molgó J, Birnbaum Morris J, Rothberg Brad S, Mak D-On D, Foskett JK, Madesh M (2012) MICU1 Is an essential gatekeeper for MCU-mediated mitochondrial Ca2+ uptake that regulates cell survival. Cell 151(3):630–644
70. Perocchi F, Gohil VM, Girgis HS, Bao XR, McCombs JE, Palmer AE, Mootha VK (2010) MICU1 encodes a mitochondrial EF hand protein required for Ca(2+) uptake. Nature 467 (7313):291–296
71. Mallilankaraman K, Cardenas C, Doonan PJ, Chandramoorthy HC, Irrinki KM, Golenar T, Csordas G, Madireddi P, Yang J, Muller M, Miller R, Kolesar JE, Molgo J, Kaufman B, Hajnoczky G, Foskett JK, Madesh M (2012) MCUR1 is an essential component of mitochondrial Ca2+ uptake that regulates cellular metabolism. Nat Cell Biol 14(12):1336–1343
72. Plovanich M, Bogorad RL, Sancak Y, Kamer KJ, Strittmatter L, Li AA, Girgis HS, Kuchimanchi S, De Groot J, Speciner L, Taneja N, Oshea J, Koteliansky V, Mootha VK (2013) MICU2, a Paralog of MICU1, resides within the mitochondrial uniporter complex to regulate calcium handling. PLoS ONE 8(2):e55785
73. Raffaello A, De Stefani D, Sabbadin D, Teardo E, Merli G, Picard A, Checchetto V, Moro S, Szabo I, Rizzuto R (2013) The mitochondrial calcium uniporter is a multimer that can include a dominant-negative pore-forming subunit. EMBO J 32(17):2362–2376
74. Sancak Y, Markhard AL, Kitami T, Kovács-Bogdán E, Kamer KJ, Udeshi ND, Carr SA, Chaudhuri D, Clapham DE, Li AA, Calvo SE, Goldberger O, Mootha VK (2013) EMRE is an essential component of the mitochondrial calcium uniporter complex. Science 342 (6164):1379–1382
75. Hoffman NE, Chandramoorthy HC, Shanmughapriya S, Zhang XQ, Vallem S, Doonan PJ, Malliankaraman K, Guo S, Rajan S, Elrod JW, Koch WJ, Cheung JY, Madesh M (2014) SLC25A23 augments mitochondrial Ca2+ uptake, interacts with MCU, and induces oxidative stress–mediated cell death. Mol Biol Cell 25(6):936–947
76. Baines CP, Kaiser RA, Purcell NH, Blair NS, Osinska H, Hambleton MA, Brunskill EW, Sayen MR, Gottlieb RA, Dorn GW, Robbins J, Molkentin JD (2005) Loss of cyclophilin D reveals a critical role for mitochondrial permeability transition in cell death. Nature 434 (7033):658–662
77. Basso E, Fante L, Fowlkes J, Petronilli V, Forte MA, Bernardi P (2005) Properties of the permeability transition pore in mitochondria devoid of Cyclophilin D. J Biol Chem 280 (19):18558–18561
78. Gunter TE, Pfeiffer PD (1990) Mechanisms by which mitochondria transport calcium. Am J Physiol 258(255 Pt 251):C755–C286
79. Bernardi P (1999) Mitochondrial transport of cations: channels, exchangers, and permeability transition. Physiol Rev 79(4):1127–1155
80. Foskett JK, Philipson B (2015) The mitochondrial Ca2 + uniporter complex. J Mol Cell Cardiol 78:3–8
81. Kamer KJ, Sancak Y, Mootha VK (2014) The uniporter: from newly identified parts to function. Biochem Biophys Res Commun 449(4):370–372

82. Lee Y, Min CK, Kim TG, Song HK, Lim Y, Kim D, Shin K, Kang M, Kang JY, Youn H-S, Lee J-G, An JY, Park KR, Lim JJ, Kim JH, Kim JH, Park ZY, Kim Y-S, Wang J, Kim DH, Eom SH (2015) Structure and function of the N-terminal domain of the human mitochondrial calcium uniporter. EMBO Rep 16(10):1318–1333
83. Csordás G, Golenár T, Seifert EL, Kamer KJ, Sancak Y, Perocchi F, Moffat C, Weaver D, Perez SF, Bogorad R, Koteliansky V, Adijanto J, Mootha VK, Hajnóczky G (2013) MICU1 controls both the threshold and cooperative activation of the mitochondrial Ca(2+) uniporter. Cell Metab 17(6):976–987
84. Qiu J, Tan Y-W, Hagenston AM, Martel M-A, Kneisel N, Skehel PA, Wyllie DJA, Bading H, Hardingham GE (2013) Mitochondrial calcium uniporter Mcu controls excitotoxicity and is transcriptionally repressed by neuroprotective nuclear calcium signals. Nat Commun 4 (2034):1–12
85. Pozzan T, Magalhaes P, Rizzuto R (2000) The comeback of mitochondria to calcium signalling. Cell Calcium 28(5-6):279–283
86. Xu S, Chisholm AD (2014) C. elegans epidermal wounding induces a mitochondrial ROS burst that promotes wound repair. Dev Cell 31(1):48–60
87. Alam MR, Groschner LN, Parichatikanond W, Kuo L, Bondarenko AI, Rost R, Waldeck-Weiermair M, Malli R, Graier WF (2012) Mitochondrial Ca2+ uptake 1 (MICU1) and mitochondrial Ca2+ uniporter (MCU) contribute to metabolism-secretion coupling in clonal pancreatic β-cells. J Biol Chem 287(41):34445–34454
88. Drago I, De Stefani D, Rizzuto R, Pozzan T (2012) Mitochondrial Ca2+ uptake contributes to buffering cytoplasmic Ca2+ peaks in cardiomyocytes. Proc Nat Acad Sci 109 (32):12986–12991
89. Pan X, Liu J, Nguyen T, Liu C, Sun J, Teng Y, Fergusson MM, Rovira II, Allen M, Springer DA, Aponte AM, Gucek M, Balaban RS, Murphy E, Finkel T (2013) The physiological role of mitochondrial calcium revealed by mice lacking the mitochondrial calcium uniporter. Nat Cell Biol 15(12):1464–1472
90. Quan X, Nguyen TT, Choi S-K, Xu S, Das R, Cha S-K, Kim N, Han J, Wiederkehr A, Wollheim CB, Park K-S (2015) Essential role of mitochondrial Ca2+ uniporter in the generation of mitochondrial ph gradient and metabolism-secretion coupling in insulin-releasing cells. J Biol Chem 290(7):4086–4096
91. Rasmussen TP, Wu Y, Joiner M-LA, Koval OM, Wilson NR, Luczak ED, Wang Q, Chen B, Gao Z, Zhu Z, Wagner BA, Soto J, McCormick ML, Kutschke W, Weiss RM, Yu L, Boudreau RL, Abel ED, Zhan F, Spitz DR, Buettner GR, Song L-S, Zingman LV, Anderson ME (2015) Inhibition of MCU forces extramitochondrial adaptations governing physiological and pathological stress responses in heart. Proceedings of the National Academy of Sciences 112 (29):9129–9134
92. Murphy E, Pan X, Nguyen T, Liu J, Holmstrom KM, Finkel T (2014) Unresolved questions from the analysis of mice lacking MCU expression. Biochem Biophys Res Commun 449 (4):384–385
93. Kwong JQ, Lu X, Correll RN, Schwanekamp JA, Vagnozzi RJ, Sargent MA, York AJ, Zhang J, Bers DM, Molkentin JD (2015) The mitochondrial calcium uniporter selectively matches metabolic output to acute contractile stress in the heart. Cell Rep 12(1):15–22
94. Luongo TS, Lambert JP, Yuan A, Zhang X, Gross P, Song J, Shanmughapriya S, Gao E, Jain M, Houser SR, Koch WJ, Cheung JY, Madesh M, Elrod JW (2015) The mitochondrial calcium uniporter matches energetic supply with cardiac workload during stress and modulates permeability transition. Cell Rep 12(1):23–34
95. Holmström KM, Pan X, Liu JC, Menazza S, Liu J, Nguyen TT, Pan H, Parks RJ, Anderson S, Noguchi A, Springer D, Murphy E, Finkel T (2015) Assessment of cardiac function in mice lacking the mitochondrial calcium uniporter. J Mol Cell Cardiol 85:178–182
96. Mailloux RJ, Harper M-E (2011) Uncoupling proteins and the control of mitochondrial reactive oxygen species production. Free Radic Biol Med 51(6):1106–1115

97. Nowikovsky K, Pozzan T, Rizzuto R, Scorrano L, Bernardi P (2012) Perspectives on: SGP symposium on mitochondrial physiology and medicine: the pathophysiology of LETM1. J Gen Physiol 139(6):445–454
98. Jiang D, Zhao L, Clish CB, Clapham DE (2013) Letm1, the mitochondrial Ca2+/H+ antiporter, is essential for normal glucose metabolism and alters brain function in Wolf-Hirschhorn syndrome. Proc Natl Acad Sci U S A 110(24):E2249–E2254
99. Doonan PJ, Chandramoorthy HC, Hoffman NE, Zhang X, Cardenas C, Shanmughapriya S, Rajan S, Vallem S, Chen X, Foskett JK, Cheung JY, Houser SR, Madesh M (2014) LETM1-dependent mitochondrial Ca2+ flux modulates cellular bioenergetics and proliferation. FASEB J 28(11):4936–4949
100. Beutner G, Sharma VK, Giovannucci DR, Yule DI, Sheu SS (2001) Identification of a ryanodine receptor in rat heart mitochondria. J Biol Chem 276(24):21482–21488
101. Beutner G, Sharma VK, Lin L, Ryu SY, Dirksen RT, Sheu SS (2005) Type 1 ryanodine receptor in cardiac mitochondria: transducer of excitation-metabolism coupling. Biochim Biophys Acta 1717(1):1–10
102. Altschafl BA, Beutner G, Sharma VK, Sheu SS, Valdivia HH (2007) The mitochondrial ryanodine receptor in rat heart: a pharmaco-kinetic profile. Biochim Biophys Acta 1768 (7):1784–1795
103. Ryu SY, Beutner G, Dirksen RT, Kinnally KW, Sheu SS (2010) Mitochondrial ryanodine receptors and other mitochondrial Ca2+ permeable channels. FEBS Lett 584(10):1948–1955
104. Palty R, Hershfinkel M, Sekler I (2012) Molecular identity and functional properties of the mitochondrial Na+/Ca2+ Exchanger. J Biol Chem 287(38):31650–31657
105. Ad A, Satrústegui J (2005) New mitochondrial carriers: an overview. Cell Mol Life Sci 62 (19):2204–2227
106. McCormack JG, Denton RM (1993) Mitochondrial Ca2+ transport and the role of intramitochondrial Ca2+ in the regulation of energy metabolism. Dev Neurosci 15 (3-5):165–173
107. Sekler I (2015) Standing of giants shoulders the story of the mitochondrial Na+Ca2+ exchanger. Biochem Biophys Res Commun 460(1):50–52
108. Murphy E, Eisner DA (2009) Regulation of intracellular and mitochondrial Na in health and disease. Circ Res 104(3):292–303
109. Palty R, Ohana E, Hershfinkel M, Volokita M, Elgazar V, Beharier O, Silverman WF, Argaman M, Sekler I (2004) Lithium-calcium exchange is mediated by a distinct potassium-independent sodium-calcium exchanger. J Biol Chem 279(24):25234–25240
110. Murphy E, Cross H, Steenbergen C (1999) Sodium regulation during ischemia versus reperfusion and its role in injury. Circ Res 84(12):1469–1470
111. Babsky A, Doliba N, Doliba N, Savchenko A, Wehrli S, Osbakken M (2001) Na+ effects on mitochondrial respiration and oxidative phosphorylation in diabetic hearts. Exp Biol Med 226 (6):543–551
112. Zu Y, Wan L-J, Cui S-Y, Gong Y-P, Li C-L (2015) The mitochondrial Na(+)/Ca(2+) exchanger may reduce high glucose-induced oxidative stress and nucleotide-binding oligomerization domain receptor 3 inflammasome activation in endothelial cells. J Geriatr Cardiol 12(3):270–278
113. Tsujimoto Y, Shimizu S (2007) Role of the mitochondrial membrane permeability transition in cell death. Apoptosis 12(5):835–840
114. Rasola A, Bernardi P (2011) Mitochondrial permeability transition in Ca2+-dependent apoptosis and necrosis. Cell Calcium 50(3):222–233
115. Shoshan-Barmatz V, Gincel D (2003) The voltage-dependent anion channel: characterization, modulation, and role in mitochondrial function in cell life and death. Cell Biochem Biophys 39 (3):279–292
116. Kinnally KW, Peixoto PM, Ryu SY, Dejean LM (2011) Is mPTP the gatekeeper for necrosis, apoptosis, or both? Biochim Biophys Acta 1813(4):616–622

117. Biasutto L, Azzolini M, Szabò I, Zoratti M (2016) The mitochondrial permeability transition pore in AD 2016: an update. Biochim Biophys Acta 1863(10):2515–2530
118. Hurst S, Hoek J, Sheu S-S (2016) Mitochondrial Ca2+ and regulation of the permeability transition pore. J Bioenerg Biomembr 49:1–21
119. Denton RM (2009) Regulation of mitochondrial dehydrogenases by calcium ions. Biochim Biophys Acta 1787(11):1309–1316
120. Nichols BJ, Denton RM (1995) Towards the molecular basis for the regulation of mitochondrial dehydrogenases by calcium ions. Mol Cell Biochem 149-150:203–212
121. Cardenas C, Miller RA, Smith I, Bui T, Molgo J, Muller M, Vais H, Cheung KH, Yang J, Parker I, Thompson CB, Birnbaum MJ, Hallows KR, Foskett JK (2010) Essential regulation of cell bioenergetics by constitutive InsP3 receptor Ca2+ transfer to mitochondria. Cell 142 (2):270–283
122. Patron M, Raffaello A, Granatiero V, Tosatto A, Merli G, De Stefani D, Wright L, Pallafacchina G, Terrin A, Mammucari C, Rizzuto R (2013) The mitochondrial calcium uniporter (MCU): molecular identity and physiological roles. J Biol Chem 288 (15):10750–10758
123. Territo PR, Mootha VK, French SA, Balaban RS (2000) Ca(2+) activation of heart mitochondrial oxidative phosphorylation: role of the F(0)/F(1)-ATPase. Am J Physiol Cell Physiol 278 (2):C423–C435
124. Gellerich FN, Gizatullina Z, Arandarcikaite O, Jerzembek D, Vielhaber S, Seppet E, Striggow F (2009) Extramitochondrial Ca2+ in the nanomolar range regulates glutamate-dependent oxidative phosphorylation on demand. PLoS One 4(12):e8181
125. Satrustegui J, Pardo B, Del Arco A (2007) Mitochondrial transporters as novel targets for intracellular calcium signaling. Physiol Rev 87(1):29–67
126. Chalmers S, McCarron JG (2008) The mitochondrial membrane potential and Ca2+ oscillations in smooth muscle. J Cell Sci 121(Pt 1):75–85
127. Gerencser AA, Chinopoulos C, Birket MJ, Jastroch M, Vitelli C, Nicholls DG, Brand MD (2012) Quantitative measurement of mitochondrial membrane potential in cultured cells: calcium-induced de- and hyperpolarization of neuronal mitochondria. J Physiol 590 (12):2845–2871
128. Yang R, Lirussi D, Thornton TM, Jelley-Gibbs DM, Diehl SA, Case LK, Madesh M, Taatjes DJ, Teuscher C, Haynes L, Rincón M (2015) Mitochondrial Ca2+ and membrane potential, an alternative pathway for Interleukin 6 to regulate CD4 cell effector function. eLife 4:e06376
129. Bajić A, Spasić M, Andjus PR, Savić D, Parabucki A, Nikolić-Kokić A, Spasojević I (2013) Fluctuating vs. continuous exposure to H_2O_2: the effects on mitochondrial membrane potential, intracellular calcium, and NF-κB in astroglia. PLoS ONE 8(10):e76383
130. Abu-Hamad S, Sivan S, Shoshan-Barmatz V (2006) The expression level of the voltage-dependent anion channel controls life and death of the cell. Proc Natl Acad Sci U S A 103 (15):5787–5792
131. Arif T, Vasilkovsky L, Refaely Y, Konson A, Shoshan-Barmatz V (2014) Silencing VDAC1 expression by siRNA inhibits cancer cell proliferation and tumor growth in vivo. Mol Ther Nucleic Acids 29(3):e159
132. Anis Y (2006) Involvement of Ca2+ in the apoptotic process – friends or foes. Pathways 2:2–7
133. Bonora M, Wieckowski MR, Chinopoulos C, Kepp O, Kroemer G, Galluzzi L, Pinton P (2015) Molecular mechanisms of cell death: central implication of ATP synthase in mitochondrial permeability transition. Oncogene 34(12):1475–1486
134. Keinan N, Pahima H, Ben-Hail D, Shoshan-Barmatz V (2013) The role of calcium in VDAC1 oligomerization and mitochondria-mediated apoptosis. Biochim Biophys Acta 1833 (7):1745–1754
135. Weisthal S, Keinan N, Ben-Hail D, Arif T, Shoshan-Barmatz V (2014) Ca2+- mediated regulation of VDAC1 expression levels is associated with cell death induction. Biochim Biophys Acta 1843(10):2270–2281

136. Giorgi C, Romagnoli A, Pinton P, Rizzuto R (2008) Ca2+ signaling, mitochondria and cell death. Curr Mol Med 8(2):119–130
137. Giorgi C, Baldassari F, Bononi A, Bonora M, De Marchi E, Marchi S, Missiroli S, Patergnani S, Rimessi A, Suski JM, Wieckowski MR, Pinton P (2012) Mitochondrial Ca(2+) and apoptosis. Cell Calcium 52(1):36–43
138. Sasaki K, Donthamsetty R, Heldak M, Cho YE, Scott BT, Makino A (2012) VDAC: old protein with new roles in diabetes. Am J Physiol Cell Physiol 303(10):C1055–C1060
139. Truong AH, Murugesan S, Youssef KD, Makino A (2016) Mitochondrial ion channels in metabolic disease. In: Levitan PI, Dopico MDPMA (eds) Vascular ion channels in physiology and disease. Springer, Cham, pp 397–419
140. Ben-Hail D, Begas-Shvartz R, Shalev M, Shteinfer-Kuzmine A, Gruzman A, Reina S, De Pinto V, Shoshan-Barmatz V (2016) Novel compounds targeting the mitochondrial protein VDAC1 inhibit apoptosis and protect against mitochondria dysfunction. J Biol Chem 291 (48):24986–25003
141. Huang H, Shah K, Bradbury NA, Li C, White C (2014) Mcl-1 promotes lung cancer cell migration by directly interacting with VDAC to increase mitochondrial Ca2+ uptake and reactive oxygen species generation. Cell Death Dis 23(5):e1482
142. Fouque A, Lepvrier E, Debure L, Gouriou Y, Malleter M, Delcroix V, Ovize M, Ducret T, Li C, Hammadi M, Vacher P, Legembre P (2016) The apoptotic members CD95, BclxL, and Bcl-2 cooperate to promote cell migration by inducing Ca2+ flux from the endoplasmic reticulum to mitochondria. Cell Death Differ 23(10):1702–1716
143. Nag S, Larsson M, Robinson RC, Burtnick LD (2013) Gelsolin: the tail of a molecular gymnast. Cytoskeleton (Hoboken) 70(7):360–384
144. Kusano H, Shimizu S, Koya RC, Fujita H, Kamada S, Kuzumaki N, Tsujimoto Y (2000) Human gelsolin prevents apoptosis by inhibiting apoptotic mitochondrial changes via closing VDAC. Oncogene 19(42):4807–4814
145. Qiao H, McMillan JR (2007) Gelsolin segment 5 inhibits HIV-induced T-cell apoptosis via Vpr-binding to VDAC. FEBS Lett 581(3):535–540
146. Sun J, Liao JK (2002) Functional interaction of endothelial nitric oxide synthase with a voltage-dependent anion channel. Proc Natl Acad Sci U S A 99(20):13108–13113
147. Feng X, Ching CB, Chen WN (2012) EBV up-regulates cytochrome c through VDAC1 regulations and decreases the release of cytoplasmic Ca2+ in the NPC cell line. Cell Biol Int 36(8):733–738
148. Montero M, Alonso MT, Carnicero E, Cuchillo-Ibanez I, Albillos A, Garcia AG, Garcia-Sancho J, Alvarez J (2000) Chromaffin-cell stimulation triggers fast millimolar mitochondrial Ca2+ transients that modulate secretion. Nat Cell Biol 2(2):57–61
149. Rizzuto R, Bernardi P, Pozzan T (2000) Mitochondria as all-round players of the calcium game. J Physiol 529(1):37–47
150. Csordás G, Renken C, Várnai P, Walter L, Weaver D, Buttle KF, Balla T, Mannella CA, Hajnóczky G (2006) Structural and functional features and significance of the physical linkage between ER and mitochondria. J Cell Biol 174(7):915–921
151. Shoshan-Barmatz V, Zalk R, Gincel D, Vardi N (2004) Subcellular localization of VDAC in mitochondria and ER in the cerebellum. Biochim Biophys Acta 1657(2-3):105–114
152. Krols M, Bultynck G, Janssens S (2016) ER-Mitochondria contact sites: A new regulator of cellular calcium flux comes into play. J Cell Biol 214(4):367–370
153. de Brito OM, Scorrano L (2008) Mitofusin 2 tethers endoplasmic reticulum to mitochondria. Nature 456(7222):605–610
154. De Vos KJ, Mórotz GM, Stoica R, Tudor EL, Lau K-F, Ackerley S, Warley A, Shaw CE, Miller CCJ (2012) VAPB interacts with the mitochondrial protein PTPIP51 to regulate calcium homeostasis. Hum Mol Genet 21(6):1299–1311
155. Iwasawa R, Mahul-Mellier AL, Datler C, Pazarentzos E, Grimm S (2011) Fis1 and Bap31 bridge the mitochondria-ER interface to establish a platform for apoptosis induction. EMBO J 30(3):556–568

156. Szabadkai G, Bianchi K, Varnai P, De Stefani D, Wieckowski MR, Cavagna D, Nagy AI, Balla T, Rizzuto R (2006) Chaperone-mediated coupling of endoplasmic reticulum and mitochondrial Ca2+ channels. J Cell Biol 175(6):901–911
157. de Brito OM, Scorrano L (2009) Mitofusin-2 regulates mitochondrial and endoplasmic reticulum morphology and tethering: the role of Ras. Mitochondrion 9(3):222–226
158. Rizzuto R, Pinton P, Carrington W, Fay FS, Fogarty KE, Lifshitz LM, Tuft RA, Pozzan T (1998) Close contacts with the endoplasmic reticulum as determinants of mitochondrial Ca2+ responses. Science 280(5370):1763–1766
159. Rusinol AE, Cui Z, Chen MH, Vance JE (1994) A unique mitochondria-associated membrane fraction from rat liver has a high capacity for lipid synthesis and contains pre-Golgi secretory proteins including nascent lipoproteins. J Biol Chem 269(44):27494–27502
160. Garofalo T, Matarrese P, Manganelli V, Marconi M, Tinari A, Gambardella L, Faggioni A, Misasi R, Sorice M, Malorni W (2016) Evidence for the involvement of lipid rafts localized at the ER-mitochondria associated membranes in autophagosome formation. Autophagy 12 (6):917–935
161. Raturi A, Gutierrez T, Ortiz-Sandoval C, Ruangkittisakul A, Herrera-Cruz MS, Rockley JP, Gesson K, Ourdev D, Lou PH, Lucchinetti E, Tahbaz N, Zaugg M, Baksh S, Ballanyi K, Simmen T (2016) TMX1 determines cancer cell metabolism as a thiol-based modulator of ER-mitochondria Ca2+ flux. J Cell Biol 214(4):433–444
162. Boehning D, Patterson RL, Sedaghat L, Glebova NO, Kurosaki T, Snyder SH (2003) Cytochrome c binds to inositol (1,4,5) trisphosphate receptors, amplifying calcium-dependent apoptosis. Nat Cell Biol 5(12):1051–1061
163. Friedman JR, Lackner LL, West M, DiBenedetto JR, Nunnari J, Voeltz GK (2011) ER tubules mark sites of mitochondrial division. Science 334(6054):358–362
164. Marchi S, Giorgi C, Oparka M, Duszynski J, Wieckowski MR, Pinton P (2014) Oncogenic and oncosuppressive signal transduction at mitochondria-associated endoplasmic reticulum membranes. Mol Cell Oncol 1(2):e956469
165. Akl H, Vervloessem T, Kiviluoto S, Bittremieux M, Parys JB, De Smedt H, Bultynck G (2014) A dual role for the anti-apoptotic Bcl-2 protein in cancer: mitochondria versus endoplasmic reticulum. Biochim Biophys Acta 1843(10):2240–2252
166. Thomenius MJ, Distelhorst CW (2003) Bcl-2 on the endoplasmic reticulum: protecting the mitochondria from a distance. J Cell Sci 116(Pt 22):4493–4499
167. Bittremieux M, Parys JB, Pinton P, Bultynck G (2016) ER functions of oncogenes and tumor suppressors: modulators of intracellular Ca(2+) signaling. Biochim Biophys Acta 1863(6 Pt B):1364–1378
168. Wolff S, Erster S, Palacios G, Moll UM (2008) p53's mitochondrial translocation and MOMP action is independent of Puma and Bax and severely disrupts mitochondrial membrane integrity. Cell Res 18(7):733–744
169. Banerjee J, Ghosh S (2004) Bax increases the pore size of rat brain mitochondrial voltage-dependent anion channel in the presence of tBid. Biochem Biophys Res Commun 323 (1):310–314
170. Shimizu S, Tsujimoto Y (2000) Proapoptotic BH3-only Bcl-2 family members induce cytochrome c release, but not mitochondrial membrane potential loss, and do not directly modulate voltage-dependent anion channel activity. Proc Natl Acad Sci U S A 97(2):577–582
171. Bargaje R, Gupta S, Sarkeshik A, Park R, Xu T, Sarkar M, Halimani M, Roy SS, Yates J, Pillai B (2012) Identification of novel targets for miR-29a using miRNA proteomics. PLoS One 7 (8):e43243
172. Li QQ, Zhang L, Wan HY, Liu M, Li X, Tang H (2015) CREB1-driven expression of miR-320a promotes mitophagy by down-regulating VDAC1 expression during serum starvation in cervical cancer cells. Oncotarget 6(33):34924–34940
173. Marchi S, Lupini L, Patergnani S, Rimessi A, Missiroli S, Bonora M, Bononi A, Corra F, Giorgi C, De Marchi E, Poletti F, Gafa R, Lanza G, Negrini M, Rizzuto R, Pinton P (2013) Downregulation of the mitochondrial calcium uniporter by cancer-related miR-25. Curr Biol 23(1):58–63

174. Wang F, Qiang Y, Zhu L, Jiang Y, Wang Y, Shao X, Yin L, Chen J, Chen Z (2016) MicroRNA-7 downregulates the oncogene VDAC1 to influence hepatocellular carcinoma proliferation and metastasis. Tumour Biol 37(8):10235–10246
175. Roshan R, Shridhar S, Sarangdhar MA, Banik A, Chawla M, Garg M, Singh VP, Pillai B (2014) Brain-specific knockdown of miR-29 results in neuronal cell death and ataxia in mice. RNA 20(8):1287–1297
176. Stary CM, Sun X, Ouyang Y, Li L, Giffard RG (2016) miR-29a differentially regulates cell survival in astrocytes from cornu ammonis 1 and dentate gyrus by targeting VDAC1. Mitochondrion 30:248–254
177. Perez-Gracia E, Torrejon-Escribano B, Ferrer I (2008) Dystrophic neurites of senile plaques in Alzheimer's disease are deficient in cytochrome c oxidase. Acta Neuropathol 116(3):261–268
178. Godbole A, Varghese J, Sarin A, Mathew MK (2003) VDAC is a conserved element of death pathways in plant and animal systems. Biochim Biophys Acta 1642(1-2):87–96
179. AJ L, Dong CW, CS D, Zhang QY (2007) Characterization and expression analysis of Paralichthys olivaceus voltage-dependent anion channel (VDAC) gene in response to virus infection. Fish Shellfish Immunol 23(3):601–613
180. Zaid H, Abu-Hamad S, Israelson A, Nathan I, Shoshan-Barmatz V (2005) The voltage-dependent anion channel-1 modulates apoptotic cell death. Cell Death Differ 12(7):751–760
181. Zhang G, Jiang G, Wang C, Zhong K, Zhang J, Xue Q, Li X, Jin H, Li B (2016) Decreased expression of microRNA-320a promotes proliferation and invasion of non-small cell lung cancer cells by increasing VDAC1 expression. Oncotarget 7(31):49470–49480
182. Fatima M, Prajapati B, Saleem K, Kumari R, Mohindar Singh Singal C, Seth P (2017) Novel insights into role of miR-320a-VDAC1 axis in astrocyte-mediated neuronal damage in neuroAIDS. Glia 65(2):250–263
183. Chaudhuri AD, Choi DC, Kabaria S, Tran A, Junn E (2016) MicroRNA-7 regulates the function of mitochondrial permeability transition pore by targeting VDAC1 expression. J Biol Chem 291(12):6483–6493
184. Li X, Wang H, Yao B, Xu W, Chen J, Zhou X (2016) lncRNA H19/miR-675 axis regulates cardiomyocyte apoptosis by targeting VDAC1 in diabetic cardiomyopathy. Sci Rep 6:36340
185. Manczak M, Reddy PH (2012) Abnormal interaction of VDAC1 with amyloid beta and phosphorylated tau causes mitochondrial dysfunction in Alzheimer's disease. Hum Mol Genet 21(23):5131–5146
186. Cuadrado-Tejedor M, Vilarino M, Cabodevilla F, Del Rio J, Frechilla D, Perez-Mediavilla A (2011) Enhanced expression of the voltage-dependent anion channel 1 (VDAC1) in Alzheimer's disease transgenic mice: an insight into the pathogenic effects of amyloid-beta. J Alzheimer's Dis 23(2):195–206
187. Liao Z, Liu D, Tang L, Yin D, Yin S, Lai S, Yao J, He M (2015) Long-term oral resveratrol intake provides nutritional preconditioning against myocardial ischemia/reperfusion injury: involvement of VDAC1 downregulation. Mol Nutr Food Res 59(3):454–464
188. Ahmed M, Muhammed SJ, Kessler B, Salehi A (2010) Mitochondrial proteome analysis reveals altered expression of voltage dependent anion channels in pancreatic beta-cells exposed to high glucose. Islets 2(5):283–292
189. Gong D, Chen X, Middleditch M, Huang L, Vazhoor Amarsingh G, Reddy S, Lu J, Zhang S, Ruggiero K, Phillips AR, Cooper GJ (2009) Quantitative proteomic profiling identifies new renal targets of copper(II)-selective chelation in the reversal of diabetic nephropathy in rats. Proteomics 9(18):4309–4320
190. Pan L, Huang BJ, Ma XE, Wang SY, Feng J, Lv F, Liu Y, Liu Y, Li CM, Liang DD, Li J, Xu L, Chen YH (2015) MiR-25 protects cardiomyocytes against oxidative damage by targeting the mitochondrial calcium uniporter. Int J Mol Sci 16(3):5420–5433
191. Hong Z, Chen KH, Dasgupta A, Potus F, Dunham-Snary K, Bonnet S, Tian L, Fu J, Breuils-Bonnet S, Provencher S, Wu D, Mewburn J, Ormiston ML, Archer SL (2016) miR-138 and miR-25 downregulate MCU, causing pulmonary arterial hypertension's cancer phenotype. Am J Respir Crit Care Med 195(4):515–529

192. Cárdenas C, Müller M, McNeal A, Lovy A, Jaňa F, Bustos G, Urra F, Smith N, Molgó J, Diehl JA, Ridky Todd W, Foskett JK (2016) Selective vulnerability of cancer cells by inhibition of Ca2+ transfer from endoplasmic reticulum to mitochondria. Cell Rep 14(10):2313–2324
193. Wiederkehr A, Wollheim CB (2012) Mitochondrial signals drive insulin secretion in the pancreatic β-cell. Mol Cell Endocrinol 353(1–2):128–137
194. Wiederkehr A, Szanda G, Akhmedov D, Mataki C, Heizmann Claus W, Schoonjans K, Pozzan T, Spät A, Wollheim Claes B (2011) Mitochondrial matrix calcium is an activating signal for hormone secretion. Cell Metab 13(5):601–611
195. Jitrapakdee S, Wutthisathapornchai A, Wallace JC, MacDonald MJ (2010) Regulation of insulin secretion: role of mitochondrial signalling. Diabetologia 53(6):1019–1032
196. Wang C-H, Tsai T-F, Wei Y-H (2015) Role of mitochondrial dysfunction and dysregulation of Ca2+ homeostasis in insulin insensitivity of mammalian cells. Ann N Y Acad Sci 1350 (1):66–76
197. Rimessi A, Patergnani S, Bonora M, Wieckowski MR, Pinton P (2015) Mitochondrial Ca(2+) remodeling is a prime factor in oncogenic behavior. Front Oncol 5:143
198. Park J, Li Y, Kim S-H, Yang K-J, Kong G, Shrestha R, Tran Q, Park KA, Jeon J, Hur GM, Lee C-H, Kim D-H, Park J (2014) New players in high fat diet-induced obesity: LETM1 and CTMP. Metabolism 63(3):318–327

Part IV
Annexins

Chapter 14
Annexins: Ca^{2+} Effectors Determining Membrane Trafficking in the Late Endocytic Compartment

Carlos Enrich, Carles Rentero, Elsa Meneses-Salas, Francesc Tebar, and Thomas Grewal

Abstract Despite the discovery of annexins 40 years ago, we are just beginning to understand some of the functions of these still enigmatic proteins. Defined and characterized by their ability to bind anionic membrane lipids in a Ca^{2+}-dependent manner, each annexin has to be considered a multifunctional protein, with a multitude of cellular locations and diverse activities. Underlying causes for this considerable functional diversity include their capability to associate with multiple cytosolic and membrane proteins. In recent years, the increasingly recognized establishment of membrane contact sites between subcellular compartments opens a new scenario for annexins as instrumental players to link Ca^{2+} signalling with the integration of membrane trafficking in many facets of cell physiology. In this chapter, we review and discuss current knowledge on the contribution of annexins in the biogenesis and functioning of the late endocytic compartment, affecting endo- and exocytic pathways in a variety of physiological consequences ranging from membrane repair, lysosomal exocytosis, to cell migration.

Keywords Annexins · AnxA6 · Late endosomes · Lysosomes · Cholesterol · Ca^{2+}-signaling · Membrane trafficking

C. Enrich (✉) · C. Rentero · E. Meneses-Salas · F. Tebar
Departament de Biomedicina, Unitat de Biologia Cel·lular, Centre de Recerca Biomèdica (CELLEX), Institut d'Investigacions Biomèdiques August Pi i Sunyer (IDIBAPS), Barcelona, Spain

Facultat de Medicina i Ciències de la Salut, Universitat de Barcelona, Barcelona, Spain
e-mail: enrich@ub.edu

T. Grewal
Faculty of Pharmacy, University of Sydney, Sydney, Australia
e-mail: thomas.grewal@sydney.edu.au

J. Krebs (ed.), *Membrane Dynamics and Calcium Signaling*, Advances in Experimental Medicine and Biology 981,
https://doi.org/10.1007/978-3-319-55858-5_14

14.1 Introduction

Annexins are a multi-gene protein family expressed in vertebrates, invertebrates, plants, fungi and protists that bind to biological membranes in a calcium (Ca^{2+})-dependent manner [1]. Depending on the local conditions of cytosolic free Ca^{2+}, pH and lipids in subcellular microenvironments, annexins can dynamically attach or possibly even insert into the plasma membrane or endomembranes. Hence, given the great diversity of Ca^{2+}-dependent events at cellular membranes, annexins participate in membrane trafficking and various other processes including signalling, proliferation, differentiation, and inflammation [2–5].

Over the last few decades, the Ca^{2+}-dependent membrane association of annexins has been investigated intensively in endo- and exocytosis, the spatial organization of membrane lipids (including lipid rafts), membrane repair, as well as connecting membranes to the actin cytoskeleton [1, 6–10]. Moreover, annexins interact with a plethora of other Ca^{2+}-effectors and can form Ca^{2+}-permeable ion channels in artificial membranes [11–18], linking them to Ca^{2+} homeostasis and Ca^{2+}-driven signal transduction [1, 19].

In humans, there are 12 different annexins, AnxA1–A11 and A13, with orthologues in most vertebrates [3]. Similar to the first annexin structure determined from purified AnxA5 [20–22], all annexins consist of a highly conserved core domain that comprises four structural repeats (I–IV), each 70–75 amino acid residues in length. AnxA6 is a unique member of this family, possessing two of these four-repeat core domains connected by a linker region [19, 23–26], most likely due to gene duplication. As shown in Fig. 14.1 for AnxA1, each repeat consists of five α-helices. The repeats are organized into two distinct arrangements within the core domain. The repeat pairs I/IV and II/III pack together, mostly as a result of hydrophobic interactions [27, 28], which in general are highly conserved within the annexin family. The N-terminal domain is located on the concave side of the molecule, or in the case of AnxA1 in the absence of Ca^{2+}, affiliated with the core in between the concave and the convex side [29].

The binding of Ca^{2+} to annexins promotes their binding to phospholipid-containing membranes. Remarkably, the Ca^{2+} ions all lie on the same side of the annexins [30], forming a convex surface which interacts with phospholipids (Fig. 14.1). Unlike the structures of EF-hand Ca^{2+}-binding proteins, such as troponin-C [31, 32] or S100 proteins [33, 34], annexins do not appear to undergo a significant structural change within their core domains on Ca^{2+}-binding [34].

In the course of the last 20 years we have focussed on AnxA6, dissecting and correlating its intracellular locations with membrane trafficking, cholesterol homeostasis and signalling [19, 35]. Here we will review the role of annexins, in particular AnxA6, in the late endocytic compartment as a pivotal Ca^{2+} effector for the regulation of endo- and exocytic trafficking pathways.

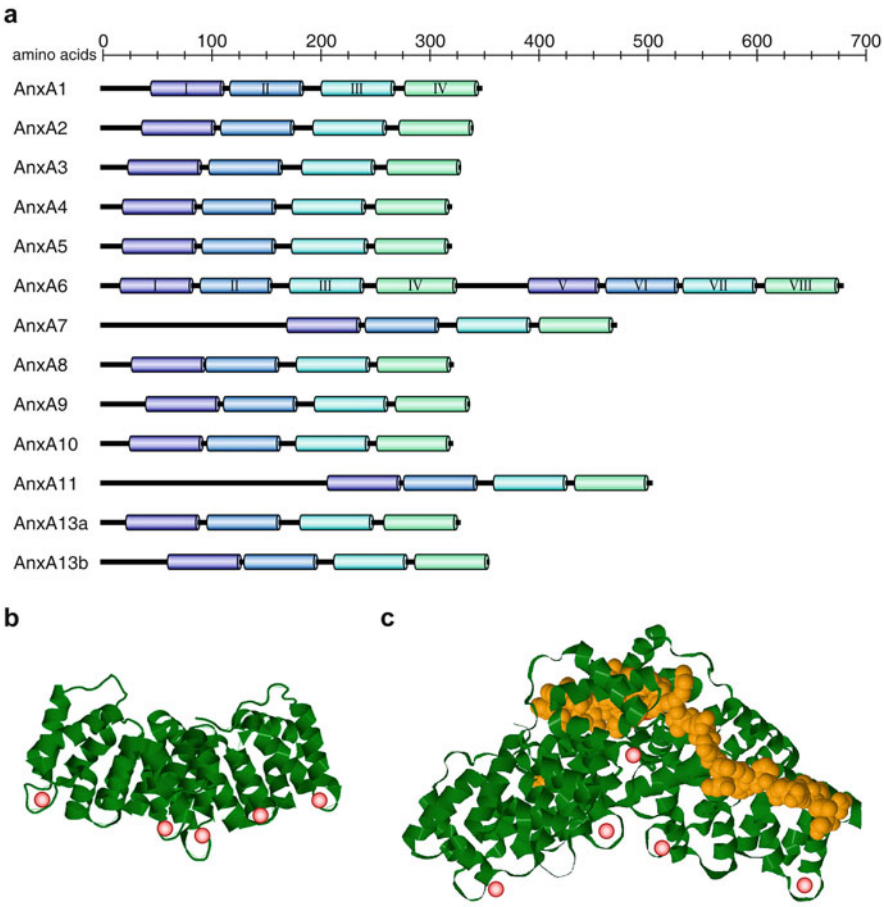

Fig. 14.1 Annexins: Domain structure. (**a**) The domain structures of human annexins AnxA1–AnxA11 and AnxA13 are illustrated. The N-terminal leader domain (solid black line), C-terminal core with annexin repeats I–IV (and I–VIII for AnxA6) and length (in amino acids) are indicated. (**b**) Structural model of AnxA1. Each annexin repeat contains five α-helices that are connected by short loops or turns. (**c**) Ribbon representation of the AnxA6 crystal structure. AnxA6 contains eight repeat segments, and the two halves of the protein, which each consist of a four-annexin-repeat unit (core), are connected by a linker (depicted in yellow). Ca^{2+} bound to annexins is shown as red spheres. Structural models for AnxA1 and AnxA6 were derived from the Protein Data Bank (http://www.rcsb.org; files 1AIN, AVC)

14.2 Annexins: Ca^{2+} Binding and Ca^{2+} Sensitivity

Ca^{2+}-binding proteins represent a heterogeneous and wide group with different structures and properties. Annexins belong to the type II Ca^{2+}-binding proteins [36], although they also contain two other types of Ca^{2+}-binding sites: type III and AB' sites [29]. Despite the large homology within annexins, X-ray crystallography

revealed striking differences in the Ca^{2+}-binding capacity of individual annexins. While AnxA1 bound six to eight Ca^{2+} ions, and AnxA2 and A3 associated with five Ca^{2+} ions, AnxA5 did bind up to ten Ca^{2+} ions. Interestingly, although containing two core domains, only three Ca^{2+} ions per lobe (six in total) were bound to AnxA6 [29]. In addition, while the EF-hand family of Ca^{2+}-binding proteins, including S100 proteins, calmodulin (CaM), and troponin-C, exhibit high affinity for Ca^{2+} with dissociation constants in the micro- and nanomolar range, annexins bind Ca^{2+} only at high concentrations. However, the Ca^{2+}-binding affinity is greatly increased in the presence of negatively charged phospholipids. Thus, Ca^{2+} ions might only serve to stabilize this interaction, bridging annexins and phospholipid headgroups [29, 34].

In this scenario, the conserved annexin core domain mediates Ca^{2+} and phospholipid interaction, yet the N-terminal domain, which is variable in sequence and length for each annexin, would facilitate different cellular functions. In human annexins, the N-terminal region ranges from a few residues to 200 or more amino acids and, based on the length of this region, can be classified into three groups. The first group consists of members with a short extension below 20–21 amino acids, including AnxA3, A4, A5, A6, A8, A10 and A13a. A second intermediate group includes AnxA1, A2, A9 and A13b containing up to 55 N-terminal residues. Finally, a third group consists of AnxA7 and A11 that possess a long N-terminus with more than 100 amino acids [reviewed in [3, 34, 37], (see scheme in Fig. 14.1)].

14.2.1 Annexin A6: Location, Signalling and Dynamics

AnxA6 has been proposed to participate in membrane trafficking, membrane and cytoskeleton organization, cholesterol homeostasis, and signal transduction [4, 23–25, 38]. Yet, how the cellular microenvironment can modulate the association of AnxA6 with biological membranes in a dynamic fashion is still not fully understood. Based on in vitro studies, the linker region (amino acids 320–378) connecting the two AnxA6 core modules allows flexible binding to one or even two separate membranes [23–25, 38], and the latter feature might contribute to the ability of AnxA6 to aggregate membranes. Ca^{2+}-sensitive membrane binding kinetics of AnxA6 are influenced predominantly by phosphatidylserine, phosphatidylinositol, phosphatidic acid [1], and to a minor extend phosphatidylethanolamine [39], all of which present in the late endosome (LE)/lysosomal (Lys) compartment [40, 41]. In addition, acidic pH and cholesterol, both critical for LE/Lys function, also contribute to the dynamic and reversible membrane binding behaviour of AnxA6 [42–52]. Indeed, while Ca^{2+} is the main determinant of membrane binding for the majority of AnxA6 proteins, an ethylenediaminetetraacetic acid-resistant pool of AnxA6 proteins is associated with LE in a cholesterol-dependent manner [42, 46].

AnxA6 is predominantly located at the plasma membrane, in the endocytic compartment, and in caveolae. In these locations, AnxA6 participates in the regulation of endo- and exocytic membrane trafficking pathways. Nevertheless, there is yet limited in vivo evidence for annexin-mediated formation of microdomains that

would enable membrane transport. We therefore recently visualized membrane order (liquid-ordered vs. disordered) using our AnxA6 cell models and the fluorescent dyes laurdan and di-4-ANEPPDHQ. High AnxA6 levels were associated with a significant decrease of condensed membrane domains [53]. Together with altered membrane order in T cells from AnxA6-deficient mice [54], this provided the first evidence from live cells that annexins have the potential to induce changes in membrane architecture [55]. Hence, AnxA6 membrane translocation and binding to phospholipids, together with the interaction to actin and the recruitment of signalling proteins (see below), might regulate lipid and protein assembly in specialized domains at the plasma membrane, and possibly endomembranes, such as the LE/Lys compartment.

Membrane trafficking events involving AnxA6 include low density lipoprotein (LDL) endocytosis [46], LDL degradation and its transport from LE/pre-lysosomes to lysosomes [56, 57], which is intimately linked to the recruitment of AnxA6 to cholesterol-laden LE [58]. In addition, AnxA6 acts as a scaffold to recruit the GTPase-activating protein p120GAP and protein kinase C to the plasma membrane to modulate Ras and EGFR signalling/trafficking pathways, respectively [4, 59]. These multifunctional features of AnxA6 are most probably a consequence of (a) its dynamic spatiotemporal behaviour in a Ca^{2+}- and/or cholesterol-dependent manner but also (b) the promiscuity to interact with a large repertoire of molecules, in particular through the N-terminal tail but also the flexible linker region (Fig. 14.1).

Alike other annexins, AnxA6 expression varies in cells, tissues and pathophysiological situations [47]. Over the years, we have focussed on two cell lines, Chinese Hamster Ovary cells (CHO), which express low AnxA6 levels [58], and AnxA6-deficient human epithelial A431 carcinoma cells [59, 60]. Stable CHO and A431 cell lines expressing high amounts of AnxA6 commonly observed in other cells and tissues served as gain-of-function models. Key findings were often validated in AnxA6 knockdown approaches in HeLa cancer cells and HuH7 hepatocytes, or upon examination of endogenous AnxA6 behaviour in various cell models of human, mouse or rat origin. Most relevant for this article, similar to the treatment with the cell-permeable amphiphilic amino-steroid U18666A, high AnxA6 levels resulted in an accumulation of cholesterol in the LE compartment, a phenotype reminiscent of mutations in Niemann–Pick Type C 1/2 (NPC1/2) proteins [58]. This blockage of LE-cholesterol egress led to reduced amounts of cholesterol in other compartments, in particular the Golgi and the plasma membrane, with drastic consequences for membrane trafficking along secretory pathways.

Initially we observed that the AnxA6-induced cholesterol imbalance inhibited caveolin export from the Golgi, affecting caveolae formation and the functioning of the secretory pathway [58, 61, 62]. The underlying mechanism could be related to vesiculation and tubulation events from the Golgi that require the activity of cholesterol-sensitive cytoplasmic phospholipase A2 ($cPLA_2$) [61]. In fact, the reduced availability of cholesterol upon AnxA6 overexpression indirectly inhibited $cPLA_2$ activity and its association with the Golgi complex. In support of AnxA6 modulating $cPLA_2$ activity required for caveolin transport to the cell surface, Ca^{2+}-dependent, but

not Ca^{2+}-independent $cPLA_2$ inhibition, mimicked the phenotype observed upon AnxA6 upregulation and led to an accumulation of caveolin in the Golgi [58, 61].

More recently, we associated elevated AnxA6 levels with mislocalization of several cholesterol-sensitive SNARE proteins, which impact on the functionality of exocytic trafficking pathways. First, syntaxin 4 (Stx4) and SNAP23, two t-SNAREs concentrated in cholesterol-rich, caveolin-containing clusters at the plasma membrane, were found to be sequestered in Golgi membranes. As the cell surface delivery of secretory vesicles highly depends on Stx4 and SNAP23 being located at the plasma membrane, their mislocalization in the Golgi upon AnxA6 overexpression inhibited exocytic transport, including fibronectin secretion [62]. Second, syntaxin 6 (Stx6), a t-SNARE predominantly located in the trans-Golgi-network, and responsible for integrin recycling to the cell surface, was mislocalized in recycling endosomes of AnxA6 expressing cells [63]. This was associated with strongly reduced integrin recycling to the cell surface. Together with our recent studies using NPC1 mutant cells [64] recognizing LE-cholesterol as a critical factor for Stx6-dependent integrin recycling, this points at elevated AnxA6 levels interfering with integrin trafficking through impaired LE-cholesterol export. Indeed, ectopic expression of NPC1 restored cell surface integrin expression in cells with high AnxA6 levels. These findings correlated with decreased cell migration and invasion upon AnxA6 upregulation, suggesting that AnxA6-dependent distribution of LE-cholesterol critically affects migratory cell behavior [65]. Beyond these observations, NPC1-induced cholesterol imbalance causes deregulation of lysosomal Ca^{2+} homeostasis [66], providing a mechanistic link between AnxA6 and LE-cholesterol export with many other Ca^{2+}-dependent cellular events (see below).

14.3 Intracellular Ca^{2+} Stores and Ca^{2+}-Binding Proteins

Most aspects of cellular life are affected by Ca^{2+}, often acting locally in subcellular micro-environments. Hence, Ca^{2+} is recognized as an evolutionarily conserved signal transducer for diverse cellular activities ranging from synaptic transmission, muscle contraction, granule secretion, to gene expression and membrane repair [67]. The common theme comprises Ca^{2+} to add charge to proteins, thereby initiating conformational changes and switching protein functions "on" and/or "off" [67, 68]. Based on this principle, hundreds of Ca^{2+}-sensor proteins with binding affinities in the nano- to millimolar range are known to trigger a wide variety of Ca^{2+}-sensitive processes [68].

Thus, tight regulation of Ca^{2+} homeostasis inside cells is critical to effectively control a plethora of molecular activities. Indeed, substantial Ca^{2+} concentration gradients exist between the extracellular space (~2 mM) and the cytosol (~100 nM) or intracellular compartments (0.5–1 mM) [67]. These gradients are established by primary and secondary Ca^{2+} transporters localized at the cell surface or on membranes of intracellular organelles, which upon stimulation, allow Ca^{2+} entry into the

cytosol [68, 69], altogether providing a complex molecular network ensuring that the cytosolic [Ca^{2+}] is tightly regulated.

The high Ca^{2+} concentrations outside cells provide an almost unlimited supply of Ca^{2+}. Consequently, stimulation of plasma membrane Ca^{2+} channels is critical to control Ca^{2+}-influx. As proper cellular functioning requires the Ca^{2+}-gradient across the cellular membrane to be maintained, pathological disruptions of the plasma membrane may cause de-regulated Ca^{2+} influxes, resulting in Ca^{2+} injury [70–72]. In addition, Ca^{2+} can also be released from specialized Ca^{2+} storage organelles, including the endoplasmic reticulum (ER), endosomes, lysosomes, Golgi, mitochondria and secretory vesicles (Fig. 14.2). Given that the nuclear envelope is continuous with the ER membrane, the nucleus may also be viewed as a Ca^{2+} store [73].

Out of the organelles listed above, the ER represents the largest intracellular Ca^{2+} store [68, 74]. In fact, in muscle, the sarco-endoplasmic reticulum is the primary source of Ca^{2+}. It is a heterogeneous organelle with a non-uniform distribution of Ca^{2+}. Luminal [Ca^{2+}] in the ER (0.3–1 mM) is established and maintained by the sarco-endoplasmic reticulum Ca^{2+} pump (SERCA) [75] and several ER Ca^{2+} channels, including ryanodine and inositol 1,4,5-trisphosphate receptors (RyRs, IP3Rs) [76, 77]. Both IP3Rs and RyRs are activated by cytosolic Ca^{2+}, a mechanism known as Ca^{2+}-induced Ca^{2+} release [78], thereby rapidly amplifying augmentation of cytosolic [Ca^{2+}]. Ca^{2+} release-activated Ca^{2+} entry can then refill depleted ER Ca^{2+} stores. For this to occur, the EF-hand domain in stromal-interacting molecule-1 (STIM1) oligomerizes to activate calcium release-activated calcium channel protein 1 (Orai1) channels in the plasma membrane [68, 73], in this manner enabling the restoration of Ca^{2+} in ER stores.

Ca^{2+} homeostasis has been intensively researched in the context of secretory pathways. The Golgi is the central player for this transport route and localized changes in Ca^{2+} concentrations in the adjacent cytosol or within the Golgi lumen regulate its function. Conversely, the Golgi can sequester Ca^{2+} to shape cytosolic Ca^{2+} signals as well as initiate them by releasing Ca^{2+} via IP3Rs located on Golgi membranes. Ca^{2+} can also regulate the passage of proteins along the secretory pathway [79]. In turn almost all of the cellular compartments of the secretory pathway can act as Ca^{2+} signalling organelles, participating in both release and uptake of Ca^{2+} [68, 80, 81]. Moreover, multiple signalling cascades, including kinases, phosphatases [82] and phosphoinositides [83] are intimately linked to components of the Ca^{2+} signalling machinery [68, 84] and are juxtaposed to the Golgi, adding another layer of Ca^{2+} sensitivity to the regulation of Golgi function.

As a result of the active ER-to-Golgi vesicular transport, the Golgi receives continuous input from ER-derived vesicles. Thus, many of the ER channels and transporters can also be found in the Golgi apparatus, including IP3Rs and SERCA pumps. In addition, specific Ca^{2+} ATPase pumps [68, 81] and several Ca^{2+}-binding proteins are also relevant in the dynamics of this early step within the secretory pathway. Apoptosis-linked gene-2 product (Alg-2), which contains five serially repetitive EF-hands, binds to protein transport protein Sec31A, a component of the outer layer of coat protein complex II (COPII), in a Ca^{2+}-dependent manner and is recruited to the endoplasmic reticulum exit sites (ERES) to stabilize Sec31A

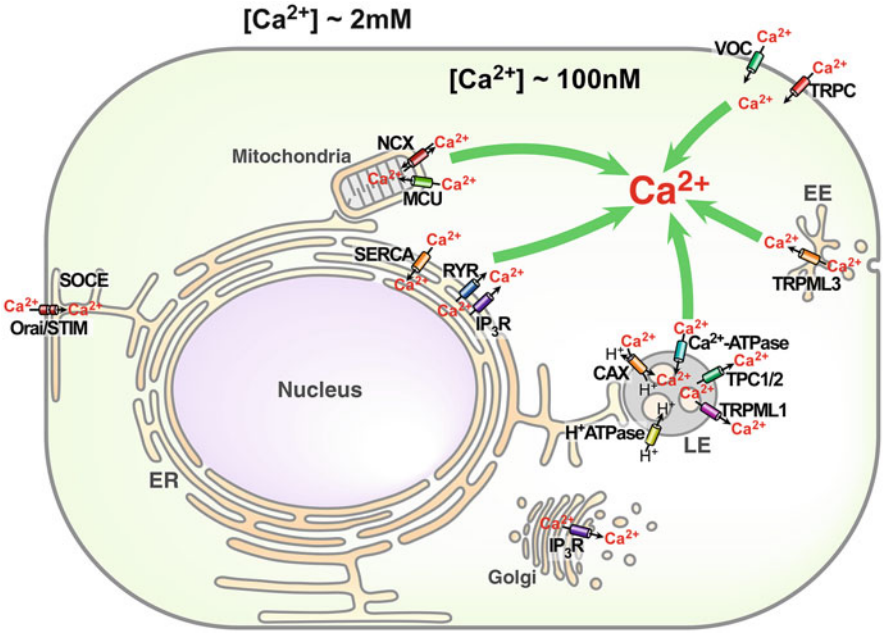

Fig. 14.2 Intracellular Ca^{2+} stores. Schematic representation of the major Ca^{2+} stores and Ca^{2+} transport routes across membranes in a mammalian cell. The plasma membrane, endoplasmic reticulum (ER), mitochondria, late endosomes (LE), Golgi and nucleus contain many different Ca^{2+} transport molecules that contribute to the control of Ca^{2+} homeostasis. For clarity only the better characterized channels and transporters are depicted. Ca^{2+} entry is controlled by store operated calcium entry (SOCE) that includes the calcium release-activated calcium channel protein 1 (Orai)/stromal-interacting molecule-1 (STIM) complex, as well as voltage operating calcium channels (VOC) or transient receptor potential channels (TRPC). Endocytosis is also relevant through caveolae, clathrin-dependent endocytosis or fluid phase. In early endosomes (EE), transient receptor potential mucolipin type 3 (TRPML3) actively releases Ca^{2+} to the cytosol. The ER is the major storage compartment with sarco/endoplasmic reticulum calcium ATPase (SERCA) and the ryanodine receptor (RyR) and inositol-1,4,5-triphosphate receptor (IP3R). Mitochondria have several transporters including sodium/calcium exchanger (NCX) and mitochondria calcium uniporter (MCU). The acidic LE/Lys compartments contain the well-characterised Ca^{2+} channels, transient receptor potential mucolipin type 1 (TRPML1) and two-pore channel (TPC1/2), and several other less-well defined Ca^{2+} pumps and exchangers such as Ca^{2+}/H^{+} exchanger (CAX) or the Ca^{2+}-ATPase (see Fig. 14.3 for more details). Finally, along the secretory pathway, the Golgi complex significantly contributes to Ca^{2+} homeostasis through Ca^{2+} transporters also located in the ER (i.e. IP3R)

[85, 86]. Interestingly, and despite the incomplete knowledge how annexins might contribute to Ca^{2+} homeostasis and membrane transport along ER-Golgi routes, several annexins including AnxA1, A2, A5, A6, A11 and A13b are found on Golgi membranes or along the early or post-Golgi trafficking pathways [35].

Besides the regulatory circuits to control $[Ca^{2+}]$ in ER/Golgi membranes, it has become increasingly evident that Ca^{2+} handling by other organelles, especially mitochondria and lysosomes, are vital to control cellular functions such as apoptosis

and/or autophagy [87]. Mitochondria exist in close proximity to the ER, allowing for a privileged Ca^{2+} transfer via IP3Rs and then voltage-dependent anion channels [88, 89]. Thus, mitochondria represent a second intracellular Ca^{2+} reservoir as they buffer Ca^{2+} released from the ER. Recent studies identified mitochondria-associated membranes (MAMs) to facilitate physical interaction between mitochondria and the ER [87]. Many proteins in these MAMs may contribute to the exchange of Ca^{2+}, reactive oxygen species and lipids between these two compartments [90]. Interestingly, AnxA6 out of the annexin family appears to be a marker for MAMs [91]. In the inner mitochondrial membrane, the mitochondria Ca^{2+} uniporter then guides the Ca^{2+} ions released from the ER stores into the mitochondrial matrix (see Fig. 14.2).

14.3.1 Ca^{2+} in Acidic Compartments

Besides the ER and mitochondria, acidic compartments also serve as Ca^{2+} stores. This includes lysosomes, LE, multivesicular bodies (MVB), pre-lysosomes, lysosomal-related organelles and secretory vesicles, all with a luminal Ca^{2+}concentration of ~0.5 mM [92, 93].

Although endosomes originate from the plasma membrane, Ca^{2+} is quickly (20 min) released from this compartment, probably through the transient receptor potential cation channel, mucolipin subfamily, member 3 (TRPML3), lowering Ca^{2+} concentrations to 3–40 μM [93–95]. Intriguingly, Ca^{2+} levels in LE are significantly higher (~500 μM) [66, 93, 96]. This implies that acidic compartments must be endowed with engines to store, retain or transfer Ca^{2+} from other sources, for example the cytosol or via membrane contact sites (MCS) with the ER or the plasma membrane (see below). Indeed, earlier work from Berg and coworkers demonstrated the release of Ca^{2+} from lysosomes using glycyl-L-phenylalanine-naphthylamide (GPN) [97]. More recently, GPN was identified to block nicotinic acid adenine dinucleotide phosphate (NAADP)-mediated Ca^{2+} signals, indicating that NAADP mobilizes Ca^{2+} from endosomes [98]. Together with several other studies, these findings established that endolysosomes are engaged in Ca^{2+} dynamics, most probably in concert with other organelles such as the ER (and Golgi). Amongst others, the two-pore channels 1 and 2 (TPC1/2) [99] and TRPML1 [100, 101] have been proposed as the two major candidates to act as Ca^{2+} channels in acidic compartments. It was first suggested that lysosomal acidification drives Ca^{2+} influx into the lysosome [102, 103]. However, more recent studies indicate that lysosomal Ca^{2+} filling requires IP3R-mediated Ca^{2+} release from the ER rather than the vacuolar H^+-ATPase [104]. The putative H^+-/Ca^{2+} -exchanger (CAX) is likely also to support lysosomal Ca^{2+} intake [105–107], although alternatively, Ca^{2+} uptake from the extracellular space via endocytosis cannot be excluded [92, 106] (Fig. 14.3).

Similar to MAMs, MCS between ER and acidic organelles have emerged as an additional mechanism for the exchange of Ca^{2+} and lipids, including sterols [108, 109]. Tether or scaffolding proteins are believed to assist to establish these close encounters. For example, AnxA1/S100A11 complexes seem to act as a tether

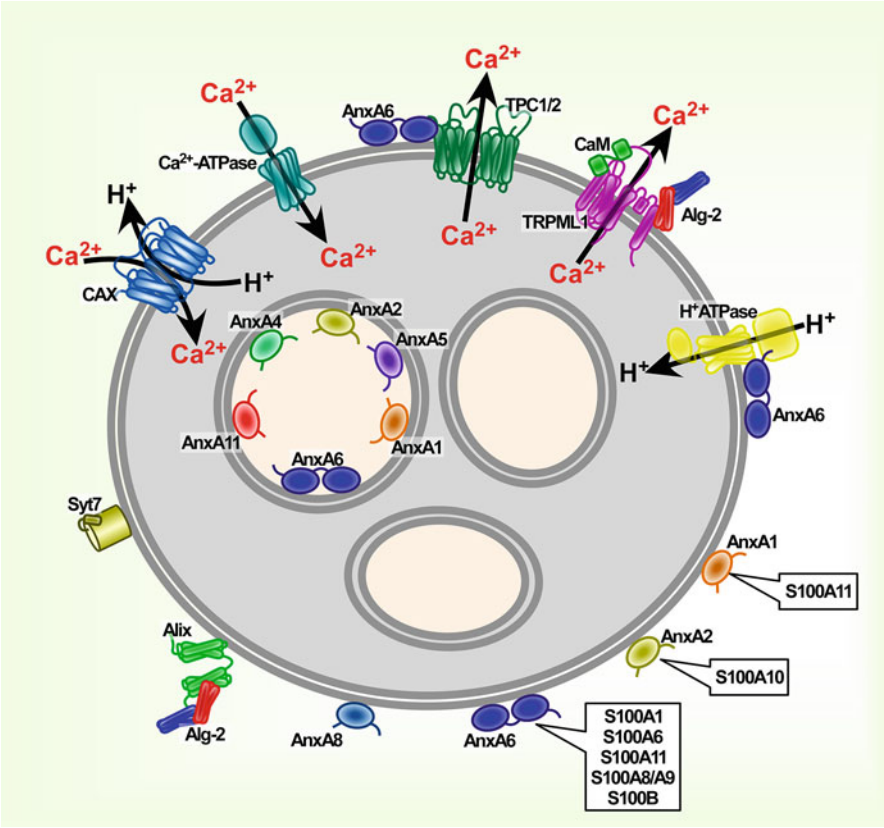

Fig. 14.3 Ca^{2+} and Ca^{2+}-binding proteins in late endosomes. Different families of Ca^{2+}-binding proteins, Ca^{2+} channels and transporters are located at the limiting membrane of late endosomes (LE) and influence Ca-influx and export from LE. In addition, a subset of annexins (Anx) identified in exosomes are depicted inside ILVs. Alg-2, Apoptosis-linked gene-2 product; Alix, Alg-2-interacting protein X; CaM, calmodulin; Syt7, synaptotagmin 7; TRPML1, transient receptor potential mucolipin type 1; TPC1/2, two-pore channel 1/2; CAX, Ca^{2+}/H^{+} exchanger; H^{+}-ATPase subunit VOa2. See text for more details

in MCS that mediate cholesterol transfer from the ER to endosomes [110]. Likewise, the AnxA6 interactome in LE suggests that this annexin might establish MCS together with several proteins engaged in LE positioning and cholesterol transport from LE to the ER (Enrich, Rentero and Grewal, unpublished studies).

Deciphering the spatio-temporal Ca^{2+} signals in subcellular microenvironments that regulate fundamental processes such as lysosomal trafficking and/or LE positioning is central to understand the integrated role of Ca^{2+} signalling. In this context, a plethora of cytosolic Ca^{2+} binding proteins can act as buffers to restrict the spread of a Ca^{2+} signal so it remains local and close to those intracellular stores [67, 68, 74]. Cytosolic buffering can produce ~10 μM to ~100 nM drops in intracellular [Ca^{2+}] over a distance of 30 nm within a few milliseconds [67–69].

Therefore, steep [Ca^{2+}] gradients around entry and release sites result in non-homogeneous activation of Ca^{2+} sensor proteins, enabling a very tight and localized control of Ca^{2+} signalling.

Ca^{2+} released by Ca^{2+} channels then binds and activates a subset of Ca^{2+}-binding proteins, inducing a change in conformation and ultimately, association with effector proteins (Fig. 14.3). In some cases, this is accompanied by a change in subcellular location. Out of the diverse group of Ca^{2+}-binding proteins, the EF-hand members served to develop the paradigm (i.e. CaM) for many Ca^{2+}-mediated effects. However, other Ca^{2+}-binding proteins such as the annexins have now been recognized as promising candidates operating in specialized membrane trafficking pathways, signalling and protein–protein complex formations. For example, annexins actively participate in autophagy, and Ca^{2+} release by lysosomes has been implicated in the autophagy process [35, 111, 112]. Other consequences of this Ca^{2+} release from acidic organelles also involving annexins include membrane repair and lysosomal exocytosis [71, 113]. As one can predict from these diverse activities, the affinity of annexins towards the various interaction partners is likely to vary significantly, and probably critically depends on both phospholipid composition and the local concentration of free Ca^{2+}.

Refilling of lysosomal Ca^{2+} is predominantly regulated through the Ca^{2+} from ER stores [104], but is intimately linked to the pH in this compartment. In fact, an acidic pH is crucial to maintain high levels of Ca^{2+} in the lysosomal lumen, and disruption of lysosomal pH by lysosomotropic agents, such as bafilomycin A1 or chloroquine, prevents Ca^{2+} storage in the lysosomal lumen and arrests the fusion of lysosomes with autophagosomes. One very refined example illustrates the link between Ca^{2+} signalling and the autophagic pathway. Under normal conditions, the transcription factor EB (TFEB) is sequestered in the cytoplasm due to mammalian target of rapamycin complex 1-mediated phosphorylation on the lysosomal surface. Starvation triggers Ca^{2+} release from the lysosome through TRPML1 to establish a Ca^{2+} microdomain in the vicinity of lysosomes. This locally activates the Ca^{2+}-binding protein calcineurin to dephosphorylate TFEB, which then translocates to the nucleus to activate the autophagic pathway [114].

Despite the extensive knowledge on cellular Ca^{2+} homeostasis that has been developed over the years, within the LE/Lys compartment two key unresolved questions still remain less well understood: (1) How does local Ca^{2+} release from acidic stores affect membrane trafficking, endolysosome positioning and dynamics? (2) How do annexins contribute to these processes?

14.3.2 Ca^{2+} and Annexins in the Endo- and Exocytic Pathways

Each annexin is generally found in multiple locations in any given cell, making it difficult to associate endosomal annexins with signalling events and protein–protein

interactions in this compartment. In addition, the transient and reversible nature of the Ca^{2+}-dependent membrane association of annexins complicates investigations aiming to address their scaffolding function in certain cellular sites. Nevertheless, it is mostly believed that a common mechanism of annexins is likely to function as organizers of membrane domains, in order to target their interaction partners to specific membrane microdomains and enable the formation of compartment-specific complexes and activities [1, 3, 4, 6, 115, 116].

Although Ca^{2+}-dependent binding to phospholipids is a fundamental property of annexins, AnxA1, A2, A5 and A6 can all be found in LE/Lys, and can interact with biological membranes in the absence of Ca^{2+} [117–120]. Also, AnxA8 in LE, similar to AnxA2 in other locations, binds to phosphatidylinositol (4,5)-biphosphate (PIP2) and actin in a Ca^{2+}-dependent manner [121, 122]. In addition, we and others demonstrated that LE membrane association of AnxA6 and AnxA2 is sensitive to LE-cholesterol [19, 42, 118, 123–126].

Irrespective of these alternative recruitment mechanisms, a well-established feature of Ca^{2+}, possibly mediated by annexins like AnxA2 and AnxA6, includes its requirement in endo-exocytosis and autophagy. In these settings, Ca^{2+} promotes vesicle fusion by inducing local segregations/re-arrangements of lipids, such as phosphatidic acid or cholesterol [123, 124]. Moreover, several annexins directly associate with merging membranes in the endolysosomal system. AnxA1 is required for early endosome fusion in a Ca^{2+}-dependent manner in vitro [10], and cell culture studies attributed AnxA2, A5 and A6 to bring together early endosomes [126], autophagosomes/lysosomes [112], and LE/lysosomes [115], respectively.

For all these membrane fusion events, local Ca^{2+} is crucial and intracellular Ca^{2+} stores are well integrated in the transduction of signalling. One excellent example for annexins linking Ca^{2+}-homeostasis with lysosomal function is the interactome of TPC1/2 proteins in which several annexins, including AnxA6, were identified [127].

Additional evidence that AnxA6 may function in endolysosomal fusion was obtained by microinjection of cells with a C-terminally truncated and non-functional AnxA6 deletion mutant, which caused the accumulation of fluorescently-labelled LDL in enlarged pre-lysosomal structures, thereby inhibiting LDL degradation [56]. As AnxA6 mediates the association of membranes in vitro, one may envisage that AnxA6, along with other players, acts as one of the tethers that have been visualized between endosomal compartments.

However, in addition to trafficking, fusion or tethering events, certain annexins also participate in the regulation of Ca^{2+} channels [12]. Evidence for annexins in direct ion channel activity is controversial and will not be discussed here, but AnxA2, A4 and A6 are potent modulators of plasma membrane chloride channels and sarcoplasmic reticulum Ca^{2+} release channels [1, 3]. On the other hand, purified AnxA6 dramatically increased the mean open time of the ryanodine-sensitive Ca^{2+} channel in sarcoplasmic membrane preparations [128]. However, the significance of this finding remains unclear because this regulatory effect was exerted from the luminal side of the sarcoplasmic reticulum. Although AnxA6, alike other annexins, is normally located on the membrane leaflet facing the cytosol, its presence in exosomes suggest that AnxA6 can also be found in intraluminal endolysosomal

locations. In fact, exosomes are endowed with a repertoire of annexins such as AnxA2, A5, A1, A6, A11 and A4, being among the 100 most abundant proteins found in exosomes (ExoCarta exosome database: www.exocarta.org) (Fig. 14.3).

Several studies also associated AnxA6 with Ca^{2+} entry at the plasma membrane. Moss and co-workers examined A431 epithelial cells, which lack endogenous AnxA6 [60]. Stable expression of AnxA6 in this cell line blocked the prolonged plasma membrane Ca^{2+} influx induced by epidermal growth factor activation, but not the Ca^{2+} release from intracellular stores [129]. More recently, we identified plasma membrane-associated AnxA6 to reduce store-operated Ca^{2+} entry (SOCE) via STIM, Orai1 and others, by stabilizing the cortical actin cytoskeleton. For these studies, AnxA6 and A1 were fused to the membrane-anchoring sequences of H- and K-Ras, thereby constitutively targeting both annexins to the plasma membrane independent of Ca^{2+} [130]. Similarly, other plasma membrane, ER- and Golgi-targeting sequences have been developed [131] and as shown for Raf-1 [132], the fusion of the 2FYVE domain to fluorescently tagged AnxA1, A2, A6, and A8 could serve as an approach to target annexins to endosomal membranes. Given their low abundance in endosomes, even upon cell stimulation, these approaches will ultimately help to improve our understanding how scaffold/targeting proteins contribute to compartmentalized signalling.

Adding to a general theme of annexins modulating localized Ca^{2+} homeostasis, it should also be mentioned that a subset of AnxA11 colocalizes with Sec31A and Alg-2 at ERES [133]. Physical association of AnxA11 with Sec31A is mediated by dimeric Alg-2 that bridges AnxA11 and Sec31A by functioning as a Ca^{2+}-dependent adaptor. Knockdown of either AnxA11 or Alg-2 accelerated ER-to-Golgi transport [85, 133]. Hence, AnxA11 may function as a Ca^{2+}-dependent membrane anchor to hold COPII vesicles at the ERES until abscission is ready. Additional yet unknown membrane-tethering proteins may also associate with Alg-2 to regulate budding and abscission. At the ER, interactions of AnxA11, but also AnxA7 not only with Alg-2, but also with sorcin, are likely to be relevant for Ca^{2+} homeostasis [134, 135].

14.4 Ca^{2+} Signalling and the Biogenesis, Function and Positioning of Acidic Compartments

Lysosomes, LE and MVB are the best-characterised structures within the acidic compartment. Lysosomes fuse with LE to form endolysosomes, which are considered the major sites of acid hydrolase activity [136]. They are morphologically and functionally heterogeneous, with intraluminal vesicles (ILV), produced by the inward invagination of the limiting membrane during maturation, and/or lamellar membranes. LE/MVBs move towards the perinuclear area, where endocytosed cargos are degraded. Alternatively, a population of MVBs can fuse with the plasma membrane inducing the secretion of ILVs, then called exosomes [137].

Multiple pathways seem to operate on endosomal membranes and give rise to different populations of endolysosomes, lysosomes and LE/MVB [138]. Moreover, diverse ILV subsets, enriched in different lipids, can coexist and form within single MVBs that can be distinguished on the basis of size and mechanism of formation [139–141]. The latter is only partially understood and endosomal-sorting complexes required for transport (ESCRT) is the best-described machinery that drives ILV formation. In this pathway, ILV formation requires ubiquitination and the sequential action of different ESCRT components [142, 143]. Yet ubiquitin and ESCRT-independent pathways, comprising tetraspanins (CD63, CD81) [144–146], ceramide [147], lysobisphosphatidic acid (LBPA) [148] as well as AnxA2 [149, 150] also exist and contribute to those different MVB subpopulations destined for either lysosomal degradation or exosomal release [151].

14.4.1 Intra-Endosomal Trafficking: ILV Back-Fusion in MVBs

ILVs can undergo "back-fusion" with the LE limiting membrane, a route exploited by some pathogens and presumably followed by proteins and lipids that need to be recycled. This process depends on LBPA and Alg-2-interacting protein X (Alix), which selectively contribute to protein and lipid export out of endosomes to destinations other than the lysosomes and perhaps exosomes [147]. However, since vesicle back-fusion with the limiting membrane also depends on the ESCRT-I subunit tumor susceptibility gene 101 (Tsg101), this may well be coupled to the ESCRT machinery [152].

Ca^{2+} also modulates back-fusion. Indeed, cytosolic proteins such as syntenin, Alg-2, Alix or annexins AnxA2, A6, A7 or A11 [153, 154], participate in ILV biogenesis and back-fusion, which raises issues regarding endosomal topology and how cytosolic (and Ca^{2+}-sensitive) proteins can contribute to the endosomal architecture. In fact, not only membrane, but also cytoplasmic proteins can be selectively packaged into ILVs through endosomal microautophagy [155]. Besides ESCRT proteins, microautophagy requires the electrostatic binding of heat shock cognate 71 kDa protein (Hsc70; also known as heat shock 70 kDa protein 8) to endosomal acidic phospholipids. Hsc70, together with Lamp2, interacts and targets cytoplasmic proteins containing KFERQ-motifs into MVBs [156]. Remarkably, nine annexins contain a constitutive canonical motif (AM Cuervo, personal communication) related to this pentapeptide sequence [157, 158]. Moreover, and linking to NPC1 as well as AnxA6-induced inhibition of LE-cholesterol egress, back-fusion of intraluminal vesicles with limiting membranes as well as chaperone-mediated autophagy in LE is dramatically impaired upon LE-cholesterol accumulation [140].

Overall, the evidence of annexins contributing to LE/Lys function is substantial, as they modulate membrane traffic, microdomain organization, interactions with the

cytoskeleton, cholesterol homeostasis, tethering, Ca^{2+} signalling and positioning of acidic compartments. In the following, some examples are given.

The tetraspanins CD63 and CD81 are enriched in internal LE membranes and, like LBPA, unlikely candidates to reside within membranes destined for degradation [141]. Here, AnxA2 coordinates the export of CD63 from LE to Weibel-Palade bodies [159]. This transport route may also require AnxA8 [160], and even extend to mannose-6-phosphate receptor trafficking, which cycles between endosomes and the Golgi, and distributes to intraluminal LE membranes [161]. Other proteins and lipids that transit through LE, including LDL-derived cholesterol, may utilize this ILV back-fusion as an escape route from lysosomes.

The actin/spectrin cytoskeleton that surrounds LE/MVBs could also participate in the back-fusion event. The LE limiting membrane has been considered to assemble actin filaments enabling fusion with neighbouring organelles [162–164]. In this context, AnxA8 on the LE limiting membrane might provide the physical link to the actin cytoskeleton through either direct interaction or the organization of specific membrane/actin attachment sites. Disruption of this interaction, for example by AnxA8 depletion, interferes with the proper localization of LE and, as a consequence, impairs cargo transport through the endocytic pathway [165].

AnxA6 has also been linked to actin and spectrin. We previously proposed a model for AnxA6-spectrin-calpain interactions in the LE compartment during LDL degradation. In this model, LDL binding to cell surface receptors induces Ca^{2+} mobilization, which then binds to CaM (or other Ca^{2+} binding proteins). Both Ca^{2+} elevation as well as LDL-cholesterol induce translocation of cytosolic AnxA6 to LE. In addition, Ca^{2+} increases binding of AnxA6 to spectrin [56]. Finally, in LE/MVBs, Ca^{2+}/CaM binds to spectrin, enhancing its sensitivity towards calpain, which then remodels the surrounding actin/spectrin cytoskeleton to facilitate the fusion to lysosomes and degradation of LDL [reviewed in [35]].

14.4.2 Lysosomal Exocytosis: A Selective Ca^{2+} Pathway

Ca^{2+}-regulated exocytosis of lysosomes is a ubiquitous process, and particularly important for the repair of plasma membrane wounds that is regulated by the Ca^{2+}-sensor synaptotagmin 7 (Syt7) on lysosomes [113, 166]. It was first assumed that the critical step in lysosomal exocytosis was the docking with the plasma membrane, but now the regulation of transport that brings lysosomes to the cell periphery is considered more decisive. In most cells, the majority of the lysosomal population resides in the centrosomal region. Yet, only a subset will be shipped to the cell surface to undergo exocytosis, via microtubule-dependent movement and a complex machinery linking motor-based kinesins with tethering and docking proteins at the plasma membrane. This repositioning of MVB/Lys is tightly regulated and remains elusive, but shares many similarities with exocytosis of synaptic vesicles.

After lysosomes are docked to the plasma membrane by the formation of the vesicle-associated membrane protein 7 (VAMP7)-Stx4-SNAP23 complex, final

fusion is triggered by a localized rise in intracellular Ca^{2+} levels [167, 168]. For lysosomal exocytosis, however, the source of Ca^{2+} and the identity of the Ca^{2+} channel(s) were unknown until recently. In vitro, LE/Lys fusion is inhibited by the Ca^{2+} chelator aminophenoxyethanetetraacetic acid (BAPTA), but not ethyleneglycoltetraacetic acid (EGTA) [138, 169]. Although BAPTA and EGTA display high Ca^{2+}-binding affinities, BAPTA binds Ca^{2+} approximately 100 times faster than EGTA [170]. Therefore, results described above suggested that the source of Ca^{2+} for LE/Lys fusion must be very close to the fusion spot, pointing at lysosomes providing the Ca^{2+} required for lysosomal fusion [171].

Various reports indicate roles for annexins in exocytosis. For example, Ca^{2+}-regulated exocytosis controls the release of hormones, digestive enzymes, immune modulators, neurotransmitters and AnxA11 and possible several other annexins appear important contributing factors [172, 173]. Sjölin et al. first detected AnxA11 fragments in neutrophil-specific granules [174]. AnxA11 was also found associated with insulin granules in a Ca^{2+}-dependent manner by proteomics and biochemical procedures. Although AnxA11 antibodies could not alter insulin release induced by calcyclin (S100A6) [175], other reports suggested that blocking AnxA11 using antibodies can inhibit Ca^{2+}-induced insulin release [176]. In addition, there is growing evidence that AnxA1 regulates hormone exocytosis [177] and AnxA2, together with SNAP23 and S100A10, mediates Ca^{2+}-dependent exocytosis in endothelial cells [178–183].

To study the consequence of differential AnxA6 expression levels in lysosomal exocytosis, we quantified the cellular release and activity of β-hexosaminidase, which is exclusively found in LE/Lys, upon knockdown (CHO-WT siAnxA6) and overexpression of AnxA6 in CHO cells (CHO-A6). Following ionomycin-induced Ca^{2+}-elevation to promote lysosomal exocytosis [184], extracellular β-hexosaminidase activity was significantly increased only with AnxA6 upregulation (Fig. 14.4). This intriguing finding suggests elevated AnxA6 levels to differentially influence exocytosis: (1) via mislocalization of the cholesterol-sensing SNARE proteins Stx4 and SNAP23, which inhibits the secretion of fibronectin [62]; (2) via enhancement of lysosomal exocytosis, most probably through the regulation of local Ca^{2+} release from acidic compartments. The molecular machinery governing these pathways are under investigation, but the dynamics of spatio-temporal formation of protein complexes between AnxA6 and a variety of partners that eventually regulate, directly or indirectly, Ca^{2+} channels seems essential.

One of the potential candidates affected by AnxA6 could be TRPML1, as gain-of-function TRPML1 mutants exhibit enhanced lysosomal exocytosis [185, 186]. Lysosomal exocytosis induced by transcription factor TFEB overexpression requires TRPML1 and fibroblasts from mucolipidosis type IV patients, an autosomal recessive lysosomal storage disorder, exhibit impaired ionomycin-induced lysosomal exocytosis [96, 113]. In primary macrophages, where TRPML1-mediated lysosomal exocytosis is believed to facilitate phagocytosis, treatment with a novel TRPML1 agonist (MS-SA1) induced Lamp1 surface staining and lysosomal enzyme release [187].

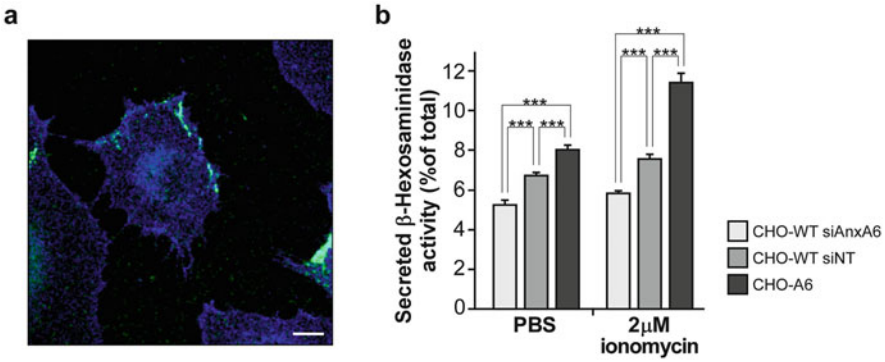

Fig. 14.4 Lysosomal exocytosis is modulated by AnxA6. Ionomycin-induced release of β-hexosaminidase and transport of Lamp1 to the plasma membrane. (**a**) NRK cells were stimulated with 2μM ionomycin and incubated on ice with anti-Lamp1 antibodies without permeabilization. Cells were fixed with paraformaldehyde and labelled with fluorescent secondary antibody (green) and co-stained for cholesterol, using filipin (blue). (**b**) Cells were stimulated with 2μM ionomycin or PBS as negative control for 10 min. Then β-hexosaminidase activity in the medium and cell lysates was determined. The secreted enzyme activity is expressed as a percentage of the total activity. Histogram shows the mean ± SEM of three independent experiments. siNT, non-target siRNA (control)

Finally, in various models to study mechanical damage, a subset of lysosomes are activated by the influx of Ca^{2+} to translocate to the site of damage in order to fuse with the damaged membrane [167, 168]. However, lysosome-mediated repair may not be conserved among all cell types or types of damage [188].

14.4.3 Ca^{2+} and Ca^{2+} Binding Proteins in Membrane Repair

A requisite for the maintenance of cell physiology is the functional integrity of the plasma membrane. However, damage and injury at the plasma membrane is common, especially in mechanically active environments, such as skeletal and cardiac muscle [70, 72]. In addition, epidermal, epithelial and endothelial cells also undergo membrane disruptions [189]. Excitingly, damaged cells seem to be able to repair the cellular lipid bilayer by adding membrane components from intracellular vesicles [71]. The repair system is complex and highly dynamic, with many protein and lipid components, including cholesterol, and involves cytoskeletal reorganization and membrane fusion events. Different mechanisms and models for plasma membrane repair have been described and we refer the reader to recent reviews for further detail [71, 190, 191].

Most relevant in the context of this review, Ca^{2+} is a fundamental component in all of these models. Membrane damage first causes rapid Ca^{2+} entry, which significantly increases intracellular Ca^{2+} concentration at injury sites [71, 190], triggering multiple Ca^{2+} sensors to initiate and promote the repair response. Importantly, while

almost all previous studies focused on extracellular Ca^{2+} injury fluxes, Ca^{2+} release from intracellular stores after injury was identified recently [reviewed in [71]]. Hence, depending on the size and type of injury, extra- and/or intracellular sources of Ca^{2+} may be used to trigger repair processes.

Consistent with Ca^{2+} triggering early responses for plasma membrane repair, a number of Ca^{2+}-binding proteins, including ferlins (with C2 domains), annexins (type II), S100 proteins (EF-hand), and Eps15 Homology Domain families contribute to membrane healing [71, 191–193]. In addition, Alg-2 is now emerging as a crucial component of the cellular repair kit [85]. As outlined above, Alg-2 binds to AnxA7 and AnxA11, Sec31A, ESCRT proteins, and Alix in a Ca^{2+}-dependent manner [135]. How AnxA7 and AnxA11 influence Alg-2 in membrane repair remains to be clarified, but luminal Ca^{2+} release from secretory organelles activates Alg-2, regulating vesicle transport in the secretory pathway [79, 133, 194]. Injury-triggered Ca^{2+} increases lead to Alg-2 dependent assembly of an ESCRT III-Alix-Vacuolar protein sorting-associated protein 4 complex at plasma membrane injury sites, resulting in cleavage and shedding of damaged membranes. Interestingly, Alg-2 requires Ca^{2+} to interact with TRPML1 and one can speculate that de-regulated Alg-2 circuits might contribute to the phenotype of TRPML1 knockout mice, which exhibit muscle repair defects and develop muscular dystrophy [85, 195].

Other proteins also participating in membrane repair include the calpains, a group of Ca^{2+}-dependent cysteine proteases that contain a “C2-like” domain near their N-terminal catalytic regions [196]. Mutations of muscle specific calpain-3 are associated with limb girdle muscular dystrophy type 2A [197]. Furthermore, the ubiquitously expressed calpains-1 and -2 also participate in plasma membrane resealing [198, 199]. Interestingly, a direct link between calpain and dysferlin was reported recently, suggesting that Ca^{2+} sensors may interact with one another in plasma membrane resealing [200].

14.4.3.1 Annexins: Masters in Membrane Repair

The first evidence for annexins contributing to membrane repair came from Lennon’s laboratory demonstrating injury-dependent interaction of AnxA1 and AnxA2 with dysferlin in muscle cells [201]. Based on their known ability to aggregate liposomes, it was proposed that annexins could facilitate plasma membrane repair by aggregating and fusing intracellular vesicles at the sites of injury. Further supporting this model, these annexins are commonly found at the plasma membrane, exhibit broad membrane trafficking roles and coordinate the assembly and organization of the cytoskeleton, another critical component required during the repair process, all of which in a Ca^{2+}-dependent manner. At “resting” cytosolic [Ca^{2+}], annexins are diffusely localized in the cytosol, only to translocate to the plasma membrane and organellar membranes upon cytosolic Ca^{2+} increase [202]. Hence, the association of AnxA1, A2, A4, A5, A6 and A8 with endosomal and secretory vesicles [149, 203–206],

together with their fusogenic properties and lipid preferences make them ideal mediators of resealing.

Despite the physical interaction of AnxA1 with dysferlin, emphasizing AnxA1 association with membrane injury sites [207] as a critical factor in membrane repair, it should also be noted that binding of extracellular AnxA1 to formyl receptors triggers a plethora of anti-inflammatory signalling cascades that substantially contribute to reparative properties of injured epithelium. This extracellular property of AnxA1 will not be discussed here and we refer the reader to recent excellent reviews [208–212].

Besides studies in mouse models and various mammalian cell types, annexins AnxA1, A2, A5, and A6 also localize to the site of muscle membrane repair in zebrafish. This localization at the sarcolemma occurs in a sequential manner with AnxA6 arriving first [188]. Several reports identified AnxA1 and AnxA2 at the site of membrane injury in muscle and various cancer cell lines [213]. Although little is known about the precise function of AnxA1 and AnxA2 in membrane repair, both of these annexins bind dysferlin and may be part of larger membrane repair complexes [188, 201, 214]. Alternatively, in the case of AnxA2, links to the secretory pathway and formation of filamentous (F)-actin may also contribute [215]. Additionally, AnxA2 binds PIP2 and cholesterol with high affinity, making the lipid bilayer at the plasma membrane a target for AnxA2 binding [6]. The Ca^{2+}-dependent binding of AnxA2 to both actin and lipids would then allow for tight control of the repair process. More recently, the influx of Ca^{2+} upon membrane damage was identified as a trigger to recruit AnxA2 to the site of membrane injury, facilitating actin reorganization near the injury lesion [213].

In addition, AnxA1 and A2 may function as diagnostic markers for a number of muscle diseases due to the strong correlation between high expression levels of AnxA1 and A2 and the clinical severity of some muscular dystrophies [216].

In human placenta, which expresses high levels of dysferlin and AnxA5, the repair of human trophoblast membranes is influenced by AnxA5 [71]. For this to occur, AnxA5 is believed to form oligomers and bind phosphatidylserine at the site of damage. This may provide stability to the injury site by reducing the movement of phosphatidylserine-containing membranes, thereby preventing the broken membrane from extending [217]. Interestingly, from these studies it also appears feasible that AnxA5 functions as a molecular repair protein from both the interior and exterior of the cell.

Several recent studies substantiated a critical function for AnxA6 in membrane repair of zebrafish and mouse skeletal muscle. During muscle membrane damage, AnxA6 translocates to the site of injury [188, 218] and supports the forming a "repair cap" structure, which facilitates healing of injured muscle fibers [193]. AnxA6 was also implicated in shedding of microvesicles from the plasma membrane upon treatment with the pore forming protein streptolysin O. Here, AnxA6 was activated and recruited to the site of injury at lower Ca^{2+} concentration compared to AnxA1, revealing a sequential recruitment of annexins for plasma membrane repair [219, 220].

Finally, the recent identification of AnxA2 and S100A11 containing complexes in plasma membrane repair [213] reinforces the contribution of the Ca^{2+}-binding S100 family in this vital cellular function. Besides the large variety of cytoplasmic proteins, S100 proteins represent prominent annexins interaction partners [34]. Their assembly seems to enable the binding of adjacent phospholipid membranes to facilitate membrane fusion [178]. Moreover, some Annexin-S100 complexes such as S100A10 and AnxA2 can bind actin cytoskeleton components and modulate actin dynamics [122, 221]. A similar interaction exists between S100A11 (also called Calgizzarin or S100C) and AnxA1 in a temporal and Ca^{2+}-dependent manner [222]. To this end, several other annexin and S100 binding pairs have been discovered and it appears likely that certain S100 proteins can bind several annexins to exert different biological functions [34, 192].

Taken together, these data emphasize a central role for annexins in the spatiotemporal coordination of membrane repair. These observations might extend to other settings beyond the resealing of membranes, as several annexins, including AnxA4, can protect cells against plasma membrane lesions induced by heat, osmotic stress or treatment with detergents [193]. Likewise, AnxA5 and AnxA6 may also provide protection to membrane permeability [223].

14.4.4 Ca^{2+} and Annexins Regulate Lysosomal Positioning

In recent years, it has become apparent that besides lysosomal exocytosis and membrane repair (see above), many other functions of lysosomes affecting cell adhesion, tumour invasion and metastasis or autophagic degradation are influenced by their positioning and motility [224, 225]. In this last section we will discuss how annexins might regulate lysosomal positioning.

While lysosomes are generally considered as a uniform compartment, there is evidence for both structural [138, 226, 227] and functional heterogeneity [136, 228], even within individual cells. Lysosome positioning, perinuclear versus peripheral, is thought to reflect the dynamic balance between centripetal and centrifugal microtubule motors. These are linked to lysosomal membrane via adapters, which in turn are associated with active GTPases. In brief, ADP-ribosylation factor-like protein 8 (Arl8b) recruits kinesin-1 via its adapter, SKI-interacting protein, pushing lysosomes away from the microtubule-organizing center (MTOC) [229, 230]. The GTPase Rab7, in contrast, has dual effects: similar to Arl8b, it promotes centrifugal motion by associating with kinesins via the FYVE and coiled-coil domain containing 1 protein (FYCO1). In addition, Rab7 also binds the Rab interacting lysosomal protein, which recruits the dynein complex, a minus end-directed motor. The net effect of Rab7 appears to be centripetal, as constitutively active Rab7 causes lysosomes to concentrate around the MTOC while dominant-negative Rab7 disperses lysosomes peripherally [231].

Ca^{2+} efflux from endosomes and lysosomes is thought to be important for signal transduction, organelle homeostasis, and organelle acidification [92, 96, 232]. But

also, lysosomes provide Ca^{2+} for membrane fusion between lysosomes and other compartments, including LEs and the plasma membrane and, the existence of multiple Ca^{2+} sensors may allow lysosomal Ca^{2+} release to regulate distinct steps of lysosomal trafficking [233]. To control these transport systems, numerous Ca^{2+}-binding proteins including annexins have been identified. Depending on the individual interaction partners and microenvironment, the recruitment of these Ca^{2+} binding proteins to the LE membrane most probably involves different strategies. Once bound to LE, one can envisage that Ca^{2+}-bound sensors may increase their association with preassembled SNARE complexes to facilitate lipid bilayer mixing.

Annexins, possibly complexed with S100 proteins, may provide tethering between vesicles and/or links to the cytoskeleton for the repositioning of lysosomes. This probably relies on the Ca^{2+}-dependent and -independent phospholipid and cholesterol binding capability of AnxA1, A2, A6 and A8 to LE membranes, and simultaneously maintaining dynamic interactions with the actin cytoskeleton. However, since annexins do not have a lysosomal targeting motif, their association with the LE/Lys membrane remains unclear. Acidic phospholipids such as phosphatidylserine, phosphatidylcholine, phosphatidylethanolamine, phosphatidic acid or cholesterol and PIP2 are present in LE and represent binding sites for annexins. Moreover, the cytosolic portion of LE/Lys membrane proteins may also, directly or indirectly, associate with annexins. Indeed, proteomic studies demonstrated that AnxA6 directly interacts with abundant ubiquitous transmembrane proteins like the proton pump H^+-ATPase subunit VOa2, [234], the TPC1/2 Ca^{2+} channels [127] or NPC1 [58].

Finally, a different view of the repositioning versus lysosomal functioning is the possibility that under certain physiological situations (i.e. endosome maturation), LE/Lys in the vicinity of the extensive ER network could establish close and functional contacts (MCS) [108, 109]. Extending these observations even further, not only MCS between LE/Lys and the ER, a recent elegant study demonstrated Syt7 to enable the transfer of cholesterol between peroxisomes and LE via MCS [235]. As outlined above (Chap. 14.3.1), the AnxA1-S100A11 complex as well as other annexins might establish MCS with other compartments, which could affect lysosomal positioning [110].

14.5 Concluding Remarks

In this review we have summarized current knowledge and discussed the possible impact of annexins in a variety of processes in the LE/Lys compartment such as membrane traffic, microdomain organization, interactions with cytoskeleton, cholesterol homeostasis, tethering, Ca^{2+} signalling and lysosomal positioning. Our knowledge regarding the way these annexins contribute to LE/Lys function is still incomplete, but seems to require the convergence of localized Ca^{2+} homeostasis in LE/Lys with direct or indirect interactions with LE membrane proteins and lipids to accomplish a variety of cellular processes.

Finally, although not within the scope of this review, disrupted cellular Ca^{2+} signaling is increasingly being associated with several inherited human diseases. In particular lysosomal storage diseases (LSD) represent a group of ≈50 malignancies caused predominantly by mutations in lysosomal proteins. These genetic defects commonly result in the accumulation of macromolecules within the lysosome. The accumulation of cholesterol and other lipids in LE/Lys from patients with mutations in NPC 1/2 genes represents the prototype of these malignancies. Strikingly, NPC1/2 disease is associated with defective lysosomal Ca^{2+} uptake and defective NAADP-mediated lysosomal Ca^{2+} release, which significantly contributes to the accumulation of cholesterol and sphingolipids [66, 92, 187, 236, 237]. In contrast, the Chediak–Higashi Syndrome is characterized by enhanced lysosomal Ca^{2+} uptake [238], whilst the TRPML1 protein is defective in mucolipidosis type IV [185].

Given the involvement of annexins in all of these regulatory circuits, one can envisage that the modulating functions of annexins in LE/Lys function, including the possibility of gene defects, could contribute to disease-related phenotypes observed in some LSD. Advanced methodology in molecular biology, live cell and intravital microscopy, mouse models and patient analysis in future studies will be needed to provide further insights into the function of individual annexins in acidic compartments.

Acknowledgements We would like to thank all members of our laboratories, past and present, for their invaluable contributions and apologize to all those researchers whose work could not be discussed owing to space limitations. C.E. was supported by grants from the Ministerio de Economía y Competitividad (BFU2015–66785-P and CSD2009–00016) and Fundació Marató TV3 (PI042182), Spain. T.G. was supported by the University of Sydney (U7042, U7113, RY253, U3367), Sydney, Australia.

References

1. Gerke V, Creutz CE, Moss SE (2005) Annexins: linking Ca2+ signalling to membrane dynamics. Nat Rev Mol Cell Biol 6(6):449–461. https://doi.org/10.1038/nrm1661
2. Gerke V, Moss SE (1997) Annexins and membrane dynamics. Biochim Biophys Acta 1357 (2):129–154
3. Gerke V, Moss SE (2002) Annexins: from structure to function. Physiol Rev 82(2):331–371. https://doi.org/10.1152/physrev.00030.2001
4. Grewal T, Enrich C (2006) Molecular mechanisms involved in Ras inactivation: the annexin A6-p120GAP complex. Bioessays 28(12):1211–1220. https://doi.org/10.1002/bies.20503
5. Grewal T, Enrich C (2009) Annexins – modulators of EGF receptor signalling and trafficking. Cell Signal 21(6):847–858
6. Hayes MJ, Rescher U, Gerke V, Moss SE (2004) Annexin-actin interactions. Traffic 5 (8):571–576. https://doi.org/10.1111/j.1600-0854.2004.00210.x
7. McNeil AK, Rescher U, Gerke V, McNeil PL (2006) Requirement for annexin A1 in plasma membrane repair. J Biol Chem 281(46):35202–35207. https://doi.org/10.1074/jbc.M606406200

8. Monastyrskaya K, Babiychuk EB, Draeger A (2009a) The annexins: spatial and temporal coordination of signaling events during cellular stress. Cell Mol Life Sci 66(16):2623–2642. https://doi.org/10.1007/s00018-009-0027-1
9. Monastyrskaya K, Babiychuk EB, Hostettler A, Rescher U, Draeger A (2007) Annexins as intracellular calcium sensors. Cell Calcium 41(3):207–219. https://doi.org/10.1016/j.ceca.2006.06.008
10. Raynal P, Pollard HB (1994) Annexins: the problem of assessing the biological role for a gene family of multifunctional calcium- and phospholipid-binding proteins. Biochim Biophys Acta 1197(1):63–93
11. Golczak M, Kicinska A, Bandorowicz-Pikula J, Buchet R, Szewczyk A, Pikula S (2001) Acidic pH-induced folding of annexin VI is a prerequisite for its insertion into lipid bilayers and formation of ion channels by the protein molecules. FASEB J 15(6):1083–1085
12. Hawkins TE, Merrifield CJ, Moss SE (2000) Calcium signaling and annexins. Cell Biochem Biophys 33(3):275–296. https://doi.org/10.1385/CBB:47:1:159
13. Hegde BG, Isas JM, Zampighi G, Haigler HT, Langen R (2006) A novel calcium-independent peripheral membrane-bound form of annexin B12. Biochemistry 45(3):934–942. https://doi.org/10.1021/bi052143+
14. Huber R, Berendes R, Burger A, Schneider M, Karshikov A, Luecke H, Romisch J, Paques E (1992) Crystal and molecular structure of human annexin V after refinement. Implications for structure, membrane binding and ion channel formation of the annexin family of proteins. J Mol Biol 223(3):683–704
15. Isas JM, Cartailler JP, Sokolov Y, Patel DR, Langen R, Luecke H, Hall JE, Haigler HT (2000) Annexins V and XII insert into bilayers at mildly acidic pH and form ion channels. Biochemistry 39(11):3015–3022
16. Kirilenko A, Pikula S, Bandorowicz-Pikula J (2006) Effects of mutagenesis of W343 in human annexin A6 isoform 1 on its interaction with GTP: nucleotide-induced oligomer formation and ion channel activity. Biochemistry 45(15):4965–4973. https://doi.org/10.1021/bi051629n
17. Kourie JI, Wood HB (2000) Biophysical and molecular properties of annexin-formed channels. Prog Biophys Mol Biol 73(2–4):91–134
18. Langen R, Isas JM, Hubbell WL, Haigler HT (1998) A transmembrane form of annexin XII detected by site-directed spin labeling. Proc Natl Acad Sci USA 95(24):14060–14065
19. Enrich C, Rentero C, de Muga SV, Reverter M, Mulay V, Wood P, Koese M, Grewal T (2011) Annexin A6-linking Ca(2+) signaling with cholesterol transport. Biochim Biophys Acta 1813(5):935–947. https://doi.org/10.1016/j.bbamcr.2010.09.015
20. Huber R, Romisch J, Paques EP (1990) The crystal and molecular structure of human annexin V, an anticoagulant protein that binds to calcium and membranes. EMBO J 9(12):3867–3874
21. Lewit-Bentley A, Morera S, Huber R, Bodo G (1992) The effect of metal binding on the structure of annexin V and implications for membrane binding. Eur J Biochem 210(1):73–77
22. Schlaepfer DD, Mehlman T, Burgess WH, Haigler HT (1987) Structural and functional characterization of endonexin II, a calcium- and phospholipid-binding protein. Proc Natl Acad Sci USA 84(17):6078–6082
23. Avila-Sakar AJ, Creutz CE, Kretsinger RH (1998) Crystal structure of bovine annexin VI in a calcium-bound state. Biochim Biophys Acta 1387(1–2):103–116
24. Avila-Sakar AJ, Kretsinger RH, Creutz CE (2000) Membrane-bound 3D structures reveal the intrinsic flexibility of annexin VI. J Struct Biol 130(1):54–62. https://doi.org/10.1006/jsbi.2000.4246
25. Benz J, Bergner A, Hofmann A, Demange P, Gottig P, Liemann S, Huber R, Voges D (1996) The structure of recombinant human annexin VI in crystals and membrane-bound. J Mol Biol 260(5):638–643. https://doi.org/10.1006/jmbi.1996.0426
26. Owens RJ, Crumpton MJ (1984) Isolation and characterization of a novel 68,000-Mr Ca2+-binding protein of lymphocyte plasma membrane. Biochem J 219(1):309–316

27. Rosengarth A, Gerke V, Luecke H (2001) X-ray structure of full-length annexin 1 and implications for membrane aggregation. J Mol Biol 306(3):489–498. https://doi.org/10.1006/jmbi.2000.4423
28. Weng X, Luecke H, Song IS, Kang DS, Kim SH, Huber R (1993) Crystal structure of human annexin I at 2.5 A resolution. Protein Sci 2(3):448–458. https://doi.org/10.1002/pro.5560020317
29. Rosengarth A, Luecke H (2004) Annexins: calcium binding proteins with unusual binding sites. In: Messerschmidt A, Bode W, Cygler M (eds) Handbook of Metalloproteins, vol 3. Wiley, Chichester, pp 649–663
30. Swairjo MA, Concha NO, Kaetzel MA, Dedman JR, Seaton BA (1995) Ca(2+)-bridging mechanism and phospholipid head group recognition in the membrane-binding protein annexin V. Nat Struct Biol 2(11):968–974
31. Herzberg O, James MN (1985) Structure of the calcium regulatory muscle protein troponin-C at 2.8 A resolution. Nature 313(6004):653–659
32. Nelson MR, Chazin WJ (1998) Structures of EF-hand Ca(2+)-binding proteins: diversity in the organization, packing and response to Ca2+ binding. Biometals 11(4):297–318
33. Maler L, Sastry M, Chazin WJ (2002) A structural basis for S100 protein specificity derived from comparative analysis of apo and Ca(2+)-calcyclin. J Mol Biol 317(2):279–290. https://doi.org/10.1006/jmbi.2002.5421
34. Rintala-Dempsey AC, Rezvanpour A, Shaw GS (2008) S100-annexin complexes – structural insights. FEBS J 275(20):4956–4966. https://doi.org/10.1111/j.1742-4658.2008.06654.x
35. Enrich C, Rentero C, Grewal T (2016) Annexin A6 in the liver: from the endocytic compartment to cellular physiology. Biochim Biophys Acta 1864(6):933–946. https://doi.org/10.1016/j.bbamcr.2016.10.017
36. Geisow MJ, Fritsche U, Hexham JM, Dash B, Johnson T (1986) A consensus amino-acid sequence repeat in Torpedo and mammalian Ca2+-dependent membrane-binding proteins. Nature 320(6063):636–638. https://doi.org/10.1038/320636a0
37. Lizarbe MA, Barrasa JI, Olmo N, Gavilanes F, Turnay J (2013) Annexin-phospholipid interactions. Functional implications. Int J Mol Sci 14(2):2652–2683. https://doi.org/10.3390/ijms14022652
38. Buzhynskyy N, Golczak M, Lai-Kee-Him J, Lambert O, Tessier B, Gounou C, Berat R, Simon A, Granier T, Chevalier JM, Mazeres S, Bandorowicz-Pikula J, Pikula S, Brisson AR (2009) Annexin-A6 presents two modes of association with phospholipid membranes. A combined QCM-D, AFM and cryo-TEM study. J Struct Biol 168(1):107–116. https://doi.org/10.1016/j.jsb.2009.03.007
39. Edwards HC, Crumpton MJ (1991) Ca(2+)-dependent phospholipid and arachidonic acid binding by the placental annexins VI and IV. Eur J Biochem 198(1):121–129
40. Kobayashi T, Beuchat MH, Chevallier J, Makino A, Mayran N, Escola JM, Lebrand C, Cosson P, Kobayashi T, Gruenberg J (2002) Separation and characterization of late endosomal membrane domains. J Biol Chem 277(35):32157–32164. https://doi.org/10.1074/jbc.M202838200
41. Tharkeshwar AK, Trekker J, Vermeire W, Pauwels J, Sannerud R, Priestman DA, Te Vruchte D, Vints K, Baatsen P, Decuypere JP, Lu H, Martin S, Vangheluwe P, Swinnen JV, Lagae L, Impens F, Platt FM, Gevaert K, Annaert W (2017) A novel approach to analyze lysosomal dysfunctions through subcellular proteomics and lipidomics: the case of NPC1 deficiency. Sci Rep 7:41408. https://doi.org/10.1038/srep41408
42. de Diego I, Schwartz F, Siegfried H, Dauterstedt P, Heeren J, Beisiegel U, Enrich C, Grewal T (2002) Cholesterol modulates the membrane binding and intracellular distribution of annexin 6. J Biol Chem 277(35):32187–32194. https://doi.org/10.1074/jbc.M205499200
43. Domon MM, Matar G, Strzelecka-Kiliszek A, Bandorowicz-Pikula J, Pikula S, Besson F (2010) Interaction of annexin A6 with cholesterol rich membranes is pH-dependent and mediated by the sterol OH. J Colloid Interface Sci 346(2):436–441. https://doi.org/10.1016/j.jcis.2010.03.015

44. Garver WS, Xie C, Repa JJ, Turley SD, Dietschy JM (2005) Niemann-Pick C1 expression is not regulated by the amount of cholesterol flowing through cells in the mouse. J Lipid Res 46 (8):1745–1754. https://doi.org/10.1194/jlr.M500130-JLR200
45. Golczak M, Kirilenko A, Bandorowicz-Pikula J, Desbat B, Pikula S (2004) Structure of human annexin a6 at the air-water interface and in a membrane-bound state. Biophys J 87 (2):1215–1226. https://doi.org/10.1529/biophysj.103.038240
46. Grewal T, Heeren J, Mewawala D, Schnitgerhans T, Wendt D, Salomon G, Enrich C, Beisiegel U, Jackle S (2000) Annexin VI stimulates endocytosis and is involved in the trafficking of low density lipoprotein to the prelysosomal compartment. J Biol Chem 275 (43):33806–33813. https://doi.org/10.1074/jbc.M002662200
47. Grewal T, Koese M, Rentero C, Enrich C (2010) Annexin A6-regulator of the EGFR/Ras signalling pathway and cholesterol homeostasis. Int J Biochem Cell Biol 42(5):580–584. https://doi.org/10.1016/j.biocel.2009.12.020
48. Hansen CG, Nichols BJ (2010) Exploring the caves: cavins, caveolins and caveolae. Trends Cell Biol 20(4):177–186. https://doi.org/10.1016/j.tcb.2010.01.005
49. Jackle S, Beisiegel U, Rinninger F, Buck F, Grigoleit A, Block A, Groger I, Greten H, Windler E (1994) Annexin VI, a marker protein of hepatocytic endosomes. J Biol Chem 269 (2):1026–1032
50. Pol A, Ortega D, Enrich C (1997) Identification of cytoskeleton-associated proteins in isolated rat liver endosomes. Biochem J 327(Pt 3):741–746
51. Sprenger RR, Speijer D, Back JW, De Koster CG, Pannekoek H, Horrevoets AJ (2004) Comparative proteomics of human endothelial cell caveolae and rafts using two-dimensional gel electrophoresis and mass spectrometry. Electrophoresis 25(1):156–172. https://doi.org/10.1002/elps.200305675
52. Sztolsztener ME, Strzelecka-Kiliszek A, Pikula S, Tylki-Szymanska A, Bandorowicz-Pikula J (2010) Cholesterol as a factor regulating intracellular localization of annexin A6 in Niemann-Pick type C human skin fibroblasts. Arch Biochem Biophys 493(2):221–233. https://doi.org/10.1016/j.abb.2009.11.001
53. Alvarez-Guaita A, Vilà de Muga S, Owen DM, Williamson D, Magenau A, Garcia-Melero A, Reverter M, Hoque M, Cairns R, Cornely R, Tebar F, Grewal T, Gaus K, Ayala-Sanmartin J, Enrich C, Rentero C (2015) Evidence for annexin A6-dependent plasma membrane remodelling of lipid domains. Br J Pharmacol 172(7):1677–1690. https://doi.org/10.1111/bph.13022
54. Cornely R, Pollock AH, Rentero C, Norris SE, Alvarez-Guaita A, Grewal T, Mitchell T, Enrich C, Moss SE, Parton RG, Rossy J, Gaus K (2016) Annexin A6 regulates interleukin-2-mediated T-cell proliferation. Immunol Cell Biol 94(6):543–553. https://doi.org/10.1038/icb.2016.15
55. Cornely R, Rentero C, Enrich C, Grewal T, Gaus K (2011) Annexin A6 is an organizer of membrane microdomains to regulate receptor localization and signalling. IUBMB Life 63 (11):1009–1017. https://doi.org/10.1002/iub.540
56. Pons M, Grewal T, Rius E, Schnitgerhans T, Jackle S, Enrich C (2001) Evidence for the involvement of annexin 6 in the trafficking between the endocytic compartment and lysosomes. Exp Cell Res 269(1):13–22. https://doi.org/10.1006/excr.2001.5268
57. Pons M, Ihrke G, Koch S, Biermer M, Pol A, Grewal T, Jackle S, Enrich C (2000) Late endocytic compartments are major sites of annexin VI localization in NRK fibroblasts and polarized WIF-B hepatoma cells. Exp Cell Res 257(1):33–47. https://doi.org/10.1006/excr.2000.4861
58. Cubells L, Vilà de Muga S, Tebar F, Wood P, Evans R, Ingelmo-Torres M, Calvo M, Gaus K, Pol A, Grewal T, Enrich C (2007) Annexin A6-induced alterations in cholesterol transport and caveolin export from the Golgi complex. Traffic 8(11):1568–1589. https://doi.org/10.1111/j.1600-0854.2007.00640.x

59. Grewal T, Evans R, Rentero C, Tebar F, Cubells L, de Diego I, Kirchhoff MF, Hughes WE, Heeren J, Rye KA, Rinninger F, Daly RJ, Pol A, Enrich C (2005) Annexin A6 stimulates the membrane recruitment of p120GAP to modulate Ras and Raf-1 activity. Oncogene 24 (38):5809–5820. https://doi.org/10.1038/sj.onc.1208743
60. Smythe E, Smith PD, Jacob SM, Theobald J, Moss SE (1994) Endocytosis occurs independently of annexin VI in human A431 cells. J Cell Biol 124(3):301–306
61. Cubells L, Vilà de Muga S, Tebar F, Bonventre JV, Balsinde J, Pol A, Grewal T, Enrich C (2008) Annexin A6-induced inhibition of cytoplasmic phospholipase A2 is linked to caveolin-1 export from the Golgi. J Biol Chem 283(15):10174–10183. https://doi.org/10.1074/jbc.M706618200
62. Reverter M, Rentero C, de Muga SV, Alvarez-Guaita A, Mulay V, Cairns R, Wood P, Monastyrskaya K, Pol A, Tebar F, Blasi J, Grewal T, Enrich C (2011) Cholesterol transport from late endosomes to the Golgi regulates t-SNARE trafficking, assembly, and function. Mol Biol Cell 22(21):4108–4123. https://doi.org/10.1091/mbc.E11-04-0332
63. Garcia-Melero A, Reverter M, Hoque M, Meneses-Salas E, Koese M, Conway JR, Johnsen CH, Alvarez-Guaita A, Morales-Paytuvi F, Elmaghrabi YA, Pol A, Tebar F, Murray RZ, Timpson P, Enrich C, Grewal T, Rentero C (2016) Annexin A6 and late endosomal cholesterol modulate integrin recycling and cell migration. J Biol Chem 291(3):1320–1335. https://doi.org/10.1074/jbc.M115.683557
64. Reverter M, Rentero C, Garcia-Melero A, Hoque M, Vilà de Muga S, Alvarez-Guaita A, Conway JR, Wood P, Cairns R, Lykopoulou L, Grinberg D, Vilageliu L, Bosch M, Heeren J, Blasi J, Timpson P, Pol A, Tebar F, Murray RZ, Grewal T, Enrich C (2014) Cholesterol regulates Syntaxin 6 trafficking at trans-Golgi network endosomal boundaries. Cell Rep 7 (3):883–897. https://doi.org/10.1016/j.celrep.2014.03.043
65. Hoque M, Rentero C, Conway JR, Murray RZ, Timpson P, Enrich C, Grewal T (2015) The cross-talk of LDL-cholesterol with cell motility: insights from the Niemann Pick Type C1 mutation and altered integrin trafficking. Cell Adh Migr 9(5):384–391. https://doi.org/10.1080/19336918.2015.1019996
66. Lloyd-Evans E, Morgan AJ, He X, Smith DA, Elliot-Smith E, Sillence DJ, Churchill GC, Schuchman EH, Galione A, Platt FM (2008) Niemann-Pick disease type C1 is a sphingosine storage disease that causes deregulation of lysosomal calcium. Nat Med 14(11):1247–1255. https://doi.org/10.1038/nm.1876
67. Berridge MJ, Bootman MD, Roderick HL (2003) Calcium signalling: dynamics, homeostasis and remodelling. Nat Rev Mol Cell Biol 4(7):517–529. https://doi.org/10.1038/nrm1155
68. Clapham DE (2007) Calcium signaling. Cell 131(6):1047–1058. https://doi.org/10.1016/j.cell.2007.11.028
69. Xu H, Martinoia E, Szabo I (2015) Organellar channels and transporters. Cell Calcium 58 (1):1–10. https://doi.org/10.1016/j.ceca.2015.02.006
70. Andrews NW, Almeida PE, Corrotte M (2014) Damage control: cellular mechanisms of plasma membrane repair. Trends Cell Biol 24(12):734–742. https://doi.org/10.1016/j.tcb.2014.07.008
71. Cheng X, Zhang X, Yu L, Xu H (2015) Calcium signaling in membrane repair. Semin Cell Dev Biol 45:24–31. https://doi.org/10.1016/j.semcdb.2015.10.031
72. McNeil PL, Kirchhausen T (2005) An emergency response team for membrane repair. Nat Rev Mol Cell Biol 6(6):499–505. https://doi.org/10.1038/nrm1665
73. Prins D, Michalak M (2011) Organellar calcium buffers. Cold Spring Harb Perspect Biol 3(3). https://doi.org/10.1101/cshperspect.a004069
74. Krebs J, Agellon LB, Michalak M (2015) Ca(2+) homeostasis and endoplasmic reticulum (ER) stress: an integrated view of calcium signaling. Biochem Biophys Res Commun 460 (1):114–121. https://doi.org/10.1016/j.bbrc.2015.02.004
75. Strehler EE, Treiman M (2004) Calcium pumps of plasma membrane and cell interior. Curr Mol Med 4(3):323–335

76. Fill M, Copello JA (2002) Ryanodine receptor calcium release channels. Physiol Rev 82 (4):893–922. https://doi.org/10.1152/physrev.00013.2002
77. Lam AK, Galione A (2013) The endoplasmic reticulum and junctional membrane communication during calcium signaling. Biochim Biophys Acta 1833(11):2542–2559. https://doi.org/10.1016/j.bbamcr.2013.06.004
78. Missiaen L, Van Acker K, Van Baelen K, Raeymaekers L, Wuytack F, Parys JB, De Smedt H, Vanoevelen J, Dode L, Rizzuto R, Callewaert G (2004) Calcium release from the Golgi apparatus and the endoplasmic reticulum in HeLa cells stably expressing targeted aequorin to these compartments. Cell Calcium 36(6):479–487. https://doi.org/10.1016/j.ceca.2004.04.007
79. Bentley M, Nycz DC, Joglekar A, Fertschai I, Malli R, Graier WF, Hay JC (2010) Vesicular calcium regulates coat retention, fusogenicity, and size of pre-Golgi intermediates. Mol Biol Cell 21(6):1033–1046. https://doi.org/10.1091/mbc.E09-10-0914
80. Dolman NJ, Tepikin AV (2006) Calcium gradients and the Golgi. Cell Calcium 40 (5–6):505–512. https://doi.org/10.1016/j.ceca.2006.08.012
81. Pizzo P, Lissandron V, Capitanio P, Pozzan T (2011) Ca(2+) signalling in the Golgi apparatus. Cell Calcium 50(2):184–192. https://doi.org/10.1016/j.ceca.2011.01.006
82. Yang Z, Kirton HM, MacDougall DA, Boyle JP, Deuchars J, Frater B, Ponnambalam S, Hardy ME, White E, Calaghan SC, Peers C, Steele DS (2015) The Golgi apparatus is a functionally distinct Ca2+ store regulated by the PKA and Epac branches of the beta1-adrenergic signaling pathway. Sci Signal 8(398):ra101. https://doi.org/10.1126/scisignal.aaa7677
83. Mayinger P (2009) Regulation of Golgi function via phosphoinositide lipids. Semin Cell Dev Biol 20(7):793–800. https://doi.org/10.1016/j.semcdb.2009.03.016
84. Jha A, Ahuja M, Patel S, Brailoiu E, Muallem S (2014) Convergent regulation of the lysosomal two-pore channel-2 by Mg(2)(+), NAADP, PI(3,5)P(2) and multiple protein kinases. EMBO J 33(5):501–511. https://doi.org/10.1002/embj.201387035
85. Maki M, Takahara T, Shibata H (2016) Multifaceted roles of ALG-2 in Ca(2+)-regulated membrane trafficking. Int J Mol Sci 17(9). https://doi.org/10.3390/ijms17091401
86. Yamasaki A, Tani K, Yamamoto A, Kitamura N, Komada M (2006) The Ca2+-binding protein ALG-2 is recruited to endoplasmic reticulum exit sites by Sec31A and stabilizes the localization of Sec31A. Mol Biol Cell 17(11):4876–4887. https://doi.org/10.1091/mbc.E06-05-0444
87. La Rovere RM, Roest G, Bultynck G, Parys JB (2016) Intracellular Ca(2+) signaling and Ca(2+) microdomains in the control of cell survival, apoptosis and autophagy. Cell Calcium 60 (2):74–87. https://doi.org/10.1016/j.ceca.2016.04.005
88. Csordas G, Thomas AP, Hajnoczky G (1999) Quasi-synaptic calcium signal transmission between endoplasmic reticulum and mitochondria. EMBO J 18(1):96–108. https://doi.org/10.1093/emboj/18.1.96
89. Rizzuto R, Brini M, Murgia M, Pozzan T (1993) Microdomains with high Ca2+ close to IP3-sensitive channels that are sensed by neighboring mitochondria. Science 262 (5134):744–747
90. Giorgi C, Missiroli S, Patergnani S, Duszynski J, Wieckowski MR, Pinton P (2015) Mitochondria-associated membranes: composition, molecular mechanisms, and physiopathological implications. Antioxid Redox Signal 22(12):995–1019. https://doi.org/10.1089/ars.2014.6223
91. Sala-Vila A, Navarro-Lerida I, Sanchez-Alvarez M, Bosch M, Calvo C, Lopez JA, Calvo E, Ferguson C, Giacomello M, Serafini A, Scorrano L, Enriquez JA, Balsinde J, Parton RG, Vazquez J, Pol A, Del Pozo MA (2016) Interplay between hepatic mitochondria-associated membranes, lipid metabolism and caveolin-1 in mice. Sci Rep 6:27351. https://doi.org/10.1038/srep27351
92. Morgan AJ, Platt FM, Lloyd-Evans E, Galione A (2011) Molecular mechanisms of endolysosomal Ca2+ signalling in health and disease. Biochem J 439(3):349–374. https://doi.org/10.1042/BJ20110949

93. Patel S, Docampo R (2010) Acidic calcium stores open for business: expanding the potential for intracellular Ca2+ signaling. Trends Cell Biol 20(5):277–286. https://doi.org/10.1016/j.tcb.2010.02.003
94. Gerasimenko JV, Tepikin AV, Petersen OH, Gerasimenko OV (1998) Calcium uptake via endocytosis with rapid release from acidifying endosomes. Curr Biol 8(24):1335–1338
95. Yamaguchi S, Jha A, Li Q, Soyombo AA, Dickinson GD, Churamani D, Brailoiu E, Patel S, Muallem S (2011) Transient receptor potential mucolipin 1 (TRPML1) and two-pore channels are functionally independent organellar ion channels. J Biol Chem 286(26):22934–22942. https://doi.org/10.1074/jbc.M110.210930
96. Xu H, Ren D (2015) Lysosomal physiology. Annu Rev Physiol 77:57–80. https://doi.org/10.1146/annurev-physiol-021014-071649
97. Berg TO, Stromhaug E, Lovdal T, Seglen O, Berg T (1994) Use of glycyl-L-phenylalanine 2-naphthylamide, a lysosome-disrupting cathepsin C substrate, to distinguish between lysosomes and prelysosomal endocytic vacuoles. Biochem J 300(Pt 1):229–236
98. Menteyne A, Burdakov A, Charpentier G, Petersen OH, Cancela JM (2006) Generation of specific Ca(2+) signals from Ca(2+) stores and endocytosis by differential coupling to messengers. Curr Biol 16(19):1931–1937. https://doi.org/10.1016/j.cub.2006.07.070
99. Grimm C, Hassan S, Wahl-Schott C, Biel M (2012) Role of TRPML and two-pore channels in endolysosomal cation homeostasis. J Pharmacol Exp Ther 342(2):236–244. https://doi.org/10.1124/jpet.112.192880
100. Cheng X, Shen D, Samie M, Xu H (2010) Mucolipins: intracellular TRPML1-3 channels. FEBS Lett 584(10):2013–2021. https://doi.org/10.1016/j.febslet.2009.12.056
101. Dong XP, Shen D, Wang X, Dawson T, Li X, Zhang Q, Cheng X, Zhang Y, Weisman LS, Delling M, Xu H (2010) PI(3,5)P(2) controls membrane trafficking by direct activation of mucolipin Ca(2+) release channels in the endolysosome. Nat Commun 1:38. https://doi.org/10.1038/ncomms1037
102. Calcraft PJ, Ruas M, Pan Z, Cheng X, Arredouani A, Hao X, Tang J, Rietdorf K, Teboul L, Chuang KT, Lin P, Xiao R, Wang C, Zhu Y, Lin Y, Wyatt CN, Parrington J, Ma J, Evans AM, Galione A, Zhu MX (2009) NAADP mobilizes calcium from acidic organelles through two-pore channels. Nature 459(7246):596–600. https://doi.org/10.1038/nature08030
103. Christensen KA, Myers JT, Swanson JA (2002) pH-dependent regulation of lysosomal calcium in macrophages. J Cell Sci 115(Pt 3):599–607
104. Garrity AG, Wang W, Collier CM, Levey SA, Gao Q, Xu H (2016) The endoplasmic reticulum, not the pH gradient, drives calcium refilling of lysosomes. Elife 5. https://doi.org/10.7554/eLife.15887
105. Brailoiu GC, Brailoiu E (2016) Modulation of calcium entry by the endo-lysosomal system. Adv Exp Med Biol 898:423–447. https://doi.org/10.1007/978-3-319-26974-0_18
106. Li X, Garrity AG, Xu H (2013) Regulation of membrane trafficking by signalling on endosomal and lysosomal membranes. J Physiol 591(18):4389–4401. https://doi.org/10.1113/jphysiol.2013.258301
107. Melchionda M, Pittman JK, Mayor R, Patel S (2016) Ca2+/H+ exchange by acidic organelles regulates cell migration in vivo. J Cell Biol 212(7):803–813. https://doi.org/10.1083/jcb.201510019
108. Burgoyne T, Patel S, Eden ER (2015) Calcium signaling at ER membrane contact sites. Biochim Biophys Acta 1853(9):2012–2017. https://doi.org/10.1016/j.bbamcr.2015.01.022
109. Eden ER (2016) The formation and function of ER-endosome membrane contact sites. Biochim Biophys Acta 1861(8 Pt B):874–879. https://doi.org/10.1016/j.bbalip.2016.01.020
110. Eden ER, Sanchez-Heras E, Tsapara A, Sobota A, Levine TP, Futter CE (2016) Annexin A1 tethers membrane contact sites that mediate ER to endosome cholesterol transport. Dev Cell 37(5):473–483. https://doi.org/10.1016/j.devcel.2016.05.005
111. Ghislat G, Aguado C, Knecht E (2012) Annexin A5 stimulates autophagy and inhibits endocytosis. J Cell Sci 125(Pt 1):92–107. https://doi.org/10.1242/jcs.086728

112. Ghislat G, Knecht E (2012) New Ca(2+)-dependent regulators of autophagosome maturation. Commun Integr Biol 5(4):308–311. https://doi.org/10.4161/cib.20076
113. Samie MA, Xu H (2014) Lysosomal exocytosis and lipid storage disorders. J Lipid Res 55 (6):995–1009. https://doi.org/10.1194/jlr.R046896
114. Medina DL, Di Paola S, Peluso I, Armani A, De Stefani D, Venditti R, Montefusco S, Scotto-Rosato A, Prezioso C, Forrester A, Settembre C, Wang W, Gao Q, Xu H, Sandri M, Rizzuto R, De Matteis MA, Ballabio A (2015) Lysosomal calcium signalling regulates autophagy through calcineurin and TFEB. Nat Cell Biol 17(3):288–299. https://doi.org/10.1038/ncb3114
115. Futter CE, White IJ (2007) Annexins and endocytosis. Traffic 8(8):951–958. https://doi.org/10.1111/j.1600-0854.2007.00590.x
116. Rescher U, Gerke V (2004) Annexins – unique membrane binding proteins with diverse functions. J Cell Sci 117(Pt 13):2631–2639. https://doi.org/10.1242/jcs.01245
117. Futter CE, Felder S, Schlessinger J, Ullrich A, Hopkins CR (1993) Annexin I is phosphorylated in the multivesicular body during the processing of the epidermal growth factor receptor. J Cell Biol 120(1):77–83
118. Harder T, Kellner R, Parton RG, Gruenberg J (1997) Specific release of membrane-bound annexin II and cortical cytoskeletal elements by sequestration of membrane cholesterol. Mol Biol Cell 8(3):533–545
119. Liu L, Tao JQ, Zimmerman UJ (1997) Annexin II binds to the membrane of A549 cells in a calcium-dependent and calcium-independent manner. Cell Signal 9(3–4):299–304
120. Trotter PJ, Orchard MA, Walker JH (1995) EGTA-resistant binding of annexin V to platelet membranes can be induced by physiological calcium concentrations. Biochem Soc Trans 23 (1):37S
121. Goebeler V, Ruhe D, Gerke V, Rescher U (2006) Annexin A8 displays unique phospholipid and F-actin binding properties. FEBS Lett 580(10):2430–2434. https://doi.org/10.1016/j.febslet.2006.03.076
122. Rescher U, Ruhe D, Ludwig C, Zobiack N, Gerke V (2004) Annexin 2 is a phosphatidylinositol (4,5)-bisphosphate binding protein recruited to actin assembly sites at cellular membranes. J Cell Sci 117(Pt 16):3473–3480. https://doi.org/10.1242/jcs.01208
123. Ayala-Sanmartin J (2001) Cholesterol enhances phospholipid binding and aggregation of annexins by their core domain. Biochem Biophys Res Commun 283(1):72–79. https://doi.org/10.1006/bbrc.2001.4748
124. Ayala-Sanmartin J, Henry JP, Pradel LA (2001) Cholesterol regulates membrane binding and aggregation by annexin 2 at submicromolar Ca(2+) concentration. Biochim Biophys Acta 1510(1–2):18–28
125. Domon MM, Besson F, Tylki-Szymanska A, Bandorowicz-Pikula J, Pikula S (2013) Interaction of AnxA6 with isolated and artificial lipid microdomains; importance of lipid composition and calcium content. Mol Biosyst 9(4):668–676. https://doi.org/10.1039/c3mb25487a
126. Emans N, Gorvel JP, Walter C, Gerke V, Kellner R, Griffiths G, Gruenberg J (1993) Annexin II is a major component of fusogenic endosomal vesicles. J Cell Biol 120(6):1357–1369
127. Lin-Moshier Y, Keebler MV, Hooper R, Boulware MJ, Liu X, Churamani D, Abood ME, Walseth TF, Brailoiu E, Patel S, Marchant JS (2014) The two-pore channel (TPC) interactome unmasks isoform-specific roles for TPCs in endolysosomal morphology and cell pigmentation. Proc Natl Acad Sci USA 111(36):13087–13092. https://doi.org/10.1073/pnas.1407004111
128. Diaz-Munoz M, Hamilton SL, Kaetzel MA, Hazarika P, Dedman JR (1990) Modulation of Ca2+ release channel activity from sarcoplasmic reticulum by annexin VI (67-kDa calcimedin). J Biol Chem 265(26):15894–15899
129. Fleet A, Ashworth R, Kubista H, Edwards H, Bolsover S, Mobbs P, Moss SE (1999) Inhibition of EGF-dependent calcium influx by annexin VI is splice form-specific. Biochem Biophys Res Commun 260(2):540–546. https://doi.org/10.1006/bbrc.1999.0915

130. Monastyrskaya K, Babiychuk EB, Hostettler A, Wood P, Grewal T, Draeger A (2009b) Plasma membrane-associated annexin A6 reduces Ca2+ entry by stabilizing the cortical actin cytoskeleton. J Biol Chem 284(25):17227–17242. https://doi.org/10.1074/jbc.M109.004457
131. Matallanas D, Sanz-Moreno V, Arozarena I, Calvo F, Agudo-Ibanez L, Santos E, Berciano MT, Crespo P (2006) Distinct utilization of effectors and biological outcomes resulting from site-specific Ras activation: Ras functions in lipid rafts and Golgi complex are dispensable for proliferation and transformation. Mol Cell Biol 26(1):100–116. https://doi.org/10.1128/MCB.26.1.100-116.2006
132. Tebar F, Gelabert-Baldrich M, Hoque M, Cairns R, Rentero C, Pol A, Grewal T, Enrich C (2014) Annexins and endosomal signaling. Methods Enzymol 535:55–74. https://doi.org/10.1016/B978-0-12-397925-4.00004-3
133. Shibata H, Kanadome T, Sugiura H, Yokoyama T, Yamamuro M, Moss SE, Maki M (2015) A new role for annexin A11 in the early secretory pathway via stabilizing Sec31A protein at the endoplasmic reticulum exit sites (ERES). J Biol Chem 290(8):4981–4993. https://doi.org/10.1074/jbc.M114.592089
134. Maki M, Kitaura Y, Satoh H, Ohkouchi S, Shibata H (2002) Structures, functions and molecular evolution of the penta-EF-hand Ca^{2+}-binding proteins. Biochim Biophys Acta 1600(1–2):51–60
135. Satoh H, Nakano Y, Shibata H, Maki M (2002) The penta-EF-hand domain of ALG-2 interacts with amino-terminal domains of both annexin VII and annexin XI in a Ca2+-dependent manner. Biochim Biophys Acta 1600(1–2):61–67
136. Wartosch L, Bright NA, Luzio JP (2015) Lysosomes. Curr Biol 25(8):R315–R316. https://doi.org/10.1016/j.cub.2015.02.027
137. Mittelbrunn M, Sanchez-Madrid F (2012) Intercellular communication: diverse structures for exchange of genetic information. Nat Rev Mol Cell Biol 13(5):328–335. https://doi.org/10.1038/nrm3335
138. Luzio JP, Pryor PR, Bright NA (2007b) Lysosomes: fusion and function. Nat Rev Mol Cell Biol 8(8):622–632. https://doi.org/10.1038/nrm2217
139. Falguieres T, Luyet PP, Gruenberg J (2009) Molecular assemblies and membrane domains in multivesicular endosome dynamics. Exp Cell Res 315(9):1567–1573. https://doi.org/10.1016/j.yexcr.2008.12.006
140. Sobo K, Le Blanc I, Luyet PP, Fivaz M, Ferguson C, Parton RG, Gruenberg J, van der Goot FG (2007) Late endosomal cholesterol accumulation leads to impaired intra-endosomal trafficking. PLoS One 2(9):e851. https://doi.org/10.1371/journal.pone.0000851
141. van der Goot FG, Gruenberg J (2006) Intra-endosomal membrane traffic. Trends Cell Biol 16(10):514–521. https://doi.org/10.1016/j.tcb.2006.08.003
142. Hurley JH (2015) ESCRTs are everywhere. EMBO J 34(19):2398–2407. https://doi.org/10.15252/embj.201592484
143. Raiborg C, Stenmark H (2009) The ESCRT machinery in endosomal sorting of ubiquitylated membrane proteins. Nature 458(7237):445–452. https://doi.org/10.1038/nature07961
144. Bari R, Guo Q, Xia B, Zhang YH, Giesert EE, Levy S, Zheng JJ, Zhang XA (2011) Tetraspanins regulate the protrusive activities of cell membrane. Biochem Biophys Res Commun 415(4):619–626. https://doi.org/10.1016/j.bbrc.2011.10.121
145. Edgar JR, Eden ER, Futter CE (2014) Hrs- and CD63-dependent competing mechanisms make different sized endosomal intraluminal vesicles. Traffic 15(2):197–211. https://doi.org/10.1111/tra.12139
146. van Niel G, Charrin S, Simoes S, Romao M, Rochin L, Saftig P, Marks MS, Rubinstein E, Raposo G (2011) The tetraspanin CD63 regulates ESCRT-independent and -dependent endosomal sorting during melanogenesis. Dev Cell 21(4):708–721. https://doi.org/10.1016/j.devcel.2011.08.019

147. Trajkovic K, Hsu C, Chiantia S, Rajendran L, Wenzel D, Wieland F, Schwille P, Brugger B, Simons M (2008) Ceramide triggers budding of exosome vesicles into multivesicular endosomes. Science 319(5867):1244–1247. https://doi.org/10.1126/science.1153124
148. Matsuo H, Chevallier J, Mayran N, Le Blanc I, Ferguson C, Faure J, Blanc NS, Matile S, Dubochet J, Sadoul R, Parton RG, Vilbois F, Gruenberg J (2004) Role of LBPA and Alix in multivesicular liposome formation and endosome organization. Science 303(5657):531–534. https://doi.org/10.1126/science.1092425
149. Mayran N, Parton RG, Gruenberg J (2003) Annexin II regulates multivesicular endosome biogenesis in the degradation pathway of animal cells. EMBO J 22(13):3242–3253. https://doi.org/10.1093/emboj/cdg321
150. Morel E, Parton RG, Gruenberg J (2009) Annexin A2-dependent polymerization of actin mediates endosome biogenesis. Dev Cell 16(3):445–457. https://doi.org/10.1016/j.devcel.2009.01.007
151. Desdin-Mico G, Mittelbrunn M (2017) Role of exosomes in the protection of cellular homeostasis. Cell Adh Migr 11(2):127–134. https://doi.org/10.1080/19336918.2016.1251000
152. Luyet PP, Falguieres T, Pons V, Pattnaik AK, Gruenberg J (2008) The ESCRT-I subunit TSG101 controls endosome-to-cytosol release of viral RNA. Traffic 9(12):2279–2290. https://doi.org/10.1111/j.1600-0854.2008.00820.x
153. Bissig C, Gruenberg J (2014) ALIX and the multivesicular endosome: ALIX in Wonderland. Trends Cell Biol 24(1):19–25. https://doi.org/10.1016/j.tcb.2013.10.009
154. Ghossoub R, Lembo F, Rubio A, Gaillard CB, Bouchet J, Vitale N, Slavik J, Machala M, Zimmermann P (2014) Syntenin-ALIX exosome biogenesis and budding into multivesicular bodies are controlled by ARF6 and PLD2. Nat Commun 5:3477. https://doi.org/10.1038/ncomms4477
155. Sahu R, Kaushik S, Clement CC, Cannizzo ES, Scharf B, Follenzi A, Potolicchio I, Nieves E, Cuervo AM, Santambrogio L (2011) Microautophagy of cytosolic proteins by late endosomes. Dev Cell 20(1):131–139. https://doi.org/10.1016/j.devcel.2010.12.003
156. Cuervo AM, Dice JF (1996) A receptor for the selective uptake and degradation of proteins by lysosomes. Science 273(5274):501–503
157. Cuervo AM, Gomes AV, Barnes JA, Dice JF (2000) Selective degradation of annexins by chaperone-mediated autophagy. J Biol Chem 275(43):33329–33335. https://doi.org/10.1074/jbc.M005655200
158. Gomes AV, Barnes JA (1995) Pest sequences in EF-hand calcium-binding proteins. Biochem Mol Biol Int 37(5):853–860
159. Kobayashi T, Vischer UM, Rosnoblet C, Lebrand C, Lindsay M, Parton RG, Kruithof EK, Gruenberg J (2000) The tetraspanin CD63/lamp3 cycles between endocytic and secretory compartments in human endothelial cells. Mol Biol Cell 11(5):1829–1843
160. Poeter M, Brandherm I, Rossaint J, Rosso G, Shahin V, Skryabin BV, Zarbock A, Gerke V, Rescher U (2014) Annexin A8 controls leukocyte recruitment to activated endothelial cells via cell surface delivery of CD63. Nat Commun 5:3738. https://doi.org/10.1038/ncomms4738
161. Griffiths G, Hoflack B, Simons K, Mellman I, Kornfeld S (1988) The mannose 6-phosphate receptor and the biogenesis of lysosomes. Cell 52(3):329–341
162. Jahraus A, Egeberg M, Hinner B, Habermann A, Sackman E, Pralle A, Faulstich H, Rybin V, Defacque H, Griffiths G (2001) ATP-dependent membrane assembly of F-actin facilitates membrane fusion. Mol Biol Cell 12(1):155–170
163. Kjeken R, Egeberg M, Habermann A, Kuehnel M, Peyron P, Floetenmeyer M, Walther P, Jahraus A, Defacque H, Kuznetsov SA, Griffiths G (2004) Fusion between phagosomes, early and late endosomes: a role for actin in fusion between late, but not early endocytic organelles. Mol Biol Cell 15(1):345–358. https://doi.org/10.1091/mbc.E03-05-0334
164. Taunton J, Rowning BA, Coughlin ML, Wu M, Moon RT, Mitchison TJ, Larabell CA (2000) Actin-dependent propulsion of endosomes and lysosomes by recruitment of N-WASP. J Cell Biol 148(3):519–530

165. Goebeler V, Poeter M, Zeuschner D, Gerke V, Rescher U (2008) Annexin A8 regulates late endosome organization and function. Mol Biol Cell 19(12):5267–5278. https://doi.org/10.1091/mbc.E08-04-0383
166. Jaiswal JK, Andrews NW, Simon SM (2002) Membrane proximal lysosomes are the major vesicles responsible for calcium-dependent exocytosis in nonsecretory cells. J Cell Biol 159 (4):625–635. https://doi.org/10.1083/jcb.200208154
167. Reddy A, Caler EV, Andrews NW (2001) Plasma membrane repair is mediated by Ca(2+)-regulated exocytosis of lysosomes. Cell 106(2):157–169
168. Rodriguez A, Webster P, Ortego J, Andrews NW (1997) Lysosomes behave as Ca2+--regulated exocytic vesicles in fibroblasts and epithelial cells. J Cell Biol 137(1):93–104
169. Pryor PR, Mullock BM, Bright NA, Gray SR, Luzio JP (2000) The role of intraorganellar Ca(2+) in late endosome-lysosome heterotypic fusion and in the reformation of lysosomes from hybrid organelles. J Cell Biol 149(5):1053–1062
170. Steinhardt RA, Bi G, Alderton JM (1994) Cell membrane resealing by a vesicular mechanism similar to neurotransmitter release. Science 263(5145):390–393
171. Luzio JP, Bright NA, Pryor PR (2007a) The role of calcium and other ions in sorting and delivery in the late endocytic pathway. Biochem Soc Trans 35(Pt 5):1088–1091. https://doi.org/10.1042/BST0351088
172. Creutz CE (1992) The annexins and exocytosis. Science 258(5084):924–931
173. Donnelly SR, Moss SE (1997) Annexins in the secretory pathway. Cell Mol Life Sci 53 (6):533–538
174. Sjölin C, Dahlgren C (1996) Isolation by calcium-dependent translation to neutrophil-specific granules of a 42-kD cytosolic protein, identified as being a fragment of annexin XI. Blood 87 (11):4817–4823
175. Wang J, Guo C, Liu S, Qi H, Yin Y, Liang R, Sun MZ, Greenaway FT (2014) Annexin A11 in disease. Clin Chim Acta 431:164–168. https://doi.org/10.1016/j.cca.2014.01.031
176. Iino S, Sudo T, Niwa T, Fukasawa T, Hidaka H, Niki I (2000) Annexin XI may be involved in Ca2+ – or GTP-gammaS-induced insulin secretion in the pancreatic beta-cell. FEBS Lett 479 (1–2):46–50
177. McArthur S, Yazid S, Christian H, Sirha R, Flower R, Buckingham J, Solito E (2009) Annexin A1 regulates hormone exocytosis through a mechanism involving actin reorganization. FASEB J 23(11):4000–4010. https://doi.org/10.1096/fj.09-131391
178. Bharadwaj A, Bydoun M, Holloway R, Waisman D (2013) Annexin A2 heterotetramer: structure and function. Int J Mol Sci 14(3):6259–6305. https://doi.org/10.3390/ijms14036259
179. Faure AV, Migne C, Devilliers G, Ayala-Sanmartin J (2002) Annexin 2 "secretion" accompanying exocytosis of chromaffin cells: possible mechanisms of annexin release. Exp Cell Res 276(1):79–89. https://doi.org/10.1006/excr.2002.5512
180. Gabel M, Delavoie F, Demais V, Royer C, Bailly Y, Vitale N, Bader MF, Chasserot-Golaz S (2015) Annexin A2-dependent actin bundling promotes secretory granule docking to the plasma membrane and exocytosis. J Cell Biol 210(5):785–800. https://doi.org/10.1083/jcb.201412030
181. Gerke V (2016) Annexins A2 and A8 in endothelial cell exocytosis and the control of vascular homeostasis. Biol Chem 397(10):995–1003. https://doi.org/10.1515/hsz-2016-0207
182. Umbrecht-Jenck E, Demais V, Calco V, Bailly Y, Bader MF, Chasserot-Golaz S (2010) S100A10-mediated translocation of annexin-A2 to SNARE proteins in adrenergic chromaffin cells undergoing exocytosis. Traffic 11(7):958–971. https://doi.org/10.1111/j.1600-0854.2010.01065.x
183. Wang P, Chintagari NR, Gou D, Su L, Liu L (2007) Physical and functional interactions of SNAP-23 with annexin A2. Am J Respir Cell Mol Biol 37(4):467–476. https://doi.org/10.1165/rcmb.2006-0447OC
184. Coorssen JR, Schmitt H, Almers W (1996) Ca2+ triggers massive exocytosis in Chinese hamster ovary cells. EMBO J 15(15):3787–3791

185. Venkatachalam K, Wong CO, Zhu MX (2015) The role of TRPMLs in endolysosomal trafficking and function. Cell Calcium 58(1):48–56. https://doi.org/10.1016/j.ceca.2014.10.008
186. Wang W, Gao Q, Yang M, Zhang X, Yu L, Lawas M, Li X, Bryant-Genevier M, Southall NT, Marugan J, Ferrer M, Xu H (2015) Up-regulation of lysosomal TRPML1 channels is essential for lysosomal adaptation to nutrient starvation. Proc Natl Acad Sci USA 112(11):E1373–E1381. https://doi.org/10.1073/pnas.1419669112
187. Weiss N (2012) Cross-talk between TRPML1 channel, lipids and lysosomal storage diseases. Commun Integr Biol 5(2):111–113. https://doi.org/10.4161/cib.20373
188. Roostalu U, Strähle U (2012) In vivo imaging of molecular interactions at damaged sarcolemma. Dev Cell 22(3):515–529. https://doi.org/10.1016/j.devcel.2011.12.008
189. Yu QC, McNeil PL (1992) Transient disruptions of aortic endothelial cell plasma membranes. Am J Pathol 141(6):1349–1360
190. Cooper ST, McNeil PL (2015) Membrane repair: mechanisms and pathophysiology. Physiol Rev 95(4):1205–1240. https://doi.org/10.1152/physrev.00037.2014
191. Demonbreun AR, McNally EM (2016) Plasma membrane repair in health and disease. Curr Top Membr 77:67–96. https://doi.org/10.1016/bs.ctm.2015.10.006
192. Jaiswal JK, Nylandsted J (2015) S100 and annexin proteins identify cell membrane damage as the Achilles heel of metastatic cancer cells. Cell Cycle 14(4):502–509. https://doi.org/10.1080/15384101.2014.995495
193. Lauritzen SP, Boye TL, Nylandsted J (2015) Annexins are instrumental for efficient plasma membrane repair in cancer cells. Semin Cell Dev Biol 45:32–38. https://doi.org/10.1016/j.semcdb.2015.10.028
194. Helm JR, Bentley M, Thorsen KD, Wang T, Foltz L, Oorschot V, Klumperman J, Hay JC (2014) Apoptosis-linked gene-2 (ALG-2)/Sec31 interactions regulate endoplasmic reticulum (ER)-to-Golgi transport: a potential effector pathway for luminal calcium. J Biol Chem 289(34):23609–23628. https://doi.org/10.1074/jbc.M114.561829
195. Scheffer LL, Sreetama SC, Sharma N, Medikayala S, Brown KJ, Defour A, Jaiswal JK (2014) Mechanism of Ca(2)(+)-triggered ESCRT assembly and regulation of cell membrane repair. Nat Commun 5:5646. https://doi.org/10.1038/ncomms6646
196. Ono Y, Sorimachi H (2012) Calpains: an elaborate proteolytic system. Biochim Biophys Acta 1824(1):224–236. https://doi.org/10.1016/j.bbapap.2011.08.005
197. Nigro V, Savarese M (2014) Genetic basis of limb-girdle muscular dystrophies: the 2014 update. Acta Myol 33(1):1–12
198. Mellgren RL, Miyake K, Kramerova I, Spencer MJ, Bourg N, Bartoli M, Richard I, Greer PA, McNeil PL (2009) Calcium-dependent plasma membrane repair requires m- or mu-calpain, but not calpain-3, the proteasome, or caspases. Biochim Biophys Acta 1793(12):1886–1893. https://doi.org/10.1016/j.bbamcr.2009.09.013
199. Mellgren RL, Zhang W, Miyake K, McNeil PL (2007) Calpain is required for the rapid, calcium-dependent repair of wounded plasma membrane. J Biol Chem 282(4):2567–2575. https://doi.org/10.1074/jbc.M604560200
200. Redpath GM, Woolger N, Piper AK, Lemckert FA, Lek A, Greer PA, North KN, Cooper ST (2014) Calpain cleavage within dysferlin exon 40a releases a synaptotagmin-like module for membrane repair. Mol Biol Cell 25(19):3037–3048. https://doi.org/10.1091/mbc.E14-04-0947
201. Lennon NJ, Kho A, Bacskai BJ, Perlmutter SL, Hyman BT, Brown RH Jr (2003) Dysferlin interacts with annexins A1 and A2 and mediates sarcolemmal wound-healing. J Biol Chem 278(50):50466–50473. https://doi.org/10.1074/jbc.M307247200
202. Draeger A, Wray S, Babiychuk EB (2005) Domain architecture of the smooth-muscle plasma membrane: regulation by annexins. Biochem J 387(Pt 2):309–314. https://doi.org/10.1042/BJ20041363

203. Diakonova M, Gerke V, Ernst J, Liautard JP, van der Vusse G, Griffiths G (1997) Localization of five annexins in J774 macrophages and on isolated phagosomes. J Cell Sci 110 (Pt 10):1199–1213
204. Merrifield CJ, Moss SE, Ballestrem C, Imhof BA, Giese G, Wunderlich I, Almers W (1999) Endocytic vesicles move at the tips of actin tails in cultured mast cells. Nat Cell Biol 1 (1):72–74. https://doi.org/10.1038/9048
205. Rambotti MG, Spreca A, Donato R (1993) Immunocytochemical localization of annexins V and VI in human placentae of different gestational ages. Cell Mol Biol Res 39(6):579–588
206. Zobiack N, Rescher U, Ludwig C, Zeuschner D, Gerke V (2003) The annexin 2/S100A10 complex controls the distribution of transferrin receptor-containing recycling endosomes. Mol Biol Cell 14(12):4896–4908. https://doi.org/10.1091/mbc.E03-06-0387
207. Demonbreun AR, Quattrocelli M, Barefield DY, Allen MV, Swanson KE, McNally EM (2016) An actin-dependent annexin complex mediates plasma membrane repair in muscle. J Cell Biol 213(6):705–718. https://doi.org/10.1083/jcb.201512022
208. Gavins FN, Hickey MJ (2012) Annexin A1 and the regulation of innate and adaptive immunity. Front Immunol 3:354. https://doi.org/10.3389/fimmu.2012.00354
209. Leoni G, Alam A, Neumann PA, Lambeth JD, Cheng G, McCoy J, Hilgarth RS, Kundu K, Murthy N, Kusters D, Reutelingsperger C, Perretti M, Parkos CA, Neish AS, Nusrat A (2013) Annexin A1, formyl peptide receptor, and NOX1 orchestrate epithelial repair. J Clin Invest 123(1):443–454. https://doi.org/10.1172/JCI65831
210. Perretti M, D'Acquisto F (2009) Annexin A1 and glucocorticoids as effectors of the resolution of inflammation. Nat Rev Immunol 9(1):62–70. https://doi.org/10.1038/nri2470
211. Perretti M, Dalli J (2009) Exploiting the Annexin A1 pathway for the development of novel anti-inflammatory therapeutics. Br J Pharmacol 158(4):936–946. https://doi.org/10.1111/j.1476-5381.2009.00483.x
212. Sugimoto MA, Vago JP, Teixeira MM, Sousa LP (2016) Annexin A1 and the resolution of inflammation: modulation of neutrophil recruitment, apoptosis, and clearance. J Immunol Res 2016:8239258. https://doi.org/10.1155/2016/8239258
213. Jaiswal JK, Lauritzen SP, Scheffer L, Sakaguchi M, Bunkenborg J, Simon SM, Kallunki T, Jaattela M, Nylandsted J (2014) S100A11 is required for efficient plasma membrane repair and survival of invasive cancer cells. Nat Commun 5:3795. https://doi.org/10.1038/ncomms4795
214. Defour A, Van der Meulen JH, Bhat R, Bigot A, Bashir R, Nagaraju K, Jaiswal JK (2014) Dysferlin regulates cell membrane repair by facilitating injury-triggered acid sphingomyelinase secretion. Cell Death Dis 5:e1306. https://doi.org/10.1038/cddis.2014.272
215. Hayes MJ, Shao D, Bailly M, Moss SE (2006) Regulation of actin dynamics by annexin 2. EMBO J 25(9):1816–1826. https://doi.org/10.1038/sj.emboj.7601078
216. Cagliani R, Magri F, Toscano A, Merlini L, Fortunato F, Lamperti C, Rodolico C, Prelle A, Sironi M, Aguennouz M, Ciscato P, Uncini A, Moggio M, Bresolin N, Comi GP (2005) Mutation finding in patients with dysferlin deficiency and role of the dysferlin interacting proteins annexin A1 and A2 in muscular dystrophies. Hum Mutat 26(3):283. https://doi.org/10.1002/humu.9364
217. Saurel O, Cezanne L, Milon A, Tocanne JF, Demange P (1998) Influence of annexin V on the structure and dynamics of phosphatidylcholine/phosphatidylserine bilayers: a fluorescence and NMR study. Biochemistry 37(5):1403–1410. https://doi.org/10.1021/bi971484n
218. Swaggart KA, Demonbreun AR, Vo AH, Swanson KE, Kim EY, Fahrenbach JP, Holley-Cuthrell J, Eskin A, Chen Z, Squire K, Heydemann A, Palmer AA, Nelson SF, McNally EM (2014) Annexin A6 modifies muscular dystrophy by mediating sarcolemmal repair. Proc Natl Acad Sci USA 111(16):6004–6009. https://doi.org/10.1073/pnas.1324242111
219. Draeger A, Monastyrskaya K, Babiychuk EB (2011) Plasma membrane repair and cellular damage control: the annexin survival kit. Biochem Pharmacol 81(6):703–712. https://doi.org/10.1016/j.bcp.2010.12.027

220. Potez S, Luginbuhl M, Monastyrskaya K, Hostettler A, Draeger A, Babiychuk EB (2011) Tailored protection against plasmalemmal injury by annexins with different Ca2+ sensitivities. J Biol Chem 286(20):17982–17991. https://doi.org/10.1074/jbc.M110.187625
221. Morel E, Gruenberg J (2007) The p11/S100A10 light chain of annexin A2 is dispensable for annexin A2 association to endosomes and functions in endosomal transport. PLoS One 2(10): e1118. https://doi.org/10.1371/journal.pone.0001118
222. Seemann J, Weber K, Gerke V (1997) Annexin I targets S100C to early endosomes. FEBS Lett 413(1):185–190
223. Creutz CE, Hira JK, Gee VE, Eaton JM (2012) Protection of the membrane permeability barrier by annexins. Biochemistry 51(50):9966–9983. https://doi.org/10.1021/bi3013559
224. Li X, Rydzewski N, Hider A, Zhang X, Yang J, Wang W, Gao Q, Cheng X, Xu H (2016) A molecular mechanism to regulate lysosome motility for lysosome positioning and tubulation. Nat Cell Biol 18(4):404–417. https://doi.org/10.1038/ncb3324
225. Pu J, Guardia CM, Keren-Kaplan T, Bonifacino JS (2016) Mechanisms and functions of lysosome positioning. J Cell Sci 129(23):4329–4339. https://doi.org/10.1242/jcs.196287
226. Huotari J, Helenius A (2011) Endosome maturation. EMBO J 30(17):3481–3500. https://doi.org/10.1038/emboj.2011.286
227. Saftig P, Klumperman J (2009) Lysosome biogenesis and lysosomal membrane proteins: trafficking meets function. Nat Rev Mol Cell Biol 10(9):623–635. https://doi.org/10.1038/nrm2745
228. Kurz T, Terman A, Gustafsson B, Brunk UT (2008) Lysosomes and oxidative stress in aging and apoptosis. Biochim Biophys Acta 1780(11):1291–1303. https://doi.org/10.1016/j.bbagen.2008.01.009
229. Khatter D, Raina VB, Dwivedi D, Sindhwani A, Bahl S, Sharma M (2015a) The small GTPase Arl8b regulates assembly of the mammalian HOPS complex on lysosomes. J Cell Sci 128 (9):1746–1761. https://doi.org/10.1242/jcs.162651
230. Khatter D, Sindhwani A, Sharma M (2015b) Arf-like GTPase Arl8: moving from the periphery to the center of lysosomal biology. Cell Logist 5(3):e1086501. https://doi.org/10.1080/21592799.2015.1086501
231. Bucci C, Thomsen P, Nicoziani P, McCarthy J, van Deurs B (2000) Rab7: a key to lysosome biogenesis. Mol Biol Cell 11(2):467–480
232. Kilpatrick BS, Eden ER, Schapira AH, Futter CE, Patel S (2013) Direct mobilisation of lysosomal Ca2+ triggers complex Ca2+ signals. J Cell Sci 126(Pt 1):60–66. https://doi.org/10.1242/jcs.118836
233. Marchant JS, Patel S (2015) Two-pore channels at the intersection of endolysosomal membrane traffic. Biochem Soc Trans 43(3):434–441. https://doi.org/10.1042/BST20140303
234. Huttlin EL, Ting L, Bruckner RJ, Gebreab F, Gygi MP, Szpyt J, Tam S, Zarraga G, Colby G, Baltier K, Dong R, Guarani V, Vaites LP, Ordureau A, Rad R, Erickson BK, Wuhr M, Chick J, Zhai B, Kolippakkam D, Mintseris J, Obar RA, Harris T, Artavanis-Tsakonas S, Sowa ME, De Camilli P, Paulo JA, Harper JW, Gygi SP (2015) The BioPlex network: a systematic exploration of the human interactome. Cell 162(2):425–440. https://doi.org/10.1016/j.cell.2015.06.043
235. Chu BB, Liao YC, Qi W, Xie C, Du X, Wang J, Yang H, Miao HH, Li BL, Song BL (2015) Cholesterol transport through lysosome-peroxisome membrane contacts. Cell 161 (2):291–306. https://doi.org/10.1016/j.cell.2015.02.019
236. Luo J, Jiang L, Yang H, Song BL (2017) Routes and mechanisms of post-endosomal cholesterol trafficking: a story that never ends. Traffic 18(4):209–217. https://doi.org/10.1111/tra.12471
237. Shen D, Wang X, Li X, Zhang X, Yao Z, Dibble S, Dong XP, Yu T, Lieberman AP, Showalter HD, Xu H (2012) Lipid storage disorders block lysosomal trafficking by inhibiting a TRP channel and lysosomal calcium release. Nat Commun 3:731. https://doi.org/10.1038/ncomms1735
238. Styrt B, Pollack CR, Klempner MS (1988) An abnormal calcium uptake pump in Chediak-Higashi neutrophil lysosomes. J Leukoc Biol 44(2):130–135

Part V
Cytokinesis and Ca^{2+} Signaling

Chapter 15
Ca^{2+} Signalling and Membrane Dynamics During Cytokinesis in Animal Cells

Sarah E. Webb and Andrew L. Miller

Abstract Interest in the role of Ca^{2+} signalling as a possible regulator of the combinatorial processes that result in the separation of the daughter cells during cytokinesis, extend back almost a 100 years. One of the key processes required for the successful completion of cytokinesis in animal cells (especially in the large holoblastically and meroblastically dividing embryonic cells of a number of amphibian and fish species), is the dynamic remodelling of the plasma membrane. Ca^{2+} signalling was subsequently demonstrated to regulate various different aspects of cytokinesis in animal cells, and so here we focus specifically on the role of Ca^{2+} signalling in the remodelling of the plasma membrane. We begin by providing a brief history of the animal models used and the research accomplished by the early twentieth century investigators, with regards to this aspect of animal cell cytokinesis. We then review the most recent progress made (i.e., in the last 10 years), which has significantly advanced our current understanding on the role of cytokinetic Ca^{2+} signalling in membrane remodelling. To this end, we initially summarize what is currently known about the Ca^{2+} transients generated during animal cell cytokinesis, and then we describe the latest findings regarding the source of Ca^{2+} generating these transients. Finally, we review the current evidence about the possible targets of the different cytokinetic Ca^{2+} transients with a particular emphasis on those that either directly or indirectly affect plasma membrane dynamics. With regards to the latter, we discuss the possible role of the early Ca^{2+} signalling events in the deformation of the plasma membrane at the start of cytokinesis (i.e., during furrow positioning), as well as the role of the subsequent Ca^{2+} signals in the trafficking and fusion of vesicles, which help to remodel the plasma membrane during the final stages of cell division. As it is becoming clear that each of the cytokinetic Ca^{2+} transients might have multiple, integrated targets, deciphering the precise role of each transient represents a significant (and ongoing) challenge.

S. E. Webb · A. L. Miller (✉)
Division of Life Science & State Key Laboratory of Molecular Neuroscience, HKUST, Clear Water Bay, Hong Kong
e-mail: almiller@ust.hk

J. Krebs (ed.), *Membrane Dynamics and Calcium Signaling*, Advances in Experimental Medicine and Biology 981,
https://doi.org/10.1007/978-3-319-55858-5_15

Keywords Ca^{2+} signalling · Membrane dynamics · Cytokinesis · Cleavage furrow · Exocytosis · IP_3 receptor · Store-operated Ca^{2+} entry (SOCE) · Vesicle trafficking · Microtubule arrays · Zebrafish

15.1 Introduction

15.1.1 Historical Perspective

Cytokinesis is the final step of the cell cycle in both animal and plant cells when a 'mother' cell divides into two 'daughter' cells. Over the last decade, a number of excellent general reviews on cytokinesis have been published (for example, see [1–6]). Here, however, we provide a more focussed review of what is known about the link between Ca^{2+} signalling and membrane dynamics during cytokinesis in animal cells. As the interest in these two specific aspects of the cell division process spans nearly 100 years, a short introduction providing a historical perspective was considered necessary. During early twentieth century investigations of the membrane dynamics during cytokinesis, the holoblastically dividing eggs of echinoderms (such as *Hemicentrotus pulcherrimus*, *Astriclypeus manni*, *Arbacia punctulata*, *Echinus esculentus,* and *Echinarachnius parma*) were some of the favoured model systems used. In these early studies, investigators recognized that the 'addition' or 'growth' of de novo plasma membrane at or near the cleavage furrow appeared to be an integral and essential part of the cytokinetic process [7–11]. Furthermore, from experiments carried out in Ca^{2+}-free media, the furrow constriction and membrane remodelling events shown to occur during cytokinesis, were suggested to somehow involve calcium ions (Ca^{2+}) [7, 12, 13]. These observations, however, were initially controversial and resulted in a certain amount of lively debate in the literature [13, 14]. Other favourite early models (due to their large size and consequent ease of manipulation and observation), were the holoblastically dividing eggs of amphibians. Once again researchers reported that new membrane addition and the remodelling of existing membrane were an integral part of the cell division process. Examples include the dividing eggs of the newts *Trituris alpestrist* [15, 16], *T. pyrrhogaster* [17] and *Cynops pyrrhogaster* [18, 19]; as well as those of the frogs *Rana pipiens* [20] and *Xenopus laevis* [21, 22]. There is, therefore, a significant record in the early literature (i.e., dating back ~50–80 years) that links plasma membrane dynamics with the first few embryonic cell divisions of holoblastically cleaving egg cells both small and large. More recently, a range of other model systems have been used to study membrane dynamics during cytokinesis. These include the zebrafish, *Danio rerio* [23] and medaka, *Oryzias latipes* [24]; the fruit fly, *Drosophila spp.* [25, 26], and the nematode, *Caenorhabditis elegans* [27].

15.1.2 General Aspects of Cytokinesis

In animal cells, cytokinesis is initiated when an actomyosin band forms and contracts, cleaving the cells in two [28]. Most of the time the cytokinesis apparatus is located in such a way that the daughter cells that form are approximately the same size [5]. This requires the precise coordination of the mitotic spindle and the cytokinetic apparatus, including the contractile band/ring and the pre-furrow plasma membrane, to ensure that the cleavage furrow is placed correctly between the segregating chromosomes and that enough new membrane can be formed to generate the two daughter cells [29, 30].

In somatic cells and small egg cells the contractile band appears to form and start contracting simultaneously around the equator of the cell [31, 32]. However, in large eggs (such as those of several fish and amphibian species), four distinct cytokinetic components can be distinguished both from a temporal and spatial viewpoint [33]. These include: The initial positioning of the furrow at the cell surface [34, 35], which is followed by the propagation of the furrow within the cell cortex with minimal initial deepening [36]; this is then followed by a phase of contractile band constriction and furrow deepening [37]. At the end of furrow deepening in these large embryonic cells, the two new daughter cells formed do not undergo abscission (or separate) as they do following cytokinesis of many unicellular species such as yeast and bacteria [38–41]; instead the fully deepened furrows undergo a process of furrow apposition (or furrow 'zipping') to maintain compaction of the early embryo [24, 42–44]. It has been suggested that a similar sequence of events might also occur during cytokinesis in somatic cells, and in small eggs such as those of certain echinoderm species [45]. It is, however, more difficult to distinguish between the sequential steps of the cytokinetic process due to these events occurring in a shorter time-frame and within a more restricted spatial domain due to the small size of the cells. Alternatively, a truncated sequence of events might occur in these small cells. It is during the latter stages of furrow deepening in both separating and non-separating daughter cells that new membrane is reported to be added [22, 27, 46–48].

It was initially assumed that the action of the actomyosin contractile ring was the main component of cytokinesis in animal cells. This is because ingression (deepening) of the cleavage furrow was considered to be the key event in the partitioning of the cytoplasm to form the two daughter cells [28]. However, it is now known that the transport and subsequent fusion of new plasma membrane is also a crucial step during cell cleavage [49, 50]. This addition of plasma membrane is necessary to allow for the increase in surface area that is required during cytokinesis. Indeed, throughout cytokinesis the plasma membrane is a highly dynamic structure (especially in the region of the cleavage furrow), as it helps to maintain the shape, volume and integrity of the cell at all times during this process [51, 52]. During furrow positioning, the cleavage furrow first appears as a shallow indentation in the plasma membrane at the animal pole. Once the furrow is positioned, a process is initiated whereby this indentation extends (or propagates) laterally in both directions. In the

case of meroblastically dividing fish eggs, once the indentation (propagating furrow) reaches the edges of the blastodisc the furrow then starts to deepen both downward and outward from the initial positioning indentation [24, 36]. In large, holoblastically dividing amphibian eggs, such as those of *Xenopus*, however, the cleavage furrow starts to deepen in the animal hemisphere before the leading edges of the propagating furrows have reached the vegetal pole [44, 53]. Finally, during the latter stages of furrow deepening, and apposition, new membrane is added via endocytosis [29, 54].

As the structural aspects of animal cell cytokinesis became better understood, so researchers began to realize that Ca^{2+} signalling was somehow involved in the overall cell division process [55–58]. In addition, with the development of better Ca^{2+} reporters and imaging techniques it became clear that cytokinesis in large eggs requires four sequential Ca^{2+} signals at furrow positioning, propagation, deepening and apposition [24, 36, 45, 59, 60]. Here, we review the most recent discoveries (i.e., those reported mainly within the last decade) regarding the mechanism of cytokinesis, especially focussing on the role of Ca^{2+} signalling on the events that lead to the dynamic reorganization of the plasma membrane. We are basing this chapter largely on the mechanisms involved in cleavage in fish embryos, as this is our major research interest. However, we also compare and contrast what is known in these large fish embryos with the mechanisms that have been identified in other embryonic systems as well as in somatic cells, highlighting the events that are conserved between the various cell types and discussing the events that might be more cell-specific.

15.2 The Cytokinetic Ca^{2+} Transients

15.2.1 Generation of Distinct Ca^{2+} Transients During Cytokinesis

The first report of intracellular changes in Ca^{2+} during cytokinesis came from Ridgway *et al.* [57] who injected medaka embryos with the luminescent Ca^{2+} reporter, aequorin, and then measured the light generated with a photomultiplier tube (PMT). Although this group were mainly investigating the large single Ca^{2+} transient that accompanies egg activation, they also reported seeing small Ca^{2+} transients that seemed to correlate with the early cell division cycles. Almost a decade after this first report, Shantz [61] demonstrated, again in medaka but this time using a Ca^{2+}-sensitive microelectrode, that the concentration of Ca^{2+} increased transiently and synchronously during two successive rounds of cell division. These early observations were confirmed in the early 1990s with the development of a specialised Photon Imaging Microscope System (PIMS; [62]) that allowed for the direct visualization of Ca^{2+} signals in the dividing embryos of medaka and other fish species.

Fluck *et al*. [24] loaded medaka embryos with aequorin and using a PIMS, confirmed that the localised increases in Ca^{2+} first reported by Ridgway *et al*. [57] occurred concurrently with cytokinesis. Fluck *et al*. [24] described the generation of two successive slow Ca^{2+} waves that accompanied the propagation then deepening of the cleavage furrows during the early meroblastic cell divisions in these embryos. The first wave was relatively confined and appeared to accompany the extension (propagation) of the furrow through the cell cortex with minimal deepening, whereas the second wave was considerably broader and accompanied furrow deepening and apposition of the newly formed daughter cells.

Following on from this initial discovery of Ca^{2+} transients in cleaving medaka embryos, subsequent investigations (using both luminescent and fluorescent Ca^{2+} reporters) quickly confirmed the existence of Ca^{2+} transients during cytokinesis in zebrafish embryos. For example, using the fluorescent Ca^{2+} reporter, calcium green-1 dextran, and laser scanning confocal microscopy, Chang and Meng [59] reported that localised elevations in free Ca^{2+} were associated with cytokinesis in these embryos, and they demonstrated that intracellular Ca^{2+} was elevated at the right time and right place to play a role in establishing the location of the furrow plane. These results were subsequently confirmed and extended using an aequorin-based imaging method somewhat similar to that used by Fluck *et al*. [24], where it was reported that a number of distinct Ca^{2+} signals accompany the sequentially-occurring cytokinetic events during the first and second cell division cycles [36]. The first Ca^{2+} signal generated was termed the 'furrow positioning' transient. This is a distinct, localised elevation of intracellular Ca^{2+}, which was demonstrated to precede the first physical manifestation of the furrow arc at the surface of the blastodisc [34]. The furrow positioning signal is followed by the 'furrow propagation signal', which takes the form of two linear sub-surface slow Ca^{2+} waves (moving at ~0.5 μm/sec), which accompany the leading edges of the furrow as they move in a linear manner to the blastodisc margins. As the propagation wave fronts approach the margins then the furrow deepening Ca^{2+} transient appears at the apex of the blastodisc in the same place as the original furrow positioning signal. Like the propagation signal, the deepening signal extends outward at ~0.5 μm/sec to the margins of the blastodisc, but it also extends deep into the blastodisc (at ~0.1 μm/sec) as it accompanies the furrow deepening process that divides the mother cell in two [36]. At the end of furrow deepening, there is a gradual decrease in the level of intracellular Ca^{2+} starting in the central base region of the furrow; this accompanies furrow apposition such that by the time the cleavage furrow is fully apposed, the $[Ca^{2+}]$ has returned to the pre-cleavage resting level [37]. The furrow positioning, propagation, deepening and apposition Ca^{2+} signals observed during the first and second cell division cycles of zebrafish embryos are shown in Fig. 15.1. The signals are shown from the side (both facial and axial views) and animal pole as (unlike confocal microscopy with fluorescent reporters) the aequorin imaging method does not provide any information with respect to the z-axis.

The generation of localised Ca^{2+} transients in zebrafish embryos during the different cytokinetic events have also been confirmed by other groups using aequorin and fluorescent reporters [60, 63, 64]. In addition, most recently, stable

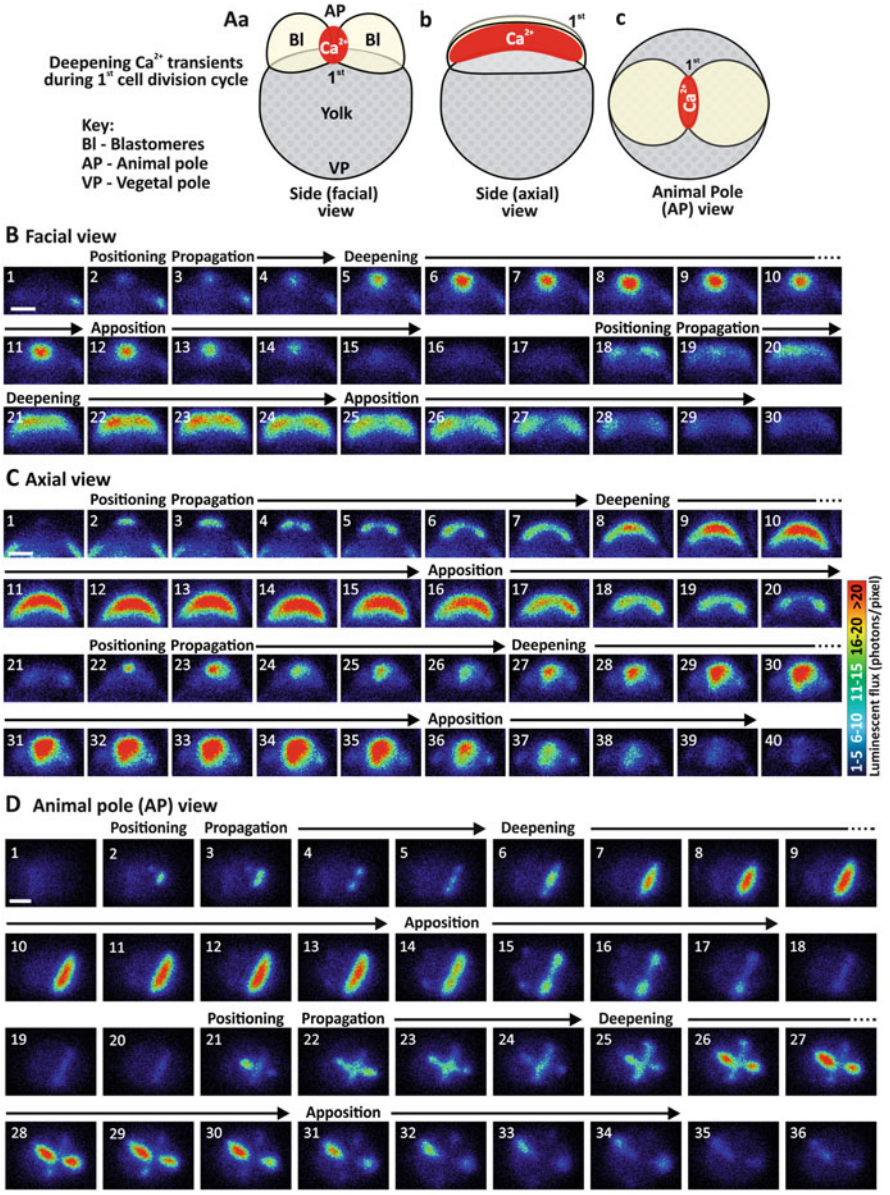

Fig. 15.1 The luminescence-generated images of three *f*-aequorin-loaded zebrafish embryos to show the changes in intracellular free Ca^{2+} that occur during the first and second cell division cycles. (**A**) Schematic illustrations of an embryo during furrow deepening of the first cell division cycle from: (**Aa**) side facial and (**Ab**) side axial views, as well as from (**Ac**) a top (animal pole; AP) view. (**B**–**D**) Pseudocolour images showing the *f*-aequorin-generated luminescence generated in embryos when viewed in a (**B**) facial, (**C**) axial, and (**D**) top orientation. Each image represents 30 s of accumulated luminescence and there is a 30-s gap between each image. For each series of images, the positioning, propagation, deepening and apposition Ca^{2+} transients are labeled. Scale bars are 200 μm. Reprinted (in a modified form) with permission from "Localized calcium transients accompany furrow positioning, propagation, and deepening during the early cleavage period of

transgenic zebrafish lines have been generated (*Tg[βactin2:GCaMP6s]stl351* and *Tg[ubi:GCaMP6s]*^{stl352}), which combine the ultra-sensitive fluorescent Ca^{2+} indicator GCaMP6s with the ubiquitously expressed *β-actin2* or *ubiquitin* genes [65]. It is possible to visualize the dynamic Ca^{2+} signalling events that are generated throughout embryogenesis and into adulthood with the *Tg[βactin2:GCaMP6s]stl351* line, but of particular interest to us with regards to this review, is the fact that the Ca^{2+} signals generated during the early cleavage stages, are the same as those visualized using injected reporter proteins [65].

In addition to zebrafish, a similar series of distinct Ca^{2+} transients have been identified to accompany furrow positioning, propagation and deepening in other fish species, such as the rosy barb (*Puntius conchonius*) and mummichog (*Fundulus heteroclitus*; [45]), as well as during furrow propagation and deepening in the *Xenopus laevis* [44, 45]. Furthermore, cytokinetic Ca^{2+} signals have also been described in species that have considerably smaller eggs than those of fish and amphibians. These include starfish (*Asterina miniata* and *Pisaster ochraceus*; [66]), sand dollar (*Echinarachnius parma*; [67]), and sea urchin (*Lytechinus pictus* and *Paracentrotus lividus*; [68, 69]).

More recently, the existence of intracellular elevations of Ca^{2+} during cytokinesis in mammalian embryos has been reported [70]. Zygote-stage (1-cell stage) mouse embryos were loaded with the ratiometric fluorescent Ca^{2+} reporter, Fura-2, and images were acquired via confocal microscopy during the first cell division cycle [70]. An elevation of intracellular Ca^{2+} was imaged in the plane of the forming cleavage furrow in a somewhat similar manner to what has been observed during cytokinesis in zebrafish that are loaded with fluorescent Ca^{2+} reporters and imaged via confocal microscopy [59]. These are very exciting findings as they provide some of the first direct evidence that Ca^{2+} signalling is a conserved feature of cytokinesis during the early embryonic stages in mammals as well as in lower invertebrate species.

15.2.2 Identifying the Source of Ca^{2+} Generating Cytokinetic Transients

To identify the source of Ca^{2+} responsible for the generation of the cytokinetic Ca^{2+} transients, embryos have been treated with antagonists of the various Ca^{2+} release channels. Chang and Meng [59] treated calcium green-1 dextran-injected zebrafish embryos with inhibitors of the IP_3 receptor (heparin), ryanodine receptor (ryanodine), or the plasma membrane Ca^{2+} channel (nifedipine or lanthanum ions, La^{3+}), and showed that heparin blocked the cytokinetic Ca^{2+} signals (and cell

Fig. 15.1 (continued) zebrafish embryos" by Webb SE, Lee KW, Karplus E, Miller AL, 1997. Developmental Biology, 192, 78–92. Academic Press

division) but the other inhibitors had no effect. The same group also demonstrated that the cytokinetic Ca^{2+} transients were still generated when Ca^{2+} was removed from the embryo bathing medium. They concluded that the transients were generated via Ca^{2+} release from IP_3 receptors most likely located in the endoplasmic reticulum (ER; [59]). Using aequorin-injected embryos, it was subsequently confirmed that the cytokinetic Ca^{2+} transients were generated in Ca^{2+}-free medium [36]. In the following sections, we describe the evidence accumulated, which demonstrates that Ca^{2+} is essential for the various specific stages of cytokinesis.

15.2.2.1 Positioning and Propagation Ca^{2+} Transients

Some of the first evidence presented for the initiation of cleavage furrow formation in embryos being dependent on Ca^{2+} comes from amphibians. Microsomal fractions were prepared from CHO-K1 cells that stably expressed SERCA-GFP, and then microinjected into dividing newt (*Cynops pyrrhogaster*) zygotes [71]. This resulted in the induction of additional cleavage furrows at the site of injection. It was also demonstrated that the Ca^{2+} transients observed in zebrafish embryos are crucial for cleavage furrow positioning and formation. Newly fertilized embryos were injected with aequorin, and then as soon as the positioning Ca^{2+} transient was observed, the weak Ca^{2+} buffer, 5,5′-dibromo-BAPTA was injected into the blastodisc [35]. This had a delocalizing effect on the normally compact positioning Ca^{2+} transient and the cleavage furrow never appeared at the surface of the blastodisc. As the positioning Ca^{2+} signal was dispersed, then the subsequent propagation, deepening and apposition Ca^{2+} signals also failed to be generated and the associated furrow propagation, deepening and apposition events were also absent.

The formation of extra furrows in newt embryos was demonstrated to be induced via IP_3-dependent Ca^{2+} release by the microinjection of microsomes prepared from the cerebella of wild-type or IP_3 receptor (type 1)- mutant mice [71]. The injection of microsomes from wild-type mice brain was shown to induce the formation of ectopic cleavage furrows; whereas the co-injection of these microsomes and heparin or an anti-IP_3 receptor antibody inhibited the formation of these extra furrows. In addition, the injection of microsomes from IP_3 receptor-deficient mice resulted in far fewer additional furrows forming [71]. It was subsequently demonstrated that when newt eggs were simultaneously labelled for IP_3 receptors and the ER (via injection of sarco/endoplasmic reticulum ATPase- (SERCA-)-tagged GFP), as well as for F-actin and DNA, the ER Ca^{2+} store and IP_3 receptors were shown to co-migrate and co-accumulate at the cleavage furrow along with F-actin [72, 73]. As migration was blocked by treatment with the microtubule-depolarizing agent, nocodazole, or the microtubule motor inhibitor, AMP-PNP, it was suggested that the ER and IP_3 receptors might accumulate in the cleavage furrow in a microtubule-dependent manner [73].

A role for IP_3-dependent Ca^{2+} release in positioning the cleavage furrow was also demonstrated in zebrafish [74]. They showed that the introduction of the IP_3 receptor antagonist, 2-aminoethoxydiphenyl borate (2-APB) just before or just

after the appearance of the furrow positioning Ca^{2+} signal, eliminated the positioning Ca^{2+} transient and the appearance of the furrow at the cell surface. On the other hand, treatment with ryanodine, or antagonists of the nicotinic acid-adenine dinucleotide phosphate (NAADP)-sensitive channel (nifedipine and verapamil), had no effect on the generation of the positioning transient or the appearance of the furrow at the blastodisc surface [35].

Following observations in the newt that furrow positioning is dependent on microtubules [72], it was subsequently reported that an array of microtubules also plays a crucial role in furrow positioning in zebrafish [34]. This so-called 'pre-furrowing microtubule array' (pf-MTA) was shown to be visible just prior to the physical deformation of the plasma membrane indicating the first appearance of the cleavage furrow. It originated between the chromosomes (i.e., at the mid-zone of the mitotic spindle) and expanded both upward toward the animal pole, and laterally toward the blastodisc surface between metaphase and telophase of the cell division cycle. It was suggested that the pf-MTA might act to transfer chromosome passenger proteins from the chromosomes to the central spindle and then to the cell cortex, and organise the cortical ER so that it is confined principally to the location of cleavage furrow formation [34].

15.2.2.2 Deepening and Apposition Ca^{2+} Transients

With regards to the deepening and apposition Ca^{2+} signals generated in zebrafish, it was reported that application of heparin or 2-APB, at a time to specifically challenge the deepening transient, inhibited the Ca^{2+} signal and blocked furrow deepening [37]. On the other hand, treatment with ryanodine, ruthenium red (another ryanodine receptor antagonist), nifedipine or verapimil had no effect on either the deepening Ca^{2+} transient or furrow deepening. It was also shown (via immunolabeling experiments) that the ER and IP_3 receptors were localised on either side of the cleavage furrow during furrow deepening. Thus, together these data support the initial suggestion of Chang and Meng [59] that the localized increase in intracellular [Ca^{2+}] observed during furrow deepening is likely to be derived mainly from the ER, and that Ca^{2+} is released into the cytoplasm via IP_3 receptors.

Since then, it has been shown in zebrafish that while furrow positioning, propagation and deepening require Ca^{2+} that is released from the ER via IP_3 receptors, for the successful apposition of the two daughter cells, the entry of extracellular Ca^{2+} is needed [23]. In support of this observation, use of a scanning ion-selective electrode [75] to measure the Ca^{2+} fluxes in the immediate vicinity of the deepening furrow, demonstrated that when embryos were maintained in normal (Ca^{2+}-containing) medium, there was a small but measureable efflux of intracellular Ca^{2+} at the base of the furrow, but there was a distinct influx of extracellular Ca^{2+} in the sides of the deepening furrow [76]. In addition, again in zebrafish embryos, store-operated Ca^{2+} entry (SOCE) has been shown to play a role in refilling the ER and thus maintaining the elevated levels of intracellular Ca^{2+} for the sustained period required for furrow

deepening and apposition to occur [76]. It was estimated that in zebrafish at 28°C, it takes ~9–13 min for deepening and apposition to be completed, and during this time the intracellular [Ca^{2+}] rises ~5-fold above the resting level of Ca^{2+} (i.e., from ~100 nM to ~500 nM). This is in contrast to the more superficially-located furrow positioning and propagation signals, which last just ~1 min and ~2–5 min, respectively (see Fig. 15.1). When embryos were treated with the STIM1 inhibitor, SKF 96365, furrow positioning and propagation occurred normally. However, although furrow deepening was initiated, it was not successfully completed to separate the two daughter cells and the cleavage furrow that was initially formed underwent regression [76]. In addition, in aequorin-loaded SKF 96365-treated embryos, a furrow positioning Ca^{2+} transient was observed and this developed into a small furrow propagation transient and thereafter into a very small (from both the volume and [Ca^{2+}] point of view) deepening transient. However, no distinct furrow apposition transient was observed [76]. Additional supporting evidence for SOCE during furrow deepening was provided by immunolabeling studies, which demonstrated that component members of SOCE (i.e., STIM1 in the ER, and both Orai1 and TRPC1 in the plasma membrane), are localised in the sides of the cleavage furrow during furrow deepening [76, 77]. The localization of the ER, IP_3 receptor, STIM1, Orai1 and TRPC1 in the deepening furrow during cytokinesis of the first cell division cycle in zebrafish embryos is shown in Fig. 15.2. Interestingly, TRPC1 has also been shown to play a key role in cytokinesis in the human grade IV D54MG glioma (brain tumour) cell line [78]. When the function of TRPC1 was genetically suppressed in these cells (via transfection with TRPC1 shRNA) or pharmacologically inhibited (by treatment with SKF 96365, 2-APB or MRS1845), SOCE was inhibited and cytokinesis was blocked. The authors went on to suggest that as the pharmacological inhibition of TRPC1 appeared to slow the growth of glioma tumours, this strategy is worth investigating as a possible therapeutic treatment for this type of highly malignant cancer [78].

15.3 Possible Targets of the Cytokinetic Ca^{2+} Transients

15.3.1 The Positioning and Propagation Ca^{2+} Transients

It was studies conducted in the 1970s–1990s with sea urchin, sand dollar, and newt embryos, which first indicated that cytokinesis involves the formation and contraction of an actomyosin ring or band at the base of the cleavage furrow [15, 79, 80]. Since then, there have been a number of suggestions with regards to the role played by Ca^{2+} in this process, including: the recruitment of microfilaments into the contractile band [24]; the regulation of binding between actin and myosin [67]; and the regulation of the contraction process itself via the Ca^{2+}/calmodulin-activated myosin light chain kinase (MLCK; [59, 81–83]). The precise function of Ca^{2+} in the assembly and/or contraction of the actomyosin contractile ring/band might prove to be species- and/or cell type-specific. For example, whereas MLCK is reported to play a key

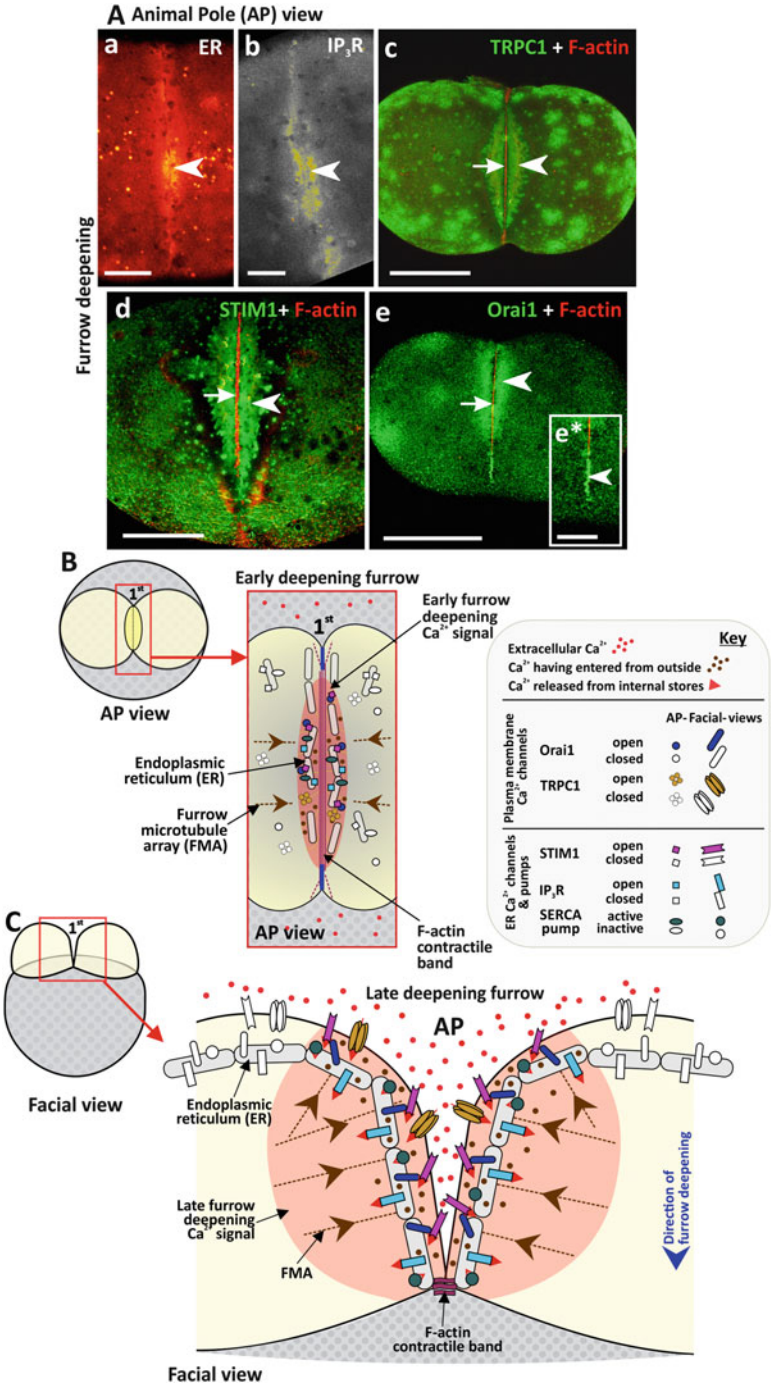

Fig. 15.2 Localization of the main Ca^{2+} store and Ca^{2+} release channel as well as components of SOCE that have been shown to play a role during furrow deepening of the first cell division cycle in zebrafish embryos. (**A**) These are series of single optical sections that have been projected as single

role in cytokinesis in *Dictyostelium discoidium* [82], crane fly (*Nephrotoma suturalis*) and *Drosophila melanogaster* spermatocytes [84]; and in human oral cancer cells [85], it does not appear to play a role in cytokinesis in early *C. elegans* embryos [86].

In zebrafish, the role of Ca^{2+} with respect to the assembly of the contractile band has not yet been fully explored. However, it was recently demonstrated that in these large embryos there is a biphasic assembly of the acto-myosin contractile apparatus [87]. Thus, initially a restricted arc of F-actin patches form along the presumptive furrow plane at the animal pole, in what was called the 'assembly phase'. These patches then fuse together to form F-actin cables, which subsequently become bundled together forming the F-actin band proper, during what was called the 'extension phase'. It was also shown that phosphorylated myosin light chain 2 (MLC2) is not associated with the initial arc of F-actin formed during the assembly phase, but that clusters of MLC2 are recruited into the extending ends of the contractile band during the extension phase. As a result, it was suggested that the MLC2-free region of the contractile band is required to position and act as a scaffold to extend the cleavage furrow, whereas the actomyosin ends generate the force required for furrow deepening [87].

It has also been suggested that the positioning Ca^{2+} transient might also play a role in the all-important adhesion of the contractile ring to the plasma membrane, an essential step for successful cytokinesis [88, 89]. Phosphatidylinositol 4,5-bisphosphate (PIP_2), an intermediate in the IP_3/diacylglycerol signalling pathway and substrate of phospholipase C (PLC), has been shown to accumulate in the furrow during cytokinesis in a variety of cells in culture, including Chinese hamster ovary (CHO), HeLa, NIH-3T3 and MDCK cells [90, 91]. In addition, when the levels of PIP_2 were reduced either genetically or pharmacologically, then the normal

Fig. 15.2 (continued) images to show the localization of the (**a**) ER, (**b**) IP_3 receptor, (**c**) TRPC1, (**d**) STIM1, and (**e**) Orai1 from an animal pole view. For panels (**a**–**e**) the arrowheads indicate the respective protein of interest, whereas in panels (**c**–**e**) the arrows indicate F-actin which is co-labeled with the various SOCE proteins. (**e***) The inset panel shows the elevated level of Orai1 in the base of the deepening furrow at the edges of the blastodisc. Scale bars are (**a,b,e***) 50 μm and (**c**–**e**) 200 μm. (**B**) Schematic illustrations of low and higher magnification animal pole views of an embryo to show the actomyosin contractile band and the associated ER, IP_3 receptor, TRPC1, STIM1, and Orai1 localized in the deepening cleavage furrow during the first cell division cycle. (**C**) Schematic illustrations of low and higher magnification facial views of an embryo showing how SOCE in combination with Ca^{2+} released from the ER via activation of IP_3 receptors might be required to maintain the high levels of Ca^{2+} in the furrow region for successful furrow deepening and apposition to take place. Panels **Aa** and **Ab** are reprinted with permission from "Ca^{2+} released via IP_3 receptors is required for furrow deepening during cytokinesis in zebrafish eggs" by Lee KW, Webb SE, Miller AL, 2003. International Journal of Developmental Biology, 47, 411–421. UBC Press. Panel **Ac** is reprinted with permission from "Inhibition of SOCE disrupts cytokinesis in zebrafish embryos mainly via inhibition of cleavage furrow deepening" by Chan CM, Chen Y, Hung TS, Miller AL, Shipley AM, Webb SE, 2015. International Journal of Developmental Biology, 59, 289–301. UBC Press. Panels **Ad** and **Ae** are reprinted with permission from "SOCE proteins, STIM1 and Orai1, are localized to the cleavage furrow during cytokinesis of the first and second cell division cycles in zebrafish embryos" by Chan CM, Aw JTM, Webb SE, Miller AL, 2016. Zygote, 24, 880-889. Cambridge University Press

adhesion between the plasma membrane and cytoskeleton was affected [90]. In an earlier report, Han *et al*. [92] demonstrated that the injection of a monoclonal anti-PIP_2 antibody into one blastomere of 2-cell stage *Xenopus* embryos, resulted in the inhibition of cleavage in that blastomere, while the uninjected sister blastomere divided normally. More recently, it has been shown that PIP_2 and PIP_2 hydrolysis are both required for cytokinesis in *Drosophila* spermatocytes [93] and that PIP_2 hydrolysis controls the actin dynamics that occur during constriction of the actomyosin contractile ring in both *Drosophila* and crane fly spermatocytes through the Ca^{2+} activation of myosin via MLCK [84]. PIP_2 is also involved in localising the scaffold protein, anillin, to the cleavage furrow [94]. Anillin links RhoA to the actomyosin contractile ring during cytokinesis [95], and it also helps to maintain the stability of the furrow by linking the actomyosin contractile band/ring with septin filaments [96], which are themselves tightly linked to the plasma membrane [97]. Indeed, in *Drosophila* spermatocytes undergoing cytokinesis, anillin has been shown to recruit septins to the cleavage furrow and to maintain F-actin and myosin II in the correct location during the later stages of cytokinesis [96]. In an earlier report in syncytial blastoderm stage *Drosophila* embryos, both F-actin and myosin II were shown to be transported along microtubules and then co-localize in regions where pseudocleavage furrows form [98]. In addition, in sea urchin (*Lytechinus pictus*) eggs, myosin II has been shown to be transiently activated globally before the cleavage plane is specified, and during cell division it is activated by both the MLCK and Rho-kinase pathways [99].

Calmodulin is another Ca^{2+}-binding protein, which appears to play a role in the earliest stages of cytokinesis as it is reported to determine the positioning and timing of cleavage furrow formation [100]. In HeLa cells, a GFP-tagged CaM was shown to concentrate in the sub-membranous region of the cell during much of the cell cycle and it accumulated at the equatorial region just prior to the formation of the cleavage furrow. In addition, when a CaM-specific inhibitory peptide was injected into cells during early anaphase, this lead to either a partial or full inhibition of cytokinesis [100]. It was subsequently demonstrated, again in HeLa cells, that calmodulin is initially associated with the spindle microtubules, and then it accumulates at the central spindle. In addition, as treatment with the Ca^{2+}/CaM inhibitor, W7, blocked the assembly of the central spindle and prevented the formation of the cleavage furrow, it was suggested that it is the central spindle that is important for the formation of the cleavage furrow in these cells [101].

Calmodulin has also been demonstrated to accumulate in the cleavage furrow of zebrafish embryos during cytokinesis [87]. Similar to the pattern of localisation in HeLa cells, calmodulin is localised in the cortex of zebrafish embryos throughout cytokinesis and it first becomes visible prior to the indentation in the plasma membrane that indicates the positioning of the cleavage furrow. When visualizing the region of calmodulin labelling from a top view, it starts off as a small, relatively diffuse arc at the animal pole; this appears to correspond (from the timing and location) with the arc of the forming contractile band during furrow positioning. Calmodulin then continues to be localized in the contractile band as it grows across the blastodisc, and it is localized in the sides of the cleavage furrow where it grows in

length and width as the furrow propagates. The pattern of labelling then continues to grow in width (during furrow deepening), and finally it narrows and the overall level of fluorescence appears to get less intense (during furrow apposition). Calmodulin labelling in the contractile band disappears in the central region of the furrow during apposition but lingers at the lateral ends of the contractile band suggesting that these regions are responsible for generating the force required for furrow deepening [87]. While calmodulin might therefore prove to be one of the targets of the cytokinetic Ca^{2+} transients in zebrafish embryos and HeLa cells, it does not appear to play a role in cytokinesis in early *C. elegans* embryos [86]. This is an example, which appears to demonstrate that the signalling pathways involved in cytokinesis are not completely conserved between species, and thus species-specific differences do occur.

The Rho family of GTPases has been shown to regulate changes in cell shape by affecting the formation of actin structures just under the surface of the plasma membrane. It has been demonstrated that the binding of Ca^{2+} to calmodulin activates Ca^{2+}/calmodulin-dependent kinase II (CaMKII), which in turn activates RhoA and Cdc42 [102]. Interestingly, during cytokinesis in *Xenopus* embryos, Rho has been shown to regulate the assembly of F-actin in the cortex and it plays a key role in the constriction of the cleavage furrow, whereas Cdc42 plays a role in furrow deepening [103].

Annexin A2 has also been demonstrated to play a necessary role in the early stages of cytokinesis. This is a Ca^{2+}- and phospholipid-binding protein, which plays a role in remodelling actin in the cortex of cells. In HeLa cells, annexin A2 has been shown to accumulate in the equatorial cortex at the start of cytokinesis [104]. However, on the siRNA-mediated down-regulation of this protein, RhoA fails to form a compact ring around the equator of the cell, and the normal association between the equatorial cortex and central spindle is lost. This leads to the formation of defective cleavage furrows and hence a failure of cytokinesis [105].

15.3.2 The Deepening and Apposition Ca^{2+} Transients

Aside from its role in the positioning and propagation of the cleavage furrow via the assembly and contraction of the contractile band, the role played by Ca^{2+} during the later stages of cytokinesis (i.e., during furrow deepening and apposition), is becoming more apparent. In zebrafish embryos, the furrow deepening Ca^{2+} transient has been suggested to play a role in the recruitment and exocytosis of vesicles at the plasma membrane of the deepening furrow [35]. A number of groups have demonstrated that vesicle trafficking plays a crucial role in membrane remodelling during cytokinesis in various animal cells, including: in zebrafish, sea urchin, *Xenopus, Drosophila*, and *C. elegans* embryos, as well as in *Drosophila* spermatocytes and *Dictyostelium* cells [29, 43, 48, 105]. There are a number of excellent recent reviews that describe membrane trafficking during cytokinesis [29, 50, 54, 106–108], and with the latest advances in cell imaging techniques, the identity and function of the trafficking components are now starting to be revealed. In zebrafish embryos, it was

demonstrated that two cognate SNARE partners, VAMP-2 and SNAP-25, mediate vesicle fusion at the deepening and apposing cleavage furrow membranes [23]. It was also shown that VAMP-2 vesicle fusion is not required for furrow deepening but is essential for successful daughter cell apposition. In addition, starting during late deepening finger-like plasma membrane projections, which express both F-actin and VAMP-2, appear on either side of the furrow and form bridges to span the furrow (Fig. 15.3Ai, B). As the plasma membrane on either side of the furrow undergoes apposition, a VAMP-2-rich boundary forms between the adjacent blastomeres (Fig. 15.3B; [23]). Furthermore, it was shown that microtubules are required for the recruitment of VAMP-2 vesicles to the furrow [23] These data support an earlier report by Jesuthasan [43], who demonstrated that microtubules are required for the apposition of daughter blastomeres in zebrafish embryos, and he suggested that they might mediate the trafficking of intracellular vesicles to the furrow plasma membrane. Furthermore, he also reported that vesicles are exocytosed at the furrow membrane, and in this way vesicle cargos of proteins such as cadherins and catenins are delivered at the right time and in the correct location to promote Ca^{2+}-sensitive blastomere apposition.

More recently, the fusion of VAMP-2 vesicles in the deepening furrow was demonstrated to require an elevation of Ca^{2+} that is released from intracellular stores via IP_3 receptors [33]. The role of IP_3 receptors in the extensive remodelling of the membrane that takes place during furrow deepening and apposition in zebrafish is supported by a report from sea urchin embryos where Ca^{2+} released from heparin-sensitive intracellular stores was shown to be required for the addition of new membrane during cytokinesis ([48]).

Intracellular Ca^{2+} is also required for the extensive remodelling of F-actin, which takes place during furrow deepening, for example, for the assembly and extension of the contractile band and for the formation of pericleavage actin enrichments (PAEs), which are located in the cortex of the deepening furrow on either side of the contractile band [33, 109]. VAMP-2 fusion also requires the presence of the PAEs, and both VAMP-2 fusion and PAE formation require the action of calpains [33]. The latter are Ca^{2+}-dependent, cytosolic cysteine proteases, which act upstream of members of the Rho GTPase family in the integrin signalling pathway, and they play a role in cell differentiation, proliferation and apoptosis [110]. In addition, the transport of VAMP-2 vesicles along microtubules to the cleavage furrow has been shown to be dependent on the recruitment of kif23, a homologue of mitotic kinesin-like protein 1 (Mklp1) to the furrow region, and that the localization of kif23 is also Ca^{2+}-dependent [33]. This confirms an earlier report demonstrating that GFP-tagged Mklp1 colocalizes with microtubules in the cleavage furrow during the early cell division cycles in zebrafish embryos, and that when embryos were injected with dominant-negative variants of GFP-Mklp1 then cytokinesis frequently failed to complete [111]. Furthermore, other kinesin-like proteins have been shown to play a significant role in the formation of the midbody matrix and be required for the completion of cytokinesis in *C. elegans* embryos [112], as well as in CHO and HeLa cells [113–115].

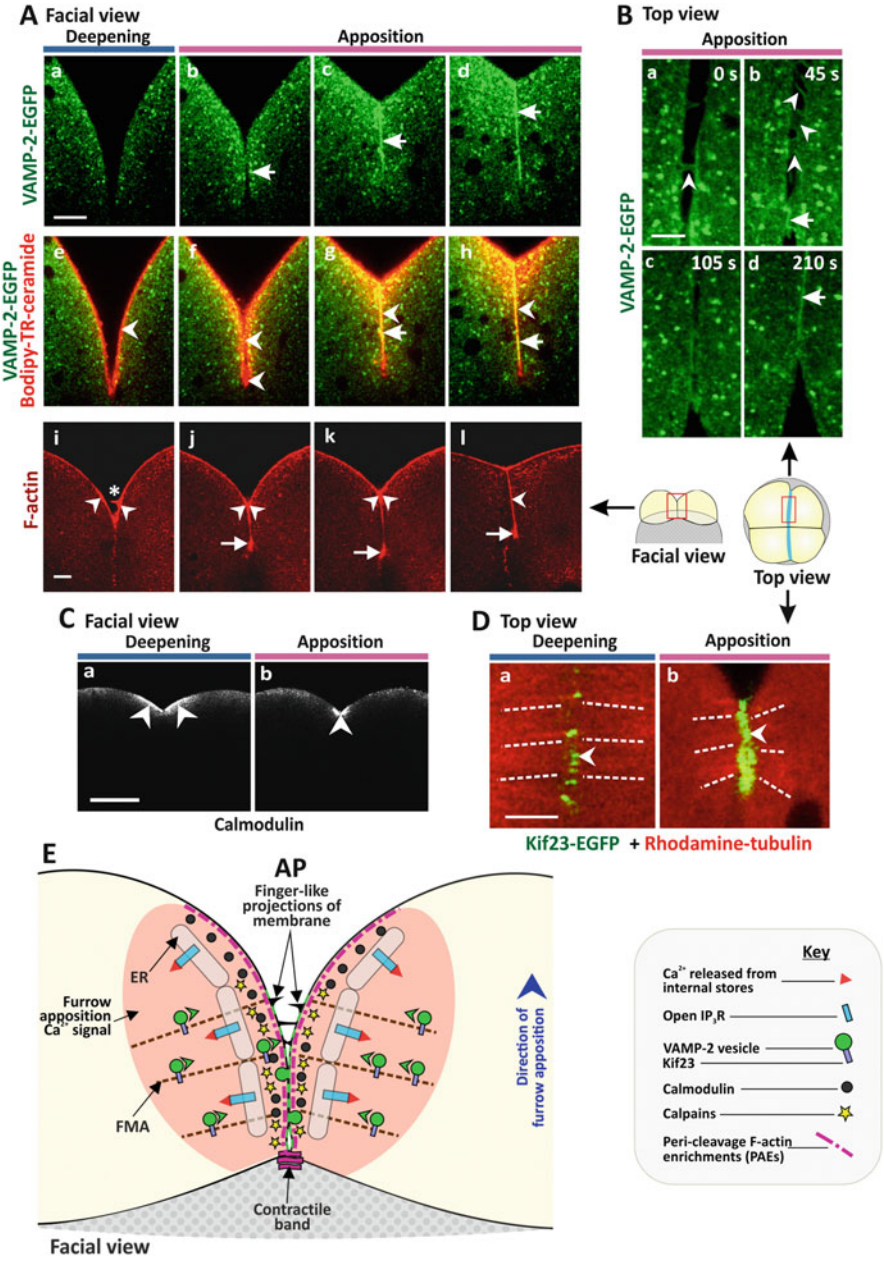

Fig. 15.3 Localization of VAMP-2 vesicles and Kif23, along with F-actin, microtubules and calmodulin in the cleavage furrow during furrow apposition of the early cell division cycles in zebrafish embryos. (**Aa**–**Ah**) Accumulation of VAMP2 in vesicles in the furrow at the end of deepening and during apposition. These images show localization of (**Aa**–**Ad**) VAMP2-EGFP alone and (**Ae**–**Ah**) both VAMP2-EGFP and Bodipy-TR-ceramide (the latter being a fluorescent lipid used to label to the plasma membrane; see arrowheads). The arrows indicate VAMP2, which accumulates in vesicles toward the end of deepening, and is then incorporated into the plasma membrane separating the two new daughter

In addition to its role in early cytokinesis, myosin II is also required for the later cleavage stages in zebrafish. Urven *et al*. [109] demonstrated that it plays a role in the recruitment of components of the adhesion junctions, i.e., β-catenin, and the pericleavage F-actin to the furrow, as well as in the remodelling of the FMA, and the disassembly of the FMA and contractile ring towards the end of cytokinesis. As myosin II did not appear to be involved in furrow deepening, they suggested that its main role is for the recruitment of cell adhesion components as well as remodelling of the cytoskeleton during the maturation of the furrow [109].

Actin depolymerizing factor (ADF)/cofilin has also been reported to play a key role in the later stages of cytokinesis. It has been shown to localize to the contractile band/ring at the end of cleavage in a number of different cell types, including *Xenopus* and *C. elegans* embryos [116, 117]. In addition, when the expression of ADF/cofilin was knocked down or inhibited in these embryos, this resulted in a failure of cytokinesis and the embryos became multinucleated [116, 117]. It has also been reported that ADF/cofilin can modulate Ca^{2+} signalling; in starfish oocytes for example, it was shown to enhance Ca^{2+} release by both IP_3 and NAADP, and in this way modulate the pattern of Ca^{2+} signalling during activation and fertilization [118]. Thus, although evidence is currently limited, ADF/cofilin associated with the contractile band in large embryos might also prove to (in some way) modulate

Fig. 15.3 (continued) cells during apposition. (**Ai–Al**) Localization of F-actin in the furrow during deepening and apposition. F-actin is localized in the sides (arrowheads) and base (arrows) of the furrow. The asterisk in panel (**Ai**) indicates an F-actin-rich finger-like membrane projection on one side of the deepening furrow. (**B**) Such finger-like membrane projections precede furrow apposition and appear from both sides of the furrow (arrowheads in panels **Ba** and **Bb**). In addition to F-actin, VAMP2-EGFP is also localized in these projections. Apposition of the blastomeres is complete when a VAMP2-EGFP-labeled boundary appears due to the cohesion of the plasma membrane from both sides of the furrow (arrows in panels **Bb** and **Bd**). (**C**) Localization of calmodulin (arrowheads) in the (**Ca**) deepening and (**Cb**) apposing cleavage furrow during the first cell division cycle. (**D**) Localization of Kif23-EGFP (arrowheads) and microtubules (labeled with rhodamine-tagged tubulin- see white dashed lines) in the (**Da**) deepening and (**Db**) apposing cleavage furrow. (**E**) Schematic illustration to show how Ca^{2+} released from intracellular stores via the IP_3 receptor might play a role in furrow apposition. We have previously shown that the fusion of VAMP2 vesicles to the plasma membrane, recruitment of Kif23 and formation of the PAEs, as well as the remodeling, stabilization and construction of the contractile band are all Ca^{2+}-dependent [33]. In addition, we have shown that VAMP2 vesicles are transported along furrow microtubule arrays (FMAs), that Kif23 plays a role in moving the vesicles along the FMAs and that calpains and the PAEs play a role in the fusion process too [33]. As calmodulin is also found in the cleavage furrow throughout cytokinesis [87], this might play some role in transducing the deepening and apposition Ca^{2+} signals to effect these various cellular activities. Scale bars are (**A**) 20 μm; (**B** and **D**) 10 μm; and (**C**) 100 μm. Panels **Aa–Ah** and **B** are reprinted with permission from "Recruitment and SNARE-mediated fusion of vesicles in furrow membrane remodeling during cytokinesis in zebrafish embryos" by Li WM, Webb SE, Lee KW, Miller AL, 2006, Experimental Cell Research, 312, 3260–3275. Elsevier Inc. Panels **Ai–Al** and **D**, are reprinted with permission from "Multiple roles of the furrow deepening Ca^{2+} transient during cytokinesis in zebrafish embryos" by Li WM, Webb SE, Chan CM, Miller AL, 2008, Developmental Biology, 316, 228–248. Elsevier Inc. Panel **C** is reprinted with permission from "Biphasic assembly of the contractile apparatus during the first two cell division cycles in zebrafish embryos" by Webb SE, Goulet C, Chan CM, Yuen MYF, Miller AL, 2014, Zygote, 22, 218–228. Cambridge University Press

the cytokinetic Ca^{2+} transients, particularly during deepening towards the end of cleavage when substantially higher levels of Ca^{2+} are generated over a relatively long-duration [37].

It has also been suggested that members of the copine family of Ca^{2+}-dependent membrane-binding proteins might play a role in cytokinesis. Copines are highly and ubiquitously expressed proteins in a wide variety of different animal (and plant) species, including *Paramecium tetraurelia*, *Dictyostelium*, *C. elegans*, mice and humans [119, 120]. In *Dictyostelium,* Damer *et al*. [120] demonstrated that copine A is localized to the plasma membrane and various intracellular vacuoles, including endolysosomal organelles. In addition, cells in which *CpnA* was knocked out exhibited cytokinesis defects. The authors suggested that during cytokinesis, CpnA might bind to vesicles that are targeted for the plasma membrane at the cleavage furrow [120]; thus they might help to regulate the addition of new membrane to the cleavage furrow during the latter stages of cytokinesis.

15.4 Conclusions

Out of the possible targets suggested for all four of the cytoplasmic Ca^{2+} transients, those associated either directly or indirectly with remodelling the plasma membrane feature prominently. Indeed it has been proposed that the cytokinetic Ca^{2+} transients might serve multiple functions at different stages of the cytokinesis process depending on the cell type in question [33]; whether they are embryonic or somatic; whether they divide evenly or unevenly, and if they are embryonic, then whether they divide holoblastically or meroblastically. We propose that for each type of cell, specific components of the so-called 'Ca^{2+} signalling toolkit' [121] are expressed along with the required Ca^{2+}-sensitive targets in order to orchestrate the form of cell division required. Furthermore, we suggest that the same Ca^{2+} signal might target several components involved in the regulation of cytokinesis either simultaneously, or at different times. A possible example of simultaneous stimulation is the IP_3 receptor-mediated deepening Ca^{2+} transient, which might serve to regulate the constriction of the actomyosin contractile band, while also promoting the transport and fusion of vesicles to add new membrane to the deepening furrow walls. We suggest that the ongoing development of super-resolution microscopy techniques that can be readily applied to living cells, as well as the continuing improvements in Ca^{2+} imaging methodologies with regards to both the reporters and detectors, bode well for the continued progress in this field.

Acknowledgments We acknowledge funding support from Hong Kong Research Grants Council (RGC) General Research Fund awards 662113, 16101714 and 16100115; the ANR/RGC joint research scheme award A-HKUST601/13 and the Hong Kong Theme-based Research Scheme award T13-706/11-1. We also acknowledge funding support from the Hong Kong Innovation and Technology Commission (ITCPD/17-9).

References

1. Atilla-Gokcumen GE, Castoreno AB, Sasse S, Eggert US (2010) Making the cut: the chemical biology of cytokinesis. ACS Chem Biol 5:79–90
2. Barr FA, Gruneberg U (2007) Cytokinesis: placing and making the final cut. Cell 131:847–860
3. Green RA, Paluch E, Oegema K (2012) Cytokinesis in animal cells. Ann Rev Cell Dev Biol 28:29–58
4. McMichael CM, Bednarek SY (2013) Cytoskeletal and membrane dynamics during higher plant cytokinesis. New Phytol 197:1039–1057
5. Oliferenko S, Chew TG, Balasubramanian MK (2009) Positioning cytokinesis. Genes Dev 23:660–674
6. Pollard TD (2010) Mechanics of cytokinesis in eukaryotes. Curr Opin Cell Biol 22:50–56
7. Dan K, Dan JC (1940) Behavior of the cell surface during cleavage III. On the formation of new surface in the eggs of *Strongylocentrotus pulcherrimus*. Biol Bull 78:486–501
8. Dan K, Yanagita T, Sugiyama M (1937) Behavior of the cell surface during cleavage I. Protoplasma 28:66–81
9. Motomura I (1940) Studies of cleavage I. Changes in the surface area of different regions of eggs of a sea urchin in the course of the first cleavage. Sci Rep Tôhoku Imp Univ Ser 4 15:121–130
10. Rappaport R, Ratner JH (1967) Cleavage of sand dollar eggs with altered patterns of new surface formation. J Exp Zool 165:89–100
11. Tilney LG, Marsland D (1969) A fine structural analysis of cleavage induction and furrowing in the eggs of *Arbacia punctulata*. J Cell Biol 42:170–184
12. Gray J (1924) The mechanism of cell-division I. The forces which control the form and cleavage of the eggs of *Echinus esculentus*. Biol Rev 1:164–188
13. Motomura I (1941) Studies of cleavage II. Cleavage of the cells of a sea urchin, *Strongylocentrotus pulcherrimus,* in calcium-free sea water. Sci Rep Tôhoku Imp Univ, Ser 4 16:283–290
14. Dan K (1954) Further study on the formation of the "new membrane" in the eggs of the sea urchin, *Hemicentrotus (Strongylocentrotus) pulcherrimus*. Embryologia 2:99–113
15. Selman GG, Perry MM (1970) Ultrastructural changes in the surface layers of the newt's egg in relation to the mechanism of its cleavage. J Cell Sci 6:207–227
16. Selman GG, Waddington CH (1955) The mechanism of cell division in the cleavage of the newt's egg. J Exp Biol 32:700–733
17. Dan K, Kuno Kojima M (1963) A study on the mechanism of cleavage in the amphibian egg. J Exp Biol 40:7–14
18. Sawai T (1976) Movement of the cell surface and change in surface area during cleavage in the newt's egg. J Cell Sci 21:537–551
19. Sawai T (1987) Surface movement in the region of the cleavage furrow of amphibian eggs. Zool Sci (Tokyo) 4:825–832
20. Woodward DJ (1968) Electrical signs of new membrane production during cleavage of *Rana pipiens* eggs. J Gen Physiol 52:509–531
21. Bluemink JG, de Latt SW (1973) New membrane formation during cytokinesis in normal and cytochalasin B-treated eggs of *Xenopus laevis* I. Electron microscope observations. J Cell Biol 59:89–108
22. Byers TJ, Armstrong PB (1986) Membrane protein redistribution during *Xenopus* first cleavage. J Cell Biol 102:2176–2184
23. Li WM, Webb SE, Lee KW, Miller AL (2006) Recruitment and SNARE-mediated fusion of vesicles in furrow membrane remodeling during cytokinesis in zebrafish embryos. Exp Cell Res 312:3260–3275
24. Fluck RA, Miller AL, Jaffe LA (1991) Slow calcium waves accompany cytokinesis in medaka fish eggs. J Cell Biol 115:1259–1265

25. Lecuit T, Wieschaus E (2000) Polarized insertion of new membrane from a cytoplasmic reservoir during cleavage of *Drosophila* embryo. J Cell Biol 150:849–860
26. Takeda T, Robinson IM, Savoian MM, Griffiths JR, Whetton AD, McMahon HT, Glover DM (2013) *Drosophila* F-BAR protein Syndapin contributes to coupling the plasma membrane and contractile ring in cytokinesis. Open Biol 3:130081. https://doi.org/10.1098/rsob.130081
27. Skop AR, Bergmann D, Mohler WA, White JG (2001) Completion of cytokinesis in *C. elegans* requires a brefeldin A-sensitive membrane accumulation at the cleavage furrow apex. Curr Biol 11:735–746
28. Rappaport R (1996) Cytokinesis in animal cells. Developmental and cell biology series. Cambridge University Press, Cambridge, UK
29. Albertson R, Riggs B, Sullivan W (2005) Membrane traffic: a driving force in cytokinesis. Trends Cell Biol 15:92–101
30. Straight AF, Field CM (2000) Microtubules, membranes and cytokinesis. Curr Biol 10: R760–RR70
31. Dan K (1988) Mechanism of equal cleavage of sea urchin egg: transposition from astral mechanism to constricting mechanism. Zool Sci 5:507–517
32. Schroeder TE (1972) The contractile ring. II Determining its brief existence, volumetric changes, and vital role in cleaving *Arbacia* eggs. J Cell Biol 53:419–434
33. Li WM, Webb SE, Chan CM, Miller AL (2008) Multiple roles of the furrow deepening Ca^{2+} transient during cytokinesis in zebrafish embryos. Dev Biol 316:228–248
34. Lee KW, Ho SM, Wong CH, Webb SE, Miller AL (2004) Characterization of mid-spindle microtubules during furrow positioning in early cleavage period zebrafish embryos. Zygote 12:221–230
35. Lee KW, Webb SE, Miller AL (2006) Requirement for a localized, IP_3R-generated Ca^{2+} transient during the furrow positioning process in zebrafish zygotes. Zygote 14:143–155
36. Webb SE, Lee KW, Karplus E, Miller AL (1997) Localized calcium transients accompany furrow positioning, propagation, and deepening during the early cleavage period of zebrafish embryos. Dev Biol 192:78–92
37. Lee KW, Webb SE, Miller AL (2003) Ca^{2+} released via IP_3 receptors is required for furrow deepening during cytokinesis in zebrafish eggs. Int J Dev Biol 47:411–421
38. Guertin DA, Trautmann S, McCollum D (2002) Cytokinesis in eukaryotes. Microbiol Mol Biol Rev 66:155–178
39. Guizetti J, Gerlich DW (2010) Cytokinetic abscission in animal cells. Sem Cell Dev Biol 21:909–916
40. Rothfield LI, Justice SS (1997) Bacterial cell division: the cycle of the ring. Cell 88:581–584
41. Yeong FM (2005) Severing all ties between mother and daughter: cell separation in budding yeast. Mol Micro 55:1325–1331
42. Danilchik MV, Brown EE (2008) Membrane dynamics of cleavage furrow closure in *Xenopus laevis*. Dev Dyn 237:565–579
43. Jesuthasan S (1998) Furrow-associated microtubule arrays are required for the cohesion of zebrafish blastomeres following cytokinesis. J Cell Sci 111:3695–3703
44. Muto A, Kume S, Inoue T, Okano H, Mikoshiba K (1996) Calcium waves along the cleavage furrows in cleavage-stage *Xenopus* embryos and its inhibition by heparin. J Cell Biol 135:181–190
45. Webb SE, Miller AL (2007) Ca^{2+} signaling during embryonic cytokinesis in animal systems. In: Krebs J, Michalak M (eds) Calcium: a matter of life and death. Elsevier, B.V., Amsterdam, The Netherlands, pp 445–470. https://doi.org/10.1016/S0167-7306(06)41017-6
46. Aimar C (1997) Formation of new plasma membrane during the first cleavage cycle in the eggs of *Xenopus laevis*: an immunocytological study. Dev Growth Dev 39:693–704
47. Danilchik MV, Funk WC, Brown EE, Larkin K (1998) Requirement for microtubules in new membrane formation during cytokinesis of *Xenopus* embryos. Dev Biol 194:47–60
48. Shuster CB, Burgess DR (2002) Targeted new membrane addition in the cleavage furrow is a late, separate event in cytokinesis. Proc Natl Acad Sci USA 99:3633–3638

49. Finger FP, White JG (2002) Fusion and fission: membrane trafficking in animal cells. Cell 108:727–730
50. Schiel JA, Prekeris R (2013) Membrane dynamics during cytokinesis. Curr Opin Cell Biol 25:92–98
51. Bezanilla M, Gladfelter AS, Kovar DR (2015) Cytoskeletal dynamics: a view from the membrane. J Cell Biol 209:329–337
52. Heng YW, Koh CG (2010) Actin cytoskeleton dynamics and the cell division cycle. Int J Biochem Cell Biol 42:1622–1633
53. Miller AL, Fluck RA, MccLaughlin JA, Jaffe LF (1993) Calcium buffer injections inhibit cytokinesis in *Xenopus* eggs. J Cell Sci 106:523–534
54. Simon GC, Prekeris R (2008) Mechanisms regulating targeting of recycling endosomes to the cleavage furrow during cytokinesis. Biochem Soc Trans 36:391–394
55. Arnold JM (1975) An effect of calcium in cytokinesis as demonstrated with ionophore A 23187. Cytobiologie 11:1–9
56. Baker PF, Warner AE (1972) Intracellular calcium and cell cleavage in early embryos of *Xenopus laevis*. J Cell Biol 53:579–581
57. Ridgway EB, Gilkey JC, Jaffe LF (1977) Free calcium increases explosively in activating medaka eggs. Proc Natl Acad Sci USA 74:623–627
58. Schroeder TE, Strickland DL (1974) Ionophore A23187, calcium and contractility in frog eggs. Exp Cell Res 83:139–142
59. Chang DC, Meng C (1995) A localized elevation of cytosolic free calcium is associated with cytokinesis in the zebrafish embryo. J Cell Biol 131:1539–1545
60. Créton R, Speksnijder JE, Jaffe LF (1998) Patterns of free calcium in zebrafish embryos. J Cell Sci 111:1613–1622
61. Shantz AR (1985) Cytosolic free calcium-ion concentration in cleaving embryonic cells of *Oryzias latipes* measured with calcium-selective microelectrodes. J Cell Biol 100:947–954
62. Miller AL, Karplus E, Jaffe LF (1994) Use of aequorin for $[Ca^{2+}]_i$ imaging. Chapter 13. In: Nuccitelli R (ed) Methods in cell biology, Vol 40: a practical guide to the study of Ca^{2+} in living cells. Academic press, San Diego, pp 305–338
63. Chang DC, Lu P (2000) Multiple types of calcium signals are associated with cell division in zebrafish embryo. Micros Res Tech 49:111–122
64. Guo YB, Wen Y, Gao WX, Li JC, Zhou P, Bai ZL, Zhang B, Wang SQ (2010) The formation of Ca^{2+} gradients at the cleavage furrows during cytokinesis of zebrafish embryos. Front Biol 5:369–377
65. Chen J, Xia L, Bruchas MR, Solnica-Krezel L (2017) Imaging early embryonic calcium activity with GCaMP6s transgenic zebrafish. Dev Biol 430(2):385–396
66. Stricker SA (1995) Time-lapse confocal imaging of calcium dynamics in starfish embryos. Dev Biol 170:496–518
67. Silver RB (1996) Calcium, BOBs, QEDs, microdomains and a cellular decision: control of mitotic cell division in sand dollar blastomeres. Cell Calc 20:161–179
68. Ciapa B, Pesando D, Wilding M, Whitaker M (1994) Cell-cycle calcium transients driven by cyclic changes in inositol trisphosphate levels. Nature 368:875–878
69. Peonie M, Alderton J, Tsien RY, Steinhardt RA (1985) Changes of free calcium levels with stages of the cell division cycle. Nature 315:147–149
70. Liu X, Wang P, Fu J, Lv D, Chen D, Li Y, Ma W (2011) Two-photon fluorescence real-time imaging on the development of early mouse embryo by stages. J Microsc 241:212–218
71. Mitsuyama F, Sawai T, Carafoli E, Furuichi T, Mikoshiba K (1999) Microinjection of Ca^{2+} store-enriched microsome fractions to dividing newt eggs induces extra-cleavage furrows via inositol 1,4,5- trisphosphate-induced Ca^{2+} release. Dev Biol 214:160–167
72. Mitsuyama F, Sawai T (2001) The redistribution of Ca^{2+} stores with inositol 1,4,5-trisphosphate receptor to the cleavage furrow in a microtubule-dependent manner. Int J Dev Biol 45:861–868

73. Mitsuyama F, Futatsugi Y, Okuya M, Karagiozov K, Kato Y, Kanno T, Sano H, Koide T, Sawai T (2008) Microinjected F-actin into dividing newt eggs moves toward the next cleavage furrow together with Ca^{2+} stores with inositol 1,4,5-trisphosphate receptor in a microtubule- and microtubule motor- dependent manner. It J Anat Embryol 113:143–152
74. Lee KW, Baker R, Galione A, Gilland EH, Miller AL (1996) Ionophore-induced calcium waves activate unfertilized zebrafish (*Danio rerio*) eggs. Biol Bull 191:265–267
75. Kühtreiber WM, Jaffe LF (1990) Detection of extracellular calcium gradients with a calcium-specific vibrating electrode. J Cell Biol 110:1565–1573
76. Chan CM, Chen Y, Hung TS, Miller AL, Shipley AM, Webb SE (2015) Inhibition of SOCE disrupts cytokinesis in zebrafish embryos mainly via inhibition of cleavage furrow deepening. Int J Dev Biol 59:289–301
77. Chan CM, Aw JTM, Webb SE, Miller AL (2016) SOCE proteins, STIM1 and Orai1, are localized to the cleavage furrow during cytokinesis of the first and second cell division cycles in zebrafish embryos. Zygote 24:880–889
78. Bomben VC, Sontheimer H (2010) Disruption of transient receptor potential canonical channel 1 causes incomplete cytokinesis and slows the growth of human malignant gliomas. Glia 58:1145–1156
79. Mabuchu I, Takano-Ohmuro H (1990) Effects of inhibitors of myosin light chain kinase and other protein kinases of the first cell division of sea urchin eggs. Develop Growth Differ 32:549–556
80. Mabuchu I, Tsukita S, Tsukita S, Sawai T (1988) Cleavage furrow isolated from newt eggs: contraction, organization of the actin filaments, and protein components of the furrow. Proc Natl Acad Sci USA 85:5966–5970
81. Murthy K, Wadsworth R (2005) Myosin-II-dependent localization and dynamics of F-actin during cytokinesis. Curr Biol 15:724–731
82. Smith JL, Silveira LA, Spudich JA (1996) Myosin light chain kinase (MLCK) gene disruption in *Dictyostelium*: a role for MLCK-A in cytokinesis and evidence for multiple MLCKs. Proc Natl Acad Sci USA 93:12321–12326
83. Yamakita Y, Yamashiro S, Matsumura F (1994) *In vivo* phosphorylation of regulatory light chain of myosin II during mitosis of cultured cells. J Cell Biol 124:129–137
84. Wong R, Fabian L, Forer A, Brill JA (2007) Phospholipase C and myosin light chain kinase inhibition define a common step in actin regulation during cytokinesis. BMC Cell Biol 8:15. https://doi.org/10.1186/1471-2121-8-15
85. Wu Q, Sahasrabudhe RM, Luo LZ, Lewis DW, Gollin SM, Saunders WS (2010) Deficiency in myosin light-chain phosphorylation causes cytokinesis failure and multipolarity in cancer cells. Oncogene 29:4183–4193
86. Batchelder EL, Thomas-Virnig CL, Hardin JD, White JG (2007) Cytokinesis is not controlled by calmodulin or myosin light chain kinase in the *Caenorhabditis elegans* early embryo. FEBS Lett 581:4337–4341
87. Webb SE, Goulet C, Chan CM, Yuen MYF, Miller AL (2014) Biphasic assembly of the contractile apparatus during the first two cell division cycles in zebrafish embryos. Zygote 22:218–228
88. Celton-Morizur S, Bordes N, Fraisier V, Tran PT, Paoletti A (2004) C-terminal anchoring of mid1p to the membrane stabilizes cytokinetic ring position in early mitosis in fission yeast. Mol Cell Biol 24:10621–10635
89. Laplante C, Huang F, Tebbs IR, Bewersdorf J, Pollard TD (2016) Molecular organization of cytokinesis nodes and contractile rings by super-resolution fluorescence microscopy of live fission yeast. Proc Natl Acad Sci USA 113(40):E5876–E5885. https://doi.org/10.1073/pnas.1608252113
90. Field SJ, Madson N, Kerr ML, Galbraith KAA, Kennedy CE, Tahiliani M, Wilkins A, Cantley LC (2005) PtdIns(4,5)P2 functions at the cleavage furrow during cytokinesis. Curr Biol 15:1407–1412

91. Naito Y, Okada M, Yagisawa H (2006) Phospholipase C isoforms are localised at the cleavage furrow during cytokinesis. J Biochem 140:785–791
92. Han JK, Fukami K, Nuccitelli R (1992) Reducing inositol lipid hydrolysis, Ins(1,4,5)P_3 receptor availability, or Ca^{2+} gradients lengthens the duration of the cell cycle in *Xenopus laevis* blastomeres. J Cell Biol 116:147–156
93. Wong R, Hadjiyanni I, Wei HC, Polevoy G, McBride R, Sem KP, Brill JA (2005) PIP2 hydrolysis and calcium release are required for cytokinesis in *Drosophila* spermatocytes. Curr Biol 15:1401–1406
94. Liu J, Fairn GD, Ceccarelli DF, Sicheri F, Wilde A (2012) Cleavage furrow organization requires PIP2- mediated recruitment of anillin. Curr Biol 22:64–69
95. Piekny AJ, Glotzer M (2007) Anillin is a scaffold protein that links RhoA, actin and myosin during cytokinesis. Curr Biol 18:30–36
96. Goldback P, Wong R, Beise N, Sarpal R, Trimble WS, Brill JA (2010) Stabilization of the actomyosin ring enables spermatocyte cytokinesis in *Drosophila*. Mol Biol Cell 21:1482–1493
97. Rodal AA, Kozubowski L, Goode BL, Drubin DG, Hartwig JH (2005) Actin and septin ultrastructures at the budding yeast cell cortex. Mol Biol Cell 16:372–384
98. Foe VE, Field CM, Odell GM (2000) Microtubules and mitotic cycle phase modulate spatiotemporal distributions of F-actin and myosin II in *Drosophila* syncytial blastoderm embryos. Development 127:1767–1787
99. Lucero A, Stack C, Bresnick AR, Shuster CB (2006) A global, myosin light chain kinase-dependent increase in myosin II contractility accompanies the metaphase-anaphase transition in sea urchin eggs. Mol Biol Cell 17:4093–4104
100. Li CJ, Heim R, Lu P, Pu Y, Tsien RY, Chang DC (1999) Dynamic redistribution of calmodulin in HeLa cells during cell division as revealed by a GFP-calmodulin fusion protein technique. J Cell Sci 112:1567–1577
101. Yu YY, Chen Y, Dai G, Chen J, Sun XM, Wen CJ, Zhao DH, Chang DC, Li CJ (2004) The association of calmodulin with central spindle regulates the initiation of cytokinesis in HeLa cells. Int J Biochem Cell Biol 36:1562–1572
102. Murakoshi H, Wang H, Yasuda R (2011) Local, persistent activation of Rho GTPases during plasticity of single dendritic spines. Nature 472:100–104
103. Drechsel DN, Hyman AA, Hall A, Glotzer M (1997) A requirement for Rho and Cdc42 during cytokinesis in *Xenopus* embryos. Curr Biol 7:12–23
104. Bernaud C, Le Dez G, Mironov S, Galli F, Reboutier D, Prigent C (2015) Annexin A2 is required for the early steps of cytokinesis. EMBO Rep 16:481–489
105. Feng B, Schwarz H, Jesuthasan S (2002) Furrow-specific endocytosis during cytokinesis of zebrafish blastomeres. Exp Cell Res 279:14–20
106. Caswell PT, Vadrevu S, Norman JC (2009) Integrins: masters and slaves of endocytic transport. Nature Rev Mol Cell Biol 10:843–853
107. McKay HF, Burgess DR (2011) 'Life is a highway': membrane trafficking during cytokinesis. Traffic 12:247–251
108. Neto H, Collins LL, Gould GW (2011) Vesicle trafficking and membrane remodeling in cytokinesis. Biochem J 437:13–24
109. Urven LE, Yabe T, Pelegri F (2006) A role for non-muscle myosin II function in furrow maturation in the early zebrafish embryo. J Cell Sci 119:4342–4352
110. Sato K, Kawashima S (2001) Calpain function in the modulation of signal transduction molecules. Biol Chem 382:743–751
111. Chen MC, Zhou Y, Detrich HW III (2002) Zebrafish mitotic kinesin-like protein 1 (Mklp1) functions in embryonic cytokinesis. Physiol Gen 8:51–66
112. Raich WB, Moran AN, Rothman JH, Hardin J (1998) Cytokinesis and midzone microtubule organization in *Caenorhabditis elegans* require the kinesin-like protein ZEN-4. Mol Biol Cell 9:2037–2049

113. Kuryama R, Gustus C, Terada Y, Uetake Y, Matuliene J (2002) CHO1, a mammalian kinesin-like protein, interacts with F-actin and is involved in the terminal phase of cytokinesis. J Cell Biol 156:783–790
114. Matuliene J, Kuriyama R (2002) Kinesin-like protein CHO1 is required for the formation of midbody matrix and the completion of cytokinesis in mammalian cells. Mol Biol Cell 13:1832–1845
115. Zhu C, Bossy-Wetzel E, Jiang W (2005) Recruitment of MKLP1 to the spindle midzone/midbody by INCENP is essential for midbody formation and completion of cytokinesis in human cells. Biochem J 389:373–381
116. Abe H, Obinata T, Minamide LS, Bamburg JR (1996) *Xenopus laevis* actin-depolarizing factor/cofilin: a phosphorylation-regulated protein essential for development. J Cell Biol 132:871–885
117. Ono K, Parast M, Alberico C, Benian GM, Ono S (2003) Specific requirement for two ADF/cofilin isoforms in distinct actin-dependent processes in *Caenorhabditis elegans*. J Cell Sci 116:2073–2085
118. Nusco GA, Chun JT, Ercolano E, Lim D, Gragnaniello G, Kyozuka K, Santella L (2006) Modulation of calcium signalling by the actin-binding protein cofilin. Biochem Biophys Res Communs 348:109–114
119. Creutz CE, Tomsig JL, Snyder SL, Gautier MC, Skouri F, Beisson J, Cohen J (1998) The copines, a novel class of C2 domain-containing, calcium-dependent, phospholipid-binding proteins conserved from *Paramecium* to humans. J Biol Chem 273:1393–1402
120. Damer CK, Bayeva M, Kim PS, Ho LK, Eberhardt ES, Socec CI, Lee JS, Bruce EA, Goldman-Yassen AE, Naliboff LC (2007) Copine A is required for cytokinesis, contractile vacuole function, and development in *Dictyostelium*. Euk Cell 6:430–442
121. Berridge MJ, Bootman MD, Llewelyn Roderick H (2003) Calcium signalling: dynamics, homeostasis and remodelling. Nature Rev Mol Cell Biol 4:517–529